frontiers | Research Topics

Cyanobacterial diversity: Environmental effect and ecosystem functioning

Edited by
Da Huo, Hua Li, Beatriz Roncero Ramos, Yueming Qu and Man Xiao

Published in
Frontiers in Microbiology

ISSN 1664-8714
ISBN 978-2-8325-5452-4
DOI 10.3389/978-2-8325-5452-4

About Frontiers

Frontiers is more than just an open access publisher of scholarly articles: it is a pioneering approach to the world of academia, radically improving the way scholarly research is managed. The grand vision of Frontiers is a world where all people have an equal opportunity to seek, share and generate knowledge. Frontiers provides immediate and permanent online open access to all its publications, but this alone is not enough to realize our grand goals.

Frontiers journal series

The Frontiers journal series is a multi-tier and interdisciplinary set of open-access, online journals, promising a paradigm shift from the current review, selection and dissemination processes in academic publishing. All Frontiers journals are driven by researchers for researchers; therefore, they constitute a service to the scholarly community. At the same time, the *Frontiers journal series* operates on a revolutionary invention, the tiered publishing system, initially addressing specific communities of scholars, and gradually climbing up to broader public understanding, thus serving the interests of the lay society, too.

Dedication to quality

Each Frontiers article is a landmark of the highest quality, thanks to genuinely collaborative interactions between authors and review editors, who include some of the world's best academicians. Research must be certified by peers before entering a stream of knowledge that may eventually reach the public - and shape society; therefore, Frontiers only applies the most rigorous and unbiased reviews. Frontiers revolutionizes research publishing by freely delivering the most outstanding research, evaluated with no bias from both the academic and social point of view. By applying the most advanced information technologies, Frontiers is catapulting scholarly publishing into a new generation.

What are Frontiers Research Topics?

Frontiers Research Topics are very popular trademarks of the *Frontiers journals series*: they are collections of at least ten articles, all centered on a particular subject. With their unique mix of varied contributions from Original Research to Review Articles, Frontiers Research Topics unify the most influential researchers, the latest key findings and historical advances in a hot research area.

Find out more on how to host your own Frontiers Research Topic or contribute to one as an author by contacting the Frontiers editorial office: frontiersin.org/about/contact

Cyanobacterial diversity: Environmental effect and ecosystem functioning

Topic editors

Da Huo — Institute of Hydrobiology, Chinese Academy of Sciences (CAS), China

Hua Li — Key Laboratory of Algal Biology, Institute of Hydrobiology, Chinese Academy of Sciences (CAS), China

Beatriz Roncero Ramos — Sevilla University, Spain

Yueming Qu — UK Centre for Ecology and Hydrology (UKCEH), United Kingdom

Man Xiao — Nanjing Institute of Geography and Limnology, Chinese Academy of Sciences (CAS), China

Citation

Huo, D., Li, H., Ramos, B. R., Qu, Y., Xiao, M., eds. (2024). *Cyanobacterial diversity: Environmental effect and ecosystem functioning*. Lausanne: Frontiers Media SA. doi: 10.3389/978-2-8325-5452-4

Table of contents

frontiers | Frontiers in Microbiology

TYPE Original Research
PUBLISHED 09 November 2023
DOI 10.3389/fmicb.2023.1284864

OPEN ACCESS

EDITED BY
Liang Peng,
Hunan Agricultural University, China

REVIEWED BY
Chongfeng Bu,
Institute of Soil and Water Conservation, Chinese Academy of Sciences (CAS), China
Lijuan Ren,
Jinan University, China

*CORRESPONDENCE
Hua Li
✉ lih@ihb.ac.cn

RECEIVED 29 August 2023
ACCEPTED 23 October 2023
PUBLISHED 09 November 2023

CITATION
Li Y, Wang F, Yang H, Li H and Hu C (2023) Balanced biogeographic and local environmental effects determine the patterns of microbial diversity in biocrusts at multi-scales.
Front. Microbiol. 14:1284864.
doi: 10.3389/fmicb.2023.1284864

Balanced biogeographic and local environmental effects determine the patterns of microbial diversity in biocrusts at multi-scales

Yuanlong Li[1,2], Fengdi Wang[3], Haijian Yang[2], Hua Li[2]* and Chunxiang Hu[2]

[1]Hunan Provincial Key Laboratory of Carbon Neutrality and Intelligent Energy, School of Resource and Environment, Hunan University of Technology and Business, Changsha, China, [2]Key Laboratory of Algal Biology, Institute of Hydrobiology, Chinese Academy of Sciences, Wuhan, China, [3]Institute of Hematology, Union Hospital, Tongji Medical College, Huazhong University of Science and Technology, Wuhan, China

Introduction: Biodiversity maintenance and its underlying mechanisms are central issues of ecology. However, predicting the composition turnovers of microbial communities at multiple spatial scales remains greatly challenging because they are obscured by the inconsistent impacts of climatic and local edaphic conditions on the assembly process.

Methods: Based on the Illumina MiSeq 16S/18S rRNA sequencing technology, we investigated soil bacterial and eukaryotic communities in biocrusts with different successional levels at a subcontinental scale of Northern China.

Results: Results showed that irrespective of spatial scale, bacterial α diversity increased but eukaryotic diversity decreased with the primary succession, whereas both β diversities decreased at the subcontinental scale compared with smaller scales, indicating that the biogeographic pattern of soil microorganisms was balanced by successional convergence and distance decay effect. We found that the convergence of bacterial and eukaryotic communities was attributed to the turnovers of generalist and specialist species, respectively. In this process, edaphic and climatic factors showed unique roles in the changes of diversity at local/subcontinental scales. Moreover, the taxonomic diversity tended to be more susceptible to climatic and edaphic conditions, while biotic factors (photosynthesis and pigments) were more important to phylogenetic diversity.

Conclusion: Taken together, our study provided comprehensive insights into understanding the pattern of microbial diversity at multiple spatial scales of drylands.

KEYWORDS

biogeography, biological soil crusts, cyanobacteria, microbial diversity, multiple spatial scales, primary succession, species turnover

1. Introduction

Efficient restoration of degraded soils is dependent on a sufficient understanding of how soil communities are generated and maintained during succession (Lan et al., 2014). It raises questions about the nature of soil biodiversity changes and the extent to which it is regulated (Miralles et al., 2020). However, exploring the interrelations among biodiversity changes, community structures, and environmental conditions remains a great challenge (Gotelli et al., 2017; Magurran et al., 2018; O'Sullivan et al., 2019). A number of previous studies have demonstrated that species diversity increases with primary succession across a wide range of

different habitats (Jessup et al., 2004; Nemergut et al., 2013; Angel Fernandez-Martinez et al., 2017). Meanwhile, the degree of differentiation between communities (i.e., β diversity) at a certain successional stage is expected to decrease with development, which is due to the selection effect under homogeneous environments (Dini-Andreote et al., 2015). However, evidence of these observed characteristics of microbial diversity is primarily achieved at a single spatial scale (Dornelas et al., 2014), which is particularly influenced by local abiotic conditions. It makes the meta-analysis of microbial diversity across individual studies unfeasible and considerably hinders the comprehensive understanding of the mechanism of diversity maintenance in this mega-diverse community. Therefore, an integrated view that depicts the diversity pattern of soil microorganisms at multiple spatial scales and assesses their co-variability with the environments is being proposed increasingly (Fierer et al., 2010; Bracken et al., 2017).

As a model system in a community (Bowker et al., 2014), biological soil crusts (biocrusts) dominate the topsoil of drylands worldwide and represent a crucial functional component of the ecosystem (Rossi et al., 2017; Li et al., 2021; Weber et al., 2022). According to the edaphic properties of development and community compositions, biocrusts can be classified into different successional stages (Lan et al., 2013). Distinct sets of microbial members reportedly constitute each successional stage of biocrusts, irrespective of geographic separation. The compositions of soil microorganisms in different stages converged at taxonomic and phylogenetic facets at a large spatial distance, whereas various biocrust components with different successional stages can be used to establish a mosaic pattern of micro-landscape at the centimeter scale (Bowker et al., 2013; Weber et al., 2016). Given the combined effect of convergence succession (Xu et al., 2020), high dispersal limitation (Li and Hu, 2021), and special patchy distribution of biocrusts (Li et al., 2016), regional species pools under different environments may contain only closely related species that adapt to the particular habitat of biocrusts. Thus, an emerging question rooted in the primary succession of biocrusts is whether the patterns of biodiversity change are idiosyncratic at local and continental scales, which is associated with the regimes of microbial assembly at multiple spatial scales.

Meanwhile, environmental factors are considered an important cause of the changes in microbial diversity (Rillig et al., 2019). However, the effect of environmental factors on diversity to a large extent is spatially autocorrelated, especially in biocrust communities. In small-scale habitats, biocrusts can tolerate limited moisture and nutrients and respond rapidly to pulsed ambient conditions (Cable and Huxman, 2004; Schwinning and Sala, 2004). A patchy micro-landscape is partly attributed to soil properties, as well as the decomposition of cyanobacterial biomass followed by the releases of exopolysaccharides (EPS), by which carbon sources accumulate unevenly and act as a repository for heterotrophic diversity (Rossi and De Philippis, 2015). At the macro-scale, regional climatic variables such as solar irradiation and precipitation are the most important factors affecting the pattern of microbial diversity on all successional components of biocrusts (Couradeau et al., 2016; Fernandes et al., 2018). Meanwhile, high climatic stresses can impede the succession and rollback of well-developed biocrusts into an early successional stage (Johnson et al., 2012; Reed et al., 2012; Ferrenberg et al., 2015), at which microbial composition significantly changes. Therefore, the heterogeneity of microbial biodiversity in biocrusts can probably be generated through interaction among climatic, edaphic, and biotic drivers. However, the relative importance and uniqueness of these influences on the pattern of microbial biodiversity in biocrusts at different scales remain unclear.

In this study, we performed the analyses on a dataset comprised of cyanobacterial, cyanobacterial-lichen, and moss-dominated crusts from 50 sites across 3,000 km in northern China (Li and Hu, 2021). These components constituted a series of successional stages from the initial to mature biocrusts (Walker et al., 2010; Ladau and Eloe-Fadrosh, 2019). We defined the local and continental scales according to the size of sampling areas (Supplementary Figure S1). Illumina MiSeq 16S/18S rRNA sequencing was used to examine the compositions of bacterial and eukaryotic communities of different successional biocrusts. Then, we further determined the characteristics and dynamics of the associations of climatic, edaphic, and biotic factors with α/β-diversity of microbial communities, to explore the underlying mechanisms of biodiversity maintenance in biocrusts. These analyses allow us to address three questions: First, does a shifting pattern of α and β diversity exist at local and continental scales along succession? Second, is there a balanced biogeographic pattern between bacterial and eukaryotic communities in soils? Third, which factors are more pivotal to underpin the change of microbial diversity in drylands?

2. Materials and methods

2.1. Sampling, definition of spatial scales, and data collection

35 cyanobacterial, 6 cyanobacteria-lichen, and 9 moss crust-dominated sites were included in a wide range of transects across seven major deserts and the Loess Plateau in northern China [see Li and Hu (2021)]. A total of 140 cyanobacterial, 24 cyanobacteria-lichen, and 36 moss crust samples were collected. Criteria of successional stages were established based on a previous study (Lan et al., 2012), and more details are described in the Supplementary Methods. Biocrusts together with apparently attached subsoil were collected with a shovel and preserved in sterilized plastic Petri dishes to ensure integrity. Macroscopic moss plants were removed from the moss-dominated biocrust to eliminate their potential influence on sequencing and physicochemical measurements.

We defined the *local scale* as the minimum area concurrently covering three successional stages (4 local areas gained) and the *continental scale* as the entire study area (Supplementary Figure S1). The environmental variables were classified into climatic and edaphic factors. Climatic factors included altitude, mean annual precipitation, mean annual sunshine duration, aridity index, windspeed, and mean annual temperature. These data are referenced from the National Meteorological Information Center (http://data.cma.cn/). Edaphic factors included soil texture, crust thickness, water content, soil pH, total phosphorus, total nitrogen, total organic carbon, and salinity. Besides, biotic factors included variable fluorescence/maximal fluorescence, gross photosynthesis/respiration, extracellular polysaccharide, bacteriochlorophyll *a*, scytonemin, chlorophyll *a*, alkaline protease, β-glucosidase, and alkaline phosphatase (see Supplementary Methods).

Total genomic DNA was extracted using the PowerSoil ®DNA Isolation Kit (Mo Bio, Carlsbad, CA, USA). The V3-V4 region of the bacterial 16S rRNA gene was amplified with the primers 338F/806R (Mori et al., 2014), and the V4 region of the eukaryotic 18S rRNA gene was amplified with the primers 3NDF/V4_euk_R2 (Amaral-Zettler et al., 2009). Sequencing was performed on the Illumina MiSeq PE300 platform (Illumina, San Diego, CA, USA). Raw FASTQ files were demultiplexed, quality filtered by Trimmomatic, and merged by FLASH with the following criteria: (i) reads were truncated at any site receiving an average quality score < 20 over a 50 bp sliding window; (ii) primers were exactly matched to allow 2-nucleotide mismatching, and reads containing ambiguous bases were removed; and (iii) sequences with overlap longer than 10 bp were merged according to their overlap sequence. Operational taxonomic units (OTUs, hereafter denoted species) were generated from defined representative sequences, with clustering at 97% similarity. The RDP classifier was used for the taxonomic annotation of representative sequences based on an identity threshold of 0.7 in the SILVA 128 database for bacteria and eukaryotic microorganisms (i.e., fungi, protozoa, and eukaryotic microalgae).

2.2. Calculations of biodiversity indices and species turnover

To study the patterns of α and β diversity along with the succession, we calculated the Shannon diversity (*H′*), phylogenetic diversity (PD), species richness, and Pielou evenness (α diversity indices) (Hurlbert, 1971), as well as the Bray-Curtis and weighted-UniFrac dissimilarities between paired samples (β diversity) (Anderson et al., 2006). At the local scale, β diversity was calculated among four adjacent parallel samples within the same successional stage. At the continental scale, the paired difference indices were calculated between the sites several kilometers apart. These analyses were performed by package vegan in *R* (Oksanen et al., 2015). ANOVA was used to analyze the significant level of α and β diversity among three successional stages (SPSS version 20, $^{*}p < 0.05$, $^{**}p < 0.01$).

To study the patterns of ubiquitous taxa, we defined the species occurring in >85% of samples as ubiquitous taxa and calculated their relative abundance in each sample. These ubiquitous taxa were selected from cyanobacterial, cyanobacterial-lichen, and moss-dominated biocrusts, respectively, and also selected from the meta-community. Then, the relationships of α diversity (*H′* and PD) with the relative abundance of ubiquitous taxa were measured.

For phylogenetic analyses, species with a cumulative abundance of 85% in bacterial and eukaryotic communities were retained. The phylogenetic tree was constructed using Fast Tree v2.2.10 with default settings having 500 iterations and 999 bootstraps (Price et al., 2009) and visualized at iTOL.[1] Meanwhile, the edge-length abundance distribution was calculated from each successional phylogeny (O'Dwyer et al., 2012).

To explore the source of community difference, the Sørensen dissimilarity (β_{sor}) in each successional stage was partitioned into the turnover (β_{sim}) and nestedness (β_{nes}) components (Baselga, 2010). The Sørensen dissimilarity was formulated as follows:

$$\beta sor = \frac{b + c}{2a + b + c};$$

Simpson dissimilarity index was used to describe spatial turnover without the influence of richness gradients, formulated as follows:

$$\beta sim = \frac{\min(b,c)}{a + \min(b,c)};$$

The β_{nes} component was calculated as follows:

$$\beta nes = \beta sor - \beta sim$$

In the equations, *a* is the number of species occurring in both paired sites of each successional stage, *b* is the number of species that occur only in one site, and *c* is the number of species occurring in the other site. They were calculated in the package betapart in *R*. βsim/βsor was considered as the turnover ratio (Baselga, 2010), and its correlations with α diversity (Spearman correlation) in the bacterial and eukaryotic community were calculated at local and continental scales, respectively. Environmental data were transformed by the Euclidean distance for the Mantel test (Spearman, permutation = 999, $^{*}p < 0.05$, $^{**}p < 0.01$), which was used to investigate the correlations between the turnover ratio and the micro-environmental (including edaphic and biotic factors) and macro-climatic (climatic factors) conditions in each successional stage (the package vegan in *R*) (Oksanen et al., 2015). Then, the highly related factors were selected at local and continental scales through Spearman correlation analysis.

2.3. Investigation of the biogeographic pattern

To compare the effects of primary succession and biogeography on community differences, we used the samples from four local scales. Community differences were calculated by analysis of similarities (ANOSIM; permutation = 999, $^{*}p < 0.05$, $^{**}p < 0.01$) based on Bray–Curtis and weighted–UniFrac dissimilarities at the species level, respectively.

We investigated community differences among three successional stages, and each successional stage contained samples from the two sample sites (termed as compared among successional stages). Meanwhile, community differences were compared between two sample sites, and each site contained three successional stages (termed as compared between sample sites). In these two ways of comparisons, vast subsets of combinations were obtained when an alterable number of samples between paired comparisons was used instead of whole samples. Here, community differences were computed using 100 randomly combinational comparisons. Finally, the community differences (R^2) with distance were studied by linear regression, and a schematic is shown in Supplementary Figure S2.

1 https://itol.embl.de/

2.4. Covariant relationships between biodiversity and the environment

Changes in the covariant relationships between α/β diversity and environmental factors with succession were assessed using multiple linear regression. Environmental factors with high multicollinearity were first excluded, and then the optimum combination of environments was selected by the all-subset regression method (the package leaps in *R*) and checked by the Global Statistical Test (the package gvlma in *R*). When the linear models had the same goodness-of-fit (GoF), the one with a lower Akaike information criterion was selected.

Partial least square path models (PLS-PMs) were also applied to demonstrate the correlations of environmental factors with α and β diversity by using the package plspm in *R*. First, climatic, edaphic, and biotic data were transformed into Z-scores and then their Euclidean distance was calculated, respectively. The distance of integrated α diversity indices (including PD, richness, and Pielou evenness) was also calculated. The Bray-Curtis and weighted–UniFrac dissimilarities were used to indicate the taxonomic and phylogenetic facets of β diversity. Dissimilarity data were introduced into initial PLS-PMs based on an *a priori* conceptual hypothesis, and paths with <0.7 loadings were removed. This process cannot be contrary to logic and was stopped until model matching achieved the optimum fit. Finally, we established PLS-PMs for bacterial and eukaryotic communities in cyanobacterial, cyanobacteria–lichen, and moss-dominated biocrusts, respectively. We quantified the relationships among these variables with path coefficients. The GoF index was used to estimate the prediction performance of models.

3. Results

3.1. Community structure and phylogenetic characteristics

To intuitively display the community structure, 140 cyanobacterial, 24 cyanobacterial-lichen, and 36 moss-dominated biocrust communities were arranged according to ascending *H′*. The bacterial communities were primarily composed of Cyanobacteria with the highest abundance (29.63%), Proteobacteria (22.14%), and Actinobacteria (21.81%) (Figure 1A), whereas the eukaryotic communities were dominated by Ascomycota (39.73%) and Phragmoplastophyta (39.15%) (Figure 1B). The number of phyla having a linear relationship with α diversity at the early successional stage was at least 1.5 times higher than that at the late stage in both communities (Supplementary Table S1), and the multiple was even larger at the class, order, family, and genus levels (Supplementary Table S2). According to the phylogenetic tree (Supplementary Figure S3), the bacterial community had more clades and branching events than eukaryotes. In bacteria and eukaryotes, nearly all branches appeared in the early successional stage, whereas some branches disappeared at the later stage primarily in firmicutes and some Cyanobacteria of bacteria, as well as Phragmoplastophyta of eukaryotes. Thus, the abundance of phyla tended to be stable and that of some branches was excluded from the phylogeny with succession.

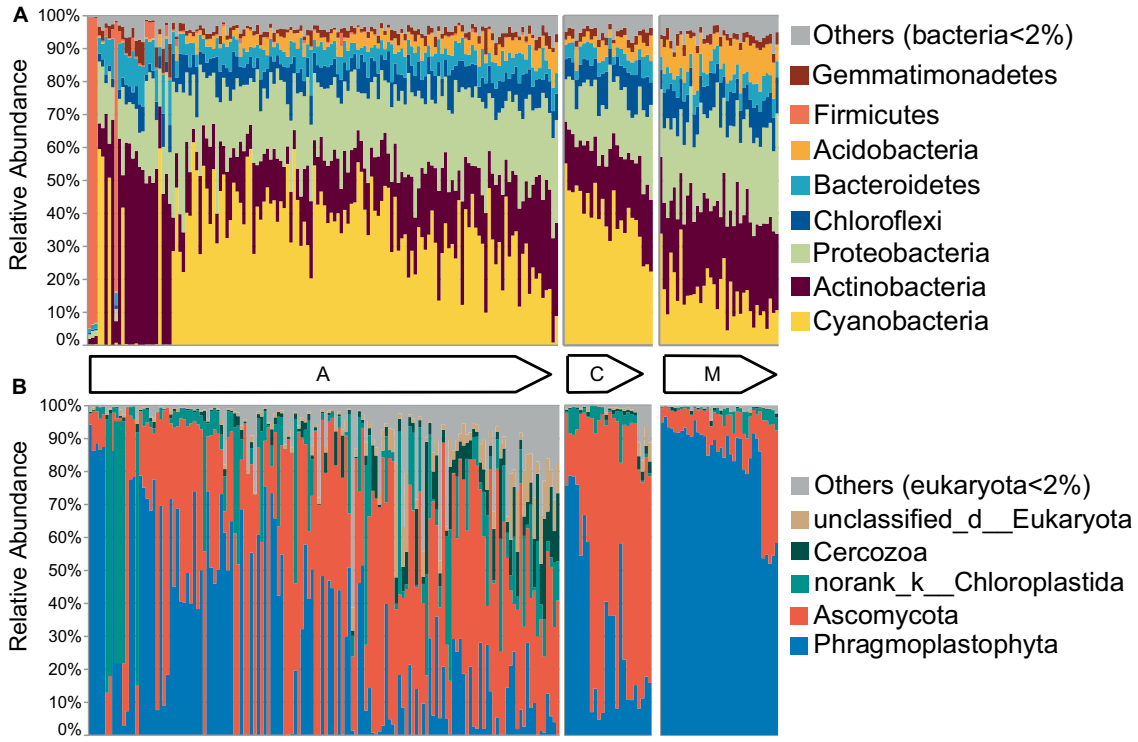

FIGURE 1
The community structures of biocrusts changed with succession. The community structures of cyanobacterial (A), cyanobacterial-lichen (C), and moss-dominated (M) crusts were separately arranged according to the increased Shannon index in bacteria **(A)** and eukaryotes **(B)** as shown by the arrow direction.

3.2. The changing pattern of α and β diversity with succession

H′ and PD were synchronously used to indicate the change feature of α diversity with successional stages (Figures 2A,B; Supplementary Table S3). At the local and continental scales, the α diversity indices in both communities gradually changed with the primary succession in a small range, whereas the α diversity of bacteria increased and that of eukaryotes decreased. In other words, α diversity of the bacterial community in moss-dominated crusts was two times higher than that of cyanobacterial crusts, whereas α diversity of the eukaryotic community in moss-dominated crusts declined by half than cyanobacterial crusts. Furthermore, we found that *H′* and PD had significant differences between cyanobacterial and moss-dominated crusts rather than between cyanobacterial and cyanobacteria-lichen for bacterial and eukaryotic communities (ANOVA, $^*p<0.05$). Regardless of the spatial scales, bacterial and eukaryotic α diversity increased and decreased with the primary succession of biocrusts, respectively.

With the succession of biocrusts, the phylogenetic and taxonomic β diversity of bacterial and eukaryotic communities both decreased nearly by half and these values became stable at the late stage (moss crusts) compared with the early stage (cyanobacterial crust) at the local and continental scales (Figures 2C,D; Supplementary Table S3). Sørensen dissimilarity was partitioned into turnover and nestedness components (Figures 2E,F), and the turnover component dominated (>85%) in each successional stage at both spatial scales. Comparison of the ratio of turnover among spatial scales (ANOVA, local scales: $n=12$; continental scale: $n=3$) revealed no significant difference in bacteria, but the turnover of eukaryotes increased at larger spatial scales. Regardless of spatial scales, consistently positive or negative correlations existed between turnover ratio and α diversity in bacteria and eukaryotes, respectively (Supplementary Table S4). The sources of community differences in each successional stage were dominated by the turnover component, but the correlations of turnover ratio with α diversity were opposite between bacterial and eukaryotic communities.

The correlations of turnover ratio with environments were explored from the perspective of succession (Supplementary Table S5) and spatial scale (Supplementary Figure S4), respectively. For the succession, the turnover ratio was negatively correlated with environmental conditions, and relatively higher with the micro-environment at the early cyanobacterial stage. Conversely, the turnover ratio was positively correlated with environmental factors, and higher with macro-climate at the late moss stage. For the spatial scale, the turnover ratio was correlated with micro-environments, especially with edaphic factors and biotic activities at the local scale. Significant correlations between turnover ratio and macro-climatic factors, specifically windspeed, primarily occurred at the continental scale.

3.3. Balanced biogeographic pattern between distance-decay and succession

Community differences among successional stages and between integral sample sites were calculated, and then the change trend of the

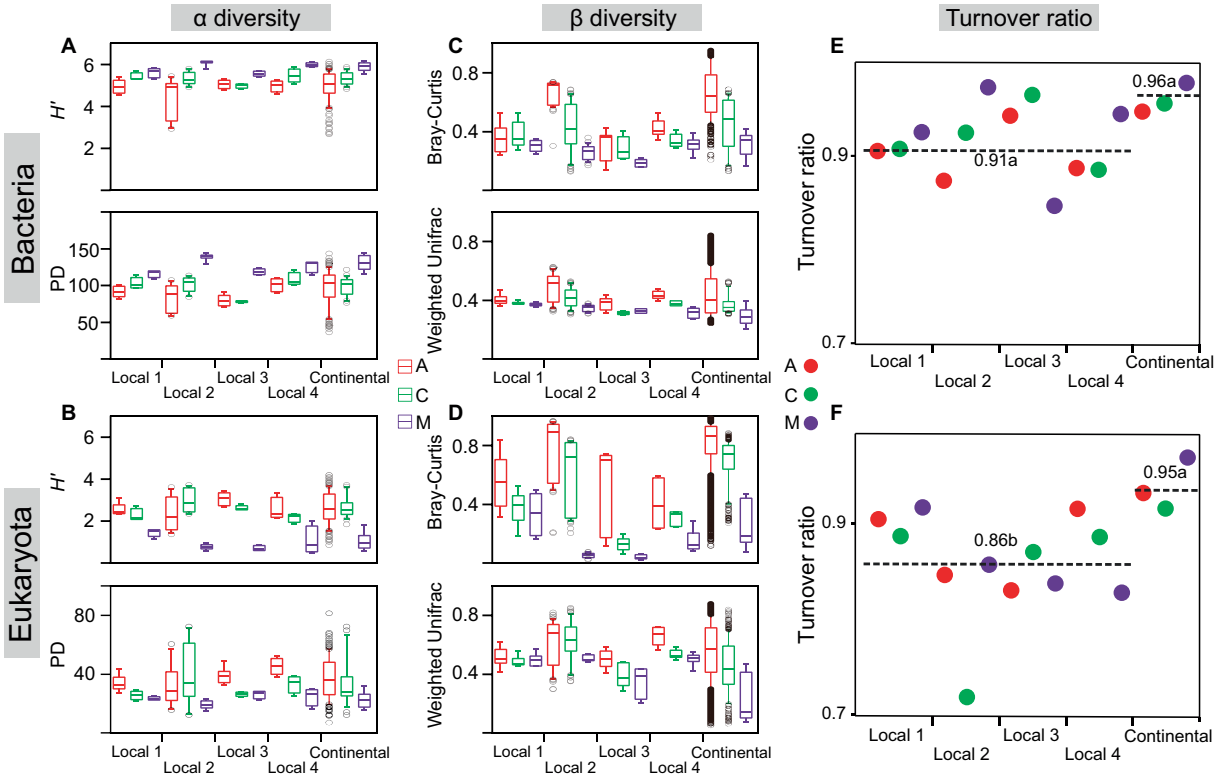

FIGURE 2
Biodiversity changed with succession. The Shannon index (*H′*) and phylogenetic diversity (PD) were calculated in cyanobacterial (A), cyanobacterial-lichen (C), and moss-dominated (M) crusts at local and continental scales **(A,B)**. Bray-Curtis and Weighted-Unifrac dissimilarities were also calculated **(C,D)**. The turnover ratio of bacteria **(E)** and eukaryotes **(F)** was calculated at different spatial scales **(E,F)**. Significant differences were tested by ANOVA (df = 2, $p<0.05$) and marked with lowercase letters as mean values decreased.

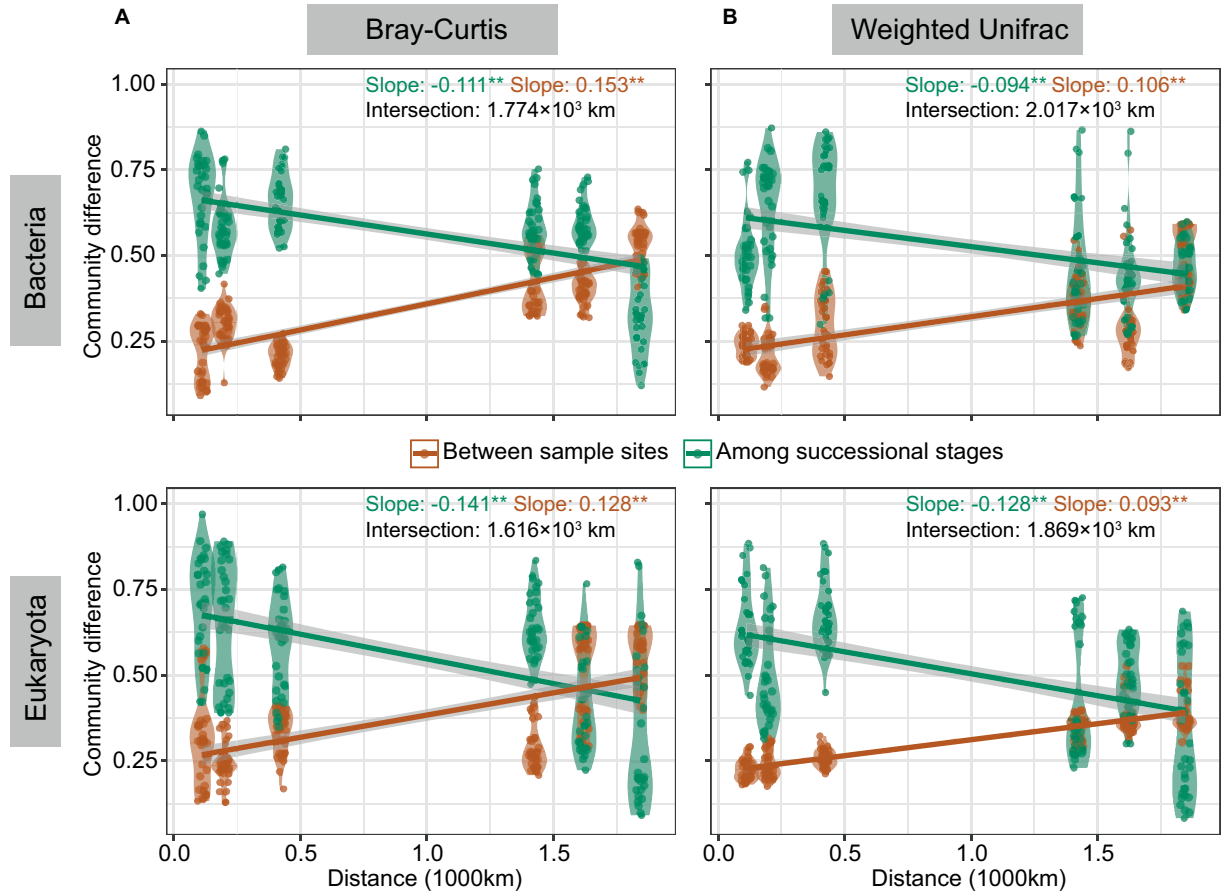

FIGURE 3
The patterns of community differences changed with distance. Community differences were studied by ANOSIM (*$p < 0.05$, **$p < 0.01$) based on Bray-Curtis **(A)** and weighted-UniFrac **(B)** dissimilarity. Linear regression was conducted between community differences and distance. The red line represents differences among successional stages, and the green line represents differences between two sample sites with kilometers of distance. The distance corresponding with the intersection of the two lines was calculated.

two difference values with distance was studied (Figure 3). Results demonstrated that community differences among the three successional stages decreased with distance and that of paired sample sites increased with distance regardless of taxonomic Bray-Curtis or phylogenetic weighted-UniFrac dissimilarity. The distance corresponding with the intersection of two opposite patterns in bacteria (1.77×10^3 and 2.01×10^3 km based on Bray-Curtis and weighted-UniFrac respectively) was larger than that in eukaryotes (1.61×10^3 and 1.86×10^3 km based on Bray-Curtis and weighted-UniFrac respectively). In summary, we found reduced community differences among successional stages with distance, as well as pronounced community differences between sample sites with distance.

3.4. Relationships of habitat environments and biodiversity with succession

At local and continental scales (Figure 4), the covariation of α diversity (*H′* and PD) with environments commonly decreased in bacteria and increased in eukaryotes, whereas the covariation of β diversity (Bray–Curtis and weighted-UniFrac) with environments mostly increased in both communities. Comparatively, the GoFs of edaphic factors with biodiversity were generally greater at local scales (α diversity: 0.69 ± 0.11, β diversity: 0.63 ± 0.16) than that at the continental scale (α diversity: 0.51 ± 0.15, β diversity: 0.46 ± 0.17). Besides, the GoFs of climatic factors (α diversity: 0.64 ± 0.14, β diversity: 0.66 ± 0.21) were greater than that of edaphic factors (α diversity: 0.51 ± 0.15, β diversity: 0.46 ± 0.17) at the continental scale. However, the covariation of biotic factors and biodiversity mostly showed no regularity with succession especially manifesting in the phylogenetic facet. In general, environmental constraints on changes in successional α diversity were opposite between bacteria and eukaryotes, whereas its constraints on changes in successional β diversity were alike in both communities. Their biodiversity changes with succession were also dominantly constrained by edaphic and climatic environments at local and continental scales, respectively.

3.5. Regulation of biodiversity maintenance in biocrusts

In bacteria, only climatic factors had a positive effect on the integrated α diversity of the early successional stage (Figures 5A,D). In eukaryotes, climatic, edaphic, and biotic factors all exerted influences. Integrated α diversity was also positively affected by β diversity. In terms of β diversity, climatic factors were the most

10.3389/fmicb.2023.1284864

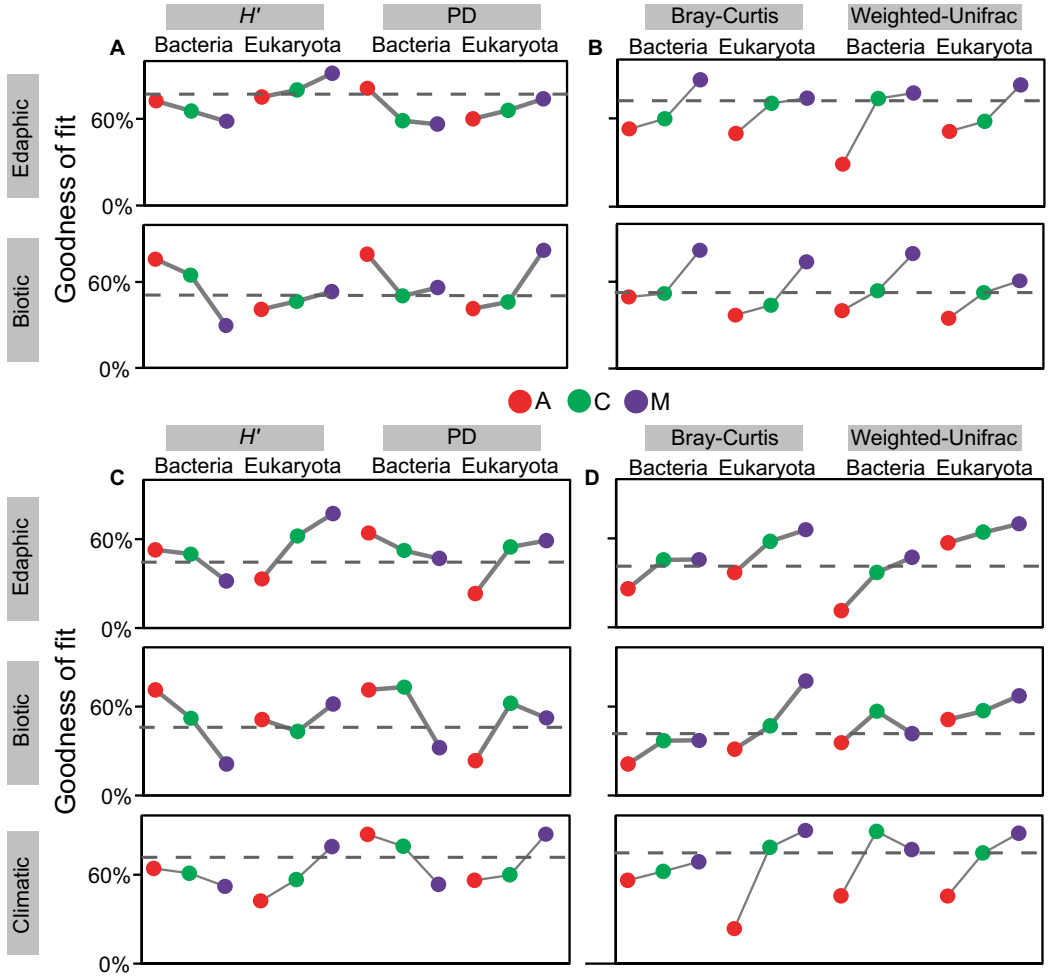

FIGURE 4
Covariant relationships existed between biodiversity and environmental factors with succession. Environmental factors were divided into three categories: edaphic, climatic, and biotic factors. The goodness-of-fits of α/β diversity and environments were calculated at the local scale **(A,B)** and continental scale **(C,D)** in cyanobacterial (A), cyanobacterial-lichen (C), and moss-dominated (M) crusts. The dashed line in the box indicates the average values.

influential environments in bacteria, which had positive and negative effects on the taxonomic and phylogenetic facets, respectively. In eukaryotes, edaphic and biotic factors had positive and negative effects on the taxonomic and phylogenetic facets, respectively.

The integrated α diversity of the middle successional stage (Figures 5B,E) was positively affected by the taxonomic facet of β diversity in both communities. In bacteria, it was additionally affected by biotic factors. In terms of β diversity, taxonomic β was positively influenced by climatic and edaphic factors in bacteria and eukaryotes, and that in bacteria was additionally affected by biotic factors. Conversely, the phylogenetic β was negatively affected by climatic factors in bacteria, and that in eukaryotes was positively affected by edaphic factors.

The integrated α diversity of the late successional stage (Figures 5C,F) was positively affected by climatic factors in both communities. In contrast to the early and middle successional stages, taxonomic β diversity negatively affected integrated α diversity in both communities. In terms of β diversity, taxonomic β was positively affected by climatic and edaphic factors in bacteria and eukaryotes, whereas phylogenetic β diversity was negatively and positively affected by edaphic factors in bacteria and eukaryotes, respectively.

In summary, climatic factors were the most conspicuous environments affecting integrated α diversity. Intriguingly, integrated α diversity tended to be negatively affected by taxonomic β diversity with succession, whereas taxonomic β diversity was consistently regulated positively by environments. Phylogenetic β diversity was the most negatively regulated by the environments.

4. Discussion

4.1. Bacterial α diversity increased but eukaryotic diversity decreased with the primary succession

Following the sequence of primary succession, α diversity often increases (Fierer et al., 2010; Dornelas et al., 2014; Maier et al., 2018; Ortiz-Alvarez et al., 2018). In biocrusts, our results showed that the α diversity of bacterial communities increased, whereas that of

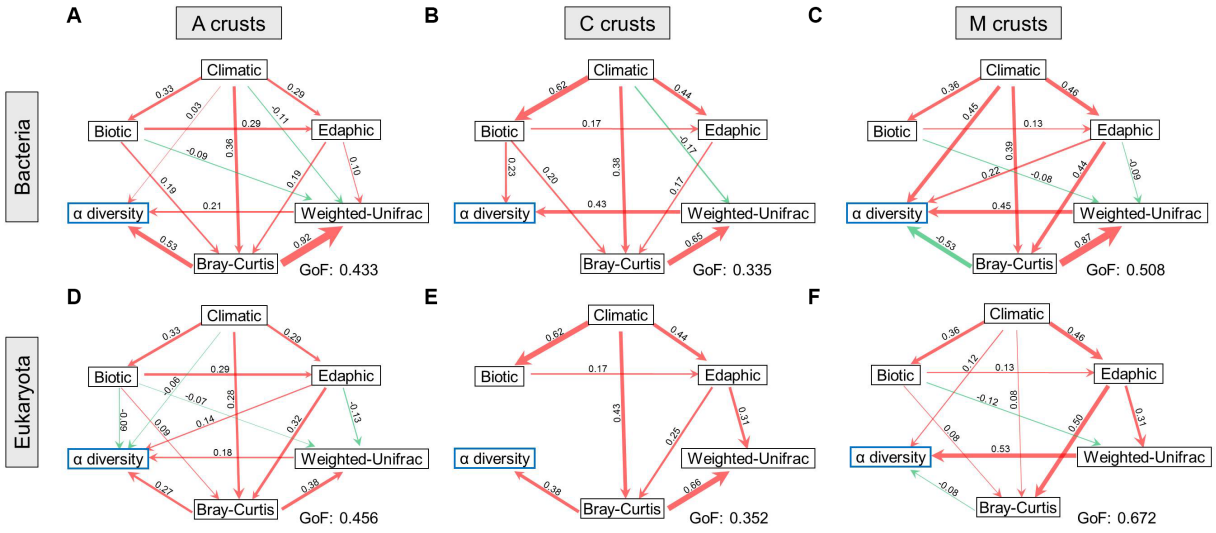

FIGURE 5
Biodiversity maintenance was regulated in biocrusts. The relationships between biodiversity and environments were demonstrated at cyanobacterial (A), cyanobacterial-lichen (C), and moss-dominated (M) crusts in bacteria **(A–C)** and eukaryotes **(D–F)**. The width of the arrow lines indicates the strength of the relationships ($p < 0.05$). Red and green arrows indicate positive and negative relationships, respectively. The values of goodness-of-fit (GoF) are marked, respectively.

eukaryotic communities decreased (Figures 2A,B). This finding implied that even microorganisms in the same succession process may have different change patterns of α diversity, which depend on different responses to environmental stresses and phylogenetic properties of different life domains (Hawkes and Keitt, 2015). Interestingly, we found that these patterns in bacteria and eukaryotes did not change with spatial scales. The α diversity of both communities also tended to fluctuate within a smaller range at the late than at the early stage (Figures 2A,B), manifesting the processes of habitat differentiation and landscape isolation (Leibold et al., 2019). Accordingly, the proportion of common OTUs tended to be larger with the forward succession, so we defined the abundance of ubiquitous taxa as precise chronosequence characteristics to show more detailed α-diversity changes (Supplementary Figure S5). On the level of integral succession (Supplementary Figure S5A), our result showed that α diversity did not increase indefinitely with the abundance of ubiquitous taxa, which can function as a threshold for determining α diversity. On the level of separated succession (Supplementary Figure S5B), the community contained a higher abundance of ubiquitous taxa at the middle-late stage corresponding with higher and lower α diversity in bacteria and eukaryotes, respectively. This finding indicated that this threshold may affect the changes in α diversity with succession, which may explain why α diversity showed hierarchical changes despite the community's continuous. A climax community could also exist in biocrusts (Meiners et al., 2015).

4.2. β diversities of both bacteria and eukaryotes decreased with succession at the subcontinental scale

β diversity decreased with succession (Figures 2C,D), proving the results of primary succession in many habitats (Purschke et al., 2013; Dornelas et al., 2014; Ortiz-Alvarez et al., 2018). This phenomenon can be considered as biotic homogenization driven by environments (Olden, 2006) and has been observed in many terrestrial assemblages (Rodrigues et al., 2013; Mori et al., 2015; Gossner et al., 2016). This result also can be explained by the successional convergence driven by self-organization in chronosequences (O'Sullivan et al., 2019; Xu et al., 2020). Moreover, the number of phyla that had a covariant relationship with α diversity decreased with succession in both communities (Supplementary Tables S1, S2). These findings indicated a tendency for a stable community structure (Vellend et al., 2017). In contrast to biocrust habitats, salt marshes had strong environmental filters that provided more niche partitions (Dini-Andreote et al., 2014), and resulted in community differences in late succession being greater than in the early stage. These contrasting results suggested biocrusts provided fewer environmental filters than expected despite the drought, like previous descriptions of them as fertile islands in dryland (Weber et al., 2016), contributing to descending community differences with succession.

Fundamentally, the sources of community differences in biocrusts were dominated by the turnover component (Figures 2E,F). Despite turnover being a common way of community assembly, it may result in diverse community structures in the same ecosystem (Soininen et al., 2018; Menegotto et al., 2019). Indeed, our results demonstrated the fact that bacterial communities contained more biodiverse phyla than eukaryotes (Figure 1). Therefore, we speculated that the generalists and specialists participated in bacterial and eukaryotic turnover, respectively. Only then can we interpret the results that the turnover ratio was positively and negatively correlated with α diversity in bacteria and eukaryotes, respectively (Supplementary Table S4). In addition, distinguished from increasing with spatial scales in eukaryotes, the turnover ratio showed no difference between local and continental scales in bacteria which may be attributed to their more versatile ecological strategies and smaller body sizes enabling the plasticity of wide distribution species pool (Farjalla et al., 2012; Wu et al., 2018). Only in the presence of a larger species pool in bacteria than in eukaryotes, can more clades be maintained in a bacterial

community even at a high turnover ratio (Wang et al., 2013). Meanwhile, larger species pools can also offer more possibilities of assemblages with multifarious microorganisms facilitating an increase of α diversity (Wang et al., 2013; Picazo et al., 2020). Briefly, under the background of gradually stable community structures in the way of a high turnover ratio, bacteria had a larger species pool than eukaryotes, which supported the view that generalists participated mostly in bacterial turnover.

Considering that more generalists participated in bacterial turnover than eukaryotes, we were motivated to further explore it from a phylogenetic perspective, which usually underlies the generation of many ecological theories (O'Dwyer et al., 2015; Graham et al., 2018). The lagging elbow in edge-length abundance distribution demonstrated (Supplementary Figure S6B) that more branching events were distributed into the tree and existing multiple lineages in the early stage than in the middle-late successional stage. This finding suggested that some clades containing more branches coalesced or were removed with succession (O'Dwyer et al., 2015). Specifically, they were Firmicutes and some Cyanobacteria in bacteria and Phragmoplastophyta in eukaryotes (Supplementary Figure S3). Combined with the fact that bacterial α diversity increased and eukaryotic α diversity decreased with succession, we speculated that more closely related species were assembled in a clade and thus exhibiting the merging of coalescence in the bacterial community, whereas, in eukaryotic phylogeny, more species were removed from the community (O'Dwyer et al., 2015). Eventually, both community structures presented successional convergence through turnover participation by different attributive microorganisms.

Furthermore, since that turnover may be driven by specific habitat differentiation (Wang et al., 2017), environmental filtering, and adaptive niche evolution (Leibold et al., 2019), we investigated environments related to turnover ratio at succession (Supplementary Table S5) and spatial scales (Supplementary Figure S4). Results showed that soil texture and biotic factors were related to turnover ratio at the early successional stage and local scale, suggesting the shaping effects of Cyanobacteria on micro-habitats and their active interaction with heterotrophs (Ratzke et al., 2020). Instead, the role of macroclimate (windspeed) and salinity-related edaphic factors (pH, HCO_3^-) were manifested at the late succession and continental scale, illustrating the process of dispersal in driving turnover, which validated the mediation of windspeed in biocrust community assembly (Li and Hu, 2021). Overall, our results elucidated that micro-environments and macroclimate alternately maintained high turnover at different spatial scales.

4.3. Balanced biogeographic and local environmental effects determined the patterns of microbial biodiversity at local and subcontinental scale

Given that the sampling transect contained complex information on environmental effects, we also studied the changes in β diversity with succession at different spatial scales. Some opinions indeed indicated that β diversity changes depended on the spatial scale (Martiny et al., 2011). Likewise, the decrease in rangeability of β diversity with succession was greater at the continental than at the local scales (Figures 2C,D). A recent study has also proposed successional convergence in biocrusts (Xu et al., 2020), suggesting that convergent communities at a late stage even with farther geographical sites can have more similarity than expected. The convergence amplified community differences among successional stages, but this effect did not remain constant. One possibility was that the force decreased with geographical distance. The reason may be the changes in species pool size across the climate zone, microorganism dispersal, and the maintenance of the environment on turnover (Bryant et al., 2016; Xu et al., 2020), which gradually concealed the effect of successional convergence on observed community differences under the high windspeed in dryland. In other words, the biocrust biogeographic pattern was balanced by distance decay and successional convergence. Furthermore, the intersectional distance of two opposite forces at the phylogenetic facet was greater than that at the taxonomic facet, and that in bacteria was larger than that in eukaryotes (Figure 3). This finding suggested a separated range of species pool in dryland, and that the differentiated species pool of bacteria had a wider spatial range than eukaryotes (Wu et al., 2018). Therefore, the size of the sampling transect-related species pool size determined the observation of biogeographic patterns.

Recent advances have shown the versatile effects on biodiversity from different categories of environments (Garcia-Pichel et al., 2013; Gotelli et al., 2017; Rillig et al., 2019), but whether the consistency of environmental effects on different facets of biodiversity remains unclear. Accordingly, we investigated the correlations of edaphic, climatic, and biotic factors with biodiversity at the taxonomic and phylogenetic facets in biocrusts to improve our understanding of environmental regulation. We found that the relationships of edaphic and climatic factors with bacterial α diversity weakened with succession, but grew strongly in eukaryotes (Figure 4A). Thus, the distinct direction of environmental force between the two communities may contribute to different change patterns of α diversity (Figures 2A,B). The covariant relationship of edaphic and climatic factors with Bray-Curtis increased with succession in bacteria and eukaryotes (Figure 4B), suggesting more distinguished environmental filtering may result in β diversity decline with succession in both communities (Figures 2C,D; Whittaker and Rynearson, 2017). These results implied that the change patterns of taxonomic biodiversity were likely governed by deterministic ecological processes (i.e., edaphic and climatic factors) (Purschke et al., 2013). In this way, in terms of the phylogenetic facets including PD and Weighted-Unifrac dissimilarity, no corresponding relationships existed between biodiversity change patterns and their environmental covariant trends with succession. These discordances suggested that phylogenetic α diversity may be explained by unquantified factors rather than edaphic and climatic ones (Purschke et al., 2013; Le Bagousse-Pinguet et al., 2019). Given that regulations of biotic factors for PD were the strongest in cyanobacterial-lichen crusts, we speculated that complex Cyanobacteria-Ascomycota interactions in symbionts may be unquantified and poorly understood parts of phylogenetic α diversity (Grube et al., 2015). In general, edaphic and climatic factors can provide more useful insights into taxonomic-biodiversity changes, whereas biotic factors probably underlie the pattern of phylogenetic biodiversity.

In dryland, microbial diversity is affected by wind and aridity directly (Bowker et al., 2010), as well as by edaphic and biotic factors (Hu and Liu, 2003; Tighe et al., 2012; Chen et al., 2020), which widely control the abundance of photoautotrophic organisms (Maier et al., 2018). Accordingly, climatic, edaphic, and biotic factors were introduced to study their effects on different aspects of biodiversity-maintenance

mechanisms in biocrusts (Figure 5). Previous studies have shown that climates can affect cyanobacterial population size and community structure (Fernandes et al., 2018). This view was further verified by our results that climatic and edaphic factors are continuously dedicated to taxonomic β diversity with succession in both communities (Figure 5). Combined with the fact that bacteria had more biodiverse taxa than eukaryotes, our results suggested climates probably played a vital role in assembling microorganisms throughout biocrust successional stages, corresponding with the finding of windspeed-mediated community assembly pattern in our previous study (Li and Hu, 2021). Notably, biotic factors in biocrusts primarily included photosynthetic pigments and EPS that had non-negligible impacts on shaping microhabitat gradients by providing organic carbon resources for heterotrophs (Colica et al., 2015) and facilitating sand consolidation (Lan et al., 2014). In particular, symbionts in cyanobacterial-lichen crusts can provide more niches for species colonization (Maier et al., 2014), which can be demonstrated by biotic factors promoting bacterial α diversity (Figure 5B). Furthermore, from the perspective of β diversity, environments mostly inhibited phylogenetic β diversity, as crucially embodied in biotic factors. One possible explanation was that biotic factors may affect the ways microbial interactions and further change community functions. Microorganisms with similar ecological adaptability are frequently retained (Leibold et al., 2019), leading to specific assemblages under the context of drought in this process (Neilson et al., 2017). Conversely, edaphic and climatic factors mostly facilitated the taxonomic β diversity, suggesting that assemblage compositions and distribution patterns had significant responses to environmental gradients. In summary, climatic and edaphic factors mostly facilitated α and taxonomic β diversity, and biotic factors mostly inhibited phylogenetic β diversity.

In conclusion, this study demonstrated the biodiversity of bacterial and eukaryotic communities in biocrusts at multispatial scales. First, the sources of biodiversity in biocrusts were dominated by turnover, primarily with the participation of generalists in bacteria and by specialists in eukaryotes. This factor fundamentally contributed to α diversity changes with succession. Microenvironments and macroclimates were also alternately related to high turnover at different successional stages and spatial scales. Second, the α diversity of bacteria increased even in convergent succession, whereas the impact of distance decay on β diversity gradually exceeded successional convergence at a large spatial scale. The two opposite drivers balanced the biogeography of biocrusts and emphasized the importance of sampling transect-related species pool size. Third, environmental constraints affected successional α and β diversity changes, which were more influenced by edaphic factors at the local scale, and by climatic factors at continental scales, respectively. Moreover, edaphic and climatic factors can be focused on studying taxonomic biodiversity, whereas biotic factors can provide more useful insights into phylogenetic biodiversity. Overall, our study provided important insights into understanding the change patterns of biodiversity at multispatial scales.

Data availability statement

The datasets presented in this study can be found in online repositories. All sequencing reads generated in this study are publicly available through the SRA database under accession number PRJNA640847. The environmental dataset (DOI: 10.6084/m9.figshare.13172411.v1) and the OTU tables based on the bacterial 16S and eukaryotic 18S rDNA amplicon sequencing (DOI: 10.6084/m9.figshare.24523276) can be found in FigShare.

Author contributions

YL: Data curation, Formal analysis, Funding acquisition, Investigation, Resources, Writing – original draft. FW: Writing – review & editing. HY: Data curation, Investigation, Writing – review & editing. HL: Funding acquisition, Methodology, Supervision, Writing – review & editing. CH: Conceptualization, Funding acquisition, Methodology, Supervision, Project administration, Writing – review & editing.

Funding

The author(s) declare financial support was received for the research, authorship, and/or publication of this article. This work was financially supported by the National Natural Science Foundation of China (41877419 and 41877339), the Strategic Priority Research Program of the Chinese Academy of Sciences (XDA17010502), the Featured Institute Service Projects from the Institute of Hydrobiology, the Chinese Academy of Sciences (Y85Z061601), and Natural Science Foundation of Hunan Province, China (2023JJ40221 and 2023JJ 40233).

Acknowledgments

We thank Qiong Wang, Yingchun Han, Qi Li, Jingyi Wei, Mengjiao Wang, and Denghua Wu for their help with the measurements.

Conflict of interest

The authors declare that the research was conducted in the absence of any commercial or financial relationships that could be construed as a potential conflict of interest.

Publisher's note

Supplementary material

The Supplementary material for this article can be found online at: https://www.frontiersin.org/articles/10.3389/fmicb.2023.1284864/full#supplementary-material

References

Amaral-Zettler, L. A., McCliment, E. A., Ducklow, H. W., and Huse, S. M. (2009). A method for studying protistan diversity using massively parallel sequencing of V9 hypervariable regions of small-subunit ribosomal RNA genes. *PLoS One* 4:e6372. doi: 10.1371/journal.pone.0006372

Anderson, M. J., Ellingsen, K. E., and McArdle, B. H. (2006). Multivariate dispersion as a measure of beta diversity. *Ecol. Lett.* 9, 683–693. doi: 10.1111/j.1461-0248.2006.00926.x

Angel Fernandez-Martinez, M., Perez-Ortega, S., Pointing, S. B., Allan Green, T. G., Pintado, A., Rozzi, R., et al. (2017). Microbial succession dynamics along glacier forefield chronosequences in Tierra del Fuego (Chile). *Polar Biol.* 40, 1939–1957. doi: 10.1007/s00300-017-2110-7

Baselga, A. (2010). Partitioning the turnover and nestedness components of beta diversity. *Glob. Ecol. Biogeogr.* 19, 134–143. doi: 10.1111/j.1466-8238.2009.00490.x

Bowker, M. A., Maestre, F. T., Eldridge, D., Belnap, J., Castillo-Monroy, A., Escolar, C., et al. (2014). Biological soil crusts (biocrusts) as a model system in community, landscape and ecosystem ecology. *Biodivers. Conserv.* 23, 1619–1637. doi: 10.1007/s10531-014-0658-x

Bowker, M. A., Maestre, F. T., and Mau, R. L. (2013). Diversity and patch-size distributions of biological soil crusts regulate dryland ecosystem multifunctionality. *Ecosystems* 16, 923–933. doi: 10.1007/s10021-013-9644-5

Bowker, M. A., Soliveres, S., and Maestre, F. T. (2010). Competition increases with abiotic stress and regulates the diversity of biological soil crusts. *J. Ecol.* 98, 551–560. doi: 10.1111/j.1365-2745.2010.01647.x

Bracken, M. E. S., Douglass, J. G., Perini, V., and Trussell, G. C. (2017). Spatial scale mediates the effects of biodiversity on marine primary producers. *Ecology* 98, 1434–1443. doi: 10.1002/ecy.1812/suppinfo

Bryant, J. A., Aylward, F. O., Eppley, J. M., Karl, D. M., Church, M. J., and DeLong, E. F. (2016). Wind and sunlight shape microbial diversity in surface waters of the North Pacific subtropical gyre. *ISME J.* 10, 1308–1322. doi: 10.1038/ismej.2015.221

Cable, J. M., and Huxman, T. E. (2004). Precipitation pulse size effects on Sonoran Desert soil microbial crusts. *Oecologia* 141, 317–324. doi: 10.1007/s00442-003-1461-7

Chen, N., Yu, K. L., Jia, R. L., Teng, J. L., and Zhao, C. M. (2020). Biocrust as one of multiple stable states in global drylands. *Sci. Adv.* 6:eaay3763. doi: 10.1126/sciadv.aay3763

Colica, G., Li, H., Rossi, F., De Philippis, R., and Liu, Y. (2015). Differentiation of the characteristics of excreted extracellular polysaccharides reveals the heterogeneous primary succession of induced biological soil crusts. *J. Appl. Phycol.* 27, 1935–1944. doi: 10.1007/s10811-015-0532-6

Couradeau, E., Karaoz, U., Lim, H. C., da Rocha, U. N., Northen, T., Brodie, E., et al. (2016). Bacteria increase arid-land soil surface temperature through the production of sunscreens. *Nat. Commun.* 7:10373. doi: 10.1038/ncomms10373

Dini-Andreote, F., Silva, M. D. C. P. E., Triado-Margarit, X., Casamayor, E. O., van Elsas, J. D., and Salles, J. F. (2014). Dynamics of bacterial community succession in a salt marsh chronosequence: evidences for temporal niche partitioning. *ISME J.* 8, 1989–2001. doi: 10.1038/ismej.2014.54

Dini-Andreote, F., Stegen, J. C., van Elsas, J. D., and Salles, J. F. (2015). Disentangling mechanisms that mediate the balance between stochastic and deterministic processes in microbial succession. *Proc. Natl. Acad. Sci. U. S. A.* 112, E1326–E1332. doi: 10.1073/pnas.1414261112

Dornelas, M., Gotelli, N. J., McGill, B., Shimadzu, H., Moyes, F., Sievers, C., et al. (2014). Assemblage time series reveal biodiversity change but not systematic loss. *Science* 344, 296–299. doi: 10.1126/science.1248484

Farjalla, V. F., Srivastava, D. S., Marino, N. A. C., Azevedo, F. D., Dib, V., Lopes, P. M., et al. (2012). Ecological determinism increases with organism size. *Ecology* 93, 1752–1759. doi: 10.1890/11-1144.1

Fernandes, V. M. C., Machado de Lima, N. M., Roush, D., Rudgers, J., Collins, S. L., and Garcia-Pichel, F. (2018). Exposure to predicted precipitation patterns decreases population size and alters community structure of cyanobacteria in biological soil crusts from the Chihuahuan Desert. *Environ. Microbiol.* 20, 259–269. doi: 10.1111/1462-2920.13983

Ferrenberg, S., Reed, S. C., and Belnap, J. (2015). Climate change and physical disturbance cause similar community shifts in biological soil crusts. *Proc. Natl. Acad. Sci. U. S. A.* 112, 12116–12121. doi: 10.1073/pnas.1509150112

Fierer, N., Nemergut, D., Knight, R., and Craine, J. M. (2010). Changes through time: integrating microorganisms into the study of succession. *Res. Microbiol.* 161, 635–642. doi: 10.1016/J.resmic.2010.06.002

Garcia-Pichel, F., Loza, V., Marusenko, Y., Mateo, P., and Potrafka, R. M. (2013). Temperature drives the continental-scale distribution of key microbes in topsoil communities. *Science* 340, 1574–1577. doi: 10.1126/science.1236404

Gossner, M. M., Lewinsohn, T. M., Kahl, T., Grassein, F., Boch, S., Prati, D., et al. (2016). Land-use intensification causes multitrophic homogenization of grassland communities. *Nature* 540:266-+. doi: 10.1038/nature20575

Gotelli, N. J., Shimadzu, H., Dornelas, M., McGill, B., Moyes, F., and Magurran, A. E. (2017). Community-level regulation of temporal trends in biodiversity. *Sci. Adv.* 3:e1700315. doi: 10.1126/sciadv.1700315

Graham, C. H., Storch, D., and Machac, A. (2018). Phylogenetic scale in ecology and evolution. *Glob. Ecol. Biogeogr.* 27, 175–187. doi: 10.1111/geb.12686

Grube, M., Cernava, T., Soh, J., Fuchs, S., Aschenbrenner, I., Lassek, C., et al. (2015). Exploring functional contexts of symbiotic sustain within lichen-associated bacteria by comparative omics. *ISME J.* 9, 412–424. doi: 10.1038/ismej.2014.138

Hawkes, C. V., and Keitt, T. H. (2015). Resilience vs. historical contingency in microbial responses to environmental change. *Ecol. Lett.* 18, 612–625. doi: 10.1111/ele.12451

Hu, C. X., and Liu, Y. D. (2003). Primary succession of algal community structure in desert soil. *Acta Bot. Sin.* 45, 917–924.

Hurlbert, S. H. (1971). The nonconcept of species diversity: a critique and alternative parameters. *Ecology* 52, 577–586. doi: 10.2307/1934145

Jessup, C. M., Kassen, R., Forde, S. E., Kerr, B., Buckling, A., Rainey, P. B., et al. (2004). Big questions, small worlds: microbial model systems in ecology. *Trends Ecol. Evol.* 19, 189–197. doi: 10.1016/j.tree.2004.01.008

Johnson, S. L., Kuske, C. R., Carney, T. D., Housman, D. C., Gallegos-Graves, L. V., and Belnap, J. (2012). Increased temperature and altered summer precipitation have differential effects on biological soil crusts in a dryland ecosystem. *Glob. Chang. Biol.* 18, 2583–2593. doi: 10.1111/j.1365-2486.2012.02709.x

Ladau, J., and Eloe-Fadrosh, E. A. (2019). Spatial, temporal, and phylogenetic scales of microbial ecology. *Trends Microbiol.* 27, 662–669. doi: 10.1016/j.tim.2019.03.003

Lan, S., Wu, L., Zhang, D., and Hu, C. (2012). Successional stages of biological soil crusts and their microstructure variability in Shapotou region (China). *Environ. Earth Sci.* 65, 77–88. doi: 10.1007/s12665-011-1066-0

Lan, S., Wu, L., Zhang, D., and Hu, C. (2013). Assessing level of development and successional stages in biological soil crusts with biological indicators. *Microb. Ecol.* 66, 394–403. doi: 10.1007/s00248-013-0191-6

Lan, S., Zhang, Q., Wu, L., Liu, Y., Zhang, D., and Hu, C. (2014). Artificially accelerating the reversal of desertification: cyanobacterial inoculation facilitates the succession of vegetation communities. *Environ. Sci. Technol.* 48, 307–315. doi: 10.1021/es403785j

Le Bagousse-Pinguet, Y., Soliveres, S., Gross, N., Torices, R., Berdugo, M., and Maestre, F. T. (2019). Phylogenetic, functional, and taxonomic richness have both positive and negative effects on ecosystem multifunctionality. *Proc. Natl. Acad. Sci. U. S. A.* 116, 8419–8424. doi: 10.1073/pnas.1815727116

Leibold, M. A., Urban, M. C., De Meester, L., Klausmeier, C. A., and Vanoverbeke, J. (2019). Regional neutrality evolves through local adaptive niche evolution. *Proc. Natl. Acad. Sci. U. S. A.* 116, 2612–2617. doi: 10.1073/pnas.1808615116

Li, H., Chen, Y. S., Yu, G., Rossi, F., Huo, D., Philippis, R. D., et al. (2021). Multiple diversity facets of crucial microbial groups in biological soil crusts promote soil multifunctionality. *Glob. Ecol. Biogeogr.* 30, 1204–1217. doi: 10.1111/geb.13295

Li, Y., and Hu, C. (2021). Biogeographical patterns and mechanisms of microbial community assembly that underlie successional biocrusts across northern China. *NPJ Biofilms Microb.* 7:15. doi: 10.1038/s41522-021-00188-6

Li, H., Li, R., Rossi, F., Li, D., De Philippis, R., Hu, C., et al. (2016). Differentiation of microbial activity and functional diversity between various biocrust elements in a heterogeneous crustal community. *Catena* 147, 138–145. doi: 10.1016/j.catena.2016.07.008

Magurran, A. E., Deacon, A. E., Moyes, F., Shimadzu, H., Dornelas, M., Phillip, D. A. T., et al. (2018). Divergent biodiversity change within ecosystems. *Proc. Natl. Acad. Sci. U. S. A.* 115, 1843–1847. doi: 10.1073/pnas.1712594115

Maier, S., Schmidt, T. S. B., Zheng, L., Peer, T., Wagner, V., and Grube, M. (2014). Analyses of dryland biological soil crusts highlight lichens as an important regulator of microbial communities. *Biodivers. Conserv.* 23, 1735–1755. doi: 10.1007/s10531-014-0719-1

Maier, S., Tamm, A., Wu, D., Caesar, J., Grube, M., and Weber, B. (2018). Photoautotrophic organisms control microbial abundance, diversity, and physiology in different types of biological soil crusts. *ISME J.* 12, 1032–1046. doi: 10.1038/s41396-018-0062-8

Martiny, J. B. H., Eisen, J. A., Penn, K., Allison, S. D., and Horner-Devine, M. C. (2011). Drivers of bacterial beta-diversity depend on spatial scale. *Proc. Natl. Acad. Sci. U. S. A.* 108, 7850–7854. doi: 10.1073/pnas.1016308108

Meiners, S. J., Cadotte, M. W., Fridley, J. D., Pickett, S. T. A., and Walker, L. R. (2015). Is successional research nearing its climax? New approaches for understanding dynamic communities. *Funct. Ecol.* 29, 154–164. doi: 10.1111/1365-2435.12391

Menegotto, A., Dambros, C. S., and Netto, S. A. (2019). The scale-dependent effect of environmental filters on species turnover and nestedness in an estuarine benthic community. *Ecology* 100:e02721. doi: 10.1002/ecy.2721

Miralles, I., Lazaro, R., Sanchez-Maranon, M., Soriano, M., and Ortega, R. (2020). Biocrust cover and successional stages influence soil bacterial composition and diversity in semiarid ecosystems. *Sci. Total Environ.* 709:134654. doi: 10.1016/j.scitotenv.2019.134654

Mori, H., Maruyama, F., Kato, H., Toyoda, A., Dozono, A., Ohtsubo, Y., et al. (2014). Design and experimental application of a novel non-degenerate universal primer set that amplifies prokaryotic 16S rRNA genes with a low possibility to amplify eukaryotic rRNA genes. *DNA Res.* 21, 217–227. doi: 10.1093/dnares/dst052

Mori, A. S., Ota, A. T., Fujii, S., Seino, T., Kabeya, D., Okamoto, T., et al. (2015). Biotic homogenization and differentiation of soil faunal communities in the production forest landscape: taxonomic and functional perspectives. *Oecologia* 177, 533–544. doi: 10.1007/s00442-014-3111-7

Neilson, J. W., Califf, K., Cardona, C., Copeland, A., van Treuren, W., Josephson, K. L., et al. (2017). Significant impacts of increasing aridity on the arid soil microbiome. *mSystems* 2:e00195-16. doi: 10.1128/mSystems.00195-16

Nemergut, D. R., Schmidt, S. K., Fukami, T., O'Neill, S. P., Bilinski, T. M., Stanish, L. F., et al. (2013). Patterns and processes of microbial community assembly. *Microbiol. Mol. Biol. Rev.* 77, 342–356. doi: 10.1128/mmbr.00051-12

O'Dwyer, J. P., Kembel, S. W., and Green, J. L. (2012). Phylogenetic diversity theory sheds light on the structure of microbial communities. *PLoS Comput. Biol.* 8:e1002832. doi: 10.1371/journal.pcbi.1002832

O'Dwyer, J. P., Kembel, S. W., and Sharpton, T. J. (2015). Backbones of evolutionary history test biodiversity theory for microbes. *Proc. Natl. Acad. Sci. U. S. A.* 112, 8356–8361. doi: 10.1073/pnas.1419341112

Oksanen, J. B. F., Kindt, R., Legendre, P., Minchin, P. R., and O'Hara, R. (2015). Vegan: community ecology package. R package version 22-1.

Olden, J. D. (2006). Biotic homogenization: a new research agenda for conservation biogeography. *J. Biogeogr.* 33, 2027–2039. doi: 10.1111/j.1365-2699.2006.01572.x

Ortiz-Alvarez, R., Fierer, N., de los Rios, A., Casamayor, E. O., and Barberan, A. (2018). Consistent changes in the taxonomic structure and functional attributes of bacterial communities during primary succession. *ISME J.* 12, 1658–1667. doi: 10.1038/s41396-018-0076-2

O'Sullivan, J. D., Knell, R. J., and Rossberg, A. G. (2019). Metacommunity-scale biodiversity regulation and the self-organised emergence of macroecological patterns. *Ecol. Lett.* 22, 1428–1438. doi: 10.1111/ele.13294

Picazo, F., Vilmi, A., Aalto, J., Soininen, J., Casamayor, E. O., Liu, Y., et al. (2020). Climate mediates continental scale patterns of stream microbial functional diversity. *Microbiome* 8:92. doi: 10.1186/s40168-020-00873-2

Price, M. N., Dehal, P. S., and Arkin, A. P. (2009). FastTree: computing large minimum evolution trees with profiles instead of a distance matrix. *Mol. Biol. Evol.* 26, 1641–1650. doi: 10.1093/molbev/msp077

Purschke, O., Schmid, B. C., Sykes, M. T., Poschlod, P., Michalski, S. G., Durka, W., et al. (2013). Contrasting changes in taxonomic, phylogenetic and functional diversity during a long-term succession: insights into assembly processes. *J. Ecol.* 101, 857–866. doi: 10.1111/1365-2745.12098

Ratzke, C., Barrere, J., and Gore, J. (2020). Strength of species interactions determines biodiversity and stability in microbial communities. *Nat. Ecol. Evolut.* 4:376. doi: 10.1038/s41559-020-1099-4

Reed, S. C., Coe, K. K., Sparks, J. P., Housman, D. C., Zelikova, T. J., and Belnap, J. (2012). Changes to dryland rainfall result in rapid moss mortality and altered soil fertility. *Nat. Clim. Chang.* 2, 752–755. doi: 10.1038/nclimate1596

Rillig, M. C., Ryo, M., Lehmann, A., Aguilar-Trigueros, C. A., Buchert, S., Wulf, A., et al. (2019). The role of multiple global change factors in driving soil functions and microbial biodiversity. *Science* 366:886. doi: 10.1126/science.aay2832

Rodrigues, J. L. M., Pellizari, V. H., Mueller, R., Baek, K., Jesus, E. D., Paula, F. S., et al. (2013). Conversion of the Amazon rainforest to agriculture results in biotic homogenization of soil bacterial communities. *Proc. Natl. Acad. Sci. U. S. A.* 110, 988–993. doi: 10.1073/pnas.1220608110

Rossi, F., and De Philippis, R. (2015). Role of cyanobacterial exopolysaccharides in phototrophic biofilms and in complex microbial mats. *Life Basel* 5, 1218–1238. doi: 10.3390/life5021218

Rossi, F., Li, H., Liu, Y., and De Philippis, R. (2017). Cyanobacterial inoculation (cyanobacterisation): perspectives for the development of a standardized multifunctional technology for soil fertilization and desertification reversal. *Earth Sci. Rev.* 171, 28–43. doi: 10.1016/j.earscirev.2017.05.006

Schwinning, S., and Sala, O. E. (2004). Hierarchy of responses to resource pulses in and and semi-arid ecosystems. *Oecologia* 141, 211–220. doi: 10.1007/s00442-004-1520-8

Soininen, J., Heino, J., and Wang, J. (2018). A meta-analysis of nestedness and turnover components of beta diversity across organisms and ecosystems. *Glob. Ecol. Biogeogr.* 27, 96–109. doi: 10.1111/geb.12660

Tighe, M., Haling, R. E., Flavel, R. J., and Young, I. M. (2012). Ecological succession, hydrology and carbon acquisition of biological soil crusts measured at the micro-scale. *PLoS One* 7:e48565. doi: 10.1371/journal.pone.0048565

Vellend, M., Dornelas, M., Baeten, L., Beausejour, R., Brown, C. D., De Frenne, P., et al. (2017). Estimates of local biodiversity change over time stand up to scrutiny. *Ecology* 98, 583–590. doi: 10.1002/ecy.1660

Walker, L. R., Wardle, D. A., Bardgett, R. D., and Clarkson, B. D. (2010). The use of chronosequences in studies of ecological succession and soil development. *J. Ecol.* 98, 725–736. doi: 10.1111/j.1365-2745.2010.01664.x

Wang, X.-B., Lu, X.-T., Yao, J., Wang, Z.-W., Deng, Y., Cheng, W.-X., et al. (2017). Habitat-specific patterns and drivers of bacterial beta-diversity in China's drylands. *ISME J.* 11, 1345–1358. doi: 10.1038/ismej.2017.11

Wang, J., Soininen, J., and Shen, J. (2013). Habitat species pools for phylogenetic structure in microbes. *Environ. Microbiol. Rep.* 5, 464–467. doi: 10.1111/1758-2229.12034

Weber, B., Belnap, J., Budel, B., Antoninka, A. J., Barger, N. N., Chaudhary, V. B., et al. (2022). What is a biocrust? A refined, contemporary definition for a broadening research community. *Biol. Rev. Camb. Philos. Soc.* 97, 1768–1785. doi: 10.1111/brv.12862

Weber, B., Büdel, B., and Belnap, J. (2016) *Biological soil crusts: an organizing principle in drylands. Ecological studies* (Cham, Switzerland: Springer),

Whittaker, K. A., and Rynearson, T. A. (2017). Evidence for environmental and ecological selection in a microbe with no geographic limits to gene flow. *Proc. Natl. Acad. Sci. U. S. A.* 114, 2651–2656. doi: 10.1073/pnas.1612346114

Wu, W., Lu, H.-P., Sastri, A., Yeh, Y.-C., Gong, G.-C., Chou, W.-C., et al. (2018). Contrasting the relative importance of species sorting and dispersal limitation in shaping marine bacterial versus protist communities. *ISME J.* 12, 485–494. doi: 10.1038/ismej.2017.183

Xu, L., Zhu, B., Li, C., Yao, M., Zhang, B., and Li, X. (2020). Development of biological soil crust prompts convergent succession of prokaryotic communities. *Catena* 187:104360. doi: 10.1016/j.catena.2019.104360

frontiers | Frontiers in Microbiology

TYPE Correction
PUBLISHED 01 February 2024
DOI 10.3389/fmicb.2024.1374406

OPEN ACCESS

APPROVED BY
Frontiers Editorial Office,
Frontiers Media SA, Switzerland

*CORRESPONDENCE
Hua Li
✉ lih@ihb.ac.cn

RECEIVED 22 January 2024
ACCEPTED 23 January 2024
PUBLISHED 01 February 2024

CITATION
Li Y, Wang F, Yang H, Li H and Hu C (2024) Corrigendum: Balanced biogeographic and local environmental effects determine the patterns of microbial diversity in biocrusts at multi-scales. *Front. Microbiol.* 15:1374406. doi: 10.3389/fmicb.2024.1374406

Corrigendum: Balanced biogeographic and local environmental effects determine the patterns of microbial diversity in biocrusts at multi-scales

Yuanlong Li[1,2], Fengdi Wang[3], Haijian Yang[2], Hua Li[2]* and Chunxiang Hu[2]

[1]Hunan Provincial Key Laboratory of Carbon Neutrality and Intelligent Energy, School of Resource and Environment, Hunan University of Technology and Business, Changsha, China, [2]Key Laboratory of Algal Biology, Institute of Hydrobiology, Chinese Academy of Sciences, Wuhan, China, [3]Institute of Hematology, Union Hospital, Tongji Medical College, Huazhong University of Science and Technology, Wuhan, China

KEYWORDS

biogeography, biological soil crusts, cyanobacteria, microbial diversity, multiple spatial scales, primary succession, species turnover

A corrigendum on
Balanced biogeographic and local environmental effects determine the patterns of microbial diversity in biocrusts at multi-scales

by Li, Y., Wang, F., Yang, H., Li, H., and Hu, C. (2023). *Front. Microbiol.* 14:1284864. doi: 10.3389/fmicb.2023.1284864

In the published article, there were two spelling mistakes in the abstract and introduction. The term MiSeq was displayed as "MeSeq". The correct statement is "MiSeq".

A correction has been made to the method section of the Abstract. The sentence previously stated:

"(Based on the Illumina MeSeq 16S/18S rRNA sequencing technology, we…)"

The corrected sentence appears below:

"(Based on the Illumina MiSeq 16S/18S rRNA sequencing technology, we…)"

A correction has been made to paragraph 4 of the Introduction. The sentence previously stated:

"(Illumina MeSeq 16S/18S rRNA sequencing was used to examine the…)"

The corrected sentence appears below:

"(Illumina MiSeq 16S/18S rRNA sequencing was used to examine the…)"

The authors apologize for this error and state that this does not change the scientific conclusions of the article in any way. The original article has been updated.

Publisher's note

All claims expressed in this article are solely those of the authors and do not necessarily represent those of their affiliated organizations, or those of the publisher, the editors and the reviewers. Any product that may be evaluated in this article, or claim that may be made by its manufacturer, is not guaranteed or endorsed by the publisher.

frontiers | Frontiers in Microbiology

TYPE Original Research
PUBLISHED 16 November 2023
DOI 10.3389/fmicb.2023.1292277

OPEN ACCESS

EDITED BY
Da Huo,
Chinese Academy of Sciences (CAS), China

REVIEWED BY
Mauro Vilar,
Federal University of Rio de Janeiro, Brazil
Yunfei Sun,
Nanjing Normal University, China

*CORRESPONDENCE
Yali Tang
✉ yalitang@jnu.edu.cn

RECEIVED 11 September 2023
ACCEPTED 25 October 2023
PUBLISHED 16 November 2023

CITATION
Lei L, Lai S, Liu W, Li Y, Zhang H and Tang Y (2023) *Chlorella pyrenoidosa* mitigated the negative effect of cylindrospermopsin-producing and non-cylindrospermopsin-producing *Raphidiopsis raciborskii* on *Daphnia magna* as a dietary supplement. *Front. Microbiol.* 14:1292277. doi: 10.3389/fmicb.2023.1292277

Chlorella pyrenoidosa mitigated the negative effect of cylindrospermopsin-producing and non-cylindrospermopsin-producing *Raphidiopsis raciborskii* on *Daphnia magna* as a dietary supplement

Lamei Lei, Shuyan Lai, Wei Liu, Yaokai Li, Huiping Zhang and Yali Tang*

Department of Ecology, Jinan University, Guangzhou, China

Feeding effects are crucial for evaluating the capacity of zooplankton to regulate phytoplankton populations within freshwater ecosystems. To examine the impact of the bloom-forming cyanobacteria *Raphidiopsis raciborskii*, which occurs in tropical and subtropical freshwaters, on the growth of zooplankton *Daphnia* in relation to toxins, filament length and fatty acid content, we fed *D. magna* with *R. raciborskii* only (cylindrospermopsin (CYN)-producing and non-CYN-producing, as the negative controls), *Chlorella pyrenoidosa* only (as the positive control) and a mixed diet containing *R. raciborskii* (CYN-producing and non-CYN-producing) and *C. pyrenoidosa*. Consequently, our findings revealed that the toxic effect of CYN-producing *R. raciborskii* strains on *Daphnia* was mitigated by the coexistence of *C. pyrenoidosa* containing stearidonic acid (SDA, C18:4 ω3) in mixed diets. This was evident in the elevated survival rate compared that from diets containing only *R. raciborskii* and a significantly higher reproduction and population intrinsic increase rate compared to diets consisting of only *R. raciborskii* or *C. pyrenoidos*. Additionally, a strong positive correlation was observed between arachidonic acid (ARA, 20:4ω6) and the population intrinsic increase rate of *Daphnia*; notably, *R. raciborskii* strains were found to be rich in the ω6 polyunsaturated fatty acid ARA. These outcomes reinforce the crucial role of polyunsaturated fatty acids in predicting the population increase of crustacean zooplankton, which has long been neglected. Furthermore, our results underscore the potential effectiveness of zooplankton, particularly in temperate lakes, in controlling CYN-producing *R. raciborskii* populations.

KEYWORDS

***Raphidiopsis raciborskii*, zooplankton, essential fatty acids, feeding experiments, nutritional supplements**

Introduction

The outbreak of cyanobacterial blooms, a symptom of eutrophication in water bodies, disrupts the balance of aquatic ecosystems. Certain harmful cyanobacteria have the ability to produce hepatotoxins or neurotoxins, as well as other unknown toxic compounds, which have a serious negative impact on the safety of aquatic organisms and human health (Dittmann and Wiegand, 2006; Buratti et al., 2017). *Raphidiopsis raciborskii* (previously known as *Cylindrospermopsis raciborskii*), recognized as one of the most successful bloom-forming cyanobacteria in freshwater, has been described as a tropical species. However, its recent expansion into temperate regions has made it a cosmopolitan species in freshwater systems around the world (Antunes et al., 2015; Wu et al., 2022). Notably, *R. raciborskii* can produce diverse cyanotoxins, including cynlindrospermopsin (CYN) and saxitoxin. Exposure to CYN may result in severe cytotoxicity, genotoxicity, and reproductive toxicity, posing a serious risk to the health of both humans and animals (Buratti et al., 2017).

Zooplankton, encompassing a vital group of primary consumers, play an important role as effective grazers of phytoplankton; nevertheless, they are assumed to be negatively affected by cyanobacterial metabolites (toxicity hypothesis) (Codd, 2000; Ger et al., 2014; Lyu et al., 2016a,b). Initially, this toxicity only referred to microcystins, and currently, the focus has shifted toward other cyanotoxins (Wilson et al., 2006; Schwarzenberger, 2022). Among these, CYN is the most commonly reported compound produced by *R. raciborskii* (Rzymski and Poniedziałek, 2014). Feeding zooplankton with a CYN-producing *R. raciborskii* led to higher mortality and lower growth in *D. magna* juveniles compared to feeding them a non-CYN-producing strain (Nogueira et al., 2004, 2006). Intriguingly, a CYN-producing strain did not exhibit lethal toxicity toward three *Daphnia* species (Hawkins and Lampert, 1989). Due to limited studies, the effects of CYN-producing *R. raciborskii* on *Daphnia* remain elusive (Schwarzenberger, 2022). Toxic effects seem to be strain specific, and different *Daphnia* species display different sensitivities to cyanotoxin exposure (Wilson et al., 2006; Ferrão-Filho et al., 2008; Costa et al., 2013). Additionally, it is noteworthy that zooplankton possess the ability to gradually develop desensitization to toxins through a series of adaptive mechanisms when coexisting with cyanobacteria (Kirk and Gilbert, 1992; Ka et al., 2012; Lyu et al., 2016a), minimizing adverse effects arising from toxin exposure.

The reduced feeding activity of *Daphnia* when fed *R. raciborskii* has been attributed to potential mechanical interference caused by long filaments impeding the feeding apparatus of grazers (Gliwicz and Lampert, 1990; DeMott et al., 2001; Bednarska et al., 2014), hence leading to negative effects on the growth and reproduction of *Daphnia*. However, Rangel et al. (2016) argued that toxicity may override morphology regarding the effects of toxic *R. raciborskii* on zooplankton. Some laboratory experiments even demonstrated that the filament length of *R. raciborskii* did not have a distinct influence on the clearance rates of *D. magna* (Panosso and Lürling, 2010). *D. galeata* actually benefits from the presence of filaments in the food suspension (Abrusán, 2004). Furthermore, by synthesizing data from 66 published laboratory studies, representing 597 experimental comparisons, Wilson et al. (2006) revealed that filamentous cyanobacteria were indeed found to be notably better food sources for grazers than single-celled cyanobacteria across all the studies. Thus, feeding inhibition by filaments may not hold the same level of significance as previously described.

Apart from filament length or toxins, the poor food quality offered by cyanobacteria may also exert adverse effects on the growth and reproduction of zooplankton. iTRAQ-Based proteomic profiling indicated that when exposing to microcystin-producing and microcystin-free *Microcystis aeruginosa*, *Daphnia* showed 94 and 117 differentially expressed proteins respectively, all of which correspond to changes in metabolism necessary to adjust the body growth rate of *Daphnia* (Lyu et al., 2016b). Food quality, including various essential elements and biochemicals, may constrain consumer performance by specifically affecting physiological processes and thus disrupt energy flow in aquatic food webs (Becker and Boersma, 2005; Ruiz et al., 2021). The essential biochemicals cyanobacteria lack but are vital for consumers include polyunsaturated fatty acids (PUFAs), especially eicosapentaenoic acid (EPA, C20: 5ω3, Gulati and DeMott, 1997), or alternative resources, such as an effective EPA enhancing fatty acid, namely, stearidonic acid (SDA, C18:4 ω3, Lenihan-Geels et al., 2013; Abonyi et al., 2023). These PUFAs play a crucial role in maintaining membrane structure and function and serve as precursors for bioactive compounds in both vertebrates and invertebrates, and their *de novo* synthesis is very scarce (Kainz et al., 2009; Twining et al., 2021). In addition, these ω3 fatty acids have been reported to attenuate the toxic effects of various oxidative stresses in mammals (Haimeur et al., 2012; Sakai et al., 2017). The deficiency of EPA in diets restricts the growth of zooplankton (Müller-Navarra, 1995a; Brett et al., 2009; Tang et al., 2019), impacting the performance of crustacean grazers within aquatic ecosystems according to lake investigations and experimental studies (Müller-Navarra et al., 2000; Tang et al., 2023). More importantly, the lack of dietary supply of both EPA and SDA can dramatically affect the reproduction of *Daphnia* due to the high investment of EPA in eggs (Wacker and Martin-Creuzburg, 2007; Kainz et al., 2009). Consequently, cyanobacteria can hardly support the somatic growth and reproduction of zooplankton even in the absence of toxins (Lampert, 1987). To date, no research has revealed the fatty acid profile of *R. raciborskii*. However, we assume that *R. raciborskii* strains, being cyanobacteria, also lack EPA or SDA.

Despite the shortage of EPA or SDA, *R. raciborskii* strains could provide essential nutritional components necessary for zooplankton. These components encompass carbohydrates, proteins, and common saturated and unsaturated fatty acids. It is noted that feeding *Daphnia* with *R. raciborskii* cells only is rarely seen in nature. Concurrently, other phytoplankton species of considerable nutritional value coexist with *R. raciborskii,* even during *Raphidiopsis* blooms (Soares et al., 2009; Chislock et al., 2014; Frau et al., 2018). Given the relatively low EPA need in zooplankton (Müller-Navarra et al., 2000; Becker and Boersma, 2005; Tang et al., 2019). Wenzel et al. (2021) proposed that food sources, such as bacteria, which may not fully meet grazers' dietary needs, could still confer nutritional benefits if other complementary food components are available in sufficient quantities to compensate for any biochemical deficiencies. Interestingly, even lower-quality food such as vascular plants can be utilized by zooplankton when simultaneously provided with algal food (Taipale et al., 2016; Tang et al., 2021). Considering the role of ω3 fatty acids in detoxication, we hypothesized that the performance of zooplankton feeding *R. raciborskii* would be dramatically improved by the concurrent feeding of good-quality algae. Reis et al. (2023) reported

that the fitness of these small-bodied cladocerans feeding on *R. raciborskii* was improved when the supply of nutritious food increased from 10 to 50% in proportion. In natural lakes, the co-occurrence of *R. raciborskii* bloom and filter-feeding zooplankton is commonly seen as previously reported (Bouvy et al., 2001; Leonard and Paerl, 2005; Soares et al., 2009; Gao et al., 2022).

To test our hypothesis, we conducted a feeding experiment to compare the dietary effect of *R. raciborskii* only (CYN- and non-CYN-producing strains), *Chlorella pyrenoidosa* only and a mixed diet of *R. raciborskii* and *C. pyrenoidosa* on the growth, reproduction and population dynamics of *Daphnia magna*. Additionally, we analyzed the fatty acid profile of these different dietary algal strains to uncover the role of specific fatty acids in influencing the growth and reproduction of *Daphnia*. Our findings revealed that the mixed diet led to a higher survival rate of *Daphnia* compared to the *R. raciborskii* only diet and an even higher population intrinsic growth rate compared to the *C. pyrenoidos* only diet. The presence of *C. pyrenoidosa* appears to diminish the toxic effect of CYN-producing *R. raciborskii* strains. In addition, the strongly positive relationship between ω6 PUFA and the population intrinsic increase rate of *Daphnia*, as well as the rich content of ω6 PUFA ARA in *R. raciborskii,* indicates that *R. raciborskii* might be beneficial for the population increase of *Daphnia* as a nutritional supplement. Elevated zooplankton populations to phytoplankton ratios normally indicate a more robust capacity for phytoplankton control (Søndergaard et al., 2008; Jeppesen et al., 2012). Thus, our results point toward the potential for employing a top-down biomanipulation approach to control *R. raciborskii* blooms, particularly in temperate areas.

Materials and methods

Experimental algae and animals

The green algae *Chlorella pyrenoidosa* was obtained from the Institute of Hydrobiology, Jinan University. Two CYN-producing strains (*R. raciborskii* CS506 and QDH7) and one non-CYN-producing strain (*R. raciborskii* N8) were used in the experiments. *R. raciborskii* CS506 was obtained from the Australian National Algae Culture Collection (ANACC) and can produce CYN and deoxy-CYN (Willis et al., 2015). Strain QDH7 mainly produced deoxy-CYN, which was identified by LC–MS/MS analysis (Lu et al., 2020). *R. raciborskii* N8 is a nontoxic strain due to the absence of the CYN biosynthesis gene cluster in its whole genome (Chen et al., 2022). All four strains were grown on BG11 medium at 28°C at a light intensity of 60 μmol m^{-2} s^{-1} in a 12:12 h light/dark cycle. Under these conditions, *C. pyrenoidosa* grew as single-cell populations with an average diameter of 4.1 μm. Filaments of *R. raciborskii* N8, QDH7 and CS506 had average lengths of 387 μm, 902 μm and 1,214 μm, respectively (Table 1).

The cladoceran *D. magna* was maintained at 20°C and fed with the green algae *C. pyrenoidosa* in 1-L glass jars. Water from Liuxihe Reservoir in Guangzhu city was used to prepare all media after sequential filtration through a 1.2 and 0.45-μm filter. The filtrate was stored statically at 25°C for 2 days before use. Neonates (<24 h old) were randomly chosen from parthenogenetically reproducing females for the life history experiments.

Feeding experiments

Daphnia magna was fed three different kinds of diets: *C. pyrenoidosa* only, 1:1 mixtures of *C. pyrenoidosa* with either *R. raciborskii* N8, QDH7 or CS506, and *R. raciborskii* (N8, QDH7 or CS506) only. All diets had a fixed total food concentration of 2 mg C L^{-1}. The food carbon concentrations were determined using OD (optical extinction) values according to the regression curve we built for OD and carbon concentration for different algae at 682 nm.

Before the life history experiments, neonates (<24 h old) originating from the same broods were collected from beakers and starved for 4 h to empty their guts. Thirty neonates were randomly selected for each treatment. Each neonate was transferred into 50 mL of food suspension and incubated under the same conditions as the stock *D. magna* cultures. Each selected neonate was transferred daily to clean beakers with freshly prepared food suspensions. Any observed offspring were removed immediately after their presence was recorded. The experiments lasted for 15 days.

The body lengths of zooplankton were measured using a stereo binocular microscope, and the biomass was calculated based on the body length measurement. Somatic growth rates at the juvenile stage (g) were determined by assessing the increase in biomass from Day 1 (M_1) to Day 7 (M_7) within the experimental period ($t = 6$ d) using the Equation $g = (\ln M_7 - \ln M_1)/t$. In addition, the survival rate and the daily number of offspring produced were also recorded.

The intrinsic rates of increase r (d^{-1}) in the population of *D. magna* were calculated using Euler's formula as follows:

$$1 = \sum_{x=0}^{n} e^{-rx} \times l_x \times m_x$$

where x is the age or time interval (day), l_x is the proportion of individuals surviving to age x, and m_x represents the number of offspring produced per surviving female at age x.

Fatty acid analysis and CYN measurement

The fatty acids within the cells of *C. pyrenoidosa* and three *R. raciborskii* strains were extracted and esterified according to the method outlined by Wiltshire et al. (2000). Quantitative analysis was

TABLE 1 General characteristics of the algal strains used in the study.

Species	Strain	Origin	Toxin type	Mean filament length (μm)
R. raciborskii	N8	China	Nontoxic	387
	QDH7	China	Deoxy-CYN (19.8 μg mg^{-1} dry weight)	903
	CS506	Australia	CYN, deoxy-CYN (14.4 μg mg^{-1} dry weight)	1,214
C. pyrenoidosa	CP	China	Nontoxic	4.1

carried out using a gas chromatography–mass spectrometer (GC–MS) with a specific temperature configuration. The cultures of the four strains were collected by centrifugation and then subjected to freeze-drying. Approximately 20 mg of dry biomass was utilized to extract total lipids three times with dichloromethane/methanol (2:1, v/v), and the pooled cell-free extracts were evaporated to dryness. Subsequently, the extracted samples were transesterified with 3 mol L^{-1} methanolic HCl (60°C, 15 min). Fatty acids were analyzed with a Finnigan TRACE GC–MS equipped with a flame ionization detector and a DB-23 column (60 m × 0.32 mm). The fatty acid methyl esters (FAME) were quantified by comparison with standard Supelco 37 Component FAME mix or an internal standard (C12:0 methyl esters).

Total CYN concentrations in *R. raciborskii* QDH7 and CS506 cells were measured before the feeding experiments. Prior to CYN measurement, *R. raciborskii* cells were lysed by ultrasonic treatment, and insoluble cell debris was removed by centrifugation. The supernatant was then analyzed with a Cylindrospermopsin Plate Kit (Beacon Analytical Systems Inc., USA) in accordance with the manufacturer's specifications.

Data analysis

To assess and compare the fatty acid (FA) content across different diet treatments, a one-way analysis of variance (ANOVA) was employed. Significant differences among treatments were then evaluated using the least significant difference (LSD) multiple comparison test. One-way ANOVA followed by the LSD test was also performed to identify differences in the growth and reproduction of *D. magna* between different diets. Regression analyses were performed to determine the relationship between population intrinsic increase rates and PUFA content in diets. An SPSS 22.0 statistical package was used for all statistical analyses. Before the statistical analysis, data were checked using a normal probability plot of the residuals and Levene's test of homogeneity of variances for compliance of ANOVA assumptions and logarithmic transformation, if necessary. Detailed information on the statistics is presented in the Supplementary Table S1.

Results

Fatty acid composition

The green algae *C. pyrenoidosa* was characterized by high amounts of C16:0 and C18:0 saturated fatty acids, very small amounts of monounsaturated fatty acids and considerable amounts of PUFAs, mainly including C18:2ω6 (linoleic acid, LA), C18:3ω3 (linolenic acid, ALA) and C18:4ω3 (stearidonic acid, SDA) (Supplementary Table S1). All *R. raciborskii* strains lacked SDA but exhibited significantly higher levels of C20:4ω6 (arachidonic acid, ARA) than *C. pyrenoidosa* (Figure 1). Detailed information on the fatty acid profile of the algae is presented in the Supplementary Table S2.

Dietary treatment effects on the performance of *Daphnia* individuals

In the case of pure *R. raciborskii* dietary treatments, all *D. magna* exposed to 100% QDH7 and 100% CS506 strains experienced toxicity, resulting in mortality within 9 days. When *C. pyrenoidosa* was added to the diets with two toxic *R. raciborskii* strains, the survival rate was greatly elevated to above 60% (Figure 2A).

Compared with the diet comprising only *C. pyrenoidosa*, the growth rates of *D. magna* fed only *R. raciborskii* were significantly lower (Figure 2B). *D. magna* exhibited better growth when fed pure diets of non-CYN-producing N8 compared to the CYN-producing strains (QDH7 and CS506). In terms of inhibiting *D. magna* growth, no significant difference was observed between the aforementioned two toxic strains. Interestingly, *R. raciborskii* supplemented with

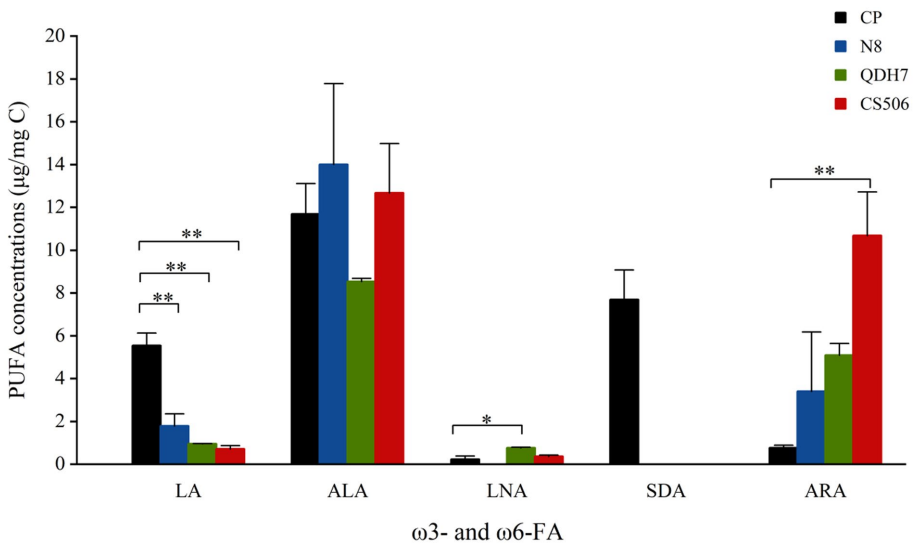

FIGURE 1
The main PUFA concentrations (μg/mg C) of *C. pyrenoidosa* (CP) and three strains of *R. raciborskii* (N8, QDH7 and CS506). Error bars indicate 1SD. The "*" above the bars are significantly different from CP, as revealed by the independent-samples *t* test (*$p < 0.05$; **$p < 0.01$).

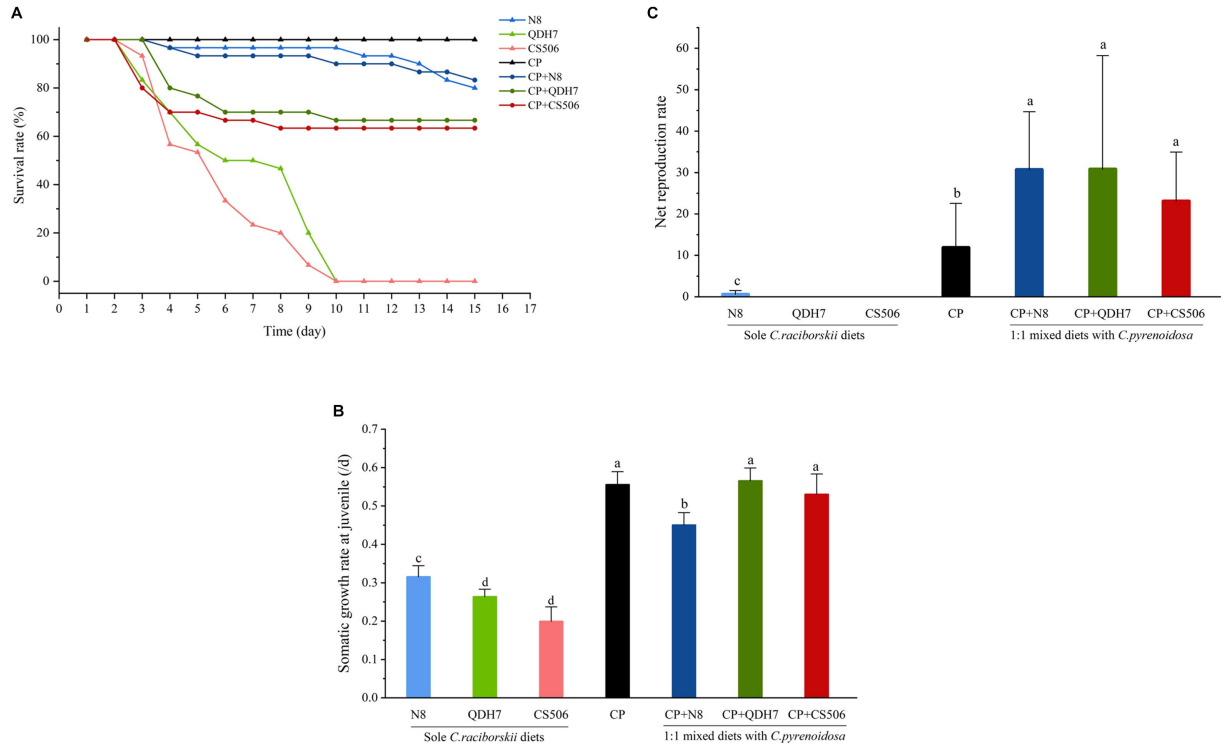

FIGURE 2
Individual performance of *D. magna* fed with pure diets of *C. pyrenoidosa*, three strains of *R. raciborskii* and 1:1 mixed diets with *C. pyrenoidosa* and *R. raciborskii* strains including survival rate **(A)** somatic growth rate at juvenile **(B)** and net reproduction rate if reproduced after juvenile **(C)**. Different letters indicate significant differences ($p < 0.05$) using the LSD multiple comparison test.

C. pyrenoidosa enhanced the growth of *D. magna*. *Daphnia* fed mixed diets displayed significantly better growth than those exclusively fed *R. raciborskii*, similar to the positive control group that was fed *C. pyrenoidosa*.

In the pure *R. raciborskii* dietary treatments, all *D. magna* exposed to 100% QDH7 and 100% CS506 strains did not reproduce. The *D. magna* on the pure diets of the non-CYN-producing N8 strain was able to reproduce successfully but showed the lowest net reproduction value. When all *Daphnia* were fed mixed diets, they exhibited robust net reproduction rates comparable to the positive control group (Figure 2C). The maximum net reproduction (net value) was observed in the 50% QDH7 treatment.

Intrinsic population increase rate of *Daphnia* and its relation with dietary PUFA supply

The intrinsic rate of population increase of *Daphnia* feeding mixed diets was found to be significantly higher than that of the positive control group feeding *C. pyrenoidosa* (Figure 3A). Among all the mixed dietary treatments, the maximal population intrinsic increase rate (mean value) was found in the 50% QDH7 treatment, and the lowest was found in the 50% N8 treatment. Since *D. magna* exposed to 100% QDH7 and 100% CS506 strains showed no reproduction, their population intrinsic increase rate could not be calculated. Regression analyses revealed a very strong correlation between the ARA content in diets and the population intrinsic increase rates of *Daphnia* in all dietary treatments containing SDA (Figure 3B).

Discussion

By setting up feeding experiments to compare the dietary impact of different food sources on the growth and reproduction of *Daphnia*, we found that the highest intrinsic population growth rate was observed in *Daphnia* fed a mixed diet, followed by those on a diet of *C. pyrenoidosa*, then non-CYN-producing *R. raciborskii*, and finally, the lowest growth rate was seen in *Daphnia* fed with CYN-producing *R. raciborskii*. Thus, a mitigation of the negative effect of CYN-producing and non-CYN-producing *R. raciborskii* on *D. magna* by *C. pyrenoidosa* as diet supplements was observed, inconsistent with our hypothesis.

In our study, the ability to produce CYN had a notable impact on the growth of *Daphnia*. Among the treatments involving a sole diet, *Daphnia* fed on two toxic strains exhibited significantly reduced growth and reproduction rates compared to those fed on nontoxic strain N8 or *C. pyrenoidosa*, consistent with the observation made by Nogueira et al. (2004, 2006), underscoring the detrimental effect of CYN toxins. Strikingly, the negative effects of the toxins produced by both toxic *R. raciborskii* strains on *Daphnia* were mitigated when *C. pyrenoidosa* was concurrently provided as part of their diets, particularly in terms of the intrinsic population increase rate.

Based on the fatty acid profiles of dietary algae, we further proposed that the differences in *Daphnia* performance across various

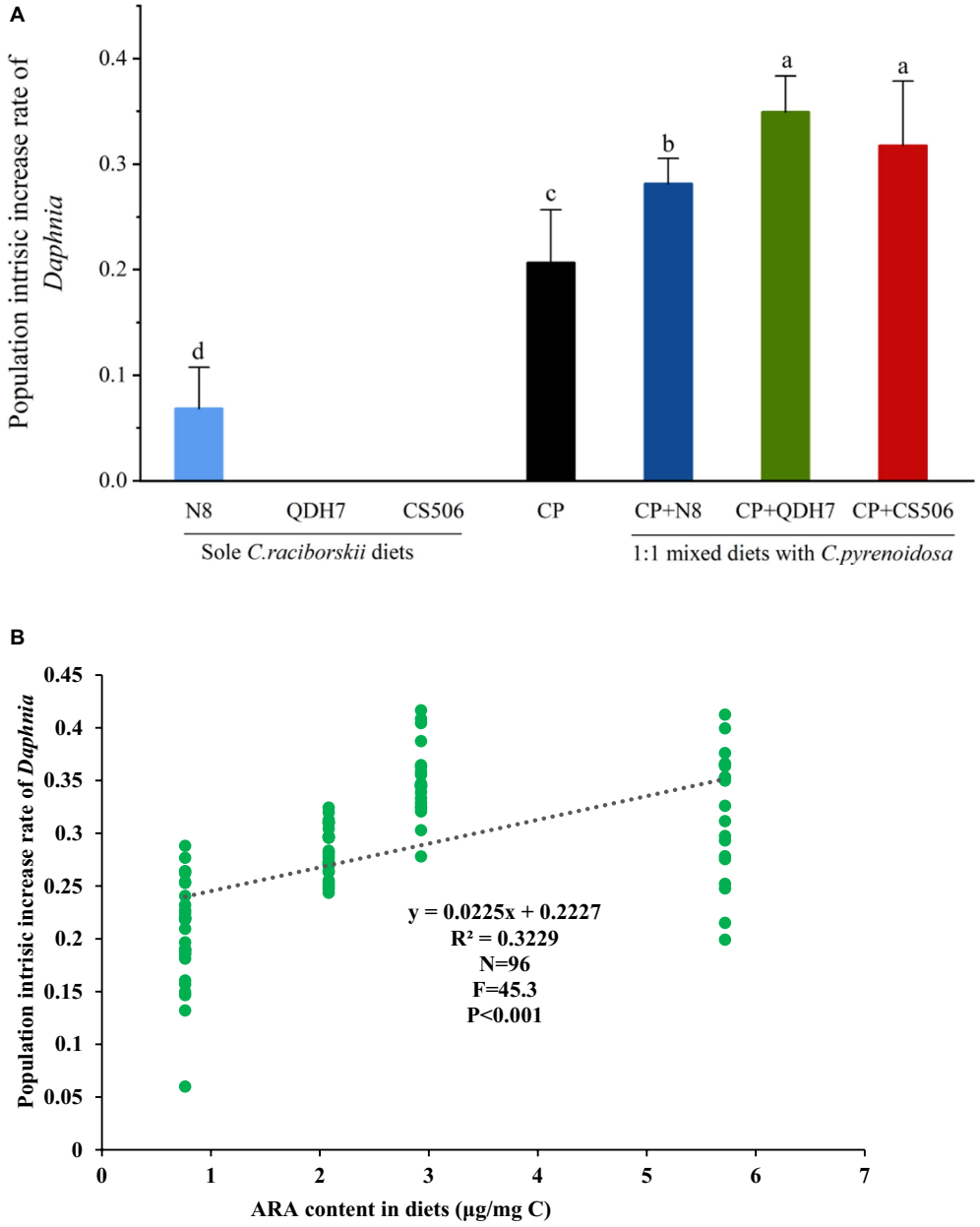

FIGURE 3
The intrinsic rate of population increase of *D. magna* fed with pure diets of *C. pyrenoidosa*, three strains of *R. raciborskii* and 1:1 mixed diets with *C. pyrenoidosa* and *R. raciborskii* strains if they reproduced **(A)** and its relation with dietary supply of arachidonic acid (ARA, 20:4 ω6) within stearidonic acid (SDA, 18:4 ω3)-containing diets **(B)**. Different letters indicate significant differences ($p < 0.05$) using the LSD multiple comparison test.

dietary treatments can be attributed to variations in the fatty acid contents. One particularly crucial fatty acid, EPA, has been shown to limit *Daphnia* growth and reproduction both in laboratory settings and in natural environments, and it also plays a predictive role in carbon transfer between primary producers and consumers (Müller-Navarra, 1995b; Müller-Navarra et al., 2000). Both SDA and ALA can be converted to EPA by consumers (Kainz et al., 2009). Due to the low conversion rate of ALA to EPA, researchers have noted that supplying SDA may increase EPA levels more effectively than ALA supplementation by bypassing a rate-limiting step (Lenihan-Geels et al., 2013; Abonyi et al., 2023). The *R. raciborskii* strains lack both the crucial ω3 PUFA EPA and the alternative EPA precursor SDA. This deficiency in essential fatty acids contributes to the poor food quality of *R. raciborskii* and significantly limited the population increase of *Daphnia* in our study. Even when fed its non-CNY-producing strain, *Daphnia* showed considerably lower growth and reproduction rates than those fed *C. pyrenoidosa*. It was evident that food containing SDA (including mixed diets and *C. pyrenoidosa* only diet) significantly supported growth and reproduction when compared to food lacking SDA (such as different strains of *R. raciborskii* as only diets).

More importantly, it is worth noting that oxidative stress, induced by the rapid increase in the production of reactive oxygen species (ROS), represents a pivotal mechanism underlying CYN

toxicity (Poniedzialek et al., 2015). EPA has been documented to attenuate oxidative stress-induced DNA damage and elevate glutathione peroxidase activity in mammals (Haimeur et al., 2012; Sakai et al., 2017). Moreover, increased levels of glutathione peroxidase have been demonstrated to participate in the detoxication of cyanotoxins, including CYN, in *Daphnia* (Nogueira et al., 2004; Lindsay et al., 2006; Schwarzenberger, 2022). Hence, it is plausible that the SDA derived from the supplemented *C. pyrenoidosa* enhanced the EPA content in zooplankton, eventually mitigating the adverse effects of toxic *R. raciborskii* strains on *Daphnia magna*. The mitigation of more dietary chlorophyte addition on the performance of *Daphnia* fed toxic *R. raciborskii* strains could also be demonstrated by data from Reis et al. (2023) for growth and reproduction, as well as Panosso and Lürling (2010) for feeding rate, supporting our view.

Unlike *Microcystis* (Ahlgren et al., 1992), *R. raciborskii* strains in our study were rich in ω6 PUFA ARA. Although most ecologists pay more attention to ω3 PUFA (Twining et al., 2021), inadequate availability of ω6 PUFA ARA can also constrain the fitness of *Daphnia* (Ilić et al., 2019), especially when EPA or EPA-enhancing fatty acid SDA is already present in their diet. ARA serves as a precursor for tissue hormones such as prostaglandin and related eicosanoids, which play critical roles in mediating reproduction (Heckmann et al., 2008; Stanley and Kim, 2019). Previously, a ω3/ω6 ratio ranging from 2.6 to 4.0 was reported for wild filtering cladoceran species (Persson and Vrede, 2006). In our study, the observed positive effects of adding *R. raciborskii* on reproduction and population increase might be attributed to nutritional supplements of ω6 PUFA. This speculation could be further demonstrated by the positive correlation between ARA content in the food and the intrinsic population increase rate of *Daphnia* when fed diets containing SDA. Other nutritional components, for example, proteins, may also work here, but we did not determine all the nutritional profiles and focused on essential fatty acids.

The observed beneficial effects of our CYN-producing and non-CYN-producing *R. raciborskii* strain in addition to *C. pyrenoidosa* as diets on the population increase of *D. magna*, however, were different from what Reis et al. (2023) observed. They reported that *R. raciborskii* constrains the fitness of *Daphnia* when this strain was added to chlorophyte as diets, by using different *R. raciborskii* strains (saxitoxin-producing strain), different *Daphnia* species (*D. laveis* and *D. gessneri*) and different chloryphyte species (*Monoraphidium capricornutum* and *Ankistrodesmus stiptatus*). A possible explanation is that algae may exhibit strain differences in their fatty acid profiles (Dunstan et al., 1993). And the fatty acid profile would eventually affected the growth of *Daphnia* if their needs for essential fatty acids were not met (Gulati and Demott, 1997). In addition, different *Daphnia* species, or even clones, may respond differently to different diets according to their different sensitivities to different or the same toxins (Ferrão-Filho et al., 2008; Costa et al., 2013) and nutritional requirements (Ferrão-Filho et al., 2019).

The poor manageability of filamentous *R. raciborskii* previously caused a reduction in both the growth rate and fecundity of *Daphnia* (Bednarska et al., 2014). In our feeding experiments, we observed that the trichomes of strain CS506 were three times longer than those of the N8 strain. Surprisingly, the length of *R. raciborskii* filaments did not appear to have a pronounced impact on *Daphnia* fitness in our study. This finding aligns with the work of Panosso and Lürling (2010), who demonstrated that longer *R. raciborskii* filaments may not necessarily cause stronger feeding inhibition than shorter ones for large-bodied *D. magna* (2–3 mm) within the range they tested. Increasing feeding inhibition in larger body-sized animals exposed to filamentous cyanobacteria were reported (Demott et al., 2001), but the conclusion was not generally-accepted for cladocerans due to their species-specific or clone-specific sensitivities when exposed to cyanobacteria (Bednarska et al., 2014). Relatively high feeding rates of *R. raciborskii* were also reported in daphnids of different body sizes, e.g., 1.1 mm *D. longispina* and 1.4 mm *D. pulicaria*, 1.6 mm *D. laevis* and 2.5 mm *D. similis* (Ferrão-Filho et al., 2017; Sikora and Dawidowicz, 2017; Ferrão-Filho et al., 2020), despite feeding inhibition being previously observed in 0.6–1.3 mm *D. galeata*, 1.2 mm *D. cucullata*, 1.9 mm *D. hyalina*, and 2.3 mm *D. pulicaria* (Schoenberg and Carlson, 1984; Gliwicz and Lampert, 1990). Notably, the *D. magna* clone used in our study might be less sensitive to clogging, as previously described (Soares et al., 2009).

Daphnia magna is a typical filter-feeding water flea and has long been used as a model for food quality and aquatic ecotoxicity studies. Most aquatic filter-feeders including cladocerans and rotifers, shared necessary requirements for polyunsaturated fatty acids such as SDA, EPA and ARA etc. (Schälicke et al., 2019; Thomas et al., 2022). Thus, our results lend further support to the idea that crustacean zooplankton may have the potential to control CYN-producing *R. raciborskii* populations in temperate lakes, as previously proposed (Gao et al., 2022), but with a particular emphasis on the nutritional perspective. Compared to temperate lakes, weak top-down effects were recorded due to the presence of fish species that spawn multiple times per year, resulting in an abundance of young-of-the-year fish all year around that prey on the large-bodied zooplankton in tropical and subtropical lakes (Liu et al., 2018; He et al., 2022), decreasing the control of large-bodied zooplankton on large-bodied zooplankton. Ferrão-Filho et al. (2020) showed the control of small-bodied zooplankton by saxitoxin-producing *R. raciborskii* in a mesocosm study; however, they suggested that high nutrient recycling other than the grazing effect by fish might weaken zooplankton's control on cyanobacteria in trophic areas. Taken together, these findings may partially explain why *R. raciborskii* is more prevalent in tropical and subtropical areas than in temperate areas.

Conclusion

In summary, *Chlorella pyrenoidosa* relieved the negative effect of cylindrospermopsin-producing and non-cylindrospermopsin-producing *Raphidiopsis raciborskii* on *D. magna* in our study. The findings underscore the potential effectiveness of zooplankton, particularly in temperate lakes, in controlling CYN-producing *R. raciborskii* populations.

Data availability statement

The original contributions presented in the study are included in the article/Supplementary material, further inquiries can be directed to the corresponding author.

Author contributions

LL: Data curation, Writing – original draft, Writing – review & editing. SL: Data curation, Writing – review & editing. WL: Methodology, Writing – review & editing. YL: Investigation, Writing – review & editing. HZ: Formal analysis, Writing – review & editing. YT: Conceptualization, Writing – original draft, Writing – review & editing.

Funding

The author(s) declare financial support was received for the research, authorship, and/or publication of this article. This study was supported financially by National Natural Science Foundation of China (Nos. 32371616 and 32371615), and Natural Science Foundation of Guangdong Province (No. 2023A1515012361).

Acknowledgments

We are grateful for the work of numerous participants who collected and analyzed samples during the experimental period.

Conflict of interest

The authors declare that the research was conducted in the absence of any commercial or financial relationships that could be construed as a potential conflict of interest.

Publisher's note

Supplementary material

The Supplementary material for this article can be found online at: https://www.frontiersin.org/articles/10.3389/fmicb.2023.1292277/full#supplementary-material

References

Abonyi, A., Rasconi, S., Ptacnik, R., Pilecky, M., and Kainz, M. J. (2023). Chytrids enhance Daphnia fitness by selectively retained chytrid-synthesised stearidonic acid and conversion of short-chain to long-chain polyunsaturated fatty acids. *Freshw. Biol.* 68, 77–90. doi: 10.1111/FWB.14010

Abrusán, G. (2004). Filamentous cyanobacteria, temperature and *Daphnia* growth: the role of fluid mechanics. *Oecologia* 141, 395–401. doi: 10.1007/s00442-004-1660-x

Ahlgren, G., Gustafsson, I. B., and Boberg, M. (1992). Fatty acid content and chemical composition of freshwater microalgae 1. *J. Phycol.* 28, 37–50. doi: 10.1111/j.0022-3646.1992.00037.x

Antunes, J. T., Leão, P. N., and Vasconcelos, V. M. (2015). *Cylindrospermopsis raciborskii*: review of the distribution, phylogeography, and ecophysiology of a global invasive species. *Front. Microbiol.* 6:473. doi: 10.3389/fmicb.2015.00473

Becker, C., and Boersma, M. (2005). Differential effects of phosphorus and fatty acids on *Daphnia magna* growth and reproduction. *Limnol. Oceanogr.* 50, 388–397. doi: 10.2307/3597910

Bednarska, A., Pietrzak, B., and Pijanowska, J. (2014). Effect of poor manageability and low nutritional value of cyanobacteria on *Daphnia magna* life history performance. *J. Plankton Res.* 36, 838–847. doi: 10.1093/plankt/fbu009

Bouvy, M., Pagano, M., and Troussellier, M. (2001). Effects of a cyanobacterial bloom (*Cylindrospermopsis raciborskii*) on bacteria and zooplankton communities in Ingazeira reservoir (Northeast Brazil). *Aquat. Microb. Ecol.* 25, 215–227. doi: 10.3354/ame025215

Brett, M. T., Kainz, M. J., Taipale, S. J., and Seshan, H. (2009). Phytoplankton, not allochthonous carbon, sustains herbivorous zooplankton production. *Proc. Natl. Acad. Sci.* 106, 21197–21201. doi: 10.1073/pnas.0904129106

Buratti, F. M., Manganelli, M., Vichi, S., Stefanelli, M., Scardala, S., Testai, E., et al. (2017). Cyanotoxins: producing organisms, occurrence, toxicity, mechanism of action and human health toxicological risk evaluation. *Arch. Toxicol.* 91, 1049–1130. doi: 10.1007/s00204-016-1913-6

Chen, Z. J., Ruan, Z. X., Cheng, N., Xiao, L. J., Peng, L., Han, B.-P., et al. (2022). Whole-genome sequencing and phosphorus uptake and transport pathway comparative analysis of *Cylindrospermopsis raciborskii* N8. *Acta Hydrobiol. Sin.* 46, 1130–1141. doi: 10.7541/2022.2021.0197

Chislock, M. F., Sharp, K. L., and Wilson, A. E. (2014). *Cylindrospermopsis raciborskii* dominates under very low and high nitrogen-to-phosphorus ratios. *Water Res.* 49, 207–214. doi: 10.1016/j.watres.2013.11.022

Codd, G. A. (2000). Cyanobacterial toxins, the perception of water quality, and the prioritisation of eutrophication control. *Ecol. Eng.* 16, 51–60. doi: 10.1016/S0925-8574(00)00089-6

Costa, S. M., Ferrão-Filho, A. S., and Azevedo, S. M. F. O. (2013). Effects of saxitoxin- and non-saxitoxin-producing strains of the cyanobacterium *Cylindrospermopsis raciborskii* on the fitness of temperate and tropical cladocerans. *Harmful Algae* 28, 55–63. doi: 10.1016/j.hal.2013.05.017

DeMott, W. R., Gulati, R. D., and Donk, E. V. (2001). Effects of dietary phosphorus deficiency on the abundance, phosphorus balance, and growth of *Daphnia cucullata* in three hypereutrophic Dutch lakes. *Limnol. Oceanogr.* 46, 1871–1880. doi: 10.2307/3069058

Dittmann, E., and Wiegand, C. (2006). Cyanobacterial toxins–occurrence, biosynthesis and impact on human affairs. *Mol. Nutr. Food Res.* 50, 7–17. doi: 10.1002/mnfr.200500162

Dunstan, G. A., Volkman, J. K., Barrett, S. M., and Garland, C. D. (1993). Changes in the lipid composition and maximisation of the polyunsaturated fatty acid content of three microalgae grown in mass culture. *J. Appl. Phycol.* 5, 71–83. doi: 10.1007/BF02182424

Ferrão-Filho, A. S., Abreu, S. S. D., Oliveira, T., Magalhães, V. F., Pflugmacher, S., and Silva, E. M. (2017). Single and combined effects of microcystin and saxitoxin producing cyanobacteria on the fitness and antioxidant defenses of cladocerans. *Environ. Toxicol. Chem.* 36, 2689–2697. doi: 10.1002/etc.3819

Ferrão-Filho, A. D. S., da Costa, S. M., Ribeiro, M. G. L., and Azevedo, S. M. (2008). Effects of a saxitoxin-producer strain of *Cylindrospermopsis raciborskii* (cyanobacteria) on the swimming movements of cladocerans. *Environ. Toxicol. Int. J.* 23, 161–168. doi: 10.1002/tox.20320

Ferrão-Filho, A. D. S., Dias, T. M., Pereira, U. J., Dos Santos, J. A. A., and Kozlowsky-Suzuki, B. (2019). Nutritional and toxicity constraints of phytoplankton from a Brazilian reservoir to the fitness of cladoceran species. *Environ. Sci. Pollut. Res.* 26, 12881–12893. doi: 10.1007/s11356-019-04851-6

Ferrão-Filho, A. S., Pereira, U. J., Vilar, M. C., de Magalhães, L., and Marinho, M. M. (2020). Can small-bodied *Daphnia* control *Raphidiopsis raciborskii* in eutrophic tropical lakes? A mesocosm experiment. *Environ. Sci. Pollut. Res.* 27, 35459–35473. doi: 10.1007/s11356-020-09737-6

Frau, D., de Tezanos Pinto, P., and Mayora, G. (2018). Are cyanobacteria total, specific and trait abundance regulated by the same environmental variables? *Ann. Limnol. - Int. J. Lim.* 54:3. doi: 10.1051/limn/2017030

Gao, X., Wang, W., Ndayishimiye, J. C., Govaert, L., Chen, H., Jeppesen, E., et al. (2022). Invasive and toxic cyanobacteria regulate allochthonous resource use and community niche width of reservoir zooplankton. *Freshw. Biol.* 67, 1344–1356. doi: 10.1111/FWB.13921

Ger, K. A., Hansson, L. A., and Lürling, M. (2014). Understanding cyanobacteria-zooplankton interactions in a more eutrophic world. *Freshw. Biol.* 59, 1783–1798. doi: 10.1111/fwb.12393

Gliwicz, Z. M., and Lampert, W. (1990). Food thresholds in *Daphnia* species in the absence and presence of blue-green filaments. *Ecology* 71, 691–702. doi: 10.2307/1940323

Gulati, R., and Demott, W. (1997). The role of food quality for zooplankton: remarks on the state-of-the-art, perspectives and priorities. *Freshw. Biol.* 38, 753–768. doi: 10.1046/j.1365-2427.1997.00275.x

Haimeur, A., Ulmann, L., Mimouni, V., Guéno, F., Pineau-Vincent, F., Meskini, N., et al. (2012). The role of *Odontella aurita*, a marine diatom rich in EPA, as a dietary supplement in dyslipidemia, platelet function and oxidative stress in high-fat fed rats. *Lipids Health Dis.* 11, 1–13. doi: 10.1186/1476-511X-11-147

Hawkins, P. R., and Lampert, W. (1989). The effect of *Daphnia* body size on fifiltering rate inhibition in the presence of a fifilamentous cyanobacterium. *Limnol. Oceanogr.* 34, 1084–1089. doi: 10.2307/2837197

He, H., Qian, T., Shen, R., Yu, J., Li, K., Liu, Z., et al. (2022). Piscivore stocking significantly suppresses small fish but does not facilitate a clear-water state in subtropical shallow mesocosms: a biomanipulation experiment. *Sci. Total Environ.* 842:156967. doi: 10.1016/J.SCITOTENV.2022.156967

Heckmann, L. H., Sibly, R. M., Timmermans, M. J., and Callaghan, A. (2008). Outlining eicosanoid biosynthesis in the crustacean Daphnia. *Front. Zool.* 5, 11–19. doi: 10.1186/1742-9994-5-11

Ilić, M., Werner, C., and Fink, P. (2019). Equal relevance of omega-3 and omega-6 polyunsaturated fatty acids for the fitness of *Daphnia* spp. *Limnol. Oceanogr.* 64, 2512–2525. doi: 10.1002/lno.11201

Jeppesen, E., Søndergaard, M., Lauridsen, T. L., Davidson, T. A., Liu, Z., Mazzeo, N., et al. (2012). Biomanipulation as a restoration tool to combat eutrophication: recent advances and future challenges. *Adv. Ecol. Res.* 47, 411–488. doi: 10.1016/B978-0-12-398315-2.00006-5

Ka, S., Mendoza-Vera, J. M., Bouvy, M., Champalbert, G., N'Gom-Kâ, R., and Pagano, M. (2012). Can tropical freshwater zooplankton graze efficiently on cyanobacteria? *Hydrobiologia* 679, 119–138. doi: 10.1007/s10750-011-0860-8

Kainz, M., Brett, M. T., and Arts, M. T. (2009). *Lipids in aquatic ecosystems*. Springer-Verlag: New York.

Kirk, K. L., and Gilbert, J. J. (1992). Variation in herbivore response to chemical defenses -zooplankton foraging on toxic cyanobacteria. *Ecology* 73, 2208–2217. doi: 10.2307/1941468

Lampert, W. (1987). Laboratory studies on zooplankton-cyanobacteria interactions. *N. Z. J. Mar. Freshw. Res.* 21, 483–490. doi: 10.1080/00288330.1987.9516244

Lenihan-Geels, G., Bishop, K. S., and Ferguson, L. R. (2013). Alternative sources of omega-3 fats: can we find a sustainable substitute for fish? *Nutrients* 5, 1301–1315. doi: 10.3390/nu5041301

Leonard, J. A., and Paerl, H. W. (2005). Zooplankton community structure, microzooplankton grazing impact, and seston energy content in the St. Johns river system, Florida as influenced by the toxic cyanobacterium *Cylindrospermopsis raciborskii*. *Hydrobiologia* 537, 89–97. doi: 10.1007/s10750-004-2483-9

Lindsay, J., Metcalf, J. S., and Codd, G. A. (2006). Protection against the toxicity of microcystin-LR and cylindrospermopsin in *Artemia salina* and *Daphnia* spp. by pre-treatment with cyanobacterial lipopolysaccharide (LPS). *Toxicon* 48, 995–1001. doi: 10.1016/j.toxicon.2006.07.036

Liu, Z., Hu, J., Zhong, P., Zhang, X., Ning, J., Larsen, S. E., et al. (2018). Successful restoration of a tropical shallow eutrophic lake: strong bottom-up but weak top-down effects recorded. *Water Res.* 146, 88–97. doi: 10.1016/j.watres.2018.09.007

Lu, Y., Lei, M., Ye, J., Lei, L. M., and Han, B.-P. (2020). Intraspecific variation of morphological traits and toxin-producing capacity and phylogenetic analysis for *Cylindrospermopsis raciborskii* from Qiandenghu Lake, Guangdong Province. *J. Lake Sci.* 32, 144–153. doi: 10.18307/2020.0114

Lyu, K., Guan, H., Wu, C., Wang, X., Wilson, A. E., and Yang, Z. (2016a). Maternal consumption of non-toxic *Microcystis*, by *Daphnia magna* induces tolerance to toxic *Microcystis* in offspring. *Freshw. Biol.* 61, 219–228. doi: 10.1111/fwb.12695

Lyu, K., Meng, Q., Zhu, X., Dai, D., Zhang, L., Huang, Y., et al. (2016b). Changes in iTRAQ-based proteomic profiling of the cladoceran *Daphnia magna* exposed to microcystin-producing and microcystin-free *Microcystis aeruginosa*. *Environ. Sci. Technol.* 50, 4798–4807. doi: 10.1021/acs.est.6b00101

Müller-Navarra, D. C. (1995a). Evidence that a highly unsaturated fatty acid limits Daphnia growth in nature. *Arch. Hydrobiol.* 132, 297–307. doi: 10.1127/ARCHIV-HYDROBIOL/132/1995/297

Müller-Navarra, D. C. (1995b). Biochemical versus mineral limitation in *Daphnia*. *Limnol. Oceanogr.* 40, 1209–1214. doi: 10.2307/2838677

Müller-Navarra, D. C., Brett, M. T., Liston, A. M., and Goldman, C. R. (2000). A highly unsaturated fatty acid predicts carbon transfer between primary producers and consumers. *Nature* 403, 74–77. doi: 10.1038/47469

Nogueira, I. C., Lobo-da-Cunha, A., and Vasconcelos, V. M. (2006). Effects of *Cylindrospermopsis raciborskii* and *Aphanizomenon ovalisporum* (cyanobacteria) ingestion on *Daphnia magna* midgut and associated diverticula epithelium. *Aquat. Toxicol.* 80, 194–203. doi: 10.1016/j.aquatox.2006.08.008

Nogueira, I. C., Saker, M. L., Pflugmacher, S., Wiegand, C., and Vasconcelos, V. M. (2004). Toxicity of the cyanobacterium *Cylindrospermopsis raciborskii* to *Daphnia magna*. *Environ. Toxicol. Int. J.* 19, 453–459. doi: 10.1002/tox.20050

Panosso, R., and Lürling, M. (2010). *Daphnia magna* feeding on *Cylindrospermopsis raciborskii*: the role of food composition, filament length and body size. *J. Plankton Res.* 32, 1393–1404. doi: 10.1093/plankt/fbq057

Persson, J., and Vrede, T. (2006). Polyunsaturated fatty acids in zooplankton: variation due to taxonomy and trophic position. *Freshw. Biol.* 51, 887–900. doi: 10.1111/j.1365-2427.2006.01540.x

Poniedzialek, B., Rzymski, P., and Karczewski, J. (2015). The role of the enzymatic antioxidant system in cylindrospermopsin-induced toxicity in human lymphocytes. *Toxicol. In Vitro* 29, 926–932. doi: 10.1016/j.tiv.2015.03.023

Rangel, L. M., Ger, K. A., Silva, L. H. S., Soares, M. C. S., Faassen, E. J., and Lürling, M. (2016). Toxicity overrides morphology on *Cylindrospermopsis raciborskii* grazing resistance to the Calanoid copepod *Eudiaptomus gracilis*. *Microb. Ecol.* 71, 835–844. doi: 10.1007/s00248-016-0734-8

Reis, G. C. D., de Carvalho, G. H. A., Vilar, M. C. P., Azevedo, S. M. F. D. O. E., and Ferrão-Filho, A. D. S. (2023). Saxitoxin-producing *Raphidiopsis raciborskii* (Cyanobacteria) constrains *Daphnia* fitness and feeding rate despite high nutritious food availability. *Toxics* 11:693. doi: 10.3390/toxics11080693

Ruiz, T., Koussoroplis, A. M., Danger, M., Aguer, J. P., Morel-Desrosiers, N., and Bec, A. (2021). Quantifying the energetic cost of food quality constraints on resting metabolism to integrate nutritional and metabolic ecology. *Ecol. Lett.* 24, 2339–2349. doi: 10.1111/ele.13855

Rzymski, P., and Poniedziałek, B. (2014). In search of environmental role of cylindrospermopsin: a review on global distribution and ecology of its producers. *Water Res.* 66, 320–337. doi: 10.1016/j.watres.2014.08.029

Sakai, C., Ishida, M., Ohba, H., Yamashita, H., Uchida, H., Yoshizumi, M., et al. (2017). Fish oil omega-3 polyunsaturated fatty acids attenuate oxidative stress-induced DNA damage in vascular endothelial cells. *PLoS One* 12:e0187934. doi: 10.1371/journal.pone.0187934

Schälicke, S., Sobisch, L. Y., Martin-Creuzburg, D., and Wacker, A. (2019). Food quantity-quality co-limitation: interactive effects of dietary carbon and essential lipid supply on population growth of a freshwater rotifer. *Freshw. Biol.* 64, 903–912. doi: 10.1111/fwb.13272

Schoenberg, S. A., and Carlson, R. E. (1984). Direct and indirect effects of zooplankton grazing on phytoplankton in a hypereutrophic lake. *Oikos* 42, 291–302. doi: 10.2307/3544397

Schwarzenberger, A. (2022). Negative effects of cyanotoxins and adaptative responses of *Daphnia*. *Toxins* 14:770. doi: 10.3390/TOXINS14110770

Sikora, A., and Dawidowicz, P. (2017). Breakage of cyanobacterial filaments by small- and large-sized *Daphnia*: are there any temperaturedependent differences? *Hydrobiologia* 798, 119–126. doi: 10.1007/s10750-015-2436-5

Soares, M. C. S., Rocha, M. I. D. A., Marinho, M. M., Azevedo, S. M., Branco, C. W., and Huszar, V. L. (2009). Changes in species composition during annual cyanobacterial dominance in a tropical reservoir: physical factors, nutrients and grazing effects. *Aquat. Microb. Ecol.* 57, 137–149. doi: 10.3354/ame01336

Søndergaard, M., Liboriussen, L., Pedersen, A. R., and Jeppesen, E. (2008). Lake restoration by fish removal: short-and long-term effects in 36 Danish lakes. *Ecosystems* 11, 1291–1305. doi: 10.1007/s10021-008-9193-5

Stanley, D., and Kim, Y. (2019). Insect prostaglandins and other eicosanoids: from molecular to physiological actions. *Adv. Insect Physiol.* 56, 283–343. doi: 10.1016/bs.aiip.2019.01.003

Taipale, S. J., Galloway, A. W., Aalto, S. L., Kahilainen, K. K., Strandberg, U., and Kankaala, P. (2016). Terrestrial carbohydrates support freshwater zooplankton during phytoplankton deficiency. *Sci. Rep.* 6:30897. doi: 10.1038/srep30897

Tang, Y., Su, L., Xu, R., Wang, S., Su, Y., Liu, Z., et al. (2023). Response of zooplankton to inputs of terrestrial dissolved organic matter: food quality constraints induced by microbes. *Limnol. Oceanogr.* 68, 709–722. doi: 10.1002/lno.12304

Tang, Y., Yang, X., Xu, R., Zhang, X., Liu, Z., Zhang, Y., et al. (2019). Heterotrophic microbes upgrade food value of a terrestrial carbon resource for *Daphnia magna*. *Limnol. Oceanogr.* 64, 474–482. doi: 10.1002/lno.11052

Tang, Y., Zhou, D., Su, L., Liu, Z., Zhang, X., and Dumont, H. J. (2021). *Vallisneria natans* detritus supports *Daphnia magna* somatic growth and reproduction under addition of periphyton. *Aquat. Ecol.* 55, 579–588. doi: 10.1007/S10452-021-09846-5

Thomas, P. K., Kunze, C., Van de Waal, D. B., Hillebrand, H., and Striebel, M. (2022). Elemental and biochemical nutrient limitation of zooplankton: a meta-analysis. *Ecol. Lett.* 25, 2776–2792. doi: 10.1111/ele.14125

Twining, C. W., Bernhardt, J. R., Derry, A. M., Hudson, C. M., Ishikawa, A., Kabeya, N., et al. (2021). The evolutionary ecology of fatty-acid variation: implications for consumer adaptation and diversification. *Ecol. Lett.* 24, 1709–1731. doi: 10.1111/ELE.13771

Wacker, A., and Martin-Creuzburg, D. (2007). Allocation of essential lipids in *Daphnia magna* during exposure to poor food quality. *Funct. Ecol.* 21, 738–747. doi: 10.1111/j.1365-2435.2007.01274.x

Wenzel, A., Vrede, T., Jansson, M., and Bergström, A. K. (2021). *Daphnia* performance on diets containing different combinations of high-quality algae, heterotrophic bacteria, and allochthonous particulate organic matter. *Freshw. Biol.* 66, 157–168. doi: 10.1111/fwb.13626

Willis, A., Adams, M. P., Chuang, A. W., Orr, P. T., O'Brien, K. R., and Burford, M. A. (2015). Constitutive toxin production under various nitrogen and phosphorus regimes of three ecotypes of *Cylindrospermopsis raciborskii* ((Wołoszyńska) Seenayya et Subba Raju). *Harmful Algae* 47, 27–34. doi: 10.1016/j.hal.2015.05.011

Wilson, A. E., Sarnelle, O., and Tillmanns, A. R. (2006). Effects of cyanobacterial toxicity and morphology on the population growth of freshwater zooplankton: meta-analyses of laboratory experiments. *Limnol. Oceanogr.* 51, 1915–1924. doi: 10.4319/lo.2006.51.4.1915

Wiltshire, K. H., Boersma, M., Möller, A., and Buhtz, H. (2000). Extraction of pigments and fatty acids from the green alga *Scenedesmus obliquus* (Chlorophyceae). *Aquat. Ecol.* 34, 119–126. doi: 10.1023/A:1009911418606

Wu, Z., Yang, S., and Shi, J. (2022). Overview of the distribution and adaptation of a bloomforming cyanobacterium *Raphidiopsis raciborskii*: integrating genomics, toxicity, and ecophysiology. *J. Oceanol. Limnol.* 40, 1774–1791. doi: 10.1007/S00343-022-2003-7

frontiers | Frontiers in Microbiology

TYPE Original Research
PUBLISHED 05 December 2023
DOI 10.3389/fmicb.2023.1285229

OPEN ACCESS

EDITED BY
Man Xiao,
Chinese Academy of Sciences (CAS), China

REVIEWED BY
Ganyu Feng,
Tongji University, China
Ming Li,
Northwest A&F University, China

*CORRESPONDENCE
Chunxiang Hu
✉ cxhu@ihb.ac.cn

RECEIVED 29 August 2023
ACCEPTED 10 November 2023
PUBLISHED 05 December 2023

CITATION
Yang H, Wu D, Li H and Hu C (2023) The extracellular polysaccharide determine the physico-chemical surface properties of *Microcystis*.
Front. Microbiol. 14:1285229.
doi: 10.3389/fmicb.2023.1285229

The extracellular polysaccharide determine the physico-chemical surface properties of *Microcystis*

Haijian Yang[1], Denghua Wu[1,2], Hua Li[1] and Chunxiang Hu[1]*

[1]Key Laboratory of Algal Biology, Institute of Hydrobiology, Chinese Academy of Sciences, Wuhan, China, [2]University of Chinese Academy of Sciences, Beijing, China

Microcystis possesses the capacity to form colonies and blooms in lakes and reservoirs worldwide, causing significant ecological challenges in aquatic ecosystems. However, little is known about the determining factors of physico-chemical surface properties that govern the competitive advantage of *Microcystis*. Here, The physico-chemical surface properties of *Microcystis wesenbergii* and *Microcystis aeruginosa*, including specific surface area (SSA), hydrophobicity, zeta potential, and functional groups were investigated. Additionally, the extracellular polysaccharide (EPS) were analyzed. Laboratory-cultured *Microcystis* exhibited hydrophilic, a negative zeta potential and negatively charged. Furthermore, no significant relationship was shown between these properties and the cultivation stage. *Microcystis wesenbergii* exhibited low free energy of cohesion, high surface free energy, high growth rate, and high EPS content during the logarithmic phase. On the other hand, *M. aeruginosa* displayed lower free energy of cohesion, high surface free energy, high EPS content, and high growth rate during the stationary phase. These characteristics contribute to their respective competitive advantage. Furthermore, the relationship between EPS and surface properties was investigated. The polysaccharide component of EPS primarily influenced the SSA and total surface energy of *Microcystis*. Likewise, the protein component of EPS influenced hydrophobicity and surface tension. The polysaccharide composition, including glucuronic acid, xylose, and fructose, mainly influenced surface properties. Additionally, hydrophilic groups such as O–H and P–O–P played a crucial role in determining hydrophobicity in *Microcystis*. This study elucidates that EPS influenced the SSA, hydrophobicity, and surface free energy of *Microcystis* cells, which in turn impact the formation of *Microcystis* blooms and the collection.

KEYWORDS

***Microcystis*, cell surface, extracellular polysaccharide, monosaccharide composition, hydrophobicity**

1 Introduction

Cyanobacterial blooms are a significant environmental issue in aquatic ecosystems (Qu et al., 2014). Common genera that form blooms include *Microcystis*, *Anabaena* (or *Dolichospermum*), *Aphanizomenon*, *Cylindrospermopsis* and others (Huisman et al., 2018). Among these, *Microcystis* is the dominant genus in eutrophic freshwaters worldwide (Xiao et al., 2018). Every year, freshwater lakes with important ecological functions in China, such as Taihu Lake, Chaohu Lake and Dianchi Lake, experience varying degrees of cyanobacterial blooms, with *Microcystis* as the predominant species (Li et al., 2018; Tang et al., 2018). *Microcystis*

exhibits a competitive advantage over other organisms in aquatic environments due to its buoyancy regulation, specialized storage strategies, efficient nitrogen uptake, and resistance to zooplankton (Xiao et al., 2018).

In several lakes and reservoirs, the predominant species responsible for the formation of blooms were *M. wesenbergii* and *M. aeruginosa*, among other common *Microcystis* species such as *M. ichthyoblabe* (Zhu et al., 2016). *Microcystis wesenbergii* and *M. aeruginosa* exhibit alternating blooms in different seasons or depths in the water column, indicating a strong competitive advantage between these two *Microcystis* species (Zhu et al., 2015). In Lake Taihu, *M. wesenbergii* dominated at water temperatures above 27°C, while *M. aeruginosa* dominated at temperature between 22°C and 25°C (Otten and Paerl, 2011). Numerous studies have investigated the relationship among light, temperature, and nutrient competition in *Microcystis* spp. (Yue et al., 2014a,b). For instance, the growth rate of *M. wesenbergii* from Japan remained relatively stable within a temperature range of 20°C–35°C. On the other hand, the growth rate of *M. aeruginosa* showed an increase as the temperature rose. Furthermore, no significant difference in the growth rate between *M. aeruginosa* and *M. wesenbergii* was observed under the same light conditions (Imai et al., 2009). The algal-bacterial relationships of different microcystic algae in nature have also been studied (Zhang et al., 2021; Le et al., 2022). Additionally, the surface characteristics of cells, including EPS, charge, and hydrophobicity play a crucial role in non-specific adhesion of *Microcystis* to various biotic and abiotic surfaces (colony formation) and competitive advantage. However, the surface characteristics of *Microcystis* have received little attention.

Physicochemical properties of microbial cell surfaces such as hydrophobicity, surface tension, contact angle, and surface energy had been studied extensively (Barros et al., 2019). Previous researches have primarily focused on energy microalgae, with the aim of efficient harvesting through flocculation (Zhang et al., 2012). However, limited research has been conducted on cyanobacteria. Liu L. et al. (2016) reported that laboratory-cultured *Microcystis* exists single cells, while wild *Microcystis* forms colonies based on the zeta potential and hydrophobicity. Additionally, the surface features of cells and colony formation are directly influenced by the characteristics of cyanobacterial extracellular polymeric substances (EPS; Liu et al., 2018). The content, composition, and monosaccharide components of EPS directly determine the surface properties of cells, including the presence of non-sugar components such as uronic acids, pyruvic acid, phosphate, and acyl groups. These non-sugar components contribute to the overall negative charge of EPS and provide binding and adsorption properties to these types of polymers (Gupta and Diwan, 2017). Surface adhesions a key factor in determining the self-aggregation capacity of cells (Zhang et al., 2020), and also affects the collection efficiency of cells (Yu et al., 2018). However, the surface characteristics of *Microcystis* are still poorly understood.

This study aimed to examine the cell surface properties of *M. wesenbergii* and *M. aeruginosa*, specifically focusing on cell surface area, hydrophobicity, zeta potential, and surface free energy. Additionally, we investigated the variations in EPS contents and composition at different cultured stages. Our analysis focused on understanding the interactions between cell surface characteristics and EPS. The findings of this study contribute to our understanding of bloom formation (*Microcystis* aggregation) and shed light on the competitive advantage of these two strains. Furthermore, the insights gained from this research may have implications for the development of flocculation collection techniques, such as co-coagulation flotation.

2 Materials and methods

2.1 *Microcystis* and cultivation

Microcystis aeruginosa and *Microcystis wesenbergii* were isolated from water samples collected from Meiliang Bay Meiliang Bay in Lake Taihu in June and November 2008 (*M. aeruginosa* was isolated by Yue Tao, and *M. wesenbergii* was isolated by Li Renhui), which are typical of single populations with different morphotypes. Single colonies were isolated using a light microscopy (Leica, Leica Microsystems, Wetzler, Germany) and purified using a series of BG-11 agar plates until the cultures were axenic. Subsequently, they were identified through 16S rRNA and gvpA-gvpC ITS sequence analysis (Supplementary Figure 5). These colonies were then maintained aseptically in BG11 medium in our laboratory (Yue et al., 2014a,b). The stock cultures were maintained in a sterilized BG11 medium containing 1.5 g $NaNO_3$, 40 mg K_2HPO_4, 75 mg $MgSO_4 \cdot 7H_2O$, 20 mg Na_2CO_3, 36 mg $CaCl_2 \cdot 2H_2O$, 6 mg ammonium ferric citrate, 6 mg ammonium citrate monohydrate, 1 mg EDTA, 2.86 μg H_3BO_3, 1.81 μg $MnCl_2 \cdot 4H_2O$, 0.222 μg $ZnSO_4 \cdot 7H_2O$, 0.39 μg $Na_2MoO_4 \cdot 2H_2O$, 0.079 μg $CuSO_4 \cdot 5H_2O$, 0.050 μg $CoCl_2 \cdot 6H_2O$ in 1 L water. *Microcystis* spp. were cultivated in 5 L Erlenmeyer flasks containing 4 L with continuous illumination under 40 μmol m^{-2} s^{-1} in a temperature-controlled incubator (25°C ± 2°C). The initial inoculum biomass was controlled at about 0.5 mg L^{-1} of Chlorophyll a (*Chl.a*) with a continuous aeration at 0.5 L min^{-1}. All the experiments were conducted in triplicate. The microalgal cells were harvested at logarithmic phase after 30-day cultivation and stationary phase after 60-day, and used for the subsequential analyses.

Microcystis colonies in the field were isolated and obtained from Lake Taihu in September 2023. The samples were collected using a plankton net positioned approximately 0.5 m above the water surface. Morphological classification using a light microscope was used to identify the *Microcystis* algal strains. Only individual *Microcystis* populations that were free of visible impurities and stray algae were selected. These populations were then rinsed with sterile water and inoculated in test tubes containing BG11 medium at 25°C. After 15 days of incubation, samples were taken for zeta potential and contact angle determination.

2.2 Physiology analysis

A 10 mL suspension of microalgal cells was centrifuged at 12,000 rpm for 5 min. The cells sediment was mechanically broken in a mortar with the addition of quartz sand and then resuspended in 2 mL 95% (v/v) ethanol. This suspension was kept in the dark at 4°C for 12 h. Subsequently, the cell suspension was centrifuged for 5 min at 10,000 rpm. The absorbencies of 663, 490, and 384 nm were measured by spectrophotometer, and the content of pigment (mg L^{-1}) was calculated using the following equations: $Chl.a = 1{,}000 \times (1.02 \times A663 - 0.027 \times A384 + 0.01 \times A490)/92.5$.

Cell diameters (d) were measured using a microscope (Nikon ECLIPSE 80i, Japan) and dry weight (DW, g L^{-1}) was measured by

difference method. The Donnan volume (DV, $m^3\ g^{-1}$) was calculated using the following equations: $DV = 1/DW \times 1{,}000$. The specific surface area (SSA, $m^2\ g^{-1}$) was calculated using the following equations: $SSA = S/m = dv \times S/V = dv \times 4\pi r^2/(4/3 \times \pi r^3) = 6 \times DV/d \times 10^6$. The surface area per cell (CSA, $\mu m^2\ cell^{-1}$) were calculated using basic geometric shapes as described by Henderson R. et al. (2008) and dry weight.

2.3 Monosaccharide composition and EPS analysis

The EPS matrix was fractionated into the soluble EPS (sEPS, or released polymeric substance, RPS) and bound EPS (bEPS, or capsular polymeric substance, CPS), which are released into the surrounding environment, and which are tightly bound to the cell surface (De Philippis, 1998). The bEPS was also fractionated into the loosely bound EPS (LB-EPS) and tightly bound EPS (TB-EPS). To extract the algae cells and supernatant, 1,000 mL of algal solution was centrifuged at 8000 rpm for 10 min. The algae cells were then washed three times with distilled water and vacuum freeze-dried (Christ ALPHA 1-2 LD plus, Germany) to obtain dry algae. The CPS were extracted from the dry algae (Supplementary material; Supplementary Figures 1–3) with less debris. 100 mg of cells was added into 10 mL of 0.05% NaCl solution, maintained at 60°C for 60 min, and then passed through GF/C Whatman glass microfiber filters (Whatman International Ltd., Maidstone, United Kingdom). Microscopic observation was conducted by staining with India ink to ensure the extract has not been contaminated from intracellular or extracellular substances. Then, the supernatant was dialyzed with distilled water in a Spectrapor dialysis tube with a molecular weight cut-off of 3,500 Daltons (Spectrum China, Shanghai, China). The polysaccharide and protein content in RPS were determined from the supernatant. EPS content refers to the total ($mg\ g^{-1}$) of RPS and CPS content (Ge et al., 2014). The polysaccharide content was determined using the phenol sulfuric acid method, with glucose as the standard sample, while the protein content was determined using the Bradford assay using bovine serum albumin. The CPS and RPS liquid was isolated to neutral part, acidic I polymers and acidic II polymers (Supplementary material; Supplementary Figure 4).

The monosaccharide composition of EPS was measured using the method by Hokputsa et al. (2003). In briefly, 1 mg of dry weight CPS and RPS samples were subjected to methanolysis using 4 M hydrochloric acid in anhydrous methanol at 80°C for 24 h. To ensure accurate measurements, mannitol was added as an internal standard prior to performing trimethylsilylation. The trimethylsilylated samples were analyzed using gas chromatographic analysis (GC-Orbitrap-MS, Thermo Scientific TRACE 1310-EXACIVE GC). The content of each monosaccharide was calculated based on its content in CPS and RPS.

2.4 Surface physicochemical parameters

2.4.1 Zeta potentials analysis

A 10 mL suspension of microalgal cells was prepared by centrifuging at 2,000 g for 20 min. The resulting pellet was washed three times with wate. The pellet was then resuspended in a 0.1 M $NaNO_3$ solution and the pH was adjusted from 2 to 8. The zeta potential was determined using a ζ-potential analyzer (Malvern, Zetasizer Nano, ZS90) at room temperature, and the value obtained represents the zeta potential in millivolts (mV).

2.4.2 Hydrophobicity characterization

The hydrophobicity of the cell surface was evaluated using the method described by Rosenberg et al. (1980). The initial content of chlorophyll a (*chl.a* 0) was determined using a 10 mL suspension of microalgal cells. The cells were then resuspended in a phosphate buffer. Subsequently, 2 mL of organic solvents (hexane, ethyl acetate, chloroform) were added to 8 mL of cell suspension. The two-phase system was vortexed for 2 min and allowed to settle for 20 min. The chlorophyll a content of the algal cells in the organic phase was measured as *Chl.a*. The percentage hydrophobicity (H) was calculated as Equation (1):

$$H = \left(Chl.a\,0 - Chl.a\right) / Chl.a\,0 \times 100\% \quad (1)$$

2.4.3 Contact angles determinations

The cells were suspended in ultrapure water and filtered through a glass fiber membrane with a pore size of 0.45 μm. The membranes were then stored in agar petri dishes containing 1% (w/v) 10% (v/v) glycerol for 2 h to ensure consistent moisture content. Afterward, the membranes were then air-dried for 60 min to achieve a relatively stable contact angle. The contact angle was determined using water (θ_W), diiodomethane (θ_D) and formamide (θ_F) as reference liquids, following the according the method described by Williams et al. (2011).

2.4.4 Free energy of adhesion determinations

The surface free energy of the algae lawns was calculated using the Lifshitz-van Waals/acid–base approach (the LW/AB method). This method decomposes the surface free energy (γ) into two components: Lifshitz-van der Waals component (γ^{LW}) and Lewis acid–base component (γ^{AB}), which further splits into a Lewis acid component (γ^+) and a Lewis base component (γ^-). The LW/AB method can be mathematically expressed as Equations (2)–(4):

$$\gamma_l\left(1+cos\theta\right) = 2\sqrt{\left(\gamma_s^{LW}\gamma_l^{LW}\right)} + 2\sqrt{\left(\gamma_s^{+}\gamma_l^{-}\right)} + 2\sqrt{\left(\gamma_s^{-}\gamma_l^{+}\right)} \quad (2)$$

$$\gamma_s^{AB} = 2\sqrt{\left(\gamma_s^{+}\gamma_l^{-}\right)} \quad (3)$$

$$\gamma = \gamma^{LW} + \gamma^{AB} \quad (4)$$

where θ is the contact angle, subscripts of "s" and "l" refer to the surface and probe liquid, respectively. In Equation (2), the contact angle of the apolar liquid, diiodomethane, was used to quantify the apolar surface energy component γ_s^{LW}, since γ_l^- and γ_l^+ are both equal to zero (van Oss, 1993). Additionally, the contact angles measured with the other two probe liquids, water and formamide, were utilized to calculate the remaining two unknown surface energy parameters, γ_s^- and γ_s^+.

According to the Derjaguin, Landau, Verwey, and Overbeek (DLVO) theory, the degree of hydrophilicity and hydrophobicity of the algae surfaces were determined by evaluating their free energy of cohesion (ΔGcoh), as described in Equation (5):

$$\Delta G_{coh} = -2\left(\sqrt{\gamma_S^{LW}} - \sqrt{\gamma_l^{LW}}\right)^2 + 4\left(\sqrt{\gamma_S^+\gamma_l^-} + \sqrt{\gamma_S^-\gamma_l^+} - \sqrt{\gamma_S^+\gamma_S^-} - \sqrt{\gamma_l^+\gamma_l^-}\right) \quad (5)$$

where subscripts s and l, respectively, refer to the surface and water. If ΔGcoh < 0, the surface–surface interaction is stronger than the interaction of the surface with water, and the material is treated as hydrophobic. In contrast, the material is hydrophilic if ΔGcoh > 0. Additionally, the free interfacial energy (or total surface tension, G^{TOT}) was calculated based on the extended Derjaguin–Landau–Verwey–Overbeek (XDLVO) theory (van Oss, 1993).

2.4.5 Fourier transform infrared spectroscopy

A 10 mL algal solution was centrifuged at 5,000 rpm for 10 min to collect the algal cells. The cells were then vacuum freeze-dried and mixed with KBr powder (1:100, wt/wt). The mixture was processed by pressing and the transmission infrared spectra were recorded using an infrared spectrometer (NEXUS, Thermo Nicolet). The spectrometer had a scanning range of 4,000 to 500 cm^{-1} and a resolution of 2 cm^{-1}. The recorded spectra were analyzed using OMNIC software.

2.5 Statistical analysis

Results are averages of triplicates, and the values in each graph and table are shown with 5% error bars. t test was performed using SPSS 24.0 package (SPSS, Chicago, IL), with values of 0.05 selected as significance.

3 Results

3.1 Microalgal growth and cells physico-chemical characterization

3.1.1 Microalgal growth and morphology

Microcystis cells are spherical or sub-spherical in shape and are enveloped by a layer of uniform, non-layered, transparent and colorless glue at different stages (Figure 1). As the culture time increased, the size of the cells also tended to increase. Both strains of *Microcystis* exhibited the similar growth rate. *Microcystis wesenbergii* exhibited a higher growth rate during the early stage of logarithmic growth, whereas *M. aeruginosa* exhibited a higher the growth rate during the late logarithmic growth stage. These findings indicated that both strains of *Microcystis* possess relatively strong competitiveness. The SSA and CSV of both strains of *Microcystis* decreased with culture time (Figure 1D). For *M. wesenbergii*, the SSA decreased from 4902.95 to 710.27 $m^2\ g^{-1}$ (a decrease of 85.5%) and for *M. aeruginosa*, the SSA decreased from 5963.65 to 1532.95 $m^2\ g^{-1}$ (a decrease of 74.3%). The CSV decreased by 16.5 and 10.7% for *M. wesenbergii* and *M. aeruginosa*, respectively. These results highlight the significant influence of biomass on SSA.

3.1.2 Cell surface hydrophobicity

Figure 2 illustrates the hydrophobicity of *Microcystis* in different solvents, namely hexane (a non-polar solvent), ethyl acetate (a polar alkaline solvent), and chloroform (a polar acidic solvent). In polar solvents, the hydrophobicity of *M. wesenbergii* increased with culture time, while in polar alkaline solvents, the hydrophobicity decreased. On the other hand, the hydrophobicity of *M. aeruginosa* showed the opposite trend. During the logarithmic phase, the hydrophobicity of *M. wesenbergii* in non-polar solvents was significantly lower than that of *M. aeruginosa*. However, during the stationary phase, the hydrophobicity of *M. wesenbergii* in non-polar solvents was significantly higher than that of *M. aeruginosa*. Additionally, *Microcystis* had a lower affinity for chloroform (a polar acidic solvent) compared to ethyl acetate (a polar alkaline solvent). The hydrophobicity of *Microcystis* cell surface in hexane was less than 50%, indicating that the cell surface of *Microcystis* was hydrophilic.

3.1.3 Contact angle and surface free energy

Contact angle and surface free energy could directly influence the hydrophobicity. As shown in Table 1, the contact angles with water (θ_W), formamide (θ_F), and diiodomethane (θ_D) on *M. wesenbergii* increased with culture time. For *M. aeruginosa*, θ_w increased with culture time, while θ_F and θ_D decreased. During the logarithmic phase, θ_w on *M. wesenbergii* was significantly higher than that of *M. aeruginosa*, whereas θ_F and θ_D on *M. wesenbergii* were significantly lower than those on *M. aeruginosa*. Conversely, during the stationary phase, θ_w on *M. wesenbergii* was not significantly different from that on *M. aeruginosa*, but θ_F and θ_D were significantly higher. In conclusion, the water contact angles on *Microcystis* were always less than 90°. Additionally, the change of θ_W in *Microcystis* from logarithmic phase to stationary phase was more than that of other algal strains (Supplementary Figure 6).

According to van Oss (1993), microalgae cells were considered hydrophobic when $\gamma_s^- \geq 28.3$ mJ m^{-2} or $\Delta G_{coh} > 0$, and hydrophilic when $\gamma_s^- < 28.3$ mJ m^{-2} or $\Delta G_{coh} < 0$. Table 1 shows that the surface of *Microcystis* cells was hydrophilic, which was not directly related to the culture stage. The ΔG_{coh} of *M. wesenbergii* and *M. aeruginosa* decreased with culture time, indicating that cells tended to gather into colonies during the stationary phase. In this phase, the hydrophobicity degree of *M. wesenbergii* (high ΔG_{coh} value) was significantly higher than that of *M. aeruginosa*. However, the change pattern of hydrophilicity reversed in the logarithmic phase. In terms of γ_s, the γ_s values of *M. aeruginosa* increased with culture time, while the γ_s values of *M. wesenbergii* decreased. Moreover, the γ_s values of both strains of *Microcystis* during the stationary phase were smaller than those during the logarithmic phase. The surface free energy of *M. aeruginosa* was lower than that of *M. wesenbergii* during the logarithmic phase. However, during the stationary phase, the opposite was observed. The nonpolar surface free energy (γ_s^{LW}) of *M. aeruginosa* remained constant throughout the culture time, with no significant difference in γ_s^{LW} between

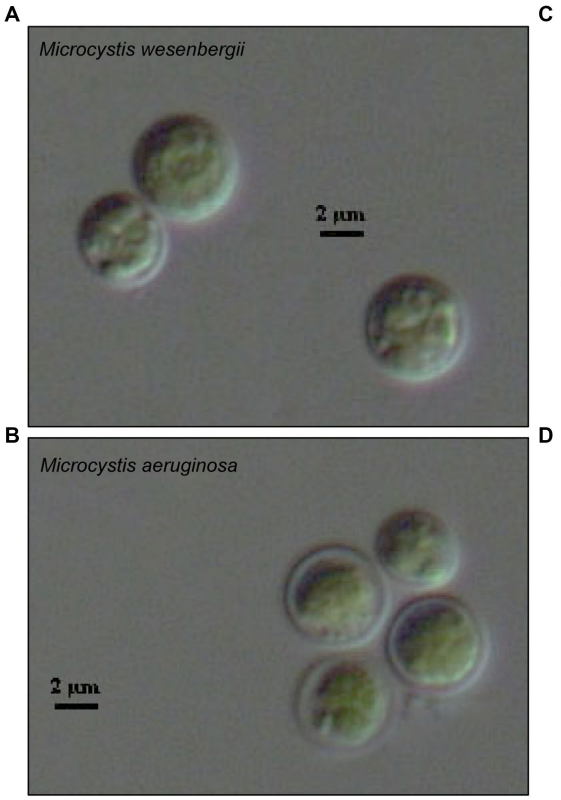

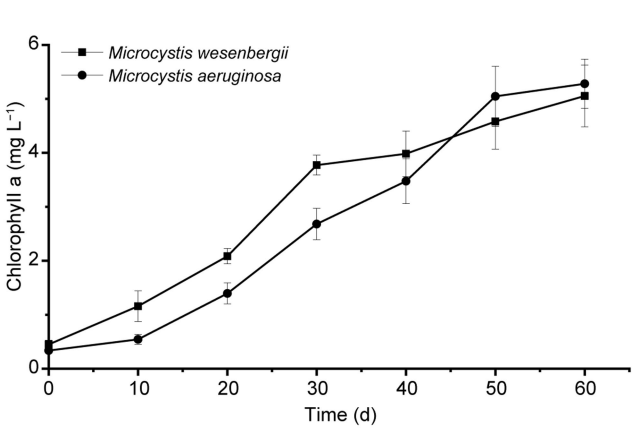

D

		M. wesenbergii	*M. aeruginosa*
Logarithmic phase	Size (μm)	4.08 ± 0.48	3.74 ± 0.29
	SSA (m^2 g^{-1})	4902.95	5963.65
	DV ($\times10^{-4}$ m^3 g^{-1})	33.33	37.04
	CSA (μm^2 $cell^{-1}$)	52.28	43.62
Stationary phase	Size (μm)	5.45 ± 0.55	5.15 ± 0.56
	SSA (m^2 g^{-1})	710.27	1532.96
	DV ($\times10^{-4}$ m^3 g^{-1})	6.45	13.16
	CSA (μm^2 $cell^{-1}$)	93.31	83.32

SSA, specific surface area. DV, Donnan volume. CSA, surface area per cell.

FIGURE 1
Growth and morphology of *Microcystis*. **(A)** *Microcystis wesenbergii*. **(B)** *Microcystis aeruginosa*. **(C)** Growth curves of *Microcystis*. **(D)** Key cell characterization data for *Microcystis*. L, Logarithmic phase; S, Stationary phases.

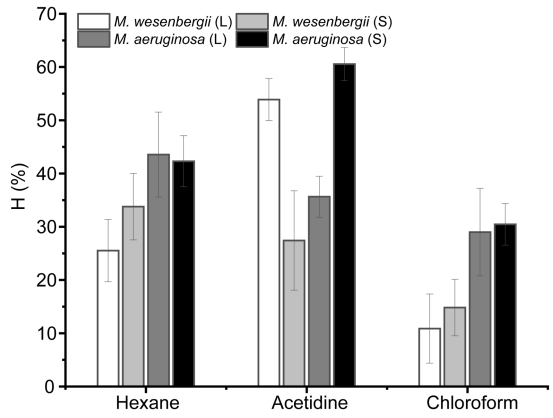

FIGURE 2
The hydrophobicity of the *Microcystis* cells under different growth phases.

M. wesenbergii and *M. aeruginosa*. These findings suggest that the overall surface free energy and adhesion free energy of *Microcystis* are determined by the polar surface free energy. Additionally, the Supplementary Figure 6 shown that *Microcystis* differed significantly from other algal strains in ΔGcoh and zeta. However, the surface of colonial *Microcystis* cells was hydrophobic ($\Delta G_{coh} < 0$; Supplementary Figure 7).

3.1.4 Physical intercellular interactions

The surface charge of microalgae is an important characteristic of the cell surface. The zeta potential, which refers to the potential of the shear layer on the surface of charged particles, is widely used to describe the electrostatic interaction between colloidal particles and is an important indicator of the stability of colloidal systems. The surface charge of microalgae is influenced by the surface structure and EPS of the cells (Zheng et al., 2019). Microalgal cells produce a significant amount of proteins and sugars both inside and outside the cell membrane, leading to an increase in the negative charges of microalgae. This increase in the absolute value of zeta potential enhances the electrostatic repulsion between microalgae cells, making it difficult for them to coagulate and promoting a more even distribution in the medium. Therefore, the absolute value of the zeta potential can serve as an indicator of the stability of the cell suspension.

Figure 3 shown the zeta potential of *Microcystis* cells at different growth stages and pH levels. The zeta potentials of *Microcystis* were consistently negative throughout different growth stages, indicating the presence of negative charges. Additionally, according to the theory of electric double layer structure (Felix et al., 2014), the binding of OH^- ions (and/or release of H^+ ions) is the main mechanism for charging the particle surface. The negative charges initially increased and then remained stable as the pH levels increased. And, the negative charges of *M. aeruginosa* and *M. wesenbergii* showed no significant change (−11.32~−12.07) from the logarithmic phase to the stationary phase. Thus, the negative charges of *Microcystis* remain relatively

TABLE 1 Contact angles and surface physicochemical properties determined for cyanobacteria.

	Contact angles of the probe liquids (°)			Free energy components (mJ m^{-2})						Zeta (mV)	
Microalgae stain	θ_w	θ_F	θ_D	γ_s^{LW}	γ_s^{AB}	γ_s	γ_s^+	γ_s^-	ΔG_{coh}	ζ	References
Microcystis wesenbergii (L)	26.0 ± 0.5	26.6 ± 0.7	31.2 ± 0.5	43.7 ± 0.2	6.6 ± 0.6	50.3 ± 0.5	0.2 ± 0.0	50.6 ± 0.7	30.3 ± 1.2	−12.07 ± 0.74	
M. wesenbergii (S)	32.3 ± 0.6	32.3 ± 0.4	32.1 ± 0.2	43.4 ± 0.1	4.4 ± 0.3	47.7 ± 0.2	0.1 ± 0.0	47.5 ± 0.5	27.6 ± 0.8	−11.93 ± 0.57	
Microcystis aeruginosa (L)	22.3 ± 0.3	31.2 ± 0.3	31.9 ± 0.4	43.4 ± 0.2	2.9 ± 0.4	46.3 ± 0.3	0.0 ± 0.0	57.6 ± 0.3	42.0 ± 0.6	−11.32 ± 0.85	
M. aeruginosa (S)	32.0 ± 0.3	27.7 ± 0.4	26.8 ± 0.3	45.5 ± 0.1	5.2 ± 0.2	50.7 ± 0.2	0.2 ± 0.0	44.9 ± 0.3	22.1 ± 0.5	−11.85 ± 0.21	This study
M. aeruginosa LEGE 91344 (L)	44.8 ± 5.5	37.1 ± 1.6	36.4 ± 8.4	35.9 ± 0.7	10.7 ± 2.8	46.6	0.5 ± 0.4	57.4 ± 7.6	43.4 ± 15.5		Gonçalves et al. (2015)
S. salina LEGE 06079 (L)	51.9 ± 8.0	37.3 ± 1.0	73.6 ± 1.1	35.8 ± 0.4	0.0 ± 0.0	35.8	0.0 ± 0.0	22.6 ± 3.2	−10.2 ± 6.6		
Synechococcus sp. ATCC 27184 (L)	64	66	61	28.3	0	28.3	0	31.7	10.9	−32.2	Ozkan and Berberoglu (2013)
A. variabilis ATCC 29413 (L)	114	71	45	37	0	37	0.3	0	−94.9	−16.80	
A. variabilis (S)	97.5 ± 1.5	74 ± 2.1 a	86 ± 3 b	29.19	0	29.19	5.47	0	−55.85	−11.00	Hao et al. (2017)
Synechocystis sp.				28.3	3.9	32.2	0.4	10.2	0.1		Volpe and Siboni (1997)
A. variabilis				37	0	37	0.2	0	−100.3		

[A]contact angle with glycol; [b]contact angle with glycerol; L, Logarithmic phase; S, Stationary phases; θ_w, contact angle with water; θ_F, contact angle with formamide; θ_D, contact angle with diiodomethane; γ_s^{LW}, Lifshitz-van der Waals component of the surface free energy; γ_s^{AB}, Lewis acid–base component of the surface free energy; γ_s, surface free energy; γ_s^-, electron donor component; γ_s^+, electron acceptor component; ΔG_{coh}, the free energy of cohesion; AB, refers to acid–base, i.e., polar component; LW, refers to Lifshitz-van der Waals, i.e., dispersive component; +, refers to electron acceptor parameter; −, refers to electron donor parameter; ξ, Zeta potential (mV).

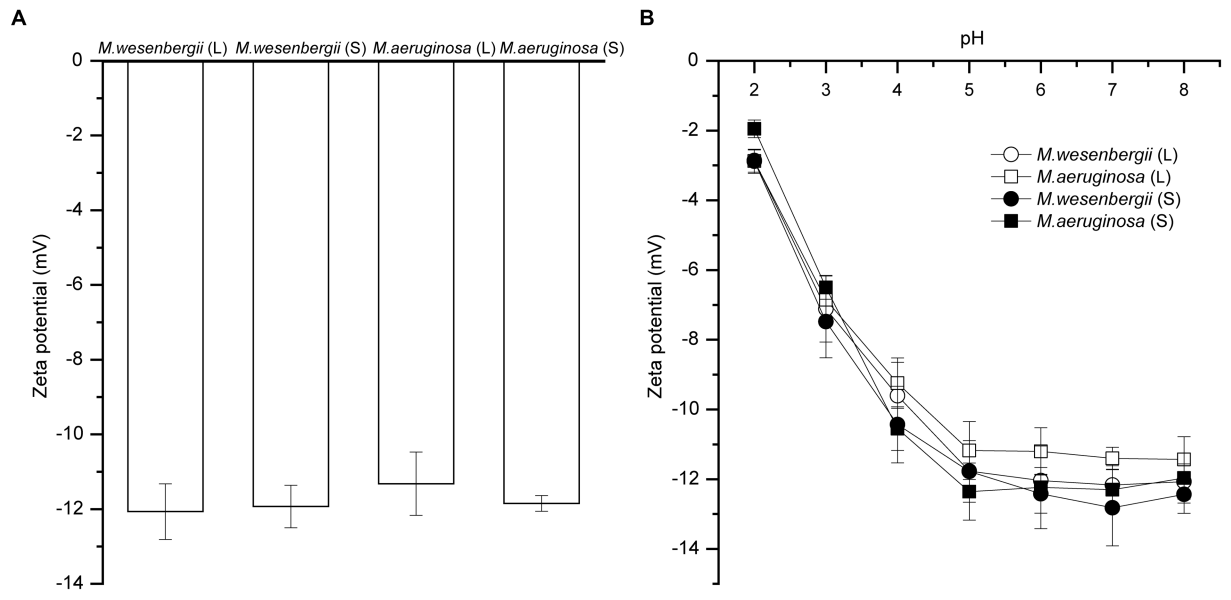

FIGURE 3
The zeta potential of *Microcystis* under different growth phases **(A)**, and pH **(B)**. L, Logarithmic phase; S, Stationary phases.

stable and do not vary with the duration of growth. Furthermore, there was no significant difference in the zeta potential between these both strains of *Microcystis* ($p > 0.05$). However, the absolute value of zeta was higher in the colonial *Microcystis* compared to the unicellular cells. Additionally, the absolute value of zeta in *M. wesenbergii* was slightly higher than that in *M. aeruginosa*.

3.2 Cell surface functional groups under different growth stage

Cell surface functional groups were analyzed using ATR-FTIR spectroscopy (Ferro et al., 2019). There were no marked differences in the spectra characteristic bands of strains corresponding to lipids, including—CH_3, CH_2, C–H functional groups [3,050–2,800 and 1,480–1,330 cm^{-1} (Wood et al., 2008)], carbohydrates, including C–O–C, C–OH, and P–O–P functional groups [1,200–950 cm^{-1} (Castro et al., 2010)], nucleic acid backbone conformations, including P=O [1,250–1,000 and 1,000–800 cm^{-1}(Liu Y. K. et al., 2016)], and amide I, II, and III, including NH, C–N, C=O [1,660–1,500 cm^{-1}, 1,385–1,300 cm^{-1} (Yee et al., 2004)].

The absorption peaks of various functional groups on the surface of *Microcystis* cells were observed within the spectral ranges of 918–1,737 cm^{-1} and 2,855–3,304 cm^{-1} (Figure 4). Comparatively, the absorption peaks of groups in the stationary phase were stronger than those in the logarithmic phase, indicating the presence of more functional groups involved in cell aggregation during the stationary phase. Notably, the increase in absorption peaks of all groups on *M. aeruginosa* during the stationary phase was significantly higher than that on *M. wesenbergii*. The absorption peak of the O–H group on *M. wesenbergii* remained unchanged throughout the growth stages, whereas the absorption peak of the O–H functional group on *M. aeruginosa* during the stationary phase was significantly higher than that during the logarithmic phase. Additionally, the content of functional groups on *M. aeruginosa* was lower than that on *M. wesenbergii*, with a reversed stability period (Supplementary Table 1). These results showed that more O–H functional groups were present on *M. aeruginosa* cell surface during the stationary phase, which could result in a more negatively charged cell surface. This enhanced negative charge would promote the adsorption of metal ions in the solution, leading to the colony formation. The absorption peak of alkyl group (CH_2/CH_3 vibrations) on *M. wesenbergii* remained by the growth stage. However, in the case of *M. aeruginosa*, the alkyl absorption peak during the stationary phase was significantly higher compared to the logarithmic phase. During the logarithmic phase, the alkyl group on *M. aeruginosa* was lower than that on *M. wesenbergii*, whereas the opposite was observed during the stationary phase. The alkyl group plays a crucial role as the primary hydrophobic component. Although the entire cell surface is hydrophilic, the decrease in hydrophilicity during the stationary phase may be attributed to the increased presence of alkyl groups. The absorption peaks of carbonyl groups (C=O) were predominantly observed at 1,622–1,657 and 1,685–1,789 cm^{-1}. The range of 1,622–1,657 cm^{-1} could be assigned to the C=O double-bond stretching vibration in the amide I band, while the range of 1,685–1,789 cm^{-1} corresponds to the C=O bond stretching vibration in the free carboxyl group. Peaks representing C–N/N–H group were present at 1,622–1,657 cm^{-1}, which were associated with the amide II band. Peaks representing P=O double-bond asymmetric stretching were observed at 1,239 cm^{-1}, and are characteristic of nucleic acid or phosphorylated polysaccharides. The absorption peaks corresponding to the C–O–C, C–O–P, and P–O–P ring vibrations of polysaccharides were mainly observed in the range of 900–1,200 cm^{-1}, which can be attributed to the mixed peaks of carbohydrates. These changes are similar to the alterations observed in the aforementioned alkyl and OH groups.

3.3 EPS and monosaccharide composition

EPS, a viscous substance produced by cyanobacteria cells, serves as a protective barrier against the external environment, such as drought resistance, high salt resistance, ultraviolet radiation resistance, colony formation, and protozoan predation (Pereira et al., 2009; Sun et al., 2020). The dominance of polysaccharide content in EPS was shown in Figure 5A. The EPS content of *M. wesenbergii* decreased significantly with culture time, while the EPS content of *M. aeruginosa* increased significantly. Moreover, during the logarithmic phase, the EPS content of *M. wesenbergii* was significantly higher than that of *M. aeruginosa*, but this trend reversed during the stationary phase. These observations aligned with changes in cell surface free energy and surface functional groups, but contradicts the law of cell adhesion free energy. In term of EPS fraction (Supplementary Figure 4), the neutral fraction of CPS in *Microcystis* cells decreased with culture time, while acidic fractions increased, mainly acidic I polymers. Additionally, the proportion of acidic fraction in EPS was higher during the stationary phase. The main monosaccharide components of the both *Microcystis* strains (Figure 5B; Supplementary Figure 8) include alduronic acid, glucose, arabinose, and galactose. The

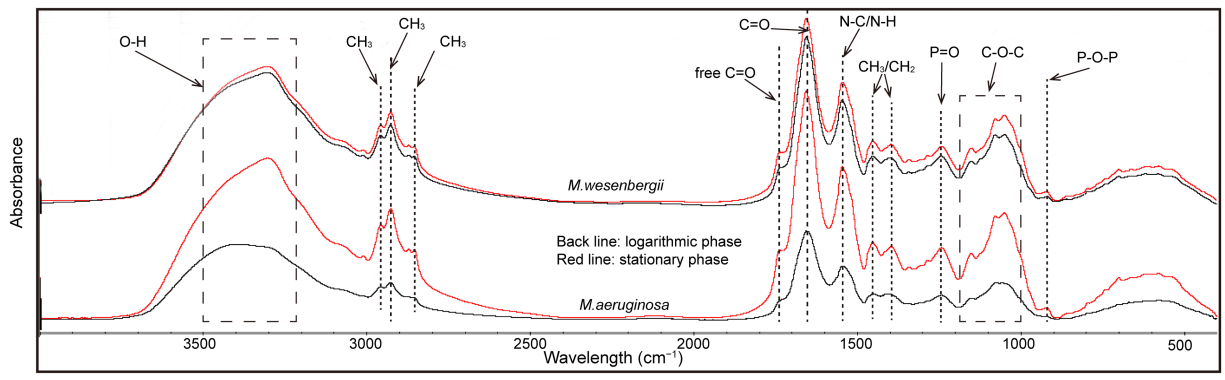

FIGURE 4
ATR-FTIR spectrum of *Microcystis wesenbergii* and *Microcystis aeruginosa* under different growth phases.

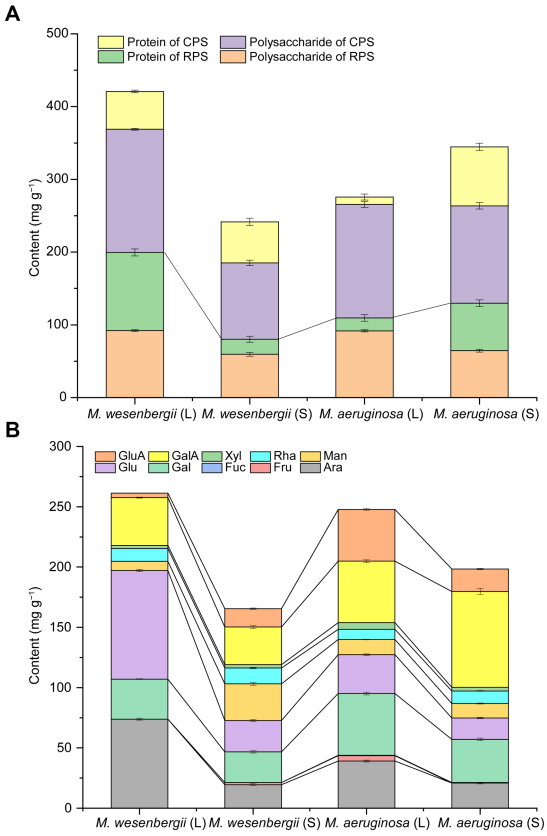

FIGURE 5
EPS contents **(A)** and monosaccharide composition contents of EPS **(B)** for *Microcystis* at different growth phases. GluA, glucuronic acid; GalA, galacturonic acid; Xyl, xylose; Rha, rhamnose; Man, mannose; Glu, glucose; Gal, galactose; Fuc, Fucose; Fru, fructose; Ara, arabinose. L, Logarithmic phase; S, Stationary phases.

glucuronic acid abundance of EPS in *M. wesenbergii* increased with culture time, whereas decreased in *M. aeruginosa*. Furthermore, the glucuronic acid abundance of EPS in *M. wesenbergii* was significantly higher than that in *M. aeruginosa* during the logarithmic phase, but becomes equal during the stationary phase. On the other hand, the galacturonic acid concentration increased with culture time in both strains of *Microcystis*. However, the content of galacturonic acid in *M. wesenbergii* consistently remained lower than that in *M. aeruginosa*, regardless of the growth phase.

Figure 5B demonstrated that the total uronic acid content was notably higher during the stationary phase compared to the logarithmic phase. Furthermore, the uronic acid content in *M. wesenbergii* consistently remained lower than that in *M. aeruginosa*. Conversely, the glucose and arabinose contents of EPS during the stable period were significantly lower than those during the logarithmic period. Moreover, the glucose and arabinose contents of EPS in *M. wesenbergii* consistently remained higher than those in *M. aeruginosa*, which contradicted the trend observed for uronic acid. The galactose content of EPS in *M. wesenbergii* increased with culture time, while decreased in *M. aeruginosa*. Moreover, the galactose content in *M. wesenbergii* during the logarithmic phase was significantly higher than that in *M. aeruginosa*. In the stationary phase, the proportion of galactose in both *Microcystis* strains was identical, reflecting the change observed in glucuronic acid. In summary, as the culture time, the monosaccharides that significantly decreased were glucose and arabinose, while galacturonic acid showed a significant increase. Additionally, glucuronic acid and galactose increased in *M. wesenbergii* but decreased in *M. aeruginosa*.

3.4 Interrelationship of EPS and functional groups with cell surface properties

The relationship between the characteristics of EPS (including content, composition, and functional groups) and the cell surface properties of *Microcystis* (such as SSA, charges, surface free energy, surface tension, and hydrophobicity) was depicted in Figure 6. Regarding hydrophobicity, the surface hydrophobicity of *Microcystis* was found to be negatively correlated with EPS content, mainly due to the protein content in EPS. This suggests a higher abundance of hydrophilic amino acids in the protein, along with the arabinose and glucose concentrations in EPS, as well as O–H and P–O–P groups (Supplementary Figure 9). On the other hand, the surface hydrophobicity of *Microcystis* showed a significant positive correlation with xylose, glucuronic acid, and fructose. Notably, *M. wesenbergii* exhibited a significant positive correlation between hydrophobicity and most functional groups, whereas *M. aeruginosa* displayed the opposite trend. Finally, two hydrophilic groups, O–H and P–O–P, were identified as key factors influencing the hydrophobicity of *Microcystis*, with P–O–P primarily found in lipopolysaccharides.

The SSA of *Microcystis* showed a significant positive correlation with the polysaccharide content in EPS and neutral fraction of CPS, as well as with arabinose and galactose concentrations in EPS. Meanwhile, SSA of *Microcystis* exhibited a significant negative correlation with most relevant functional groups and acidic fractions of CPS, as well as with the presence of rhamnose and mannose. The relationship between the surface tension of *Microcystis* and the protein content in EPS, as well as the most relevant functional groups, was found to be significantly positive. On the other hand, there were significant negative correlations with the monosaccharide composition of fructose, xylose, and glucuronic acid. The adhesion free energy of *Microcystis* and G^{TOT} showed a significant positive correlation with the polysaccharide content in EPS, as well as with the monosaccharide composition of fructose, galactose, xylose, and glucuronic acid. On the other hand, there was a significant negative correlation with rhamnose and most functional groups. Therefore, the presence of polysaccharides in EPS primarily influenced the SSA and total surface energy of *Microcystis* cells, while proteins in EPS influenced hydrophobicity and surface tension. Glucuronic acid, xylose, and fructose in the polysaccharide composition mainly impacted the surface properties. The hydrophilic groups O–H and P–O–P were identified as key factors influencing the hydrophobicity of *Microcystis*.

4 Discussion

Microcystis sp. is a unicellular microorganism with remarkable phenotypic plasticity, which frequently causes the formation of colonies and algal blooms in lakes and reservoirs worldwide (Xiao et al., 2018). In addition to particular adaptation characteristics like buoyancy regulation, cell surface charge and hydrophobicity, notably

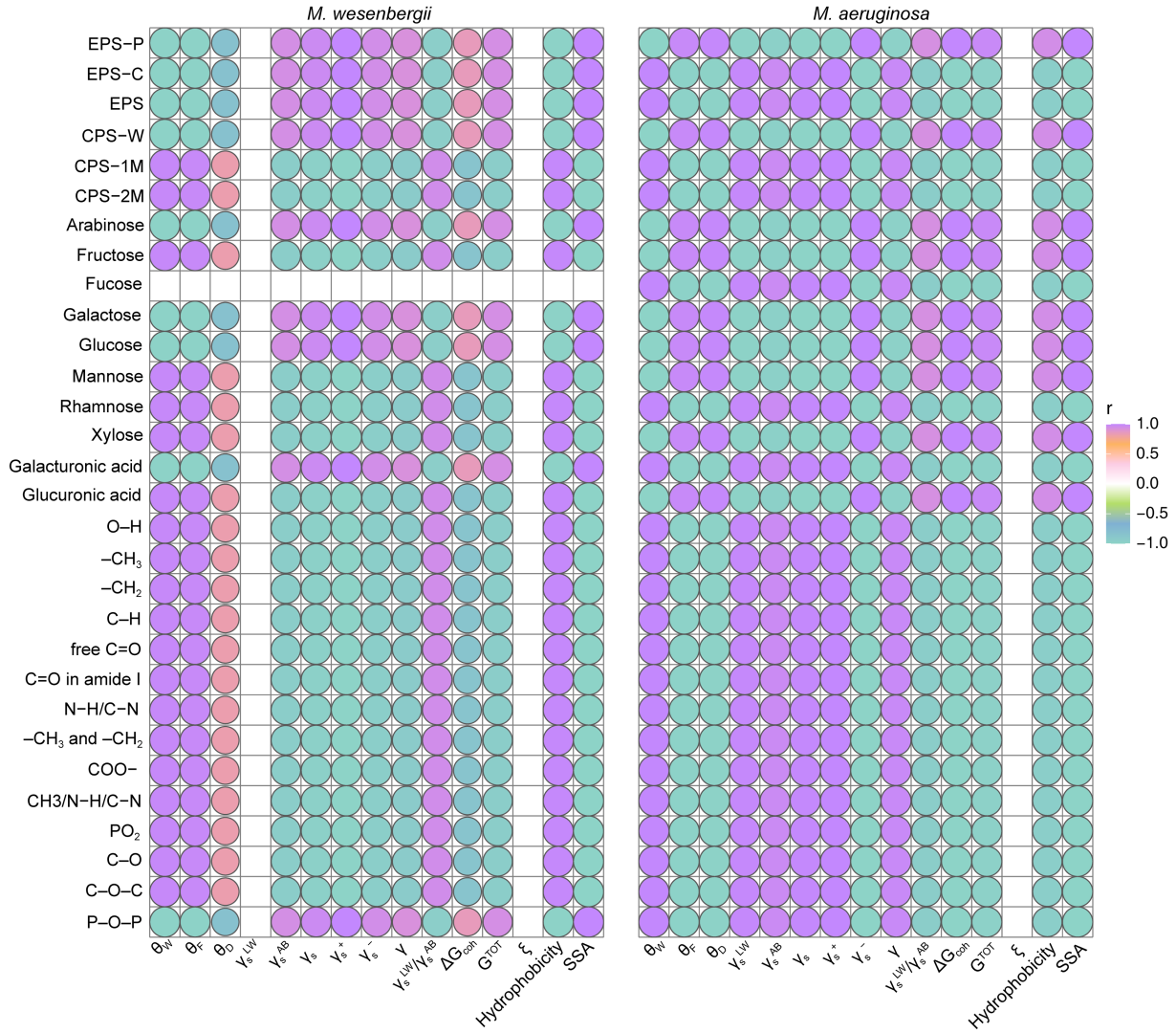

FIGURE 6
The relation between cell surface characterization and EPS content, composition and functional groups for *Microcystis*. EPS-C, the carbohydrate content in EPS; EPS-P, the protein content in EPS. CPS-W, neutral part in CPS; CPS-1M, acidic I polymers in CPS; CPS-2M, acidic II polymers in CPS. θ_W, contact angle with water; θ_F, contact angle with formamide; θ_D, contact angle with diiodomethane; γ_s^{LW}, Lifshitz-van der Waals component of the surface free energy; γ_s^{AB}, Lewis acid–base component of the surface free energy; γ_s, surface free energy; γ_s^-, electron donor component; γ_s^+, electron acceptor component; ΔG_{coh}, the free energy of cohesion; AB, refers to acid–base, i.e., polar component; LW, refers to Lifshitz-van der Waals, i.e., dispersive component; +, refers to electron acceptor parameter; −, refers to electron donor parameter; ξ, Zeta potential (mV).

EPS, also play a role in the development of *Microcystis* colonies or blooms. Additionally, different morphologies of *Microcystis* can result in successional blooms in lakes. This begs the question of how *Microcystis* achieves a competitive edge.

4.1 Physico-chemical surface properties of *Microcystis*

In terms of cell growth, size and morphology, *M. wesenbergii* had a higher growth rate in the pre-logarithmic phase and a lower growth rate in the late-logarithmic phase. Additionally, biomass had a significant impact on SSA. The SSA of *Microcystis* was 50 times more than that of the unicellular *Synechococcus* sp. (76 and 88 $m^2\ g^{-1}$; Dittrich and Sibler, 2005). The CSV values of the two *Microcystis* strains were similar to those reported by Henderson R. et al. (2008), indicating that the large SSA can enhance the ability of *Microcystis* to adsorb substances in the liquid phase (Cheng et al., 2019). The SSA was widely recognized as an initial parameter for evaluating the flocculation potential. In the context of *Microcystis* removal through flocculation, a higher SSA value indicates a greater demand for flocculant dosage (Henderson R. et al., 2008). The analysis of contact angle, adhesion free energy, and surface free energy (Table 1) revealed that both strains of *Microcystis* cultivated in the laboratory exhibit hydrophilic characteristics. However, there were noticeable variations in hydrophobicity between *M. wesenbergii* and *M. aeruginosa*, especially in the composition of the non-polar region of the cell surface. The discrepancy may contribute to the differential occurrence of *Microcystis* blooms in different seasons. Notably,

during the logarithmic phase, the contact angles of *Microcystis* with solvent were smaller than that of *M. aeruginosa* LEGE 91344 (less than 90°; Gonçalves et al., 2015), and *A. variabilis* (greater than 90°; Volpe and Siboni, 1997; Ozkan and Berberoglu, 2013; Hao et al., 2017). Compared with other freshwater cyanobacteria, *S. salina* LEGE 06079, *Synechocystis* sp., and *A. variabilis* are all hydrophobic (Table 1).

Cell-to-cell interactions can be evaluated using the free energy of adhesion (ΔG_{coh}; Yu et al., 2018), which measures the change in free energy before and after adhesion. A higher ΔGcoh suggest a weaker adhesion effect, indicating a stronger repulsive force (or higher mutual absorption) between cells. In this study, *M. wesenbergii* exhibited a lower free energy of adhesion during the logarithmic phase, leading to a higher likelihood of adsorbing substrate and cells. Similarly, *M. aeruginosa* exhibited a lower free energy of adhesion during the stationary phase, making it more prone to adsorb substrate and cells. Both species displayed distinct competitive advantages in this study.

In this study, the zeta potential of *Microcystis* cells remained negative during throughout the cultivation stage and under different pH conditions. This finding is consistent with previous studies on various algal strains, including eukaryotic freshwater single-celled green algae and cyanobacteria (Gonçalves et al., 2015; Xia et al., 2016), marine green algae and diatoms (Ozkan and Berberoglu, 2013), and field *Microcystis* algae (Liu L. et al., 2016). These findings further support the notion that *Microcystis* cells can maintain a stable electronegativity, and that the electrostatic interactions can promote the surface adhesion of cells and metal cations to *Microcystis* cells. However, Liu L. et al. (2016) observed that the absolute value of the zeta potential on the cell surface of *Microcystis* algae was higher during the stationary phase compared to the logarithmic phase, and this difference was influenced by pH. Nonetheless, no significant difference in the absolute values of the zeta potential was observed between the two algal strains during the cultivation period (pH range of from 7 to 8).

4.2 EPS and functional groups of *Microcystis*

The cell surface functional groups of *Microcystis* were determined by the composition and content of EPS secreted by the cells. Ionizable functional groups in EPS, such as carboxyl, phosphorus, amino, and hydroxyl groups, can serve as binding sites for divalent cations. These functional groups play a crucial role in determining the properties of the cell surface (Bhunia et al., 2018). The content of hydrophilic groups (including amino groups, hydroxyl groups, carboxyl groups, sulfonic acid groups, aldehyde groups, and phosphoric acid groups) increased during the stationary phase. Similarly, the hydrophobic groups (including hydrocarbon groups, ester groups, and alkanes) also undergo similar changes. These results indicated that the hydrophilicity of the both *Microcystis* strains decreased with culture time. Therefore, the hydrophobic groups play a significant role in the change of hydrophilicity of the algal strains during the culture time. Pringle and Fletcher (1983) demonstrated that an increase in the surface hydrophobicity of microorganisms promoted their mutual approach, facilitating adsorption between microorganisms or with adsorption carriers. In our study, the hydrophobic group contents of *M. aeruginosa* were significantly lower than those of *M. wesenbergii* during the logarithmic phase. However, this trend reversed during the stationary phase, with *M. wesenbergii* exhibiting lower adhesion free energy during the logarithmic phase, making cells easier to adsorb matrix and cells. Conversely, *M. aeruginosa* had lower free adhesion energy during the stationary phase, making cells easier to adsorb matrix and cells. These findings suggested that both strains of *Microcystis* have competitive advantages at different growth stages.

The types of EPS components, such as uronic acid, phosphate, and sulfate (P=O functional group, Figure 4), along with unique connection to sugar groups, give EPS important characteristics (Bhunia et al., 2018). Uronic acids, phosphates, and acetylated sugars primarily contribute to the overall negative charge of EPS, which give EPS its binding and adsorption properties (Gupta and Diwan, 2017). During the stationary phase, the concentration of uronic acid significantly increased, usually in the form of glycosidic bonds. Additionally, the EPS monosaccharide profiles in *Microcystis* were influenced by different culture conditions of distinct algal strains (Forni et al., 1997). However, the polysaccharide content in EPS consistently exceeds that of protein in EPS (Costa et al., 2018). Notably, galacturonic acid was prevalent in *M. flos-aquae*. Among the neutral sugars, fucose, mannose, rhamnose, glucose, uronic acid, and xylose are present in the EPS of *M. flos-aquae*, *M. viridis*, and *M. aeruginosa*, while *M. wesenbergii* contains only uronic acid (Le et al., 2022). The variation in growth rate and the variability in EPS content could potentially shed light on the seasonal succession of *Microcystis*. This may also explain why *M. aeruginosa* blooms were both the larger and last longer in the lake, as well as its predominance in terms of abundance and frequency (Zhai et al., 2013).

4.3 Determinants of surface properties of *Microcystis*

The protein content in EPS of unicellular *Microcystis* was hydrophilic in this study. Previous research have shown that an increase in C−(O, N) group content indicated the presence of polysaccharides, which can reduce cell hydrophobicity and increase cell surface energy. Conversely, an increase in C−(C, H) group content indicated the presence of hydrocarbons, which can increase cell hydrophobicity and decrease cell surface energy. Other studies have also demonstrated a relationship between the abundance of phosphodiester-linked and the exposure of hydrophobic regions on the cell surface (Masuoka and Hazen, 1997). In this study, it was found that the C−(O, N) group could effectively reduced the hydrophobicity of *M. aeruginosa*, but had no impact on the hydrophobicity of *M. wesenbergii*. Meanwhile, the C−(C, H) group increased the hydrophobicity of *M. aeruginosa*, but did not have the same effect on *M. wesenbergii*. These findings suggest that the changes in hydrophobicity during different growth stages vary between *M. wesenbergii* and *M. wesenbergii*, and the functional groups involved in these changes also differ. Furthermore, as depicted in Supplementary Figure 5, the O–H and

P–O–P groups are shown to play a significant role in influencing the hydrophobicity of *Microcystis*.

The surface free energy of microorganisms is a reflection of the intermolecular force on the surface of microorganisms. It provides insight into the inherent characteristics of microorganisms and serves as a measure of the adhesion between cells and substrates or between cells themselves. Changes in cell surface components and chemical groups can result in alterations in cell free energy. Various substances [such as protein, peptidoglycan, teichoic acid, lipopolysaccharide, EPS, etc. (Liu et al., 2011; Li et al., 2014)] facilitate the interaction of the cell surface with other substances through Lewis acid–base interactions, electrostatic interactions, and hydrophobic interactions. These interactions ultimately influence cell adhesion. Among these components, EPS has been found to have the most significant impact, as supported by numerous studies. For example, EPS can inhibit the adhesion of *Rhodococcus*, while the protein-rich EPS on the surfaces of strains *Sphingobium* and *Micrococcus* has minimal effect on bacterial adhesion to silicone oil (Iwabuchi et al., 2003; Zhang et al., 2011). Sheng and Yu (2006) demonstrated a positive correlation between the γ_b^{AB} and γb of *Rhodopseudomonas acidophila* with EPS content, as well as a positive correlation with protein/polysaccharide content. In our study, we also observed positive correlations between the γ_s^{AB} and γ_s values and the EPS content on *Microcystis*. Additionally, we found positive correlations between the γ_s^{AB} and γ_s values and the polysaccharide content in EPS on *M. wesenbergii*, as well as a positive correlation with the protein content in EPS on *M. aeruginosa*. Previous studies have already demonstrated the impact of EPS on the formation of *Microcystis* blooms (Zhang et al., 2018; Le et al., 2022).

4.4 Determinants of surface properties on colony formation and the contribution of *Microcystis* ecology

Xiao et al. (2017) demonstrated that *Microcystis* colonies formation involves two mechanisms: cell division formation (e.g., *M. ichthyoblabe* colonies formation), and cell adhesion (e.g., *M. wesenbergii* colonies formation). However, cell adhesion leads to faster colony formation. The surface properties of *Microcystis*, such as zeta potential, hydrophobicity, and EPS, play a crucial role in cell adhesion. These properties have a significant impact on the morphology, structure, and function of cyanobacterial colonies (Devasia et al., 1993). Algal cell surface have a negatively charged (zeta < 0), making somewhat hydrophobicity. In the field of *Microcystis* removal, cations are commonly employed as flocculants, due to neutralize the negative surface charge of *Microcystis*. Therefore, Zeta potential as an important index to characterize the surface charge has been applied in wastewater treatment (Henderson R. K. et al., 2008). Furthermore, cations are a factor in the colony formation of *Microcystis*. In addition to neutralize the negative surface charge, divalent Ca^{2+} and Mg^{2+} exhibited a strong binding capability with phenolic −OH, aromatic C − C, and polysaccharide C − O groups to promote forming colonies (Xu et al., 2016; Masumoto et al., 2023). Thus, EPS plays a crucial role in population formation, especially TB-EPS (Xu et al., 2014). Meanwhile, a study indicated that most organic matters were located in the TB–EPS (Xu et al., 2013). This finding aligns with the results of our study, which also observed a higher content of bEPS compared to sEPS, particularly in terms of polysaccharides. Duan et al. (2022) further explain that the protein component of EPS has a negative effect on colony formation, while the sugar component has a positive effect.

The surface properties of colonial *Microcystis* differ from those of unicellular *Microcystis*, and the colonial *Microcystis* cells produce more EPS, which is more conducive to the stabilization of the colonies. Additionally, when *Microcystis* cells form a colony, various environmental factors can influence the physical and chemical properties of the colony. For instance, light and temperature not only impact the photosynthesis of *Microcystis* cells, but also influence parameters such as dissolved oxygen (DO), pH, and Eh (oxidation–reduction potential) of the colony. Then, these factors affect the buoyancy of the colony, where Eh represents the Zeta potential of the colony (Fang et al., 2014). Additionally, influencing factors (nutrient limits and turbulent shear) can induce structural changes within the colonies, enabling to acquire survival strategies (Feng et al., 2020). This study further elucidates that EPS influences the SSA, hydrophobicity, and surface free energy, thereby affecting the formation of *Microcystis* bloom colonies and the efficiency of algal cell collection.

5 Conclusion

This study examines the factors that influence the physico-chemical surface properties of *Microcystis*, including EPS polysaccharides, monosaccharide composition and functional groups. The polysaccharide in EPS primarily impacts the surface area and total surface energy of *Microcystis* cells, while the protein in EPS affects hydrophobicity and surface tension. The composition of EPS, specifically glucuronic acid, xylose, and fructose, plays a significant role in determining surface properties. Additionally, during the stationary phase, the content of hydrophilic groups (including amino groups, hydroxyl groups, carboxyl groups, sulfonic acid groups, aldehyde groups, and phosphoric acid groups) increased. Similarly, the hydrophobic groups (including hydrocarbon groups, ester groups, and alkanes) also exhibited similar changes. The hydrophilic group O–H and P–O–P were identified as key groups that influence the hydrophobicity of *Microcystis*. Variations in growth rate, surface properties, and EPS between *M. wesenbergii* and *M. aeruginosa* provide a competitive advantage.

Data availability statement

The original contributions presented in the study are included in the article/Supplementary material, further inquiries can be directed to the corresponding author.

Author contributions

HY: Formal analysis, Writing – original draft, Writing – review & editing, Data curation, Software. DW: Data curation, Writing

– original draft. HL: Supervision, Writing – review & editing. CH: Conceptualization, Funding acquisition, Writing – review & editing.

Funding

The author(s) declare financial support was received for the research, authorship, and/or publication of this article. This work was funded by the Featured Institute Service Projects from the Institute of Hydrobiology, Chinese Academy of Sciences (Y85Z061601), the Knowledge Innovation Program of Wuhan-Basic Research (2022020801010142), National Key R&D Program of China (2021YFE0112000), and Natural Science Foundation for Distinguished Young Scholars of Hubei Province (2022CFA105).

Acknowledgments

The authors would like to thank Yanxia Zuo at The Analysis and Testing Center of Institute of Hydrobiology, Chinese Academy of Sciences for her assistance with monosaccharide composition analysis.

Conflict of interest

The authors declare that the research was conducted in the absence of any commercial or financial relationships that could be construed as a potential conflict of interest.

Publisher's note

Supplementary material

The Supplementary material for this article can be found online at: https://www.frontiersin.org/articles/10.3389/fmicb.2023.1285229/full#supplementary-material

References

Barros, A. C., Goncalves, A. L., and Simoes, M. (2019). Microalgal/cyanobacterial biofilm formation on selected surfaces: the effects of surface physicochemical properties and culture media composition. *J. Appl. Phycol.* 31, 375–387. doi: 10.1007/s10811-018-1582-3

Bhunia, B., Prasad Uday, U. S., Oinam, G., Mondal, A., Bandyopadhyay, T. K., and Tiwari, O. N. (2018). Characterization, genetic regulation and production of cyanobacterial exopolysaccharides and its applicability for heavy metal removal. *Carbohydr. Polym.* 179, 228–243. doi: 10.1016/j.carbpol.2017.09.091

Castro, F. D., Sedman, J., Ismail, A. A., Asadishad, B., and Tufenkji, N. (2010). Effect of dissolved oxygen on two bacterial pathogens examined using ATR-FTIR spectroscopy, microelectrophoresis, and potentiometric titration. *Environ. Sci. Technol.* 44, 4136–4141. doi: 10.1021/es903692u

Cheng, Z., Zhang, X., Kennes, C., Chen, J., Chen, D., Ye, J., et al. (2019). Differences of cell surface characteristics between the bacterium *pseudomonas veronii* and fungus *Ophiostoma stenoceras* and their different adsorption properties to hydrophobic organic compounds. *Sci. Total Environ.* 650, 2095–2106. doi: 10.1016/j.scitotenv.2018.09.337

Costa, O. Y. A., Raaijmakers, J. M., and Kuramae, E. E. (2018). Microbial extracellular polymeric substances: ecological function and impact on soil aggregation. *Front. Microbiol.* 9:1636. doi: 10.3389/fmicb.2018.01636

De Philippis, R. (1998). Exocellular polysaccharides from cyanobacteria and their possible applications. *FEMS Microbiol. Rev.* 22, 151–175. doi: 10.1016/s0168-6445(98)00012-6

Devasia, P., Natarajan, K. A., Sathyanarayana, D. N., and Rao, G. R. (1993). Surface chemistry of *Thiobacillus ferrooxidans* relevant to adhesion on mineral surfaces. *Appl. Environ. Microbiol.* 59, 4051–4055. doi: 10.1128/aem.59.12.4051-4055.1993

Dittrich, M., and Sibler, S. (2005). Cell surface groups of two picocyanobacteria strains studied by zeta potential investigations, potentiometric titration, and infrared spectroscopy. *J. Colloid Interface Sci.* 286, 487–495. doi: 10.1016/j.jcis.2005.01.029

Duan, Z., Tan, X., and Zeng, Q. (2022). Key physiological traits and chemical properties of extracellular polymeric substances determining colony formation in a cyanobacterium. *J. Oceanol. Limnol.* 40, 1720–1731. doi: 10.1007/s00343-022-1353-5

Fang, F., Yang, L., Gan, L., Guo, L., Hu, Z., Yuan, S., et al. (2014). DO, pH, and eh microprofiles in cyanobacterial granules from Lake Taihu under different environmental conditions. *J. Appl. Phycol.* 26, 1689–1699. doi: 10.1007/s10811-013-0211-4

Felix, C., Yaroshchuk, A., Pasupathi, S., Pollet, B. G., Bondarenko, M. P., Kovalchuk, V. I., et al. (2014). Electrophoresis and stability of nano-colloids: history, theory and experimental examples. *Adv. Colloid. Interfac.* 211, 77–92. doi: 10.1016/j.cis.2014.06.005

Feng, G., Zhu, W., Xue, Z., Hu, S., Wang, R., Zhao, S., et al. (2020). Structural variations increase the upper limit of colony size of *Microcystis*: implications from laboratory cultures and field investigations. *J. Phycol.* 56, 1676–1686. doi: 10.1111/jpy.13054

Ferro, L., Gojkovic, Z., Gorzsas, A., and Funk, C. (2019). Statistical methods for rapid quantification of proteins, lipids, and carbohydrates in nordic microalgal species using ATR–FTIR spectroscopy. *Molecules* 24:3237. doi: 10.3390/molecules24183237

Forni, C., Telo, F. R., and Caiola, M. G. (1997). Comparative analysis of the polysaccharides produced by different species of *Microcystis* (Chroococcales, Cyanophyta). *Phycologia* 36, 181–185. doi: 10.2216/i0031-8884-36-3-181.1

Ge, H. M., Zhang, J., Zhou, X. P., Xia, L., and Hu, C. X. (2014). Effects of light intensity on components and topographical structures of extracellular polymeric substances from *Microcoleus vaginatus* (Cyanophyceae). *Phycologia* 53, 167–173. doi: 10.2216/13-163.1

Gonçalves, A. L., Ferreira, C., Loureiro, J. A., Pires, J. C. M., and Simões, M. (2015). Surface physicochemical properties of selected single and mixed cultures of microalgae and cyanobacteria and their relationship with sedimentation kinetics. *Bioresourc Bioprocess* 2:21. doi: 10.1186/s40643-015-0051-y

Gupta, P., and Diwan, B. (2017). Bacterial exopolysaccharide mediated heavy metal removal: a review on biosynthesis, mechanism and remediation strategies. *Biotechnol. Rep.* 13, 58–71. doi: 10.1016/j.btre.2016.12.006

Hao, W., Yanpeng, L., Zhou, S., Xiangying, R., Wenjun, Z., and Jun, L. (2017). Surface characteristics of microalgae and their effects on harvesting performance by air flotation. *Int. J. Agr. Biol. Eng.* 10, 125–133. doi: 10.3965/j.ijabe.20171001.2698

Henderson, R., Parsons, S. A., and Jefferson, B. (2008). The impact of algal properties and pre-oxidation on solid-liquid separation of algae. *Water Res.* 42, 1827–1845. doi: 10.1016/j.watres.2007.11.039

Henderson, R. K., Parsons, S. A., and Jefferson, B. (2008). Successful removal of algae through the control of zeta potential. *Sep. Sci. Technol.* 43, 1653–1666. doi: 10.1080/01496390801973771

Hokputsa, S., Hu, C. X., Paulsen, B. S., and Harding, S. E. (2003). A physico-chemical comparative study on extracellular carbohydrate polymers from five desert algae. *Carbohydr. Polym.* 54, 27–32. doi: 10.1016/S0144-8617(03)00136-X

Huisman, J., Codd, G. A., Paerl, H. W., Ibelings, B. W., Verspagen, J. M. H., and Visser, P. M. (2018). Cyanobacterial blooms. *Nat. Rev. Microbiol.* 16, 471–483. doi: 10.1038/s41579-018-0040-1

Imai, H., Chang, K.-H., and Nakano, S.-I. (2009). "Growth responses of harmful algal species *Microcystis* (Cyanophyceae) under various environmental conditions" in *Interdisciplinary studies on environmental chemistry—Environmental research in Asia*. eds. Y. Obayashi, T. Isobe, A. Subramanian, S. Suzuki and S. Tanabe (Tokyo, Japan: TerraPub), 269–275.

Iwabuchi, N., Sunairi, M., Anzai, H., Morisaki, H., and Nakajima, M. (2003). Relationships among colony morphotypes, cell-surface properties and bacterial adhesion to substrata in *Rhodococcus*. *Colloid. Surface. B.* 30, 51–60. doi: 10.1016/S0927-7765(03)00036-5

Le, V. V., Srivastava, A., Ko, S. R., Ahn, C. Y., and Oh, H. M. (2022). *Microcystis* colony formation: extracellular polymeric substance, associated microorganisms, and its application. *Bioresour. Technol.* 360:127610. doi: 10.1016/j.biortech.2022.127610

Li, L., Wang, Z., Rietveld, L. C., Gao, N., Hu, J., Yin, D., et al. (2014). Comparison of the effects of extracellular and intracellular organic matter extracted from *Microcystis aeruginosa* on ultrafiltration membrane fouling: dynamics and mechanisms. *Environ. Sci. Technol.* 48, 14549–14557. doi: 10.1021/es5035365

Li, M., Xiao, M., Zhang, P., and Hamilton, D. P. (2018). Morphospecies-dependent disaggregation of colonies of the cyanobacterium *Microcystis* under high turbulent mixing. *Water Res.* 141, 340–348. doi: 10.1016/j.watres.2018.05.017

Liu, Y. X., Alessi, D. S., Owttrim, G. W., Kenney, J. P. L., Zhou, Q. X., Lalonde, S. V., et al. (2016). Cell surface acid-base properties of the cyanobacterium *Synechococcus*: influences of nitrogen source, growth phase and N:P ratios. *Geochim. Cosmochim. Acta* 187, 179–194. doi: 10.1016/j.gca.2016.05.023

Liu, L. Z., Huang, Q., and Qin, B. Q. (2018). Characteristics and roles of *Microcystis* extracellular polymeric substances (EPS) in cyanobacterial blooms: a short review. *J. Freshwater Ecol.* 33, 183–193. doi: 10.1080/02705060.2017.1391722

Liu, L., Huang, Q., Qin, B., Zhu, G., Wu, P., and Wu, Y. (2016). Characterizing cell surface of blooming *Microcystis* in Lake Taihu, China. *Water Sci. Technol.* 73, 2731–2738. doi: 10.2166/wst.2016.069

Liu, J., Lu, L. J., Huang, X. F., Shang, J. J., Li, M. X., Xu, J. C., et al. (2011). Relationship between surface physicochemical properties and its demulsifying ability of an alkaliphilic strain of *Alcaligenes* sp. S-XJ-1. *Process Biochem.* 46, 1456–1461. doi: 10.1016/j.procbio.2011.03.018

Masumoto, A., Amano, Y., and Machida, M. (2023). Enhancement of cyanobacterial blooms buoyancy by controlling extracellular polysaccharides content and cation concentration under light-limited condition. *Int. J. Environ. Sci. Technol.* doi: 10.1007/s13762-023-05014-4

Masuoka, J., and Hazen, K. C. (1997). Cell wall protein mannosylation determines *Candida albicans* cell surface hydrophobicity. *Microbiology* 143, 3015–3021. doi: 10.1099/00221287-143-9-3015

Otten, T. G., and Paerl, H. W. (2011). Phylogenetic inference of colony isolates comprising seasonal *Microcystis* blooms in Lake Taihu, China. *Microb. Ecol.* 62, 907–918. doi: 10.1007/s00248-011-9884-x

Ozkan, A., and Berberoglu, H. (2013). Physico-chemical surface properties of microalgae. *Colloid. Surface. B.* 112, 287–293. doi: 10.1016/j.colsurfb.2013.08.001

Pereira, S., Zille, A., Micheletti, E., Moradas-Ferreira, P., De Philippis, R., and Tamagnini, P. (2009). Complexity of cyanobacterial exopolysaccharides: composition, structures, inducing factors and putative genes involved in their biosynthesis and assembly. *FEMS Microbiol. Rev.* 33, 917–941. doi: 10.1111/j.1574-6976.2009.00183.x

Pringle, J. H., and Fletcher, M. (1983). Influence of substratum wettability on attachment of freshwater bacteria to solid surfaces. *Appl. Environ. Microbiol.* 45, 811–817. doi: 10.1128/aem.45.3.811-817.1983

Qu, M., Lefebvre, D. D., Wang, Y., Qu, Y., Zhu, D., and Ren, W. (2014). Algal blooms: proactive strategy. *Science* 346, 175–176. doi: 10.1126/science.346.6206.175-b

Rosenberg, M., Gutnick, D., and Rosenberg, E. (1980). Adherence of bacteria to hydrocarbons: a simple method for measuring cell-surface hydrophobicity. *FEMS Microbiol. Lett.* 9, 29–33. doi: 10.1016/0378-1097(80)90106-8

Sheng, G. P., and Yu, H. Q. (2006). Relationship between the extracellular polymeric substances and surface characteristics of *Rhodopseudomonas acidophila*. *Appl. Microbiol. Biotechnol.* 72, 126–131. doi: 10.1007/s00253-005-0225-1

Sun, F., Zhang, H., Qian, A., Yu, H., Xu, C., Pan, R., et al. (2020). The influence of extracellular polymeric substances on the coagulation process of cyanobacteria. *Sci. Total Environ.* 720:137573. doi: 10.1016/j.scitotenv.2020.137573

Tang, X., Krausfeldt, L. E., Shao, K., LeCleir, G. R., Stough, J. M. A., Gao, G., et al. (2018). Seasonal gene expression and the Ecophysiological implications of toxic *Microcystis aeruginosa* blooms in Lake Taihu. *Environ. Sci. Technol.* 52, 11049–11059. doi: 10.1021/acs.est.8b01066

van Oss, C. J. (1993). Acid—base interfacial interactions in aqueous media. *Colloids Surf. A Physicochem. Eng. Asp.* 78, 1–49. doi: 10.1016/0927-7757(93)80308-2

Volpe, C. D., and Siboni, S. (1997). Some reflections on Acid–Base solid surface free energy theories. *J. Colloid Interface Sci.* 195, 121–136. doi: 10.1006/jcis.1997.5124

Williams, D., Kuhn, A., O'Bryon, T., Konarik, M., and Huskey, J. (2011). Contact angle measurements using cellphone cameras to implement the Bikerman method. *Galvanotechnik* 102, 1718–1725.

Wood, B. R., Chernenko, T., Matthäus, C., Diem, M., Chong, C., Bernhard, U., et al. (2008). Shedding new light on the molecular architecture of oocytes using a combination of synchrotron Fourier transform-infrared and Raman spectroscopic mapping. *Anal. Chem.* 80, 9065–9072. doi: 10.1021/ac8015483

Xia, L., Li, H. Q., and Song, S. X. (2016). Cell surface characterization of some oleaginous green algae. *J. Appl. Phycol.* 28, 2323–2332. doi: 10.1007/s10811-015-0768-1

Xiao, M., Li, M., and Reynolds, C. S. (2018). Colony formation in the cyanobacterium *Microcystis*. *Biol. Rev. Camb. Philos. Soc.* 93, 1399–1420. doi: 10.1111/brv.12401

Xiao, M., Willis, A., Burford, M. A., and Li, M. (2017). Review: a meta-analysis comparing cell-division and cell-adhesion in *Microcystis* colony formation. *Harmful Algae* 67, 85–91. doi: 10.1016/j.hal.2017.06.007

Xu, H., Jiang, H., Yu, G., and Yang, L. (2014). Towards understanding the role of extracellular polymeric substances in cyanobacterial *Microcystis* aggregation and mucilaginous bloom formation. *Chemosphere* 117, 815–822. doi: 10.1016/j.chemosphere.2014.10.061

Xu, H., Lv, H., Liu, X., Wang, P., and Jiang, H. (2016). Electrolyte cations binding with extracellular polymeric substances enhanced *Microcystis* aggregation: implication for *Microcystis* bloom formation in eutrophic freshwater lakes. *Environ. Sci. Technol.* 50, 9034–9043. doi: 10.1021/acs.est.6b00129

Xu, H., Yu, G., and Jiang, H. (2013). Investigation on extracellular polymeric substances from mucilaginous cyanobacterial blooms in eutrophic freshwater lakes. *Chemosphere* 93, 75–81. doi: 10.1016/j.chemosphere.2013.04.077

Yee, N., Benning, L. G., Phoenix, V. R., and Ferris, F. G. (2004). Characterization of metal-cyanobacteria sorption reactions: a combined macroscopic and infrared spectroscopic investigation. *Environ. Sci. Technol.* 38, 775–782. doi: 10.1021/es0346680

Yu, G., Cai, X., Shen, L., Chen, J., Hong, H., Lin, H., et al. (2018). A novel integrated method for quantification of interfacial interactions between two rough bioparticles. *J. Colloid Interface Sci.* 516, 295–303. doi: 10.1016/j.jcis.2018.01.075

Yue, T., Zhang, D., and Hu, C. X. (2014a). Utilization of phosphorus in four forms of the three dominant *Microcystis* morphospecies in Lake Taihu. *J. Lake Sci.* 26, 379–384. doi: 10.18307/2014.0307

Yue, T., Zhang, D. L., and Hu, C. X. (2014b). Comparative studies on phosphate utilization of two bloom-forming *Microcystis* spp. (cyanobacteria) isolated from Lake Taihu (China). *J. Appl. Phycol.* 26, 333–339. doi: 10.1007/s10811-013-0067-7

Zhai, C. M., Song, S., Zou, S. H., Liu, C. H., and Xue, Y. R. (2013). The mechanism of competition between two bloom-forming *Microcystis* species. *Freshw. Biol.* 58, 1831–1839. doi: 10.1111/fwb.12172

Zhang, X., Amendola, P., Hewson, J. C., Sommerfeld, M., and Hu, Q. (2012). Influence of growth phase on harvesting of Chlorella zofingiensis by dissolved air flotation. *Bioresour. Technol.* 116, 477–484. doi: 10.1016/j.biortech.2012.04.002

Zhang, P. L., Chen, M. Z., Zhang, Y. P., Li, Y. M., Lu, S., and Li, P. F. (2018). Autoaggregation and adhesion abilities in bacteria associated with colonies of *Microcystis*. *Hydrobiologia* 823, 205–216. doi: 10.1007/s10750-018-3706-9

Zhang, J. Y., Nawaz, M. Z., Zhu, D. C., Yan, W., Alghamdi, H. A., and Lu, Z. H. (2021). Diversity, seasonal succession and host specificity of bacteria associated with cyanobacterial aggregates in a freshwater lake. *Environ. Technol. Innov.* 24:101988. doi: 10.1016/j.eti.2021.101988

Zhang, Y., Wang, F., Yang, X., Gu, C., Kengara, F. O., Hong, Q., et al. (2011). Extracellular polymeric substances enhanced mass transfer of polycyclic aromatic hydrocarbons in the two-liquid-phase system for biodegradation. *Appl. Microbiol. Biotechnol.* 90, 1063–1071. doi: 10.1007/s00253-011-3134-5

Zhang, X., Yuan, H., Wang, Y., Guan, L., Zeng, Z., Jiang, Z., et al. (2020). Cell surface energy affects the structure of microalgal biofilm. *Langmuir* 36, 3057–3063. doi: 10.1021/acs.langmuir.0c00274

Zheng, Y., Huang, Y., Xia, A., Qian, F., and Wei, C. (2019). A rapid inoculation method for microalgae biofilm cultivation based on microalgae-microalgae co-flocculation and zeta-potential adjustment. *Bioresour. Technol.* 278, 272–278. doi: 10.1016/j.biortech.2019.01.083

Zhu, W., Li, M., Dai, X. X., and Xiao, M. (2015). Differences in vertical distribution of *Microcystis* morphospecies composition in a shallow hypertrophic Lake (lake Taihu, China). *Environ. Earth Sci.* 73, 5721–5730. doi: 10.1007/s12665-014-3826-0

Zhu, W., Zhou, X., Chen, H., Gao, L., Xiao, M., and Li, M. (2016). High nutrient concentration and temperature alleviated formation of large colonies of *Microcystis*: Evidence from field investigations and laboratory experiments. *Water Res.* 101, 167–175. doi: 10.1016/j.watres.2016.05.080

frontiers | Frontiers in Microbiology

TYPE Original Research
PUBLISHED 13 December 2023
DOI 10.3389/fmicb.2023.1283073

OPEN ACCESS

EDITED BY
Hua Li,
Key Laboratory of Algal Biology, Institute of Hydrobiology, Chinese Academy of Sciences (CAS), China

REVIEWED BY
Federico Rossi,
University of Pisa, Italy
Weibo Wang,
Wuhan Botanical Garden, Chinese Academy of Sciences (CAS), China

*CORRESPONDENCE
Jie Li
lijietaren@scsio.ac.cn
Si Zhang
zhsimd@scsio.ac.cn

†These authors have contributed equally to this work

RECEIVED 04 September 2023
ACCEPTED 27 November 2023
PUBLISHED 13 December 2023

CITATION
Wang L, Huang Y, Yang Q, Mai Z, Xie F, Lyu L, Zhang S and Li J (2023) Biocrust reduces the soil erodibility of coral calcareous sand by regulating microbial community and extracellular polymeric substances on tropical coral island, South China Sea. *Front. Microbiol.* 14:1283073. doi: 10.3389/fmicb.2023.1283073

Biocrust reduces the soil erodibility of coral calcareous sand by regulating microbial community and extracellular polymeric substances on tropical coral island, South China Sea

Lin Wang[1†], Yu Huang[1,2†], Qingsong Yang[1], Zhimao Mai[1], Feiyang Xie[1], Lina Lyu[1], Si Zhang[1,3*] and Jie Li[1*]

[1]CAS Key Laboratory of Tropical Marine Bio-resources and Ecology, South China Sea Institute of Oceanology, Chinese Academy of Sciences, Guangzhou, China, [2]University of Chinese Academy of Sciences, Beijing, China, [3]Southern Marine Science and Engineering Guangdong Laboratory (Guangzhou), Guangzhou, China

Tropical coral islands assume a pivotal role in the conservation of oceanic ecosystem biodiversity. However, their distinctive environmental attributes and limited vegetation render them highly susceptible to soil erosion. The biological soil crust (biocrust), owing to its significant ecological role in soil stabilization and erosion prevention, is deemed an effective means of mitigating soil erosion on coral island. However, existing research on the mechanisms through which biocrusts resist soil erosion has predominantly concentrated on arid and semi-arid regions. Consequently, this study will specifically delve into elucidating the erosion-resistant mechanisms of biocrusts in tropical coral island environments, South China Sea. Specifically, we collected 16 samples of biocrusts and bare soil from Meiji Island. High-throughput amplicon sequencing was executed to analyze the microbial community, including bacteria, fungi, and archaea. Additionally, quantitative PCR was utilized to assess the abundance of the bacterial 16S rRNA, fungal ITS, archaeal 16S rRNA, and cyanobacterial 16S rRNA genes within these samples. Physicochemical measurements and assessments of extracellular polymeric substances (EPSs) were conducted to characterize the soil properties. The study reported a significantly decreased soil erodibility factor after biocrust formation. Compared to bare soil, soil erodibility factor decreased from 0.280 to 0.190 t h MJ^{-1} mm^{-1} in the biocrusts. Mechanistically, we measured the microbial EPS contents and revealed a negative correlation between EPS and soil erodibility factor. Consistent with increased EPS, the abundance of bacteria, fungi, archaea, and cyanobacteria were also detected significantly increased with biocrust formation. Correlation analysis detected Cyanobacteria, Chloroflexi, Deinococcota, and Crenarchaeota as potential microbials promoting EPSs and reducing soil erosion. Together, our study presents the evidence that biocrust from tropical coral island in the South China Sea promotes resistance to soil erosion, pinpointing key EPSs-producing microbials against soil erosion. The findings would provide insights for island soil restoration.

KEYWORDS

tropical coral island, biological soil crust, microbial community, extracellular polymeric substances, soil erodibility factor, soil nutrients

Introduction

Tropical coral islands hold a pivotal role in upholding the biodiversity of the oceanic ecosystem, as they serve as crucial waystations for migratory avifauna and marine mammals. Furthermore, they make significant contributions to the preservation of freshwater reserves and local climate regulation (Blackburn et al., 2004; Whittaker and Fernández-Palacios, 2007; Li et al., 2021). Coral calcareous sand stands as the predominant constituent of these islands; however, it poses challenges to the spontaneous growth of vegetation. Furthermore, the vegetation found on tropical coral islands is highly susceptible to degradation and notoriously challenging to restore once disrupted (Prabakaran and Paramasivam, 2014; Wolfe et al., 2015; Zong et al., 2021). This predicament arises due to a combination of distinctive environmental attributes, including a scarcity of soil clay and essential nutrients, elevated levels of salinity and alkalinity, intense heat and solar radiation, as well as recurrent periods of drought (Zhang et al., 2019). Without ecological function of vegetations, coral islands are highly prone to soil erosion. Therefore, erosion prevention and control are urgent issues that need to be addressed in the region currently. The employment of biological soil crusts (biocrusts) as a strategy to mitigate soil erosion on tropical coral islands bears resemblance to their efficacious implementation in desert ecosystems and other extreme habitats (Weber et al., 2016).

Biocrusts constitute a significant assemblage of soil particles and organisms, encompassing different species of cyanobacteria, microalgae, bacteria, microfungi, lichens, and bryophytes (Maier et al., 2018; Wang et al., 2022). Biocrusts thrive within the uppermost layer of the soil and serve as prominent biotic constituents within arid regions (Rodríguez-Caballero et al., 2022). According to the research by Rodriguez-Caballero et al. (2018), biocrusts approximately span 12% of the Earth's surface area. As multifunctional communities, biocrusts could impact energy cycling, water retention, biogeochemical fluxes on a global scale, with crucial impacts on soil fertility, regional hydrology, and the soil's resilience against erosive forces (Chamizo et al., 2012, 2016; Belnap et al., 2014; Couradeau et al., 2016; Mogul et al., 2017; Eldridge et al., 2020; Rodríguez-Caballero et al., 2022). The functions performed by biocrusts exert a beneficial influence on various aspects, including the germination and establishment of seeds, the performance of plants, as well as the population dynamics and behavior of animals (Lan et al., 2015; Couradeau et al., 2016; Weber et al., 2016). Among the ecosystem functions offered by biocrusts, their pivotal role in stabilizing soil and mitigating soil erosion stands as the most vital ecological services in numerous ecoregions (Belnap et al., 2003, 2009; Gao et al., 2017). Munson et al. (2011) documented that biocrusts have the capacity to prevent soil loss caused by wind erosion. Moreover, biocrust also has a significantly inhibitory effect on water erosion. The study conducted by Gao et al. (2017) reported well-developed biocrusts could reduce soil loss by up to 100% in areas experiencing water erosion. Similarly, in the region of semi-arid watersheds, despite large amounts of runoff, the least erosion was observed in areas where biocrusts were present (Rodríguez-Caballero et al., 2014). Furthermore, the magnitude of biocrust coverage is considered the foremost predictor of site stability within local ecosystems (Belnap et al., 2009). Despite the widespread acknowledgment of the soil erosion-reducing capacity of biocrusts, current research on the erosion-resistant mechanisms of biocrusts predominantly centers on arid regions, with virtually no exploration in the realm of tropical coral islands.

In general, the protective impact of biocrusts against erosion is directly related to the extent of their coverage on the soil surface. Biocrusts possess the capacity to shield the erodible surface layer physically or create aggregates through their biomass. The initial aggregation of the biocrust is facilitated by the secretion of extracellular polymeric substances (EPSs) from biocrust organisms. EPSs comprise a combination of polysaccharides, proteins, nucleic acids, lipids, and humic substances, each present in varying proportions and possessing diverse chemical properties and structures (Flemming and Wingender, 2010; Rossi et al., 2018). Indeed, a significant proportion of the organisms found in biocrusts, such as cyanobacteria, green microalgae, and microfungi, possess the ability to produce EPSs that become incorporated within the soil mineral particles and cellular structures (Belnap et al., 2003). Hence, the synthesis of EPSs exhibit a strong correlation with the abundance and diversity of microorganisms (Meng et al., 2006; Zhang et al., 2015). Microbial EPSs could promote the formation of soil aggregates by owing to their viscosity, so that it has a high structural stability (Costa et al., 2018). Belnap et al. (1993) and Bowker et al. (2008) also reported that biocrusts can decrease soil loss mainly due to microbial EPSs bind soil particles smaller than 65 μm together and physically weave them together by filamentous cyanobacteria. Further, the EPSs secreted by the biocrust and the formation of biofilms could relatively increase soil crust thickness with resulting increase in stability against wind force (Kheirfam and Asadzadeh, 2020). Regarding biocrusts, there is a notable variation in microbial abundance and diversity across various biocrust types (Büdel et al., 2009; Weber et al., 2012; Maier et al., 2018; Wang et al., 2022). This variation in microbial composition potentially contributes to the divergence observed in EPSs contents and synthesis. Notably, changes in the environmental conditions (e.g., nutrient elements, contaminants, pH, temperature, and salinity) also had strongly influence in EPSs synthesis (Yang et al., 2018, 2020). Might the variances in environmental conditions engender distinctions in the erosion-resistant mechanisms of biocrusts between arid regions and tropical coral islands?

Meiji Island is a typical coral island in Nansha Archipelagos, South China Sea, and the primary constituents of the soil are coral calcareous sand (Li et al., 2013). Further, Meiji Island highly susceptible to soil erosion due to abundant rainfall, loose coral sand, and extreme environmental conditions, including high salt, alkali, temperature, light, and radiation intensity. Recent years, with the development and utilization of coral islands, the role of biocrusts in reducing soil erosion of coral islands has gradually attracted attention. Despite the widely acknowledged barrier function of biocrusts (Munson et al., 2011; Zhao and Xu, 2013; Gao et al., 2017), the precise mechanism governing the interplay between EPSs concentration, soil erosion resistance, and microbial composition associated with biocrusts remains inadequately comprehended. In this study, our focus lies on examining the alterations induced by biocrusts in the inherent properties of soil that are linked to erodibility, and evaluate the potential impact of biocrusts on soil resistance to erosion throughout the region. Therefore, we aim to address two questions: (1) how biocrust formation affects soil properties, microbial community, and EPSs contents on tropical coral island? (2) does biocrust formation affect the soil erodibility? The outcomes of this

study will not only showcase the extent of influence exerted by biocrusts in reducing soil erodibility but also offer a fresh perspective on the ecological restoration of tropical coral islands.

Materials and methods

Sampling and storage

The samples of biocrust and bare soil were meticulously gathered from Meiji Island, South China Sea, during October, 2020. This island is influenced by a tropical marine climate, characterized by an average temperature surpassing 27°C and an annual precipitation exceeding 2,000 mm. The coverage of biocrusts on Meiji Island is approximately 6.25%, predominantly composed of cyanobacterium-crust, with almost no presence of lichen-or moss-dominated types (Figure 1; Wang et al., 2022). The surface texture of the biocrust was very similar, all of which were rugose. For per sampling site, precise collection of biocrust (uppermost 0–1 cm layer) and bare soil (uppermost 0–1 cm of adjacent soil lacking evident indications of biocrusts) was performed using sterile equipment. We inserted a sterilized foil sampler into the sampling site and used sterile spatulas and spoons to separate the surface biocrust and bare soil from the underlying soil sample, followed by appropriate preservation methods. In sum, 12 samples were used for sequencing, including 6 bare soil and 6 biocrust samples; a total of 16 samples were used for soil properties testing, including 8 bare soil and 8 biocrust samples. The collection of samples, including biocrusts and bare soil, was carried out with a minimum distance of 100 meters between each sample location.

The samples intended for soil properties assays were meticulously obtained and placed in sealed plastic bags, ensuring a secure environment. These bags were subsequently stored in a temperature-controlled freezer at −20°C. As for the samples designated for DNA extraction, sterile equipment was employed during collection, and the samples were then placed in tubes that containing LifeGuard™ Soil Preservation Solution (MO BIO Laboratories, Carlsbad, CA, United States). These tubes were suitably preserved at a temperature of-80°C until subsequent processing.

Measurement of the soil physicochemical parameters

The collected samples underwent a process of air-drying at ambient room temperature. Subsequently, they were meticulously sieved through 35 mesh screens to eliminate any coarse impurities. The remaining fine particles were then finely ground using a mortar and pestle. To determine the soil pH, a 1:2.5 (w/w) suspension of the soil samples was prepared, and the pH analysis was conducted using a pH meter (pH 211, Hanna Instruments, Germany), adhering to the method outlined by Acosta-Martínez et al. (2007). Furthermore, the analysis of total organic carbon (TOC) and total nitrogen content (TN) was carried out utilizing an advanced Elemental Analyzer (Flash EA 3000 Thermo Scientific, Milan, Italy), following the methodology established by Zhao et al. (2019). Total phosphorus (TP) was determined by the H_2SO_4–$HClO_4$ digestion method (Kuo, 1996). Chl *a* content was measured based on described by Wang et al. (2022). The grain-size components of samples were analyzed using a laser particle

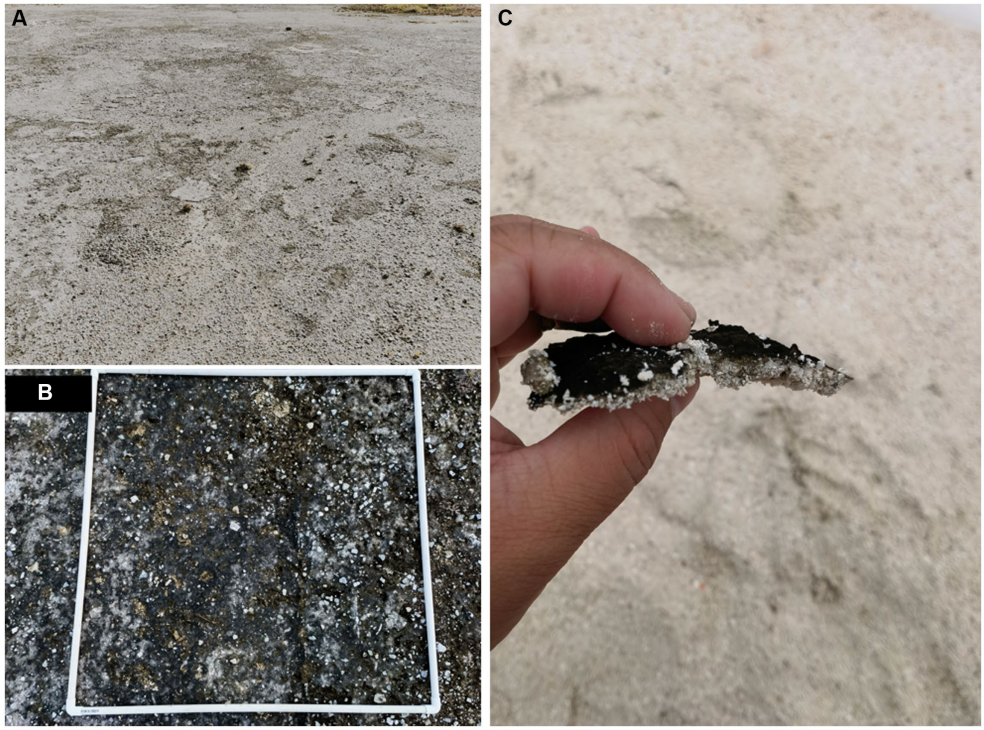

FIGURE 1
The representative coral land biocrust samples. The landscape view of the study site **(A)**, cyanobacteria-dominated biocrust **(B)**, and the filamentous cyanobacteria associated with sand particles **(C)** were investigated.

sizer (Malvern Mastersizer 2000) as previously described (Tian et al., 2019).

Analysis of EPSs concentrations

EPSs extraction was conducted using a cation exchange resin method with minor modifications, as previously described by Takahashi et al. (2009) and Mai et al. (2022). In summary, artificial seawater with a salinity of 30‰ was added to tubes containing 30 grams of fresh soil sample and mixed in a shaker for 1 h at 4°C in the absence of light. The supernatant was collected after centrifugation at 3,500 rpm at 4°C for 10 min to obtain colloidal EPSs. Subsequently, 20 mL of artificial seawater and 2 grams of activated cation exchange Dowex 50 WX8 resin (in hydrogen form, with a mesh size of 200–400, from Sigma-Aldrich, MO, United States) were added to the remaining soil sample. This mixture was then mixed for 1 h at 4°C in the dark and subsequently centrifuged at 3,500 rpm at 4°C for 10 min to obtain bound EPSs. Both the supernatants of the two EPSs subfractions were purified using dialysis bags (with a 3.5 kDa molecular weight cutoff, incubated at 4°C for 24 h). The purified EPSs samples were then subjected to freeze-drying. Concurrently, the determination of extracellular protein content (EP) and polysaccharide content (EPS) involved the reconstitution of freeze-dried colloidal and bound EPSs powder in 10 mL of deionized water, respectively. The EP concentration was quantified using a modified bicinchoninic acid protein assay kit (Sangon Biotech, Shanghai, China), with bovine serum albumin serving as the standard (Smith et al., 1985). For the evaluation of EPS content, the phenol-sulfuric acid method, as described by DuBois et al. (1956), was employed with glucose as the standard reference. The unit of EPS and EP content is μg/g.

Estimation of the soil erodibility factor on biocrust

The soil erodibility factor (K) was usually applied for represent soil erodibility (Sharpley and Williams, 1990). This factor has found extensive application in various models utilized for the prediction of soil erosion (Liu et al., 1999; Parysow et al., 2003; Ouyang et al., 2018). The K embodies the inherent susceptibility of soil to undergo denudation and migration when subjected to the erosive forces of raindrop splash and runoff. In total, we collected 16 samples for the determination of the soil erosion coefficient. These samples comprise 8 biocrust and 8 bare soil samples. We employed the foil sampler method for field sampling, followed by laboratory analysis of the collected samples' soil mechanical composition, which includes the proportion of sand (0.05–2.00 mm, %), silt (0.002–0.05 mm, %), and clay (<0.002 mm, %). Subsequently, we conducted measurements of the organic carbon content for each sample. Finally, we calculated the K (t h MJ^{-1} mm^{-1}) for each sample using the formula described by Sharpley and Williams (1990):

$$K = \left\{0.2 + 0.3\exp\left[-0.0256 S_a\left(1 - S_i/100\right)\right]\right\} * \left(S_i/\left(C_l + S_i\right)\right)^{0.3} * \left[1 - 0.25C/\left(C + \exp\left(3.72 - 2.95C\right)\right)\right] * \left[1 - 0.7S_n/\left(S_n + \exp\left(-5.51 + 22.9S_n\right)\right)\right]$$

and

$$S_n = 1 - S_a/100,$$

where S_a represents the sand content (0.05–2.00 mm, %); S_i reflects the silt content (0.002–0.05 mm, %); C_l reflects the clay content (< 0.002 mm, %); and C is the total organic carbon content (%).

DNA extraction, amplification, and sequencing

Extraction of total environmental DNA was carried out utilizing DNeasy® PowerSoil® Pro Kit (QIAGEN, United States), followed by monitoring its concentration using a NanoVuePlus Spectrophotometer (GE Healthcare, Little Chalfont, United Kingdom). The primers for amplification of the V4 region of the bacterial 16S rRNA gene, ITS1 region of fungal ITS, and V4-V5 region of archaeal 16S rRNA gene were designed based on Wang et al. (2022). Specifically, the primer of the V4 region of the bacterial 16S rRNA gene was: 515F 5′-GTGCCAGCMGCCGCGGTAA-3′, 806R 5′-GGACTACHV GGGTWTCTAAT-3′; the primer of ITS1 region of fungal ITS was: ITS1f 5′-CTTGGTCATTTAGAGGAAGTAA-3′, ITS2 5′-GCT GCGTTCTTCATCGATGC-3′; and the primer of the V4-V5 region of archaeal 16S rRNA gene was: Arch519F 5′-CAGCCGCCGCGGTAA-3′, Arch915R 5′-GTGCTCCCCCGC CAATTCCT-3′. The products derived from standard thermocycling, involving an annealing temperature of 53°C with 30 cycles for bacterial V4 and archaeal V4-V5 regions, and 53°C with 35 cycles for the ITS1 region, were consolidated and subsequently sequenced on an Illumina Miseq PE300 platform (Majorbio Bio-Pharm Technology, Shanghai, China). The raw sequencing data have been deposited in the National Center for Biotechnology Information.[1]

De-multiplexing raw FASTQ files by applying the in-house perl scripts, filtered by fastp v0.19.6 and merged by FLASH v1.2.7 (Magoč and Salzberg, 2011). The flashed reads were processed using the Quantitative Insights into Microbial Ecology (QIIME) v1.8.0 and UCHIME algorithm-based Gold database to obtain effective tags (Bates et al., 2010; Bokulich et al., 2012). Next, we applied UPARSE 7.1 to cluster the optimized sequences into operational taxonomic units (OTUs) at a 97% sequence similarity level (Edgar, 2013). For each representative sequence, the Silva v138 (for 16S) and Unite 8.0 (for ITS) databases were used to annotate taxonomic information with a confidence threshold of ≥0.5.

Quantitative PCR

The abundance of bacterial 16S rRNA, fungal ITS, archaeal 16S rRNA, and cyanobacterial 16S rRNA gene were measured by Quantitative PCR (qPCR). The primer used were: for bacteria, 338F (5′- ACTCCTACGGGAGGCAGCAG-3′) and 518R (5′- ATTACCGCGGCTGCTGG-3′) (Maier et al., 2018); for fungi, ITS7 (5′-GTGARTCATCGARTCTTTG-3′) and ITS4 (5′-TCCTCCG

1 http://www.ncbi.nlm.nih.gov/bioproject/1008893

CTTATTGATATGC-3′) (Zhang et al., 2018); for archaea, Arch349F (5′-GYGCASCAGKCGMGAAW-3′) and Arch806R (5′-GGACT ACVSGGGTATCTAAT-3′) (Zhao et al., 2020); for cyanobacteria, CYA 359F (5′-GGGGAATYTTCCGCAATGGG-3′) and an equimolar mixture of CYA-781RA (5′-GACTACTGGGGTATCTAATCC CATT-3′) and CYA-781RB (5′-GACTACAGGGGTATCTAAT CCCTTT-3′) (Nübel et al., 1997), respectively. The qPCR reactions were conducted in triplicate using a CFX96 Real-Time System (Bio-Rad Inc., United States). The thermal profile comprised an initial denaturation step at 95°C for 30 s, succeeded by 40 cycles of 95°C for 10 s, 55°C for 30 s, and 72°C for 30 s. Notably, the assay efficiency for all targeted genes was recorded as 98%, accompanied by a standard curve regression coefficient (R^2) exceeding 0.995.

Statistical analyses

A *t*-test was performed to analysis the soil characteristics between biocrust and bare soil, employing SPSS 18 software. Correlations between EPSs contents and the soil erodibility factor K were evaluated with logistic regression. Permutational multivariate analysis of variance determined the statistical significance of differences between biocrusts and bare soils (Vegan v2.5–3 in R). The canonical correlation analysis (CCA) and redundancy analysis (RDA) investigated the impact of soil properties on the microbial composition (Vegan v2.5–3 package in R). The selection principle of RDA or CCA model: first use the abundance matrix data to do DCA (Detrended Correspondence Analysis), and look at the size of the Axis Lengths of gradient in the analysis results. If it is greater than 4.0, CCA is recommended; if it is between 3.0–4.0, both RDA and CCA are acceptable; if it is less than 3.0, RDA is recommended. Monte Carlo permutation tests inferred the forward selection (permutations = 9,999). The heatmap depicted the correlation between microbial relative abundance and environmental factors through Spearman's rank correlations (Wang et al., 2022).

Results

Determination of soil properties

By determining soil properties that serve as indicators of the biocrust formation process, we found that the biocrusts' pH values were significantly lower, but TOC, TP, TN, and Chl *a* content exhibited significant increases in biocrusts (Supplementary Table S1). With biocrust formation, biocrusts had more fine particles, including clay and silt compared to bares soil, but the opposite result for sand (0.05–2 mm) content (Supplementary Table S2). The gravel ratio has no significantly difference between biocrust and bare soil.

Microbial diversity and composition

Employing qPCR to quantify the abundance of microbiome in bare soil and biocrust, including bacteria, fungi, archaea, and cyanobacteria. The gene copy numbers of these microbial groups were found to be significantly lower in bare soil than that in the biocrusts (Figure 2). Meanwhile, bacterial abundance was significantly higher

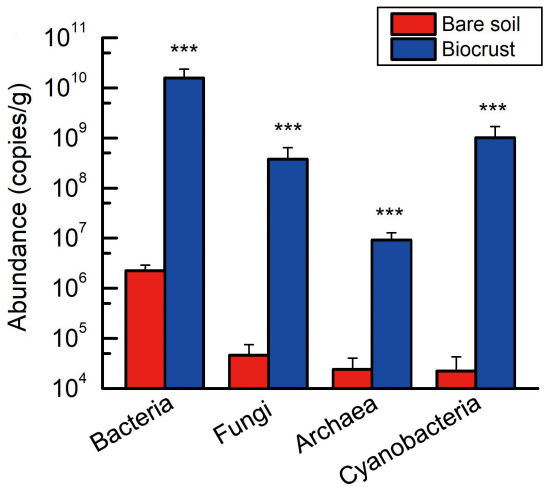

FIGURE 2
The absolute abundance of bacteria, fungi, archaea, and cyanobacteria within both the bare soil and biocrust samples. All data are presented as Mean ± SD calculated from biological repetition. Significant differences: ***$P < 0.001$.

than that of fungi and archaea in both biocrust and bare soil samples. Moreover, the abundance of cyanobacterial community changed from the lowest to the second highest (Figure 2).

A comparison of alpha diversity (chao 1 and Shannon index) was conducted across all samples. In the bacterial community, the Chao 1 was no significantly difference between the biocrust and bare soil, while the Shannon index was higher in the bare soil (Figure 3A). In addition, the Chao 1 of the fungal community was lower in the bare soil compared to the biocrusts (Figure 3B). In contrast, the Chao 1 and Shannon index of archaeal community were significantly higher in the bare soil than that in biocrusts (Figure 3C).

Within the bacterial community, the most abundant taxa in the biocrust at the phylum level were Cyanobacteria (average relative abundance of 40.90%), followed by Chloroflexi (35.69%), Proteobacteria (10.97%), and Actinobacteriota (5.20%) (Figure 4A). Notably, Cyanobacteria and Chloroflexi were significantly higher in biocrust than that in bare soil (Figure 4B). Among the bare soil samples, phyla Proteobacteria was dominant (63.91%), followed by Actinobacteriota (10.32%), Cyanobacteria (6.73%), and Chloroflexi (6.16%) (Figure 4A). At the genus level, the most prevalent taxa in the biocrust were *Chroococcidiopsis* (33.62%) and *norank_f__Roseiflexaceae* (22.67%) (Figure 4C), both exhibiting a substantial abundance over the bare soil samples (Figure 4D). Conversely, the most abundant genera in the bare soil were *Rhodobacter* (7.87%), *Porphyrobacter* (7.80%), and *Phreatobacter* (6.76%) (Figure 4C). In the fungal community, the most prevalent phylum is Ascomycota (57.84%), yet it displays no significant variance between the biocrust and bare soil (Supplementary Figures S2A,B). However, at the genus level, the biocrust exhibits higher abundance of *unclassified_k__Fungi* (40.94%), *Emericellopsis* (28.01%), and *unclassified_p__Ascomycota* (25.63%), all of which significantly higher compared to bare soil (Supplementary Figures S1C,D). For archaeal community, the most abundant taxa within the biocrust were Crenarchaeota (86.21%) and Halobacterota (9.22%), both significantly higher compared to bare soil

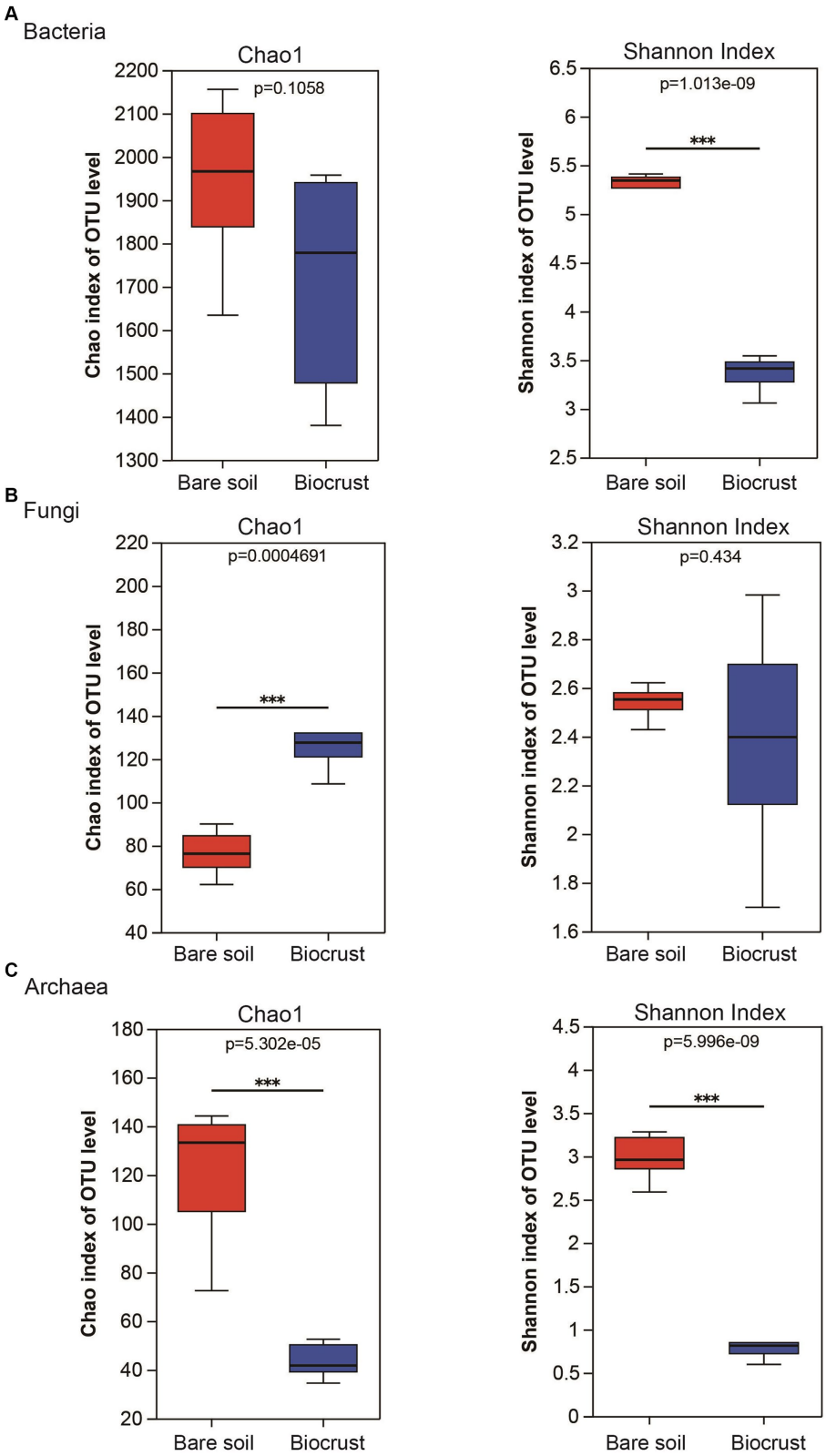

FIGURE 3
Alteration of richness and diversity of bacterial, fungal and archaeal communities in the biocrust and bare soil samples. The boxplot demonstrates the alpha diversity parameters, Chao1 and Shannon index, across three types of microbial communities, bacteria **(A)**, fungi **(B)**, and archaea **(C)**. Boxes limit the 25th-and 75th percentile with the median presented as line inside. Error bars present the 1st and 99th percentile and outliers are shown as dots below and above. Significant differences: ***$P < 0.001$.

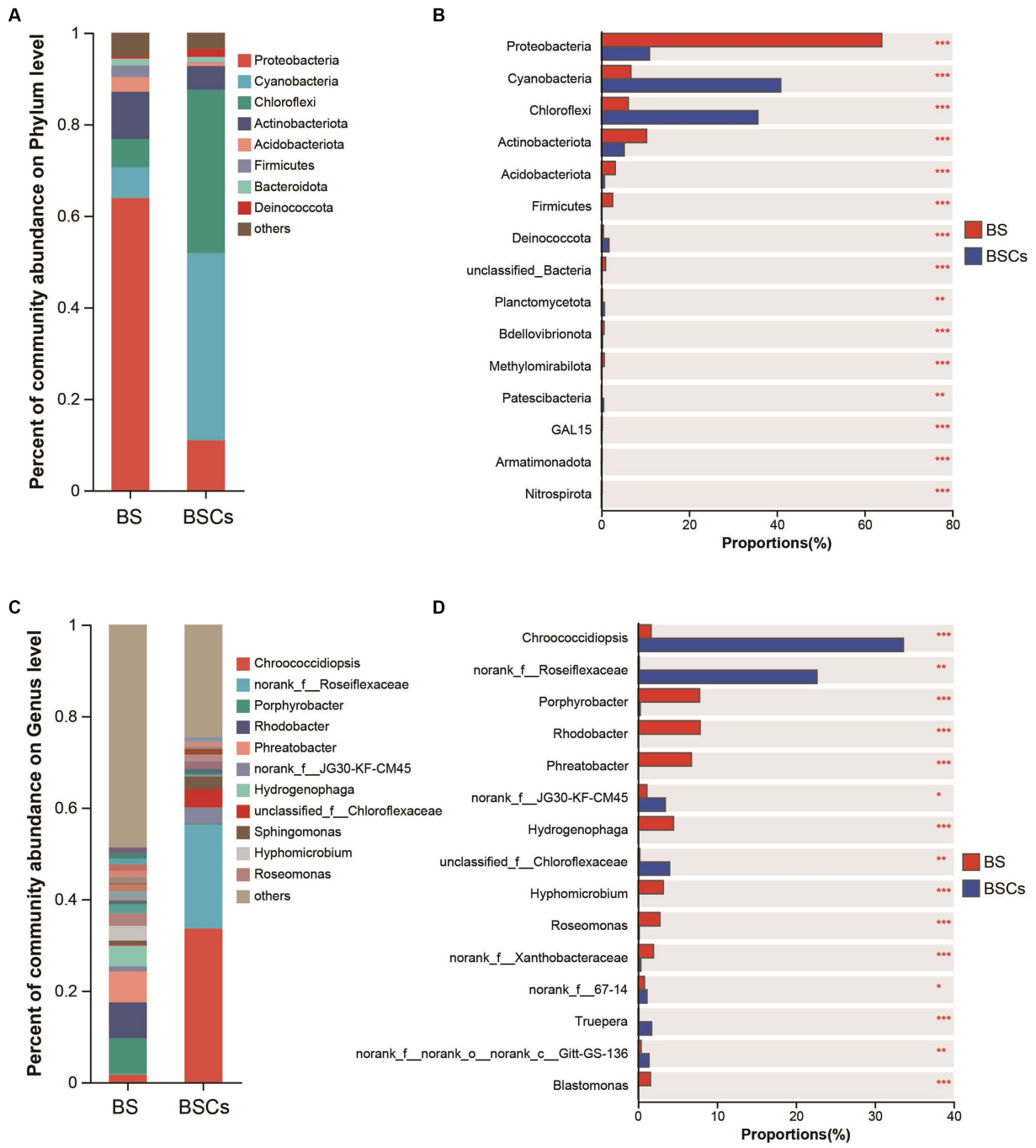

FIGURE 4
Analysis of differences of microbial composition between bare soil and biocrusts. **(A)** Relative abundance of the major bacterial taxa in biocrust and bare soil; **(B)** difference analysis of dominant bacterial taxa at phylum level; **(C)** relative abundance of the major bacterial taxa in biocrust and bare soil at genus level; **(D)** difference analysis of dominant bacterial taxa at genus level. Based on amplicon 16S rRNA gene data. Significant differences: ***$p < 0.001$, **$p < 0.01$, *$p < 0.05$. BS, bare soil; BSCs, biocrusts.

(Supplementary Figures S2A,B). The biocrust was dominated by *Candidatus_Nitrocosmicus* (82.22%) at genus level, followed by *Haladaptatus* (8.88%), with both genera substantially surpassing the abundance found in bare soil (Supplementary Figures S3C,D). Based on the 16S rRNA sequencing results, we conducted an annotative analysis of the species composition within the phylum Cyanobacteria. The relative abundance of dominant cyanobacterial taxa significantly increased with biocrust formation. Specifically, the abundance of *Chroococcidiopsis* (80.65%) was significantly higher in biocrust than that in bare soil (Supplementary Figure S4), while *unclassified_o_Thermosynechococcales* (21%), *unclassified_f_Nostocaceae* (11.57%), and *Chlorogloeopsis* (11.11%) were significantly higher in bare soil (Supplementary Figure S4). This portion of the findings aligns with the outcomes obtained through the amplification utilizing cyanobacterial-specific primers. Relevant data is accessible in Supplementary Table S3 (unpublished data).

Through PERMANOVA, we found significant differences in the microbiome between bare soil and the biocrusts, including bacterial, fungal, and archaeal communities (Supplementary Table S3). In addition, the results of CCA and RDA showed that microbial composition and structure (e.g., bacteria, fungi, and archaea) was highly correlated to the soil properties, including Chl *a*, TOC, TN, pH, and TP (Figure 5). Changes in nutrients might have contributed to changes in microbial composition of the biocrusts.

Measurement of soil erodibility factor

The soil erodibility factor (*K*-value) ranged from 0.264 to 0.280 t h MJ^{-1} mm^{-1}, and 0.190 to 0.221 t h MJ^{-1} mm^{-1} on bare soils and biocrusts, respectively. On tropical coral island, the K-value exhibited a notable decrease of approximately 25% in soils influenced by biocrust compared to bare soils, as illustrated in Figure 5. A *t*-test analysis revealed that the K-value in biocrust-influenced soils was significantly lower than that in bare soils (Figure 6).

Relationship among the soil erodibility factor, EPSs, microbial components, and soil properties

We observed that EPSs contents, including EP and EPS, in biocrusts were significantly higher than that in bare soil. Notably, both EPS and EP exhibited a significant negative correlation with the soil erodibility factor (Figures 7C,D).

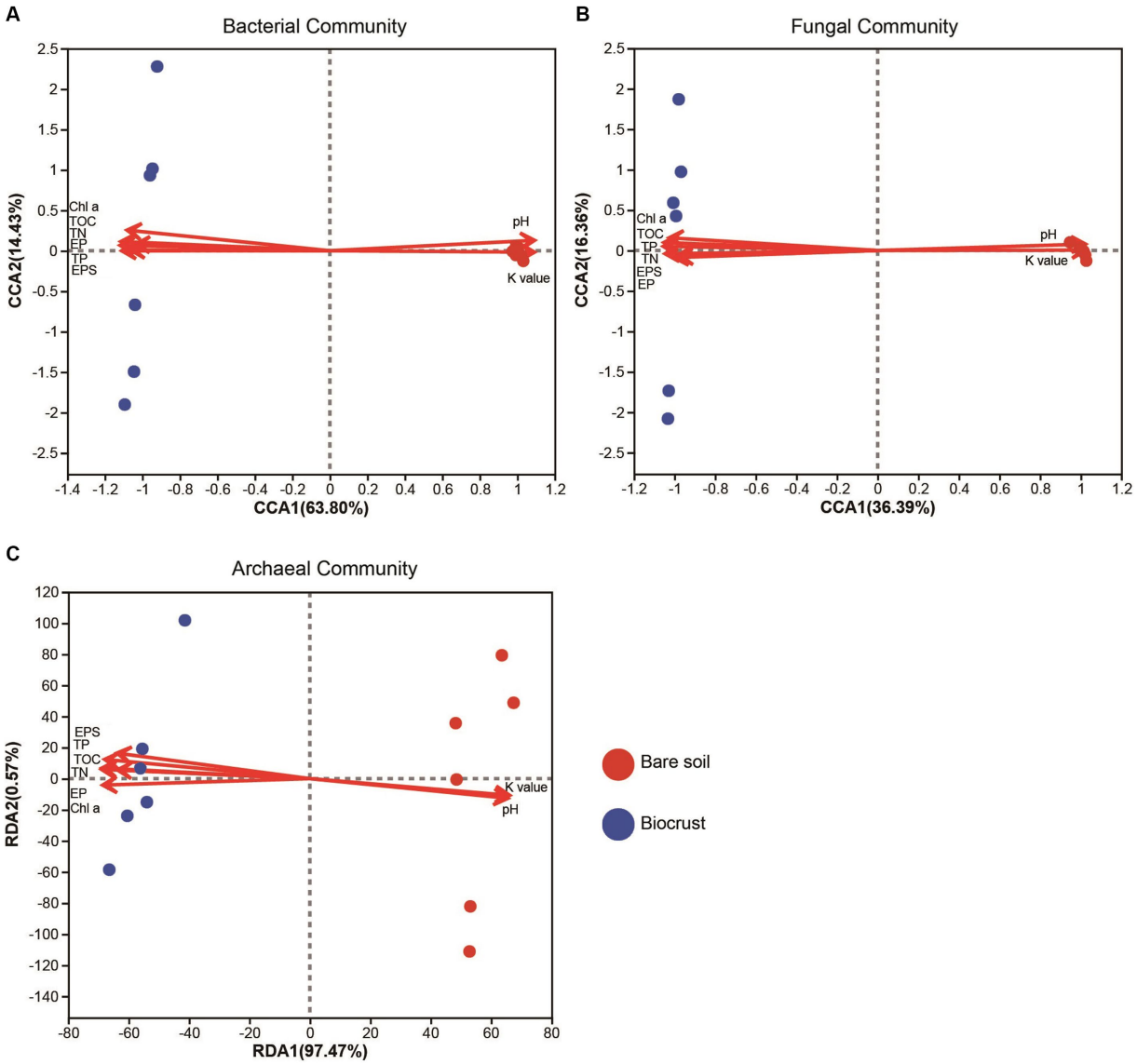

FIGURE 5
The canonical correlation analysis of bacterial **(A)** and fungal **(B)** community structure and its correlation with environmental factors. The redundancy analysis of archaeal **(C)** community and its correlation with environmental factors. Circle shape represents soil sample. TN, total nitrogen; TOC, total organic carbon; TP, total phosphorus; EP, extracellular protein; EPS, extracellular polysaccharide; Chl a, chlorophyll a; K value, soil erodibility factor.

Through the analysis of the spearman correlation heatmap, we found that the dominant phyla Proteobacteria, Actinobacteria, Acidobacteriota, Basidiomycota, and Thermoplasmatota were significantly negatively correlated to EPSs content, but the other phyla, including Cyanobacteria, Chloroflexi, Deinococcota, and Crenarchaeota were significantly positively correlated to EPSs contents (Figures 8A,C; Supplementary Figure S5A). At genus level, the dominant taxa, including *Chroococcidiopsis*, *norank_f_Roseiflexaceae*, *Emericellopsis*, and *Candidatus_Nitrocosmicus*, were observed to be significantly positively correlated to EPSs contents (Figures 8B,D; Supplementary Figure S5B). In addition, we also found that these microbial taxa were significantly positively associated with soil properties, including TOC, TN, and Chl a, but not pH and soil erodibility factor (Figure 8; Supplementary Figure S5).

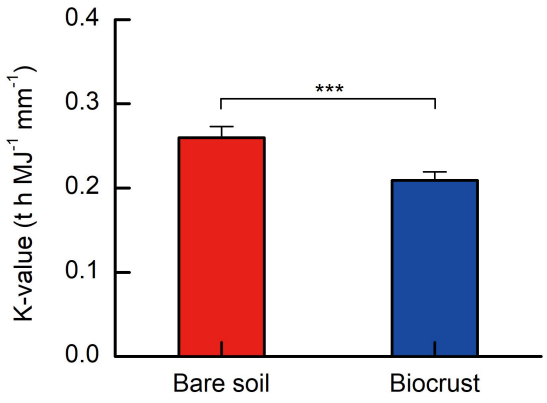

FIGURE 6
Soil erodibility factor (K) from biocrusts and bare soils. All data are presented as Mean ± SD calculated from biological repetition. Significant differences: ***P < 0.001.

Discussion

Biocrust formation enhances EPSs and reduces the soil erodibility factor in the tropical coral island

The study clearly demonstrated that soil erodibility factor was significantly decreased with biocrust formation (Figure 6). Similar protective characteristics (e.g., alleviation of erosion) have likewise been documented for alternative vegetative cover and mangrove ecosystems (Zhou and Shangguan, 2005; Mai et al., 2022). Furthermore, our findings demonstrated a notable negative correlation between the K-value and the abundance of EPSs, including EP and EPS (Figures 7C,D). Consistently, we also observed that EPSs content was rose after biocrust formation (Figures 7A,B). Diminished soil erodibility can be attributed in part to the adhesion of EPS and EP, which, in turn, promote the coalescence of microbial cells and microparticles (Meng et al., 2019). In this investigation, the proportion of silt (0.002–0.05 mm, %) and clay (<0.002 mm, %) were significantly higher in the biocrusts compared to bare soil. This signifies that, under the influence of EPS and EP adsorption, the formation of stable aggregate structures in the biocrusts is rendered more attainable. Simultaneously, EP bolster the architecture of EPSs, thereby facilitating the amalgamation of cells and upholding the steadfastness of biofilms

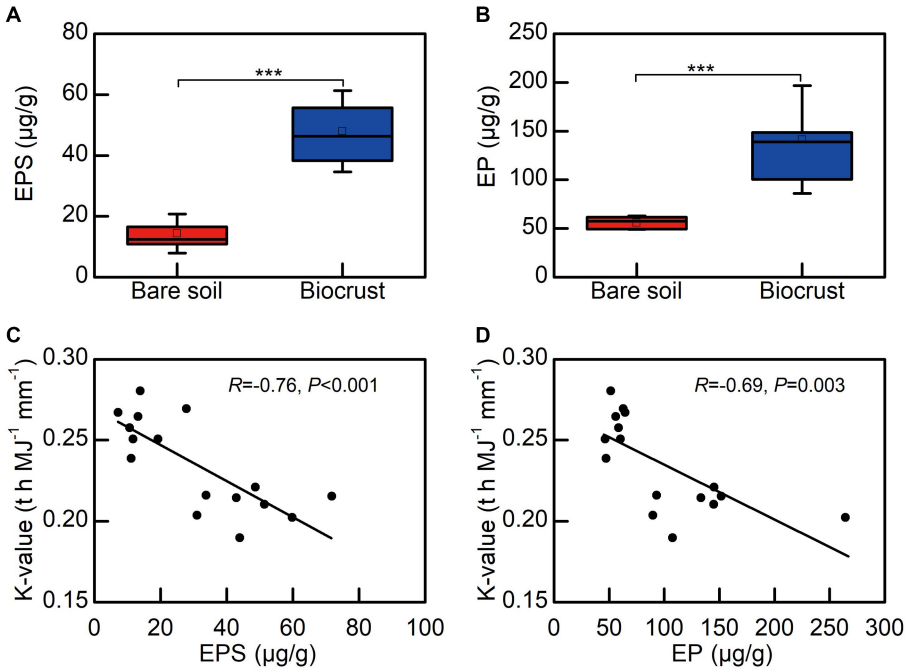

FIGURE 7
The relationship between EPS and soil erodibility factor (K). **(A)** The content of extracellular polysaccharide, **(B)** the content of extracellular protein, **(C)** the correlation between extracellular polysaccharide and K, **(D)** the correlation between extracellular protein and K. Each circle shape represents different soil sample. EPS, extracellular polysaccharide; EP, extracellular protein.

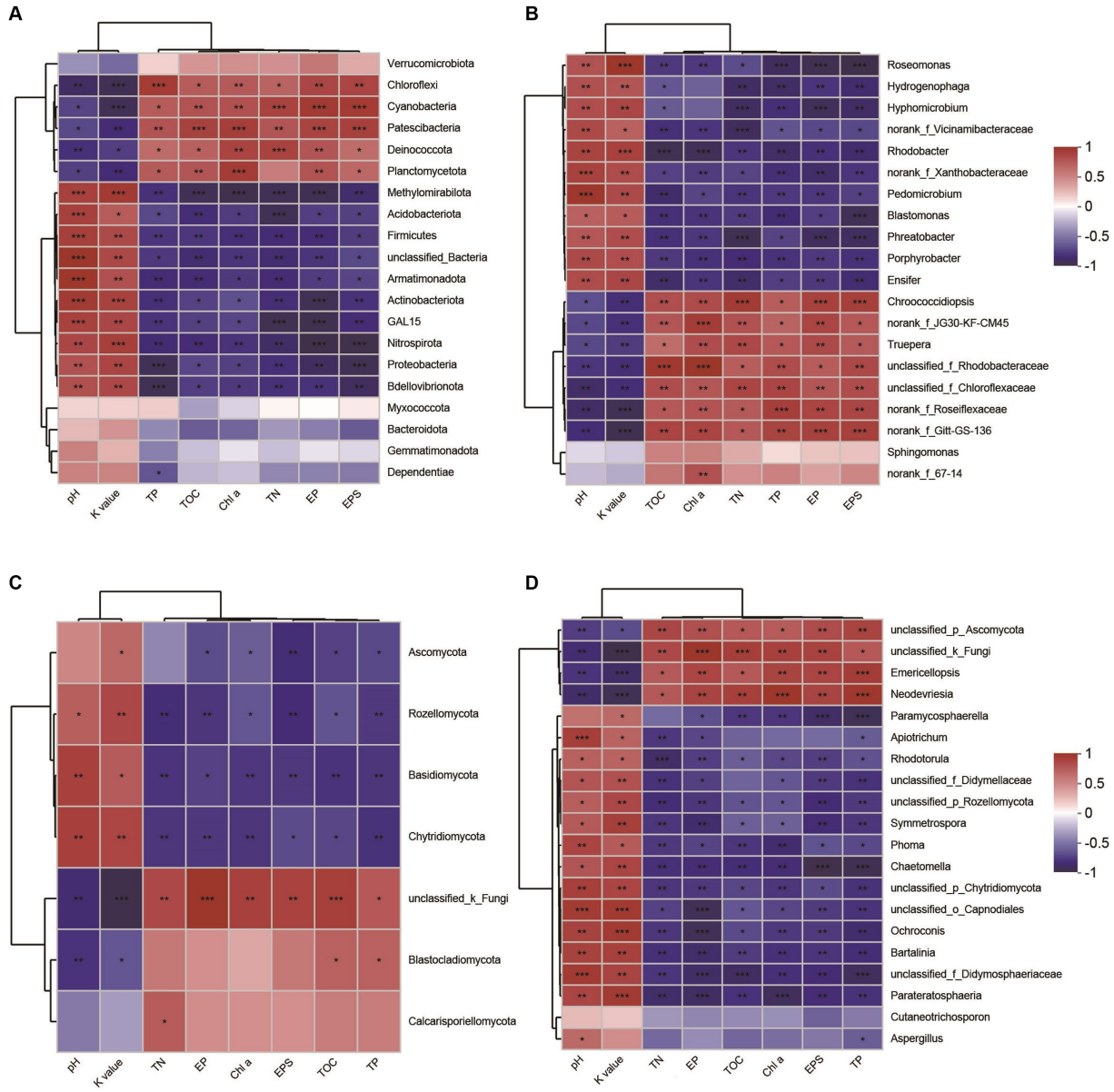

FIGURE 8
Spearman's correlation analysis between microbial taxa and soil properties. Bacterial taxa and its correlations with soil parameters **(A)** phylum level, **(B)** genus level. Fungal taxa and tis correlations with soil properties **(C)** phylum level, **(D)** genus level. Red illustrates positive correlations, while blue indicates negative correlations, significant differences: ***$p < 0.001$, **$p < 0.01$, *$p < 0.05$. TN, total nitrogen; TOC, total organic carbon; TP, total phosphorus; EP, extracellular protein; EPS, extracellular polysaccharide; Chl a, chlorophyll a; K value, soil erodibility factor.

(Flemming et al., 2007; Mai et al., 2022). Both neutral and hydrophobic EPS, on the other hand, heighten the ionic strength and play pivotal roles in the adsorption of EPS (Adav et al., 2008; Sharma and Sarkar, 2013). Therefore, the amplified quantities of EP and EPS engendered by the formation of biocrusts contribute to the promotion of microparticle adsorption and aggregation. Furthermore, the investigation conducted by Flemming and Wingender (2010) further elucidated that EPSs possesses a multitude of binding sites due to its varied functional groups. These binding sites enable the interaction and attachment of macromolecules through forces such as hydrogen bonds and electrostatic interactions, thereby fostering enhanced cohesion (Flemming and Wingender, 2010). Bowker et al. (2008) also reported that the concentration of EPSs could be used as a proxy measure of soil stability in the field. Additionally, the excretion of EPSs by biocrusts contributes to the formation of an exopolymeric matrix, which facilitates the cohesive bonding of bacterial filaments to agglomerated soil particles, as demonstrated by Garcia-Pichel and Wojciechowski (2009). This process establishes a conducive microenvironment for nutrient availability and utilization (Garcia-Pichel and Wojciechowski, 2009). Simultaneously, the exopolymeric matrix, which is an intricate network of EPSs, exhibits varying degrees of attachment to cells and sediments. It can manifest as loosely affiliated material or adopt a more compact configuration, such as tightly bound substances or cyanobacterial sheaths (Rossi et al., 2018). This elaborate framework contributes to enhanced soil stability and fortifies resistance against erosion, as emphasized by Rossi et al.

(2018). In the current investigation, we have noted that the EPSs generated by biocrusts possess the capacity to exert influence over the adsorption and aggregation of soil microparticles. Consequently, this phenomenon facilitates the promotion and sustenance of soil macroaggregate formation while concurrently bolstering the overall stability of the soil structure. Ultimately, these mechanisms culminate in the enhancement of soil's resistance against erosion.

In arid desert regions, the adhesion mechanisms of biocrusts are widely acknowledged. During their initial developmental stages, certain bacterial constituents of biocrusts, such as Cyanobacteria and Chloroflexi, have been observed to foster soil aggregate formation through the production of EPSs (Mager and Thomas, 2011; Cania et al., 2020). These EPSs served as the "adhesive agents" binding soil particles together. Furthermore, the filamentous structures and EPSs produced by cyanobacteria can create intricate network structures (Zhang, 2005). This network not only binds mineral particles and finer particles but also captures them on the filamentous surfaces, thereby promoting the formation and development of biocrusts (Zhang, 2005). In this study, as biocrusts formed, there was a significant increase in the relative abundance of Cyanobacteria and Chloroflexi, along with a noticeable elevation in EPSs content. Consequently, we hypothesize that the adhesion mechanism of tropical coral island biocrusts shares similarities with those in arid desert areas. However, in this investigation, we observed a significant decrease in pH values as biocrusts formed, which contrasts with conditions in arid regions (Maier et al., 2018; Ghiloufi et al., 2019). The substantial pH reduction suggests an abundance of H^+ ions within the EPSs secreted by island biocrusts. Given that the calcium carbonate proportion in coral calcareous sand reaches as high as 95%, these H^+ ions can alter the ion balance of carbonate salts in the soil, thereby promoting mineral precipitation (Zheng and Qian, 2020). This, in turn, leads to an increase in soil particle size. Furthermore, the presence of carbonate salt precipitation in the soil enhances the interparticle adhesion, creating a consolidation effect akin to what is observed in the process of cement solidification (Al-Salloum et al., 2017). This disparity represents the distinguishing feature between the adhesion process of tropical island biocrusts and traditional biocrusts.

Furthermore, EPSs could also create a nutrient-rich microenvironment by capturing airborne silt and clay particles through exploiting its adhesion (Souza-Egipsy et al., 2004). Prior research has extensively documented that the efficacy of biocrusts in capturing dust particles exhibits a progressive increase during the maturation process of these intricate ecosystems (Williams et al., 2012). Notably, among the diverse biocrust types, moss-lichen pinnacled crusts have been found to possess the highest degree of dust capture efficiency and exhibit significant potential in this regard (Williams et al., 2012). Furthermore, apart from their ability to ensnare airborne dust particles, EPSs also have the capacity to accumulate various nutrients and molecules. The incorporation of extracellular enzymes within the EPSs matrix facilitates the establishment of an extracellular digestive system, wherein compounds from the aqueous phase are captured and utilized as nourishing elements and sources of energy (Flemming and Wingender, 2010). Concurrently, a series of studies has provided compelling evidence regarding the remarkable capacity of EPSs to adsorb metal ions, thereby contributing to the remediation of heavy metal contamination and the restoration of polluted environments (Gadd, 2010; Costa et al., 2018).

However, the anti-erosion mechanism of biocrusts is very complex. In addition to EPSs, hydrodynamics, topography, soil particle distribution, and nutrient status may also affect soil erodibility (Gao et al., 2017; Yang et al., 2022). Undertaking more comprehensive investigations that specifically delve into the role of biocrust formation in mitigating run-off and preventing erosion would undoubtedly be a valuable pursuit.

Potential microbial taxa contributing to EPSs production and erosion resistance

In general, alterations in microbial composition and structure wield a pivotal influence over the secretion and production of EPSs. Enhanced nutrient content and elevated microbial abundance could promote protein and polysaccharide synthesis, result in increased EPSs accumulation in biocrusts (Mager and Thomas, 2011). Lan et al. (2022) reported that different microorganisms have different EPSs secretion capabilities, implying that shifts in microbial composition and structure could consequently induce alterations in EPSs content within biocrusts. In this study, our findings demonstrated that microbial abundance, including bacteria, fungi, archaea, and cyanobacteria, was significantly increased with biocrust formation (Figure 2), which is in line with the results of the study conducted at the Colorado Plateau and Succulent Karoo (Garcia-Pichel et al., 2003; Maier et al., 2018). Moreover, we conducted an analysis of environmental drivers affecting microbial composition in the coral islands. The CCA and RDA showed that microbial composition was significantly correlated to Chl *a* contents, TOC, TP, and TN (Figure 5). As important nutrients for the development of biocrusts, TOC, TP, and TN have been indicated to shape the microbial composition of biocrusts (Schulz et al., 2016; Zhang et al., 2016). Our results indicated that phylum Cyanobacteria, Chloroflexi, and Crenarchaeota might be essential and effective in EPSs secretion through differential analysis at the phylum level (Figure 8; Supplementary Figure S3). Notably, the relative abundances of biocrusts' major microbial phyla were significantly increased with biocrust formation (Figure 8; Supplementary Figure S3), which similar to our recent publication (Wang et al., 2022). Thus, we speculated that these three major microbial phyla were the main contributors. Specifically, cyanobacteria were the most important microbial phyla in the cyanobacterium-biocrust (Belnap et al., 2016), which produced EPSs that increase soil carbon pools as carbohydrates through CO_2 fixation. Moreover, the EPSs secreted by cyanobacteria serve as architectural elements, enveloping bacterial cells and intermingling with soil particles. This collaborative interplay results in the formation of heterogeneous clumps or aggregates within the topsoil (Mager and Thomas, 2011). Besides, filamentous cyanobacteria had a greater ability to entangle surface soil particles, as they could reach between soil particles or into deeper biocrusts, facilitated the formation of aggregates and maintained the stability, so that decreased carbon loss from erosion (Mager and Thomas, 2011). Therefore, cyanobacteria, especially filamentous cyanobacterial EPSs, play a key role in stabilizing coral calcareous sand, and preventing the adverse consequences of erosion (such as nutrient and organic matter loss, and dust production). Phototrophic filamentous Chloroflexi thrive in compatible anaerobic environments (Xian et al., 2020), are acknowledged for their copious production of EPSs within their habitat, and possess the capability to

fix CO_2 through a multitude of avenues, encompassing the Calvin cycle, Arnon–Buchanan cycle, and 3-hydroxypropionate bicycle (Ma et al., 2019; Xian et al., 2020). The EPSs secreted by Chloroflexi have the propensity to stimulate the aggregation of soil particles and the formation of soil aggregates, thus effectively mitigating soil erosion (Mager and Thomas, 2011). Further, the dominant archaeal phylum, Crenarchaeota, exhibits high enrichment within biocrusts and plays a significant role as a biogeochemical catalyst in the global nitrogen cycling (Nicol and Schleper, 2006). Meanwhile, the protein or glycoprotein subunits were found in the Crenarchaeota surface layer (Huber and Stetter, 2001). Significantly, the filamentous structure and the secretion of EPSs are shared attributes among the phyla Cyanobacteria and Chloroflexi. These characteristics assume a crucial role in both the formation and the preservation of soil aggregates, thereby contributing to the overall stability of the soil structure. Although all these microorganisms have the capacity to produce EPSs, we are not certain about the primary source of EPSs in this study. Based on the qPCR results, we observed that the abundances of bacteria and cyanobacteria were significantly higher than that of fungi and archaea, leading us to speculate that bacteria are the major contributors to EPSs content in this study. Prior research has indicated that cyanobacteria prefer alkaline environments (Belnap et al., 2003), while Chloroflexi thrive in acidic conditions (Jones et al., 2009; Santofimia et al., 2013; Cania et al., 2020). This accounts for the significantly higher relative abundance of cyanobacteria in the biocrusts of this study, as the alkaline soil environment of the coral island is more conducive to their growth, facilitating greater EPSs production. Therefore, we hypothesize that EPSs primarily originates from cyanobacteria. The amount of EPSs produced by bacterial communities in natural environments can vary depending on soil types (Hu et al., 2002). Moreover, the biochemical composition of EPSs is not specific to particular bacterial groups but rather controlled by environmental conditions and nutrient levels (Nicolaus et al., 1999). Thus, predicting the quantity of EPSs produced by soil microorganisms and tracing its sources presents a challenge. Nevertheless, in the initial stages of biocrust development, EPSs production is predominantly associated with the dominant members of the bacterial community within the biocrust (Cania et al., 2020). In addition, Genus *Chroococcidiopsis* belonged to Phylum Cyanobacteria, is widely described for its ability to metabolize carbon and nitrogen and to secrete polysaccharide and scytonemin (Dineshbabu et al., 2019; Assunção et al., 2021). Genus *Emericellopsis* belongs to Phylum Ascomycota and possesses the myceliar structure. This organism exhibits the capacity to generate substantial quantities of EPSs, thereby offering crucial assistance in enhancing the stability of soil aggregates (Elíades et al., 2006; Gonçalves et al., 2020; Agrawal and Saha, 2022). In our results, the abundance of *Chroococcidiopsis* and *Emericellopsis* in biocrusts was higher, coinciding with increased EPSs concentrations. Nevertheless, within the microbial communities of biocrusts in arid regions, the predominant taxa of cyanobacteria are filamentous or sheath-forming species, such as *Microcoleus vaginatus* and *M. steenstrupii*, contrary to the findings in this study (Mager and Thomas, 2011; Fernandes et al., 2018; Couradeau et al., 2019). This implies a divergence in the assembly mechanisms of biocrusts between tropical coral islands and arid regions. The exploration of these distinct assembly modes will be a focal point of our future investigations, bearing crucial scientific significance in elucidating the formation patterns of tropical coral island biocrusts.

Conclusion

In this study, we explore the anti-erosion role of biocrusts on tropical coral islands from the perspective of microbial EPSs. We found that after biocrust formation, soil erodibility factor was significantly reduced, whereas EPSs contents, specifically, extracellular protein and polysaccharides were significantly increased, demonstrating a significant negative correlation. Coinciding with an increased EPSs level, we reported increased bacterial, fungal, archaeal, and cyanobacterial abundance. Correlation analysis documented that Cyanobacteria, Chloroflexi, Deinococcota, and Crenarchaeota as potential microbials promoting EPSs and reducing soil erosion. In summation, this study furnishes substantiation of the integral function of biocrusts in averting soil erosion, while elucidating the contribution of microbial EPSs in the amelioration of soil erosion. Moreover, the evidence establishes a foundation for biocrust-directed environmental restoration on tropical coral islands, South China Sea.

Data availability statement

The datasets presented in this study can be found in online repositories. The names of the repository/repositories and accession number(s) can be found at: https://www.ncbi.nlm.nih.gov/, PRJNA1008893.

Author contributions

LW: Writing – original draft, Writing – review & editing. YH: Writing – original draft, Writing – review & editing. QY: Writing – original draft, Writing – review & editing. ZM: Writing – review & editing. FX: Writing – review & editing LL: Writing – review & editing. SZ: Writing – original draft, Writing – review & editing. JL: Writing – original draft, Writing – review & editing.

Funding

The author(s) declare financial support was received for the research, authorship, and/or publication of this article. The work was supported by the National Natural Science Foundation of China (grant nos. 41890853 and 42206155), the National Key Research and Development Project of China (grant no. 2022YFC3102103), the Natural Science Foundation of Guangdong Province, China (grant no. 2022A1515011889), and Guangzhou Science and Technology Plan Project (grant no. 202201010499).

Acknowledgments

We thank Jie Wang for helpful data analysis and suggestion to make this manuscript greatly improved, Jian Zhang for his assistance in data analysis, Jing Zhang for her assistance in environmental data detection, Testing Center of Marine Environment, South China Sea Institute of Oceanology, Chinese

Academy of Sciences, Yadong Huang and Zhiyuan Ouyang for their suggestion in sample collection, Nansha Marine Ecological and Environmental Research station, Chinese Academy of Science for sampling assistance.

Conflict of interest

The authors declare that the research was conducted in the absence of any commercial or financial relationships that could be construed as a potential conflict of interest.

The author(s) declared that they were an editorial board member of Frontiers, at the time of submission. This had no impact on the peer review process and the final decision.

Publisher's note

Supplementary material

The Supplementary material for this article can be found online at: https://www.frontiersin.org/articles/10.3389/fmicb.2023.1283073/full#supplementary-material

References

Acosta-Martínez, V., Cruz, L., Sotomayor-Ramírez, D., and Pérez-Alegría, L. (2007). Enzyme activities as affected by soil properties and land use in a tropical watershed. *Appl. Soil Ecol.* 35, 35–45. doi: 10.1016/j.apsoil.2006.05.012

Adav, S. S., Lee, D.-J., and Tay, J.-H. (2008). Extracellular polymeric substances and structural stability of aerobic granule. *Water Res.* 42, 1644–1650. doi: 10.1016/j.watres.2007.10.013

Agrawal, S., and Saha, S. (2022). The genus Simplicillium and Emericellopsis: a review of phytochemistry and pharmacology. *Biotechnol. Appl. Biochem.* 69, 2229–2239. doi: 10.1002/bab.2281

Al-Salloum, Y., Hadi, S., Abbas, H., Almusallam, T., and Moslem, M. (2017). Bio-induction and bioremediation of cementitious composites using microbial mineral precipitation–a review. *Constr. Build. Mater.* 154, 857–876. doi: 10.1016/j.conbuildmat.2017.07.203

Assunção, J., Amaro, H. M., Lopes, G., Tavares, T., Malcata, F. X., and Guedes, A. C. (2021). Exploration of marine genus *Chroococcidiopsis* sp.: a valuable source for antioxidant industry? *J. Appl. Phycol.* 33, 2169–2187. doi: 10.1007/s10811-021-02435-x

Bates, S. T., Berg-Lyons, D., Caporaso, J. G., Walters, W. A., Knight, R., and Fierer, N. (2010). Examining the global distribution of dominant archaeal populations in soil. *ISME J.* 5:908. doi: 10.1038/ismej.2010.171

Belnap, J., Büdel, B., and Lange, O. L. (2003). "Biological soil crusts: characteristics and distribution" in *Biological soil crusts: structure, function, and management*. eds. J. Belnap and O. L. Lange (Berlin, Heidelberg: Springer Berlin Heidelberg), 3–30.

Belnap, J., and Gardner, J. S. (1993). Soil microstructure in soils of the Colorado plateau: the role of the cyanobacterium *Microcoleus vaginatus*. *Great Basin Nat.* 53, 40–47.

Belnap, J., Reynolds, R. L., Reheis, M. C., Phillips, S. L., Urban, F. E., and Goldstein, H. L. (2009). Sediment losses and gains across a gradient of livestock grazing and plant invasion in a cool, semi-arid grassland, Colorado plateau, USA. *Aeolian Res.* 1, 27–43. doi: 10.1016/j.aeolia.2009.03.001

Belnap, J., Walker, B. J., Munson, S. M., and Gill, R. A. (2014). Controls on sediment production in two U.S. deserts. *Aeolian Res.* 14, 15–24. doi: 10.1016/j.aeolia.2014.03.007

Belnap, J., Weber, B., and Büdel, B. (2016). "Biological soil crusts as an organizing principle in drylands" in *Biological soil crusts: an organizing principle in drylands* (Cham: Springer International Publishing), 3–13.

Blackburn, T. M., Cassey, P., Duncan, R. P., Evans, K. L., and Gaston, K. J. (2004). Avian extinction and mammalian introductions on oceanic islands. *Science* 305, 1955–1958. doi: 10.1126/science.1101617

Bokulich, N. A., Subramanian, S., Faith, J. J., Gevers, D., Gordon, J. I., Knight, R., et al. (2012). Quality-filtering vastly improves diversity estimates from Illumina amplicon sequencing. *Nat. Methods* 10:57. doi: 10.1038/nmeth.2276

Bowker, M. A., Belnap, J., Bala Chaudhary, V., and Johnson, N. C. (2008). Revisiting classic water erosion models in drylands: the strong impact of biological soil crusts. *Soil Biol. Biochem.* 40, 2309–2316. doi: 10.1016/j.soilbio.2008.05.008

Büdel, B., Darienko, T., Deutschewitz, K., Dojani, S., Friedl, T., Mohr, K. I., et al. (2009). Southern African biological soil crusts are ubiquitous and highly diverse in drylands, being restricted by rainfall frequency. *Microb. Ecol.* 57, 229–247. doi: 10.1007/s00248-008-9449-9

Cania, B., Vestergaard, G., Kublik, S., Köhne, J. M., Fischer, T., Albert, A., et al. (2020). Biological soil crusts from different soil Substrates Harbor distinct bacterial groups with the potential to produce exopolysaccharides and lipopolysaccharides. *Microb. Ecol.* 79, 326–341. doi: 10.1007/s00248-019-01415-6

Chamizo, S., Cantón, Y., Miralles, I., and Domingo, F. (2012). Biological soil crust development affects physicochemical characteristics of soil surface in semiarid ecosystems. *Soil Biol. Biochem.* 49, 96–105. doi: 10.1016/j.soilbio.2012.02.017

Chamizo, S., Cantón, Y., Rodríguez-Caballero, E., and Domingo, F. (2016). Biocrusts positively affect the soil water balance in semiarid ecosystems. *Ecohydrology* 9, 1208–1221. doi: 10.1002/eco.1719

Costa, O. Y., Raaijmakers, J. M., and Kuramae, E. E. (2018). Microbial extracellular polymeric substances: ecological function and impact on soil aggregation. *Front. Microbiol.* 9:1636. doi: 10.3389/fmicb.2018.01636

Couradeau, E., Giraldo-Silva, A., De Martini, F., and Garcia-Pichel, F. (2019). Spatial segregation of the biological soil crust microbiome around its foundational cyanobacterium, Microcoleus vaginatus, and the formation of a nitrogen-fixing cyanosphere. *Microbiome* 7, 1–12. doi: 10.1186/s40168-019-0661-2

Couradeau, E., Karaoz, U., Lim, H. C., Nunes Da Rocha, U., Northen, T., Brodie, E., et al. (2016). Bacteria increase arid-land soil surface temperature through the production of sunscreens. *Nat. Commun.* 7:10373. doi: 10.1038/ncomms10373

Dineshbabu, G., Uma, V., Shylajanaciyar, M., Rashmi, V., Prabaharan, D., and Uma, L. (2019). The differential carbon-fixing and nitrogen-assimilating enzyme activities of Oscillatorian marine cyanobacterium *Phormidium valderianum* BDU 20041. *Photosynthetica* 57, 475–482. doi: 10.32615/ps.2019.062

Dubois, M., Gilles, K. A., Hamilton, J. K., Rebers, P. T., and Smith, F. (1956). Colorimetric method for determination of sugars and related substances. *Anal. Chem.* 28, 350–356. doi: 10.1021/ac60111a017

Edgar, R. C. (2013). UPARSE: highly accurate OTU sequences from microbial amplicon reads. *Nat. Methods* 10, 996–998. doi: 10.1038/nmeth.2604

Eldridge, D. J., Reed, S., Travers, S. K., Bowker, M. A., Maestre, F. T., Ding, J., et al. (2020). The pervasive and multifaceted influence of biocrusts on water in the world's drylands. *Glob. Chang. Biol.* 26, 6003–6014. doi: 10.1111/gcb.15232

Elíades, L. A., Cabello, M. N., and Voget, C. E. (2006). Contribution to the study of alkalophilic and alkali-tolerant Ascomycota from Argentina. *Darwin* 44, 64–73. doi: 10.2307/23226711

Fernandes, V. M. C., Machado de Lima, N. M., Roush, D., Rudgers, J., Collins, S. L., and Garcia-Pichel, F. (2018). Exposure to predicted precipitation patterns decreases population size and alters community structure of cyanobacteria in biological soil crusts from the Chihuahuan Desert. *Environ. Microbiol.* 20, 259–269. doi: 10.1111/1462-2920.13983

Flemming, H. C., Neu, T. R., and Wozniak, D. J. (2007). The EPS matrix: the "house of biofilm cells". *J. Bacteriol.* 189, 7945–7947. doi: 10.1128/JB.00858-07

Flemming, H. C., and Wingender, J. (2010). The biofilm matrix. *Nat. Rev. Microbiol.* 8, 623–633. doi: 10.1038/nrmicro2415

Gadd, G. M. (2010). Metals, minerals and microbes: geomicrobiology and bioremediation. *Microbiology* 156, 609–643. doi: 10.1099/mic.0.037143-0

Gao, L., Bowker, M. A., Xu, M., Sun, H., Tuo, D., and Zhao, Y. (2017). Biological soil crusts decrease erodibility by modifying inherent soil properties on the loess plateau, China. *Soil Biol. Biochem.* 105, 49–58. doi: 10.1016/j.soilbio.2016.11.009

Garcia-Pichel, F., Johnson, S. L., Youngkin, D., and Belnap, J. (2003). Small-scale vertical distribution of bacterial biomass and diversity in biological soil crusts from arid lands in the Colorado plateau. *Microb. Ecol.* 46, 312–321. doi: 10.1007/s00248-003-1004-0

Garcia-Pichel, F., and Wojciechowski, M. F. (2009). The evolution of a capacity to build supra-cellular ropes enabled filamentous Cyanobacteria to colonize highly erodible substrates. *PLoS One* 4:e7801. doi: 10.1371/journal.pone.0007801

Ghiloufi, W., Seo, J., Kim, J., Chaieb, M., and Kang, H. (2019). Effects of biological soil crusts on enzyme activities and microbial community in soils of an arid ecosystem. *Microb. Ecol.* 77, 201–216. doi: 10.1007/s00248-018-1219-8

Gonçalves, M. F., Vicente, T. F., Esteves, A. C., and Alves, A. (2020). Novel halotolerant species of Emericellopsis and Parasarocladium associated with macroalgae in an estuarine environment. *Mycologia* 112, 154–171. doi: 10.1080/00275514.2019.1677448

Hu, C., Liu, Y., Song, L., and Zhang, D. (2002). Effect of desert soil algae on the stabilization of fine sands. *J. Appl. Phycol.* 14, 281–292. doi: 10.1023/A:1021128530086

Huber, H., and Stetter, K. O. (2001). Crenarchaeota. In *eLS*. doi: 10.1038/npg.els.0000453

Jones, R. T., Robeson, M. S., Lauber, C. L., Hamady, M., Knight, R., and Fierer, N. (2009). A comprehensive survey of soil acidobacterial diversity using pyrosequencing and clone library analyses. *ISME J.* 3, 442–453. doi: 10.1038/ismej.2008.127

Kheirfam, H., and Asadzadeh, F. (2020). Stabilizing sand from dried-up lakebeds against wind erosion by accelerating biological soil crust development. *Eur. J. Soil Biol.* 98:103189. doi: 10.1016/j.ejsobi.2020.103189

Kuo, S. (1996). "Phosphorus" in *Methods of soil analysis*. ed. D. L. Sparks (Madison, WI: SSSA), 908–909.

Lan, S., Wu, L., Adessi, A., and Hu, C. (2022). Cyanobacterial persistence and influence on microbial community dynamics over 15 years in induced biocrusts. *Environ. Microbiol.* 24, 66–81. doi: 10.1111/1462-2920.15853

Lan, S., Wu, L., Zhang, D., and Hu, C. (2015). Analysis of environmental factors determining development and succession in biological soil crusts. *Sci. Total Environ.* 538, 492–499. doi: 10.1016/j.scitotenv.2015.08.066

Li, Y., Chen, Z., Peng, C., Huang, G., Niu, H., and Zhang, H. (2021). Assessment of habitat change on bird diversity and bird–habitat network of a Coral Island, South China Sea. *BMC Ecol. Evol.* 21:137. doi: 10.1186/s12862-021-01865-y

Li, J., Chen, Q., Zhang, S., Huang, H., Yang, J., Tian, X.-P., et al. (2013). Highly heterogeneous bacterial communities associated with the South China Sea reef corals *Porites lutea*, Galaxea fascicularis and *Acropora millepora*. *PLoS One* 8:e71301. doi: 10.1371/journal.pone.0071301

Liu, B., Zhang, K., and Jiao, J. (1999). Soil erodibility and its use in soil erosion prediction model. *J. Nat. Resour.* 14, 345–350.

Ma, H., Guo, C. Y., Wu, M., Liu, H., Wang, Z., and Wang, S. (2019). Use of extracellular polymer substances as additives for improving biogas yield and digestion performance. *bioRxiv*:699314. doi: 10.1101/699314

Mager, D. M., and Thomas, A. D. (2011). Extracellular polysaccharides from cyanobacterial soil crusts: a review of their role in dryland soil processes. *J. Arid Environ.* 75, 91–97. doi: 10.1016/j.jaridenv.2010.10.001

Magoč, T., and Salzberg, S. L. (2011). FLASH: fast length adjustment of short reads to improve genome assemblies. *Bioinformatics* 27, 2957–2963. doi: 10.1093/bioinformatics/btr507

Mai, Z., Zeng, X., Wei, X., Sun, C., Niu, J., Yan, W., et al. (2022). Mangrove restoration promotes the anti-scouribility of the sediments by modifying inherent microbial community and extracellular polymeric substance. *Sci. Total Environ.* 811:152369. doi: 10.1016/j.scitotenv.2021.152369

Maier, S., Tamm, A., Wu, D., Caesar, J., Grube, M., and Weber, B. (2018). Photoautotrophic organisms control microbial abundance, diversity, and physiology in different types of biological soil crusts. *ISME J.* 12, 1032–1046. doi: 10.1038/s41396-018-0062-8

Meng, D., Wu, J., Chen, K., Li, H., Jin, W., Shu, S., et al. (2019). Effects of extracellular polymeric substances and microbial community on the anti-scouribility of sewer sediment. *Sci. Total Environ.* 687, 494–504. doi: 10.1016/j.scitotenv.2019.05.387

Meng, F., Zhang, H., Yang, F., Li, Y., Xiao, J., and Zhang, X. (2006). Effect of filamentous bacteria on membrane fouling in submerged membrane bioreactor. *J. Membr. Sci.* 272, 161–168. doi: 10.1016/j.memsci.2005.07.041

Mogul, R., Vaishampayan, P., Bashir, M., Mckay, C. P., Schubert, K., Bornaccorsi, R., et al. (2017). Microbial community and biochemical dynamics of biological soil crusts across a gradient of surface coverage in the Central Mojave Desert. *Front. Microbiol.* 8:1974. doi: 10.3389/fmicb.2017.01974

Munson, S. M., Belnap, J., and Okin, G. S. (2011). Responses of wind erosion to climate-induced vegetation changes on the Colorado plateau. *Proc. Natl. Acad. Sci. U. S. A.* 108, 3854–3859. doi: 10.1073/pnas.1014947108

Nicol, G. W., and Schleper, C. (2006). Ammonia-oxidising Crenarchaeota: important players in the nitrogen cycle? *Trends Microbiol.* 14, 207–212. doi: 10.1016/j.tim.2006.03.004

Nicolaus, B., Panico, A., Lama, L., Romano, I., Manca, M. C., Giulio, D., et al. (1999). Chemical composition and production of exopolysaccharides from representative members of heterocystous and non-heterocystous cyanobacteria. *Phytochemistry* 52, 639–647. doi: 10.1016/S0031-9422(99)00202-2

Nübel, U., Garcia-Pichel, F., and Muyzer, G. (1997). PCR primers to amplify 16S rRNA genes from Cyanobacteria. *Appl. Environ. Microbiol.* 63, 3327–3332. doi: 10.1128/aem.63.8.3327-3332.1997

Ouyang, W., Wu, Y., Hao, Z., Zhang, Q., Bu, Q., and Gao, X. (2018). Combined impacts of land use and soil property changes on soil erosion in a mollisol area under long-term agricultural development. *Sci. Total Environ.* 613-614, 798–809. doi: 10.1016/j.scitotenv.2017.09.173

Parysow, P., Wang, G., Gertner, G., and Anderson, A. B. (2003). Spatial uncertainty analysis for mapping soil erodibility based on joint sequential simulation. *Catena* 53, 65–78. doi: 10.1016/S0341-8162(02)00198-4

Prabakaran, N., and Paramasivam, B. (2014). Recovery rate of vegetation in the tsunami impacted littoral forest of Nicobar Islands, India. *For. Ecol. Manag.* 313, 243–253. doi: 10.1016/j.foreco.2013.11.023

Rodriguez-Caballero, E., Belnap, J., Büdel, B., Crutzen, P. J., Andreae, M. O., Pöschl, U., et al. (2018). Dryland photoautotrophic soil surface communities endangered by global change. *Nat. Geosci.* 11, 185–189. doi: 10.1038/s41561-018-0072-1

Rodríguez-Caballero, E., Cantón, Y., Lazaro, R., and Solé-Benet, A. (2014). Cross-scale interactions between surface components and rainfall properties. Non-linearities in the hydrological and erosive behavior of semiarid catchments. *J. Hydrol.* 517, 815–825. doi: 10.1016/j.jhydrol.2014.06.018

Rodríguez-Caballero, E., Reyes, A., Kratz, A., Caesar, J., Guirado, E., Schmiedel, U., et al. (2022). Effects of climate change and land use intensification on regional biological soil crust cover and composition in southern Africa. *Geoderma* 406:115508. doi: 10.1016/j.geoderma.2021.115508

Rossi, F., Mugnai, G., and De Philippis, R. (2018). Complex role of the polymeric matrix in biological soil crusts. *Plant Soil* 429, 19–34. doi: 10.1007/s11104-017-3441-4

Santofimia, E., González-Toril, E., López-Pamo, E., Gomariz, M., Amils, R., and Aguilera, A. (2013). Microbial diversity and its relationship to physicochemical characteristics of the water in two extreme acidic pit lakes from the Iberian Pyrite Belt (SW Spain). *PLoS One* 8:e66746. doi: 10.1371/journal.pone.0066746

Schulz, K., Mikhailyuk, T., Dreßler, M., Leinweber, P., and Karsten, U. (2016). Biological soil crusts from coastal dunes at the Baltic Sea: cyanobacterial and algal biodiversity and related soil properties. *Microb. Ecol.* 71, 178–193. doi: 10.1007/s00248-015-0691-7

Sharma, P., and Sarkar, B. (2013). Prediction of permeate flux during ultrafiltration of polysaccharide in a stirred batch cell. *Food Bioprocess Technol.* 6, 3634–3643. doi: 10.1007/s11947-012-0990-7

Sharpley, A. N., and Williams, J. R. (1990). *EPIC-Erosion/productivity impact calculator. I: model documentation. II: user manual*. Washington, DC: Technical Bulletin-United States Department of Agriculture.

Smith, P. E., Krohn, R. I., Hermanson, G. T., Mallia, A. K., Gartner, F. H., Provenzano, M., et al. (1985). Measurement of protein using bicinchoninic acid. *Anal. Biochem.* 150, 76–85. doi: 10.1016/0003-2697(85)90442-7

Souza-Egipsy, V., Wierzchos, J., Sancho, C., Belmonte, A., and Ascaso, C. (2004). Role of biological soil crust cover in bioweathering and protection of sandstones in a semi-arid landscape (Torrollones de Gabarda, Huesca, Spain). *Earth Surf. Process. Landf.* 29, 1651–1661. doi: 10.1002/esp.1118

Takahashi, E., Ledauphin, J., Goux, D., and Orvain, F. (2009). Optimising extraction of extracellular polymeric substances (EPS) from benthic diatoms: comparison of the efficiency of six EPS extraction methods. *Mar. Freshw. Res.* 60, 1201–1210. doi: 10.1071/MF08258

Tian, Y., Chen, Z., Hou, Z., Luo, Y., Xu, A., and Yan, W. (2019). Geoacoustic provinces of the northern South China Sea based on sound speed as predicted from sediment grain sizes. *Mar. Geophys. Res.* 40, 571–579. doi: 10.1007/s11001-019-09387-5

Wang, L., Li, J., and Zhang, S. (2022). A comprehensive network integrating signature microbes and crucial soil properties during early biological soil crust formation on tropical Reef Islands. *Front. Microbiol.* 13:831710. doi: 10.3389/fmicb.2022.831710

Weber, B., Belnap, J., and Büdel, B. (2016). "Synthesis on biological soil crust research" in *Biological soil crusts: an organizing principle in drylands* (Cham: Springer International Publishing), 527–534.

Weber, B., Graf, T., and Bass, M. (2012). Ecophysiological analysis of moss-dominated biological soil crusts and their separate components from the succulent Karoo, South Africa. *Planta* 236, 129–139. doi: 10.1007/s00425-012-1595-0

Whittaker, R. J., and Fernández-Palacios, J. M. (2007). *Island biogeography: ecology, evolution, and conservation* (Oxford, New York: Oxford University Press).

Williams, A. J., Buck, B. J., and Beyene, M. A. (2012). Biological soil crusts in the Mojave Desert, USA: micromorphology and pedogenesis. *Soil Sci. Soc. Am. J.* 76, 1685–1695. doi: 10.2136/sssaj2012.0021

Wolfe, B. T., Dent, D. H., Deago, J., and Wishnie, M. H. (2015). Forest regeneration under Tectona grandis and Terminalia amazonia plantation stands managed for biodiversity conservation in western Panama. *New For.* 46, 157–165. doi: 10.1007/s11056-014-9448-2

Xian, W., Zhang, X., and Li, W. (2020). Research status and prospect on bacterial phylum Chloroflexi. *Acta Microbiol Sin.* 60, 1801–1820. doi: 10.13343/j.cnki.wsxb.20200463

Yang, L., Xiao, S., Luan, T., and Tam, N. F. Y. (2018). Overproduction of microbial extracellular polymeric substances in subtropical intertidal sediments in response to endocrine disrupting chemicals. *Sci. Total Environ.* 624, 673–682. doi: 10.1016/j.scitotenv.2017.12.160

Yang, L., Xiao, S., Yang, Q., Luan, T., and Tam, N. F. Y. (2020). Recovery of subtropical coastal intertidal system prokaryotes from a destruction event and the role of

extracellular polymeric substances in the presence of endocrine disrupting chemicals. *Environ. Int.* 144:106023. doi: 10.1016/j.envint.2020.106023

Yang, K., Zhao, Y., and Gao, L. (2022). Biocrust succession improves soil aggregate stability of subsurface after "grain for green" project in the hilly loess plateau, China. *Soil Tillage Res.* 217:105290. doi: 10.1016/j.still.2021.105290

Zhang, Y. (2005). The microstructure and formation of biological soil crusts in their early developmental stage. *Chin. Sci. Bull.* 50, 117–121. doi: 10.1007/BF02897513

Zhang, T., Jia, R. L., and Yu, L. Y. (2016). Diversity and distribution of soil fungal communities associated with biological soil crusts in the southeastern Tengger Desert (China) as revealed by 454 pyrosequencing. *Fungal Ecol.* 23, 156–163. doi: 10.1016/j.funeco.2016.08.004

Zhang, M., Liao, B.-Q., Zhou, X., He, Y., Hong, H., Lin, H., et al. (2015). Effects of hydrophilicity/hydrophobicity of membrane on membrane fouling in a submerged membrane bioreactor. *Bioresour. Technol.* 175, 59–67. doi: 10.1016/j.biortech.2014.10.058

Zhang, W., Zhang, H., Jian, S., and Liu, N. (2019). Tree plantations influence the abundance of ammonia-oxidizing bacteria in the soils of a coral island. *Appl. Soil Ecol.* 138, 220–222. doi: 10.1016/j.apsoil.2019.02.014

Zhang, B., Zhang, Y., Li, X., and Zhang, Y. (2018). Successional changes of fungal communities along the biocrust development stages. *Biol. Fertil. Soils* 54, 285–294. doi: 10.1007/s00374-017-1259-0

Zhao, C., Jiang, Z., Wu, Y., Liu, S., Cui, L., Zhang, J., et al. (2019). Origins of sediment organic matter and their contributions at three contrasting wetlands in a coastal semi-enclosed ecosystem. *Mar. Pollut. Bull.* 139, 32–39. doi: 10.1016/j.marpolbul.2018.12.008

Zhao, L., Liu, Y., Yuan, S., Li, Z., Sun, J., and Li, X. (2020). Development of archaeal communities in biological soil crusts along a revegetation chronosequence in the Tengger Desert, north Central China. *Soil Tillage Res.* 196:104443. doi: 10.1016/j.still.2019.104443

Zhao, Y., and Xu, M. (2013). Runoff and soil loss from revegetated grasslands in the hilly loess plateau region, China: influence of biocrust patches and plant canopies. *J. Hydrol. Eng.* 18, 387–393. doi: 10.1061/(ASCE)HE.1943-5584.0000633

Zheng, T., and Qian, C. (2020). Influencing factors and formation mechanism of CaCO3 precipitation induced by microbial carbonic anhydrase. *Process Biochem.* 91, 271–281. doi: 10.1016/j.procbio.2019.12.018

Zhou, Z. C., and Shangguan, Z. P. (2005). Soil anti-scouribility enhanced by plant roots. *J. Integr. Plant Biol.* 47, 676–682. doi: 10.1111/j.1744-7909.2005.00067.x

Zong, J., Li, L., Yao, X., Chen, J., Wang, H., Zhao, X., et al. (2021). Performance of five typical warm-season turfgrasses and their influence on soil bacterial community under a simulated tropical coral island environment. *Land Degrad. Dev.* 32, 3920–3929. doi: 10.1002/ldr.4012

frontiers | Frontiers in Microbiology

TYPE Original Research
PUBLISHED 15 December 2023
DOI 10.3389/fmicb.2023.1295193

OPEN ACCESS

EDITED BY
Hua Li,
Chinese Academy of Sciences (CAS), China

REVIEWED BY
Ming Li,
Northwest A&F University, China
Yuxiang Yuan,
Chinese Academy of Sciences (CAS), China
Shengwei Hou,
Southern University of Science and Technology, China

*CORRESPONDENCE
Anna Carratalà
✉ anna.carratala@epfl.ch

RECEIVED 15 September 2023
ACCEPTED 28 November 2023
PUBLISHED 15 December 2023

CITATION
Carratalà A, Chappelier C, Selmoni O, Guillaume AS, Chmiel HE, Pasche N, Weil C, Kohn T and Joost S (2023) Vertical distribution and seasonal dynamics of planktonic cyanobacteria communities in a water column of deep mesotrophic Lake Geneva. *Front. Microbiol.* 14:1295193. doi: 10.3389/fmicb.2023.1295193

Vertical distribution and seasonal dynamics of planktonic cyanobacteria communities in a water column of deep mesotrophic Lake Geneva

Anna Carratalà[1]*, Coralie Chappelier[1], Oliver Selmoni[2,3], Annie S. Guillaume[3], Hannah E. Chmiel[4,5], Natacha Pasche[5], Charlotte Weil[6], Tamar Kohn[1] and Stéphane Joost[3]

[1]Environmental Chemistry Laboratory, ENAC, École Polytechnique Fédérale de Lausanne (EPFL), Lausanne, Switzerland, [2]Department of Embryology, Department of Plant Biology, Carnegie Institution for Science, Washington, DC, United States, [3]Laboratory for Biological Geochemistry (LGB), Geospatial Molecular Epidemiology Group (GEOME), ENAC Faculty, École Polytechnique Fédérale de Lausanne (EPFL), Lausanne, Switzerland, [4]Eusserthal Ecosystem Research Station (EERES), Institute for Environmental Sciences (iES), University of Kaiserslautern-Landau, Landau, Germany, [5]Limnology Center, École Polytechnique Fédérale de Lausanne (EPFL), Lausanne, Switzerland, [6]ENAC-IT4R, École Polytechnique Fédérale de Lausanne (EPFL), Lausanne, Switzerland

Background: Temperate subalpine lakes recovering from eutrophication in central Europe are experiencing harmful blooms due to the proliferation of *Planktothrix rubescens*, a potentially toxic cyanobacteria. To optimize the management of cyanobacteria blooms there is the need to better comprehend the combination of factors influencing the diversity and dominance of cyanobacteria and their impact on the lake's ecology. The goal of this study was to characterize the diversity and seasonal dynamics of cyanobacteria communities found in a water column of Lake Geneva, as well as the associated changes on bacterioplankton abundance and composition.

Methods: We used 16S rRNA amplicon high throughput sequencing on more than 200 water samples collected from surface to 100 meters deep monthly over 18 months. Bacterioplankton abundance was determined by quantitative PCR and PICRUSt predictions were used to explore the functional pathways present in the community and to calculate functional diversity indices.

Results: The obtained results confirmed that the most dominant cyanobacteria in Lake Geneva during autumn and winter was *Planktothrix* (corresponding to *P. rubescens*). Our data also showed an unexpectedly high relative abundance of picocyanobacterial genus *Cyanobium,* particularly during summertime. Multidimensional scaling of Bray Curtis dissimilarity revealed that the dominance of *P. rubescens* was coincident with a shift in the bacterioplankton community composition and a significant decline in bacterioplankton abundance, as well as a temporary reduction in the taxonomic and PICRUSt2 predicted functional diversity.

Conclusion: Overall, this study expands our fundamental understanding of the seasonal dynamics of cyanobacteria communities along a vertical column in Lake Geneva and the ecology of *P. rubescens*, ultimately contributing to improve our preparedness against the potential occurrence of toxic blooms in the largest lake of western Europe.

KEYWORDS

cyanobacteria, bacterioplankton, lake, column, *Planktothrix*

1 Introduction

Bacterial communities rapidly respond to numerous biological and environmental factors, such as protist grazing, viral infections, predatory bacteria, temperature, salinity, or nutrient concentrations (Fenchel, 2002; Berdjeb et al., 2011; Parvathi et al., 2014; Ezzedine et al., 2020). It is therefore likely that environmental changes will have a significant impact on the composition and evolution of bacteria communities in freshwater environments, both directly and indirectly (Weckström et al., 2016; Kraemer et al., 2021).

Research suggests that certain bacteria, such as cyanobacteria, may be favored by environmental conditions imposed by global warming, water eutrophication and human development (Huisman et al., 2018). Cyanobacteria are of notable importance, as some strains can produce toxins harmful to humans and other mammals and can cause large harmful cyanobacteria blooms (HAB) that deteriorate water quality, sometimes leading to widespread death of other aquatic species (Paerl and Paul, 2012; Paerl and Otten, 2013; Chorus and Welker, 2021). Therefore, it is important to accurately identify the combinations of environmental and biological factors that influence bacterial community dynamics, particularly with regards to cyanobacteria that can represent a threat to public health (Jacquet et al., 2005).

The impact of cyanobacteria proliferation on microbial community composition and functions remains elusive. While recent work has noted negative impacts of cyanobacteria blooms on zooplankton and phytoplankton diversity and function (Jia et al., 2017; Krztoń et al., 2019; Amorim and Moura, 2021), other studies have shown that cyanobacteria may cause both increases or decreases in diversity and function of aquatic communities (Sukenik et al., 2015). Less is known about the effects of cyanobacteria on bacterioplankton communities and their functions in mesotrophic and oligotrophic environments. However, studies available to date, developed mostly in eutrophic lakes and reservoirs, have noted an impact of cyanobacteria such as *Microcystis aeruginosa* on bacterioplankton composition and succession (Zheng et al., 2008; Guedes et al., 2018; Mankiewicz-Boczek and Font-Nájera, 2022).

Cyanobacteria from the *Planktothrix* genus play a crucial role in lakes where oligotrophic conditions are being restored through corrective measures (Jacquet et al., 2005; Ernst et al., 2009; Fernández Castro et al., 2021). Two examples of such lakes occur in Switzerland, where both Lake Zurich and Lake Geneva have recovered from strong eutrophication periods in the 1970s (Posch et al., 2012; Fernández Castro et al., 2021). In these restored lakes, *Planktothrix rubescens* has the potential to rapidly multiply and emerge as the dominant species among the phytoplankton communities, as bacteria of this genus are well-adapted to low light environments, regulating their position in the water column using gas vesicles and undergoing physiological adaptations (Walsby et al., 2004, 2006; Walsby, 2005; Yankova et al., 2016; Gallina et al., 2017). *Planktothrix rubescens* in Lake Zurich have been shown to accumulate as a persistent thin layer in the metalimnion during the stratified season (typically between May–October), which then disappears in autumn with the deepening of the mixed layer (Fernández Castro et al., 2021).

As the largest and deepest lake in western Europe, with a volume of 89 km^3 and a surface area of 580 km^2, Lake Geneva is of major importance for the region as a source of drinking water for 900,000 people, as well as for tourism development and fishing (Gallina et al., 2017). This monomictic lake (mixed from top to bottom during one period per year) experiences thermal stratification from spring to early winter (Minaudo et al., 2021).

Research suggests that the abundance of cyanobacteria could increase in Lake Geneva by 34% by the end of this century under future climatic conditions, potentially inducing significant changes in the microalgal composition and posing a threat for water quality (Paerl and Otten, 2013; Huisman et al., 2018; Amorim and Moura, 2021). *Planktothrix rubescens* has been shown to be a dominant cyanobacterial species in the water column of Lake Geneva since the early 2000's (Jacquet et al., 2005). However, despite extensive monitoring since 1957 as part of the international water protection program led by the "Commission Internationale pour la Protection des Eaux du Léman" (CIPEL; International Commission for the Protection of Lake Geneva Waters), the temporal dynamics and diversity of cyanobacteria, as well as their impact on microbial diversity and functions in Lake Geneva, remain unknown.

In this study we aimed to unravel the dynamics of cyanobacteria throughout the water column of Lake Geneva and assess its impacts on the microbial community of the lake. Our hypothesis was that *P. rubescens* is the most dominant cyanobacteria in Lake Geneva and that in nutrient-poor lakes outcompetes other bacteria communities reducing bacterioplankton abundance, diversity and function (Walsby, 2005). Our specific goals were to (i) identify the main cyanobacteria genera present in a water column of Lake Geneva throughout the year, (ii) to characterize their seasonal dynamics and main environmental drivers and finally, (iii) to determine changes in the bacterioplankton community that may be associated with the dominance of *P. rubescens*. The dataset obtained in this study and the initial findings reported here mark an important stride towards improving our ability to make precise predictions regarding the potential effect of climate changes on the proliferation of the diverse cyanobacteria groups in Lake Geneva and the impact on the lake's ecosystem services.

2 Materials and methods

2.1 Study location, sample methods and processing

Water samples were collected in Lake Geneva from the scientific platform LéXPLORE (46°30′0.819″ N, 6°39′39.007″ E), located 570 meters offshore from the town of Pully, Switzerland (Wüest et al., 2021a,b). Lake Geneva is a deep perialpine lake (maximum depth is 309 meters) located in the north of the Alps at 372 meters above the sea level (Supplementary Figure S1). We conducted monthly sampling campaigns between August 2019 and December 2020, collecting and processing a total of 218 samples over 18 dates. The sampling campaigns planned during the spring months of 2020 coincided with lockdown orders due to the COVID-19 pandemic such that fewer samples were collected during that period. During each sampling campaign, two-liter samples were collected using a Niskin bottle (HydroBios Kiel) and a 750 W electric winch (KC Denmark A/S). The maximum depth under the floating platform is approximately 110 meters, and samples were taken at 12 distinct depths (0, 2.5, 5, 10, 15, 20, 25, 30, 50, 60, 80, and 100 meters) (Figure 1). Upon collection, water samples were stored in polycarbonate bottles, transferred to a laboratory at EPFL, and kept at 4°C until they were filtered within the

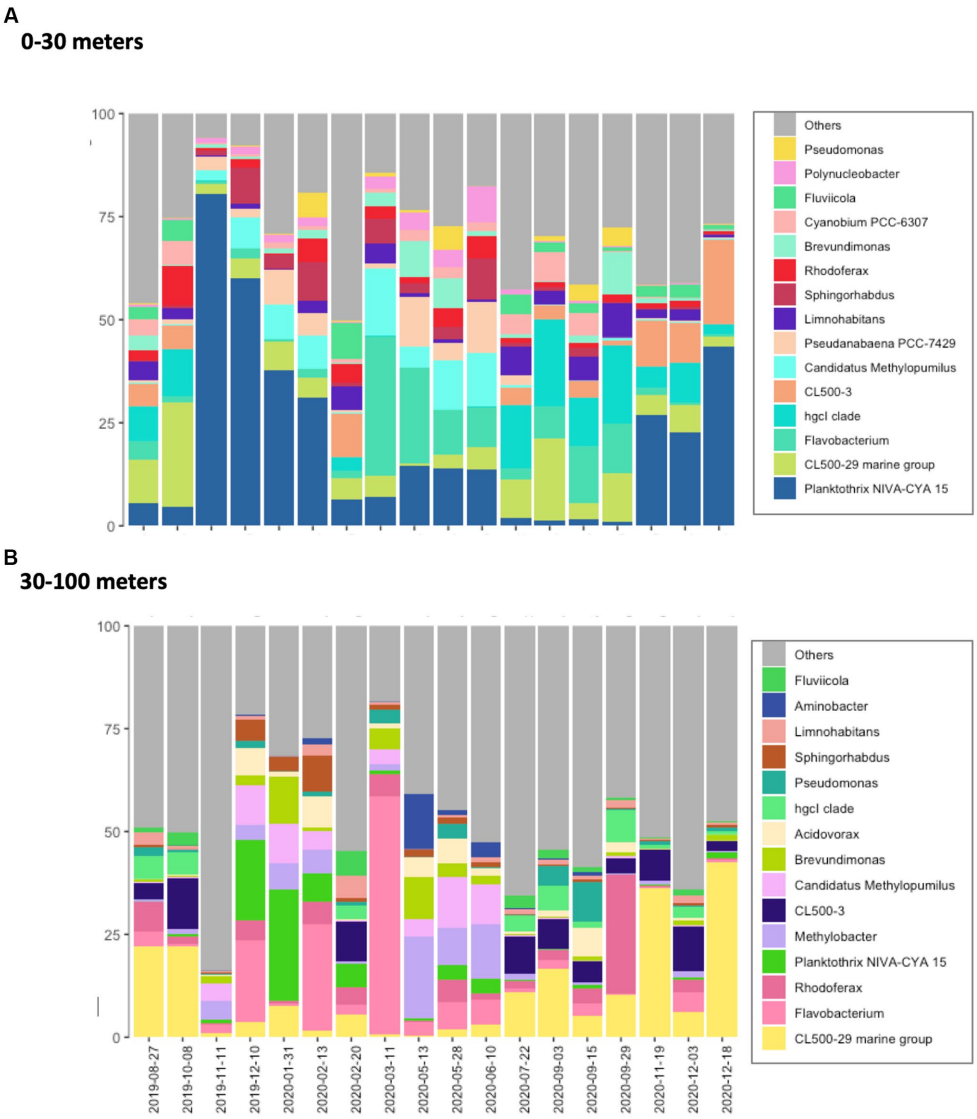

FIGURE 1
Bacterioplankton community composition in Lake Geneva. Main bacteria genus identified in the **(A)** top (0–30 m depth) and **(B)** bottom (30–100 m depth) layers of the studied water column. Compositional data was obtained by averaging the relative abundances determined in 155 and 58 water samples collected at different depths within the top and bottom layer, respectively.

next 24 h. One liter per sample collected between 0 and 50 m depth, and two liters per sample from 50 to 100 m depth, were filtered through 0.45 µm filters (Millipore) using an electrostatic pump. Filters were kept frozen at −20°C until nucleic acid extractions were performed.

2.2 Water analysis and compilation of meteorological data

The physicochemical properties of the water column were monitored during each sampling campaign using a multiparameter probe (Sea & Sun Technology GmbH), which determined vertical gradients of conductivity, temperature, pressure, pH, chlorophyll a, oxygen saturation, dissolved oxygen concentration and turbidity (data shown in Supplementary Figure S2). Nutrient concentrations [i.e., total phosphorous (TP), total nitrogen (TN), total dissolved phosphorous (TDN), total dissolved nitrogen (TDN), dissolved inorganic phosphorous (DIN), and dissolved inorganic nitrogen (DIN)] were determined from a subset of the water samples at the Department of Surface Waters of the Swiss Federal Institute of Aquatic Sciences (Eawag) following standard protocols (Supplementary Figure S3). Meteorological data (air temperature, precipitation, wind speed and irradiance) were pulled from the nearby Pully weather station for each sampling day, retrieved from the Swiss Federal Office of Meteorology and Climatology (Meteoswiss) on July 27th, 2022.

2.3 DNA extraction and determination of 16 s gene abundances by quantitative PCR

Nucleic acid extractions were performed using the DNeasy® PowerWater® kit according to the manufacturer's instructions with

minor modifications (nucleic acids eluted in 60 µL of elution buffer). To monitor the abundance of bacterioplankton biomass in the samples, quantitative real-time PCR assays (qPCR) were performed using the Femto Bacterial DNA quantification kit (Zymo Research Corporation), which includes primers and standards, following the thermocycling conditions recommended by the manufacturer. The average efficiency of all the standard curves was 0.92 and the average R^2 was 0.98. All qPCR data were retrieved using the thermocycler Mic Real-Time PCR System (LabGene Scientific, SA).

2.4 MiSeq sequencing of 16S rRNA amplicons and data processing

Prior to the DNA library preparation, 2 µL of the extracted nucleic acids from each sample were quantified using a Qubit® fluorometer (Thermo Fisher scientific United States) and the Qubit™ 1x dsDNA HS Assay kit (Thermo Fisher scientific United States). Samples were sent to Fasteris (Genesupport, SA. Geneva) for library preparation and next generation sequencing using MiSeq (Illumina). Libraries were prepared following the Metafast protocol, an in-house procedure of Fasteris (Genesupport, SA. Geneva). To obtain the library, PCR targeting the V3–V4 region of the 16S gene of bacteria were conducted for every sample. The primers used were 341F (5′-CCTACGGGNGGCWGCAG-3′) and 805R (5′-GACTACHVGGGTATCTAATCC-3′) (Klindworth et al., 2013). The obtained sequences were sorted using an in-house script property of Fasteris, trimmed using Trimmomatic and joined using the ea-utils obtaining FastQ scores for each sample. Finally, the sequences were classified as operational taxonomic units (OTUs) using the Burrows-Wheeler Alignment Tool and the taxonomically clustering was performed using Silva rRNA database based on 97% sequence similarity.

2.5 Data analysis

The data analysis and plots were conducted in RStudio (R version 4.1.3) (R Core Team, 2012). The qPCR results were visualized using the ggplot2 and lattice packages (Grothendieck, 2008; Darrin and Bryan, 2021). R functions levelplot and panel. 2dsmoother were used to plot smooth approximations of 16S rRNA abundance, environmental data and Chao1 over dates and depths using the method of locally estimated scatterplot smoothing (LOESS). An analysis of variance (ANOVA) was performed to determine the statistical significance of differences in 16S rRNA abundances between different layers and seasons. The microeco package was used for downstream analysis of the sequencing data (Liu et al., 2021). Mitochondria and chloroplast sequences were removed from the dataset, and Chao1 index was selected to assess alpha diversity. The spatiotemporal abundance of specific bacterial genera was plotted using the raster and gstat R packages (Hijmans and van Etten, 2015). The prediction of metabolic pathways and functional profiles of the identified communities was determined using QIIME2 (version 2021.2) and PICRUSt2 (version 2.4.0) (Langille et al., 2013; Bolyen et al., 2019; Douglas et al., 2020). The OTUs underwent closed reference picking in QIIME2 using a database that was trained on Greengenes version 13.5, employing a 97% identity cluster. The resulting feature table was exported as a biom format file, normalized by the predicted 16S rRNA copy number and employed in PICRUSt2 for predicting counts of metabolic functions. This prediction was accomplished by referencing the Kyoto Encyclopedia of Genes and Genome (KEGG) Orthology (KO) Database (Kanehisa and Goto, 2000). The accuracy of metagenomic prediction was assessed using the Nearest Sequenced Taxon Index (NSTI) values as previously described (Langille et al., 2013). Chao1 indices were calculated to assess functional diversity in the samples.

The Kruskal–Wallis rank sum test was employed to determine the significance of differences in alpha diversity and taxon abundance among different groups for both taxonomic and functional diversity. Bray–Curtis dissimilarity was used to measure the dissimilarities between pairs of communities, and non-metric multi-dimensional scaling (NMDS) was used to visualize differences among communities. The relative abundances of important genera were correlated with environmental factors using the Spearman correlation method. Prior to calculating Spearman correlations, autocorrelation between environmental variables was assessed using multicollinearity analysis, and variance inflation factors (VIF) were calculated using the R package car (Fox and Weisberg, 2019). Variables with VIF ≥5 were excluded from each pair, where the variable retained was based on its assumed biological relevance (James et al., 2019). Of the 22 initial measured variables included in the correlation analyses, 10 variables were retained. To identify significant biomarker functions for the productive and unproductive zones, as well as for each season at both taxonomic and functional level, linear discriminant analyses (LDA) with differential abundance tests implemented in LEfSe were applied (Segata et al., 2011).

3 Results

3.1 Environmental characterization of the water column

The environmental variables and nutrient concentrations measured in this study clearly reflect the spatiotemporal variations of the local weather conditions and in the water column throughout the year due to the stratification and deep mixing of the lake (Supplementary Figures S2, S3). The water column appeared fully mixed from December to April (Supplementary Figure S2). During deep mixing, the water temperature reached its minimum at 6°C, while the highest water temperature was 22°C, which was recorded at the surface of the water column in September 2020. Nutrient measures were determined for a subset of the 218 samples collected in the study and showed higher concentrations in the unproductive layer than in the productive layer, particularly in winter and spring (Supplementary Figure S2). Measures of TN, TDN and DIN were higher in winter at the water surface and below 30 m across the sampling period. TN, TDN and DIN were, as expected, shown to be highly correlated (Pearson's correlation index >0.75). The highest values of DIP were observed in winter in the homogenized water column reaching 5 mg/L. TDP and TP concentrations showed less variability in the water column across seasons, but concentrations were generally higher in the unproductive layer compared to the productive layer in every season.

3.2 Bacterioplankton community structure

From the 218 water samples collected in this study, 56 samples were taken in autumn, 34 in spring, 46 in summer and 82 in winter (two winter seasons were included in the study, which lasted 15 months). With regards to the physical state of the water column, 131 samples were collected during lake stratification and 81 during deep mixing. The sequencing of the collected samples produced almost 25 million of Bacteria sequences and a total of 12,748 OTUs were identified. On average each sample produced 115,621 reads and 731 OTUs.

The five most abundant bacteria phyla in Lake Geneva at the time of this study were *Proteobacteria*, *Actinobacteriota*, *Bacteroidota*, *Cyanobacteria* and *Planctomycetota*. These phyla accounted for more than 75% of the sequenced reads and were both present along the water column. The most abundant bacteria genera identified in the dataset were *CL500-29 marine group*, *Flavobacterium*, *Planktothrix*, *CL500-3*, *hgcl clade* and *Rhodoferax* (Figure 1). Most bacteria genera were observed both in the surface and the bottom layer (2,867), however certain groups appeared exclusively in the top or bottom layer (1,699 and 1,119 genera, respectively). Beta diversity analysis based on Bray–Curtis dissimilarity distances show that community dissimilarity was mostly driven by compositional changes occurring at specific dates (Figure 2; Supplementary Figure S4), with flare ups occurring from November 2019 to February 2020 and from March 2020 to June 2020.

Linear discriminant analysis (LDA) with LDA effect size analysis (LEfSe) allowed us to identify taxonomic biomarkers and functional pathways defined in the Kyoto Encyclopedia of Genes and Genomes (KEGG) that were significantly associated with the top and bottom layers of the water column. These results (Supplementary Figure S7) suggest that several cyanobacteria genera (*Planktothrix*, *Pseudoanabaena*, *Cyanobium* and *Aphanizomenon*) and the genus *Limnohabitans* were markers of the top layer of the studied column (LDA scores above 2.5) and consequently, PICRUSt2-predicted functions involving energy metabolism and photosynthesis were identified as biomarkers (LDA scores above 2). Conversely, the genera *Pedobacter*, *Undibacterium*, *Nitrospira* and *Methylobacter* were markers of the bottom layer (LDA scores from −2.5 to nearly −5). At the functional level, the bottom of the water column was enriched in pathways for the metabolism of aminoacids and carbohydrates, cell motility and transport, and the processing of environmental information (LDA scores below −2; Supplementary Figure S7).

3.3 Cyanobacteria diversity and spatiotemporal dynamics

As shown in Figure 3A, diverse cyanobacteria were identified in the lake including genera of filamentous and picocyanobacterial species. The most dominant genera were *Planktothrix* sp., *Cyanobium and Pseudoanabaena*. Less dominant genera included *Tychonema* and *Microcystis* among other. At the species level, reads belonging to genus *Planktothrix* were identified as *P. rubescens* (Supplementary Figure S5) and those identified as members of genus *Pseudoanabaena* were identified as *Pseudoanabaena foetida*. Reads associated with genus *Cyanobium,* showed higher diversity and were identified as diverse species including *Synechococcus rubescens* and *Cyanobium* sp. (Supplementary Figure S5).

The spatiotemporal abundance of the 4 genera showing highest number of reads in the dataset are shown in Figure 3B. In the top layer of the water column (0–25 meters deep), genus *Planktothrix,* reached a maximum relative abundance of approximately 90% and was dominant in the community until February 2020 (Figures 1A, 3B). The relative abundance of *P. rubescens* remained low from February 2020 (nearly 0%) until October 2020, when it surpassed 25% of all identified bacteria. The spatiotemporal distribution of the genus *Planktothrix* is shown in Figure 3B and suggests the existence of

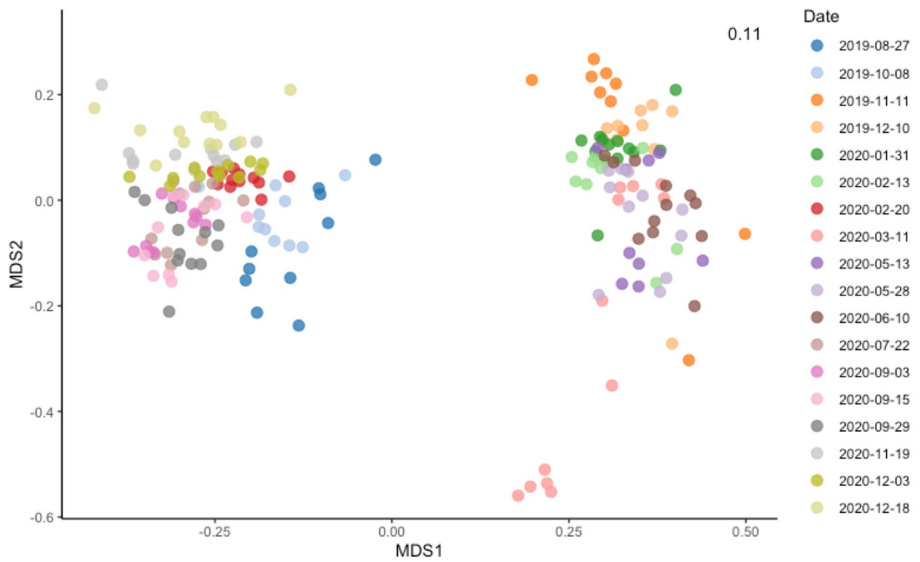

FIGURE 2
Non-metric multidimensional scaling (MDS) plot showing Bray–Curtis dissimilarity among samples. dbRDA ordinations of the bacteria communities obtained using Bray Curtis distance estimates and colored based on the sampling date.

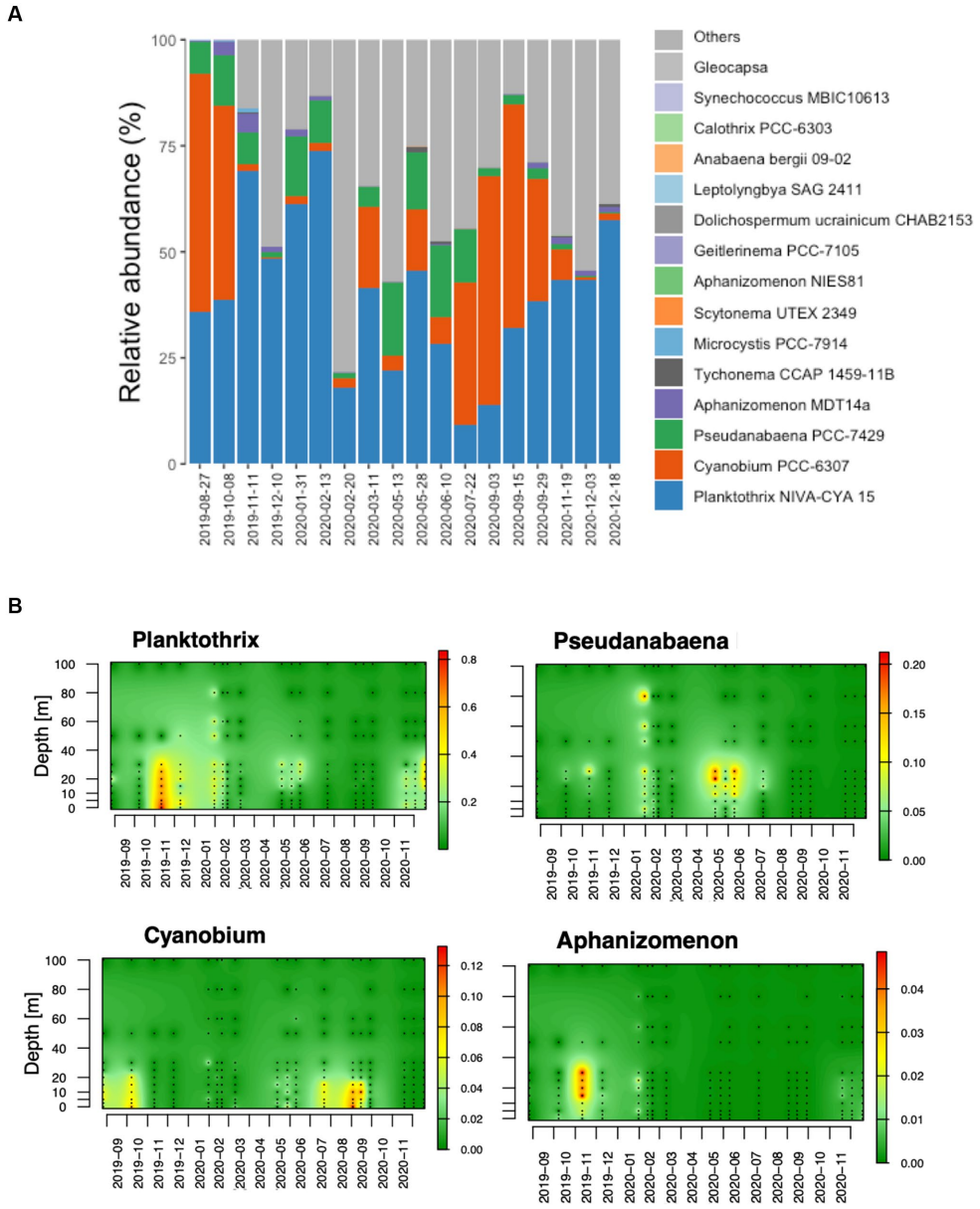

FIGURE 3
Cyanobacteria community composition in Lake Geneva. **(A)** Main cyanobacteria genus identified in the studied water column. The compositional data was obtained by averaging the relative abundance of cyanobacteria in 218 water samples. **(B)** The panel below shows the spatiotemporal abundance of genera *Planktothrix* and *Flavobacterium* as relative abundance of reads.

changing ecological niches throughout the year. In autumn and winter, *P. rubescens* was mostly located at 0 to 30 meters depth, while in May and June it became restricted to depths between 15 to 30 meters and was nearly absent from the water column during summer. From March to September 2020, the bacterioplankton communities in the productive layer were dominated by the genera *Flavobacterium*, *CL500-29* and *hgcl clade,* where the cyanobacteria that dominated the column during summertime in the absence of *Planktothrix* was genus *Cyanobium*.

The bottom layer of the water column (from 30 to 100 meters deep) was mainly dominated by the genera *CL500-29*, *Flavobacterium*, *Rhodoferax* and *Methylobacter* throughout the year (Figure 1A). Unlike the top layer, the relative abundance of cyanobacteria was quite low, even in November 2019 when *Planktothrix* bloomed in the bottom layer (maximum relative abundance of 27%). Nevertheless, the relative abundance of *Planktothrix* rapidly increased in December 2019 and January 2020. In March 2020, the bacteria community was suddenly dominated by genus *Flavobacterium* (60%), a proliferation which rapidly decreased by May 2020.

Unlike *P. rubescens*, picocyanobacterial genus *Cyanobium* was mostly restricted to the top of the water column, specifically up to 20 meters of depth and was mostly abundant from July to October (Figure 3B). Conversely, genus *Pseudoanabaena* was typically found at depths from 20 to 40 meters from May to July, although lower abundances were also observed in deeper layers of the water column in winter (February 2020). In general, genus *Aphanizomenon* showed

lower relative abundances, but sporadic dominance could be observed from 10 to 30 meters deep in November 2019.

3.4 Environmental conditions associated with *Planktothrix rubescens*

The dominance of *P. rubescens* OTUs was coincident with an observed decrease of water temperature, pH and solar irradiation, and an increase in the wind speed (Supplementary Figure S6). Figure 4 shows the specific environmental values associated with a higher number of reads identified as *P. rubescens*. Specifically, proliferation of *P. rubescens* was associated with low water temperatures (ranging from 9°C–12°C), a pH value of 7.8, low solar irradiation (50 W/m^2), conductivity values between 0.2–0.22 µS/cm, very low turbidity (0.8 NTU), oxygen saturation between 90%–100%, dissolved oxygen between 10–11 mg/L and mostly associated to the productive layer.

3.5 Bacterioplankton biomass and diversity indices

We monitored the concentration of 16S rRNA genes using qPCR analysis as a proxy of bacterioplankton biomass abundance (Figure 5A). The concentration of the 16S rRNA gene in the samples ranged from 5.97×10^3 to 5.31×10^8 genome copies (gc)/L and overall, the mean value was 5.31×10^7 gc/L (Figure 5). A peak in the concentration of 16S rRNA gene was observed in January 2020 with values ranging from 2.1×10^8 to nearly 10^9 gc/L. Bacterioplankton abundance was generally higher in the top of the water column (0–30 m) during periods of stratification (summer, autumn), but equivalent to the values of the bottom layer during deep mixing in winter. Our data shows that higher number of reads identified as *P. rubescens* coincide with the lowest abundances of 16S rRNA gene, and highest estimates of bacteria abundance were only observed when *P. rubescens* reads were very low.

The spatiotemporal distribution of the taxonomic diversity in the studied communities (measured as Chao1 indices) is shown in Figure 5B. Chao1 indices ranged from few hundred up to nearly 4,000 in March, and from July to November 2020. While occasionally higher indices were determined in the bottom layer of the water column, these differences were not statistically significant. Temporal analysis of the taxonomic diversity (Figure 5B) showed higher Chao1 values (up to almost 4,000) during lake stratification in summer and autumn. Lower Chao1 values (below 1,000) were observed from November 2019 until early February 2020 and again from March to June 2020. Taxonomic diversity was positively associated with sunlight, wind speed and phosphorus concentrations, and negatively associated with rain, dissolved oxygen, and chlorophyll a concentration (Supplementary Figure S10).

Functional diversity was also assessed using Chao1 indices and its spatiotemporal distribution along the water column is shown in Figure 5C. Higher functional diversity was observed in the bottom layer, particularly from February to June 2020 and unlike taxonomic diversity, differences observed between top and bottom layers were statistically significant in a *t*-test (p-value = 0.0019). The functional diversity of the bacteria communities was higher from January to May 2020, with one exception in March 2020. No clear trend could be identified between functional and taxonomic diversity (Supplementary Figure S9) and functional diversity was positively associated with nutrient concentrations and negatively correlated with temperature, pH, and chlorophyll a concentration (Supplementary Figure S10). As described for the abundance of 16S rRNA gene, high relative abundances of the *P. rubescens* can be associated with lower estimates of PICRUSt2-predicted functional diversity in the water column, and higher diversity was mostly observed at times when the relative abundance of *P. rubescens* was low (Figure 5C).

3.6 PICRUSt2-predicted functions associated with the dominance of *Planktothrix rubescens*

In this study, PICRUSt2 predictions were based on 12,748 OTUs and generated a total of 308 features. Low NSTI values (<0.15), suggest that the samples share a close phylogenetic relationship and are well-suited for analysis with PICRUSt2. In our extensive dataset, composed of 218 lake water samples, weighted NSTI values ranged from 0.05 to 0.347 with a mean value of 0.220 ± 0.06, suggesting a reasonable reliability of the obtained predictions (Langille et al., 2013). The most abundant KEGG pathways predicted from the sequencing results belonged to the categories of cellular processes, environmental information processing, genetic information processing and microbial metabolism. Table 1 shows a list of the PICRUSt2-predicted functional pathways that were correlated with the number of reads identified as *P. rubescens*. Overall, *P. rubescens* reads were positively correlated with diverse metabolic functions such as genetic information processing, carbohydrate metabolism, photosynthesis, glycan biosynthesis, amino acid metabolism, degradation of xenobiotics and the biosynthesis of secondary metabolites. Among all these functions, photosynthesis proteins, including antenna proteins, replication, recombination and repair proteins, carbohydrate metabolism, carotenoid biosynthesis and the biosynthesis of macrolides were the ones with higher correlation coefficients.

Differential abundance tests implemented in LefSe allowed us to identify taxonomic groups and functional pathways that characterized diverse sampling dates (LDA scores above 3; Supplementary Figure S8; Figure 6). These analyses show that in January 2020, 2 months after the start of the dominance of *P. rubescens*, functional markers in the water column were related to the processing of genetic information, including functions involved in replication and repair, as well as translation. From February 2020, the water column became enriched in functions relating to chemotaxis, cell motility and secretion. March 2020 was characterized by an enrichment in cellular processes and signaling, metabolism of amino acids, bacterial secretion and the synthesis of membrane and intracellular molecules. No functional biomarkers were identified for months between May and September 2020. In September 2020, the water column had shifted to display a wide diversity of metabolic pathways such as those involved in the degradation of xenobiotics, amino acids, lipids, and the synthesis of transporters. Later in December 2020, the water column showed a new increase in the abundance of functions related to photosynthesis, genetic information processing and repair, as well as the metabolism of amino acids, sugars, and other cofactors.

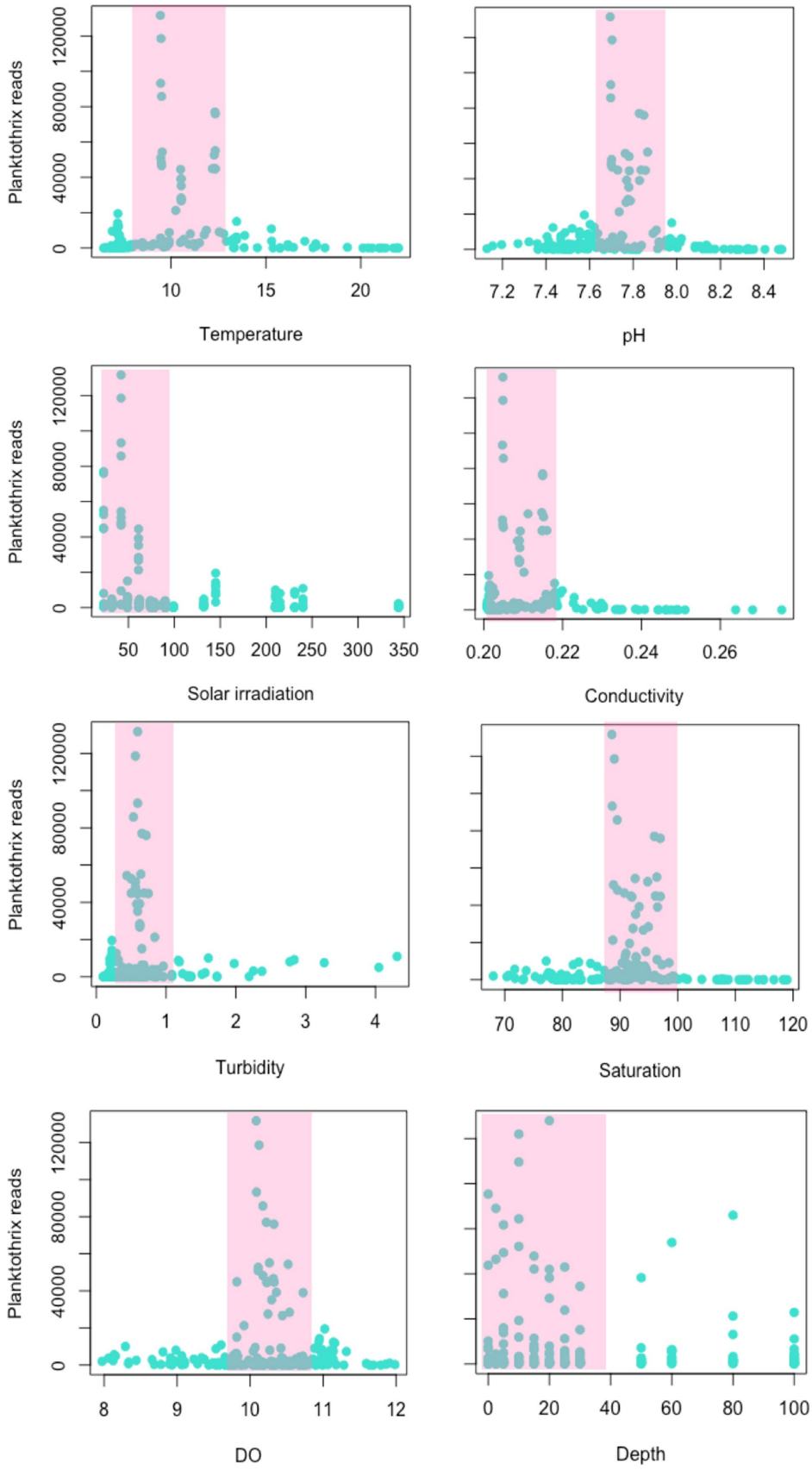

FIGURE 4
Environmental variables associated with the increase of *Planktothrix rubescens* in the current study. Temperature is presented in Celsius degrees, conductivity is in µS/cm, global solar irradiation in Wm^{-2}, turbidity in NTU, oxygen saturation in %, DO in mg/L and depth is in meters. The abundance of *Planktothrix rubescens* reads was extracted for each sample of the study ($n = 218$).

TABLE 1 PICRUSt2 predicted functional pathways showing significant correlations with *Plankthotrix rubescens* reads.

General processes	Predicted KEGG pathway	Correlation coefficient	*p*-value
Biosynthesis of secondary metabolites	Butirosin and neomycin biosynthesis	0.540521783	4.44E−16
	Isoquinoline alkaloid biosynthesis	0.521254299	7.77E−15
Carbohydrate metabolism	Starch and sucrose metabolism	0.517889545	1.24E−14
Cellular processes and signaling	Sporulation	0.590309636	0
	Signal transduction mechanisms	0.518700664	1.11E−14
Energy metabolism	**Photosynthesis—antenna proteins**	**0.812632671**	0
	Photosynthesis proteins	**0.802461181**	0
	Photosynthesis	**0.796149456**	0
	Carbon fixation in photosynthetic organisms	0.523303743	5.77E−15
Environmental information processing	Ion channels	0.534312261	1.33E−15
Genetic information processing	**Replication, recombination and repair proteins**	**0.735462236**	0
	Restriction enzyme	0.686880751	0
	RNA transport	0.565224507	0
	RNA degradation	0.514858556	1.87E−14
Glycan biosynthesis and metabolism	N-Glycan biosynthesis	0.612298906	0
	Glycosyltransferases	0.522179583	6.66E−15
Metabolism	**Carbohydrate metabolism**	**0.701319679**	0
	Others	0.637005874	0
	Amino acid metabolism	0.558735588	0
Metabolism of cofactors and vitamins	Ubiquinone and other terpenoid-quinone biosynthesis	0.597394151	0
	Porphyrin and chlorophyll metabolism	0.571232153	0
	Lipoic acid metabolism	0.549014081	0
Metabolism of terpenoids and polyketides	**Carotenoid biosynthesis**	**0.809793148**	0
	Biosynthesis of 12, 14, and 16-membered macrolides	**0.749152832**	0
	Biosynthesis of vancomycin group antibiotics	0.526431044	3.77E−15
	Polyketide sugar unit biosynthesis	0.50728973	5.13E−14
Metabolism, enzyme families	Protein kinases	0.659465394	0
	Peptidases	0.512782765	2.46E−14
Xenobiotics degradation and metabolism	Chlorocyclohexane and chlorobenzene degradation	0.65212298	0
	Atrazine degradation	0.555279076	0

All *p*-values were $<4.44e10^{-14}$ and only correlations with Pearson correlation coefficient larger than 0.50 and pertinent to prokaryotes are shown here. KEGG pathways with coefficients larger than 0.7 are highlighted in bold.

4 Discussion

In this study we characterized the diversity and spatiotemporal dynamics of cyanobacteria communities in Lake Geneva, a large deep mesotrophic lake, and explored the environmental and biological factors that may be associated with dominance of *P. rubescens* in the water column. We confirmed that *P. rubescens* is the dominant cyanobacteria in the lake and that its blooms reduce bacterioplankton abundance and diversity leading to community divergence. Our results showed that the top layer of the water column (spanning from 0 to 30 meters depth) was particularly enriched with three genera of cyanobacteria (*Planktothrix*, *Cyanobium* and *Pseudoanabaena*), as well as *Limnohabitans* (a member of phylum *Verrucomicrobia*) (Kraemer et al., 2021). The most abundant bacteria genera were *CL500-29 marine group*, *Flavobacterium*, *Planktothrix*, *CL500-3*, *hgcl clade* and *Rhodoferax*, which are consistent with genera typically found in other freshwater ecosystems (Newton et al., 2011). Reads belonging to genus *Planktothrix* were exclusively identified as *P. rubescens*, confirming the widespread and dominance of this potentially toxic cyanobacteria in Lake Geneva, as previously described in Lake Zurich and other lakes recovering from eutrophication in the area (Jacquet et al., 2005; Fernández Castro et al., 2021). Our results also highlighted the previously unknown dominance of diverse picocyanobacterial species in the lake belonging to genus *Cyanobium*, which appear particularly abundant in the top of the water column during stratification periods. Reads classified as members of genus *Pseudoanabaena* could be identified as *Pseudoanabaena foetida* and were mostly abundant during May and June at depths from 10 to 30 meters.

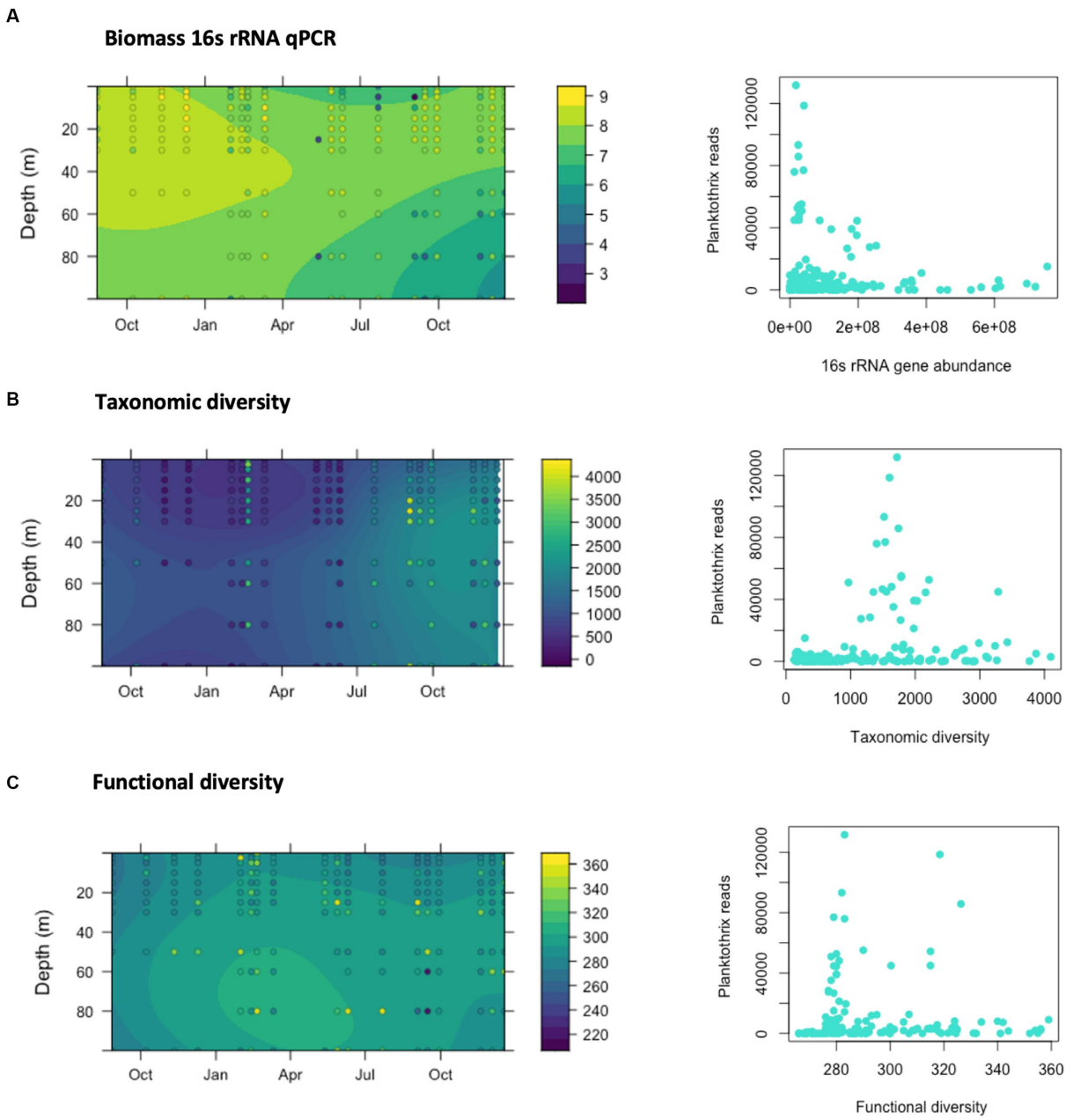

FIGURE 5
Relationship between the dominance of *Planktothrix rubescens* reads, 16srRNA gene abundance and diversity estimations. **(A)** Abundance of the 16S rRNA gene determined by qPCR in lake samples collected across different depths and dates from August 2019 to December 2020. Results are represented as Log10 genomic copies per liter of lake water. **(B)** Estimates of taxonomic diversity according to Chao1 indices. **(C)** Estimates of functional diversity according to Chao1 indices, calculated from the predicted KEGG pathways obtained using PICRUST2.

As expected from these sequencing observations, a high abundance of PICRUSt2-predicted functional pathways dedicated to photosynthesis and the metabolism of cofactors and vitamins was identified in top layers of the water column, where light conditions are favorable for the proliferation of cyanobacteria. While cyanobacteria were dominant in shallow water layers, the bottom layer (from 30 to 100 meters deep) was instead characterized by a high relative abundance of non-photosynthetic bacteria such as genera *Nitrospira* (important in nitrification) and *Methylobacter* (motile bacteria involved in methane metabolism) (Tsagkari and Sloan, 2018; van Grinsven et al., 2020; Bayer et al., 2021). At the functional level, bacteria in this layer appeared particularly active in cellular processes including cell motility, membrane transport and the metabolism of carbohydrates, which may be released from the lake's sediments due to the degradation of organic matter and during the sedimentation process (She et al., 2021). Previous research in Lake Baikal (Russia) Soutourina et al. (2001) has shown that warm temperatures may inhibit the motility of bacteria isolates, thus it possible that bacteria motility in Lake Geneva's bottom layers is favored by cold and stable temperatures.

The study revealed seasonal variations in the abundance of different genera. *Planktothrix* dominated during late autumn and

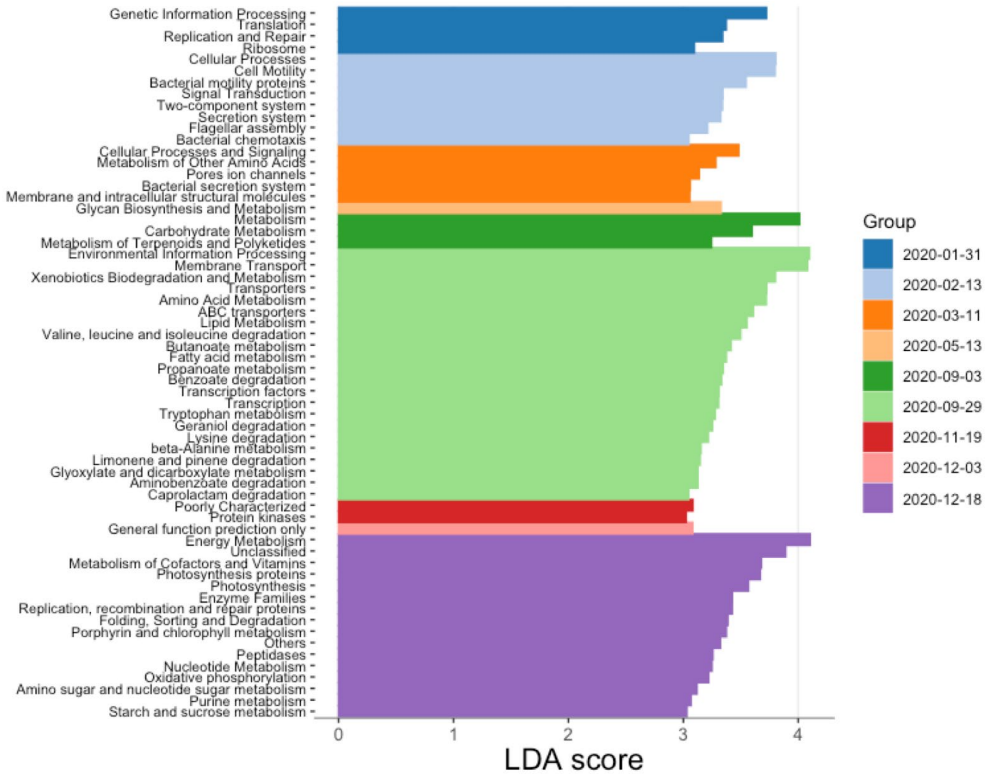

FIGURE 6
PICRUSt-predicted functional markers for different dates. The determination of the markers was done using Lefse algorithm based on KEGG pathway predictions obtained with PICRUSt2. LDA stands for linear discriminant analysis.

winter, followed by an increase in *Pseudanabaena* towards the end of winter. In spring, there was a notable increase in the relative abundance of *Cyanobium*, especially in the upper water layers, which continued to dominate during the summer across different depths. Previous research conducted investigating the competitive dynamics between *Planktothrix* and *Pseudoanabaena* provided insights indicating that temperature alone does not emerge as the primary determinant influencing the displacement one genus by the other (Su et al., 2022). Instead, this observation suggests that the ecological succession may, in part, be elucidated by the differential light requirements of these two genera. Notably, previous monitoring campaigns conducted by the International Commission for the protection of the waters of Lake Geneva (CIPEL) have demonstrated a late-winter augmentation in phytoplankton abundance in the lake (CIPEL, 2020). The biomass of phytoplankton in water bodies impacts the light extinction coefficient, thereby influencing the distribution of short-wave radiation (Rinke et al., 2010). Although both genera were identified as specialists adapted to low-irradiance conditions, *Pseudanabaena* may exhibit lower light requirements compared to *Planktothrix*.

In stratified lakes, nutrient availability may be diminished in the epilimnion due to their confinement in deeper layers (Zhang et al., 2021). The observed rise in the relative prevalence of genus *Cyanobium* during late spring could be attributed to the scarcity of nutrients within the upper regions of the water column. The small size of picocyanobacteria, combined with their relatively expansive surface area, endows them with exceptional efficiency and resilience, potentially accounting for their widespread distribution and prevalence (Callieri and Stockner, 2000). Their cell size, in conjunction with minimal diffusion boundary layers and a heightened surface area per unit volume, confers upon these minuscule phytoplankton cells a competitive advantage in nutrient poor waters, facilitating enhanced nutrient absorption and efficient utilization for growth and maintenance (Davey et al., 2008). Moreover, owing to their prokaryotic cellular structure, they demand less energy for metabolic upkeep (Quiroga et al., 2021). To provide a comparative perspective, research by Padisák et al. (2003) underscores that the surface-to-volume ratio of *Planktothrix* stands at 0.57, whereas that of *Cyanobium* is substantially higher at 6.73 (Padisák et al., 2003). This disparity might elucidate the inverse correlation observed between *Cyanobium* and nutrient levels, implying that nutrient availability may not act as a limiting factor for this genus, in contrast to its potential impact on *Pseudanabaena* and *Planktothrix*.

Beta-diversity analyses revealed that an increase of community dissimilarity was coincident with sampling dates in which genera *Planktothrix* and *Flavobacterium* were dominant in number of reads. *Planktothrix* is a potentially toxic cyanobacteria known in temperate freshwater ecosystems for its capacity of producing harmful blooms and cyanotoxins, such as microcystins, that cause significant ecological and human health impacts (Blom et al., 2003; Knapp et al., 2021). In this study, dominance (understood as high relative abundance of reads) of *P. rubescens* began in November 2019, associated with a decrease in water temperature, pH and solar irradiation, and an increase in wind speed, which may have contributed to the dispersion of *Planktothrix* filaments from a metalimnetic refuge layer to the rest of the water column, as described for Lake Zurich (Fernández Castro

et al., 2021). In this study, the proliferation of *Planktothrix* was associated with very specific environmental conditions: water temperatures ranging from 9°C to 12°C, pH of 7.8, solar irradiation of around 50 W/m^2, conductivity values between 0.2–0.22 µS/cm, very low turbidity (0.8 NTU), oxygen saturation between 90%–100% and dissolved oxygen values between 10–11 mg/L. In consistence, other authors have also identified the role of solar irradiance and light winds as drivers for the seasonal cycling of *P. rubescens* in Lake Zurich (Fernández Castro et al., 2021; Knapp et al., 2021).

Our results showed that the proliferation of *Planktothrix* was associated with lower 16S rRNA gene abundances, and lower taxonomic and functional diversity estimates as determined by Chao1 indices. Notably, both taxonomic and functional diversity recovered to achieve their maximum annual values upon resolution of the *Planktothrix* bloom. This may suggest that the effects of *Planktothrix* proliferation on bacterioplankton diversity may be only observed over short time periods, and that blooms could ultimately promote functional diversity in the community. This is a novel hypothesis that requires further research. In agreement with the observations of this study, cyanobacteria blooms in lakes have been previously known to have a significant impact on the diversity and functions of bacteria communities. For instance, a study conducted on Lake Agawam (United States) found that cyanobacteria and bacteria abundances have an inverse relationship (Jankowiak and Gobler, 2020). Similarly, recent studies have linked the dynamics of certain cyanobacterial species with microbial community successions, changes in diversity, and dynamic functions during harmful cyanobacterial blooms in a freshwater lake and in lake sediments (Woodhouse et al., 2016; Li et al., 2020; Yang et al., 2021).

The effects of cyanobacteria, and more specifically *Planktothrix*, on specific bacterioplankton functions have previously received less attention in the literature. Here, proliferation of *P. rubescens* was associated with higher abundance PICRUSt2-predicted pathways involved in photosynthesis, replication and repair pathways, metabolism of carbohydrates and the biosynthesis of carotenoid and macrolides [compounds that are share similarities of structure, assembly, and chemical composition with microcystins (Tillett et al., 2000; Barboza et al., 2017; Bouaïcha et al., 2019)]. These functions are consistent with the function of *Planktothrix* as a photosynthetic bacterium, which may need to replicate efficiently to produce blooms and repair its genome from the harmful effects of sunlight, thus producing microcystins and accumulating carbohydrates for modulating buoyancy in the water column (Utkilen et al., 1985). LefSe analyses showed that the proliferation of *Planktothrix* induced seasonal changes on the functional profile of the studied water column. For example, in winter we found an increase in PICRUSt2-predicted functions involving genetic information processing, cell motility and chemotaxis, as well as photosynthesis and sugar metabolism. Conversely, in summer, the bacteria communities in the water column were associated with the metabolism of certain compounds such as xenobiotics, amino acids and lipids. During its autumn proliferation, *Planktothrix* was mostly found in the top 30 meters, progressing down the water column through winter deep mixing. During spring and summer, *Planktothrix* likely regulated its vertical position in the water column using gas vesicles and other physiological changes (Utkilen et al., 1985) to find refuge at deeper layers (around 20–30 meters), close to the metalimnion with suitable irradiation conditions (Knapp et al., 2021).

Our sequencing results suggest an increase of the dominance of genus Flavobacterium after the bloom of *P. rubescens*. Increase of *Flavobacterium* reads was associated with higher pH conditions, abundant precipitations, low water temperatures and low solar irradiation. *Flavobacteria* (family Flavobacteriaceae, phylum Bacteroidota), are non-spore-forming, strictly aerobic, motile by gliding and can degrade complex organic compounds such as polysaccharides (Fernández-Gómez et al., 2013; Waśkiewicz and Irzykowska, 2014; Kraut-Cohen et al., 2021). *Flavobacterium* have been previously described as main responders to phytoplankton blooms and were the dominant heterotrophic bacteria in the cyanobacteria phycosphere during blooms (Kim et al., 2019, 2020; Bartlau et al., 2022). We hypothesize that the proliferation of genus *Flavobacterium* observed in this study occurred as a response to the bloom of *P. rubescens* and an increase of water temperature and sunlight irradiation, and that they contributed to the degradation of dead *P. rubescens* filaments. The increase of *Flavobacterium* was associated with PICRUSt2-predicted functional pathways involved in the metabolism of amino acids, secretion systems and the synthesis of membrane and intracellular structural molecules, which may serve *Flavobacterium* to degrade organic matter in the water column.

To conclude, our study has shed light on the diversity and dynamics of cyanobacteria communities in Lake Geneva and confirmed the dominance of *P. rubescens* in this mesotrophic lake. In addition, our study has also shown that picocyanobacteria may be more relevant for the lake's ecology than previously thought. Overall, these observations emphasize the need for further cyanobacteria monitoring in Lake Geneva, which serves a source of drinking water for approximately 900,000 people (Huisman et al., 2018). Particularly, with regards to the production of cyanotoxins by the herein identified species. Moreover, we have identified environmental conditions that may favor the proliferation of *P. rubescens* and established a link between dominance of *P. rubescens* and community dissimilarity, and the bacterioplankton biomass and diversity. These observations have some implications for the biological consequences of climate change. Global warming is expected to prolong lake stratification periods, which may induce abnormal oxygenation and nutrient dynamics within the water column (Weckström et al., 2016). Our findings suggest that summer stratification and winter deep mixing are important events that influence the proliferation of *P. rubescens*, as well as the abundance, composition, diversity and functioning of a deep mesotrophic lake such as Lake Geneva. In Lake Geneva, the proliferation of *P. rubescens* led to a loss of bacteria diversity along the entire water column in the short-term. While we were able to show that the functional richness of the community was maintained, and even stimulated by the bloom of *P. rubescens*, it is still necessary to better understand the environmental drivers and ecological consequences of these blooms to better anticipate the potential biological consequences of climate change in non-eutrophic freshwater ecosystems.

Data availability statement

Raw sequence data are available at NCBI with a BioProject ID PRJNA974682 and accession numbers from SAMN36273484 to SAMN36273698. The obtained OTU table, taxon identification table

and environmental data on the water column are deposited in Zenodo repository with number (doi: 10.5281/zenodo.7957172).

Author contributions

AC: Conceptualization, Funding acquisition, Investigation, Supervision, Writing – original draft, Writing – review & editing. CC: Methodology, Writing – review & editing. OS: Formal analysis, Writing – review & editing. AG: Data curation, Writing – review & editing. HC: Methodology, Writing – review & editing. NP: Methodology, Writing – review & editing. CW: Data curation, Writing – review & editing. TK: Formal analysis, Resources, Writing – review & editing. SJ: Writing – review & editing.

Funding

The author(s) declare financial support was received for the research, authorship, and/or publication of this article. This project, entitled "Local adaptation of bacteria communities in Lake Geneva (LAC)" was funded by the Limnology Center (EPFL) in 2019.

Acknowledgments

The authors would like to thank the entire team from LéXPLORE platform, for their administrative and technical support and for LéXPLORE core dataset. The authors specially acknowledge Sébastien Lavanchy and Guillaume Cunillera for their technical assistance during our sampling campaigns. The authors also recognize LéXPLORE five partner institutions: Eawag, EPFL, University of Geneva, University of Lausanne and CARRTEL (INRAE-USMB). In addition, we thank Patrick Katriner for carrying out the nutrient analysis.

Conflict of interest

The authors declare that the research was conducted in the absence of any commercial or financial relationships that could be construed as a potential conflict of interest.

Publisher's note

All claims expressed in this article are solely those of the authors and do not necessarily represent those of their affiliated organizations, or those of the publisher, the editors and the reviewers. Any product that may be evaluated in this article, or claim that may be made by its manufacturer, is not guaranteed or endorsed by the publisher.

Supplementary material

The Supplementary material for this article can be found online at: https://www.frontiersin.org/articles/10.3389/fmicb.2023.1295193/full#supplementary-material

References

Amorim, C. A., and Moura, A. N. (2021). Ecological impacts of freshwater algal blooms on water quality, plankton biodiversity, structure, and ecosystem functioning. *Sci. Total Environ.* 758:143605. doi: 10.1016/j.scitotenv.2020.143605

Barboza, G., Gorlach-Lira, K., Sassi, C., and Sassi, R. (2017). Microcystins production and antibacterial activity of cyanobacterial strains of *Synechocystis*, *Synechococcus* and *Romeria* isolated from water and coral reef organisms of Brazilian coast. *Rev. Biol. Trop.* 65:890. doi: 10.15517/rbt.v65i3.29437

Bartlau, N., Wichels, A., Krohne, G., Adriaenssens, E. M., Heins, A., Fuchs, B. M., et al. (2022). Highly diverse flavobacterial phages isolated from North Sea spring blooms. *ISME J.* 16, 555–568. doi: 10.1038/s41396-021-01097-4

Bayer, B., Saito, M. A., McIlvin, M. R., Lücker, S., Moran, D. M., Lankiewicz, T. S., et al. (2021). Metabolic versatility of the nitrite-oxidizing bacterium *Nitrospira marina* and its proteomic response to oxygen-limited conditions. *ISME J.* 15, 1025–1039. doi: 10.1038/s41396-020-00828-3

Berdjeb, L., Ghiglione, J. F., and Jacquet, S. (2011). Bottom-up versus top-down control of hypo- and epilimnion free-living bacterial community structures in two neighboring freshwater lakes. *Appl. Environ. Microbiol.* 77, 3591–3599. doi: 10.1128/AEM.02739-10

Blom, J. F., Bister, B., Bischoff, D., Nicholson, G., Jung, G., Süssmuth, R. D., et al. (2003). Oscillapeptin J, a new grazer toxin of the freshwater cyanobacterium *Planktothrix rubescens*. *J. Nat. Prod.* 66, 431–434. doi: 10.1021/np020397f

Bolyen, E., Rideout, J. R., Dillon, M. R., Bokulich, N. A., Abnet, C. C., Al-Ghalith, G. A., et al. (2019). Reproducible, interactive, scalable and extensible microbiome data science using QIIME 2. *Nat. Biotechnol.* 37, 852–857. doi: 10.1038/s41587-019-0209-9

Bouaïcha, N., Miles, C., Beach, D., Labidi, Z., Djabri, A., Benayache, N., et al. (2019). Structural diversity, characterization and toxicology of microcystins. *Toxins* 11:714. doi: 10.3390/toxins11120714

Callieri, C., and Stockner, J. (2000). Picocyanobacteria success in oligotrophic lakes: fact or fiction? *J. Limnol.* 59:72. doi: 10.4081/jlimnol.2000.72

Chorus, I., and Welker, M. *Toxic cyanobacteria in water* (2021) London CRC Press

CIPEL. *Rapport-scientifique CIPEL 2020–2021* (2020).

Darrin, S., and Bryan, C. (2021). "Data visualization with ggplot" in *Probability, statistics, and data*

Davey, M., Tarran, G. A., Mills, M. M., Ridame, C., Geider, R. J., and LaRoche, J. (2008). Nutrient limitation of picophytoplankton photosynthesis and growth in the tropical North Atlantic. *Limnol. Oceanogr.* 53, 1722–1733. doi: 10.4319/lo.2008.53.5.1722

Douglas, G. M., Maffei, V. J., Zaneveld, J. R., Yurgel, S. N., Brown, J. R., Taylor, C. M., et al. (2020). PICRUSt2 for prediction of metagenome functions. *Nat. Biotechnol.* 38, 685–688. doi: 10.1038/s41587-020-0548-6

Ernst, B., Hoeger, S. J., O'Brien, E., and Dietrich, D. R. (2009). Abundance and toxicity of *Planktothrix rubescens* in the pre-alpine Lake Ammersee, Germany. *Harmful Algae* 8, 329–342. doi: 10.1016/j.hal.2008.07.006

Ezzedine, J. A., Jacas, L., Desdevises, Y., and Jacquet, S. (2020). *Bdellovibrio* and like organisms in Lake Geneva: an unseen elephant in the room? *Front. Microbiol.* 11:98. doi: 10.3389/fmicb.2020.00098

Fenchel, T. (2002). Microbial behavior in a heterogeneous world. *Science* 296, 1068–1071. doi: 10.1126/science.1070118

Fernández Castro, B., Sepúlveda Steiner, O., Knapp, D., Posch, T., Bouffard, D., and Wüest, A. (2021). Inhibited vertical mixing and seasonal persistence of a thin cyanobacterial layer in a stratified lake. *Aquat. Sci.* 83, 351–365. doi: 10.1007/s00027-021-00785-9

Fernández-Gómez, B., Richter, M., Schüler, M., Pinhassi, J., Acinas, S. G., González, J. M., et al. (2013). Ecology of marine bacteroidetes: a comparative genomics approach. *ISME J.* 7, 1026–1037. doi: 10.1038/ismej.2012.169

Fox, J., and Weisberg, S. *An R companion to applied regression*, *3*. Thousand Oaks, CA: Sage. (2019).

Gallina, N., Beniston, M., and Jacquet, S. (2017). Estimating future cyanobacterial occurrence and importance in lakes: a case study with *Planktothrix rubescens* in Lake Geneva. *Aquat. Sci.* 79, 249–263. doi: 10.1007/s00027-016-0494-z

Grothendieck, G. (2008). Lattice: multivariate data visualization with R. *J. Stat. Softw.* 25, 1–3. doi: 10.18637/jss.v025.b02

Guedes, I. A., Rachid, C. T. C. C., Rangel, L. M., Silva, L. H. S., Bisch, P. M., Azevedo, S. M. F. O., et al. (2018). Close link between harmful cyanobacterial dominance and associated bacterioplankton in a tropical eutrophic reservoir. *Front. Microbiol.* 9:424. doi: 10.3389/fmicb.2018.00424

Hijmans, R. J., and van Etten, J. *raster: geographic analysis and modeling with raster data*. R package version 2.5-2 (2015).

Huisman, J., Codd, G. A., Paerl, H. W., Ibelings, B. W., Verspagen, J. M. H., and Visser, P. M. (2018). Cyanobacterial blooms. *Nat. Rev. Microbiol.* 16, 471–483. doi: 10.1038/s41579-018-0040-1

Jacquet, S., Briand, J. F., Leboulanger, C., Avois-Jacquet, C., Oberhaus, L., Tassin, B., et al. (2005). The proliferation of the toxic cyanobacterium *Planktothrix rubescens* following restoration of the largest natural French lake (Lac du Bourget). *Harmful Algae* 4, 651–672. doi: 10.1016/j.hal.2003.12.006

James, G., Witten, D., and Hastie, T. *Introduction to statistical learning with applications in R. Synthesis lectures on mathematics and statistics volume 11* (2019).

Jankowiak, J. G., and Gobler, C. J. (2020). The composition and function of microbiomes within *Microcystis* colonies are significantly different than native bacterial assemblages in two north American Lakes. *Front. Microbiol.* 11:1016. doi: 10.3389/fmicb.2020.01016

Jia, J., Shi, W., Chen, Q., and Lauridsen, T. L. (2017). Spatial and temporal variations reveal the response of zooplankton to cyanobacteria. *Harmful Algae* 64, 63–73. doi: 10.1016/j.hal.2017.02.008

Kanehisa, M., and Goto, S. K. E. G. G. (2000). Kyoto encyclopedia of genes and genomes. *Nucleic Acids Res.* 28, 27–30. doi: 10.1093/nar/28.1.27

Kim, M., Lee, J., Yang, D., Park, H. Y., and Park, W. (2020). Seasonal dynamics of the bacterial communities associated with cyanobacterial blooms in the Han River. *Environ. Pollut.* 266:115198. doi: 10.1016/j.envpol.2020.115198

Kim, M., Shin, B., Lee, J., Park, H. Y., and Park, W. (2019). Culture-independent and culture-dependent analyses of the bacterial community in the phycosphere of cyanobloom-forming *Microcystis aeruginosa*. *Sci. Rep.* 9:20416. doi: 10.1038/s41598-019-56882-1

Klindworth, A., Pruesse, E., Schweer, T., Peplies, J., Quast, C., Horn, M., et al. (2013). Evaluation of general 16S ribosomal RNA gene PCR primers for classical and next-generation sequencing-based diversity studies. *Nucleic Acids Res.* 41:e1. doi: 10.1093/nar/gks808

Knapp, D., Fernández Castro, B., Marty, D., Loher, E., Köster, O., Wüest, A., et al. (2021). The red harmful plague in times of climate change: blooms of the cyanobacterium *Planktothrix rubescens* triggered by stratification dynamics and irradiance. *Front. Microbiol.* 12:705914. doi: 10.3389/fmicb.2021.705914

Kraemer, B. M., Pilla, R. M., Woolway, R. I., Anneville, O., Ban, S., Colom-Montero, W., et al. (2021). Climate change drives widespread shifts in lake thermal habitat. *Nat. Clim. Chang.* 11, 521–529. doi: 10.1038/s41558-021-01060-3

Kraut-Cohen, J., Shapiro, O. H., Dror, B., and Cytryn, E. (2021). Pectin induced colony expansion of soil-derived *Flavobacterium* strains. *Front. Microbiol.* 12:065981. doi: 10.3389/fmicb.2021.651891

Krztoń, W., Kosiba, J., Pociecha, A., and Wilk-Woźniak, E. (2019). The effect of cyanobacterial blooms on bio- and functional diversity of zooplankton communities. *Biodivers. Conserv.* 28, 1815–1835. doi: 10.1007/s10531-019-01758-z

Langille, M. G. I., Zaneveld, J., Caporaso, J. G., McDonald, D., Knights, D., Reyes, J. A., et al. (2013). Predictive functional profiling of microbial communities using 16S rRNA marker gene sequences. *Nat. Biotechnol.* 31, 814–821. doi: 10.1038/nbt.2676

Li, H., Barber, M., Lu, J., and Goel, R. (2020). Microbial community successions and their dynamic functions during harmful cyanobacterial blooms in a freshwater lake. *Water Res.* 185:116292. doi: 10.1016/j.watres.2020.116292

Liu, C., Cui, Y., Li, X., and Yao, M. (2021). Microeco: an R package for data mining in microbial community ecology. *FEMS Microbiol. Ecol.* 97:fiaa255. doi: 10.1093/femsec/fiaa255

Mankiewicz-Boczek, J., and Font-Nájera, A. (2022). Temporal and functional interrelationships between bacterioplankton communities and the development of a toxigenic *Microcystis* bloom in a lowland European reservoir. *Sci. Rep.* 12:19332. doi: 10.1038/s41598-022-23671-2

Minaudo, C., Odermatt, D., Bouffard, D., Rahaghi, A. I., Lavanchy, S., and Wüest, A. (2021). The imprint of primary production on high-frequency profiles of Lake optical properties. *Environ. Sci. Technol.* 55, 14234–14244. doi: 10.1021/acs.est.1c02585

Newton, R. J., Jones, S. E., Eiler, A., McMahon, K., and Bertilsson, S. (2011). A guide to the natural history of freshwater lake bacteria. *Microbiol. Mol. Biol. Rev.* 75, 14–49. doi: 10.1128/MMBR.00028-10

Padisák, J., Barbosa, F., Koschel, R., and Krienitz, L. (2003). Deep layer cyanoprokaryota maxima in temperate and tropical lakes. *Adv. Limnol.* 58, 175–199.

Paerl, H. W., and Otten, T. G. (2013). Harmful cyanobacterial blooms: causes, consequences, and controls. *Microb. Ecol.* 65, 995–1010. doi: 10.1007/s00248-012-0159-y

Paerl, H. W., and Paul, V. J. (2012). Climate change: links to global expansion of harmful cyanobacteria. *Water Res.* 46, 1349–1363. doi: 10.1016/j.watres.2011.08.002

Parvathi, A., Zhong, X., Ram, A. S. P., Jacquet, S., and Jacquet, S. (2014). Dynamics of auto-and heterotrophic picoplankton and associated viruses in Lake Geneva. *Hydrol. Earth Syst. Sci.* 18, 1073–1087. doi: 10.5194/hess-18-1073-2014

Posch, T., Köster, O., Salcher, M. M., and Pernthaler, J. (2012). Harmful filamentous cyanobacteria favoured by reduced water turnover with lake warming. *Nat. Clim. Chang.* 2, 809–813. doi: 10.1038/nclimate1581

Quiroga, M. V., Huber, P., Ospina-Serna, J., Diovisalvi, N., Odriozola, M., Cueto, G. R., et al. (2021). The dynamics of picocyanobacteria from a hypereutrophic shallow lake is affected by light-climate and small-bodied zooplankton: a 10 years cytometric time-series analysis. *FEMS Microbiol. Ecol.* 97:fiab055. doi: 10.1093/femsec/fiab055

R Core Team. *R: A language and environment for statistical computing* (R foundation for statistical computing, Vienna, (2012). Available at: http://www.R-project.org (2015).

Rinke, K., Yeates, P., and Rothhaupt, K. O. (2010). A simulation study of the feedback of phytoplankton on thermal structure via light extinction. *Freshw. Biol.* 55, 1674–1693. doi: 10.1111/j.1365-2427.2010.02401.x

Segata, N., Izard, J., Waldron, L., Gevers, D., Miropolsky, L., Garrett, W. S., et al. (2011). Metagenomic biomarker discovery and explanation. *Genome Biol.* 12:R60. doi: 10.1186/gb-2011-12-6-r60

She, Z., Wang, J., He, C., Pan, X., Li, Y., Zhang, S., et al. (2021). The stratified distribution of dissolved organic matter in an AMD lake revealed by multi-sample evaluation procedure. *Environ. Sci. Technol.* 55, 8401–8409. doi: 10.1021/acs.est.0c05319

Soutourina, O. A., Semenova, E. A., Parfenova, V., Danchin, A., and Bertin, P. (2001). Control of bacterial motility by environmental factors in polarly flagellated and peritrichous bacteria isolated from Lake Baikal. *Appl. Environ. Microbiol.* 67, 3852–3859. doi: 10.1128/AEM.67.9.3852-3859.2001

Su, M., Zhu, Y., Andersen, T., Wang, X., Yu, Z., Lu, J., et al. (2022). Light-dominated selection shaping filamentous cyanobacterial assemblages drives odor problem in a drinking water reservoir. *npj Clean Water* 5:37. doi: 10.1038/s41545-022-00181-2

Sukenik, A., Quesada, A., and Salmaso, N. (2015). Global expansion of toxic and non-toxic cyanobacteria: effect on ecosystem functioning. *Biodivers. Conserv.* 24, 889–908. doi: 10.1007/s10531-015-0905-9

Tillett, D., Dittmann, E., Erhard, M., von Döhren, H., Börner, T., and Neilan, B. A. (2000). Structural organization of microcystin biosynthesis in *Microcystis aeruginosa* PCC7806: an integrated peptide-polyketide synthetase system. *Chem. Biol.* 7, 753–764. doi: 10.1016/S1074-5521(00)00021-1

Tsagkari, E., and Sloan, W. T. (2018). The role of the motility of methylobacterium in bacterial interactions in drinking water. *Water* 10:1386. doi: 10.3390/w10101386

Utkilen, H. C., Oliver, R. L., and Walsby, A. E. (1985). Buoyancy regulation in a red Oscillatoria unable to collapse gas vacuoles by turgor pressure. *Arch. Hydrobiol.* 102, 319–329. doi: 10.1127/archiv-hydrobiol/102/1985/319

van Grinsven, S., Sinninghe Damsté, J. S., Abdala Asbun, A., Engelmann, J. C., Harrison, J., and Villanueva, L. (2020). Methane oxidation in anoxic lake water stimulated by nitrate and sulfate addition. *Environ. Microbiol.* 22, 766–782. doi: 10.1111/1462-2920.14886

Walsby, A. E. (2005). Stratification by cyanobacteria in lakes: a dynamic buoyancy model indicates size limitations met by *Planktothrix rubescens* filaments. *New Phytol.* 168, 365–376. doi: 10.1111/j.1469-8137.2005.01508.x

Walsby, A. E., Ng, G., Dunn, C., and Davis, P. A. (2004). Comparison of the depth where *Planktothrix rubescens* stratifies and the depth where the daily insolation supports its neutral buoyancy. *New Phytol.* 162, 133–145. doi: 10.1111/j.1469-8137.2004.01020.x

Walsby, A. E., Schanz, F., and Schmid, M. (2006). The Burgundy-blood phenomenon: a model of buoyancy change explains autumnal waterblooms by *Planktothrix rubescens* in Lake Zürich. *New Phytol.* 169, 109–122. doi: 10.1111/j.1469-8137.2005.01567.x

Waśkiewicz, A., and Irzykowska, L. (2014). "*Flavobacterium* spp.—characteristics, occurrence, and toxicity" in *Encyclopedia of food microbiology*. 2nd ed

Weckström, K., Weckström, J., Huber, K., Kamenik, C., Schmidt, R., Salvenmoser, W., et al. (2016). Impacts of climate warming on alpine lake biota over the past decade. *Arct. Antarct. Alp. Res.* 48, 361–376. doi: 10.1657/AAAR0015-058

Woodhouse, J. N., Kinsela, A. S., Collins, R. N., Bowling, L. C., Honeyman, G. L., Holliday, J. K., et al. (2016). Microbial communities reflect temporal changes in cyanobacterial composition in a shallow ephemeral freshwater lake. *ISME J.* 10, 1337–1351. doi: 10.1038/ismej.2015.218

Wüest, A., Bouffard, D., Guillard, J., Ibelings, B. W., Lavanchy, S., Perga, M. E., et al. (2021a). LéXPLORE: a floating laboratory on Lake Geneva offering unique lake research opportunities. *Wiley Interdiscip. Rev. Water* 8:e1544. doi: 10.1002/wat2.1544

Wüest, A., Bouffard, D., Guillard, J., Ibelings, B. W., Lavanchy, S., Perga, M.-E., et al. (2021b). A floating laboratory on Lake Geneva offering unique lake research opportunities. *Wiley Interdiscip. Rev. Water* 8:2022:e1572. doi: 10.1002/wat2.1572, (Erratum)

Yang, Y., Chen, J., Chen, X., Jiang, Q., Liu, Y., and Xie, S. (2021). Cyanobacterial bloom induces structural and functional succession of microbial communities in eutrophic lake sediments. *Environ. Pollut.* 284:117157. doi: 10.1016/j.envpol.2021.117157

Yankova, Y., Villiger, J., Pernthaler, J., Schanz, F., and Posch, T. (2016). Prolongation, deepening and warming of the metalimnion change habitat conditions of the harmful filamentous cyanobacterium *Planktothrix rubescens* in a prealpine lake. *Hydrobiologia* 776, 125–138. doi: 10.1007/s10750-016-2745-3

Zhang, J., Kong, J. D., Shi, J., and Wang, H. (2021). Phytoplankton competition for nutrients and light in a stratified lake: a mathematical model connecting epilimnion and hypolimnion. *J. Nonlinear Sci.* 31:35. doi: 10.1007/s00332-021-09693-6

Zheng, X., Xiao, L., Ren, J., and Yang, L. (2008). The effect of a *Microcystis aeruginosa* bloom on the bacterioplankton community composition of lake Xuanwa. *J. Freshw. Ecol.* 23, 297–304. doi: 10.1080/02705060.2008.9664202

frontiers | Frontiers in Microbiology

TYPE Original Research
PUBLISHED 11 January 2024
DOI 10.3389/fmicb.2023.1322548

OPEN ACCESS

EDITED BY
Yueming Qu,
UK Centre for Ecology and Hydrology (UKCEH), United Kingdom

REVIEWED BY
Jiwen Liu,
Ocean University of China, China
Isabelle Fournier,
UK Centre for Ecology and Hydrology (UKCEH), United Kingdom

*CORRESPONDENCE
Li Zhao
✉ zhaoli@qdio.ac.cn
Wuchang Zhang
✉ wuchangzhang@qdio.ac.cn

†These authors have contributed equally to this work and share first authorship

RECEIVED 20 November 2023
ACCEPTED 29 December 2023
PUBLISHED 11 January 2024

CITATION
Li S, Dong Y, Sun X, Zhao Y, Zhao L, Zhang W and Xiao T (2024) Seasonal and spatial variations of *Synechococcus* in abundance, pigment types, and genetic diversity in a temperate semi-enclosed bay. *Front. Microbiol.* 14:1322548. doi: 10.3389/fmicb.2023.1322548

Seasonal and spatial variations of *Synechococcus* in abundance, pigment types, and genetic diversity in a temperate semi-enclosed bay

Suheng Li[1,2,3,4†], Yi Dong[1,2,3†], Xiaoxia Sun[1,2,3,5], Yuan Zhao[1,2,3], Li Zhao[1,2,3*], Wuchang Zhang[1,2,3*] and Tian Xiao[1,2,3]

[1]CAS Key Laboratory of Marine Ecology and Environmental Sciences, Institute of Oceanology, Chinese Academy of Sciences, Qingdao, China, [2]Laboratory for Marine Ecology and Environmental Science, Qingdao National Laboratory for Marine Science and Technology, Qingdao, China, [3]Center for Ocean Mega-Science, Chinese Academy of Sciences, Qingdao, China, [4]University of Chinese Academy of Sciences, Beijing, China, [5]Jiaozhou Bay Marine Ecosystem Research Station, Institute of Oceanology, Chinese Academy of Sciences, Qingdao, China

Synechococcus is abundant and globally widespread in various marine environments. Seasonal and spatial variations in *Synechococcus* abundance, pigment types, and genetic diversity were investigated based on flow cytometric analysis and high-throughput sequencing of *cpcBA* operon (encoding phycocyanin) and *rpoC1* gene (encoding RNA polymerase) in a temperate semi-enclosed bay. *Synechococcus* abundance exhibited seasonal variations with the highest value in summer and the lowest value in winter, which was consistent with temperature variation. Three pigment types of *Synechococcus* type 1, type 2, and type 3 were distinguished based on *cpcBA* operon, which displayed obvious variations spatially between the inner and the outer bay. Freshwater discharge and water turbidity played important roles in regulating *Synechococcus* pigment types. *Synechococcus* assemblages were phylogenetically diverse (12 different lineages) based on *rpoC1* gene and dominated by three core lineages S5.1-I, S5.1-IX, and S5.2-CB5 in different seasons. Our study demonstrated that *Synechococcus* abundance, pigment types, and genetic diversity displayed variations seasonally and spatially by different techniques, which were mainly driven by temperature, salinity, nutrients, and turbidity. The combination of more technical means provides more information for studying *Synechococcus* distribution. In this study, three pigment types of *Synechococcus* were discriminated simultaneously by dual lasers flow cytometer for the first time.

KEYWORDS

***Synechococcus*, pigment types, cpcBA operon, genetic diversity, rpoC1 gene, co-dominate, temperate semi-enclosed bay**

Introduction

Synechococcus is abundant and globally widespread in various marine environments from coastal waters to open ocean, from equatorial to polar seas, and generally reaches its highest abundance in nutrient-rich coastal waters (Farrant et al., 2016; Paulsen et al., 2016; Doré et al., 2022). As an important component of the marine microbial food web, *Synechococcus* contributes significantly in carbon biomass and primary productivity (Olson et al., 1990; Flombaum et al., 2013).

Synechococcus assemblages are both phenotypically and phylogenetically diverse. Three main pigment types of *Synechococcus* were divided depending on different phycobiliprotein (PBP) compositions, including type 1, type 2 and type 3. Type 1 merely contains phycocyanin (PC, encoded by *cpcBA* operon), which binds the phycocyanobilin (PCB, A_{max} = 620 nm). Type 2 contains both PC and phycoerythrin-I (PE-I, encoded by *cpeBA* operon), which binds both PCB and phycoerythrobilin (PEB, A_{max} = 550 nm). In addition to PC and PE-I, type 3 also contains phycoerythrin-II (PE-II, encoded by *mpeBA*), which binds PCB, PEB and phycourobilin (PUB, A_{max} = 495 nm). Studies have revealed that different pigment types prefer different light niches (Voros et al., 1998; Stomp et al., 2004, 2007). Type 1 was usually abundant in turbid estuarine waters where red light dominates (Stomp et al., 2007; Wang et al., 2011). Type 2 usually appears in the coastal and shelf waters where yellow-green light prevails, whereas type 3 appears in the oceanic waters with high transparency (Wood et al., 1998). The phylogeny of *cpcBA* and *cpeBA* operons encoding for PC and PE-I, respectively, has been widely applied to distinguish different pigment types (Larsson et al., 2014; Xia et al., 2017a; Wang et al., 2021, 2022a). Based on flow cytometric analysis, PC-only (type 1) and PE-rich (type 2 + type 3) *Synechococcus* could also be discriminated with 488 nm and 640 nm lasers (Liu et al., 2014).

Synechococcus strains also display a wide genetic diversity (Grébert et al., 2018). Various gene markers such as 16S rRNA gene (Dufresne et al., 2008), the 16S-23S rRNA gene internal transcribed spacer (ITS, Choi and Noh, 2009), the nitrate reductase gene (*narB*, Paerl et al., 2008), the nitrogen regulatory gene (*ntcA*, Post et al., 2011), and the ribulose-1,5-bisphosphate carboxylase/oxygenase large subunit gene (*rbcL*, Chen et al., 2006), and the RNA polymerase gene (*rpoC1*, Xia et al., 2015) have been gradually developed to study the genetic diversity of *Synechococcus*. The *rpoC1* gene is able to distinguish most of the *Synechococcus* lineages, which has been proven to be a robust gene marker (Wang et al., 2022b). Based on 16S rRNA phylogeny, *Synechococcus* strains can be classified into three subclusters, labeled subclusters 5.1, 5.2, and 5.3 (namely S5.1, S5.2 and S5.3). S5.1 is the most widespread and abundant, and contains at least 20 lineages with Clades I, II, III, and IV being the most common lineages. Clades I always coexists with Clades IV in cold and temperate nutrient-rich coastal environments (Zwirglmaier et al., 2008; Tai and Palenik, 2009; Sohm et al., 2016). Clades II and III preferentially thrive in subtropical/tropical warm waters (Post et al., 2011). S5.2 is mainly found in estuarine and brackish waters, which always copes with variations in salinity (Xia et al., 2017a, 2023). It is more abundant in river-influenced coastal waters such as in the Chesapeake Bay (Chen et al., 2004, 2006; Cai et al., 2010), Pearl River estuary (Xia et al., 2015, 2017a), and Baltic Sea (Haverkamp et al., 2008). S5.3 was less studied than S5.1 and S5.2, which has been reported in various marine and freshwater environments, with relatively low abundance in the global ocean (Farrant et al., 2016; Xia et al., 2023). Environmental factors such as temperature (Doré et al., 2022), salinity (Xia et al., 2017a, 2023), and nutrients (Sohm et al., 2016) are known to influence the distribution of *Synechococcus* lineages.

Temporal and spatial variations of *Synechococcus* pigment types and phylogenetic clades have been reported in coastal and estuarine waters (Tai and Palenik, 2009; Post et al., 2011; Liu et al., 2014; Chung et al., 2015; Xia et al., 2015). The dominance of *Synechococcus* pigment types shifted from PC-rich (type 1) to PE-rich (type 2 + type 3) along salinity/turbidity gradients. In the subtropical Pearl River estuary, PC-rich *Synechococcus* dominated in a turbid estuary in summer, whereas PE-rich *Synechococcus* dominated in coastal waters all over the year (Liu et al., 2014). A similar phenomenon has also been observed in the subtropical estuary in the Gulf of Mexico (Murrel and Lores, 2004). *Synechococcus* assemblages exhibited distinct seasonal variations in the estuarine and coastal waters. A study conducted in the Pearl River estuary has shown that S5.1-II and S5.1-IX dominated in winter. Whereas in summer S5.1-II and S5.1-VI co-occurred in the coastal water and S5.2, freshwater *Synechococcus*, and *Cyanobium* co-occurred in the estuary owing to high temperature, freshwater input during summer monsoon (Xia et al., 2015). In the California Current, S5.1-II and S5.1-III co-occurred in the months leading to the *Synechococcus* spring bloom whereas S5.1-I and S5.1-IV co-dominated during the bloom (Tai and Palenik, 2009).

The temperate Jiaozhou Bay (35°8′–36°18′N, 120°04′–120°23′E) is a typical shallow semi-enclosed bay in the western Yellow Sea, southeast of Shandong Peninsula (Xing et al., 2017). The bay is connected with the Yellow Sea through a narrow bay mouth (~2.5 km). More than 10 small rivers enter the bay and become the major sources of external nutrient input. Freshwater discharge exhibits seasonal fluctuation with the highest discharge in summer and the lowest discharge in spring and winter (Cui et al., 2021). Connected with the Yellow Sea and surrounded by Qingdao City (population > 10 million), Jiaozhou Bay is affected by both natural and anthropogenic factors, such as East Asian monsoon, Yellow Sea Water Mass, seasonal freshwater inflow, half-day tidal exchange with the open sea (Feng et al., 2018) and rapid economic development, aquaculture, and pollutions from the land. Due to the interaction between natural changes and human activities, as well as long-term monitoring and systematic investigation, Jiaozhou Bay has become a "model" bay of temperate coastal ecosystem for ecological investigation (Zhao et al., 2020; Cui et al., 2021).

The importance of *Synechococcus* in the temperate Jiaozhou Bay has been realized and seasonal variations of PE-rich *Synechococcus* abundance have been studied (Zhao et al., 2005; Yang et al., 2012). However, little is known about PC-only *Synechococcus*, which has long been overlooked and might be an important component in the studied area. It is worth noting that the distribution of PC-only *Synechococcus* abundance in the temperate Jiaozhou Bay is still unknown. Studies have revealed that freshwater discharge plays an important role in determining the proportion of PC/PE *Synechococcus* in the surface water of ECS (Chung et al., 2015) and Pearl River Estuary (Xia et al., 2015). Similarly, Jiaozhou Bay is connected with several small rivers, seasonal freshwater discharge might be an important factor influencing the variation of PE-rich and PC-only *Synechococcus* in this area. It is necessary to further study *Synechococcus* in multiple aspects. Besides, the pigmentation and genetic diversity of *Synechococcus* are still unclear in this temperate coastal ecosystem. Therefore, seasonal and spatial variations of *Synechococcus* abundance, pigment types and genetic diversity were conducted among three selected stations over a seasonal cycle using dual lasers of flow cytometry and high-throughput sequencing of *cpcBA* operon (encoding phycocyanin) and *rpoC1* gene (encoding RNA polymerase). The relationship between environmental variables (temperature, salinity, turbidity, and nutrients) and *Synechococcus* abundance, pigmentation and lineages will be discussed in temperate coastal ecosystems.

Materials and methods

Sample collection

Three stations were sampled in February (winter), May (spring), August (summer) and October (autumn) in 2021 in Jiaozhou Bay. The estuarine station A5 and central bay station C1 locate inside the bay, whereas the coastal station D7 locates outside the bay (Figure 1). All samples were taken during daytime. Surface seawater was collected at each station and divided for analysis. The samples for flow cytometric analyses (4 mL) were fixed with paraformaldehyde (final concentration 1%) after collection and then frozen in liquid nitrogen until analysis in the laboratory (Marie et al., 2000). For molecular study, 1.2 L of water was pre-filtered by 200 μm sieve, then filtered onto a 0.22 μm (50 mm) mixed cellulose membrane. The membrane was flash-frozen in liquid nitrogen and then frozen at −80°C until used for DNA extraction.

Temperature and salinity were measured by a AAQ1183-1F CTD probe (Alec, Japan). Chlorophyll *a* (Chl *a*) concentration was determined using a Turner Designs model-10 fluorometer. The measurement of nutrient concentrations (NO_3^-, NO_2^-, NH_4^+ and PO_4^{3-}) were conducted by a QuAAtro-SFA Analyzer (Bran-Lubbe Co., Germany). The concentration of suspended particulate matter (SPM) was measured using the method outlined by Shi et al. (2023). SPM data in October was missing (unsampled). All of the temperature, salinity, Chl *a*, nutrients, and SPM concentrations data were provided by the Jiaozhou Bay National Marine Ecosystem Research Station.

Flow cytometric analysis of *Synechococcus* abundance

Synechococcus cells were detected using a BD FACSJazz™ flow cytometer (Becton Dickinson) equipped with dual lasers of 488 nm and 640 nm. Forward scatter (FSC), side scatter (SSC), 3 fluorescence signals (green: 530/40 nm, orange: 585/29 nm, red: 692/40 nm) induced by 488 nm laser and red fluorescence (660/20 nm) induced by 640 nm laser were recorded with BD FACS™ Sortware Sorter software. PC-only (type 1) and PE-rich (type 2 + type 3) *Synechococcus* were distinguished from other eukaryotic picoplankton by orange fluorescence and red fluorescence induced by 488 nm laser. No *Prochlorococcus* was detected in Jiaozhou Bay. Type 1 (PC-only) *Synechococcus* was recognized by red fluorescence induced by 488 nm and 640 nm, respectively (Liu et al., 2014). Type 1, type 2, and type 3 *Synechococcus* were separated at the same time using green fluorescence induced by 488 nm and red fluorescence induced by 640 nm (Figure 2). Fluorescent beads (2 μm, Polysciences) were added to each sample as the internal standard. Flow cytometric data were analyzed with Flowjo V10 software.

DNA extraction, PCR amplification

DNA was extracted according to the phenol-chloroform-isoamyl alcohol (25:24:1) method in Haverkamp et al. (2008). For the *cpcBA* operon, the PCR process followed the protocol of Xia et al. (2017a). The *cpcBA* operon was amplified by PCR (94°C for 5 min, followed by 40 cycles at 94°C for 30 s, 55°C for 30 s, and 72°C for 60 s and a final extension at 72°C for 1 min) using primers SyncpcB-Fw (5'-ATGGCTGCTTGCCTGCG-3') and SyncpcA-Rev (5'-ATCTGGGTGGTGTAGGG-3').

For the *rpoC1* gene, a nested PCR process was used (Muhling et al., 2006). Two independent PCRs used the same procedure (95°C for 5 min, followed by 30 cycles at 95°C for 60 s, 51°C for 60 s, and 72°C for 60 s and a final extension at 72°C for 10 min) with different primer sets. The first round's primers were *rpoC1*-N5 and the C-terminal, while the second round's primers were *rpoC1*-39F (5'-GGNATYGTYTGYG AGCGYTG) and *rpoC1*-462R (5'-CGY AGRCFCTTGRTCAGCTT) (Muhling et al., 2006; Xia et al., 2015), where barcode is an eight-base sequence unique to each sample.

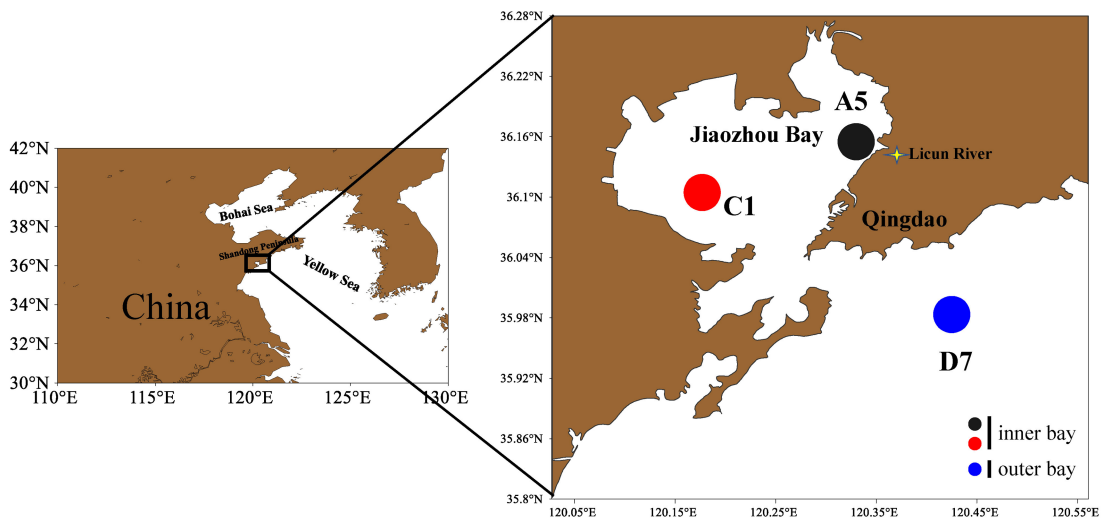

FIGURE 1
Sampling stations in Jiaozhou Bay. Stations A5 and C1 are inner bay and station D7 is outer bay.

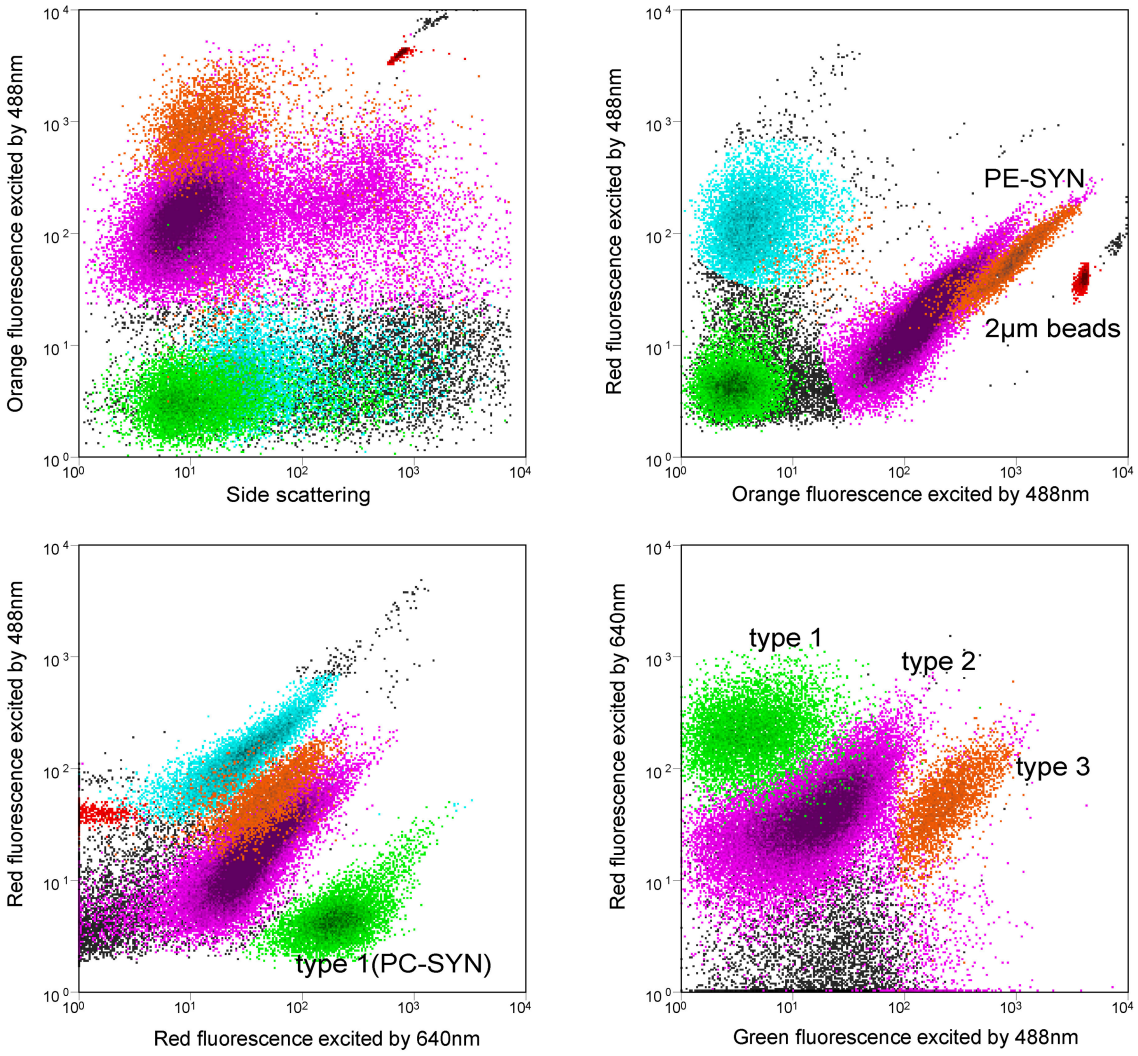

FIGURE 2
Flow cytometric signatures of type 1, type 2, and type 3 *Synechococcus* using a flow cytometer with 488 nm and 640 nm dual lasers. Orange fluorescence represents phycoerythrin (PE); Red fluorescence excited by 488 nm laser indicates chlorophyll *a*, and red fluorescence excited by 640 nm comes from phycocyanin (PC). Note that PUB-containing cells (type 3) have relatively higher green fluorescence than the non-PUB-containing cells (type 2).

Amplicons were extracted from 2% agarose gels and purified using the AxyPrep DNA Gel Extraction Kit (Axygen Biosciences, Union City, CA, United States) according to the manufacturer's instructions.

Library construction and sequencing

SMRTbell libraries were prepared from the amplified DNA by blunt-ligation according to the manufacturer's instructions (Pacific Biosciences). Purified SMRTbell libraries from the Zymo and HMP mock communities were sequenced on dedicated PacBio Sequel II 8 M cells using the Sequencing Kit 2.0 chemistry. All amplicon sequencing was performed by Shanghai Biozeron Biotechnology Co. Ltd. (Shanghai, China).

Processing of sequencing data

PacBio raw reads were processed using the SMRT Link Analysis software version 9.0 to obtain demultiplexed circular consensus sequence (CCS) reads with the following settings: minimum number of passes = 3, minimum predicted accuracy = 0.99. Raw reads were processed through SMRT Portal to filter sequences for length (<300 bp and >700 bp) and quality. Sequences were further filtered by removing barcode, primer sequences, chimeras and sequences if they contained 10 consecutive identical bases. OTUs were clustered with 95% (*cpcBA*); 97% (*rpoC1*), similarity cutoff using UPARSE (version 7.1 http://drive5.com/uparse/) and chimeric sequences were identified and removed using UCHIME (Amato et al., 2013). Representative sequences of OTU were identified using BLASTn against the nt database with an expectation value 1e-50, of which not belonging to

Cyanobacteria were picked out. Reference sequences were listed in the Supplementary Tables S1, S2. There are three copies of the *cpcBA* operon in the genomic sequence of type 1 *Synechococcus* (Six et al., 2007; Xia et al., 2017a). Regarding calculation of the relative abundance of each *Synechococcus* pigment type, the OTU numbers of type 1 were divided by three. For *rpoC1* gene, sequences with less than 90% consistency with the reference sequence are assigned as unclassified.

Phylogenetic analysis of the *rpoC1* and *cpcBA* sequences

The representative sequences of the 30 and 50 most abundant OTUs for the *cpcBA* operon (covered 99.8% of total reads) and *rpoC1* gene (covered 97.9% of total reads) were aligned with the reference sequence (Supplementary Tables S1, S2). Maximum likelihood phylogenetic trees were constructed by Mega-X with the model T92+G (200 bootstraps) and GTR+G+I (200 bootstraps), respectively (Xia et al., 2017a). A heatmap showing the relative abundance of each OTU was formed with TBtools (Wang et al., 2021).

Statistical analyses

The relative abundance of each pigment type and lineage was transformed by square root transformation. Environmental data were transformed by square root transformation and then normalized. Season and station variations of pigment composition and *Synechococcus* assemblages structure were investigated by the UPGMA (unweighted pair-group method with arithmetic means) cluster analysis based on the Bray–Curtis similarity matrix. ANOSIM was used to test differences in pigment composition and *Synechococcus* assemblage structure between groups. SIMPER (similarity percentage procedure) analysis was used to ascertain *Synechococcus* pigment type contributing most to the inner-outer area *Synechococcus* pigment composition dissimilarities and *Synechococcus* lineage contributing most to the four-groups *Synechococcus* assemblage dissimilarities. All the above analyses were conducted by PRIMER 6 (Clarke, 1993). The Spearman correlation analysis of *Synechococcus* abundance and environmental variables was processed by Past 4.06b. The relationships between environmental parameters and pigment composition and *Synechococcus* assemblage were studied by Mantel test using the OmicStudio tools[1] and redundancy analysis (RDA) using CANOCO V5, Monte Carlo permutation tests (500 permutations) can be used to test significant correlations of environmental variables with assemblage structure (Cookson et al., 2006).

Accession numbers

All sequences obtained from this study have been deposited in the National Center for Biotechnology Information (NCBI) Sequence Read Archive (SRA). The BioProject accession number PRJNA996355 (based on *cpcBA*) and PRJNA995918 (based on *rpoC1*).

1 https://www.omicstudio.cn/tool/62

Results

Environmental conditions

Seasonal and spatial variations of environmental variables in Jiaozhou Bay are shown in Figure 3. Three stations A5, C1, and D7 exhibited similar hydrographic features in temperature and salinity. Temperature was highest in summer (August) (27.7–29.2°C) and lowest in winter (February) (3.4–4.7°C). Salinity in summer and autumn (October) was slightly lower than in winter and spring (May). The lowest salinity (27.2) in the estuarine station A5 in summer was mainly attributed to freshwater discharge and summer rainfall. Spatial variations of Chl *a*, SPM and nutrient concentrations (NO_3^-, NO_2^-, NH_4^+, and PO_4^{3-}) differed among three stations with A5 > C1 > D7. SPM was much higher at stations A5 and C1, indicating higher turbidity of the stations. Seasonally, the highest nutrient concentrations including NO_3^-, NO_2^-, NH_4^+, and PO_4^{3-} were mostly detected in autumn, suggesting a relatively nutrient-rich environment in autumn.

Synechococcus abundance based on flow cytometry

Total abundances of *Synechococcus* measured by flow cytometry displayed similar seasonal patterns among three stations (Figure 4). Total *Synechococcus* had the highest abundances in summer and the lowest abundances in winter, which was consistent with temperature variation (Figure 3A). Our data showed that abundances in summer were 2–3 orders of magnitude higher than those in winter. Total *Synechococcus* abundances were positively correlated with temperature ($r = 0.93$, $p < 0.01$; Supplementary Table S3). The highest abundance of *Synechococcus* occurred at station C1 in summer (231.54×10^3 cells mL^{-1}), and the lowest abundance occurred at station C1 in winter (0.1×10^3 cells mL^{-1}) (Figure 4). Flow cytometry allowed us to separate three pigment types of *Synechococcus*, namely type 1 (PC-only *Synechococcus*), type 2, and type 3 (PE-containing *Synechococcus*) (Figure 2). Type 2 was predominant in Jiaozhou Bay and exhibited similar seasonal pattern as total *Synechococcus* abundance, while type 1 and type 3 had the lower abundance with different seasonal variations compared to type 2. Type 2 was more abundant in summer and autumn, with abundances ranging from 10.71×10^3 cells mL^{-1} to 203.76×10^3 cells mL^{-1}. In winter and spring, type 2 was almost negligible (≦41 cells mL^{-1}). Type 1 was less abundant than type 2 with higher abundances in summer. In winter and spring, type 1 was nearly undetected (<20 cells mL^{-1}). Type 3 was less abundant than type 2 and type 1. Seasonal variation of type 3 abundance was similar to type 2 while varied among three stations. Type 2 and type 1 were more abundant at stations A5 and C1, whereas type 3 was slightly more abundant at station D7 (Figure 4). The significance test for the comparison of *Synechococcus* abundance is shown in Supplementary Table S4.

In general, type 1 was more abundant in summer at stations A5 and C1. Type 2 dominated in summer and autumn, which seemed more important at stations A5 and C1. Spearman correlation analysis showed that type 1 and type 2 were positively correlated with temperature ($r = 0.84$, $p < 0.01$ and $r = 0.94$, $p < 0.01$, respectively, Supplementary Table S3), and negatively correlated with salinity ($r = -0.86$, $p < 0.01$ and $r = -0.80$, $p < 0.01$ respectively,

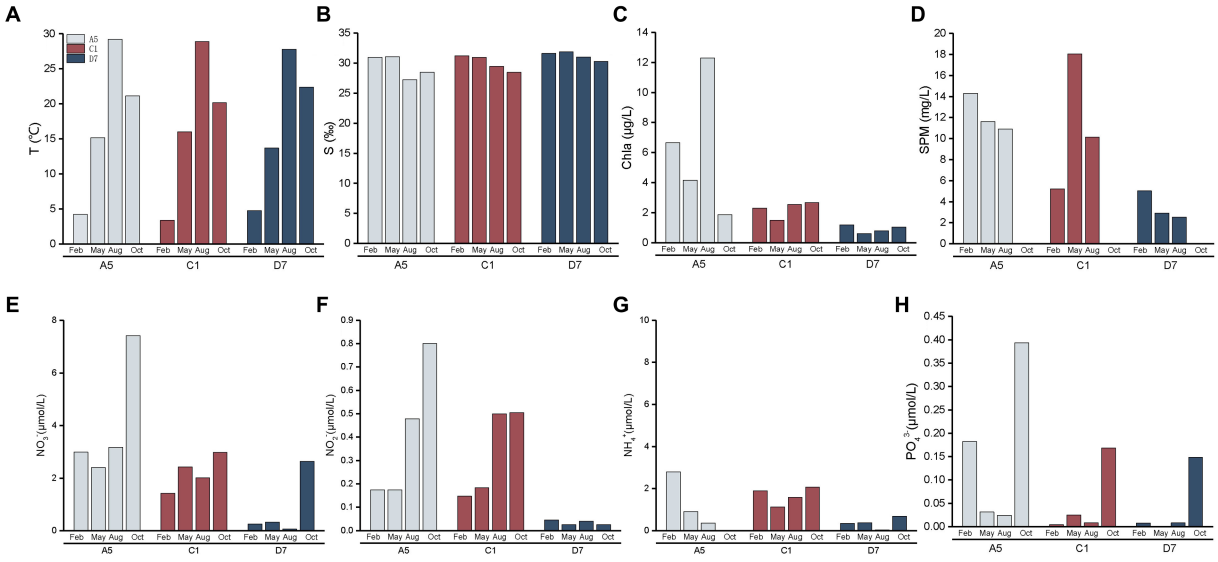

FIGURE 3
Spatial and seasonal variations of environment parameters **(A)**: temperature, **(B)**: salinity, **(C)**: Chl *a*, **(D)**: suspended particulate matter, **(E)**: NO_3^-, **(F)**: NO_2^-, **(G)**: NH_4^+, **(H)**: PO_4^{3-} in Jiaozhou Bay. The data of suspended particulate matter was missing in October.

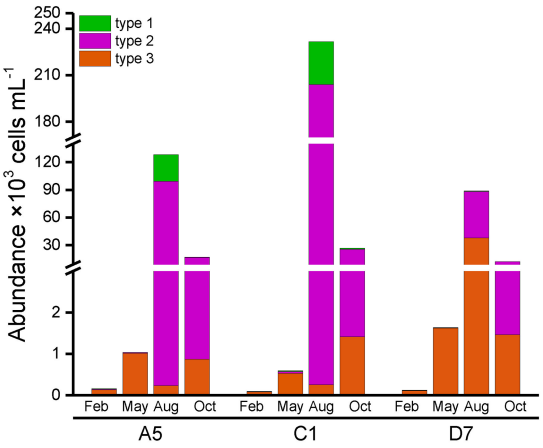

FIGURE 4
Synechococcus abundance measured by flow cytometric analysis.

Supplementary Table S3). On the contrary, type 3 dominated in winter and spring, and was more important at station D7 (Figure 4).

Synechococcus pigment composition based on *cpcBA* gene

The *cpcBA* gene was sequenced for 12 samples (4 seasons × 3 stations) from Jiaozhou Bay. A total of 125,309 high-quality sequences were generated with an average of 10,442 sequences per sample. The diversity of *Synechococcus cpcBA* operon was estimated by the Shannon diversity index, which ranged from 1.21 to 3.98 (Supplementary Table S5). In general, the diversity of *Synechococcus cpcBA* operon differed among stations, with A5 and C1 showing higher diversity and D7 showing lower diversity. Seasonally, the diversity of *Synechococcus cpcBA* operon at station A5 was highest in autumn (3.11) and lowest in spring (1.82). Similarly, station C1 had the highest and lowest diversities in winter (3.98) and spring (1.59), respectively. Station D7 showed lower and less obvious variations, with highest and lowest diversities in summer (2.63) and winter (1.21), respectively.

In the phylogenetic tree based on the *cpcBA* operon, three well-separated clusters (type 1, type 2 and type 3) were formed (Supplementary Figure S1). According to the similarity of pigment composition recognized by UPGMA clustering, 12 samples were classified into two groups: the inner bay and the outer bay (Figure 5). The pigment composition of the two groups were significantly different (ANOSIM, $p < 0.01$). The group in the inner bay was mainly composed of samples from stations A5 and C1, except for Oct-D7. In the inner bay, type 2 was the dominant pigment type, followed by type 1 in summer and spring. The group in the outer bay was mostly composed of samples from station D7, except for Feb-A5. In the outer bay in winter and spring, type 3 was the major pigment type, and followed by type 2. Whereas in sample Aug-D7, type 2 and type 3 co-dominated (Figure 5). The dissimilarities of SIMPER analysis identified the contribution of each pigment type in the inner bay and outer bay. The average dissimilarity between two groups was 39.9%. In the inner bay (station A5 and station C1), *Synechococcus* pigment types were mainly composed of type 2 and type 1. In the outer bay (station D7), it was mainly composed of type 3 and type 2 (Table 1).

Three pigment types of *Synechococcus* type 1, type 2, and type 3 were distinguished based on the phylogenetic analysis of *cpcBA* operon. On the other hand, flow cytometric analysis was also able to separate type 1, type 2, and type 3 (Figure 2; Supplementary Figure S2A) (Olson et al., 1988; Liu et al., 2014). Comparing the relative abundance of type 1, type 2, and type 3 with the two mentioned methods, 9 of 12 samples exhibited a similar distribution pattern. The dissimilarity mainly comes from three samples in the winter and spring in the inner

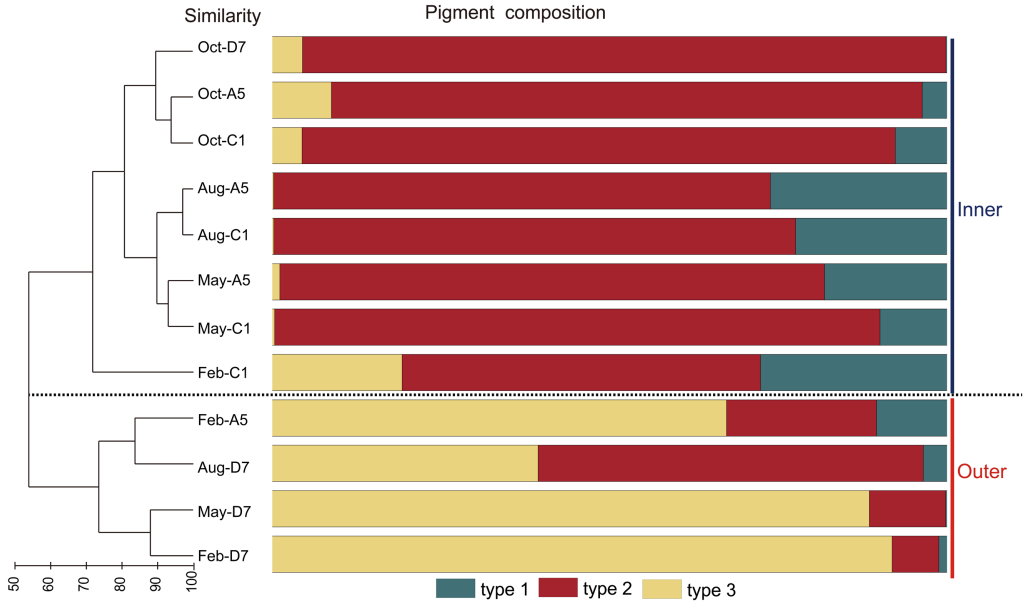

FIGURE 5
Results of UPGMA cluster analysis. *Synechococcus* pigment composition based on the relative abundance of each *Synechococcus* pigment type. The samples formed two groups, inner and outer.

TABLE 1 *Synechococcus* pigment types that contribute most to the *Synechococcus* pigment composition dissimilarities between the inner (stationC1 and stationA5) and outer (station D7) bay stations in Jiaozhou Bay (SIMPER results with a cut-off at 100% cumulative contribution).

Synechococcus pigment types	Contribution (%)	Cumulative contribution (%)	Average abundance (%)	
			Inner	Outer
Type 3	54.21	54.21	19.66	73.37
Type 2	24.35	78.56	69.56	56.48
Type 1	21.44	100	31.11	9.97

bay (Feb-C1, May-C1, and May-A5) with low abundances (Supplementary Figure S2).

Synechococcus genetic diversity based on *rpoC1* gene

The *rpoC1* gene was sequenced for 12 samples (4 seasons × 3 stations) in Jiaozhou Bay. A total of 64,031 high-quality sequences were obtained with an average of 5,336 sequences per sample. The Shannon diversity index of *Synechococcus* assemblages ranged from 3.76 to 4.87. Seasonally, the diversity of *Synechococcus* assemblages was more pronounced in autumn than in other seasons, with the highest and lowest diversity both observed in autumn. Spatially, stations C1 and A5 showed higher diversity than station D7. The Shannon diversity based on the *rpoC1* operon was much higher than that based on the *cpcBA* operon in all the samples (Supplementary Table S5).

Based on our database, 97.6% of the sequences were classified. All three marine *Synechococcus* subclusters (S5.1, S5.2, and S5.3) were detected based on *rpoC1* gene. S5.1 was most abundant in 9 samples with relative abundances ranging from 48.0 to 88.3%. S5.2 was less abundant than S5.1, whereas in samples May-C1, Aug-C1, and Aug-A5, S5.2 outnumbered S5.1 with relative abundances ranging from 50 to 61.4%. S5.3 was a minor component and merely detected in autumn with relative abundances from 6.7 to 18.1%. Freshwater *Synechococcus* (FS) and *Cyanobium* were found in the inner bay with relative abundance ≤4.5% (Supplementary Table S6).

In the phylogenetic tree (Figure 6), 10 clades in total were detected, with S5.1-I, S5.1-IX, and S5.2-CB5 being the most abundant lineages in Jiaozhou Bay. S5.1-I was dominant in winter and spring, whereas S5.1-IX was dominant in autumn. S5.2-CB5 was widespread and abundant (11.2–61.4%) in all the samples and predominant in summer. Most OTUs of S5.1-I in winter and spring were affiliated with *Synechococcus* sp. st235. However, OTU18 and OTU28 merely occurred in spring, which were affiliated with *Synechococcus* sp. CC9311 and CC9617. OTUs belonging to S5.1-IX in summer and autumn were affiliated with *Synechococcus* sp. RS9901 and 59. S5.1-II and S5.1-III were merely observed in summer and autumn, especially in autumn. OTUs of S5.2-CB5 were affiliated with *Synechococcus* sp. WH8007. OTU2, OTU7 and OTU12 of S5.2-CB5 occurred in all the samples, whereas OTU8 and OTU63 mainly occurred in summer and autumn. OTUs of S5.3 were affiliated with *Synechococcus* sp. Minos01 and Minos11, which merely occurred in autumn.

The *Synechococcus* assemblages structure was recognized by UPGMA clustering. According to the similarity of taxonomic composition, 12 samples were classified into four groups:

10.3389/fmicb.2023.1322548

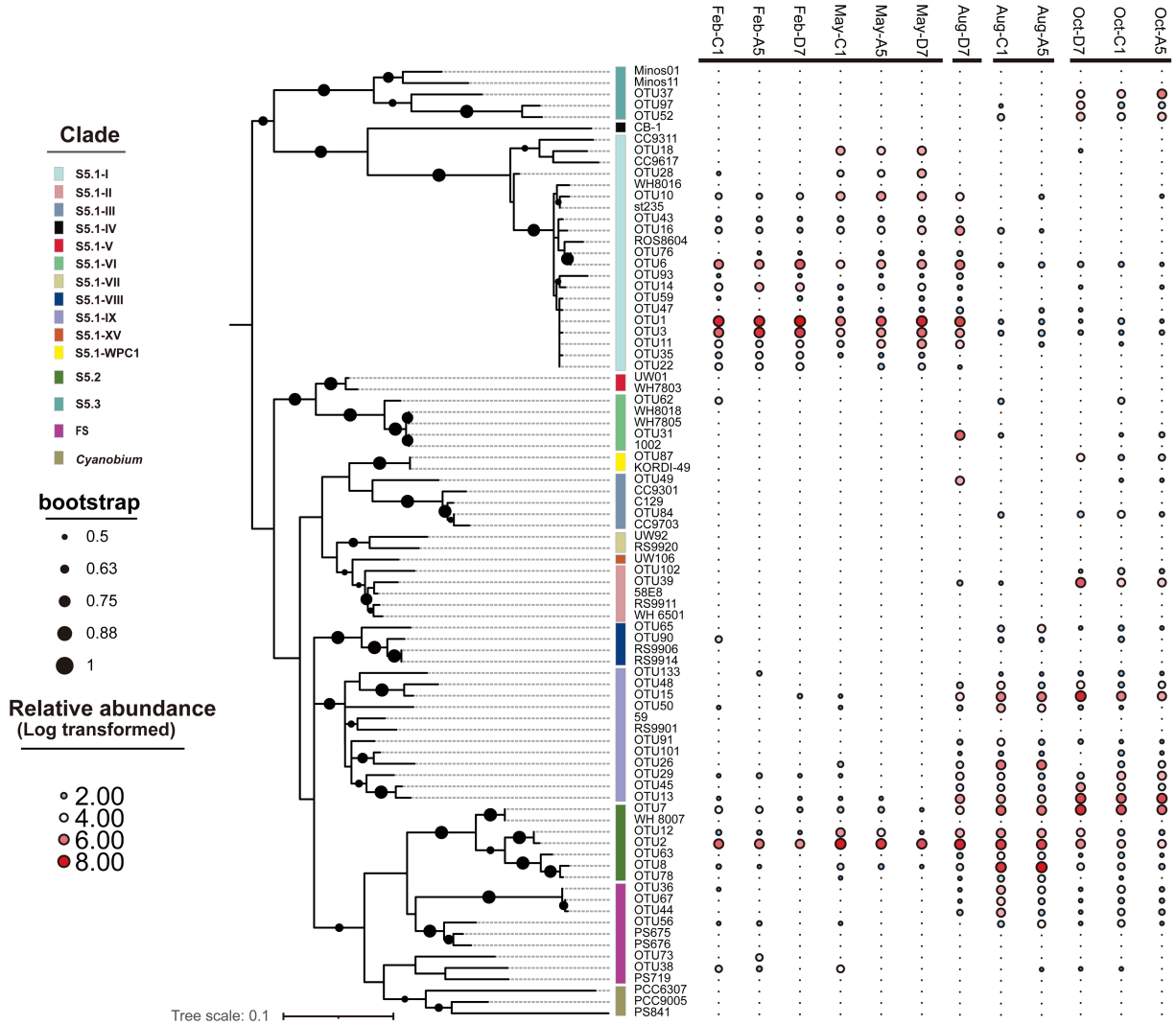

FIGURE 6
Maximum likelihood phylogenetic tree of the 50 most abundant *rpoC1* OTUs across all samples. The heatmap on the right-hand side shows the relative abundance of OTUs in each library (Log transformed). Only nodes with bootstrap values higher than 50% are shown.

Group 1-samples in winter and spring, Group 2-sample in summer at station D7 (Aug-D7), Group 3-samples in summer at stations C1 and A5 (Aug-C1 and Aug-A5), Group 4-samples in autumn (Oct-C1, Oct-A5, and Oct-D7) (Figure 7A). In Group 1, S5.1-I was predominant in most samples and followed by S5.2-CB5. They co-dominated in winter and spring with relative total abundances ranging from 89.6 to 99.5%. The importance of S5.1-I decreased from winter to spring whereas S5.2-CB5 exhibited an opposite trend. In Group 2, S5.1-I and S5.2-CB5 dominated at station D7 in summer with relative abundance of 42.1 and 28.7%, respectively. Besides, S5.1-IX, S5.1-VI, and S5.1-III also contributed to the high abundance with relative abundances of 13.3, 9.4, and 4.9%, respectively. In Group 3, S5.2-CB5 and S5.1-IX co-dominated in summer with their relative total abundances of 79.8 and 87.5% at stations C1 and A5, respectively. Furthermore, S5.1-VIII and S5.1-I were also detected with proportions <3.2%. In Group 4, S5.1-IX became the core lineage, and followed by S5.2-CB5 in autumn. Other *Synechococcus* lineages including S5.1-II, S5.1-III, S5.1-WPC1 and S5.3 also made minor contributions to *Synechococcus* abundance (Supplementary Table S6).

In general, three dominant lineages of *Synechococcus* exhibited distinct seasonal variations in Jiaozhou Bay. S5.1-I decreased gradually from winter to spring (Group 1), and almost disappeared in summer (Group 3) and autumn (Group 4), except for the sample Aug-D7 (Group 2). On the contrary, S5.1-IX was negligible from winter to spring (Group 1), increased gradually from summer (Group 2, 3) and became dominant in autumn (Group 4). S5.2-CB5 was widespread in all the samples and became predominant in summer at station A5 and C1 (Group 3) (Figure 7B).

Impact of environmental variables on *Synechococcus* pigment composition (*cpcBA*) and genetic diversity (*rpoC1*)

Environmental variables and distribution of the *Synechococcus* pigment composition were analyzed by the Mantel test. Temperature (Mantel test, $p = 0.014$) had a significant impact on *Synechococcus*

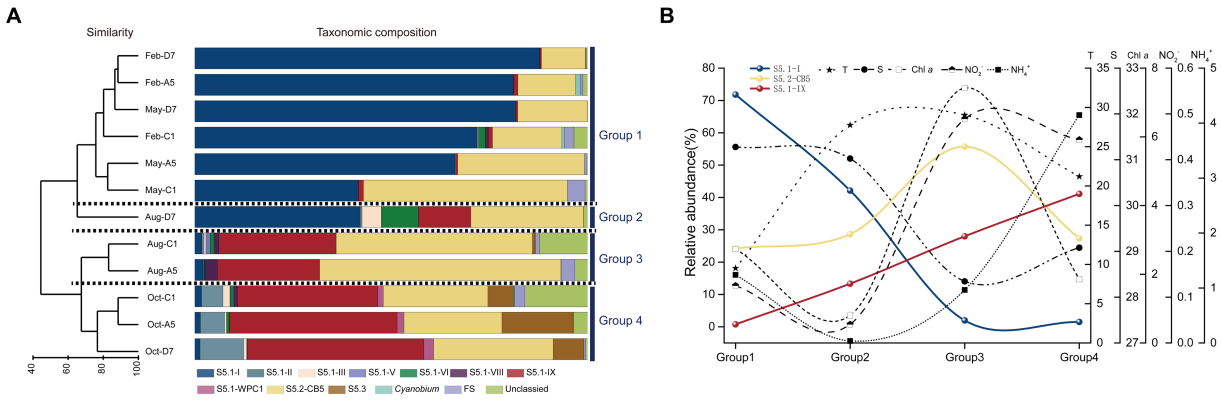

FIGURE 7
Results of UPGMA cluster analysis. *Synechococcus* assemblages composition based on the relative abundance of each *Synechococcus* lineage. The samples formed four groups, Group 1, Group 2, Group 3, and Group 4 **(A)**. The trends in the relative abundance of dominant lineages S5.1-I, S5.1-IX, and S5.2-CB and typical environmental factors-T, S, Chl *a*, NO_2^-, NH_4^+ in the above four groups. The data in each group is the average of the total sample data in the corresponding group. T, temperature; S, salinity **(B)**.

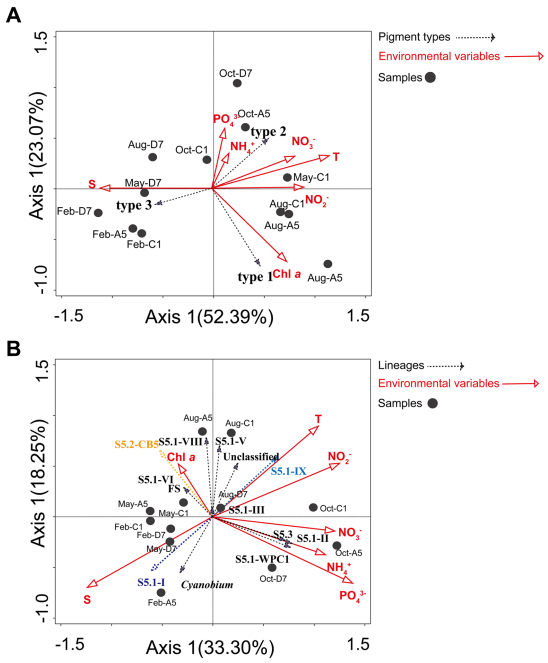

FIGURE 8
RDA analysis. **(A)** The relationship between the distribution of *Synechococcus* pigment types (*cpcBA*) and environmental factors in Jiaozhou Bay. **(B)** The relationship between the distribution of *Synechococcus* lineages (*rpoC1*) and environmental factors in Jiaozhou Bay.

pigment composition. RDA analysis reflects the relationships between *Synechococcus* pigment types and environmental variables (Figure 8A). A Monte Carlo test (499 permutations) showed a high significance for the whole model ($p < 0.001$) and demonstrated that environmental factors affect pigment type distribution. The first two axes explained 52.4 and 23.1% of *Synechococcus* pigment variance, respectively. *Synechococcus* type 1 was positively correlated with Chl *a*. Type 2 was positively correlated with temperature, NO_3^-, NO_2^-, NH_4^+, and PO_4^{3-}, and negatively correlated with salinity. On the contrary, type 3 was positively correlated with salinity, and negatively correlated with temperature and NO_3^-, NO_2^-, NH_4^+, and PO_4^{3-}.

Environmental variables and distribution of the *Synechococcus* assemblages were analyzed by the Mantel test. Temperature ($p < 0.05$), salinity ($p < 0.01$), and PO_4^{3-} ($p < 0.05$) had significant impacts on the distribution of *Synechococcus* assemblages. RDA analysis (Figure 8B) reflects the relationships between *Synechococcus* lineages and environmental variables. A Monte Carlo test (499 permutations) showed a high significance for the whole model ($p < 0.001$) and demonstrated that environmental factors affect lineages distribution. The first two axes explained 33.3 and 18.3% of lineages variance, respectively. S5.1-I was positively correlated with salinity, and negatively correlated with temperature and NO_2^-. On the contrary, S5.1-IX was positively correlated with temperature and NO_2^-, and negatively correlated with salinity. S5.2-CB5 and FS were positively correlated with Chl *a*, and negatively correlated with NO_3^-, NH_4^+, and PO_4^{3-}, whereas S5.1-II, S5.3, and S5.1-WPC1 were positively correlated with NO_3^-, NH_4^+, and PO_4^{3-} and negatively correlated with Chl *a*.

Discussion

Distribution of *Synechococcus* abundance (FCM)

In the temperate Jiaozhou Bay, a clear seasonality in *Synechococcus* abundance was observed, with maximum abundance in summer and minimum abundance in winter (Figure 4). A strong positive correlation was found between temperature and *Synechococcus* abundance ($r = 0.93$, $p < 0.01$), indicating the importance of temperature in regulating *Synechococcus* abundance (Agawin et al., 1998; Mitbavkar et al., 2009). Similar temperature-driven pattern has been reported in Bohai Sea (Wang et al., 2022a), Chesapeake Bay (Cai et al., 2010), and Martha's Vineyard Coastal Observatory

(Hunter-Cevera et al., 2016). High temperature could support rapid growth rate of *Synechococcus* (Wang et al., 2011). In the present study, the optimum temperature range of 27.5–29.5°C in summer seemed to be favorable for high abundance of *Synechococcus* (Figure 3). Under the circumstance of global warming, surface temperature in Jiaozhou Bay showed a rising trend over the past decades. Larger phytoplankton showed a downward trend in species composition and cell abundance (Chen et al., 2023). Accordingly, phytoplankton tend to be small-sized in Jiaozhou Bay and *Synechococcus* may become more and more important in the future.

Besides temperature, salinity could be another important influencing factor. The ratio of PC-only: PE-rich *Synechococcus* abundances decreased with salinity gradient. PC-only *Synechococcus* was more abundant in lower salinity waters whereas PE-rich *Synechococcus* dominated in higher salinity waters (Wang et al., 2011; Rajaneesh and Mitbavkar, 2013; Xia et al., 2017a). Widespread coexistence of PC-only (type 1) and PE-rich (type 2 + type 3) *Synechococcus* have been found in turbid estuarine and coastal waters, such as in the Chesapeake Bay (Wang et al., 2011), Martha's Vineyard Coastal Observatory (Hunter-Cevera et al., 2016), and Pearl River Estuary (Xia et al., 2017a). Similarly in Jiaozhou Bay, type 1 (PC-only) abundance decreased from the inner bay to the outer bay along with salinity increase mainly owing to freshwater discharge (Figures 3, 4). A negative correlation was observed between type 1 abundance and salinity, implying the importance of salinity on type 1 distribution. In the subtropical Hong Kong waters, PC-only *Synechococcus* dominated in the estuarine station in summer, whereas PE-rich *Synechococcus* dominated in the coastal waters all over the year (Liu et al., 2014). Our observations did not agree well with the results in Hong Kong waters, with a much lower abundance of type 1, perhaps owing to lower temperature and lower freshwater discharge in Jiaozhou Bay.

Spatio-temporal variation of *Synechococcus* pigment composition (*cpcBA*)

Niche partitions of *Synechococcus* pigment types have been widely studied (Liu et al., 2014; Xia et al., 2017a; Grébert et al., 2018; Wang et al., 2022a). Type 1 is abundant in low salinity, nutrient-rich, turbid coastal and estuarine waters. Type 2 is preferred in coastal and shelf waters, whereas type 3 dominates in oligotrophic open oceans (Xia et al., 2017b; Grébert et al., 2018). The phylogeny of *cpcBA* operon (encoding PC) and *cpeBA* operon (encoding PE) were applied to distinguish *Synechococcus* pigment types. Since type 1 (PC-only *Synechococcus*) could not be recognized by *cpeBA* operon because of lacking PE, in this study *cpcBA* operon was applied and three pigment types type 1, type 2, and type 3 were thus distinguished in Jiaozhou Bay (Supplementary Figure S1). Studies have reported that different pigment types usually co-occur and one phenotype generally predominates in marine environments (Xia et al., 2017b). Similar in Jiaozhou Bay, type 1, type 2, and type 3 co-occurred, with type 2 being predominant in the majority of samples (Supplementary Figure S2B). Type 1 was more abundant in summer at stations A5 and C1 with low salinity of 27.23 and 29.47, respectively (Figure 3). Low salinity in the inner bay was mainly attributed to freshwater discharge and summer rainfall (Cui et al., 2021). Lower salinity and higher temperature seemed to be favorable for the higher growth rate of type 1 *Synechococcus* in the inner bay in summer.

Type 2 is prevalent in turbid waters, and type 3 is usually distributed in clearer water with high transparency. It has been proposed that the dominant pigment type shifted from type 2 to type 3 following a decrease in turbidity in the marine environment (Everroad and Wood, 2012; Xia et al., 2018). A similar phenomenon was observed in Jiaozhou Bay. Type 2 was predominant in the inner bay with lower salinity, higher nutrients, and higher turbidity (Figure 3; Supplementary Figure S2B). SPM in the inner bay was much higher than those in the outer bay, implying higher turbidity in the inner bay (Figure 3D). The dominance of type 2 in the inner bay indicated that it was well adapted to harvest light in the turbid waters. In the outer bay, type 3 was predominant in winter and spring with higher salinity, lower nutrients, and lower turbidity (Figure 3; Supplementary Figure S2B). The outer bay is connected to the Yellow Sea with clearer water, which is suitable for the survival of type 3. We found that the dominant pigment type not only varied with locations from the inner bay to the outer bay, but also varied with seasons from the winter to the autumn (Supplementary Figure S2B). In the outer bay, the dominant pigment type shifted from type 3 to type 2 from the winter to the autumn. In winter and spring, type 3 predominated, whereas type 2 co-dominated with type 3 in summer and even became the predominant pigment type in autumn. It is necessary to find out the possible reason. The proportion of type 3 decreased with increasing temperature (Figure 3; Supplementary Figure S2B). RDA analysis also showed that type 3 was negatively correlated with temperature (Figure 8A), implying the importance of temperature in regulating the variation of type 3. Salinity was also an important factor in the composition of *Synechococcus* pigmentation. Compared to type 1 and type 2 with a higher tolerance for salinity variations, type 3 seemed to be less tolerant in low-salinity environments (Xia et al., 2017a). In the outer bay, salinity was lower in summer and autumn compared to winter and spring. The lowest salinity and smallest proportion of type 3 coincided in October. RDA analysis exhibited a positive correlation between type 3 and salinity, indicating the importance of salinity in type 3 distribution. Although the relationship between type 3 and nutrients is still unclear, RDA analysis exhibited a negative correlation between type 3 and nutrients NO_3^-, NO_2^-, NH_4^+, and PO_4^{3-}. Nutrients in summer and autumn were generally higher than those in winter and spring, especially for PO_4^{3-}, phosphorus stress was obvious in winter and spring and relieved in October. The mechanisms of temperature, salinity, and nutrients influencing *Synechococcus* pigment types are still unclear, which is necessary to figure out the next step.

Synechococcus pigment types comparison measured by different methods (FCM and *cpcBA* sequencing)

Flow cytometry has been widely used for the measurement of *Synechococcus* abundance since the 1980s (Olson et al., 1988; Liu et al., 2014). PC-only *Synechococcus* (type 1) and PE-rich *Synechococcus* (type 2 + type 3) can be separated using flow cytometer with dual lasers of 488 nm and 640 nm (Murrel and Lores, 2004; Liu et al., 2014). Type 1 could be recognized by red fluorescence induced by 640 nm

laser because of the binding phycocyanobilin (PCB, Amax = 620 nm) (Six et al., 2007; Liu et al., 2014). PE-*Synechococcus* type 2 and type 3 could be separated by green fluorescence induced by 488 nm laser since type 3 showed higher green fluorescence than type 2 because of the binding phycourobilin (PUB, A_{max} = 495 nm) (Olson et al., 1988). In this study, *Synechococcus* type 1, type 2, and type 3 were clearly discriminated by dual lasers of a flow cytometer in Jiaozhou Bay (Figure 2). This was the first time three pigment types of *Synechococcus* were simultaneously distinguished. In the Hong Kong coastal waters and Pearl River Estuary, PC-only (type 1) and PE-rich (type 2 + type 3) *Synechococcus* were detected, whereas, in the Bohai Sea, Yellow Sea, and the East China Sea, only PE-Synechococcus was detected (Liu et al., 2014; Xia et al., 2017a, 2018; Wang et al., 2021, 2022a, 2022c).

In this study, both flow cytometric analysis and phylogenetic analysis of the *cpcBA* operons were applied to distinguish *Synechococcus* pigment types type 1, type 2, and type 3. 9 in 12 samples exhibited a similar distribution pattern, which showed 75% similarity of the two above methods, implying the reliability of *Synechococcus* pigment types analyzed by flow cytometry. The dissimilarity mainly comes from three samples in winter and spring in the inner bay (Feb-C1, May-C1, and May-A5) with low abundances (<10^3 cells/mL) (Supplementary Figure S2). A low abundance of *Synechococcus* analyzed by flow cytometer may confuse in recognizing type 2 and type 3 by operators. Besides, a small proportion of dividing cells with replicated chromosomes measured by molecular method may be detected as single cells by flow cytometer (Tai and Palenik, 2009). This may cause a slight mismatch between the two above methods. To improve the accuracy of flow cytometric detection, it is necessary to enrich *Synechococcus* abundances collected in winter and spring by filtering before analysis and increasing the acquisition time during analysis. On the other hand, there is a need to use more sensitive and efficient molecular methods, such as qPCR for quantitative analysis of specific groups of *Synechococcus*, making the results more comparable and accurate (Wang et al., 2022c).

Spatio-temporal variation of *Synechococcus* genetic diversity (*rpoC1*)

In the present study, 10 clades representing *Synechococcus* S5.1, S5.2, and S5.3 were identified (Figure 7A). S5.1 and S5.2 were abundant and widespread in the temperate Jiaozhou Bay. In comparison, 6–13 *Synechococcus* clades were identified in the temperate Chesapeake Bay (Chen et al., 2006), Gulf of Aqaba (Post et al., 2011), and Yellow Sea (Wang et al., 2021). In the subtropical Hong Kong waters, 17 clades were identified with abundant S5.1 and S5.2 in the coastal and estuarine waters (Xia et al., 2015). Our results were consistent with previous reports mentioned above.

Temporal and spatial variations in the distribution of the *Synechococcus* assemblages have been reported in various estuarine and coastal waters. *Synechococcus* population did not vary obviously and was dominated by a single clade, for instance in the Gulf of Aqaba, S5.1-II was predominant over a 3 years scale throughout the oceanic region (Fuller et al., 2005). At the Martha's Vineyard Coastal Observatory (MVCO), S5.1-I dominated *Synechococcus* populations all over the year (Hunter-Cevera et al., 2016). However, in the subtropical Hong Kong waters, dominant lineages of *Synechococcus* were multiple and varied with seasons and locations. From spring to summer, S5.2 dominated in the estuarine water whereas S5.1-II and S5.1-VI co-dominated in coastal waters. In winter S5.1-II and S5.1-IX co-dominated in the estuarine and coastal waters (Xia et al., 2015). In Jiaozhou Bay, *Synechococcus* assemblages varied mainly with seasons. The composition of *Synechococcus* assemblages shifted from two dominant lineages in winter and spring to a high genetic diversity in summer and autumn. Three major lineages S5.1-I, S5.1-IX, and S5.2-CB5 were detected, with S5.1-I and S5.1-IX being dominant in winter and spring, and in autumn, respectively. S5.2-CB5 was abundant and widespread in most samples (Figure 7A). S5.1-I was dominant in winter and spring with temperatures ≤16°C. The importance of S5.1-I decreased with increasing temperature (Figure 7B). RDA analysis showed that S5.1-I was negatively correlated with temperature, indicating the importance of temperature in regulating S5.1-I distribution (Figure 8B). Similarly at MVCO, S5.1-I has been reported to be predominant over the entire year (Hunter-Cevera et al., 2016). S5.1-I is known as a cold-water *Synechococcus*, which is primarily found in cold and temperate, nutrient-rich coastal waters at higher latitudes. Higher tolerance to cold stress together with the ability to survive in low temperatures may be favorable for the dominance of S5.1-I in cold water (Hunter-Cevera et al., 2016; Doré et al., 2022).

S5.1-I usually co-occurred with S5.1-IV in the cold water. However, in Jiaozhou Bay, S5.1-IV was not detected. S5.1-I co-dominated with S5.2-CB5 in winter and spring. S5.2-CB5 was abundant and widespread in most samples, especially in summer in the inner bay, S5.2-CB5 was predominant with relative abundance >50% (Supplementary Table S6). S5.2-CB5 was always found in coastal and estuarine waters (Cai et al., 2010; Huang et al., 2012; Hunter-Cevera et al., 2016). Temperature, salinity, and nutrient concentrations might be important in regulating S5.2-CB5 distribution. In the Chesapeake Bay, S5.2-CB5 was merely detected in summer and dominated in the upper bay, which was characterized by a higher ammonium concentration and lower salinity (Chen et al., 2006; Cai et al., 2010). At the MVCO, S5.2-CB5 was isolated during later summer and fall, when the temperature was relatively high (17–20°C) and nitrate + nitrite concentration was relatively low (<0.5 μM) (Hunter-Cevera et al., 2016). Similarly in Jiaozhou Bay, the dominant *Synechococcus* lineage S5.2-CB5 was observed in summer with high temperature (28.9–29.5°C), low salinity (27.2–29.5), and low ammonium (0.36–1.57 μM) (Figure 7B). RDA analysis showed that S5.2-CB5 was negatively correlated with NO_3^-, NH_4^+ and PO_4^{3-}, implying the importance of nutrients in S5.2-CB5 regulation (Figure 8B). Representative of S5.2-CB5 showed a pigment type 1, which may largely contribute to the presence of type 1 in Jiaozhou Bay.

S5.1-IX exhibited an opposite trend compared to S5.1-I, being dominant in summer and autumn. Especially in autumn, S5.1-IX was predominant with relative abundance >35.7% (Supplementary Table S6). Unlike S5.1-I and S5.2-CB5, S5.1-IX was not a common *Synechococcus* clade, the knowledge about S5.1-IX was rather scarce. S5.1-IX was first discovered in the Gulf of Aqaba (Fuller et al., 2003). Nevertheless, it was considered to be rare in this field (Penno et al., 2006). In the China Sea, S5.1-IX was detected as a minor component in the East China Sea and the Yellow Sea (Choi and Noh, 2009; Chung et al., 2015; Wang et al., 2021). Even in the global ocean, Clade IX was reported to have low abundance (less than 5%) (Zwirglmaier et al., 2008). However, it thrived in the

subtropical Hong Kong waters in October and December (Xia et al., 2015). Pyrosequencing analysis and growth experiment indicated that S5.1-IX (MW02) prefers to grow in low salinity waters and grows best at a salinity of 28 in Hong Kong waters (Xia et al., 2015). In the temperate Jiaozhou Bay, salinities ranged from 28.5 to 30.3 in autumn, which might be suitable for the growth of Clade IX. In autumn, phosphorus stress was largely relieved owing to higher nitrogen and phosphate concentrations. Sufficient nutrients may be another key factor for Clade IX growth in autumn. RDA analysis indicated that S5.1-IX was positively related to NO2-and temperature, and negatively related to salinity (Figure 8B). Compared to the environmental parameters, it seemed higher temperature, lower salinity, and sufficient nutrients could be the important factors for the dominance of S5.1-IX in autumn (Figure 7B). Since environmental conditions in the temperate Jiaozhou Bay are obviously different from those in the subtropical Hong Kong waters, S5.1-IX in Jiaozhou Bay might be a different subclade. It is necessary to isolate and sequence the clade S5.1-IX in Jiaozhou in the next step.

The relationship of *Synechococcus* pigment types (FCM, *cpcBA*) and genetic diversity (*rpoC1*)

In our study, *Synechococcus* pigment types based on flow cytometry analysis and phylogenetic analysis of *cpcBA* operon showed similar distribution patterns in most samples. Liu et al. (2014) also showed phylogenetic study based on *cpcBA* agreed well with flow cytometric counts, which revealed the coexistence of PC-rich and PE-rich *Synechococcus* in the subtropical coastal waters.

Our phylogenetic tree based on *cpcBA* operon sequences, formed three well-separated clusters (type 1, type 2, and type 3) (Supplementary Figure S1). Type 1 corresponds to S5.1-VIII and S5.2; Type 2 corresponds to clades II, V, and VI of S5.1; Type 3 corresponds to clades I, II, III, IV, and WPC1 of S5.1. Based on the phylogeny of *rpoC1* gene, clades I, II, III, V, VI, VIII, IX, WPC1 of S5.1, S5.2, and S5.3 were detected (Figure 6). The phylogenic tree based on the two genes showed congruency. Comparing their responses to environmental factors, type 1 *Synechococcus* (S5.1-VIII, S5.2) based on *cpcBA* operon was positively correlated with Chl *a*, which was consistent with S5.1-VIII and S5.2 based on *rpoC1* gene (Figure 8). This fully indicates that *Synechococcus* type 1 in Jiaozhou Bay was mainly contributed by S5.1-VIII and S5.2, accompanied by high Chl *a* concentration, which is consistent with the spatio-temporal distribution of *Synechococcus* type 1 mentioned above (Figures 3, 5). However, the relationship between *Synechococcus* type 2 and type 3 and environmental factors, is inconsistent with the results based on *rpoC1* gene. The reason is that the single clade of *Synechococcus* assemblages may possess phycobilisomes of different types, i.e., S5.1-II corresponds to type 2 and type 3, consistent with observations on isolates (Haverkamp et al., 2008; Everroad and Wood, 2012; Xia et al., 2017b). *Synechococcus* clades have higher diversity compare to pigment types (Supplementary Table S5). The response of different *Synechococcus* clades to environmental factors will be more detailed than that of pigment types. The combination of more technical means provides more information for studying *Synechococcus* distribution.

Conclusion

This present study investigated seasonal and spatial variations of *Synechococcus* in abundance, pigment types and genetic diversity in the temperate Jiaozhou Bay. *Synechococcus* abundance exhibited seasonal variations with highest value in summer and lowest value in winter, which was consistent with temperature variation. Three pigment types of *Synechococcus* type 1, type 2, and type 3 were discriminated simultaneously by dual lasers of flow cytometry for the first time. The phylogenetic analysis of *cpcBA* operon also revealed three pigment types of *Synechococcus* type 1, type 2, and type 3. By comparison, 75% similarity was shown between the two approaches, indicating the reliability of pigment types measured by flow cytometry. It is essential to eliminate the 25% mismatch between the two methods. We will attempt in various aspects, for instance, by increasing acquisition cells and time of flow cytometry and applying more sensitive and efficient molecular methods. Three pigment types of *Synechococcus* type 1, type 2 and type 3 were distinguished based on *cpcBA* operon, which displayed obvious variations spatially between the inner bay and the outer bay. Freshwater discharge and water turbidity played important roles in regulating *Synechococcus* pigment types. *Synechococcus* assemblages were phylogenetically diverse (12 different lineages) based on *rpoC1* gene and dominated by three core lineages S5.1-I, S5.1-IX, and S5.2-CB5 in different seasons, which were influenced by different environmental factors.

From this study, we clearly know about Synechococcus abundance, pigment types and genetic diversity on a spatio-temporal scale by different techniques in Jiaozhou Bay. The combination of more technical means provides more information for studying *Synechococcus* distribution. However, more questions are raised and need to be addressed. (1) Since S5.2-CB5 was widespread in all the seasons, it might be the best-fit genotype for Jiaohou Bay, which could be monitored as an indicator for long-term investigation. (2) The subclade of S5.1-IX in Jiaozhou Bay is still unclear. It is urgent to isolate, culture and sequence the S5.1-IX strains in Jiaozhou Bay and compare them with the subclade (NW02) in the subtropical Hong Kong strains.

Data availability statement

The datasets presented in this study can be found in online repositories. The names of the repository/repositories and accession number(s) can be found at: https://www.ncbi.nlm.nih.gov/, BioProject PRJNA996355, https://www.ncbi.nlm.nih.gov/, BioProject PRJNA995918.

Author contributions

SL: Data curation, Formal analysis, Methodology, Software, Visualization, Writing – original draft. YD: Conceptualization, Formal analysis, Methodology, Writing – original draft. XS: Conceptualization, Resources, Writing – review & editing. YZ: Conceptualization, Funding acquisition, Supervision, Writing – review & editing, Visualization. LZ: Conceptualization, Funding acquisition, Methodology, Supervision, Visualization, Writing – original draft, Writing – review & editing. WZ: Conceptualization, Supervision, Writing – review & editing. TX: Conceptualization, Supervision, Writing – review & editing.

Funding

The author(s) declare financial support was received for the research, authorship, and/or publication of this article. This work was supported by the National Natural Science Foundation of China (NSFC) (grant numbers. U22A20583 and 42076139), the Key Deployment Project of Center for Ocean Mega-Science, Chinese Academy of Sciences (grant number. COMS2020Q09), and the Sino-French International Research Project (CNR-CAS) Dynamics and Function of Marine Microorganisms (IRP-DYF2M): insight from physics and remote sensing.

Acknowledgments

We are grateful to Jiaozhou Bay National Marine Ecosystem Research Station, and captain and crew of the R/V Chuangxin for their assistance during the research. We also thank Yongfang Zhao and the Jiaozhou Bay National Marine Ecosystem Research Station for their support to share environmental data.

Conflict of interest

The authors declare that the research was conducted in the absence of any commercial or financial relationships that could be construed as a potential conflict of interest.

Publisher's note

All claims expressed in this article are solely those of the authors and do not necessarily represent those of their affiliated organizations, or those of the publisher, the editors and the reviewers. Any product that may be evaluated in this article, or claim that may be made by its manufacturer, is not guaranteed or endorsed by the publisher.

Supplementary material

The Supplementary material for this article can be found online at: https://www.frontiersin.org/articles/10.3389/fmicb.2023.1322548/full#supplementary-material

References

Agawin, N. S. R., Duarte, C. M., and Agusti, S. (1998). Growth and abundance of Synechococcus sp. in a Mediterranean Bay: seasonality and relationship with temperature. *Mar. Ecol.-Prog. Ser.* 170, 45–53. doi: 10.3354/meps170045

Amato, K. R., Yeoman, C. J., Kent, A., Righini, N., and Carbonero, F. (2013). Habitat degradation impacts black howler monkey (Alouatta pigra) gastrointestinal microbiomes. *ISME J.* 7, 1344–1353. doi: 10.1038/ismej.2013.16

Cai, H., Wang, K., Huang, S., Jiao, N., and Chen, F. (2010). Distinct patterns of Picocyanobacterial communities in winter and summer in the Chesapeake Bay. *Appl. Environ. Microbiol.* 76, 2955–2960. doi: 10.1128/AEM.02868-09

Chen, F., Wang, K., Kan, J., Bachoon, D., and Lu, J. (2004). Phylogenetic diversity of Synechococcus in the Chesapeake Bay revealed by Ribulose-1,5-bisphosphate carboxylase-oxygenase (RuBisCO) large subunit gene (rbcL) sequences. *Aquat. Microb. Ecol.* 36, 153–164. doi: 10.3354/ame036153

Chen, F., Wang, K., Kan, J. J., and Suzuki, M. T. (2006). Diverse and unique picocyanobacteria in Chesapeake Bay, revealed by 16S-23S rRNA internal transcribed spacer sequences. *Appl. Environ. Microbiol.* 72, 2239–2243. doi: 10.1128/AEM.72.3.2239-2243.2006

Chen, W., Wang, X., and Yang, S. (2023). Response of phytoplankton community structure to environmental changes in the coastal areas of northern China. *Mar. Pollut. Bull.* 195:115300. doi: 10.1016/j.marpolbul.2023.115300

Choi, D. H., and Noh, J. H. (2009). Phylogenetic diversity of Synechococcus strains isolated from the East China Sea and the East Sea. *FEMS Microbiol. Ecol.* 69, 439–448. doi: 10.1111/j.1574-6941.2009.00729.x

Chung, C.-C., Gong, G.-C., Huang, C.-Y., and Lin, J.-Y. (2015). Changes in the Synechococcus assemblage composition at the surface of the East China Sea due to flooding of the Changjiang River. *Microb. Ecol.* 70, 677–688. doi: 10.1007/s00248-015-0608-5

Clarke, K. (1993). Nonparametric multivariate analyses of changes in community structure. *Aust. J. Ecol.* 18, 117–143. doi: 10.1111/j.1442-9993.1993.tb00438.x

Cookson, W. R., Marschner, P., Clark, I. M., Milton, N., and Smirk, M. N. (2006). The influence of season, agricultural management, and soil properties on gross nitrogen transformations and bacterial community structure. *Aust. J. Soil Res.* 44, 453–465. doi: 10.1071/SR05042

Cui, K., Dong, Y., Sun, X., Zhao, L., and Du, H. (2021). Long-term temporal and spatial distribution of coliform bacteria in Jiaozhou Bay associated with human activities and environmental governance. *Front. Mar. Sci.* 8:641137. doi: 10.3389/fmars.2021.641137

Doré, H., Leconte, J., Guyet, U., Breton, S., and Farrant, G. K. (2022). Global phylogeography of marine Synechococcus in coastal areas reveals strong community shifts. *mSystems*:7. doi: 10.1128/msystems.00656-22

Dufresne, A., Ostrowski, M., Scanlan, D. J., Garczarek, L., and Mazard, S. (2008). Unraveling the genomic mosaic of a ubiquitous genus of marine cyanobacteria. *Genome Biol.* 9:R90. doi: 10.1186/gb-2008-9-5-r90

Everroad, R. C., and Wood, A. M. (2012). Phycoerythrin evolution and diversification of spectral phenotype in marine Synechococcus and related picocyanobacteria. *Mol. Phylogenet. Evol.* 64, 381–392. doi: 10.1016/j.ympev.2012.04.013

Farrant, G. K., Dore, H., Cornejo-Castillo, F. M., Partensky, F., and Ratin, M. (2016). Delineating ecologically significant taxonomic units from global patterns of marine picocyanobacteria. *Proc. Natl. Acad. Sci. U. S. A.* 113, E3365–E3374. doi: 10.1073/pnas.1524865113

Feng, M., Wang, C., Zhang, W., Zhang, G., and Xu, H. (2018). Annual variation of species richness and lorica oral diameter characteristics of tintinnids in a semi-enclosed bay of western Pacific. *Estuar. Coast. Shelf Sci.* 207, 164–174. doi: 10.1016/j.ecss.2018.04.003

Flombaum, P., Gallegos, J. L., Gordillo, R. A., Rincon, J., Zabala, L. L., Jiao, N., et al. (2013). Present and future global distributions of the marine Cyanobacteria Prochlorococcus and Synechococcus. *Proc. Natl. Acad. Sci. U. S. A.* 110, 9824–9829. doi: 10.1073/pnas.1307701110

Fuller, N. J., Marie, D., Partensky, F., Vaulot, D., and Post, A. F. (2003). Clade-specific 16S ribosomal DNA oligonucleotides reveal the predominance of a single marine Synechococcus clade throughout a stratified water column in the Red Sea. *Appl. Environ. Microbiol.* 69, 2430–2443. doi: 10.1128/AEM.69.5.2430-2443.2003

Fuller, N. J., West, N. J., Marie, D., Yallop, M., and Rivlin, T. (2005). Dynamics of community structure and phosphate status of picocyanobacterial populations in the Gulf of Aqaba, Red Sea. *Limnol. Oceanogr.* 50, 363–375. doi: 10.4319/lo.2005.50.1.0363

Grébert, T., Dore, H., Partensky, F., Farrant, G. K., and Boss, E. S. (2018). Light color acclimation is a key process in the global ocean distribution of Synechococcus cyanobacteria. *Proc. Natl. Acad. Sci. U. S. A.* 115, E2010–E2019. doi: 10.1073/pnas.1717069115

Haverkamp, T., Acinas, S. G., Doeleman, M., Stomp, M., Huisman, J., and Stal, L. J. (2008). Diversity and phylogeny of Baltic Sea picocyanobacteria inferred from their ITS and phycobiliprotein operons. *Environ. Microbiol.* 10, 174–188. doi: 10.1111/j.1462-2920.2007.01442.x

Huang, S., Wilhelm, S. W., Harvey, H. R., Taylor, K., and Jiao, N. (2012). Novel lineages of Prochlorococcus and Synechococcus in the global oceans. *ISME J.* 6, 285–297. doi: 10.1038/ismej.2011.106

Hunter-Cevera, K. R., Post, A. F., Peacock, E. E., and Sosik, H. M. (2016). Diversity of Synechococcus at the Martha's vineyard coastal observatory: insights from culture isolations, clone libraries, and flow cytometry. *Microb. Ecol.* 71, 276–289. doi: 10.1007/s00248-015-0644-1

Larsson, J., Celepli, N., Ininbergs, K., Dupont, C. L., and Yooseph, S. (2014). Picocyanobacteria containing a novel pigment gene cluster dominate the brackish water Baltic Sea. *ISME J.* 8, 1892–1903. doi: 10.1038/ismej.2014.35

Liu, H., Jing, H., Wong, T. H. C., and Chen, B. (2014). Co-occurrence of phycocyanin- and phycoerythrin-rich Synechococcus in subtropical estuarine and coastal waters of Hong Kong. *Environ. Microbiol. Rep.* 6, 90–99. doi: 10.1111/1758-2229.12111

Marie, D., Simon, N., Guillou, L., Partensky, Frédéric, and Vaulot, D.. (2000). Flow cytometry analysis of marine picoplankton, *Living color*, Eds. R. A. Diamond and S. Demaggiopp (Berlin, Heidelberg: Springer Berlin Heidelberg), 421–454.

Mitbavkar, S., Saino, T., Horimoto, N., Kanda, J., and Ishimaru, T. (2009). Role of environment and hydrography in determining the picoplankton community structure of Sagami Bay. *Japan. J. Oceanogr.* 65, 195–208. doi: 10.1007/s10872-009-0019-7

Muhling, M., Fuller, N. J., Somerfield, P. J., Post, A. F., and Wilson, W. H. (2006). High resolution genetic diversity studies of marine Synechococcus isolates using rpoC1-based restriction fragment length polymorphism. *Aquat. Microb. Ecol.* 45, 263–275. doi: 10.3354/ame045263

Murrel, M. C., and Lores, E. M. (2004). Phytoplankton and zooplankton seasonal dynamics in a subtropical estuary: importance of cyanobacteria. *J. Plankton Res.* 26, 371–382. doi: 10.1093/plankt/fbh038

Olson, R. J., Chisholm, S. W., Zettler, E. R., and Armbrust, E. V. (1988). Analysis of Synechococcus pigment types in the sea using single and dual beam flow cytometry. Deep Sea research part a. *Oceanogr. Res. Papers* 35, 425–440. doi: 10.1016/0198-0149(88)90019-2

Olson, R., Chisholm, S., Zettler, E., and Armbrust, E. (1990). Pigments, size, and distribution of Synechococcus in the North-Atlantic and Pacific oceans. *Limnol. Oceanogr.* 35, 45–58. doi: 10.4319/lo.1990.35.1.0045

Paerl, R. W., Foster, R. A., Jenkins, B. D., and Montoya, J. P. (2008). Phylogenetic diversity of cyanobacterial narB genes from various marine habitats. *Environ. Microbiol.* 10, 3377–3387. doi: 10.1111/j.1462-2920.2008.01741.x

Paulsen, M. L., Dore, H., Garczarek, L., Seuthe, L., and Mueller, O. (2016). Synechococcus in the Atlantic gateway to the Arctic Ocean. *Front. Mar. Sci.* 3:191. doi: 10.3389/fmars.2016.00191

Penno, S., Lindell, D., and Post, A. F. (2006). Diversity of Synechococcus and Prochlorococcus populations determined from DNA sequences of the N-regulatory gene ntcA. *Environ. Microbiol.* 8, 1200–1211. doi: 10.1111/j.1462-2920.2006.01010.x

Post, A. F., Penno, S., Zandbank, K., Paytan, A., Huse, S. M., and Welch, D. M. (2011). Long term seasonal dynamics of Synechococcus population structure in the Gulf of Aqaba. *Northern Red Sea. Front. Microbiol.* 2:131. doi: 10.3389/fmicb.2011.00131

Rajaneesh, K. M., and Mitbavkar, S. (2013). Factors controlling the temporal and spatial variations in Synechococcus abundance in a monsoonal estuary. *Mar. Environ. Res.* 92, 133–143. doi: 10.1016/j.marenvres.2013.09.010

Shi, X., Wang, Z., Gao, W., and Huang, H. (2023). Distribution of suspended particulate matter in the Caroline M4 seamount in the western Pacific Ocean and its influencing factors. *Oceanologia et Limnologia Sinica* 54, 703–717. doi: 10.11693/hyhz20220800219

Six, C., Thomas, J.-C., Garczarek, L., Ostrowski, M., and Dufresne, A. (2007). Diversity and evolution of phycobilisomes in marine Synechococcus spp.: a comparative genomics study. *Genome Biol.* 8:R259. doi: 10.1186/gb-2007-8-12-r259

Sohm, J. A., Ahlgren, N. A., Thomson, Z. J., Williams, C., and Moffett, J. W. (2016). Co-occurring Synechococcus ecotypes occupy four major oceanic regimes defined by temperature, macronutrients and iron. *ISME J.* 10, 333–345. doi: 10.1038/ismej.2015.115

Stomp, M., Huisman, J., de Jongh, F., Veraart, A. J., and Gerla, D. (2004). Adaptive divergence in pigment composition promotes phytoplankton biodiversity. *Nature* 432, 104–107. doi: 10.1038/nature03044

Stomp, M., Huisman, J., Voros, L., Pick, F. R., and Laamanen, M. (2007). Colourful coexistence of red and green picocyanobacteria in lakes and seas. *Ecol. Lett.* 10, 290–298. doi: 10.1111/j.1461-0248.2007.01026.x

Tai, V., and Palenik, B. (2009). Temporal variation of Synechococcus clades at a coastal Pacific Ocean monitoring site. *ISME J.* 3, 903–915. doi: 10.1038/ismej.2009.35

Voros, L., Callieri, C., Balogh, K. V., and Bertoni, R. (1998). Freshwater picocyanobacteria along a trophic gradient and light quality range. *Hydrobiologia* 370, 117–125. doi: 10.1007/978-94-017-2668-9_10

Wang, T., Chen, X., Li, J., and Qin, S. (2022a). Distribution and phenogenetic diversity of Synechococcus in the Bohai Sea. *China. J. Oceanol. Limnol.* 40, 592–604. doi: 10.1007/s00343-021-1005-1

Wang, T., Chen, X., Qin, S., and Li, J. (2021). Phylogenetic and Phenogenetic diversity of Synechococcus along a Yellow Sea section reveal its environmental dependent distribution and co-occurrence microbial pattern. *J. Mar. Sci. Eng.* 9:1018. doi: 10.3390/jmse9091018

Wang, T., Li, J., Jing, H., and Qin, S. (2022b). Picocyanobacterial Synechococcus in marine ecosystem: insights from genetic diversity, global distribution, and potential function. *Mar. Environ. Res.* 177:105622. doi: 10.1016/j.marenvres.2022.105622

Wang, K., Wommack, K. E., and Chen, F. (2011). Abundance and distribution of Synechococcus spp. and cyanophages in the Chesapeake Bay. *Appl. Environ. Microbiol.* 77, 7459–7468. doi: 10.1128/AEM.00267-11

Wang, T., Xia, X., Chen, J., Liu, H., and Jing, H. (2022c). Spatio-temporal variation of Synechococcus assemblages at DNA and cDNA levels in the tropical estuarine and coastal waters. *Front. Microbiol.* 13:837037. doi: 10.3389/fmicb.2022.837037

Wood, A. M., Phinney, D. A., and Yentsch, C. S. (1998). Water column transparency and the distribution of spectrally distinct forms of phycoerythrin-containing organisms. *Mar. Ecol.-Prog. Ser.* 162, 25–31. doi: 10.3354/meps162025

Xia, X., Guo, W., Tan, S., and Liu, H. (2017a). Synechococcus assemblages across the salinity gradient in a salt wedge estuary. *Front. Microbiol.* 8:1254. doi: 10.3389/fmicb.2017.01254

Xia, X., Liao, Y., Liu, J., Leung, S. K., and Lee, P. Y. (2023). Genomic and transcriptomic insights into salinity tolerance-based niche differentiation of Synechococcus clades in estuarine and coastal waters. *mSystems*:8. doi: 10.1128/msystems.01106-22

Xia, X., Liu, H., Choi, D., and Noh, J. H. (2018). Variation of Synechococcus pigment genetic diversity along two turbidity gradients in the China seas. *Microb. Ecol.* 75, 10–21. doi: 10.1007/s00248-017-1021-z

Xia, X., Partensky, F., Garczarek, L., Suzuki, K., and Guo, C. (2017b). Phylogeography and pigment type diversity of Synechococcus cyanobacteria in surface waters of the northwestern Pacific Ocean. *Environ. Microbiol.* 19, 142–158. doi: 10.1111/1462-2920.13541

Xia, X., Vidyarathna, N. K., Palenik, B., Lee, P., and Liu, H. (2015). Comparison of the seasonal variations of Synechococcus assemblage structures in estuarine waters and coastal waters of Hong Kong. *Appl. Environ. Microbiol.* 81, 7644–7655. doi: 10.1128/AEM.01895-15

Xing, J., Song, J., Yuan, H., Wang, Q., and Li, X. (2017). Atmospheric wet deposition of dissolved trace elements to Jiaozhou Bay, North China: fluxes, sources and potential effects on aquatic environments. *Chemosphere* 174, 428–436. doi: 10.1016/j.chemosphere.2017.02.004

Yang, L., Wang, M., Liu, G., Wang, J., and Lu, L. (2012). The abundance of picophytoplankton and correlation analysis with environmental factors in Jiaozhou Bay. *Oceanologia et Limnologia Sinica* 43, 967–975. doi: 10.11693/hyhz201205014014

Zhao, S., Xiao, T., Li, H., and Xu, J. (2005). Distribution of Synechococcus spp. in Jiaozhou Bay. *Oceanologia et Limnologia Sinica* 36, 534–540.

Zhao, Y., Zhao, Z., and Sun, X. (2020). A dataset of nutrient structure and limiting factors of phytoplankton growth in Jiaozhou Bay from 1997 to 2010. *China Scientific Data* 5:e1. doi: 10.11922/csdata.2019.0056.zh

Zwirglmaier, K., Jardillier, L., Ostrowski, M., Mazard, S., and Garczarek, L. (2008). Global phylogeography of marine Synechococcus and Prochlorococcus reveals a distinct partitioning of lineages among oceanic biomes. *Environ. Microbiol.* 10, 147–161. doi: 10.1111/j.1462-2920.2007.01440.x

frontiers | Frontiers in Microbiology

TYPE Original Research
PUBLISHED 16 February 2024
DOI 10.3389/fmicb.2024.1349322

OPEN ACCESS

EDITED BY
Beatriz Roncero Ramos,
Sevilla University, Spain

REVIEWED BY
Yuu Hirose,
Toyohashi University of Technology, Japan
Lisa Wiltbank,
Weber State University, United States

*CORRESPONDENCE
Frédéric Partensky
frederic.partensky@sb-roscoff.fr

RECEIVED 04 December 2023
ACCEPTED 30 January 2024
PUBLISHED 16 February 2024

CITATION
Dufour L, Garczarek L, Gouriou B, Clairet J, Ratin M and Partensky F (2024) Differential acclimation kinetics of the two forms of type IV chromatic acclimaters occurring in marine *Synechococcus* cyanobacteria. *Front. Microbiol.* 15:1349322. doi: 10.3389/fmicb.2024.1349322

Differential acclimation kinetics of the two forms of type IV chromatic acclimaters occurring in marine *Synechococcus* cyanobacteria

Louison Dufour, Laurence Garczarek, Bastian Gouriou, Julia Clairet, Morgane Ratin and Frédéric Partensky*

Sorbonne Université, CNRS, UMR 7144 Adaptation and Diversity in the Marine Environment (AD2M), Station Biologique de Roscoff (SBR), Roscoff, France

Synechococcus, the second most abundant marine phytoplanktonic organism, displays the widest variety of pigment content of all marine oxyphototrophs, explaining its ability to colonize all spectral niches occurring in the upper lit layer of oceans. Seven *Synechococcus* pigment types (PTs) have been described so far based on the phycobiliprotein composition and chromophorylation of their light-harvesting complexes, called phycobilisomes. The most elaborate and abundant PT (3d) in the open ocean consists of cells capable of type IV chromatic acclimation (CA4), i.e., to reversibly modify the ratio of the blue light-absorbing phycourobilin (PUB) to the green light-absorbing phycoerythrobilin (PEB) in phycobilisome rods to match the ambient light color. Two genetically distinct types of chromatic acclimaters, so-called PTs 3dA and 3dB, occur at similar global abundance in the ocean, but the precise physiological differences between these two types and the reasons for their complementary niche partitioning in the field remain obscure. Here, photoacclimation experiments in different mixes of blue and green light of representatives of these two PTs demonstrated that they differ by the ratio of blue-to-green light required to trigger the CA4 process. Furthermore, shift experiments between 100% blue and 100% green light, and *vice-versa*, revealed significant discrepancies between the acclimation pace of the two types of chromatic acclimaters. This study provides novel insights into the finely tuned adaptation mechanisms used by *Synechococcus* cells to colonize the whole underwater light field.

KEYWORDS

marine picocyanobacteria, *Synechococcus*, chromatic acclimation, spectral niche, phycobilisome, comparative physiology

Introduction

Phytoplanktonic cells have an obligate requirement for light to perform photosynthesis. Yet in the marine environment, this energy source is highly variable quantitatively and qualitatively with depth but also along coast-offshore gradients, leaving aside daily oscillations (Kirk, 1994; Holtrop et al., 2021). This variability has triggered an extensive structural and pigment diversification of phytoplankton light-harvesting antennae, which enable cells to considerably enhance the wavelength range they can collect and therefore the number of

photons reaching photosystems. Despite their apparent simplicity compared to algae and higher plants, cyanobacteria possess the most elaborated form of antennae known in oxyphototrophs, called phycobilisomes (PBS). PBS are huge water-soluble complexes composed of six to eight rods radiating around a central core. Both core and rods are constituted of phycobiliproteins that bind open-chain tetrapyrroles, called phycobilins (Sidler, 1994). While the PBS core is always made of allophycocyanin and is highly conserved, PBS rods display a very large structural flexibility since they can be made of phycocyanin (PC) only, or of PC and one or two phycoerythrin (PE) types, PE-I and PE-II (Ong and Glazer, 1991; Six et al., 2007). Additionally, each phycobiliprotein can bind up to three different kinds of phycobilins. The ultimate degree of sophistication is the capacity for some cyanobacterial cells to modify the composition of their PBS in response to changes in the ambient light color. This process called "chromatic acclimation" (CA)—the initial term was actually "chromatic adaptation," but was recently replaced in order to best describe this physiological process (Shukla et al., 2012)—was first observed in the early 20th century in freshwater cyanobacteria shifted from red to green light (Engelmann, 1902; Gaidukov, 1903). CA was later on attributed to changes in the phycobiliprotein composition of PBS rods: in red light, rods are entirely composed of PC and cells look green, whereas in green light PC is restricted to the base of the rods and the distal part is made of PE, causing cells to exhibit a bright red color (Boresch, 1922). This type of complementary chromatic acclimation (CCA, also called type 3 chromatic acclimation or CA3) is one among the seven different types of CA known so far in cyanobacteria (Tandeau de Marsac, 1977; Hirose et al., 2019; Sanfilippo et al., 2019a). While CA2—a simple type of CA where PE production is induced in green light, generating longer PBS rods, and repressed in red light—and CA3 occur mainly in freshwater and brackish cyanobacteria, CA4 is the main type occurring in the open ocean and is specific to marine *Synechococcus* cyanobacteria (Palenik, 2001; Everroad et al., 2006; Humily et al., 2013). Contrary to CA2 and CA3, CA4 does not involve changes in the phycobiliprotein composition of PBS rods, but in their phycobilin composition. In response to shifts between green light (GL) and blue light (BL), chromatic acclimaters can indeed modify the relative amount of the two phycobilins bound to PE-I and PE-II in order to match the predominant ambient light color. More specifically, they exhibit in BL a high ratio of the BL-absorbing phycourobilin (PUB, $\lambda_{max} \approx 495$ nm) to the GL-absorbing phycoerythrobilin (PEB, $\lambda_{max} \approx 545$ nm), and *vice-versa* in GL (Everroad et al., 2006; Shukla et al., 2012). Variations in PUB and PEB cell content are generally assessed by measuring the relative ratio of whole cell fluorescence excitation at 495 and 545 nm ($Exc_{495:545}$) with emission set at 580 nm, which in chromatic acclimaters changes from 0.6–0.7 in GL to 1.6–1.7 in BL (Palenik, 2001; Everroad et al., 2006). In the nomenclature of *Synechococcus* pigment types (PTs) established by Six et al. (2007) and later modified by Humily et al. (2013), chromatic acclimaters are classified as "PT 3d" cells, meaning that they possess PBS rods made of PC, PE-I and PE-II, a feature shared by all PT 3 representatives, and can modify their $Exc_{495:545}$ ratio. In contrast, PTs 3a, 3b, and 3c display a constitutively low, medium and high $Exc_{495:545}$ ratio, respectively. For this reason, PT 3a strains are often referred to as "green light specialists" and PT 3c as "blue light specialists" (Grébert et al., 2018, 2022).

Two genetically different types of chromatic acclimaters have been described so far: PTs 3dA and 3dB (Humily et al., 2013). Both possess a small genomic island involved in the CA4 process, yet the CA4-A and CA4-B islands differ genetically and structurally (Humily et al., 2013; Sanfilippo et al., 2019b; Grébert et al., 2021). Although long overlooked, CA4 appears to be an ecologically important process since chromatic acclimaters were shown to account for more than 40% of the whole marine *Synechococcus* population along the *Tara* oceans expedition transect (Grébert et al., 2018). Moreover, PTs 3dA and 3dB were found to be equally abundant (22.6% and 18.9%, respectively) but distributed in complementary ecological niches in the field. The former was indeed predominant in cold, nutrient-rich and highly productive waters at high latitude, as well as in other vertically mixed environments, while the latter was mostly found in nitrogen and phosphorus-poor oceanic areas and appeared to be more abundant at depth. The emergence and maintenance of two CA4 types over the course of evolution, as well as the differential distribution of PTs 3dA and 3dB in the environment (Grébert et al., 2018), strongly suggest that they may not be as phenotypically equivalent as previously thought (Humily et al., 2013). To check this hypothesis, we acclimated three representatives of each PT 3dA and 3dB in batch culture under two conditions of temperature, two light irradiances and five light colors in order to compare their growth rates and PBS properties. Furthermore, we performed shifts from BL to GL (and *vice-versa*) at two irradiances to compare the CA4 kinetics between five strains of each PT. These experiments demonstrated that PT 3dA and 3dB strains actually differ in the blue-to-green light ratio necessary to trigger the CA4 process, and revealed some significant discrepancies in their acclimation pace.

Materials and methods

Biological material and culture conditions

Ten *Synechococcus* strains, of which five PT 3dA and five PT 3dB representatives (Table 1), were retrieved from the Roscoff Culture Collection.[1] These strains were isolated from diverse environments and selected based on their genome availability (Doré et al., 2020) and clade affiliation, in order to include the CA4-A model strain RS9916 (Shukla et al., 2012; Sanfilippo et al., 2016, 2019b) as well as representatives from all five major clades (I to IV and CRD1) in the global ocean (Farrant et al., 2016).

Cells were grown in 50 mL polystyrene flasks (Sarstedt, Germany) in PCR-S11 medium (Rippka et al., 2000) supplemented with 1 mM sodium nitrate. All were pre-acclimated prior to measurements for at least 3 weeks in continuous light provided by blue and/or green LEDs (Alpheus, France) in temperature-controlled chambers.

Acclimation experiments

A selection of six out of the 10 abovementioned strains (BL107, RS9916 and WH8020 for PT 3dA and A15-62, PROS-U-1 and RS9915 for PT 3dB; Table 1) were grown in the following conditions: (i) two temperatures: 18°C and 25°C; (ii) two irradiances: low light (LL,

1 https://roscoff-culture-collection.org/

TABLE 1 Characteristics of the different *Synechococcus* strains used in this study.

Strain name	RCC #[a]	Subcluster[b]	Clade[b]	Subclade[c]	Pigment type[d]	Isolation region
BIOS-U3-1	2,533	5.1	CRD1	n.a.	3dA	Chile upwelling
BL107	515	5.1	IV	IVa	3dA	Balearic Sea
MITS9220	2,571	5.1	CRD1	n.a.	3dA	Equatorial Pacific
RS9916	555	5.1	IX	n.a.	3dA	Gulf of Aqaba
WH8020	751	5.1	I	Ia	3dA	Sargasso Sea
A15-62	2,374	5.1	II	IIa	3dB	Off Mauritania
A18-40	n.a.	5.1	III	IIIa	3dB	Atlantic Ocean
MINOS11	2,319	5.3	n.a.	n.a.	3dB	Mediterranean Sea
PROS-U-1	2,369	5.1	II	IIh	3dB	Moroccan upwelling
RS9915	2,553	5.1	III	IIIa	3dB	Gulf of Aqaba

[a]Roscoff Culture Collection.
[b]Farrant et al. (2016).
[c]Mazard et al. (2012).
[d]Humily et al. (2013).

15 µmol photons m^{-2} s^{-1}) and high light (HL, 75 µmol photons m^{-2} s^{-1}); (iii) five light qualities: blue light (100% BL), green light (100% GL), as well as three mixes of blue-green light: 25% BL–75% GL, 50% BL–50% GL and 75% BL–25% GL. Both temperatures were selected based on Ferrieux et al. (2022), which recently demonstrated that 18 and 25°C were the lowest and highest temperatures at which a selection of *Synechococcus* strains belonging to the five major clades in the environment were capable of growing. The two irradiances were chosen as being similar to those used in a previous study by Humily et al. (2013), for easier comparison of results between the two studies.

The light intensity and visible spectra of LEDs were measured using a PG200N Spectral PAR Meter (UPRtek, Taiwan; Supplementary Figure S1). Each strain was grown in triplicate and inoculated at an initial cell density of 3×10^6 cells mL^{-1}. Samples were harvested every day to measure cell concentration and fluorescence parameters by flow cytometry, and once during the exponential phase to measure phycobilin and phycobiliprotein contents by spectrofluorimetry (see below).

Shift experiments

Shift experiments between 100% low BL (LBL) and 100% low GL (LGL) and *vice-versa*, and between 100% high BL (HBL) and 100% high GL (HGL) and *vice-versa*, were performed on all 10 *Synechococcus* strains mentioned in Table 1, but only at 25°C. Each strain was diluted with fresh medium before the beginning of the experiments and regularly transferred in order to avoid limitation by nutrients. Aliquots were collected two to three times a day, depending on light intensity, to measure phycobilin content by spectrofluorimetry (see below).

Flow cytometry

Culture aliquots were sampled twice a day, fixed with 0.25% (v/v) glutaraldehyde (grade II, Sigma Aldrich, United States) and stored at −80°C until analysis (Marie et al., 1999). Cell density was determined using a Guava easyCyte flow cytometer equipped with a 488 nm laser and the Guavasoft software (Luminex Corporation, Texas). Average orange (583 nm) and red (695 nm) fluorescence signals were used as proxies of the phycoerythrin (PE) and chlorophyll *a* (Chl *a*) contents per cell, respectively. Both signals were normalized to that of standard fluorescent 0.95 µm silica beads.

Spectrofluorimetry

In vivo fluorescence spectra were recorded at 240 nm min^{-1} with slits fixed at 10 nm once during the exponential phase using a spectrofluorimeter FL6500 (Perkin-Elmer, United-States). Excitation spectra were acquired between 450 and 560 nm with emission set at 580 nm, corresponding to the PE emission maximum. Emission spectra were recorded between 550 and 750 nm with excitation set at 530 nm, close to the PEB excitation maximum. Spectra were monitored and analyzed with the Fluorescence software (Perkin-Elmer). The $Exc_{495:545}$ fluorescence excitation ratio was used as a proxy for the PUB:PEB ratio. The $Em_{560:650}$ and $Em_{650:680}$ fluorescence emission ratios were used as proxies of the PE to PC and PC to PBS terminal acceptor (TA) ratios, respectively. The first parameter provided information about the electron transfer efficiency within the PBS and/or the length of PBS rods, and the second one about the coupling of PBS to PSII reaction center chlorophylls.

Statistical analyses

All statistical analyses were conducted using the R software (version 4.2.3; R Core Team, 2021) in order to test for significant differences between PTs 3dA and 3dB. The potential influence of growing conditions (temperature, light quality and quantity) was also investigated.

For acclimation experiments, a linear mixed model (nlme package version 3.1-164; Pinheiro et al., 2023) was fit to each variable (growth rate, flow cytometry fluorescence signals, fluorescence excitation and emission ratios), by considering the temperature, light intensity, light color and pigment type as fixed factors, and the strain as a random factor.

For shift experiments, the slopes of the linear parts of $Exc_{495:545}$ vs. time curves were compared between PTs 3dA and 3dB representatives using *t*-tests. As the number of strains used for shift experiments was reduced ($n = 3$ for PT 3dA and $n = 5$ for PT 3dB), the significance level was raised to 0.1 in order to confer more power to statistical analyses.

Results

Acclimation experiments

A first set of experiments was performed to investigate the effect of temperature, light intensity and color on various physiological characteristics including growth rate, flow cytometric red and orange fluorescence signals, as well as phycobilin and phycobiliprotein content, of six *Synechococcus* strains (BL107, RS9916 and WH8020 for PT 3dA and A15-62, PROS-U-1 and RS9915 for PT 3dB; Table 1) pre-acclimated for at least 3 weeks to the different tested conditions.

Growth rate

The growth rate (μ) of the six *Synechococcus* strains was lower at 18°C than at 25°C (*p*-value <0.05; Figure 1; Supplementary Table S1). Maximal μ values were reached at 25°C in HL, with all strains except WH8020 achieving more than one cell division per day ($\mu > 0.69\ day^{-1}$; Supplementary Figure S2). While a clear increase in growth rates of both PTs was seen between LL and HL at 25°C, a less marked difference was noted at 18°C, suggesting that temperature and light intensity had a synergistic effect on μ. This was confirmed by the mixed model, which highlighted an interaction effect between the two factors (*p*-value <0.05; Supplementary Table S1). While for any given strain, the growth rate varied little between the different light colors (Supplementary Figure S2), PT 3dA representatives globally grew faster than their PT 3dB counterparts (*p*-value <0.05; Figure 1; Supplementary Table S1).

Chlorophyll *a* and phycoerythrin fluorescence

A significant downward trend in both flow cytometric red (Chl *a*) and orange (PE) fluorescence signals was observed from 100% BL to 100% GL for both PTs in all conditions (*p*-value <0.05; Figures 2, 3; Supplementary Figures S3, S4; Supplementary Table S1). Besides light quality, temperature and light intensity strongly impacted Chl *a* and PE fluorescence signals (*p*-value <0.05; Supplementary Table S1). Both variables were indeed higher in LL than HL, but also at 25°C compared to 18°C (Figures 2, 3). Due to the synergistic effect of temperature and irradiance (*p*-value <0.05; Supplementary Table S1), maximum values were measured at 25°C in LL, and conversely minima were associated with the 18°C and HL condition.

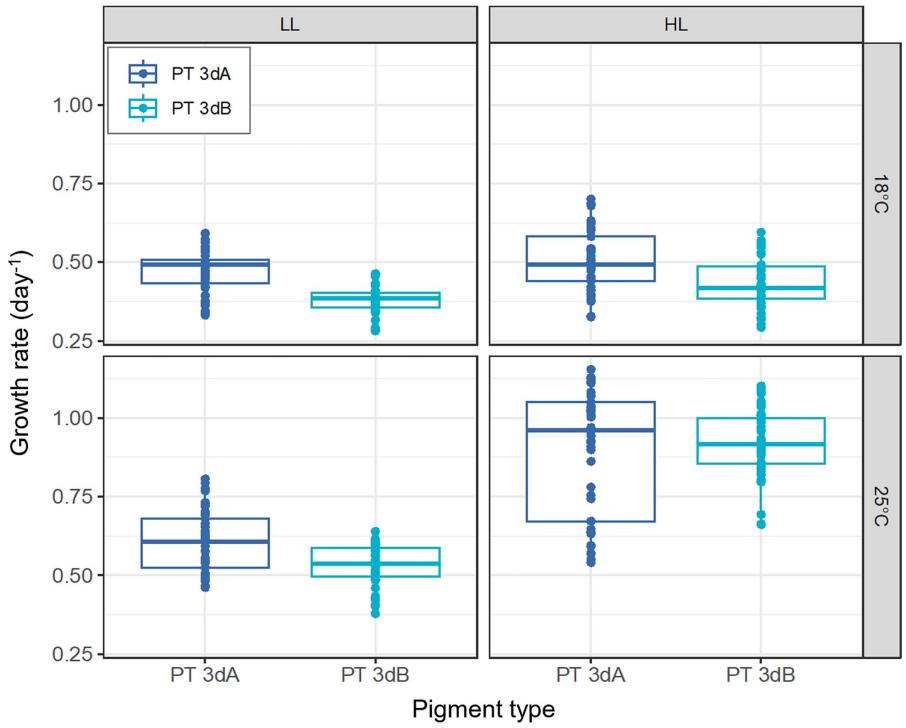

FIGURE 1
Growth rates of six PT 3dA and 3dB representatives acclimated to the different conditions of temperature and light intensity used for acclimation experiments. Each boxplot represents the measurements performed for all representatives of each pigment type in the five light colors tested in this study ($n = 45$). The light quality factor is not shown, as it had no significant effect on growth rate (*p*-value >0.05). LL, 15 µmol photons m^{-2} s^{-1}; HL, 75 µmol photons m^{-2} s^{-1}; PT, pigment type.

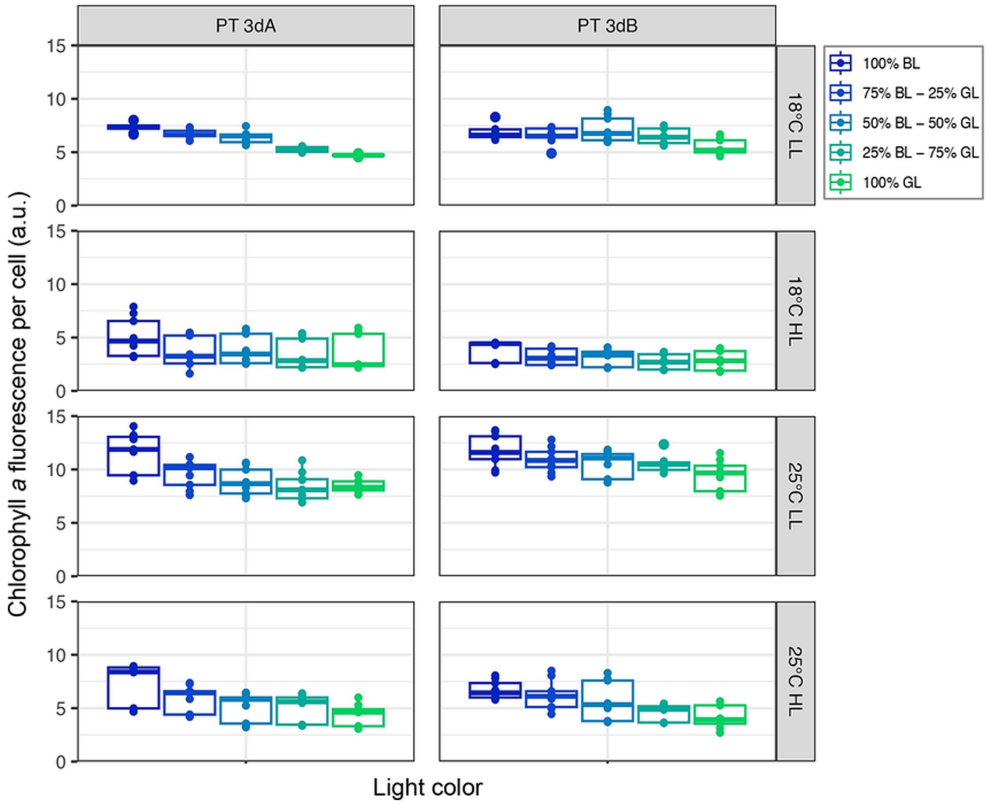

FIGURE 2
Flow cytometric chlorophyll *a* fluorescence per cell of six PT 3dA and 3dB representatives acclimated to the different conditions of temperature, light intensity and quality used for acclimation experiments. Each boxplot represents the measurements performed for all representatives of each pigment type in one light color condition ($n = 9$). LL, 15 µmol photons m^{-2} s^{-1}; HL, 75 µmol photons m^{-2} s^{-1}; PT, pigment type; BL, blue light; GL, green light.

Phycobilin content

All strains globally displayed $Exc_{495:545}$ fluorescence excitation ratio, a proxy of the whole cell PUB:PEB ratio, typical of chromatic acclimaters when grown in 100% GL ($Exc_{495:545} \approx 0.6–0.7$) or 100% BL ($Exc_{495:545} \approx 1.6–1.7$; Humily et al., 2013; Supplementary Figure S5). It is important to note that the LEDs used to get the 100% GL condition actually peaked at 515 nm, which is at the blue edge of the green wavelength range (Supplementary Figure S1). Yet, the fact that all tested strains exhibited the lowest possible $Exc_{495:545}$ ratio for chromatic acclimaters shows that they did sense this light quality as being full GL.

The light quality had the strongest impact on the $Exc_{495:545}$ fluorescence excitation ratio (p-value <0.05; Supplementary Table S1), the latter expectedly decreasing from 100% BL to 100% GL. Interestingly, the two PTs did not respond in the same way to the light color (p-value <0.05; Supplementary Table S1). PT 3dB representatives indeed exhibited higher $Exc_{495:545}$ ratios than their PT 3dA counterparts in most intermediate blue-green conditions (Figure 4), due to a more progressive decrease of their ratio from the BL- to the GL-acclimated state. This trend was more pronounced in LL than HL conditions, as confirmed by the significant interaction effect between PT and light quantity (p-value <0.05; Supplementary Table S1).

Phycobiliprotein content

PT 3dA and 3dB representatives exhibited different patterns of variation with light color of the $Em_{560:650}$ fluorescence emission ratio, a proxy of the whole cell PE:PC ratio (p-value <0.05; Figure 5; Supplementary Figure S6; Supplementary Table S1). The $Em_{560:650}$ ratio was indeed generally higher in PT 3dA than PT 3dB strains and often decreased from 100% BL to 100% GL in the former, while it remained fairly stable whatever the light quality in the latter. Although less obvious, the mixed model demonstrated that the $Em_{560:650}$ fluorescence emission ratio was also significantly influenced by the temperature and light intensity (p-value <0.05; Supplementary Table S1).

The $Em_{650:680}$ fluorescence emission ratio, a proxy of the whole cell PC:TA ratio, was only impacted by the temperature factor, which was found to interact with the PT (p-value <0.05; Supplementary Table S1). PT 3dA representatives were indeed able to achieve higher values than PT 3dB strains in all conditions, but the difference was even greater at 25°C (Figure 6; Supplementary Figure S7). Moreover, the PTs were not similarly affected by the light quantity (p-value <0.05; Supplementary Table S1) as increasing irradiance seemed to induce an increase in the $Em_{650:680}$ ratio in PT 3dA strains and a decrease in PT 3dB cells.

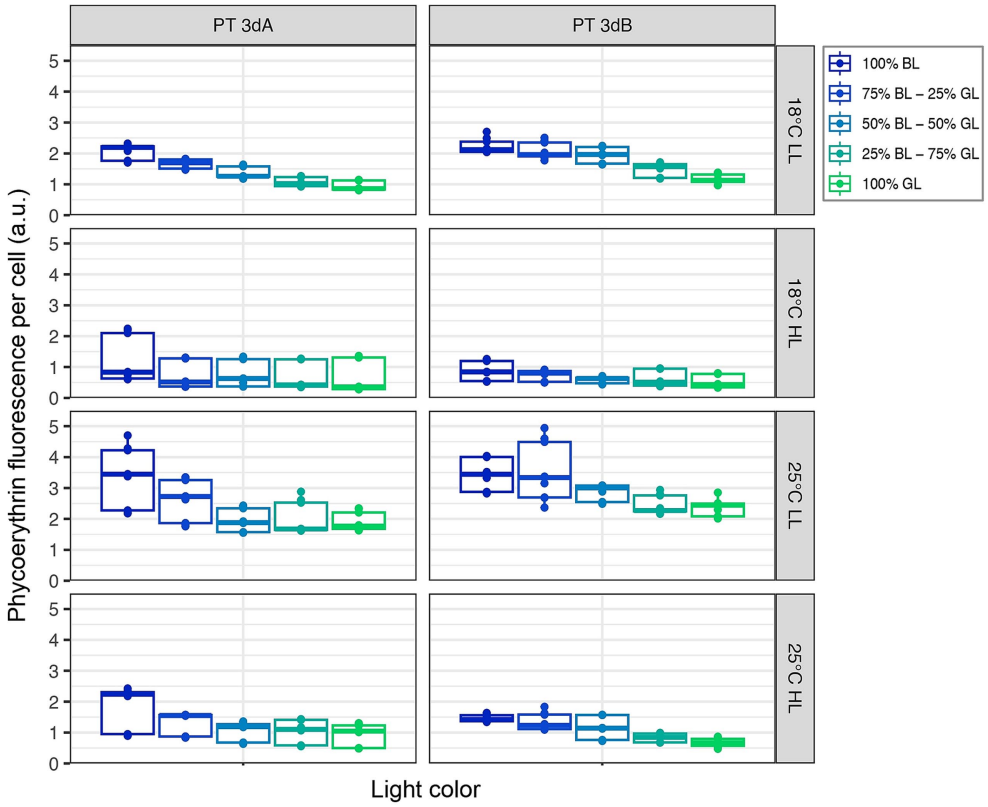

FIGURE 3
Same as Figure 2 but for the flow cytometric phycoerythrin fluorescence per cell.

Shift experiments

A second set of experiments consisted in studying the CA4 kinetics following shifts from BL to GL, and *vice-versa*, for 10 *Synechococcus* strains (BIOS-U3-1, BL107, MITS9220, RS9916 and WH8020 for PT 3dA and A15-62, A18-40, MINOS11, PROS-U-1 and RS9915 for PT 3dB; Table 1) pre-acclimated for at least 3 weeks to either LL or HL at 25°C. As expected, all strains exhibited slower chromatic acclimation kinetics in LL than HL, regardless of the initial light color, since the CA4 process took about 7 days in the former condition and 4 days in the latter.

Consistent with a previous study (Humily et al., 2013), the BIOS-U3-1 strain could not fully acclimate to HBL, never exceeding an $Exc_{495:545}$ ratio of about 1.2, and the same observation was made for the other representative of the CRD1 clade, MITS9220. We therefore excluded these two strains before comparing the kinetics of $Exc_{495:545}$ variations between PTs. To do so, we compared the slopes of linear regressions computed from the linear parts of the kinetics between the shift time (T_0) and the time needed for the cells to reach a plateau (Figure 7; 50 h for HGL to HBL, 75 h for HBL to HGL, 125 h for both LL shifts). These slopes (Supplementary Figures S8A–D), which reflected the rate of $Exc_{495:545}$ variation over time, were then compared between PTs (Supplementary Figures S9A,B). This comparison demonstrated that the rate of $Exc_{495:545}$ variation was significantly higher for PT 3dB than PT 3dA cells from HBL to HGL (p-value <0.1; Supplementary Figure S9A). Conversely, PT 3dA strains displayed a significantly faster acclimation pace than their PT 3dB counterparts after the shifts from LGL to LBL and HGL to HBL (p-value <0.1; Supplementary Figure S9B).

Discussion

The marine environment was recently shown to shelter five distinct spectral niches, based on the absorption properties of water molecules as well as the variable concentrations of colored dissolved organic matter and non-algal particles (Holtrop et al., 2021). Thanks to their specific antenna complexes binding divinyl derivatives of Chl *a* and *b* (Goericke and Repeta, 1992), cells of the tiny cyanobacterium *Prochlorococcus* appear to be well adapted to the violet niche (401–449 nm), which encompasses the central oceanic gyres. In contrast, *Synechococcus* BL specialists (PT 3c), i.e., cells possessing a high content in PUB ($\lambda_{max} \approx 495$ nm), are best suited for the blue niche (449–514 nm) that comprises most other open ocean zones. As concerns *Synechococcus* GL specialists (PT 3a), i.e., cells possessing a high content in PEB ($\lambda_{max} \approx 545$ nm), they preferentially thrive in the green niche (514–605 nm) that is essentially found in coastal and upwelling areas (Holtrop et al., 2021). In this context, *Synechococcus* cells capable of CA4, i.e., to match their $Exc_{495:545}$ ratio to the ambient light color in order to optimize photon collection, expectedly colonize both blue and green niches, where they can constitute a large part of the whole *Synechococcus* population, especially at high latitude (Xia et al., 2017; Grébert

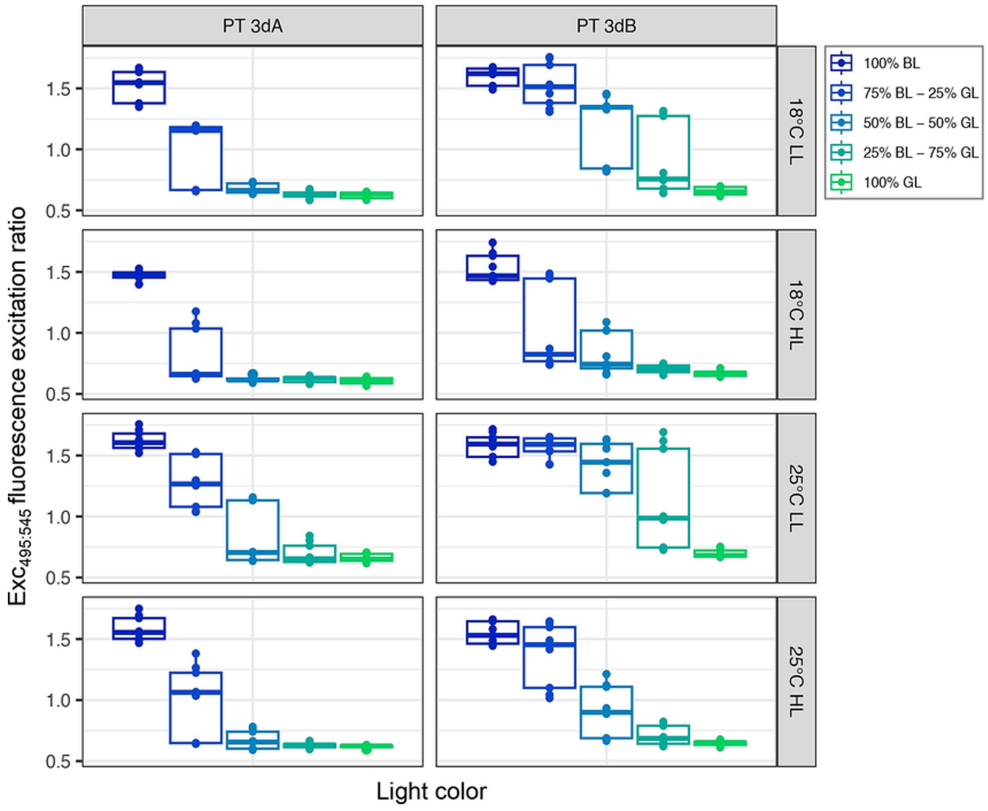

FIGURE 4
Same as Figure 2 but for the $Exc_{495:545}$ fluorescence excitation ratio, a proxy of the whole cell PUB:PEB ratio.

et al., 2018). The occurrence of two genetically distinct types of chromatic acclimaters colonizing different habitats in the field (Humily et al., 2013; Grébert et al., 2018, 2021, 2022) however made us wonder whether they displayed phenotypic differences that may partly explain their different spatial distributions.

Here, we looked at the interplay between light quality, light quantity and temperature, and we managed to unveil subtle but significant differences between PTs 3dA and 3dB. Comparisons of cultures acclimated to various light colors ranging from 100% BL to 100% GL at two temperatures and two irradiance levels revealed that, in intermediate blue-green light conditions, PT 3dB strains displayed significantly higher $Exc_{495:545}$ ratios than their PT 3dA counterparts (Figure 4). The observed differences are notably due to a more progressive decrease of the $Exc_{495:545}$ ratio for PT 3dB than PT 3dA representatives from BL to GL. The latter were indeed more frequently found in the GL-acclimated state with some of them, such as RS9916 in most conditions, even shifting their $Exc_{495:545}$ ratio to the BL-acclimated state only in 100% BL (Supplementary Figure S5). In contrast, PT 3dB cells tended to remain longer in the BL-acclimated state, even when the proportion of GL in the incident light was important, an extreme case being A15-62 at 25°C and LL that shifted to the GL-acclimated state only in 100% GL. Based on the phenotypes of knock-out mutants of genes involved in the CA4 process, it has been previously hypothesized that the PT 3dA genotype may have derived from a former GL specialist having acquired the CA4 capacity by integrating a CA4-A island, while the PT 3dB genotype may have been derived from a former BL specialist having integrated a CA4-B island (Sanfilippo et al., 2019b; Grébert et al., 2021). Interestingly, our results are in good agreement with this hypothesis since they suggest that PT 3dA strains need a large proportion of blue photons to induce the CA4-A response, while on the contrary PT 3dB cells require a larger proportion of green photons to induce the CA4-B response. In other words, the two PTs seemingly differ in the blue-to-green ratio necessary to trigger the CA4 process, even though there is some strain-to-strain variability.

The molecular basis of the difference in $Exc_{495:545}$ ratio between chromatic acclimaters fully acclimated to either 100% BL or 100% GL has been well documented, and was found to be the same in the PT 3dA model strain RS9916 (Shukla et al., 2012; Sanfilippo et al., 2016, 2019b) and the PT 3dB model strain A15-62 (Grébert et al., 2021). Both CA4-A and -B processes indeed consist in an exchange of one out of the five phycobilins bound to the α-PE-I subunit (Cys-139) and two out of the six phycobilins bound to the α-PE-II subunit (Cys-83 and Cys-140), with PUB molecules being bound to these three positions in BL, and PEB in GL. However, the observation of intermediate $Exc_{495:545}$ ratios in blue-green light mixes (Figure 4; see also Sanfilippo et al., 2019b) remains difficult to interpret as it may translate different, but not mutually exclusive, sources of variability. More precisely, this observation may be explained by: (i) heterogeneous populations of *Synechococcus* cells with PBS either fully acclimated to BL (PUB-rich) or to GL (PEB-rich); (ii)

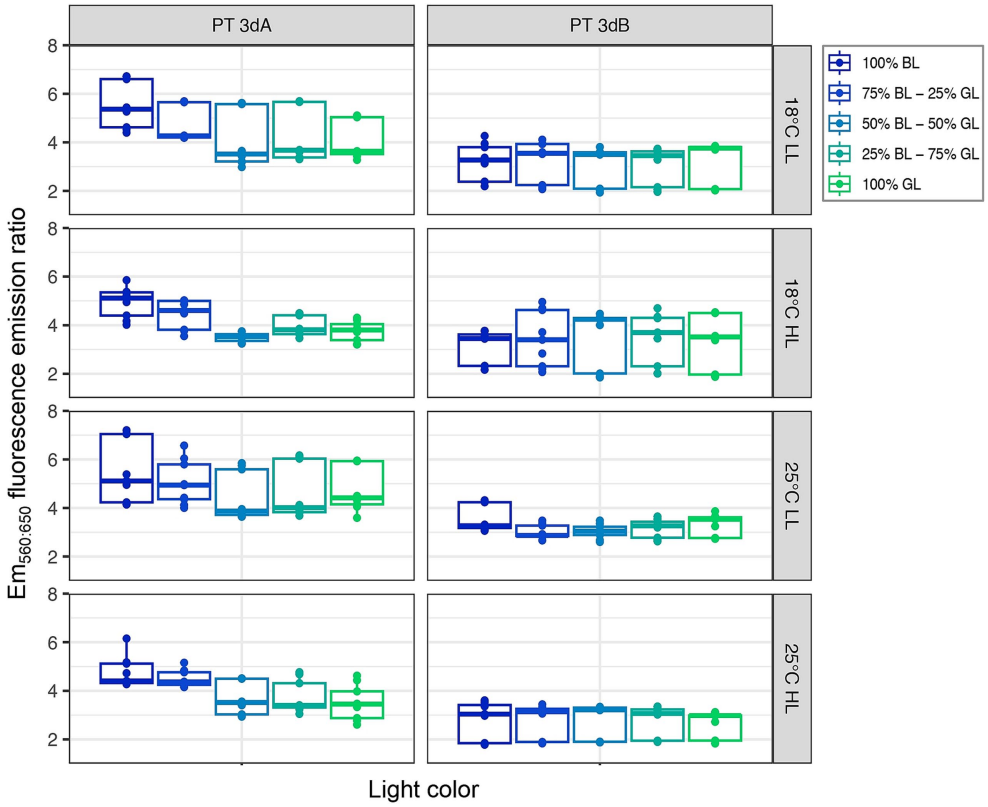

FIGURE 5
Same as Figure 2 but for the $Em_{560:650}$ fluorescence emission ratio, a proxy of the whole cell PE:PC ratio.

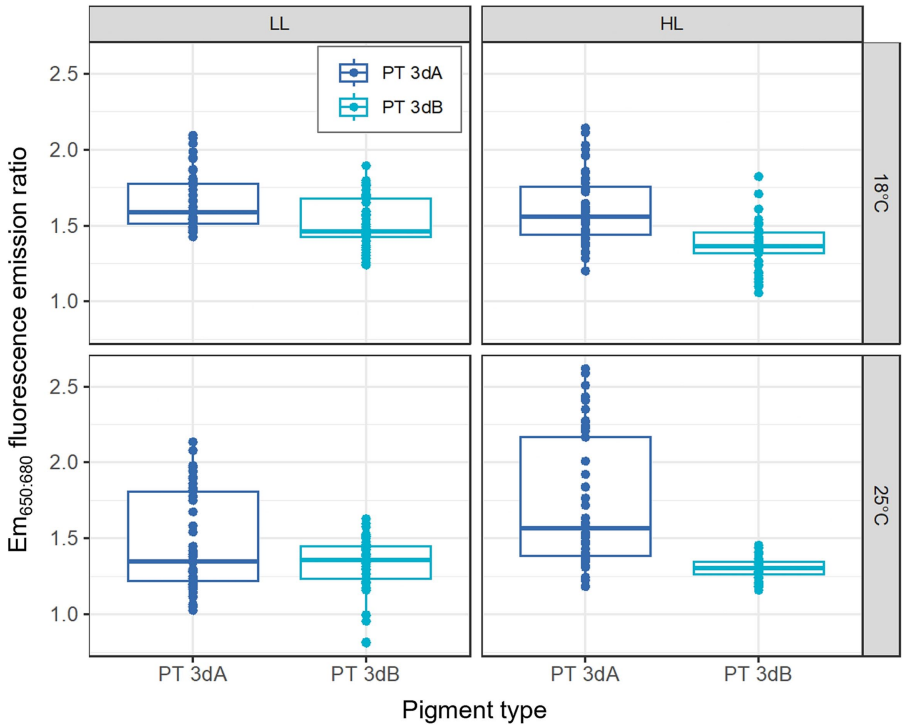

FIGURE 6
Same as Figure 1 but for the $Em_{650:680}$ fluorescence emission ratio, a proxy of the whole cell PC:TA ratio.

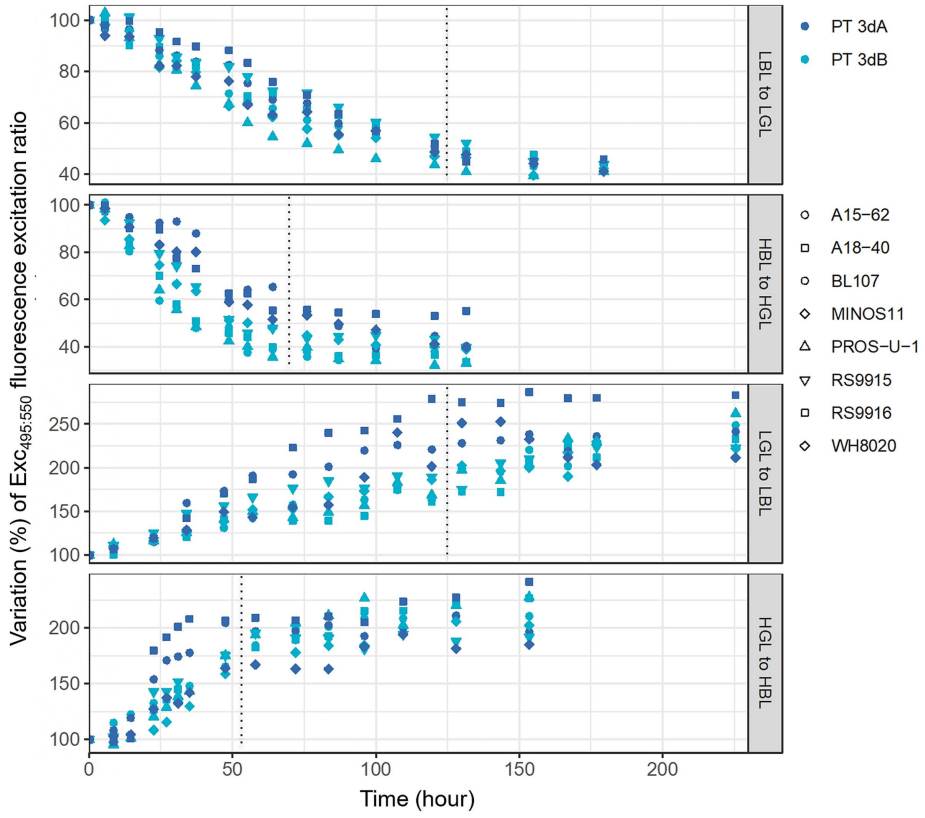

FIGURE 7
Time course variations of the $Exc_{495:545}$ fluorescence excitation ratio, a proxy of the whole cell PUB:PEB ratio, of eight PT 3dA and 3dB representatives after an abrupt shift of light quality from 100% blue to 100% green light, and *vice-versa*, in low and high light. Data are normalized to the initial value at time zero. Each point represents one measurement performed for one strain. LL, 15 µmol photons m^{-2} s^{-1}; HL, 75 µmol photons m^{-2} s^{-1}; PT, pigment type; BL, blue light; GL, green light.

homogeneous populations of *Synechococcus* cells all having different phycobilins at the three swing sites in a given light color; (iii) individual cells containing PBS with different chromophorylation states; and/or (iv) heterogeneity in phycobiliprotein chromophorylation within single PBS, i.e., PBS having rods with different chromophorylation states. Unfortunately, there is currently no simple experimental way to demonstrate which of these hypotheses is most likely.

In contrast to $Exc_{495:545}$ ratios, light quality had no significant effect on growth rates, while the latter varied with PT, temperature and light quantity. In HL, the growth rates of all six chromatic acclimaters used for acclimation experiments were significantly higher at 25°C than 18°C, the former being an optimal growth temperature for most marine *Synechococcus* strains tested so far (Figure 1; Mackey et al., 2013; Pittera et al., 2014; Breton et al., 2020; Doré et al., 2022; Ferrieux et al., 2022). The impact of increasing temperature on growth rate was however much less important at LL, confirming that temperature and irradiance have a synergistic effect on growth, as previously observed in the model strain WH7803 (Guyet et al., 2020). Of note, whatever the temperature, all cells were also able of typical photoacclimation, i.e., to adjust the surface of their photosynthetic membranes to reduce the incoming photon flux (Kana and Glibert, 1987; Moore et al., 1995; Six et al., 2004), as shown by the decrease of both Chl *a* and PE fluorescence signals between LL and HL (Figures 2, 3). Interestingly, both parameters also slightly decreased in all representatives in response to progressive changes in light quality from 100% BL to 100% GL (Figures 2, 3; Supplementary Figures S3, S4), suggesting that chromatic acclimaters used GL more efficiently than BL, at least in our experimental setup. Consequently, all strains needed to slightly adjust their thylakoid surface (and thus the number of both photosystems and PBS) in BL in order to maximize the collection of available photons and maintain similar growth rate (Supplementary Figure S2).

Another parameter that differentiated PTs 3dA from 3dB in the present study is the $Em_{560:650}$ fluorescence emission ratio, which is often interpreted as a proxy of the PE:PC ratio. This ratio exhibited higher values and tended to decrease from 100% BL to 100% GL in PT 3dA strains, while it was more stable in PT 3dB representatives (Figure 5). Since PE fluorescence per cell decreased in PT 3dA from BL to GL (Figure 3) and the PC:TA ratio was somewhat constant (Supplementary Figure S7), this may indicate a lower within-rod photon energy transfer efficiency in PT 3dA cells in GL compared to BL. Another possibility is that PBS rod length decreased by disconnection of the distal PUB-rich PE-II hexamers, as previously observed in *Synechococcus* sp. WH8102 as a result of photoacclimation (Six et al., 2004). In PT

3dB representatives, the PE:PC ratio stability, associated with decreasing PE fluorescence, rather suggests that other kinds of structural changes occurred, such as a reduction of the PBS number per cell or of the thylakoidal surface area.

Shift experiments in both LL and HL conditions from 100% BL to 100% GL, and *vice-versa*, confirmed previous observations by Humily et al. (2013) that PT 3dA cells generally exhibit a more variable acclimation kinetics than PT 3dB cells. Two PT 3dA strains belonging to the CRD1 clade (BIOS-U3-1 and MITS9220) were indeed stuck at an $Exc_{495:545}$ ratio of around 1.2 in HBL (corresponding to "phenotypic group 2" in Humily et al., 2013). Moreover, MITS9220 and another PT 3dA strain (BL107) showed a delay in the initiation of CA4 from LBL to LGL, but not in the reverse condition, as previously reported by these authors for BL107, a behavior they designed as "phenotypic group 3." Some PT 3dA representatives common to both studies (RS9916 and WH8020) exhibited different behaviors. Both strains indeed reached a significantly lower $Exc_{495:545}$ ratio in HBL than LBL in the previous study but not in the present one, strengthening the idea that PT 3dA cells display a more variable acclimation phenotype than PT 3dB cells, at least in some conditions. In contrast, most PT 3dB representatives exhibited a "typical" CA4 dynamics in both studies, designed by Humily et al. (2013) as "phenotypic group 1." The only exceptions are strains such as WH8103 that have a typical CA4-B region but, for a yet unknown reason, have completely lost their CA4 ability and thus display a fixed $Exc_{495:545}$ ratio. Interestingly in this context, the WH8109 strain that was reported to display this fixed phenotype in Humily et al. (2013) was found to have recovered its CA4 ability in a more recent study (Lovindeer et al., 2021). The wider phenotypic variability observed in PT 3dA representatives might be attributed to the erratic genomic localization of the CA4-A island, which can be found virtually anywhere in the genome of PT 3dA strains, including the 5′-end of the PBS region, while the CA4-B island is systematically located in the middle of the PBS rod region in PT 3dB cells (Humily et al., 2013; Grébert et al., 2022).

The most striking outcome of our shift experiments was certainly the discrepancy in acclimation paces between the two types of chromatic acclimaters in three out of the four tested conditions. Indeed, after the LGL to LBL and HGL to HBL shifts, the PT 3dA representatives acclimated faster than their PT 3dB counterparts, while the opposite pattern was observed after the HBL to HGL shift (Figure 7; Supplementary Figures S8, S9). Altogether, our results showed that while PT 3dA and PT 3dB cells preferentially remain in their respective basal state (i.e., low and high $Exc_{495:545}$ ratio, respectively) when grown in a blue-green light mix (Figure 4), they can reach the acclimation state opposite to their basal state faster than the other PT once the CA4 process has been triggered (Figure 7; Supplementary Figures S8, S9). These distinct acclimation paces might be due to differences in the organization and gene content of the CA4-A and CA4-B islands. While both share two genes in tandem encoding the regulatory proteins FciA and FciB (Sanfilippo et al., 2016), as well as a gene encoding a protein of unknown function (Unk10), they also contain specific genes. A third putative regulatory gene, *fciC*, is indeed only found in PT 3dA representatives, possibly explaining why the two CA4 processes are opposite, CA4-A being activated in BL and CA4-B in GL (Shukla et al., 2012; Humily et al., 2013; Sanfilippo et al 2019b; Grébert et al., 2021). Additionally, the CA4-A and CA4-B islands encode distinct enzymes, the PEB lyase-isomerase MpeZ and the PEB lyase MpeW, respectively. Both compete with another enzyme, encoded in the main PBS genomic region, for binding either a PUB in BL or a PEB in GL at Cys-83 of the α-PE-II subunit (Sanfilippo et al., 2019b; Grébert et al., 2021). Functional studies are needed to determine whether these mechanistic discrepancies are responsible for the phenotypic differences between PT 3dA and 3dB strains reported in the present study.

In conclusion, PTs 3dA and 3dB cells exhibit subtle but significant phenotypic differences that may explain why, in a spectral niche encompassing both blue and green light, they can coexist not only with BL and/or GL specialists, but also with their CA4-able counterpart (Huisman et al., 2002; Stomp et al., 2004; Grébert et al., 2018; Luimstra et al., 2020; Holtrop et al., 2021). Future studies should allow one to confirm this hypothesis, either using co-cultures of different PTs grown in various light colors, or by correlation analyses of the variations of the relative abundance of the different PTs with changes in the underwater light field.

Data availability statement

The original contributions presented in the study are included in the article/Supplementary material, further inquiries can be directed to the corresponding author.

Author contributions

LD: Conceptualization, Data curation, Formal analysis, Investigation, Methodology, Resources, Validation, Writing – original draft, Writing – review & editing, Software, Visualization. LG: Conceptualization, Data curation, Formal analysis, Investigation, Methodology, Resources, Validation, Writing – review & editing, Funding acquisition, Project administration, Supervision. BG: Investigation, Methodology, Writing – review & editing. JC: Investigation, Methodology, Writing – review & editing. MR: Investigation, Methodology, Resources, Writing – review & editing. FP: Conceptualization, Data curation, Formal analysis, Investigation, Methodology, Resources, Supervision, Validation, Writing – review & editing, Funding acquisition, Project administration, Visualization.

Funding

The author(s) declare financial support was received for the research, authorship, and/or publication of this article. This work was supported by the French "Agence Nationale de la Recherche" Program EFFICACY (ANR-19-CE02-0019).

Acknowledgments

The authors would like to thank Priscillia Gourvil, Martin Gachenot, and Michele Grego from the Roscoff Culture Collection (http://roscoff-culture-collection.org/) for maintaining the *Synechococcus* strains used in this study, and Maela Kloareg (Kuzulia) for performing statistical analyses.

Conflict of interest

The authors declare that the research was conducted in the absence of any commercial or financial relationships that could be construed as a potential conflict of interest.

Publisher's note

All claims expressed in this article are solely those of the authors and do not necessarily represent those of their affiliated organizations, or those of the publisher, the editors and the reviewers. Any product that may be evaluated in this article, or claim that may be made by its manufacturer, is not guaranteed or endorsed by the publisher.

Supplementary material

The Supplementary material for this article can be found online at: https://www.frontiersin.org/articles/10.3389/fmicb.2024.1349322/full#supplementary-material

References

Boresch, K. (1922). Photokatalysen in Pflanzen. *Naturwissenschaften* 10, 505–512. doi: 10.1007/BF01565117

Breton, S., Jouhet, J., Guyet, U., Gros, V., Pittera, J., Demory, D., et al. (2020). Unveiling membrane thermoregulation strategies in marine picocyanobacteria. *New Phytol.* 225, 2396–2410. doi: 10.1111/nph.16239

Doré, H., Farrant, G. K., Guyet, U., Haguait, J., Humily, F., Ratin, M., et al. (2020). Evolutionary mechanisms of long-term genome diversification associated with niche partitioning in marine picocyanobacteria. *Front. Microbiol.* 11:567431. doi: 10.3389/fmicb.2020.567431

Doré, H., Leconte, J., Guyet, U., Breton, S., Farrant, G. K., Demory, D., et al. (2022). Global phylogeography of marine *Synechococcus* in coastal areas reveals strong community shifts. *mSystems* 7, e00656–e00622. doi: 10.1128/msystems.00656-22

Engelmann, T. W. (1902). Über experimentelle Erzeugung zweckmässiger Änderungen der Färbung pflanzlicher Chromophylle durch farbiges Licht. Bericht über Versuche von N. Gaidukow. *Arch. Anat. Physiol*, 333–335.

Everroad, C., Six, C., Partensky, F., Thomas, J.-C., Holtzendorff, J., and Wood, A. M. (2006). Biochemical bases of type IV chromatic adaptation in marine *Synechococcus* spp. *J. Bacteriol.* 188, 3345–3356. doi: 10.1128/JB.188.9.3345-3356.2006

Farrant, G. K., Doré, H., Cornejo-Castillo, F. M., Partensky, F., Ratin, M., Ostrowski, M., et al. (2016). Delineating ecologically significant taxonomic units from global patterns of marine picocyanobacteria. *Proc. Natl. Acad. Sci. USA* 113, E3365–E3374. doi: 10.1073/pnas.1524865113

Ferrieux, M., Dufour, L., Doré, H., Ratin, M., Guéneuguès, A., Chasselin, L., et al. (2022). Comparative thermophysiology of marine *Synechococcus* CRD1 strains isolated from different thermal niches in iron-depleted areas. *Front. Microbiol.* 13:893413. doi: 10.3389/fmicb.2022.893413

Gaidukov, N. (1903). Weitere Untersuchungen über den Einfluss farbigen Lichtes auf die Färbung der Oscillarien. *Ber. Dtsch. Bot. Ges.* 21, 484–492. doi: 10.1111/j.1438-8677.1903.tb05185.x

Goericke, R., and Repeta, D. J. (1992). The pigments of *Prochlorococcus marinus*: the presence of divinyl-chlorophyll *a* and *b* in a marine procaryote. *Limnol. Oceanogr.* 37, 425–433. doi: 10.4319/lo.1992.37.2.0425

Grébert, T., Doré, H., Partensky, F., Farrant, G. K., Boss, E. S., Picheral, M., et al. (2018). Light color acclimation is a key process in the global ocean distribution of *Synechococcus* cyanobacteria. *Proc. Natl. Acad. Sci. USA* 115, E2010–E2019. doi: 10.1073/pnas.1717069115

Grébert, T., Garczarek, L., Daubin, V., Humily, F., Marie, D., Ratin, M., et al. (2022). Diversity and evolution of pigment types in marine *Synechococcus* cyanobacteria. *Genome Biol. Evol.* 14:evac035. doi: 10.1093/gbe/evac035

Grébert, T., Nguyen, A. A., Pokhrel, S., Joseph, K. L., Ratin, M., Dufour, L., et al. (2021). Molecular bases of an alternative dual-enzyme system for light color acclimation of marine *Synechococcus* cyanobacteria. *Proc. Natl. Acad. Sci. USA* 118:e2019715118. doi: 10.1073/pnas.2019715118

Guyet, U., Nguyen, N. A., Doré, H., Haguait, J., Pittera, J., Conan, M., et al. (2020). Synergic effects of temperature and irradiance on the physiology of the marine *Synechococcus* strain WH7803. *Front. Microbiol.* 11:1707. doi: 10.3389/fmicb.2020.01707

Hirose, Y., Chihong, S., Watanabe, M., Yonekawa, C., Murata, K., Ikeuchi, M., et al. (2019). Diverse chromatic acclimation processes regulating phycoerythrocyanin and rod-shaped phycobilisome in cyanobacteria. *Mol. Plant* 12, 715–725. doi: 10.1016/j.molp.2019.02.010

Holtrop, T., Huisman, J., Stomp, M., Biersteker, L., Aerts, J., Grébert, T., et al. (2021). Vibrational modes of water predict spectral niches for photosynthesis in lakes and oceans. *Ecol. Evol.* 5, 55–66. doi: 10.1038/s41559-020-01330-x

Huisman, J., Matthijs, H. C. P., Visser, P. M., Balke, H., Sigon, C. A. M., Passarge, J., et al. (2002). Principles of the light-limited chemostat: theory and ecological applications. *Antonie Van Leeuwenhoek* 81, 117–133. doi: 10.1023/A:1020537928216

Humily, F., Partensky, F., Six, C., Farrant, G. K., Ratin, M., Marie, D., et al. (2013). A gene island with two possible configurations is involved in chromatic acclimation in marine *Synechococcus*. *PLoS One* 8:e84459. doi: 10.1371/journal.pone.0084459

Kana, T. M., and Glibert, P. M. (1987). Effect of irradiances up to 2000 μE m^{-2} s^{-1} on marine *Synechococcus* WH7803—I. Growth, pigmentation, and cell composition. *Deep Sea Res.A* 34, 479–495. doi: 10.1016/0198-0149(87)90001-X

Kirk, J. T. (1994). *Light and photosynthesis in aquatic ecosystems. 2* Cambridge University Press. Cambridge

Lovindeer, R., Abbott, L., Medina, H., and Mackey, K. R. M. (2021). Costs and limitations of marine *Synechococcus* blue-green chromatic acclimation. *Front. Mar. Sci.* 8:689998. doi: 10.3389/fmars.2021.689998

Luimstra, V. M., Verspagen, J. M. H., Xu, T., Schuurmans, J. M., and Huisman, J. (2020). Changes in water color shift competition between phytoplankton species with contrasting light-harvesting strategies. *Ecology* 101:e02951. doi: 10.1002/ecy.2951

Mackey, K. R. M., Paytan, A., Caldeira, K., Grossman, A. R., Moran, D., McIlvin, M., et al. (2013). Effect of temperature on photosynthesis and growth in marine *Synechococcus* spp. *Plant Physiol.* 163, 815–829. doi: 10.1104/pp.113.221937

Marie, D., Partensky, F., Vaulot, D., and Brussaard, C. (1999). Enumeration of phytoplankton, bacteria, and viruses in marine samples. *Curr. Prot. Cytom.* 11:11.11. doi: 10.1002/0471142956.cy1111s10

Moore, L. R., Goericke, R., and Chisholm, S. W. (1995). Comparative physiology of *Synechococcus* and *Prochlorococcus*: influence of light and temperature on growth, pigments, fluorescence and absorptive properties. *Mar. Ecol. Prog. Ser.* 116, 259–275. doi: 10.3354/MEPS116259

Mazard, S., Ostrowski, M., Partensky, F., and Scanlan, D. J. (2012). Multi-locus sequence analysis, taxonomic resolution and biogeography of marine. *Synechococcus. Environ. Microbiol.* 14, 372–386. doi: 10.1111/j.1462-2920.2011.02514.x

Ong, L. J., and Glazer, A. N. (1991). Phycoerythrins of marine unicellular cyanobacteria. I. Bilin types and locations and energy transfer pathways in *Synechococcus* spp. phycoerythrins. *J. Biol. Chem.* 266, 9515–9527. doi: 10.1016/S0021-9258(18)92851-6

Palenik, B. (2001). Chromatic adaptation in marine *Synechococcus* strains. *Appl. Environ. Microbiol.* 67, 991–994. doi: 10.1128/AEM.67.2.991-994.2001

Pinheiro, J., Bates, D., DebRoy, S., Sarkar, D., Heisterkamp, S., and Van Willigen, B., et al R Core Team. (2023). *nlme: Linear and nonlinear mixed effects models*. R package version 3.1-164.Available at: https://CRAN.R-project.org/package=nlme

Pittera, J., Humily, F., Thorel, M., Grulois, D., Garczarek, L., and Six, C. (2014). Connecting thermal physiology and latitudinal niche partitioning in marine *Synechococcus*. *ISME J.* 8, 1221–1236. doi: 10.1038/ismej.2013.228

R Core Team (2021). *R: A language and environment for statistical computing*. R Foundation for Statistical Computing, Vienna, Austria. Available at: https://www.R-project.org/

Rippka, R., Coursin, T., Hess, W., Lichtlé, C., Scanlan, D. J., Palinska, K. A., et al. (2000). *Prochlorococcus marinus* Chisholm et al. 1992 subsp. *pastoris* subsp. nov. strain PCC 9511, the first axenic chlorophyll a_2/b_2-containing cyanobacterium (*Oxyphotobacteria*). *Int. J. Syst. Evol. Microbiol.* 50, 1833–1847. doi: 10.1099/00207713-50-5-1833

Sanfilippo, J. E., Garczarek, L., Partensky, F., and Kehoe, D. M. (2019a). Chromatic acclimation in cyanobacteria: a diverse and widespread process for optimizing photosynthesis. *Ann. Rev. Microbiol.* 73, 407–433. doi: 10.1146/annurev-micro-020518-115738

Sanfilippo, J. E., Nguyen, A. A., Garczarek, L., Karty, J. A., Pokhrel, S., Strnat, J. A., et al. (2019b). Interplay between differentially expressed enzymes contributes to light color acclimation in marine *Synechococcus*. *Proc. Natl. Acad. Sci. USA* 116, 6457–6462. doi: 10.1073/pnas.1810491116

Sanfilippo, J. E., Nguyen, A. A., Karty, J. A., Shukla, A., Schluchter, W. M., Garczarek, L., et al. (2016). Self-regulating genomic island encoding tandem regulators confers chromatic acclimation to marine *Synechococcus*. *Proc. Natl. Acad. Sci. USA* 113, 6077–6082. doi: 10.1073/pnas.1600625113

Shukla, A., Biswas, A., Blot, N., Partensky, F., Karty, J. A., Hammad, L. A., et al. (2012). Phycoerythrin-specific Bilin lyase–isomerase controls blue-green chromatic acclimation in marine *Synechococcus*. *Proc. Natl. Acad. Sci. USA* 109, 20136–20141. doi: 10.1073/pnas.121177710

Sidler, W. A. (1994). "Phycobilisome and phycobiliprotein structures" in *The molecular biology of cyanobacteria advances in photosynthesis* (Dordrecht: Springer), 139–216.

Six, C., Thomas, J. C., Brahamsha, B., Lemoine, Y., and Partensky, F. (2004). Photophysiology of the marine cyanobacterium *Synechococcus* sp. WH8102, a new model organism. *Aquat. Microb. Ecol.* 35, 17–29. doi: 10.3354/ame035017

Six, C., Thomas, J.-C., Garczarek, L., Ostrowski, M., Dufresne, A., Blot, N., et al. (2007). Diversity and evolution of phycobilisomes in marine *Synechococcus* spp.: a comparative genomics study. *Genome Biol.* 8:R259. doi: 10.1186/gb-2007-8-12-r259

Stomp, M., Huisman, J., de Jongh, F., Veraart, A. J., Gerla, D., Rijkeboer, M., et al. (2004). Adaptive divergence in pigment composition promotes phytoplankton biodiversity. *Nature* 432, 104–107. doi: 10.1038/nature03044

Tandeau de Marsac, N. (1977). Occurrence and nature of chromatic adaptation in cyanobacteria. *J. Bacteriol.* 130, 82–91. doi: 10.1128/jb.130.1.82-91.1977

Xia, X., Partensky, F., Garczarek, L., Suzuki, K., Guo, C., Yan Cheung, S., et al. (2017). Phylogeography and pigment type diversity of *Synechococcus* cyanobacteria in surface waters of the northwestern Pacific Ocean. *Environ. Microbiol.* 19, 142–158. doi: 10.1111/1462-2920.13541

frontiers | Frontiers in Microbiology

TYPE Original Research
PUBLISHED 08 April 2024
DOI 10.3389/fmicb.2024.1377732

OPEN ACCESS

EDITED BY
Beatriz Roncero Ramos,
Sevilla University, Spain

REVIEWED BY
Nathali Maria Machado De Lima,
University of New South Wales, Australia
Sonia Chamizo,
University of Almeria, Spain

*CORRESPONDENCE
Lanzhou Chen
✉ chenlz@whu.edu.cn

RECEIVED 28 January 2024
ACCEPTED 27 March 2024
PUBLISHED 08 April 2024

CITATION
Zhou X, Liang B, Zhang T, Xiong Q, Ma X and Chen L (2024) Co-inoculation of fungi and desert cyanobacteria facilitates biological soil crust formation and soil fertility.
Front. Microbiol. 15:1377732.
doi: 10.3389/fmicb.2024.1377732

Co-inoculation of fungi and desert cyanobacteria facilitates biological soil crust formation and soil fertility

Xiangjun Zhou[1,2], Bin Liang[1], Tian Zhang[1], Qiao Xiong[1], Xiao Ma[1] and Lanzhou Chen[2]*

[1]Huangshi Key Laboratory of Prevention and Control of Soil Pollution, College of Urban and Environmental Sciences, Hubei Normal University, Huangshi, China, [2]Hubei Key Laboratory of Biomass-Resources Chemistry and Environmental Biotechnology, School of Resource and Environmental Sciences, Wuhan University, Wuhan, China

The inoculation of cyanobacteria for enriching soil nutrients and forming biological soil crusts (BSCs) is considered an effective means to restore degraded soil. However, there are limited studies on the application of co-inoculation of fungi and cyanobacteria for degraded soil remediation. In this study, a high exopolysaccharide-secreting fungi Zh2 was isolated from lichen BSCs in Hobq Desert, and co-inoculated with a cyanobacterial strain identified as *Phormidium tenue* in different proportions to form BSCs on sand during a 35 days incubation period. Results revealed significant differences in crust biomass and soil properties among crusts with different cyanobacterial/fungal inoculation ratios. Microbial biomass, soil nutrient content and enzyme activities in crusts co-inoculated with cyanobacteria and fungi were higher than those inoculated with cyanobacteria and fungi alone. The inoculation of cyanobacteria contributed to the fulvic-like accumulation, and the inoculated fungi significantly increased the humic-like content and soil humification. Redundancy analysis showed that the inoculation of cyanobacteria was positively correlated with the activities of urease and phosphatase, and the content of fulvic-like. Meanwhile, the inoculation of fungi was positively correlated with the contents of total carbon, total nitrogen and humic-like, the activities of catalase and sucrase. Cyanobacteria and fungi play distinct roles in improving soil fertility and accumulating dissolved organic matter. This study provides new insights into the effects of cyanobacteria and fungi inoculations on the formation and development of cyanobacterial-fungus complex crusts, offering a novel method for accelerating induced crust formation on the surface of sand.

KEYWORDS

biological soil crusts, co-inoculation, fungi, cyanobacteria, dissolved organic matter

1 Introduction

Desertification is a serious global environmental challenge, with approximately 40% of the Earth's land experiencing its adverse effects, imperiling the livelihoods, and living conditions of a billion individuals (Dregne et al., 1991; Verón et al., 2006). This phenomenon is exacerbated by climate change, overgrazing, unsustainable agricultural practices, and the excessive exploitation of water resources (Wang et al., 2023; Ren et al., 2024). In China, the

government has adopted the "Grain for Green" program (Segura et al., 2020) and "Soil and Water Conservation Engineering" (Karlen et al., 2014; Li et al., 2020). These initiatives involve measures such as reducing agricultural activities, slope protection, afforestation, artificial grass planting, and windbreak construction. These engineering projects entail substantial economic investment and manual maintenance (He et al., 2023), yet the desertification recovery process remains slow. The development of desertification control technology continues to be a global concern.

Biological soil crusts (BSCs) living within or on top of the uppermost millimeter of soil are soil particle-associated communities of cyanobacteria, algae, fungi, lichens, liverworts, mosses and bacteria in different proportions, and form coherent layers at the soil surface (Belnap et al., 2016; Ferrenberg et al., 2017). BSCs have long been known as "pioneers" or "ecosystem engineers" in drylands because of their multifunction on water reservation, carbon and nitrogen cycles, soil stabilization and preparation for the establishment and performance of vascular plants (Bowker et al., 2014; Rodriguez-Caballero et al., 2022; Marasco et al., 2023). BSCs are widely distributed in semiarid and arid areas, which constitute up to 40% of the terrestrial land surface (Weber et al., 2016). As 10–20% of these drylands are currently suffering from severe degradation (Maestre et al., 2016), the restoration of drylands is an urgent issue and one way to achieve this goal can be through the rehabilitation of BSC (Bowker, 2007; Antoninka et al., 2020; Rossi et al., 2022).

The biological crust can be classified into algae crust, lichen crust, and moss crust based on the primary components present in the biological soil crust (Weber et al., 2022). Among them, the lichen crust is a typical symbiont formed by cyanobacteria or green algae and fungi, performing multiple functions derived from a variety of microbial attributes and metabolic pathways (Li et al., 2017; Grimm et al., 2021). Cyanobacteria or green algae in lichen contribute energy and nutrients to the symbiotic organism through photosynthesis and nitrogen fixation, while fungi utilize mycorrhizae to absorb water and inorganic salts from cyanobacteria or green algae. Additionally, fungi play a role in converting inorganic substances into organic matter through saprophytic decomposition (Cao et al., 2024). The fungal hyphae can envelop algal cells, providing protection against external stress, and their tightly interwoven structure facilitates the storage of air and moisture. Lichen crusts have been reported to be more efficient to algal crusts in terms of soil improvement, fertilization, windbreak, and sand fixation (Atashpaz et al., 2023).

Previous studies have demonstrated that cyanobacterial inoculation could assist in induced BSC (IBSC) formation and development by overcoming crust organisms' dispersal limitation (Lan et al., 2014; Chamizo et al., 2018; Kheirfam et al., 2020). There are numerous works demonstrating successful cultivation of mosses (Antoninka et al., 2016; Bu et al., 2018; Liao et al., 2024), but very limited works on lichen cultivation. One study involved the translocation of lichens from a quarry to a degraded gypsum area, where researchers tested various adhesives to improve lichen attachment to the substrate, to enhance the restoration of gypsum soils (Ballesteros et al., 2017). Bacterial and fungal inoculants can be considered as potential choices in strategies for restoring degraded soils (Rashid et al., 2016). The addition of nitrogen-fixing bacteria (Rezasoltani and Champagne, 2023), phosphorus-solubilizing bacteria (Liu et al., 2023), mycorrhizal fungi (Chaudhary et al., 2020) and fungi with high extracellular polysaccharide production significantly enhances soil fertility (Rashid et al., 2016; Mao et al., 2024). Notably, the incorporation of fungi with high extracellular polysaccharide production not only increases soil organic matter but also forms aggregates by secreting extracellular polymers, effectively binding soil particles and minerals. The co-inoculation of cyanobacteria and high extracellular polysaccharide-producing fungi holds the potential to enhance the conversion of soil organic matter and facilitate the restoration of degraded soils in arid regions.

The structural composition and stability of soil organic matter are important indicators of desertification soil restoration (Jensen et al., 2020). Soil microorganisms could convert new carbon in the soil into stable carbon, i.e., humus, through their metabolic activities, thereby improving soil ecological functions (Yang et al., 2022). Dissolved organic matter (DOM) in the soil mainly originates from plant residues, root exudates, and microbial metabolic activities and is the most active component of soil organic matter. DOM consists of highly heterogeneous components with different molecular weights and structures, which not only affect the bioavailability of soil nutrients such as carbon, nitrogen, sulfur, and phosphorus but also play a significant role in microbial growth, metabolism, and soil formation processes (Li et al., 2023). Liu et al. (2021) used three-dimensional fluorescence spectroscopy to investigate soil DOM biodegradation at different successional stages of vegetation recovery, demonstrating the sensitivity of DOM as an indicator reflecting the degree of soil recovery. Swenson et al. (2015, 2018) revealed the link between microbial metabolism and soil environmental chemistry by understanding the DOM composition and abundance changes in the inoculation experiment. Assuming that the inoculated microorganisms contribute to desert soil nutrition, DOM composition and characteristics can respond quickly and potentially reveal differences in the roles of cyanobacteria and fungi.

This study draws inspiration from the lichen mutualistic symbiosis model to investigate the effects of different proportions of filamentous cyanobacteria and high-yield exopolysaccharide fungi inoculation on: (i) the growth of IBSC and variations in cyanobacterial and fungal biomass; (ii) improvements in soil properties, including carbon, nitrogen, and soil enzyme activity; and (iii) alterations in soil dissolved organic matter (DOM) composition and characteristics. The objective is to elucidate the contributions of cyanobacteria and fungi to the soil restoration process and to provide a novel method for accelerating IBSC formation on the surface of sand.

2 Materials and methods

2.1 Soil collection

The soil samples were obtained from moving sandy dunes in Hobq Desert, Dalateqi County, Inner Mongolia, China (44°21′N; 109°50′E). The Hobq Desert is a hyper plateau at an elevation of 1,230 m and characterized by mass moving sandy dunes in an arid to semi-arid climate (Chen et al., 2014). The average annual temperature is 7.4°C, and the prevailing wind direction is WNW, with an average annual speed of 2.7 m/s. The mean annual evaporation (2,448 mm) far exceeds the mean annual precipitation (293 mm). Sand samples was carried from 10 cm of the surface layer. The sand was air-dried and sieved by 2 mm-sized mesh. Subsequently, 500 g sand were analysed for soil physicochemical properties (Supplementary Table S1), and the remaining portion was

utilized as soil substrates for inoculation. Additionally, there are experimental areas where cyanobacteria were inoculated onto the sandy surface between 2002 and 2008 for desertification control, as documented in our previous study (Deng et al., 2020). Dark lichen BSCs were gathered from this experimental area to screen strains.

2.2 Screening and taxonomic identification of strain

Dark lichen BSCs with three replicates were added to flasks with enrichment medium (5 g/L tryptone, 5 g/L yeast extract, 1 g/L K_2HPO_4, and 1 g/L glucose), and shaken at 30°C for 20 min to obtain the soil suspension. Next, the microbial suspension was diluted with sterile water at a ratio of 1: 10, and further diluted to 10^{-6}. Afterwards, 200 μL of the solutions from dilution gradients of 10^{-4}, 10^{-5}, and 10^{-6} were evenly spread onto PDA, Ashby nitrogen-free, and phosphate-solubilizing solid media. The plates were then inverted and incubated at 30°C in a constant temperature incubator for 24 h. Following incubation, distinct single colonies of various types were selected, streaked multiple times for purification on agar plates, and preserved at 4°C on PDA slants for future use.

To test the ability of the strain to produce exopolysaccharides, 2 volumes of 95% ethanol was added to the fermentation, and after 2 h reaction, the mixture was centrifuged at 7000 rpm for 10 min. Next, 1 mL deionized water was added to dissolve the precipitate and the solution was fully reacted in a boiled water bath for 5 min after added 1 mL DNS reagent. The strain in which the cooled solution turned reddish brown was recognized as a polysaccharide producing strain. One highly polysaccharide-excreting fungus designated Zh2 was isolated and used for further research.

The fungal Zh2 was identified by sequencing 18S rDNA gene. DNA extraction was carried out following the instruction of Genomic DNA Extraction Kit (TianGen, China). The universal primers used in PCR amplification were as follows: ITS1 (5'-TCCGTAGGTG AACCTGCGC-3') and ITS4 (5'-TCCTCCGCTTATTGATATGC-3'). The amplication results were sequenced by the BGI Gene Co. (Wuhan, China). A BLAST search was conducted at the National Center for Biotechnology Information (NCBI, https://www.ncbi.nlm.nih.gov/). Sequencing data were phylogenetically analysed using Mega 5 and submitted to NCBI database with the sequence number MH973233. The results indicated the strain Zh2 belongs to *Exophiala oligosperma* (Supplementary Figure S1).

The genus *Phormidium tenue*, affiliated with the order Oscilatoriaceae, is commonly found in BSC communities within arid regions (Hu et al., 2003). The strains were kindly provided by Institute of Hydrobiology, Chinese Academy of Sciences. It was isolated from the Tengger Desert in Shapotou, Zhongwei County, Ningxia, China (37°27′N, 104°57′E), and deposited at the Freshwater Algae Culture Collection at the Institute of Hydrobiology (FACHB-collection), with deposit number FACHB886. The genus *Phormidium tenue* has been successfully used for inoculation in the Hobq Desert (Xie et al., 2007). Additionally, it has been found to dominate in natural biocrusts in the Hobq Desert (Deng et al., 2020) and the Loess Plateau (Zhang et al., 2018). Furthermore, *Phormidium tenue* has been reported to perform well in resisting UV damage (Wang et al., 2017), water stress (Chen et al., 2012), and promoting shrub growth (Xu et al., 2013). Therefore, it is suitable for inoculation onto the surface of shifting sand dunes.

2.3 Inoculum preparation and cultivation

The *Exophiala oligosperma* Zh2 were inoculated into sterile PDA medium and cultured in a constant temperature shaking incubator at 28°C and 150 rpm for 48 h. After homogenizing, the filamentous cyanobacterium *Phormidium tenue* was transferred to sterile BG11 medium and cultured in a light incubator at a constant temperature of 25 ± 2°C under 24-h continuous illumination with a light intensity of 50 $\mu Em^{-2}s^{-1}$ for 4 days with aeration. The fungal and cyanobacterial cultures were then centrifuged, the supernatant was discarded, and the pellets were washed several times with sterile water. The pellets were then resuspended in sterile water to serve as stock solutions for both cyanobacteria and fungi, and the concentrations were determined for subsequent inoculation.

For fungal biomass determination, the hemocytometer counting method was employed. Specifically, a small volume of well-shaken fungal suspension was drawn up with a pipette and dropped into the grooves on both sides of the central platform of a counting chamber. Excess fungal suspension in the grooves was removed using absorbent paper. After a brief settling period, the cells were counted under a microscope, and the results were expressed as CFU/mL.

The biomass of *Phormidium tenue* was characterized by the content of chlorophyll *a* (Chl *a*). The measurement method for Chl *a* in cyanobacteria was as follows: 5 mL of cyanobacterial solution was centrifuged at 8000 rpm for 10 min, the supernatant was discarded, and the algal cells were collected. Then, 5 mL of 95% ethanol was added, and the mixture was extracted and soaked in a refrigerator at 4°C for 24 h, shaking 2–3 times in between to ensure full dissolution of Chl *a*. The supernatant was collected after centrifugation (8,000 rpm, 10 min), and the absorbance values (OD) at 665 nm and 649 nm were measured using a UV-2000 spectrophotometer. The Chl *a* content was calculated using the formula: Chl *a* (mg/L) = $13.95 \times OD_{665}$-$6.88 \times OD_{649}$.

Finally, based on the concentrations of the cyanobacterial and fungal stock solutions, the dilution factors were calculated, and the stock solutions were diluted to the desired concentrations using sterile water.

After the *Exophiala oligosperma* Zh2 and *Phormidium tenue* FACHB886 were cultured to the logarithmic phase, the biomass was determined by hemocytometer and Chl *a* method, respectively, as a stock solution. The stock solution was diluted to target concentration with sterile water and mixed to obtain a mixed cyanobacterial-fungal inoculum. Sand, sieved, sterilized, dried, and distributed into Petri dishes (90 mm × 12 mm), each containing 60 g, served as the growth substrate.

Five treatment groups were established, with 5 Petri dishes in each group as replicates. After extensive preliminary experiments, the inoculation amounts of cyanobacteria and fungi were set at 1 ± 0.1 μg (Chl *a*)/cm² and 10^7 CFU/cm², respectively. Thus, the sand surface of the Cya group was inoculated with 1 ± 0.1 μg (Chl *a*)/cm² of *Phormidium tenue*; the Cya + Fun group was simultaneously inoculated with 1 ± 0.1 μg (Chl *a*)/cm² of *Phormidium tenue* and 10^7 CFU/cm² of the *Exophiala oligosperma* Zh2; The 2Cya + Fun group was simultaneously inoculated with 2 ± 0.15 μg (Chl *a*)/cm² of *Phormidium tenue* and 10^7 CFU/cm² of the *Exophiala oligosperma* Zh2; The Cya + 2Fun group was simultaneously inoculated with 1 ± 0.1 μg (Chl *a*)/cm² of *Phormidium tenue* and $2*10^7$ CFU/cm² of the *Exophiala oligosperma* Zh2; the Fun group was inoculated with 10^7 CFU/cm² of the *Exophiala oligosperma* Zh2.

The inoculated Petri dishes were incubated in a light incubator at at a constant temperature of 25 ± 2°C under 24-h continuous illumination with a light intensity of 50 μEm^{-2}s^{-1}. Throughout this period, water was added daily at 9:00 according to the soil moisture content to maintain a water content of 15%. The culture period spanned 35 days, during which samples were collected six times, weekly, to assess crust Chl *a* content, DNA content, cyanobacterial and fungal gene copy numbers, as well as soil properties and dissolved organic matter (DOM) characteristics.

2.4 Analysis of BSC biomass

Chl *a* extraction from 1.0 g of soil samples involved using 5 mL of ethanol at 80°C for 5 min. The samples were subsequently incubated at 4°C for 8 h and then centrifuged at 3500 × g for 15 min. The extraction process was repeated twice to ensure complete pigment recovery. The supernatant, containing the pigments, was measured at 655 nm and 750 nm using a spectrophotometer (UV-1700 PharmaSpec, Japan). The Chl *a* concentration was calculated using the formula reported by Mugnai et al. (2018).

Soil DNA was extracted from 0.5 g of soil of each BSC sample using a FastDNA Spin Kit for Soil (MP Biomedical, LLC) and an MP FastPrep-24 Instrument (MP Biomedical, LLC) according to the supplied protocols. DNA extracts were examined on 0.9% agarose gels in 1× Tris-acetic acid-EDTA with GelRed and quantified using a Nanodrop 2000c (Thermo Scientific, United States). The fungal 25-28S rRNA genes and cyanobacterial 16S rRNA gene were quantified with a StepOne Real-Time PCR System (Applied Biosystems, United States) using the primers NL1f and LS2r, and CYA359F and CYA781A/B (Deng et al., 2016), respectively. Further details of qPCR procedures were outlined in our previous study (Zhou et al., 2020).

2.5 Measurement of soil properties

Following the 35-day culture period, the crust was air-dried at 25°C. The cyanobacterial-fungal composite crust underwent analysis for its C/N/H element content, along with assessments of catalase, sucrase, urease, and phosphatase activities. Soil elemental content was determined using an elemental analyzer (Vario Macro Cube, Elementar, Germany). Soil enzyme activities were conducted according to the method described by references (Liu et al., 2014; Yang et al., 2018). Catalase activity in the soil was determined using the $KMnO_4$ titration method, sucrase activity was assessed through the dinitrosalicylic acid colorimetric method, urease activity was measured via the sodium phenolate-sodium hypochlorite colorimetric method, and phosphatase activity was determined using the disodium benzene phosphate colorimetric method.

2.6 Fluorescence emission-excitation matrix (EEM) spectroscopy

Subsequently, 5.0 g of the sieved soil, mixed with 30 mL of deionized water, underwent shaking at 200 rpm for 30 min at 25°C. The resulting aqueous extracts were subjected to centrifugation and filtration to isolate the dissolved organic matter (DOM). The carbon content in DOM, also known as dissolved organic carbon (DOC), was measured using a TOC analyser (Vario TOC, Elementar, Germany) (Zhou et al., 2019). DOM fluorescence was measured in a 1.0 cm quartz cell using a spectrofluorometer (Edinburgh, FS5) equipped with continuous (150 W) and pulsed xenon lamps. Scanning ranges were configured at 200–500 nm with 5 nm sampling intervals for excitation (Ex), and at 250–600 nm with 5 nm sampling intervals in emission (Em). This setup allowed for comprehensive information gathering about all organic compounds present (Chen et al., 2003). Spectra were recorded at a scan rate of 1,200 nm/min with a dwell time of 0.01 s, utilizing excitation and emission slit bandwidths of 10 nm. The spectra underwent blank subtraction, correction for inner filter effects (for both excitation and emission wavelengths), and masking with first-and second-order Rayleigh scattering (±10 nm at $\lambda ex = \lambda em$ and $2\lambda ex = \lambda em$) (Fox et al., 2017). Deionized water blanks were analyzed under the same conditions as the samples.

In EEM spectra, three indices are commonly used to reflect the degree of humification and the bioavailability of DOM (Ye et al., 2020; Xue et al., 2022). The Humification Index (HIX) is used to characterize the content of humic substances. It is the ratio of the integrated values between the regions of Em 435–480 nm and Em 300–345 nm under an Ex of 254 nm. The Biological Index (BIX) refers to the ratio of fluorescence intensity at Em 380 nm and Em 430 nm when Ex is set to 310 nm, indicating the bioavailability of organic matter. The Fluorescence Index (FI) represents the ratio of fluorescence intensity at Em 470 nm and Em 520 nm when Ex is 520 nm, primarily reflecting the source of dissolved organic matter (DOM). Microbial activity is considered the main source of DOM when $1.7 < FI < 2.0$, while microbial contribution is lower when FI is less than 1.5.

2.7 Statistical analyses

A one-way ANOVA was conducted to assess the significance of differences across the analyses for soil property indicators, including soil C/N content and enzyme activity. Tukey's test ($p < 0.05$) was subsequently employed to ascertain the statistical significance of the variables (IBM SPSS Statistics v20). A repeated-measures ANOVA was used to determine the effects of cultivation time and treatment on Chl *a*, cyanobacterial and fungal abundance. Parallel Factor Analysis (PARAFAC) was conducted to separate distinct fluorescent components, and DOM indices, including FI, BIX, and HIX, were determined using MATLAB 7.0 (Mathworks, Natick, MA). The analysis utilized the DOM Fluor toolbox.[1] The outcomes wwpere then compared with previous findings on soil environments accessible in the OpenFluor database.[2] To investigate the effects of algae and fungi inoculation levels on the biomass of composite crusts and soil properties, the redundancy analysis (RDA) was conducted in R (Version 3.5.1, MathSoft, United States) with the "vegan" package. The inoculation levels of cyanobacteria and fungi were assigned values of 0, 1, 2, where the Cya group is denoted as Cya = 1, Fun = 0; the Cya + Fun group as Cya = 1, Fun = 1; the 2Cya + Fun group as Cya = 2, Fun = 1; the Cya + 2Fun group as Cya = 1, Fun = 2; and the Fun group

1 http://www.models.life.ku.dk/

2 https://openfluor.lablicate.com

as Cya = 0, Fun = 1. Data representation and graphical fittings were generated using OriginPro 2023.

3 Results

3.1 Growth of IBSCs with different inoculum biomass

As shown in Figure 1, both cyanobacteria and fungi exhibited viability in sand, forming IBSCs. Notably, the distribution of cyanobacterial coverage varied among crusts inoculated with different inoculum biomass. Cya and Cya + Fun were characterized by a more even layer, whereas Cya + 2Fun displayed a patchy distribution (Figure 1). A repeated-measures ANOVA showed that there were significant differences in Chl *a* content, cyanobacterial and fungal abundance between different cultural time or inoculation treatment. Cyanobacterial abundance in cyanobacteria-fungi co-inoculated crusts showed an adaptive decline after the initial inoculation. Throughout the 35-day cultivation period, the Chl *a* content and cyanobacterial abundance in crusts co-inoculated with cyanobacteria and fungi surpassed those in the singly inoculated cyanobacteria. Among all experimental groups, Cya + Fun exhibited the most rapid growth rate in terms of Chl *a* content and cyanobacterial abundance. The abundance of fungi in cyanobacteria-fungi co-inoculated crusts displayed an overall growth trend, with the growth rate slightly lower than that of cyanobacteria. While fungi could sustain growth in the co-inoculated scenario, the abundance of fungi was observed to gradually decrease in the later stages of cultivation when the fungus was inoculated alone.

3.2 Soil C, N and enzymes activity

After a 35-day inoculation period, significant differences in soil C, N content and enzyme activity were observed between crusts with varing cyanobacterial/fungal inoculation ratios (Table 1). The Cya + Fun group exhibited the highest soil C and N content, while the Cya group had the lowest. The treatments involving the combined inoculation of cyanobacterial and fungal strains showed a significant augmentation in both soil C, N content, and enzyme activity. Specifically, soil catalase, sucrase, urease, and phosphatase activities in crusts co-inoculated with cyanobacteria and fungi surpassed those of the Cya and Fun groups, which were singly inoculated with cyanobacteria or fungi. Notably, the Cya + Fun and Cya + 2Fun groups displayed elevated soil catalase and sucrase activities compared to other groups.

3.3 Soil DOM characteristics and components

Dynamic variations in three-dimensional fluorescence spectra of DOM in cyanobacteria-fungi crusts with different inoculum biomass are depicted in Figure 2. The fluorescence intensity of each group exhibited a gradual increase during the cultivation process. In

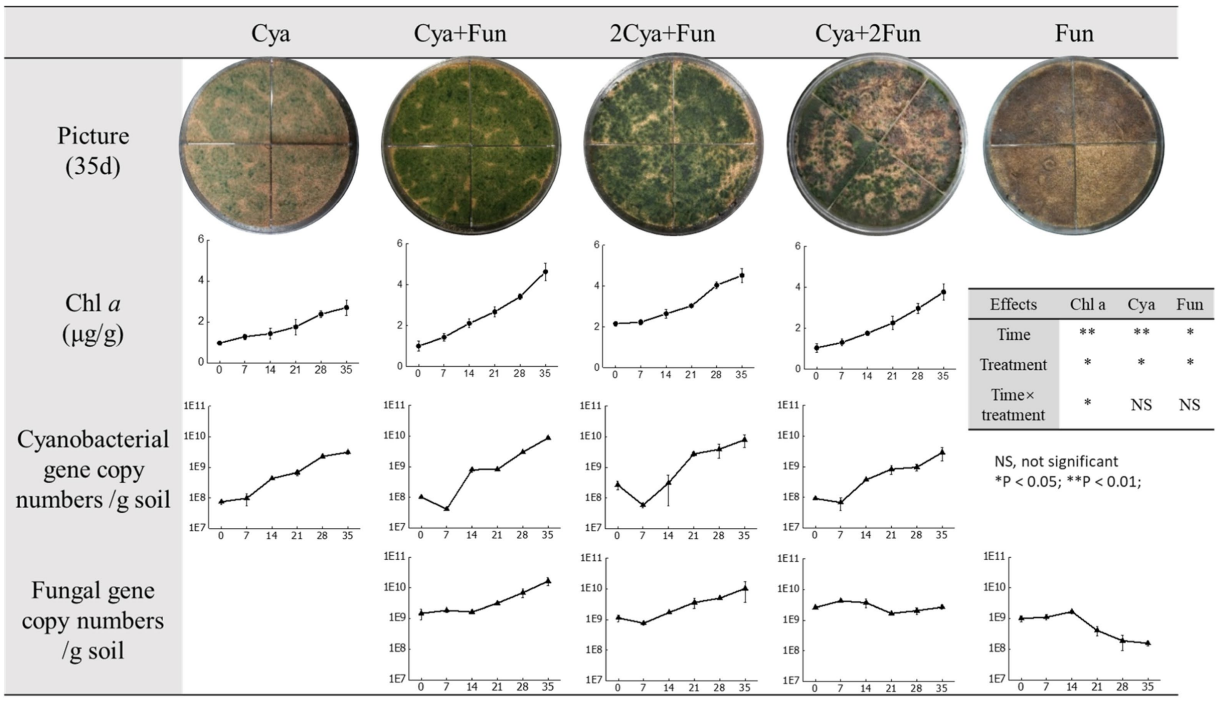

FIGURE 1
Images depicting crusts with varying inoculum biomass after 35 days of inoculation, along with the biomass growth curve during the culture period. Lines 4 and 5 represent changes in cyanobacterial and fungal gene copy numbers per gram of soil, respectively. The x-axis of the line chart corresponds to the cultivation time (days). Effects of cultivation time and treatment on Chl *a*, cyanobacterial and fungal abundance on the basis of the repeated-measures ANOVA analyses also shown.

TABLE 1 Soil nutrient contents and enzyme activities in cyanobacteria-fungi crusts with varying inoculum biomass.

	Cya	Cya + Fun	2Cya + Fun	Cya + 2Fun	Fun
Soil C	1.01 ± 0.16c	1.33 ± 0.07a	1.12 ± 0.03bc	1.28 ± 0.04ab	0.97 ± 0.02c
Soil N	0.09 ± 0.01b	0.14 ± 0.02a	0.12 ± 0.02ab	0.12 ± 0.01ab	0.11 ± 0.01ab
Catalase activity (U/g)	5.27 ± 0.32c	6.21 ± 0.3ab	5.83 ± 0.06b	6.37 ± 0.11a	5.14 ± 0.07c
Sucrase activity (U/g)	0.34 ± 0.004e	0.47 ± 0.007b	0.42 ± 0.008c	0.48 ± 0.006a	0.38 ± 0.006d
Urease activity (U/g)	1.68 ± 0.05b	1.79 ± 0.04a	1.78 ± 0.02a	1.75 ± 0.05ab	1.39 ± 0.02c
Phosphatase activity (U/g)	1.39 ± 0.1c	1.59 ± 0.02b	1.93 ± 0.07a	1.5 ± 0.09bc	1.34 ± 0.07c

Different letters (a,b,c,d,e) indicate significant differences between treatment groups.

comparison with the Cya group, which was solely inoculated with *Phormidium tenue*, the soil DOM's fluorescence intensity significantly increased after the addition of fungal Zh2, accompanied by the appearance of fluorescence peaks in the humus area (Em > 350 nm). The DOM fluorescence intensity in the Cya group was comparatively weaker in the humus, while cyanobacteria-fungi crusts displayed distinct fluorescence peaks in the humus area after 1 week of culture, gradually intensifying with the culture time. In the case of sole inoculation with Zh2, the fluorescence peak emerged in the humus area during the initial inoculation, and its intensity continued to increase in the later stages of the culture.

For a more in-depth investigation into the photochemical characterization of DOM, PARAFAC analysis was performed to separate dissimilar fluorescent components from the DOM (Figure 3). Two fluorescent components were isolated from the DOM in the Fun group, and three components were obtained in the remaining four groups. The models for each component were consistent with previous reports or well-matched with the OpenFluor database, exhibiting similarity scores of >0.95. The C1 component (Ex/Em = 205–210/390–400) in the ultraviolet region, present in all five groups, was attributed to fulvic substances with low molecular weight. The C2 component (Ex/Em = 210–220/405–420) in the Cya, Cya + Fun, and 2Cya + Fun groups, and the C3 component in the Cya group (Ex/Em = 225/420), could be considered as fulvic-like substances. The C2 component in the Cya + Fun and 2Cya + Fun groups, and the C3 component in the Cya +2Fun and Fun groups (Ex/Em = 230–250, 340–345/420–435) belonged to the visible region and could be categorized as relatively stable humic-like substances with higher molecular weight. The fulvic-like component in DOM consisted of two components, with C1 present in all five treatment groups, showing small fluctuations in relative intensity. The C2 component only appeared in the Cya, Cya + Fun, and 2Cya + Fun groups. In comparison with the Cya group, the C2 component in the Cya + Fun and 2Cya + Fun groups exhibited a red-shift and decreased light intensity (Table 2).

3.4 Soil DOC content and DOM fluorescence parameters

As shown in Figure 4, soil DOC content exhibited an upward trend with cultivation time in all crusts, but the accumulation rates varied with different cyanobacterial/fungal inoculation ratios. Following 35 days of inoculation, the soil DOC content demonstrated the following trend: Cya + 2Fun > 2Cya + Fun > Cya + Fun > Fun > Cya. Additionally, EEM was employed to assess the humification and bioavailability of DOM, as indicated by BIX, FI, and HIX. The BIX and HIX values of DOM exhibited significant differences in crusts with different inoculum biomass, while the FI values showed comparatively less variation. As the cultivation time increased, the BIX and HIX values of DOM demonstrated an upward trend, while the FI value decreased. After 35 days of cultivation, the BIX values of DOM in Cya + 2Fun and Cya + Fun were significantly higher than in the other groups. Moreover, the HIX values were notably higher in treatments involving the combination of cyanobacterial and fungal strains than in those of the Cya and Fun groups, which were inoculated solely with cyanobacteria or fungi.

3.5 Redundancy analysis between inoculum biomass and soil properties

RDA was employed to explore the impact of inoculum biomass on crust growth and soil properties (Figure 5). The inoculation quantity of cyanobacteria accounted for 26.2% of the total variation in all crust and soil indices, while the fungal inoculum contributed to 37.9%. The five groups with different inoculum biomass exhibited an even distribution across four quadrants, with the Cya + Fun group situated in the middle and displaying correlations with the measured indicators. In addition to the expected positive correlation with Chl *a* content and cyanobacterial abundances, cyanobacterial inoculum demonstrated positive correlations with fulvic-like content, urease activity, and phosphatase activity. On the other hand, the quantity of fungal inoculum exhibited positive correlations with soil C, N content, catalase activity, invertase activity, and HIX, BIX value and humic-like content of soil DOM.

4 Discussion

The success of constructing the lichen bionic system relies on the potential mutual symbiosis between cyanobacteria and fungi (Frey-Klett et al., 2011; Scharnagl et al., 2023). The *Exophiala oligosperma* Zh2, belongs to Ascomycetes, which is consistent with the reported results that 90% of fungi in biological crusts are Ascomycetes (Bates et al., 2012; Abed et al., 2013). Fungi of the phylum Ascomycetes are found in the soil in parasitic, saprophytic, or symbiotic forms. In this study, *Exophiala oligosperma* Zh2 acting as a heterotrophic fungus, exhibited a gradual biomass decrease in the absence of external nutrient input (Figure 1). Co-inoculation with *Phormidium tenue* resulted in a continuous increase in fungal abundance in the soil, suggesting that *Phormidium tenue* could serve as a nutrient source for fungal growth. Concurrently, gene abundance and Chl *a* content of cyanobacteria increased with the addition of fungi, demonstrating a mutualistic symbiosis. Fungal Zh2 was characterized by high-yield

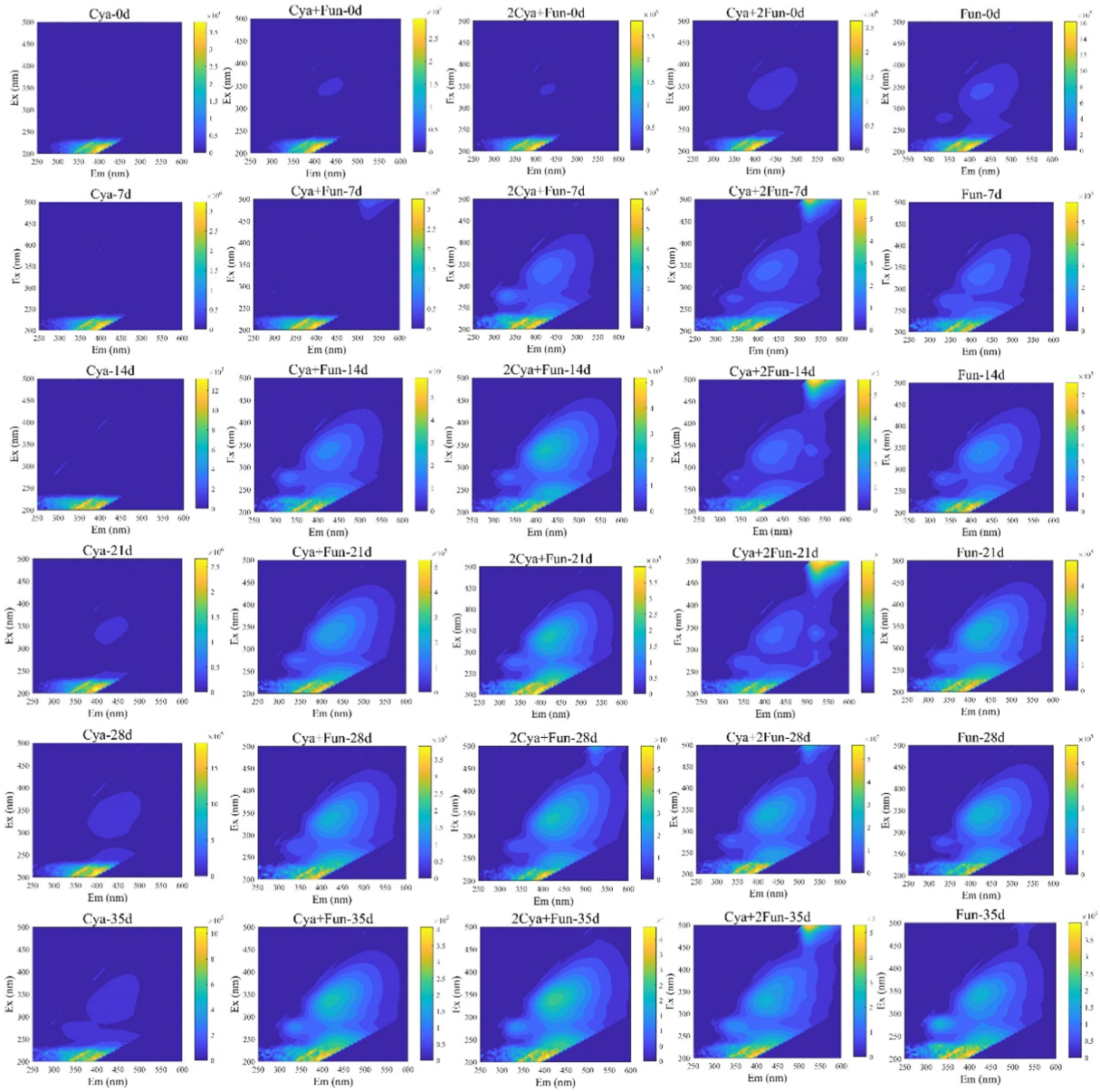

FIGURE 2
Dynamic changes in three-dimensional fluorescence spectra of DOM in cyanobacteria-fungi crusts with different inoculum biomass.

exopolysaccharide, and exopolysaccharides are known to be beneficial for the growth of cyanobacteria and cyanobacterial BSCs (Colica et al., 2014; Rossi et al., 2018; Dabravolski and Isayenkov, 2022). Fungi transformed inorganic substances inaccessible to cyanobacteria into organic matter, while cyanobacteria supplied organic nutrients from photosynthesis to fungi (Guo and Tong, 2014; Li et al., 2022). The symbiotic dynamics in the cyanobacterial-fungal system were influenced by the inoculation ratio of cyanobacteria and fungi (Chu et al., 2021). After a 35-day culture, no significant differences were observed in cyanobacterial biomass between the 2Cya + Fun group and the Cya + Fun group, indicating that the inoculation ratio in the Cya + Fun group favored cyanobacterial-fungal symbiosis more than the 2Cya + Fun group. Cyanobacterial inoculation biomass positively influenced fungal growth to varying extents (Marks et al., 2019), with the promoting effect diminishing as the inoculum biomass increased. This could be attributed to an excess of cyanobacterial inoculum occupying the fungal niche, subsequently affecting fungal growth space (Zhang et al., 2014). An appropriate spatial structure is conducive to nutrient and gas exchange between microalgae and fungi, facilitating mutual growth (Li and Zhu, 2023).

Soil C, N, and enzyme activity serve as crucial indicators for restoring desert soil structure and function (Zhang et al., 2023). Significant differences in soil property indicators were observed between crusts with different cyanobacterial/fungal inoculation ratios (Table 1). In comparison to other groups, the C and N contents of the Cya + Fun group were higher, aligning with its elevated biomass, confirming the well-developed biological crust induced by the consortium of cyanobacteria and fungi. Soil enzyme activities, known for their sensitivity to environmental changes (Aponte et al., 2020; Wang et al., 2022), were notably higher after the coinoculation of

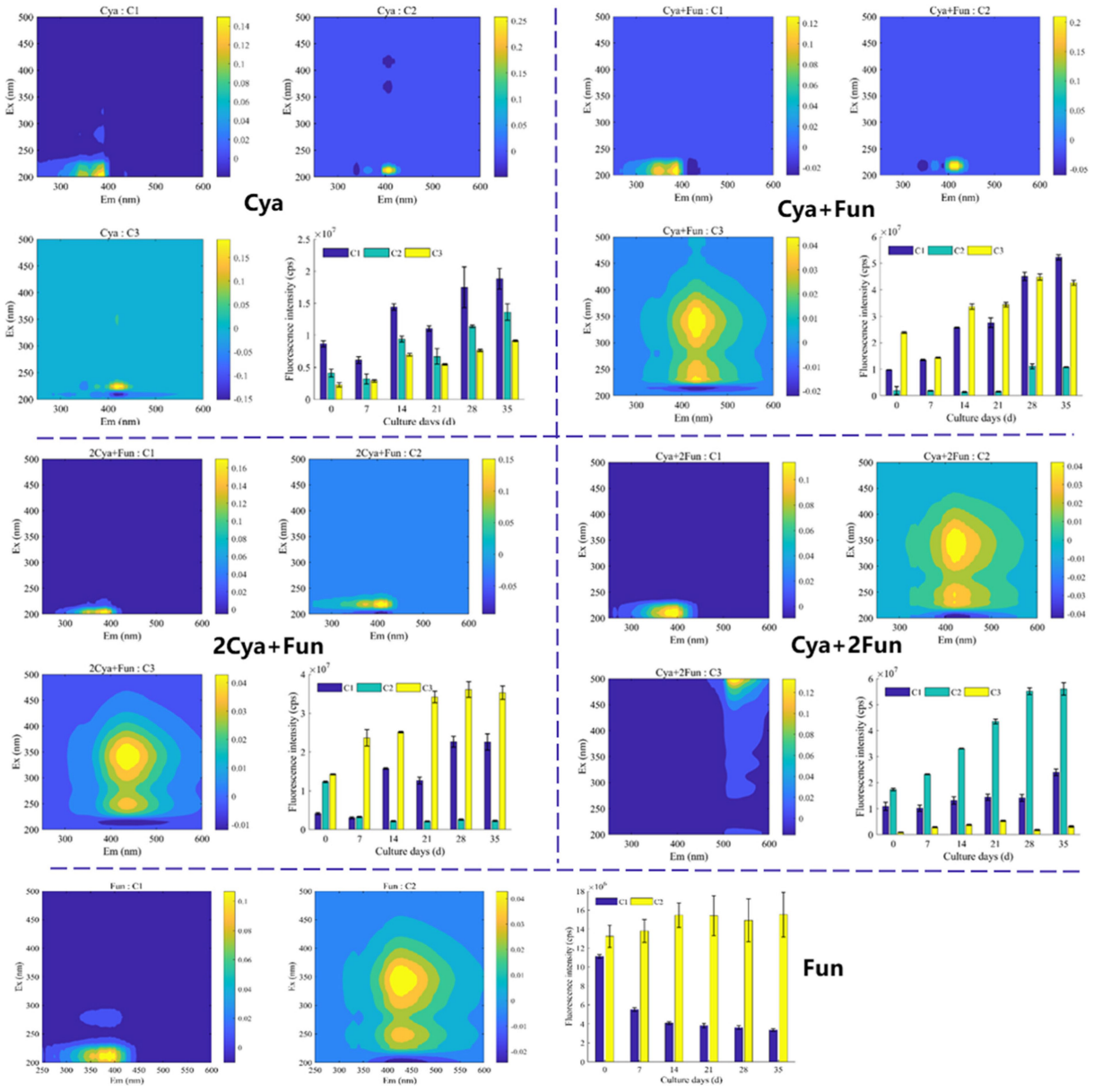

FIGURE 3
Spectral characteristics and fluorescence intensity of the two/three primary fluorescent components identified through EEM-PARAFAC analysis in cyanobacteria-fungi crusts with varying inoculum biomass.

cyanobacteria and fungi compared to single inoculation groups of Cya and Fun, showcasing the contribution of the cyanobacteria-fungi crust to soil enzyme activities. Furthermore, the Cya + Fun group exhibited the highest activities of catalase and sucrase. Catalase, an oxidoreductase in soil, is frequently employed to characterize soil humification intensity and organic matter conversion rate. It plays a pivotal role in the oxidation of organic matter and humus formation (Liu et al., 2020). The significantly higher catalase activity in the Cya + Fun group reflected its robust microbial activity (Prasanna et al., 2012). Soil sucrase enhances soluble nutrients in soil and is closely associated with the transformation of organic matter and respiration intensity (Xiao et al., 2022; Yang et al., 2024). In this study, sucrase activity notably increased with fungal addition, possibly linked to the substantial exopolysaccharide secretion by *Exophiala oligosperma* Zh2. Consequently, the cyanobacterial-fungal mixture in this study may contribute to humus formation and the transformation of organic matter structure.

Soil humus, derived mainly from microbial metabolism and biotransformation, plays a pivotal role in regulating soil carbon and nitrogen cycling, microbial growth, and structural stability in ecological processes (Schmidt et al., 2011; Vikram et al., 2022). It serves as a crucial indicator for assessing the effectiveness of degraded soil restoration. Throughout the incubation process, the fluorescence intensity of DOM in all groups increased, indicating that DOM mainly originated from microorganisms such as cyanobacteria and fungi in the soil (Meng et al., 2016; Li et al.,

TABLE 2 Position of DOM fluorescence peaks in cyanobacteria-fungi crusts with different inoculum biomass and a comparison with earlier reports from the OpenFluor database.

	C1		C2		C3	
	Wavelength (Ex/Em, nm)	Relative intensity	Wavelength (Ex/Em, nm)	Relative intensity	Wavelength (Ex/Em, nm)	Relative intensity
Cya	205/390	0.174	210/405	0.302	225/420	0.237
Cya + Fun	210/390	0.148	215/420	0.249	230,340/430	0.047,0.053
2Cya + Fun	205/390	0.195	220/410	0.186	250,340/435	0.039,0.051
Cya + 2Fun	210/400	0.131	345/420	0.054	500/525	0.154
Fun	210/390	0.123	250,345/430	0.039,0.052		
Component resemblances	Protein-like		Protein-like (except for Cya + 2Fun and Fun)		Humic-like (except for Cya)	
Open Fluor Study Matches	Borisover et al. (2011) and Derrien et al. (2019, 2020)				Lin and Guo (2020) and Zhuang et al. (2021)	

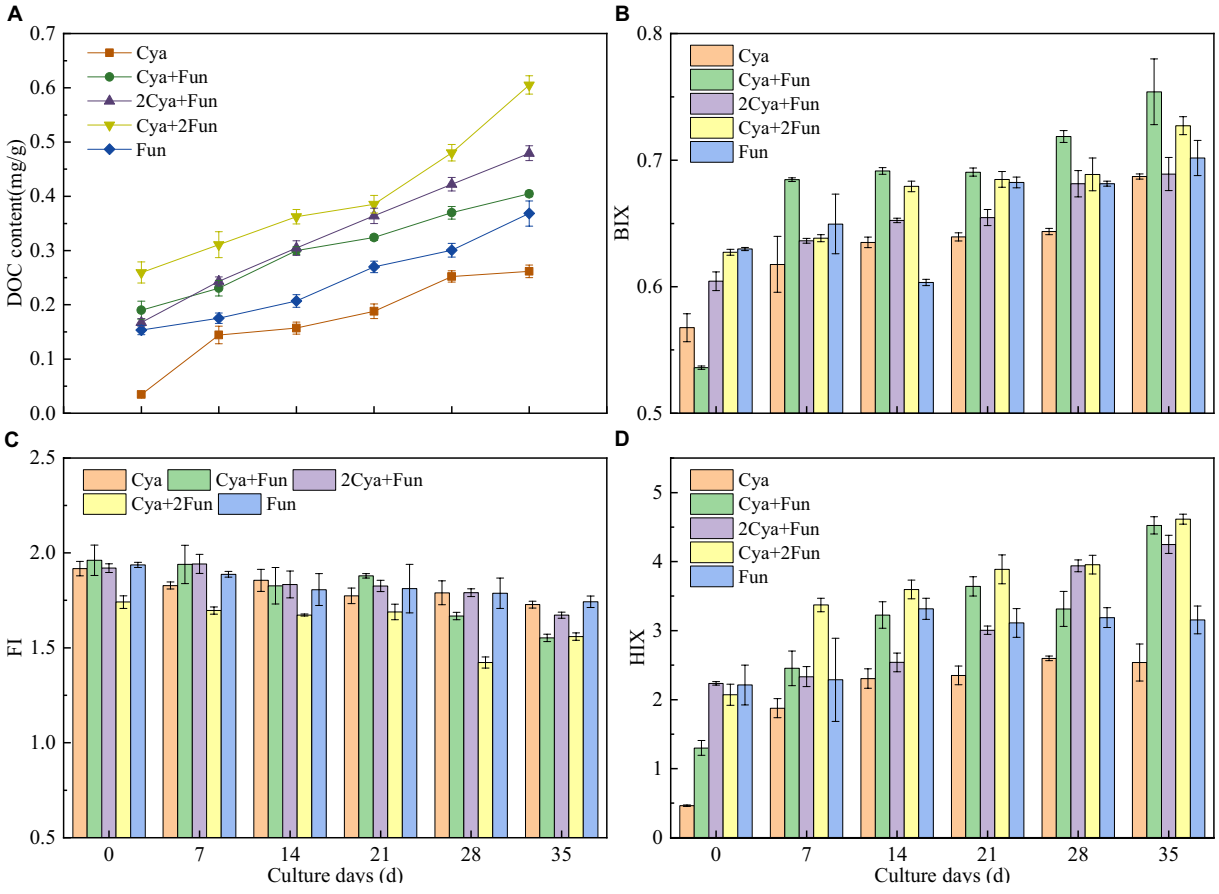

FIGURE 4
Dynamic changes in DOC content **(A)** and fluorescence parameters, including BIX **(B)**, FI **(C)** and HIX **(D)**, in cyanobacteria-fungi crusts with different inoculum biomass.

2023). Despite a decreasing trend in fungal biomass in the later stages of cultivation (Figure 1), the fluorescence intensity of soil DOM continued to rise (Figure 2). This could be attributed to the continuous accumulation of fungal metabolites during the cultivation process, with the decrease in fungal biomass having a relatively minor impact on the metabolic capacity of the remaining viable fungi. Two components—fulvic-like and humic-like—were isolated from the artificial crust DOM. Fulvic-like substances, characterized by hydrophilic small molecules, dispersed uniformly in solution at any pH, displaying strong diffusivity and instability (Canellas et al., 2015). In contrast, humic-like substances, rich in aromatic groups, indicated higher maturity and humification, forming more stable bonds with the mineral components of the soil (Mohinuzzaman et al., 2020). The high-molecular-weight

humic-like component (Ex/Em = 230, 340/430 nm) was exclusively present in treatment groups with fungal inoculation, emphasizing the fungus Zh2's capacity to contribute humic substances to soil DOM through its metabolic activities (Figure 6). The humic-like component C3 appeared in cyanobacterial-fungal and fungal crusts, albeit with relatively low intensity, possibly due to the high molecular weight and weak fluorescence intensity of humic-like substances. Besides humic components, two fulvic components were identified. Fulvic component C1 (Ex/Em = 210/390 nm) appeared in all five treatment groups with minor intensity fluctuations, suggesting it might represent a small amount of low-molecular-weight organic compounds in the sand matrix. Fulvic component C2 (Ex/Em = 210/405 nm) exhibited higher fluorescence intensity in the Cya group than in the Cya + Fun and 2Cya + Fun groups after fungal addition, indicating its potential origin from the metabolic products of filamentous cyanobacteria. Fulvic components displayed a redshift trend after fungal inoculation, typically associated with increased molecular conjugation effects and enhanced molecular condensation (Yakimov et al., 2021). This suggested an increase in the aromaticity and complexity of fulvic component C2, leading to higher humification and structural complexity post-fungal inoculation. Given that the cyanobacterial-fungal crust exhibited higher levels of humic-like and relatively lower levels of fulvic compared to the single algal crust, fungal inoculation may facilitate the gradual transformation of fulvic into humic, enhancing soil humification and stability.

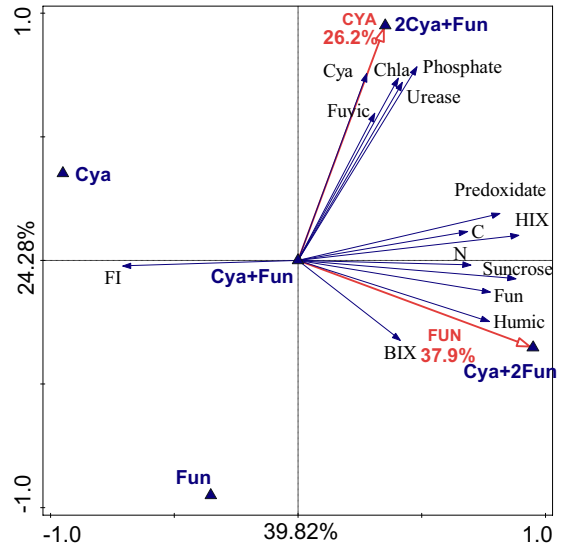

FIGURE 5
Redundancy analysis depicting the relationship between inoculum biomass and soil properties.

Soil DOC primarily originated from microbial metabolic activities and constituted an important component of total soil carbon, thus being significantly correlated with soil organic carbon content (Zhang et al., 2018). However, this study revealed inconsistent patterns between soil C and DOC content. The highest DOC content was observed in the Cya + 2Fun and 2Cya + Fun groups, while the highest C content was found in the Cya + Fun group. This discrepancy suggested that the Cya + Fun group might contain a higher proportion of water-insoluble organic compounds, such as humin. Humic substances, particularly humin, represent the most tightly bound fraction of organic matter to mineral components. Under certain conditions, like dryness, humic acid can transform into humin irreversibly (Schmidt et al., 2011). Humin constitutes the majority of soil organic carbon, playing a crucial role in soil fertility and the ecological environment (Pham et al., 2021). However, further research

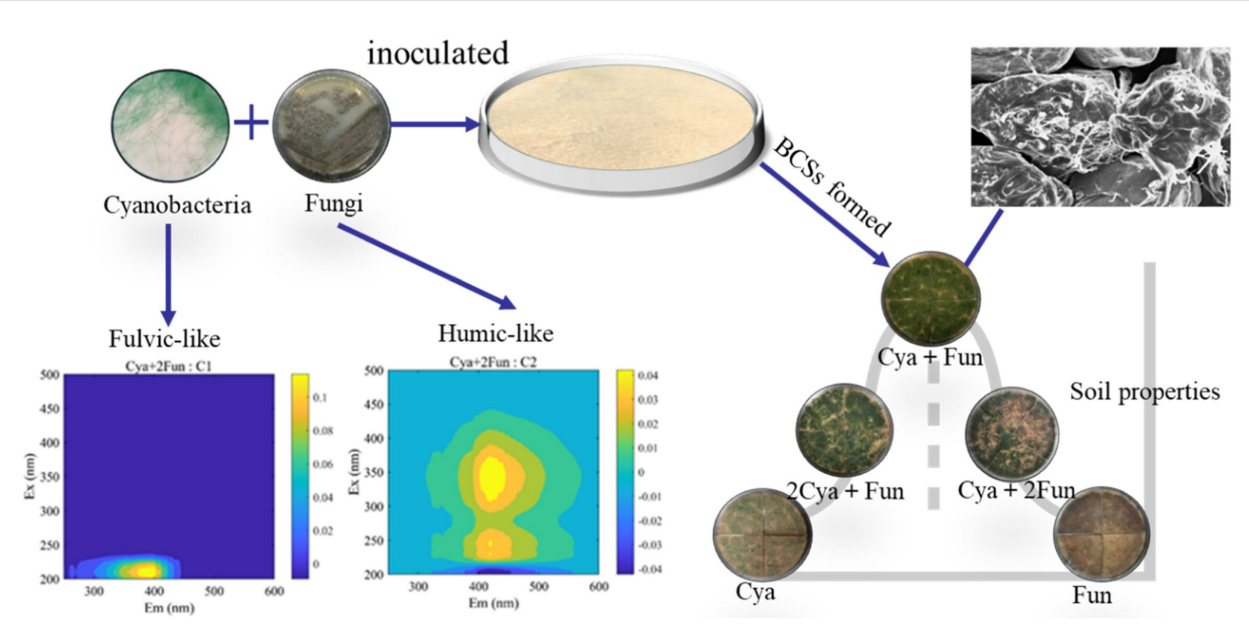

FIGURE 6
The collaborative impact of cyanobacteria and fungi enhances the accumulation of dissolved soil organic matter in the crust.

is needed to confirm whether the Cya + Fun group indeed contains a higher proportion of humin components. Changes in fluorescence parameters can reflect the characteristics of DOM. This study found that parameters BIX and HIX were more sensitive in reflecting DOM characteristics compared to FI, consistent with other studies (Zhang et al., 2018). Throughout the incubation process, the bioavailability and humification degree of crust DOM exhibited an increasing trend, confirming the contribution of cyanobacteria and fungi to soil humus. Research has demonstrated that the artificial addition of humic and fulvic acids to the soil can effectively enhance nutrient bioavailability (Delgado et al., 2002). The enhancement of humic and fulvic through cyanobacteria and fungal inoculation played an irreplaceable role in improving soil fertility, activity, and stability.

The effects of algal and fungal inoculation on composite crust biomass and soil properties were examined based on the RDA analysis. Both cyanobacteria and fungi significantly contributed to crust biomass and soil properties, but their main targets of action were different. Inoculation with cyanobacteria had a pronounced promoting effect on the content of fulvic, and the activities of urease and phosphatase. Research on the detection of humic acids released during the growth cycle of *Microcystis* found only fulvic components and did not detect the presence of humin components (Yilu et al., 2015), which was consistent with the significant correlation between cyanobacterial inoculation and fulvic content observed in this study. Moreover, the inoculation of the high exopolysaccharide-producing fungus Zh2 showed a significant positive correlation with humic-like component content. Furthermore, fungal inoculation, rather than cyanobacterial, significantly correlated with soil carbon content. This could be attributed to the fact that most of the carbon fixed by filamentous cyanobacteria through photosynthesis was stored in the soil by filamentous fungi, which could convert a substantial amount of new carbon into stable carbon (Schmidt et al., 2011). This also explained the positive correlations observed between measured crust biomass and soil properties in the Cya + Fun group. In the 2Cya + Fun group, with a higher abundance of cyanobacteria, the soil humus was predominantly composed of fulvic, indicating insufficient humification degree and stability. In the Cya + 2Fun group, with a higher abundance of fungi, the ecological niche of filamentous cyanobacteria was occupied. Filamentous cyanobacteria, as photosynthetic organisms, could only grow in the surface layer of the soil. Kheirfam and Roohi (2020) inoculated bacteria and cyanobacteria on the dried-up lakebeds to induce the formation of biological soil crusts. Their results revealed that the inoculation of the bacteria, separately or in combination with cyanobacteria, had a limited effect on accelerating crust formation. The co-inoculation of cyanobacteria and fungi in this study exhibited a synergistic effect, possibly due to the mutualistic symbiosis between cyanobacteria and fungi. The reduced photosynthetic efficiency of cyanobacteria directly affected the input of new carbon into the soil, indirectly influencing the abundance of fungi and the synthesis of stable carbon in the soil. Therefore, the cyanobacterial-fungal inoculation in the Cya + Fun group was considered to achieve the optimal synergistic effect in the symbiotic system. Chaudhary et al. (2020) co-inoculated biological crust fragments and arbuscular mycorrhizal (AM) fungi into the arid land simultaneously, but unexpectedly, no synergistic effect emerged. The authors attributed this to the presence of AM fungal propagules in the background soil and inoculated biological fragments, eliminating the need for additional AM fungal inoculation. However, in this study, the abundance of sand dune fungi was low, and we inoculated cyanobacterial inoculants, necessitating some fungal supplementation to help construct a richer soil species ecological structure.

5 Conclusion

The study explored the impacts of varying inoculation biomass on the formation and development of cyanobacterial-fungal composite crusts. The findings revealed noteworthy differences in growth conditions and soil nutrient content across different inoculation scenarios. Cyanobacteria inoculation substantially increased the content of the fulvic-like component in the soil, whereas fungal inoculation markedly elevated soil humic-like content and humification degree. Cyanobacterial inoculation demonstrated a positive correlation with fulvic-like content, urease, and phosphatase activities in the soil. Fungal inoculation exhibited a significantly positive correlation with soil C and soil N content, catalase and sucrase activities, as well as HIX and BIX. Hence, cyanobacteria and fungi played distinct roles in the cyanobacterial-fungal symbiotic system, contributing differentially to soil nutrition and stability. The optimal synergistic effect of the cyanobacterial-fungal symbiotic system was observed with an appropriate initial proportion of cyanobacterial and fungal inoculation, as evidenced by the Cya + Fun group. This study furnishes crucial theoretical support for the co-inoculation of cyanobacteria and fungi in desertification treatment.

Data availability statement

The datasets presented in this study can be found in online repositories. The names of the repository/repositories and accession number(s) can be found at: https://www.ncbi.nlm.nih.gov/genbank/, accession number: MH973233.

Author contributions

XZ: Conceptualization, Data curation, Formal analysis, Funding acquisition, Methodology, Visualization, Writing – original draft, Writing – review & editing. BL: Data curation, Formal analysis, Methodology, Writing – original draft, Writing – review & editing. TZ: Data curation, Methodology, Writing – original draft, Writing – review & editing. QX: Formal analysis, Writing – original draft, Writing – review & editing. XM: Methodology, Writing – original draft, Writing – review & editing. LC: Conceptualization, Funding acquisition, Project administration, Resources, Writing – original draft, Writing – review & editing.

Funding

The author(s) declare financial support was received for the research, authorship, and/or publication of this article. This research was supported by the National Natural Science Foundation of China (32101366).

Conflict of interest

The authors declare that the research was conducted in the absence of any commercial or financial relationships that could be construed as a potential conflict of interest.

Publisher's note

All claims expressed in this article are solely those of the authors and do not necessarily represent those of their affiliated organizations, or those of the publisher, the editors and the reviewers. Any product that may be evaluated in this article, or claim that may be made by its manufacturer, is not guaranteed or endorsed by the publisher.

Supplementary material

The Supplementary material for this article can be found online at: https://www.frontiersin.org/articles/10.3389/fmicb.2024.1377732/full#supplementary-material

References

Abed, R. M. M., Al-Sadi, A. M., Al-Shehi, M., Al-Hinai, S., and Robinson, M. D. (2013). Diversity of free-living and lichenized fungal communities in biological soil crusts of the Sultanate of Oman and their role in improving soil properties. *Soil Biol. Biochem.* 57, 695–705. doi: 10.1016/j.soilbio.2012.07.023

Antoninka, A., Bowker, M. A., Reed, S. C., and Doherty, K. (2016). Production of greenhouse-grown biocrust mosses and associated cyanobacteria to rehabilitate dryland soil function. *Restor. Ecol.* 24, 324–335. doi: 10.1111/rec.12311

Antoninka, A., Faist, A., Rodriguez-Caballero, E., Young, K. E., Chaudhary, V. B., Condon, L. A., et al. (2020). Biological soil crusts in ecological restoration: emerging research and perspectives. *Restor. Ecol.* 28, S3–S8. doi: 10.1111/rec.13201

Aponte, H., Meli, P., Butler, B., Paolini, J., Matus, F., Merino, C., et al. (2020). Meta-analysis of heavy metal effects on soil enzyme activities. *Sci. Total Environ.* 737:139744. doi: 10.1016/j.scitotenv.2020.139744

Atashpaz, B., Khormali, F., Malekzadeh, E., and Soleymanzadeh, M. (2023). The effect of different sequences of biological crusts on soil physicochemical properties in dry land. *Environ. Earth Sci.* 82:614. doi: 10.1007/s12665-023-11258-7

Ballesteros, M., Ayerbe, J., Casares, M., Cañadas, E. M., and Lorite, J. (2017). Successful lichen translocation on disturbed gypsum areas: a test with adhesives to promote the recovery of biological soil crusts. *Sci. Rep.* 7:45606. doi: 10.1038/srep45606

Bates, S. T., Nash, T. H. III, and Garcia-Pichel, F. (2012). Patterns of diversity for fungal assemblages of biological soil crusts from the southwestern United States. *Mycologia* 104, 353–361. doi: 10.3852/11-232

Belnap, J., Weber, B., and Büdel, B. (2016). "Biological soil crusts as an organizing principle in drylands" in *Biological soil crusts: an organizing principle in drylands*. eds. B. Weber, B. Büdel and J. Belnap (Berlin: Springer)

Borisover, M., Laor, Y., Saadi, I., Lado, M., and Bukhanovsky, N. (2011). Tracing organic footprints from industrial effluent discharge in recalcitrant riverine Chromophoric dissolved organic matter. *Water Air Soil Pollut.* 222, 255–269. doi: 10.1007/s11270-011-0821-x

Bowker, M. A. (2007). Biological soil crust rehabilitation in theory and practice: An underexploited opportunity. *Restor. Ecol.* 15, 13–23. doi: 10.1111/j.1526-100X.2006.00185.x

Bowker, M. A., Maestre, F. T., Eldridge, D., Belnap, J., Castillo-Monroy, A., Escolar, C., et al. (2014). Biological soil crusts (biocrusts) as a model system in community, landscape and ecosystem ecology. *Biodivers. Conserv.* 23, 1619–1637. doi: 10.1007/s10531-014-0658-x

Bu, C., Li, R., Wang, C., and Bowker, M. A. (2018). Successful field cultivation of moss biocrusts on disturbed soil surfaces in the short term. *Plant Soil* 429, 227–240. doi: 10.1007/s11104-017-3453-0

Canellas, L. P., Olivares, F. L., Aguiar, N. O., Jones, D. L., Nebbioso, A., Mazzei, P., et al. (2015). Humic and fulvic acids as biostimulants in horticulture. *Sci. Hortic. (Amsterdam)* 196, 15–27. doi: 10.1016/j.scienta.2015.09.013

Cao, T., Luo, Y., Shi, M., Tian, X., and Kuzyakov, Y. (2024). Microbial interactions for nutrient acquisition in soil: miners, scavengers, and carriers. *Soil Biol. Biochem.* 188:109215. doi: 10.1016/j.soilbio.2023.109215

Chamizo, S., Mugnai, G., Rossi, F., Certini, G., and De Philippis, R. (2018). Cyanobacteria inoculation improves soil stability and fertility on different textured soils: gaining insights for applicability in soil restoration. *Front. Environ. Sci.* 6:49. doi: 10.3389/fenvs.2018.00049

Chaudhary, V. B., Akland, K., Johnson, N. C., and Bowker, M. A. (2020). Do soil inoculants accelerate dryland restoration? A simultaneous assessment of biocrusts and mycorrhizal fungi. *Restor. Ecol.* 28, S115–S126. doi: 10.1111/rec.13088

Chen, L. Z., Rossi, F., Deng, S. Q., Liu, Y. D., Wang, G. H., Adessi, A., et al. (2014). Macromolecular and chemical features of the excreted extracellular polysaccharides in induced biological soil crusts of different ages. *Soil Biol. Biochem.* 78, 1–9. doi: 10.1016/j.soilbio.2014.07.004

Chen, W., Westerhoff, P., Leenheer, J. A., and Booksh, K. (2003). Fluorescence excitation-emission matrix regional integration to quantify spectra for dissolved organic matter. *Environ. Sci. Technol.* 37:5701. doi: 10.1021/es034354c

Chen, L. Z., Yang, Y., Deng, S. D., Xu, Y. H., Wang, G. H., and Liu, Y. D. (2012). The response of carbohydrate metabolism to the fluctuation of relative humidity (RH) in the desert soil cyanobacterium *Phormidium tenue*. *Eur. J. Soil Biol.* 48, 11–16. doi: 10.1016/j.ejsobi.2011.10.002

Chu, R., Li, S., Zhu, L., Yin, Z., Hu, D., Liu, C., et al. (2021). A review on co-cultivation of microalgae with filamentous fungi: efficient harvesting, wastewater treatment and biofuel production. *Renew. Sust. Energ. Rev.* 139:110689. doi: 10.1016/j.rser.2020.110689

Colica, G., Li, H., Rossi, F., Li, D., Liu, Y., and De Philippis, R. (2014). Microbial secreted exopolysaccharides affect the hydrological behavior of induced biological soil crusts in desert sandy soils. *Soil Biol. Biochem.* 68, 62–70. doi: 10.1016/j.soilbio.2013.09.017

Dabravolski, S. A., and Isayenkov, S. V. (2022). Metabolites facilitating adaptation of desert Cyanobacteria to extremely arid environments. *Plan. Theory* 11:3225. doi: 10.3390/plants11233225

Delgado, A., Madrid, A., Kassem, S., Andreu, L., and Del Campillo, M. D. C. (2002). Phosphorus fertilizer recovery from calcareous soils amended with humic and fulvic acids. *Plant Soil* 245, 277–286. doi: 10.1023/A:1020445710584

Deng, S., Wang, C., De Philippis, R., Zhou, X., Ye, C., and Chen, L. (2016). Use of quantitative PCR with the chloroplast gene rps4 to determine moss abundance in the early succession stage of biological soil crusts. *Biol. Fertil. Soils* 52, 595–599. doi: 10.1007/s00374-016-1107-7

Deng, S., Zhang, D., Wang, G., Zhou, X., Ye, C., Fu, T., et al. (2020). Biological soil crust succession in deserts through a 59-year-long case study in China: how induced biological soil crust strategy accelerates desertification reversal from decades to years. *Soil Biol. Biochem.* 141:107665. doi: 10.1016/j.soilbio.2019.107665

Derrien, M., Choi, H., Jardé, E., Shin, K.-H., and Hur, J. (2020). Do early diagenetic processes affect the applicability of commonly-used organic matter source tracking tools? An assessment through controlled degradation end-member mixing experiments. *Water Res.* 173:115588. doi: 10.1016/j.watres.2020.115588

Derrien, M., Shin, K. H., and Hur, J. (2019). Biodegradation-induced signatures in sediment pore water dissolved organic matter: implications from artificial sediments composed of two contrasting sources. *Sci. Total Environ.* 694:133714. doi: 10.1016/j.scitotenv.2019.133714

Dregne, H. E., Kassas, M., and Rozanov, B. (1991). A new assessment of the world status of desertification. *Desertif. Control Bull.* 2, 6–18.

Ferrenberg, S., Tucker, C. L., and Reed, S. C. (2017). Biological soil crusts: diminutive communities of potential global importance. *Front. Ecol. Environ.* 15, 160–167. doi: 10.1002/fee.1469

Fox, B. G., Thorn, R. M. S., Anesio, A. M., and Reynolds, D. M. (2017). The in situ bacterial production of fluorescent organic matter; an investigation at a species level. *Water Res.* 125, 350–359. doi: 10.1016/j.watres.2017.08.040

Frey-Klett, P., Burlinson, P., Deveau, A., Barret, M., Tarkka, M., and Sarniguet, A. (2011). Bacterial-fungal interactions: hyphens between agricultural, clinical, environmental, and food microbiologists. *Microbiol. Mol. Biol. Rev.* 75, 583–609. doi: 10.1128/MMBR.00020-11

Grimm, M., Grube, M., Schiefelbein, U., Zühlke, D., Bernhardt, J., and Riedel, K. (2021). The lichens' microbiota, still a mystery? *Front. Microbiol.* 12:623839. doi: 10.3389/fmicb.2021.623839

Guo, Z., and Tong, Y. W. (2014). The interactions between Chlorella vulgaris and algal symbiotic bacteria under photoautotrophic and photoheterotrophic conditions. *J. Appl. Phycol.* 26, 1483–1492. doi: 10.1007/s10811-013-0186-1

He, W., Di, B., Zeng, Y., Duan, Y., Li, J., Qiu, L., et al. (2023). Reconsidering the eco-economic benefits of grain for green program in Sichuan Province, China. *Ecol. Indic.* 157:111225. doi: 10.1016/j.ecolind.2023.111225

Hu, C., Zhang, D., Huang, Z., and Liu, Y. (2003). The vertical microdistribution of cyanobacteria and green algae within desert crusts and the development of the algal crusts. *Plant Soil* 257, 97–111. doi: 10.1023/A:1026253307432

Jensen, J. L., Schjønning, P., Watts, C. W., Christensen, B. T., Obour, P. B., and Munkholm, L. J. (2020). Soil degradation and recovery – changes in organic matter fractions and structural stability. *Geoderma* 364:114181. doi: 10.1016/j.geoderma.2020.114181

Karlen, D. L., Peterson, G. A., and Westfall, D. G. (2014). Soil and water conservation: our history and future challenges. *Soil Sci. Soc. Am. J.* 78, 1493–1499. doi: 10.2136/sssaj2014.03.0110

Kheirfam, H., and Roohi, M. (2020). Accelerating the formation of biological soil crusts in the newly dried-up lakebeds using the inoculation-based technique. *Sci. Total Environ.* 706:136036. doi: 10.1016/j.scitotenv.2019.136036

Kheirfam, H., Sadeghi, S. H., and Zarei Darki, B. (2020). Soil conservation in an abandoned agricultural rain-fed land through inoculation of cyanobacteria. *Catena* 187:104341. doi: 10.1016/j.catena.2019.104341

Lan, S., Zhang, Q., Wu, L., Liu, Y., Zhang, D., and Hu, C. (2014). Artificially accelerating the reversal of desertification: cyanobacterial inoculation facilitates the succession of vegetation communities. *Environ. Sci. Technol.* 48, 307–315. doi: 10.1021/es403785j

Li, T., Li, C.-T., Butler, K., Hays, S. G., Guarnieri, M. T., Oyler, G. A., et al. (2017). Mimicking lichens: incorporation of yeast strains together with sucrose-secreting cyanobacteria improves survival, growth, ROS removal, and lipid production in a stable mutualistic co-culture production platform. *Biotechnol. Biofuels* 10:55. doi: 10.1186/s13068-017-0736-x

Li, S., Li, Z., Liu, D., Yin, Z., Hu, D., Yu, Y., et al. (2022). Response of fungi-microalgae pellets to copper regulation in the removal of sulfonamides and release of dissolved organic matters. *J. Hazard. Mater.* 434:128932. doi: 10.1016/j.jhazmat.2022.128932

Li, Z., Ning, K., Chen, J., Liu, C., Wang, D., Nie, X., et al. (2020). Soil and water conservation effects driven by the implementation of ecological restoration projects: evidence from the red soil hilly region of China in the last three decades. *J. Clean. Prod.* 260:121109. doi: 10.1016/j.jclepro.2020.121109

Li, P., Wu, M., Li, T., Dumbrell, A. J., Saleem, M., Kuang, L., et al. (2023). Molecular weight of dissolved organic matter determines its interactions with microbes and its assembly processes in soils. *Soil Biol. Biochem.* 184:109117. doi: 10.1016/j.soilbio.2023.109117

Li, S., and Zhu, L. (2023). Copper regulates degradation of typical antibiotics by microalgal-fungal consortium in simulated swine wastewater: insights into metabolic routes and dissolved organic matters. *Water Res.* 245:120654. doi: 10.1016/j.watres.2023.120654

Liao, K., Tao, Y., Tu, J., Zeng, Y., Li, Y., Wang, P., et al. (2024). Induced and natural moss soil crusts accelerate the C, N, and P cycles of Pb Zn tailings. *Sci. Total Environ.* 909:168657. doi: 10.1016/j.scitotenv.2023.168657

Lin, H., and Guo, L. (2020). Variations in colloidal DOM composition with molecular weight within individual water samples as characterized by flow field-flow fractionation and EEM-PARAFAC analysis. *Environ. Sci. Technol.* 54, 1657–1667. doi: 10.1021/acs.est.9b07123

Liu, H., Huang, Y., Wang, H., Shen, Z., Qiao, C., Li, R., et al. (2020). Enzymatic activities triggered by the succession of microbiota steered fiber degradation and humification during co-composting of chicken manure and rice husk. *J. Environ. Manag.* 258:110014. doi: 10.1016/j.jenvman.2019.110014

Liu, Y., Nessa, A., Zheng, Q., Hu, D., Zhang, W., and Zhang, M. (2023). Inoculations of phosphate-solubilizing bacteria alter soil microbial community and improve phosphorus bioavailability for moso bamboo (*Phyllostachys edulis*) growth. *Appl. Soil Ecol.* 189:104911. doi: 10.1016/j.apsoil.2023.104911

Liu, H., Xu, H., Wu, Y., Ai, Z., Zhang, J., Liu, G., et al. (2021). Effects of natural vegetation restoration on dissolved organic matter (DOM) biodegradability and its temperature sensitivity. *Water Res.* 191:116792. doi: 10.1016/j.watres.2020.116792

Liu, Y., Yang, H., Li, X., and Xing, Z. (2014). Effects of biological soil crusts on soil enzyme activities in revegetated areas of the Tengger Desert. *China. Appl. Soil Ecol.* 80, 6–14. doi: 10.1016/j.apsoil.2014.03.015

Maestre, F. T., Bowker, M. A., Eldridge, D. J., Cortina, J., Lázaro, R., Gallardo, A., et al. (2016). "Biological soil crusts as a model system in ecology" in *Biological soil crusts: An organizing principle in drylands*. eds. B. Weber, B. Büdel and J. Belnap (Berlin: Springer)

Mao, Q., Xie, Z., Pinzon-Nuñez, D. A., Issaka, S., Liu, T., Zhang, L., et al. (2024). Leptolyngbya sp. XZMQ and Bacillus XZM co-inoculation reduced sunflower arsenic toxicity by regulating rhizosphere microbial structure and enzyme activity. *Environ. Pollut.* 341:123001. doi: 10.1016/j.envpol.2023.123001

Marasco, R., Ramond, J., Van Goethem, M. W., Rossi, F., and Daffonchio, D. (2023). Diamonds in the rough: dryland microorganisms are ecological engineers to restore degraded land and mitigate desertification. *Microb. Biotechnol.* 16, 1603–1610. doi: 10.1111/1751-7915.14216

Marks, E. A. N., Montero, O., and Rad, C. (2019). The biostimulating effects of viable microalgal cells applied to a calcareous soil: increases in bacterial biomass, phosphorus scavenging, and precipitation of carbonates. *Sci. Total Environ.* 692, 784–790. doi: 10.1016/j.scitotenv.2019.07.289

Meng, W., Song, M., Ming, L., Jiang, C., and Li, Z. (2016). Fungicidal activities of soil humic/fulvic acids as related to their chemical structures in greenhouse vegetable fields with cultivation chronosequence. *Sci. Rep.* 6:32858. doi: 10.1038/srep32858

Mohinuzzaman, M., Yuan, J., Yang, X., Senesi, N., Li, S.-L., Ellam, R. M., et al. (2020). Insights into solubility of soil humic substances and their fluorescence characterisation in three characteristic soils. *Sci. Total Environ.* 720:137395. doi: 10.1016/j.scitotenv.2020.137395

Mugnai, G., Rossi, F., Martin Noah Linus Felde, V. J., Colesie, C., Büdel, B., Peth, S., et al. (2018). The potential of the cyanobacterium Leptolyngbya ohadii as inoculum for stabilizing bare sandy substrates. *Soil Biol. Biochem.* 127, 318–328. doi: 10.1016/j.soilbio.2018.08.007

Pham, D. M., Kasai, T., Yamaura, M., and Katayama, A. (2021). Humin: no longer inactive natural organic matter. *Chemosphere* 269:128697. doi: 10.1016/j.chemosphere.2020.128697

Prasanna, R., Joshi, M., Rana, A., Shivay, Y. S., and Nain, L. (2012). Influence of co-inoculation of bacteria-cyanobacteria on crop yield and C–N sequestration in soil under rice crop. *World J. Microbiol. Biotechnol.* 28, 1223–1235. doi: 10.1007/s11274-011-0926-9

Rashid, M. I., Mujawar, L. H., Shahzad, T., Almeelbi, T., Ismail, I. M. I., and Oves, M. (2016). Bacteria and fungi can contribute to nutrients bioavailability and aggregate formation in degraded soils. *Microbiol. Res.* 183, 26–41. doi: 10.1016/j.micres.2015.11.007

Ren, Y., Zhang, B., Chen, X., and Liu, X. (2024). Analysis of spatial-temporal patterns and driving mechanisms of land desertification in China. *Sci. Total Environ.* 909:168429. doi: 10.1016/j.scitotenv.2023.168429

Rezasoltani, S., and Champagne, P. (2023). An integrated approach for the phycoremediation of Pb(II) and the production of biofertilizer using nitrogen-fixing cyanobacteria. *J. Hazard. Mater.* 445:130448. doi: 10.1016/j.jhazmat.2022.130448

Rodriguez-Caballero, E., Stanelle, T., Egerer, S., Cheng, Y., Su, H., Canton, Y., et al. (2022). Global cycling and climate effects of aeolian dust controlled by biological soil crusts. *Nat. Geosci.* 15, 458–463. doi: 10.1038/s41561-022-00942-1

Rossi, F., Mugnai, G., and De Philippis, R. (2018). Complex role of the polymeric matrix in biological soil crusts. *Plant Soil* 429, 19–34. doi: 10.1007/s11104-017-3441-4

Rossi, F., Mugnai, G., and De Philippis, R. (2022). Cyanobacterial biocrust induction: a comprehensive review on a soil rehabilitation-effective biotechnology. *Geoderma* 415:115766. doi: 10.1016/j.geoderma.2022.115766

Scharnagl, K., Tagirdzhanova, G., and Talbot, N. J. (2023). The coming golden age for lichen biology. *Curr. Biol.* 33, R512–R518. doi: 10.1016/j.cub.2023.03.054

Schmidt, M. W., Torn, M. S., Abiven, S., Dittmar, T., Guggenberger, G., Janssens, I. A., et al. (2011). Persistence of soil organic matter as an ecosystem property. *Nature* 478, 49–56. doi: 10.1038/nature10386

Segura, C., Navarro, F. B., Jiménez, M. N., and Fernández-Ondoño, E. (2020). Implications of afforestation vs. secondary succession for soil properties under a semiarid climate. *Sci. Total Environ.* 704:135393. doi: 10.1016/J.SCITOTENV.2019.135393

Swenson, T. L., Jenkins, S., Bowen, B. P., and Northen, T. R. (2015). Untargeted soil metabolomics methods for analysis of extractable organic matter. *Soil Biol. Biochem.* 80, 189–198. doi: 10.1016/j.soilbio.2014.10.007

Swenson, T. L., Karaoz, U., Swenson, J. M., Bowen, B. P., and Northen, T. R. (2018). Linking soil biology and chemistry in biological soil crust using isolate exometabolomics. *Nat. Commun.* 9:19. doi: 10.1038/s41467-017-02356-9

Verón, S. R., Paruelo, J. M., and Oesterheld, M. (2006). Assessing desertification. *J. Arid Environ.* 66, 751–763. doi: 10.1016/j.jaridenv.2006.01.021

Vikram, N., Sagar, A., Gangwar, C., Husain, R., and Narayan Kewat, R. (2022). "Properties of humic acid substances and their effect in soil quality and plant health" in *Humus and humic substances-recent advances*. ed. A. Makan (London: IntechOpen)

Wang, G., Deng, S., Liu, J., Ye, C., Zhou, X., and Chen, L. (2017). Cell damage caused by ultraviolet B radiation in the desert cyanobacterium Phormidium tenue and its recovery process. *Ecotoxicol. Env. Saf* 144, 315–320. doi: 10.1016/j.ecoenv.2017.06.024

Wang, G., Gao, Q., Yang, Y., Hobbie, S. E., Reich, P. B., and Zhou, J. (2022). Soil enzymes as indicators of soil function: a step toward greater realism in microbial ecological modeling. *Glob. Chang. Biol.* 28, 1935–1950. doi: 10.1111/gcb.16036

Wang, Y., Xu, D., and Li, L. (2023). Assessing the influences of natural and human factors upon desertification vulnerability in northern China during 1985–2010. *Catena* 233:107529. doi: 10.1016/j.catena.2023.107529

Weber, B., Belnap, J., Büdel, B., Antoninka, A. J., Barger, N. N., Chaudhary, V. B., et al. (2022). What is a biocrust? A refined, contemporary definition for a broadening research community. *Biol. Rev.* 97, 1768–1785. doi: 10.1111/brv.12862

Weber, B., Büdel, B., and Belnap, J. (2016). "Biological soil crusts" in *An organizing principle in drylands*. eds. B. Weber, B. Büdel and J. Belnap (Cham: Springer International Publishing)

Xiao, J., Wang, G., Liu, H., and Dai, X. (2022). Application of composted lipstatin fermentation residue as organic fertilizer: temporal changes in soil characteristics and bacterial community. *Chemosphere* 306:135637. doi: 10.1016/j.chemosphere.2022.135637

Xie, Z. M., Liu, Y. D., Hua, C. X., Chen, L. Z., and Li, D. H. (2007). Relationships between the biomass of algal crusts in fields and their compressive strength. *Soil Biol. Biochem.* 39, 567–572. doi: 10.1016/j.soilbio.2006.09.004

Xu, Y. H., Rossi, F., Colica, G., Deng, S. Q., De Philippis, R., and Chen, L. Z. (2013). Use of cyanobacterial polysaccharides to promote shrub performances in desert soils: a potential approach for the restoration of desertified areas. *Biol. Fertil. Soils* 49, 143–152. doi: 10.1007/s00374-012-0707-0

Xue, S., Liu, Z., Fan, J., Xue, R., Guo, Y., Chen, W., et al. (2022). Insights into variations on dissolved organic matter of bauxite residue during soil-formation processes following 2-year column simulation. *Environ. Pollut.* 292:118326. doi: 10.1016/j.envpol.2021.118326

Yakimov, B. P., Rubekina, A. A., Budylin, G. S., Zherebker, A. Y., Kompanets, V. O., Chekalin, S. V., et al. (2021). Ultrafast energy transfer determines the formation of fluorescence in DOM and humic substances. *Environ. Sci. Technol.* 55, 10365–10377. doi: 10.1021/acs.est.1c00998

Yang, Y., Dou, Y., Wang, B., Wang, Y., Liang, C., An, S., et al. (2022). Increasing contribution of microbial residues to soil organic carbon in grassland restoration chronosequence. *Soil Biol. Biochem.* 170:108688. doi: 10.1016/j.soilbio.2022.108688

Yang, H., Liu, C., Liu, Y., and Xing, Z. (2018). Impact of human trampling on biological soil crusts determined by soil microbial biomass, enzyme activities and nematode communities in a desert ecosystem. *Eur. J. Soil Biol.* 87, 61–71. doi: 10.1016/j.ejsobi.2018.05.005

Yang, X., Yan, R., Yang, C., Zhang, H., Lyu, H., Li, S., et al. (2024). Soil accelerates the humification involved in co-composting of wheat straw and cattle manure by promoting humus formation. *Chem. Eng. J.* 479:147583. doi: 10.1016/j.cej.2023.147583

Ye, Q., Wang, Y.-H., Zhang, Z.-T., Huang, W.-L., Li, L.-P., Li, J., et al. (2020). Dissolved organic matter characteristics in soils of tropical legume and non-legume tree plantations. *Soil Biol. Biochem.* 148:107880. doi: 10.1016/j.soilbio.2020.107880

Yilu, G., Xiaofeng, G., and Renhui, L. (2015). Characterization of humic acid release during the growth of Microcystis flos-aquae. *J. Lake Sci.* 27, 623–628. doi: 10.18307/2015.0409

Zhang, Y., Duan, P., Zhang, P., and Li, M. (2018). Variations in cyanobacterial and algal communities and soil characteristics under biocrust development under similar environmental conditions. *Plant Soil* 429, 241–251. doi: 10.1007/s11104-017-3443-2

Zhang, Y., Fu, Z., Zhou, W., Min, M., Ma, X., Cheng, Y., et al. (2014). Effect of wastewater-borne bacteria on algal growth and nutrients removal in wastewater-based algae cultivation system. *Bioresour. Technol.* 167, 8–13. doi: 10.1016/j.biortech.2014.05.087

Zhang, K., Li, Y., Wang, K., Liu, D., Dou, S., Chen, Y., et al. (2023). Response of soil enzymes to soil properties and seasonal characteristics of cyanobacteria-dominated crusts in a dryland ecosystem. *J. Soils Sediments* 23, 2756–2765. doi: 10.1007/s11368-023-03514-x

Zhou, X., An, X., De Philippis, R., Ye, C., Ke, T., Zhang, Y., et al. (2019). The facilitative effects of shrub on induced biological soil crust development and soil properties. *Appl. Soil Ecol.* 137, 129–138. doi: 10.1016/j.apsoil.2019.02.010

Zhou, X., Ke, T., Li, S., Deng, S., An, X., Ma, X., et al. (2020). Induced biological soil crusts and soil properties varied between slope aspect, slope gradient and plant canopy in the Hobq desert of China. *Catena* 190:104559. doi: 10.1016/j.catena.2020.104559

Zhuang, W.-E., Chen, W., Cheng, Q., and Yang, L. (2021). Assessing the priming effect of dissolved organic matter from typical sources using fluorescence EEMs-PARAFAC. *Chemosphere* 264:128600. doi: 10.1016/j.chemosphere.2020.128600

frontiers | Frontiers in Microbiology

TYPE Original Research
PUBLISHED 15 April 2024
DOI 10.3389/fmicb.2024.1370334

OPEN ACCESS

EDITED BY
Da Huo,
Chinese Academy of Sciences (CAS), China

REVIEWED BY
Elżbieta Zębek,
University of Warmia and Mazury in Olsztyn, Poland
Xinxin Lu,
Harbin Normal University, China
Hang Zhang,
Hubei Water Resources Research Institute, China

*CORRESPONDENCE
Junmei Jia
jiadao_mei@126.com

RECEIVED 14 January 2024
ACCEPTED 25 March 2024
PUBLISHED 15 April 2024

CITATION
Gu P, Jia J, Qi D, Gao Q, Zhang C, Yang X, Nie M, Liu D and Luo Y (2024) Response of phytoplankton composition to environmental stressors under humidification in three alpine lakes on the Qinghai-Tibet Plateau, China. *Front. Microbiol.* 15:1370334. doi: 10.3389/fmicb.2024.1370334

Response of phytoplankton composition to environmental stressors under humidification in three alpine lakes on the Qinghai-Tibet Plateau, China

Peiwen Gu[1], Junmei Jia[1]*, Delin Qi[1], Qiang Gao[1], Cunfang Zhang[1], Xi Yang[2], Miaomiao Nie[1], Dan Liu[1] and Yule Luo[2]

[1]State Key Laboratory of Plateau Ecology and Agriculture, Qinghai University, Xining, China, [2]College of Eco-Environmental Engineering, Qinghai University, Xining, China

Owning to their extreme environmental conditions, lakes on the Qinghai-Tibet Plateau have typically displayed a simplistic food web structure, rendering them more vulnerable to climate change compared to lakes in plains. Phytoplankton, undergoing a changing aquatic environment, play a crucial role in the material cycle and energy flow of the food chain, particularly important for the unique fish species of the Tibetan Plateau. To identify the changing environment indexes and determine the response of phytoplankton composition to the environment change in alpine lakes, three lakes—Lake Qinghai, Lake Keluke and Lake Tuosu—were selected as study areas. Seasonal sampling surveys were conducted in spring and summer annually from 2018 to 2020. Our findings revealed there were significant changes in physicochemical parameters and phytoplankton in the three lakes. Bacillariophyta was the predominant phytoplankton in Lake Qinghai from 2018 to 2020, with the genera *Synedra* sp., *Navicula* sp., *Cymbella* sp. and *Achnanthidium* sp. predominated alternately. Lake Keluke alternated between being dominated by Bacillariophyta and cyanobacteria during the same period. *Dolichospermum* sp., a cyanobacteria, was prevalent in the summer of 2018 and 2019 and in the spring of 2020. In Lake Tuosu, Bacillariophyta was the predominant phytoplankton from 2018 to 2020, except in the summer of 2019, which was dominated by cyanobacteria. *Synedra* sp., *Oscillatoria* sp., *Pseudoanabaena* sp., *Chromulina* sp. and *Achnanthidium* sp. appeared successively as the dominant genera. Analysis revealed that all three lakes exhibited higher phytoplankton abundance in 2018 that in 2019 and 2020. Concurrently, they experienced higher average temperatures in 2018 than in the subsequent years. The cyanobacteria, Bacillariophyta, Chlorophyta and overall phytoplankton increased with temperature and decreased with salinity and NH_4-N. Besides, the ratios of cyanobacteria, and the ratios of Bacillariophyta accounted in total phytoplankton increased with temperature. These findings suggest that cyanobacteria and phytoplankton abundance, especially Bacillariophyta, may have an increase tendency in the three alpine lakes under warm and wet climate.

KEYWORDS

phytoplankton, succession, biodiversity, environmental response, eutrophication, alpine lakes

1 Introduction

Phytoplankton serve as primary producers in aquatic ecosystems, playing a critical role in the material cycle and energy flow of food chains (Zhang et al., 2021). Biological production serves as an indicator of the trophic status and potential of fishery resources in aquatic organisms. The productivity of an aquatic environment is closely linked to the density of phytoplankton (Jakhar, 2013). The structure of the phytoplankton community is a sensitive indicator for assessing water quality changes, and its composition offers valuable insights into these shifts (Ger et al., 2014). A large amount of nutrients is discharged into freshwater systems along with surface runoff and domestic sewage (Carpenter et al., 1998a). Consequently, the phytoplankton community becomes overpopulated, aquatic plants gradually diminish or even disappear, and cyanobacterial blooms drive the deterioration of water quality and aquatic ecosystems in eutrophic lakes worldwide (Conley et al., 2009). The degradation of water resources through eutrophication can lead to the loss of the amenities or services that these aquatic resources provide (Smith, 2003). Climate change accelerated the degradation rate in aquatic systems (Huang et al., 2021). Qinghai-Tibetan Plateau is one of the most sensitive regions to global warming worldwide. Even though the rare species on the Tibetan Plateau has received widespread attention due to its unique geographical location and climatic conditions, the primary producers phytoplankton was seldom considered in those areas.

Extensive researches had done to explore driving factors of phytoplankton succession under climate change (Winder and Sommer, 2012; Li et al., 2016; Cao et al., 2018; Li et al., 2023). Temperature was one of the most important drivers. High temperatures favor phytoplankton growth, since temperature affects life activities such as metabolism by influencing enzyme activity in phytoplankton. Phytoplankton had different temperature optimum. Bacillariophyta are able to grow rapidly when temperatures are low, while cyanobacteria and Chlorophyta may become dominant genera in summer as temperatures rise (Chen et al., 2003; Ke et al., 2008). Beyond temperature, nutrients are indispensable for phytoplankton growth and reproduction, and appropriate concentrations will promote phytoplankton growth and reproduction. Commonly, nutrient enrichment fosters the growth of specific phytoplankton like *Microcystis*, *Dolichospermum* sp., *Nostoc* and *Aphanizomenon*, which can be detrimental to both aquatic and terrestrial life (Chen et al., 2008; Lv et al., 2011). Nitrogen (N) and Phosphorus (P) are often identified as the primary nutrients limiting aquatic algal growth (Lv et al., 2011). The P essential for summer algal blooms originates from rapid water column P cycling and sediment P release, a process accelerated by increased salinity, which supplies sulfate reducing sediment *microorganism* populations and triggers substantial P release (Conley, 1999; Blomqvist et al., 2004). Long-term analysis in Lake Geneva demonstrated that phytoplankton photosynthetic efficiency is directly proportional to water temperature given adequate phosphorus, a relationship amplified at elevated nutrient concentrations. In phosphorus-limited scenarios, the correlation between photosynthetic efficiency and temperature diminishes (Tadonléke, 2010). Excessive P in the water column causes cyanobacterial blooms in the summer. Concurrently, N is essential for the growth of cyanobacteria. Phytoplankton communities experience regular variation in response to nutrient stress. Previous studies have shown that nitrogen deficiency induces nitrogen fixation by phytoplankton, favoring the growth and reproduction of nitrogen-fixing algae. This in turn favors the growth and reproduction of nitrogen-fixing algae (Dokulil and Teubner, 2000). In a high mountain lake, nutrient enrichment bioassays indicated that phytoplankton growth was severely limited by phosphorus due to overgrazing by pastoralists and ongoing climate change (Ren et al., 2019; Jia et al., 2022). In contrast, nitrogen did not significantly impact phytoplankton growth, but excessive nitrogen is toxic to phytoplankton. In addition, phytoplankton growth is affected by environmental factors such as salinity and NH_4-N and is able to react quickly by responding to changes in the environment, which some previous studies might have overlooked. Each species of planktonic plants has a specific salinity range optimal for its growth and reproduction. Therefore, the variations of physicochemical parameters such as temperature, salinity and nutrient may favor some of phytoplankton genera and become stressors for others under climate change.

The Qinghai-Tibet Plateau, known as the world's highest and most expansive plateau, encompasses a significant cluster of plateau lake systems (Li et al., 2021). The Tibetan Plateau is very sensitive to climate change and the lakes undergone expansion on surface water in recent years (Lei and Yang, 2017). This situation may alters the physico-chemical properties of water bodies and lake nutrient concentrations since increasing terrestrial inflow (Liu, 2013; Lu et al., 2017). These changes in environmental factors will inevitably have a profound impact on the composition and structure of phytoplankton (Abirhire et al., 2015; Jia et al., 2022). Previous studies had demonstrated that cyanobacteria were boosted in many aquatic systems under climate change. Alpine lakes, characterized by their special geographical location and extreme environmental conditions, form an integral part of mountain systems and typically feature simpler aquatic ecosystems compared to other lakes. Lakes like Lake Qinghai, Lake Keluke and Lake Tuosu, all situated on the Tibetan Plateau, are distinguished by their extreme conditions and presented low phytoplankton abundance without blooms. Although alpine lakes have a low percentage of cyanobacteria, cyanobacteria may increase as the increase of temperatures and nutrients load and pose some threat to rare fish and birds in the lakes under climate change. In recent years, Lake Qinghai, Lake Keluke and Lake Tuosu all had undone an marked increase of surface water. For example, the water level of Lake Qinghai decreased by 3.35 m, 2.77 m and 0.58 m from 1959 to 2000, 1959 to 1986, and 1986 to 2000, respectively. Compared to 1989, the water area of Lake Qinghai had shrunk by 129 km^2 in 2004. The lake's area has expanded due to climate-induced increases in rainfall since 2005, reaching 4,476 km^2 in 2017, and it is expected that the water area will continue to increase from 2021 to 2050 in Lake Qinghai (Li et al., 2007; Dong et al., 2018). This had resulted in a series of ecological environmental problems in littoral zone of Lake Qinghai, for example the blooming of Cladophora (Wu et al., 2023). However, seldom had research focused on the changes in aquatic environment and the phytoplankton on the Tibetan Plateau. In present study, we intended to identify those changing aquatic indexes and phytoplankton succession in the typical alpine lakes under climate change, and response of phytoplankton communities to changing aquatic indexes. This research would provide the basic information of sensitive environment indexes to climate change in alpine lakes and the response of phytoplankton composition to the environment

change, which is imperative for the lake protection on the Tibetan Plateau under climate change.

2 Materials and methods

2.1 Study area and sampling locations

Lake Qinghai (36°32′–37°15′N; 99°36′–100°16′E) is located in northeastern (Jia et al., 2022) Qinghai-Tibetan Plateau, and is the largest lake in China (Figure 1). It covers an area of approximately 4,300 km^2 (Tang et al., 2018), has a maximum depth of 30 m, and a mean surface elevation of 3,194 m. The lake is bordered by Qilian Mountains, AltynTagh Mountains, and the Kunlun Mountains (Abirhire et al., 2015; Li et al., 2021). This region has an alpine and continental climate with an annual average temperature of 1.2°C (Cao et al., 2020). With the unique beauty of the plateau lakes, it is known as the "China's most beautiful lake" and is a famous tourist destination in China. With the increase in popularity of Qinghai Lake tourism, the number of tourists has been increased year by year, greatly contributing to Qinghai Province's economic growth. However, tourism has brought economic benefits, but also the ecological environment of the tourist sites have been damaged by the increasing tourists (Zhang, 2019). Lake Keluke (37°10′–37°20′N; 96°49′–97°30′E) is a small salty water in Qinghai Province and the habitat and breeding place of many important waterfowls (Tang and Ju, 2011). It spans an area of about 56.7 km^2, boasts a mean water depth of 4 m, and reaches a maximum depth of 13.3 m. The lake is rich in Chinese mitten crabs, or hairy crabs, and is also dominated by the habitat of crane birds. Due to the large number of people living in the neighborhood of Lake Qinghai and Lake Keluke, the area of farming in the reserve is also large. The density of settlements directly affects the habitat of birds and destroys the aquatic vegetation of wetlands, while surface farming has a tendency to cause eutrophication of lake water. Around the lake area, tens of thousands of livestock graze annually, and a large amount of animal manure is washed into the lake, making the lake mud and water very fertile, providing nutritious growth conditions for aquatic plants, and also causing a certain degree of water pollution (Guo, 2013). Lake Tuosu (37°04′–37°13′N; 96°50′–97°03′E) is situated in the east of the Qaidam Basin, holding an average elevation of 2,800 meters. Its annual average temperature at 3°C (Song and Sun, 2020). Lake Tuosu primarily receives water from Lake Leluke, with the two lakes being linked by a river (Chen et al., 2003). Lake Keluke and Lake Tuosu have the same ecological environment and history of change but had different characteristic. Lake Tuosu is a typical inland saltwater lake and surrounded by the vast Gobi Desert. The temperature is relative high and the water evaporation of the lake is very high. There is very little aquatic flora and fauna in Lake Tuosu (Sheng, 2022).

2.2 Sample collection and processing

Water samples of Lake Qinghai, Lake Keluke and Lake Tuosu were collected during the spring and summer of 2018 (Jia et al., 2022), 2019 and 2020. Samples were taken from 10, 5 and 4 sites in Lake Qinghai, Lake Keluke and Lake Tuosu, respectively (Figure 1). The sampling time is listed in Table 1. Surface water samples, from a depth of 0.5 meters, were collected in 1 L plastic containers. All samples were stored in polyethylene barrels at 4°C, kept cool and shaded, and transported to the laboratory for analysis within 24 h (Ke et al., 2008). Analysis of the water parameters for the three lakes included temperature, pH, salinity, TN, TP and NH_4-N. Water temperature, pH and salinity were measured on-site at each location using a YSI 6600

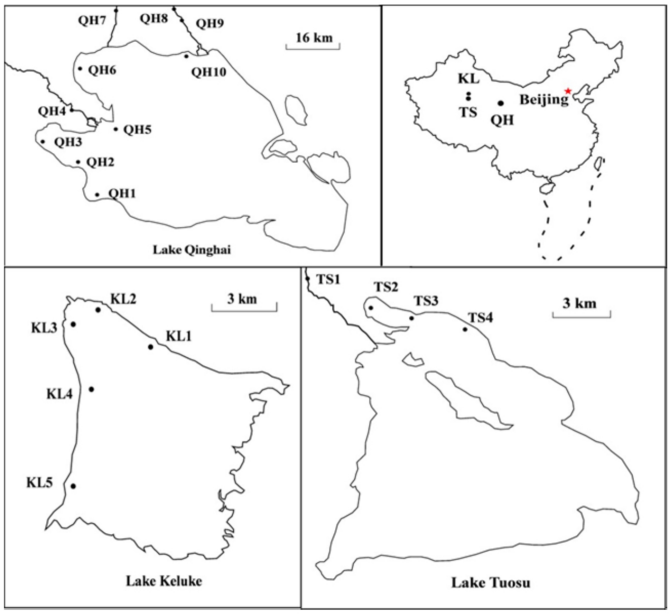

Sample site	longitude	latitude
QH1	99°49'4"E	36°42'19"N
QH2	99°45'42"E	36°49'51"N
QH3	99°38'27"E	36°53'31"N
QH4	99°44'23"E	37°1'55"N
QH5	99°51'10"E	36°59'22"N
QH6	99°45'15"E	37°8'40"N
QH7	99°53'54"E	37°16'16"N
QH8	99°52'52"E	37°13'56"N
QH9	100°7'30"E	37°19'43"N
QH10	100°9'5"E	37°18'24"N
KL1	96°54'4"E	37°18'55"N
KL2	96°52'1"E	37°19'52"N
KL3	96°51'2"E	37°19'12"N
KL4	96°51'35"E	37°17'31"N
KL5	96°50'57"E	37°15'0"N
TS1	96°49'57"E	37°14'9"N
TS2	96°52'16"E	37°12'58"N
TS3	96°54'8"E	37°12'33"N
TS4	96°56'8"E	37°12'14"N

FIGURE 1
Sampling sites of Lake Qinghai, Lake Keluke, and Lake Tuosu, in China.

TABLE 1 The sample collection times in the three lakes in China.

Years	Season	Lake Qinghai	Lake Keluke	Lake Tuosu
2018	Spring	28-29th May	1th June	2th June
	Summer	20-21th August	18th August	19th August
2019	Spring	10-11th June	8th June	9th June
	Summer	1-2th September	30th August	31th August
2020	Spring	10-11th June	8th June	9th June
	Summer	10-11th September	8th September	9th September

multi-probe sonde (YSI, Yellow Springs, OH, United States). Total nitrogen (TN) and total phosphorus (TP) were measured using Chinese standard methods HJ/T 636-2012 and GB/T 11983-1989, respectively. NH_4-N was measured following the Chinese standard method HJ 535-2009.

Quantitative water samples were stored in clean plastic containers, and phytoplankton genera were fixed with Lugol's iodine solution (1.5% v/v). Phytoplankton were allowed to settle for 48 h. Based on monographs, phytoplankton were identified and enumerated under 20 × 20 magnification using light microscopy for cell density (Lv et al., 2011; Zhang et al., 2016). The Shannon-wiener index (H) of phytoplankton diversity were computed (Chen et al., 2008). Biodiversity of phytoplankton in the three lakes was calculated according to groups such as cyanobacteria, Bacillariophyta, Chlorophyta, Cryptophyta, Euglenophyta, Pyrrophyta and Chrysophyta (Liu et al., 2016; Li et al., 2021).

2.3 Statistical analysis

All physical and chemical parameters were analyzed using SPSS software, version 26.0 for Windows (Chicago, United States). The data approximately conformed to a normal distribution. Analysis of variance was employed to assess the differences in water parameters and phytoplankton both temporally and spatially. RDA analyzed was applied to assess relationships between phytoplankton and environmental factors using canoco 5. Detrended correspondence analysis (DCA) was conducted to assess the length of the dominant gradient of environmental factors and phytoplankton and the first axis of lengths of gradient was <3.0. Thusly, RDA analysis was chosen in present study. Linear regression models were applied to environmental indexes and phytoplankton based on yearly average data. Water parameters and phytoplankton showing a p value <0.05 were considered to be significantly different or related.

3 Results

3.1 Water parameter and nutrients in the three lakes

Table 2 displays the annual changes in water parameters and nutrient levels. Lake Qinghai had significantly higher temperature in 2018 than in 2020 ($p < 0.05$). Lake Keluke and Lake Tuosu recorded significantly higher temperatures in 2018 than in 2019 and 2020 ($p < 0.05$). Over the three-year period, Lake Tuosu had the highest average temperature, followed by Lake Keluke, with Lake Qinghai having the lowest ($p < 0.05$). In terms of salinity, Lake Tuosu exhibited the highest levels among the three lakes ($p < 0.05$), followed by Lake Keluke, with Lake Qinghai recording the lowest salinity ($p < 0.05$). There were notable differences in the NH_4-N levels among the lakes. Lake Tuosu had the highest NH_4-N, followed by Lake Keluke, while Lake Qinghai had the lowest. Compared to Lake Qinghai, Lake Tuosu demonstrated higher levels of temperature, salinity and NH_4-N. The TP concentrations in all three lakes remained below 0.1 mg/L. Lake Keluke exhibited elevated TP levels compared to Lake Qinghai and Lake Tuosu. Fluctuations in TP concentrations between Lake Qinghai and Lake Tuosu over different years were minimal. Conversely, Lake Tuosu had higher TP concentrations than both Lake Qinghai and Lake Keluke during those years.

3.2 Phytoplankton composition and biodiversity in the three lakes

The phytoplankton composition varied among the three lakes (Figure 2). Cyanobacteria, Bacillaiophyta, Chlorophyta, Pyrrophyta, Cryptophyta, Chrysophyta and Euglenophyta have been found both in Lake Qinghai and Lake Keluke. Cyanobacteria, Bacillaiophyta, Chlorophyta, Pyrrophyta, Cryptophyta and Chrysophyta were found in Lake Tuosu. Cyanobacteria, Bacillariophyta and Chlorophyta were dominated across all sampling sites in Lake Qinghai, Lake Keluke and Lake Tuosu in 2018, 2019 and 2020. Lake Qinghai recorded phytoplankton abundances of 1.3×10^5 cells/L, 1.6×10^4 cells/L and 2.9×10^5 cells/L in 2018, 2019 and 2020, respectively. Within this lake, Bacillariophyta contributed to 73, 88 and 66% of the total, cyanobacteria made up 24, 3% and 14%. For Lake Keluke, the figures stood at 2.7×10^5 cells/L, 1.8×10^5 cells/L and 2.3×10^5 cells/L for those respective years. Between 2018 and 2020, cyanobacteria represented 58%, 32%, and 46%, while Bacillariophyta made up 23%, 56%, and 46% of the phytoplankton. In Lake Tuosu, the numbers were 1.22×10^5 cells/L, 1.43×10^4 cells/L and 1.13×10^5 cells/L over the 3 years. Bacillariophyta made up 65, 40 and 43% of the phytoplankton, cyanobacteria contributed 24%, 34%, and 2% in 2018, 2019, and 2020, and Chrysophyta accounted for 29% in 2020. Both Bacillariophyta and total phytoplankton abundance in Lake Qinghai were significantly higher in 2018 than in 2019 and 2020 ($p < 0.05$) and cyanobacteria in 2018 had a significantly higher abundance than in 2019 ($p < 0.05$). Lake Tuosu exhibited significantly higher Bacillariophyta abundance in 2018 compared to 2019 and 2020 ($p < 0.05$) along with a higher cyanobacteria abundance in 2018 than 2020 ($p < 0.05$).

Table 3 displays the percentage of dominant phytoplankton and genera. Bacillariophyta was dominanted in Lake Qinghai from 2018 to 2020. The *Synedra* sp., *Navicula* sp., *Cymbella* sp., *Synedra* sp., *Synedra* sp., and *Achnanthidium* sp. were emerging successively as the dominant genera, which accounted for 33%, 35%, 24%, 21%, 23%, and 41% of the total phytoplankton, respectively. In addition, there was a higher percentage of *Dolichospermum* sp. in spring 2018 and *Spirogyra* sp. in summer 2019 in Lake Qinghai, which accounted for 25% and 15% of the total phytoplankton. Cyanobacteria and Bacillariophyta were alternated dominanted in Lake Keluke during the same period, the genus *Dolichospermum* sp., was dominanted in the summer of 2018 and 2019 and in the spring of 2020, which accounted for 44%, 31%, and 32%, respectively. In Lake Tuosu, Bacillariophyta was dominant from 2018 to 2020, except in the summer of 2019, which

TABLE 2 Means and standard deviations of several water parameters of lakes in China.

Lakes	Years	Water parameters							
		Temperature (°C)	DO (mg/L)	C (mS/cm)	Salinity (ppt)	pH	TN (mg/L)	TP (mg/L)	NH_4-N (mg/L)
Qinghai(12)	2018	15.0±4.4	3.6 ±3.7	5.1 ±5.8	4.3 ±4.9	8.8 ±0.4	4.6 ±6.0	0.02 ±0.03	NA ± NA
	2019	13.4 ±5.3	5.8±1.8	5.9±6.9	4.2±4.9	8.2±2.5	3.8±3.4	0.06±0.09	1.5 ±2.5
	2020	10.4 ±6.9	4.7±3.1	4.9±6.8	3.5±5.0	6.8±4.4	0.9±0.8	0.03±0.04	0.2 ± 0.2
	Mean	13.0 ±5.9	4.7±3.1	5.3±6.5	4.0±4.9	7.9±3.1	3.1±4.2	0.04±0.06	0.6 ± 1.6
Keluke(6)	2018	20.8 ±2.5	3.6±4.0	6.0±13.1	5.6±13.2	8.4±0.2	4.6±4.9	0.04±0.04	NA ± NA
	2019	16.0 ±1.3	6.3 ±2.9	5.9 ±16.0	4.7 ±13.4	8.5 ±0.3	5.4 ±8.9	0.09 ±0.11	2.9 ±6.6
	2020	11.7±7.1	4.5 ±2.8	5.8 ±15.6	4.8 ±13.7	6.7 ±4.1	6.1 ±9.8	0.05 ±0.08	3.1±6.8
	Mean	16.2 ±5.7	4.8 ±3.4	5.9 ±14.5	5.0 ±13.0	7.9 ±2.4	5.4 ±7.9	0.06 ±0.08	2.0±5.5
Tuosu(4)	2018	21.1 ±2.5	3.7 ±4.0	12.9 ±10.5	11.7 ±10.1	8.9 ±0.3	1.4 ±1.0	0.02 ±0.006	NA ± NA
	2019	17.2 ±1.3	6.2 ±0.05	19.5 ±11.1	14.1 ±8.2	9.0 ±0.2	10.6 ±7.6	0.05 ±0.06	8.8 ±6.9
	2020	18.8 ±3.0	6.1 ±0.3	19.3 ±11.3	13.3 ±7.8	9.5 ±0.2	6.8 ±4.7	0.03 ±0.04	4.9 ± 4.8
	Mean	19.0 ±2.8	5.4 ±2.5	17.2 ±11.0	13.0 ±8.4	9.1 ±0.3	6.3 ±6.3	0.03 ±0.04	4.6 ±5.9

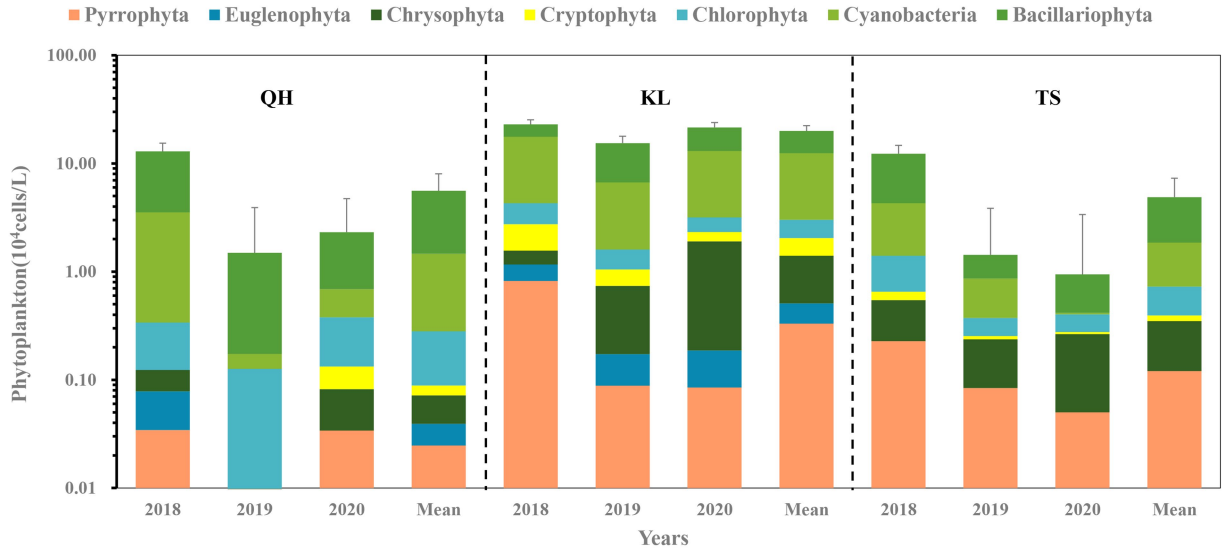

FIGURE 2
Phytoplankton composition based on the abundance in different seasons in Lake Qinghai (QH), Lake Keluke (KL), Lake Tuosu (TS). The standard deviations of phytoplankton abundance in each lake are indicated by the error bars.

was dominated by cyanobacteria, the dominant genera *Synedra* sp., *Oscillatoria* sp., *Pseudoanabaena* sp. and *Achnanthidium* sp. were appeared successively, which accounted for 28%, 26%, 23%, 24%, and 62%, respectively. Chlorophyta was the second dominant in the spring of 2020, which was dominated by the genus of *Chromulina* sp. accounted for 22% in Tuosu.

The phytoplankton biodiversity of the three lakes exhibited significant variances. In 2018, 2019 and 2020, Lake Qinghai's phytoplankton diversity was 0.26 ±0.33, 0.19 ± 0.31 and 0.19 ± 0.42, respectively. In 2018, 2019 and 2020, Lake Keluke's phytoplankton diversity was 0.81 ± 0.59, 0.79 ± 0.55 and 0.55 ± 0.61, respectively. Additionally, in 2018, 2019 and 2020, Lake Tuosu's phytoplankton diversity was 0.83 ± 0.53, 0.48 ± 0.60, and 0.44 ±0.61, respectively.

3.3 RDA analyses in the three lakes

The relationship among phytoplankton and water parameters was analyzed by redundancy analysis (RDA), as shown in Figure 3. Based on the results of the RDA analysis, it can be seen that the eigenvalue of axis 1 is 0.37, and the eigenvalue of axis 2 is 0.19, and the two axes can explain 56.0% of the variation rate. RDA analyses showed that cyanobacteria, Chlorophyta, phytoplankton abundance, and the ratio of cyanobacteria/phytoplankton were positively correlated with temperature in Lake Qinghai, Lake Keluke and Lake Tuosu in 2018–2020 ($p < 0.05$). Bacillariophyta, phytoplankton abundance and the ratio of Chlorophyta/phytoplankton were all negatively correlated with salinity ($p < 0.05$). Meanwhile, cyanobacteria, Bacillariophyta, Chlorophyta and phytoplankton abundance were all negatively

TABLE 3 Percentage of dominant phytoplankton genera in several lakes in China.

Years	Season	Lake Qinghai			Lake Keluke			Lake Tuosu		
		Dominant genera	Pi (%)	phytoplankton	Dominant genera	Pi (%)	phytoplankton	Dominant genera	Pi (%)	phytoplankton
2018	Spring	*Synedra* sp.	33	Bacillariophyta	*Synedra* sp.	21	Bacillariophyta	*Synedra* sp.	28	Bacillariophyta
		Dolichospermum sp.	25	Cyanobacteria	*Oscillatoria* sp.	21	Cyanobacteria	*Nitzschia* sp.	18	Bacillariophyta
		Navicula sp.	18	Bacillariophyta	*Navicula* sp.	11	Bacillariophyta	*Merismopedia* sp.	15	Cyanobacteria
	Summer	*Navicula* sp.	35	Bacillariophyta	*Dolichospermum* sp.	44	Cyanobacteria	*Synedra* sp.	26	Bacillariophyta
		Synedra sp.	17	Bacillariophyta	*Merismopedia* sp.	7	Cyanobacteria	*Dactylococcopsis* sp.	16	Cyanobacteria
		Oscillatoria sp.	8	Cyanobacteria	*Synedra* sp.	4	Bacillariophyta	*Chlorella* sp.	6	Chlorophyta
2019	Spring	*Cymbella* sp.	24	Bacillariophyta	*Synedra* sp.	34	Bacillariophyta	*Oscillatoria* sp.	23	Cyanobacteria
		Synedra sp.	18	Bacillariophyta	*Navicula* sp.	16	Bacillariophyta	*Synedra* sp.	15	Bacillariophyta
		Navicula sp.	10	Bacillariophyta	*Diatoma* sp.	16	Bacillariophyta	*Cymbella* sp.	15	Bacillariophyta
	Summer	*Synedra* sp.	21	Bacillariophyta	*Dolichospermum* sp.	31	Cyanobacteria	*Pseudoanabaena* sp.	24	Cyanobacteria
		Spirogyra sp.	15	Chlorophyta	*Oscillatoria* sp.	19	Cyanobacteria	*Dactylococcopsis* sp.	20	Cyanobacteria
		Navicula sp.	9	Bacillariophyta	*Pseudoanabaena* sp.	15	Cyanobacteria	*Synedra* sp.	19	Bacillariophyta
2020	Spring	*Synedra* sp.	23	Bacillariophyta	*Dolichospermum* sp.	32	Cyanobacteria	*Chromulina* sp.	22	Chlorophyta
		Cyclotella sp.	16	Bacillariophyta	*Synedra* sp.	28	Bacillariophyta	*Synedra* sp.	19	Bacillariophyta
		Merismopedia sp.	9	Cyanobacteria	*Oscillatoria* sp.	11	Cyanobacteria	*Cyclotella* sp.	7	Bacillariophyta
	Summer	*Achnanthidium* sp.	41	Bacillariophyta	*Fragilaria* sp.	35	Bacillariophyta	*Achnanthidium* sp.	62	Bacillariophyta
		Fragilaria sp.	20	Bacillariophyta	*Cyclotella* sp.	22	Bacillariophyta	*Fragilaria* sp.	17	Bacillariophyta
		Cyclotella sp.	1	Bacillariophyta	*Navicula* sp.	13	Bacillariophyta	*Gomphonema* sp.	9	Bacillariophyta

10.3389/fmicb.2024.1370334

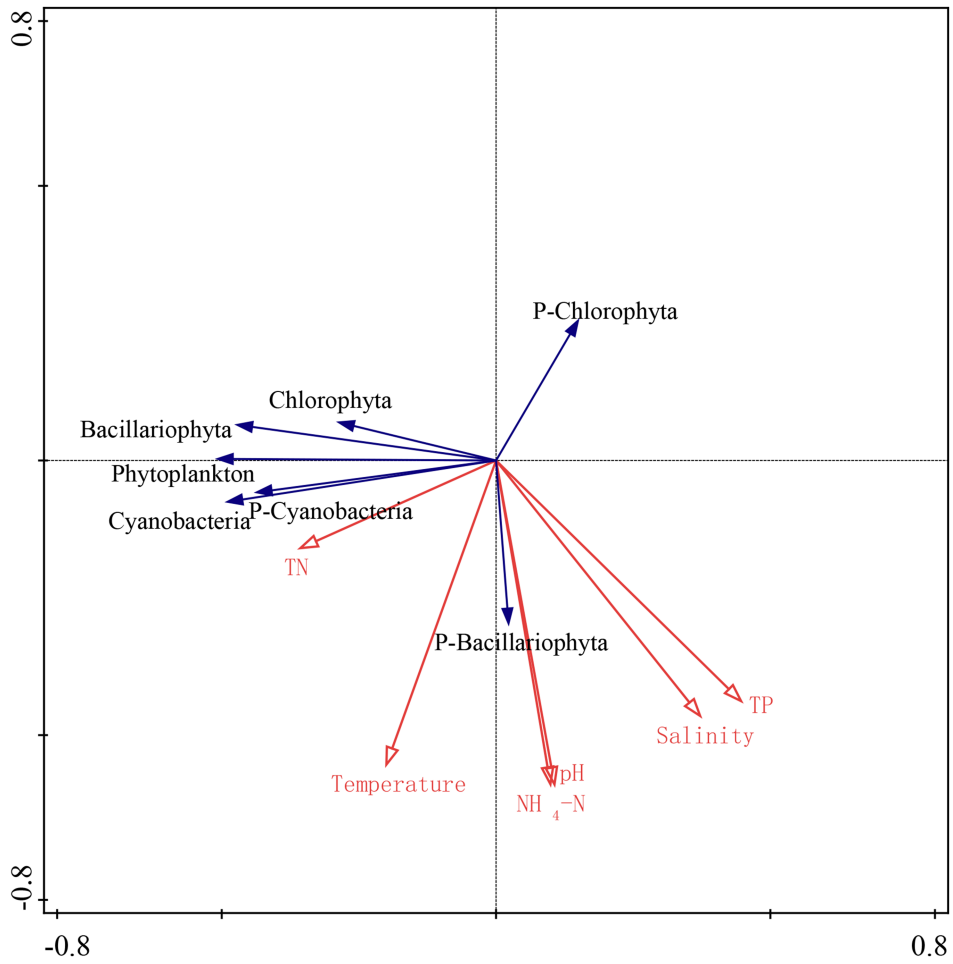

FIGURE 3
RDA analyses of biological and environmental factors in Lake Qinghai, Lake Keluke and lake Tuosu.

correlated with NH_4-N ($p < 0.05$). Besides, the ratio of Bacillariophyta /phytoplankton and the ratio of cyanobacteria/phytoplankton were all negatively correlated with NH_4-N ($p < 0.05$).

3.4 Linear regression analysis based on annual average values of water parameters and phytoplankton in the three lakes

According to the annual average data from Lake Qinghai, Lake Keluke and Lake Tuosu, phytoplankton had clear responses to water parameters, such as temperature, salinity and NH_4-N in Figures 4–6. Cyanobacteria, Bacillariophyta, Chlorophyta and phytoplankton abundance all increased with temperature with $R^2 = 0.25$, 0.25, 0.25 and 0.30, respectively ($p < 0.01$). Additionally, the ratio of cyanobacteria/phytoplankton and the ratio of Bacillariophyta/ phytoplankton both increased with temperature ($p < 0.01$).

Significant responses were also observed between phytoplankton and salinity based on the annual average data from Lake Qinghai, Lake Keluke and Lake Tuosu (Figure 5). Cyanobacteria, Bacillariophyta, Chlorophyta and phytoplankton abundance all decreased with salinity under $R^2 = 0.27$, 0.20, 0.36 and 0.40, respectively ($p < 0.01$). In addition, the ratio of Bacillariophyta/ phytoplankton, the ratio of Chlorophyta/phytoplankton and the ratio of cyanobacteria/phytoplankton all decreased with the salinity ($p < 0.05$). Furthermore, based on the annual average data from the three alpine lakes, phytoplankton had clear response to NH_4-N (Figure 6). Cyanobacteria, Bacillariophyta, Chlorophyta and phytoplankton abundance declined with NH_4-N ($p < 0.05$; Figure 6). In addition, the ratio of cyanobacteria/phytoplankton, the ratio of Bacillariophyta/phytoplankton and the ratio of Chlorophyta/ phytoplankton all decreased with NH_4-N ($p < 0.05$).

4 Discussion

Previous studies had indicated that the Tibetan Plateau are sensitive to climate change, which was two-three times of the average level (Lan, 2024). In present study, physicochemical parameters variations showed that there were clear responses of aquatic environment to climate change, especially in temperature, salinity and nutrients. This would inevitably affect the phytoplankton genera and community structure, and have a profound impact on the structure and function of the ecosystem in alpine lakes. Previous studies have shown that the increased of temperatures changed the phytoplankton composition and structure (Trombetta et al., 2019), the maximum

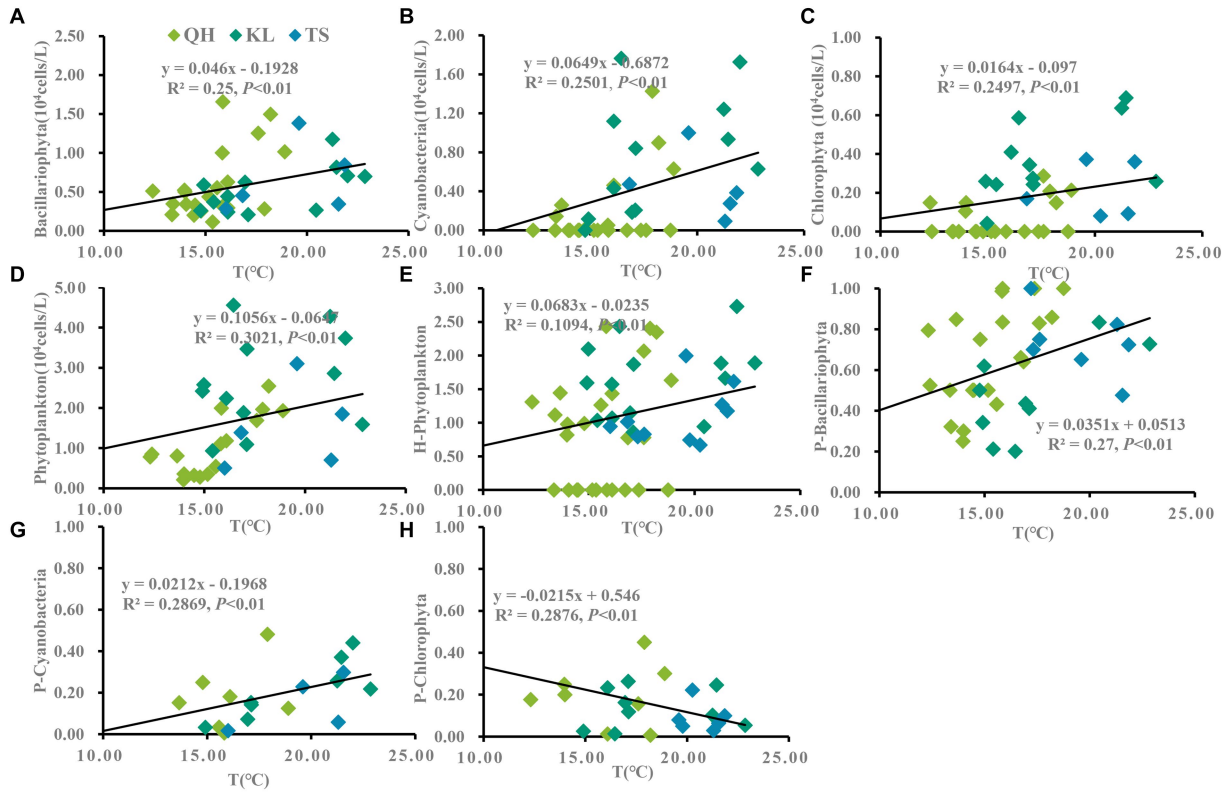

FIGURE 4
Linear regression models was applied to temperature (T) and phytoplankton based on yearly average data from each site of Lake Qinghai, Lake Keluke and Lake Tuosu. The response of phytoplankton to T were shown in **(A–D)** and response of phytoplankton composition to T were shown in **(E–H)**. Bacillariophyta, cyanobacteria, Chlorophyta and phytoplankton abundance were changed via Log (X + 1). P-i represents the i/phytoplankton ratio based on abundance. H-phytoplankton indicates the biodiversity of phytoplankton.

biomass, and promoted the growth of cyanobacteria and Chlorophyta. Moreover, the temperature elevation can enhance the competitiveness of the dominant genera, while accelerating the process of succession in different trophic phytoplankton in the water, and also making eutrophication water appear the common dominant genera in even heavy eutrophic water (Winder and Sommer, 2012; Yang, 2016). In current study, linear regression analysis showed that cyanobacteria, Bacillariophyta, Chlorophyta and overall phytoplankton all increase with temperature. Besides, the ratio of cyanobacteria/phytoplankton and the ratio of Bacillariophyta/phytoplankton both increased with temperature. Those results indicated that phytoplankton abundance would increase if water temperature rise under climate change. Both cyanobacteria and Bacillariophyta are sensitive to temperature change and the phytoplankton composition would tend to shift toward cyanobacteria and Bacillariophyta in alpine lakes with temperature rise. The inferences were consistent with the results of both temporal and spatial variations in temperature and phytoplankton. The three lakes exhibited cyanobacteria, Bacillariophyta, Chlorophyta and phytoplankton showed significantly higher abundances in 2018 compared to 2019 and 2020. Concurrently, higher average temperatures in 2018 than in the subsequent years. Besides, elevated temperatures particularly benefit cyanobacteria growth. Lake Keluke and Lake Tuosu displayed greater average cyanobacteria abundance and a higher cyanobacteria/phytoplankton ratio compared to Lake Qinghai.

Extreme environmental changes can limit species richness. Halotolerance, which determines species diversity in hypersaline lakes, restricts species diversity. Many saline lakes worldwide exhibit a negative correlation between species richness and salinity. However, hypersaline lakes remain under-studied compared to their freshwater counterparts (Williams et al., 1990; Williams, 1998; Williams, 2002; Larson and Belovsky, 2013). The lakes on Tibetan Plateau may undergo a decline in salinity since the balance of precipitation and evaporation was broken as reflected by the expansion of the surface water in many alpine lakes under climate change (Song et al., 2022). A study by Li et al. (2021) found that salinity was the dominant factor controlling phytoplankton community abundance and biomass in lake systems on the Qinghai-Tibet Plateau. Phytoplankton communities were analyzed along salinity, revealing that phytoplankton and overall abundance was significantly and negatively correlated to salinity ($p < 0.05$). High salinity levels make phytoplankton unable to maintain normal cell osmotic pressure, resulting in low phytoplankton abundance and biomass in high-salinity lake. This is consistent with our findings. In this study, cyanobacteria, Bacillariophyta, Chlorophyta and overall phytoplankton abundance tend to decline with increase of salinity. Besides, the ratios of cyanobacteria to phytoplankton, the ratios of Bacillariophyta and Chlorophyta to phytoplankton were decrease with salinity. Those results indicate that the abundance of cyanobacteria, Bacillariophyta and Chlorophyta may increase if the

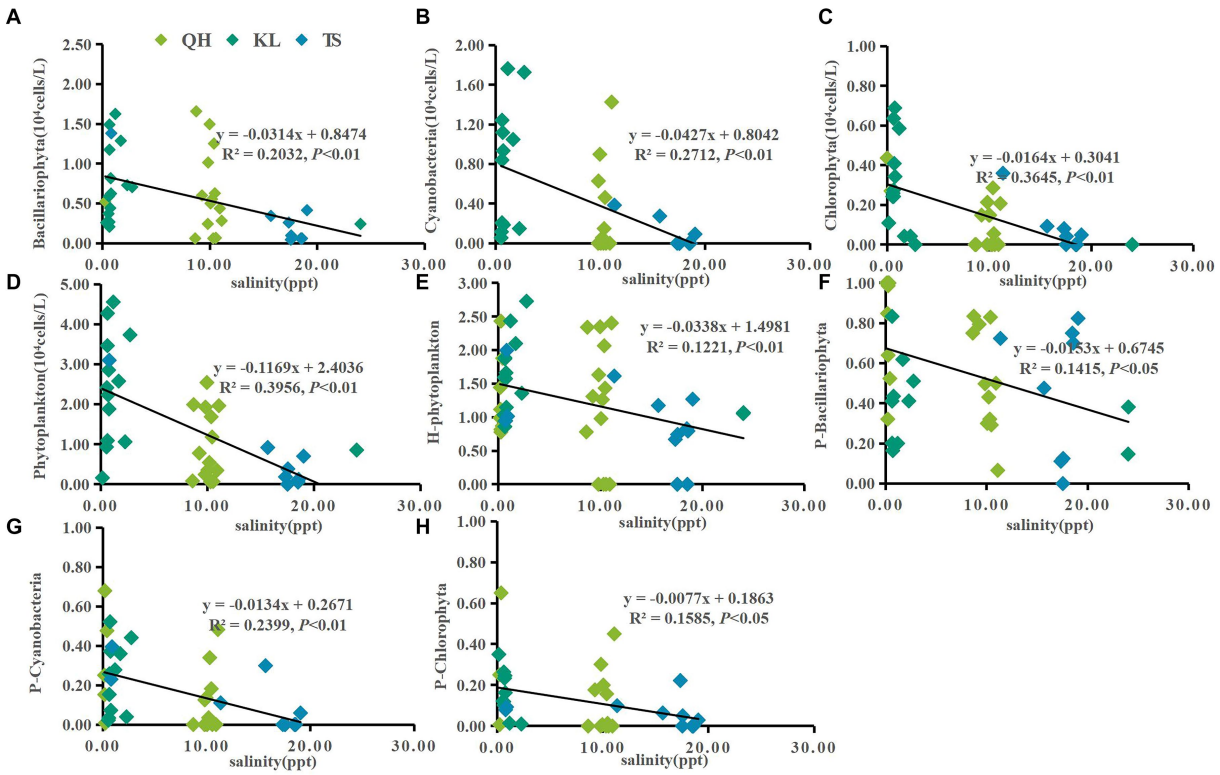

FIGURE 5
Linear regression models was applied to salinity and phytoplankton based on yearly average data from each site of Lake Qinghai, Lake Keluke and Lake Tuosu. The response of phytoplankton to salinity were shown in **(A–D)** and response of phytoplankton composition to salinity were shown in **(E–H)**. Bacillariophyta, cyanobacteria, Chlorophyta and phytoplankton abundance were changed via the Log (X + 1). P-i represents the i/phytoplankton ratio based on abundance. H-phytoplankton indicates the biodiversity of phytoplankton.

salinity decreased under climate change. Moreover, the low phytoplankton abundance in certain lakes is not solely due to salinity but also nutrients and other growth-limiting elements, such as light and temperature. *Microcystis aeruginosa*, a common freshwater blooming genus, could endure salinities as high as 17.5 for 9 days under laboratory (Preece et al., 2017; Georges des Aulnois et al., 2019). Meanwhile, *Microcystis* blooms toxicity was highest at low salinity in estuary (Lehman et al., 2005). Therefore, the phytoplankton growth could be affected by high salinity, but the salinity was not the determinant factor responsible for the low phytoplankton. In our study, while the salinity in Lake Keluke was below the maximum tolerance observed in laboratory conditions, phytoplankton abundance remained low. Therefore, Lake Keluke does not necessarily have low phytoplankton abundance due to high salinity. Lake Tuosu has a salinity of 13.08 ± 0.4, which may negatively affect various phytoplankton genera. This also verifies that phytoplankton abundance in Lake Tuosu is relatively high in low salinity years.

Despite the salinity change under precipitation augments in alpine lakes, the nutrient had a significant variations due to the increasing amount of nitrogen and phosphorus along with runoff (Wu et al., 2012). Ammonia was one of important compositions in the nutrient, which significantly affect lake phytoplankton biomass (Dai et al., 2008; Drath et al., 2008). Its concentration typically depends on environmental pH, salinity and temperature. At a pH below 8.75, ammonia predominantly exists in the form of NH_4-N. There is a significant relationship between ammonia concentration and organisms, directly affecting their normal activities (Zhao et al., 2020). In lake ecosystem, ammonia serves as a nutrient salt and is a key indicator for monitoring environmental pollution, reflecting the survival of aquaculture animals and phytoplankton (Wu et al., 2006; O'Connor Šraj et al., 2018; Zhao et al., 2020). Previous studies have indicated that phosphorus substantially enhances total phytoplankton biomass and growth rates, with nitrogen exerting secondary effects. However, excessive nitrogen can be detrimental to phytoplankton (Dai et al., 2008; Drath et al., 2008). It has been noted that cyanobacteria and Chlorophyta typically have greater NH_4-N tolerance thresholds than Bacillariophyta. Therefore, cyanobacteria and Chlorophyta are less affected by high concentrations of NH_4-N and are not outcompeted by other taxa when NH_4-N is the sole nitrogen source (Esparza et al., 2014). In this study, correlation analyses showed that NH_4-N with cyanobacteria, Bacillariophyta, Chlorophyta and overall phytoplankton abundance were all significantly negatively correlated. This was also found in Lake Keluke before that the both TN and NH_4-N had very high concentration and were negative for phytoplankton growth (Wang et al., 2018). NH_4-N is the most readily absorbed nitrogen source by phytoplankton since the absorption of NH_4-N by phytoplankton is passive diffusion and does not require energy consumption. However, the absorption of other forms of nitrogen is active transport and requires energy consumption. Previous articles have indicated that as NH_4-N decreases, inflow to lake NH_4-N concentrations also decreases, thereby reducing or eliminating phytoplankton sensitivity to NH_4-N. For current highland

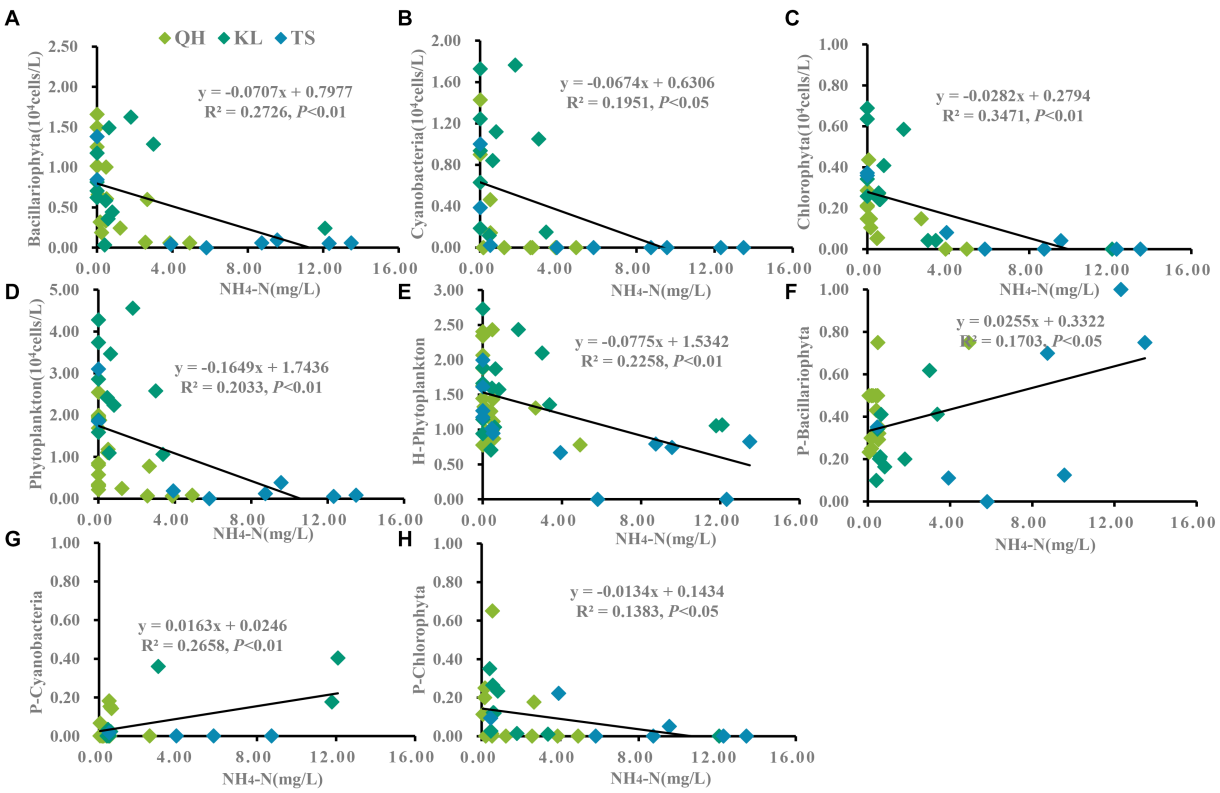

FIGURE 6
Linear regression models was applied to NH_4-N and phytoplankton based on yearly average data from each site of Lake Qinghai, Lake Keluke and Lake Tuosu. The response of phytoplankton to NH_4-N were shown in **(A–D)** and response of phytoplankton composition to NH_4-N were shown in **(E–H)**. Bacillariophyta, cyanobacteria, Chlorophyta and phytoplankton abundance were changed via the Log (X + 1). P-i represents the i/phytoplankton ratio based on abundance. H-phytoplankton indicates the biodiversity of phytoplankton.

lakes such as Keluke and Tuosu, ammonia nitrogen levels are high and cyanobacteria levels are gradually rising, threatening the survival of fish (Dugdale et al., 2013). In aquaculture, ammonia produced by fish is absorbed by phytoplankton. With the proliferation of phytoplankton, ammonia levels increase continuously, leading to water body eutrophication and moderate fish kills (Collos and Harrison, 2014). Meanwhile, ammonia is a major water pollutant and its rapidly increase escalates the mortality rate of fish and shrimp, causing substantial economic losses to farmers (Zhao et al., 2020).

Algal bloom in plateau lakes are increasingly frequent globally, especially in nutrient-poor lakes (Zhang et al., 2020). Alterations in nutrients such as nitrogen and phosphorus can affect phytoplankton growth. Several studies have shown that the addition of phosphorus significantly increases phytoplankton biomass and growth rates (Carpenter et al., 1998b). TN is a crucial indicator for assessing a lake's eutrophication level and is vital for phytoplankton growth and metabolism. Inappropriate TN content can affect phytoplankton growth and community structure succession (Paparazzo et al., 2017; Le et al., 2019). In this study, high TN concentrations were observed in all three lakes, with little variation in TP concentrations. The dominant phytoplankton's growth was not nitrogen-limited, but phosphorus limited, with TP levels considerably below 0.06 mg/L. Hence, TP did not determine the differences in phytoplankton abundance across the lakes. In Lake Taihu, where ammonia levels peak during spring and winter (non-growing season), bloom-forming *Microcystis* spp. might experience growth inhibition due to NH_4-N toxicity (Dai et al., 2012). In contrast, Chlorophyta, less sensitive to ammonia, could flourish (Xu et al., 2010). Excessive nitrogen can be toxic to phytoplankton (Dai et al., 2008). In all three alpine lakes of this study, phytoplankton in both Lakes Keluke and Tuosu struggled to thrive under elevated NH_4-N conditions. Thus, NH_4-N is key to regulating the distribution of cyanobacterial blooms and common algae group, both as a nutrient and a toxin in cyanobacterial blooms (Dai et al., 2012).

The sensitivity of phytoplankton to the aquatic environment leads to the vulnerability of their community characteristics to changes in aquatic systems. The dominant phytoplankton groups were cyanobacteria, Bacillariophyta and Chlorophyta in the three lakes during the survey. The moderate temperature and nutrient levels of Lake Qinghai make it easier to form dominant taxa Bacillariophyta. In general, *Synedra* sp. and *Navicula* sp. (Bacillariophyta) were the dominant genera in Lake Qinghai from 2018 to 2020, whereas the dominant genus *Spirogyra* sp. of the Chlorophyta appeared in the summer of 2019 up to 15% of the total phytoplankton. This was due to the high NH_4-N content of Lake Qinghai in the summer of 2019, since Chlorophyta are more likely to grow in a nitrogen-rich, phosphorus-rich, and temperature-suitable condition (Gamier et al., 1995). This phenomenon could be seen in Lake Tuosu in the spring of 2020. The seasonal phytoplankton composition of Lake Keluke showed a clear seasonal succession, with moderate spring

temperatures in 2018 and 2019, resulting in the emergence of Bacillariophyta as dominant phytoplankton group, then the dominant was evolved from Bacillariophyta to cyanobacteria during the summer of 2018–2019 and the spring of 2020 due to increasing temperatures, include the genera *Dolichospermum* sp., *Oscillatoria* sp. and *Pseudoanabaena* sp., which preferred high temperatures (Nalley et al., 2018). Cyanobacteria reproduce fast in the high temperature season, while Bacillariophyta have strong adaptability in the low temperature season. This is in accordance with the change process of Bacillariophyta in spring and peak cyanobacteria in summer in Lake Keluke (Chomérat et al., 2007; Ding et al., 2023). In the present study, phytoplankton were dominated by cyanobacteria in Lake Keluke in the summer of 2019 and spring of 2020, and in Lake Tuosu in the summer of 2019. This was consistent with the previous research that cyanobacteria tended to dominate when the water body was high in nutrients (Sun, 2023).

The response of phytoplankton in alpine lakes to environmental factors is mainly expressed in changes of temperature increase, salinity, and nutrients. The impact of rising temperature is notably significant in the lakes of the Tibetan Plateau, and precipitation tends to increase in the east and north. As a result, the lakes in the Tibetan Plateau experience a warm and wet climate (Zong-Xue et al., 2006; Yao et al., 2007; Liao et al., 2013; Lin et al., 2017). This leads to increases in lake water temperature and nutrients, but a decrease in salinity, potentially facilitating the growth of nuisance algae such as cyanobacteria (Jeppesen et al., 2010). Lake Qinghai had experienced a gradual increase of phytoplankton abundance in the past decades. The phytoplankton average abundance was 7.0×10^4 cells/L in the summer of 1961–1962 (Yao et al., 2007). The abundance was up to 1.22×10^5 cells/L during 2006–2010 (Yao et al., 2011). In present study, the phytoplankton abundances was upward 2.9×10^5 cells/L in 2020, which more than two times higher than 2006–2010. Both the ratios of Bacillariophyta and cyanobacteria accounted for phytoplankton were increased from 2006–2010 to 2018–2010. The ratios of Bacillariophyta reached 77% from 71% and the ratios of cyanobacteria was up to 14% from 6% (Yao et al., 2011). In Lake Keluke, there was an increase of 22 phytoplankton species in 2018–2020 compared to 2007 (Wang and Li, 2014), and cyanobacteria are the majority. The phytoplankton average densities were 3.2×10^5 cells/L in 1977–1980 (Zhao et al., 1990), which were similar with 2018–2020. However, the ratios of cyanobacteria were up to 46% (2018–2020) from 10% (2007).

Lake Qinghai, renowned as a popular tourist destination, attracts a significant number of residents and tourists. Lake Keluke, additionally, stands as a small salty water in Qinghai Province. The density of residents, coupled with overgrazing and surface farming, is progressively damaging the aquatic vegetation of the wetlands and thereby continuously promoting eutrophication in the lake. A study focused on a typical brackish lake with ample nutrients on the Qinghai-Tibet Plateau found that with increased eutrophication due to climate change, phytoplankton blooms might also emerge (Wu et al., 2021). Human activity on the plateau has steadily increased with ongoing socio-economic growth, impacting the water quality and evolution of many plateau lakes. The Qinghai-Tibet Plateau is a habitat for numerous rare birds and native plateau fish. Thus, managing brackish lakes on the Qinghai-Tibet Plateau should be a priority. Furthermore, the primary sources of nitrate in the groundwater near lakes such as Lake Qinghai and Lake Tuosu originate from animal feces and sewage (Li et al., 2021). Therefore, establishing buffer zones is crucial for the effective planning, design, and management of livestock waste and wastewater from the grazing industry. The ongoing expansion of tourism at Lake Qinghai and aquaculture at Lake Keluke, while generating increased economic revenue, also undeniably exacerbates the ecological burden on these scenic areas. This added pressure impairs the self-regulation capabilities of their ecological environments. Consequently, it is imperative for relevant management authorities to undertake effective planning, commit to the protection of the ecological environment, and embrace a strategy of sustainable development.

5 Conclusion

There were significant changes in physicochemical parameters and phytoplankton in the three lakes. The significant variations of parameters were mainly in temperature, salinity and nutrients. Phytoplankton presented different successions in the three lakes. Bacillariophyta was predominant in Lake Qinghai from 2018 to 2020, with *Synedra* sp., *Navicula* sp., *Cymbella* sp. and *Achnanthidium* sp. emerging altertively as the dominant genera. Lake Keluke alternated between being dominated by cyanobacteria and Bacillariophyta during the same period. The genus *Dolichospermum* sp., a cyanobacteria, was dominanted in the summer of 2018 and 2019 and in the spring of 2020. In Lake Tuosu, Bacillariophyta was predominant from 2018 to 2020, except in the summer of 2019, which was dominated by cyanobacteria. The dominant genera *Synedra* sp., *Oscillatoria* sp., *Pseudoanabaena* sp., *Chromulina* sp. and *Achnanthidium* sp. were appeared successively. Both temporal and spatial variations showed that phytoplankton had a relative high abundance under high temperature, especially cyanobacteria. Linear regression analysis showed the abundance of cyanobacteria, Bacillariophyta, Chlorophyta and overall phytoplankton increased with temperature and decreased with salinity and NH_4-N. Besides, the ratios of cyanobacteria, and the ratios of Bacillariophyta accounted in total phytoplankton increased with temperature. These findings suggest that cyanobacteria and phytoplankton abundance, especially Bacillariophyta may have an increase tendency in the three alpine lakes under warm and wet climate.

Data availability statement

The original contributions presented in the study are included in the article/supplementary material, further inquiries can be directed to the corresponding author.

Author contributions

PG: Data curation, Formal analysis, Writing – original draft. JJ: Funding acquisition, Investigation, Writing – review & editing. DQ: Writing – review & editing. QG: Writing – review & editing. CZ: Writing – review & editing. XY: Writing – review & editing. MN: Writing – review & editing. DL: Writing – review & editing. YL: Writing – review & editing.

Funding

The author(s) declare that financial support was received for the research, authorship, and/or publication of this article. This research was supported by the National Natural Science Foundation of China (no. 42167012) and the Open Project of the State Key Laboratory of Plateau Ecology and Agriculture, Qinghai University (2017-ZZ-19).

Acknowledgments

The authors are deeply grateful for the technical assistance provided by the Hydrobiological Data Analysis Center, Institute of Hydrobiology, Chinese Academy of Sciences, Wuhan, China.

Conflict of interest

The authors declare that the research was conducted in the absence of any commercial or financial relationships that could be construed as a potential conflict of interest.

Publisher's note

All claims expressed in this article are solely those of the authors and do not necessarily represent those of their affiliated organizations, or those of the publisher, the editors and the reviewers. Any product that may be evaluated in this article, or claim that may be made by its manufacturer, is not guaranteed or endorsed by the publisher.

References

Abirhire, O., North, R. L., Hunter, K., Vandergucht, D. M., Sereda, J., and Hudson, J. J. (2015). Environmental factors influencing phytoplankton communities in Lake Diefenbaker, Saskatchewan, Canada. *J. Great Lakes Res.* 41, 118–128. doi: 10.1016/j.jglr.2015.07.002

Blomqvist, S., Gunnars, A., and Elmgren, R. (2004). Why the limiting nutrient differs between temperate coastal seas and freshwater lakes: a matter of salt. *Limnol. Oceanogr.* 49, 2236–2241. doi: 10.4319/lo.2004.49.6.2236

Cao, J., Hou, Z., Li, Z., Chu, Z., Yang, P., and Zheng, B. (2018). Succession of phytoplankton functional groups and their driving factors in a subtropical plateau lake. *Sci. Total Environ.* 631-632, 1127–1137. doi: 10.1016/j.scitotenv.2018.03.026

Cao, Y., Lin, C., Zhang, X., Liu, X., He, M., and Ouyang, W. (2020). Distribution, source, and ecological risks of polycyclic aromatic hydrocarbons in Lake Qinghai, China. *Environ. Pollut.* 266:115401. doi: 10.1016/j.envpol.2020.115401

Carpenter, S. R., Caraco, N. F., Correll, D. L., Howarth, R. W., Sharpley, A. N., and Smith, V. H. (1998a). Nonpoint pollution of surface waters with phosphorus and nitrogen. *Ecol. Appl.* 8, 559–568. doi: 10.1890/1051-0761(1998)008[0559:NPOSWW]2.0.CO;2

Carpenter, S. R., Cole, J. J., Kitchell, J. F., and Pace, M. L. (1998b). Impact of dissolved organic carbon, phosphorus, and grazing on phytoplankton biomass and production in experimental lakes. *Limnol. Oceanogr.* 43, 73–80. doi: 10.4319/lo.1998.43.1.0073

Chen, Y., Qin, B., Teubner, K., and Dokulil, M. (2003). Long-term dynamics of phytoplankton assemblages: Microcystis-domination in Lake Taihu, a large shallow lake in China. *J. Plankton Res.* 25, 445–453. doi: 10.1093/plankt/25.4.445

Chen, W., Song, L., Peng, L., Wan, N., Zhang, X., and Gan, N. (2008). Reduction in microcystin concentrations in large and shallow lakes: water and sediment-interface contributions. *Water Res.* 42, 763–773. doi: 10.1016/j.watres.2007.08.007

Chomérat, N., Garnier, R., Bertrand, C., and Cazaubon, A. (2007). Seasonal succession of cyanoprokaryotes in a hypereutrophic oligo-mesohaline lagoon from the south of France. *Estuar. Coast. Shelf Sci.* 72, 591–602. doi: 10.1016/j.ecss.2006.11.008

Collos, Y., and Harrison, P. J. (2014). Acclimation and toxicity of high ammonium concentrations to unicellular algae. *Mar. Pollut. Bull.* 80, 8–23. doi: 10.1016/j.marpolbul.2014.01.006

Conley, D. J. (1999). Biogeochemical nutrient cycles and nutrient management strategies. *Hydrobiol. J.* 410, 87–96. doi: 10.1023/A:1003784504005

Conley, D. J., Paerl, H. W., Howarth, R. W., Boesch, D. F., Seitzinger, S. P., Havens, K. E., et al. (2009). Controlling eutrophication: nitrogen and phosphorus. *Science* 323, 1014–1015. doi: 10.1126/science.1167755

Dai, G., Deblois, C., Liu, S., Juneau, P., and Qiu, B. (2008). Differential sensitivity of five cyanobacterial strains to ammonium toxicity and its inhibitory mechanism on the photosynthesis of rice-field cyanobacterium Ge–Xian–mi (Nostoc). *Aquat. Toxicol.* 89, 113–121. doi: 10.1016/j.aquatox.2008.06.007

Dai, G. Z., Shang, J. L., and Qiu, B. S. (2012). Ammonia may play an important role in the succession of cyanobacterial blooms and the distribution of common algal species in shallow freshwater lakes. *Glob. Chang. Biol.* 18, 1571–1581. doi: 10.1111/j.1365-2486.2012.02638.x

Ding, L., Xinghua, W., and Xu, L. (2023). Dynamic simulation seasonal succession of different species of phytoplankton in reservoir-type water(in Chinese). *J. Hydraul. Eng.* 54, 554–562. doi: 10.13243/j.cnki.slxb.20211015

Dokulil, M. T., and Teubner, K. (2000). Cyanobacterial dominance in lakes. *Hydrobiol. J.* 438, 1–12. doi: 10.1023/A:1004155810302

Dong, H., Song, Y., and Zhang, M. (2018). Hydrological trend of Qinghai Lake over the last 60 years: driven by climate variations or human activities? *J Water Climate Change* 10, 524–534. doi: 10.2166/wcc.2018.033

Drath, M., Kloft, N., Batschauer, A., Marin, K., Novak, J., and Forchhammer, K. (2008). Ammonia triggers Photodamage of photosystem II in the cyanobacterium Synechocystis sp. strain PCC 6803. *Plant Physiol.* 147, 206–215. doi: 10.1104/pp.108.117218

Dugdale, R. C., Wilkerson, F. P., and Parker, A. E. (2013). A biogeochemical model of phytoplankton productivity in an urban estuary: the importance of ammonium and freshwater flow. *Ecol. Model.* 263, 291–307. doi: 10.1016/j.ecolmodel.2013.05.015

Esparza, M. L., Farrell, A. E., Craig, D. J., Swanson, C., Dhaliwal, B. S., and Berg, G. M. (2014). Impact of atypical ammonium concentrations on phytoplankton abundance and composition in fresh versus estuarine waters. *Aquat. Biol.* 21, 191–204. doi: 10.3354/ab00588

Gamier, J., Billen, G., and Coste, M. (1995). Seasonal succession of diatoms and Chlorophyceae in the drainage network of the Seine River: observation and modeling. *Limnol. Oceanogr.* 40, 750–765. doi: 10.4319/lo.1995.40.4.0750

Georges des Aulnois, M., Roux, P., Caruana, A., Réveillon, D., Briand, E., Hervé, F., et al. (2019). Physiological and metabolic responses of freshwater and brackish strains of *Microcystis aeruginosa* acclimated to a salinity gradient: insight into salt tolerance. *ASM J CD* 85:19. doi: 10.1128/AEM.01614-19

Ger, K. A., Hansson, L. A., and Lürling, M. (2014). Understanding cyanobacteria-zooplankton interactions in a more eutrophic world. *Freshwater Biol* 59, 1783–1798. doi: 10.1111/fwb.12393

Guo, Y. (2013). Protection measures of wetland in Qinghai Keluke Lake-Tuosu Lake nature reserve(in Chinese). *Agric Technol* 33:80. doi: 10.3969/j.issn.1671-962X.2013.07.068

Huang, J., Xu, Q., Wang, X., Ji, H., Quigley, E. J., Sharbatmaleki, M., et al. (2021). Effects of hydrological and climatic variables on cyanobacterial blooms in four large shallow lakes fed by the Yangtze River. *Environ Sci Ecotechnol* 5:100069. doi: 10.1016/j.ese.2020.100069

Jakhar, P. (2013). Role of phytoplankton and zooplankton as health indicators of aquatic ecosystem: a review. *Int J Innov Res Stud* 2, 489–500.

Jeppesen, E., Meerhoff, M., Holmgren, K., González-Bergonzoni, I., Teixeira-de Mello, F., Declerck, S. A. J., et al. (2010). Impacts of climate warming on lake fish community structure and potential effects on ecosystem function. *Hydrobiol. J.* 646, 73–90. doi: 10.1007/s10750-010-0171-5

Jia, J., Chen, Q., Ren, H., Lu, R., He, H., and Gu, P. (2022). Phytoplankton composition and their related factors in five Different Lakes in China: implications for Lake management. *Int. J. Environ. Res. Public Health* 19:3135. doi: 10.3390/ijerph19053135

Ke, Z., Xie, P., and Guo, L. (2008). Controlling factors of spring–summer phytoplankton succession in Lake Taihu (Meiliang Bay, China). *Hydrobiol. J.* 607, 41–49. doi: 10.1007/s10750-008-9365-5

Lan, C. (2024). Progresses and deficiencies in land surface modeling under the global warming-hydrology, vegetation and soil modeling on the Qinghai-Xizang plateau(in Chinese). *Adv. Earth Science* 39, 46–55. doi: 10.11867/j.issn.1001-8166.2023.079

Larson, C. A., and Belovsky, G. E. (2013). Salinity and nutrients influence species richness and evenness of phytoplankton communities in microcosm experiments from great salt Lake, Utah, USA. *J. Plankton Res.* 35, 1154–1166. doi: 10.1093/plankt/fbt053

Le, D., Jing, Q. I., Yongjun, S., Huacong, L., Yaohui, B., Huijuan, L., et al. (2019). Characteristics of phytoplankton functional groups and their influencing factors in Chenghai Lake in summer. *Ecol Environ Sci.* 28, 2281–2288. doi: 10.16258/j.cnki.1674-5906.2019.11.018

Lehman, P. W., Boyer, G., Hall, C., Waller, S., and Gehrts, K. (2005). Distribution and toxicity of a new colonial *Microcystis aeruginosa* bloom in the San Francisco Bay estuary, California. *Hydrobiol. J.* 541, 87–99. doi: 10.1007/s10750-004-4670-0

Lei, Y. B., and Yang, K. (2017). The cause of rapid lake expansion in the Tibetan plateau: climate wetting or warming? *Wiley Interdisciplin Rev* 4:1236. doi: 10.1002/wat2.1236

Li, D. S., Cui, B. L., Wang, Y., Wang, Y. X., and Jiang, B. F. (2021). Source and quality of groundwater surrounding the Qinghai Lake, NE Qinghai-Tibet plateau. *Groundwater* 59, 245–255. doi: 10.1111/gwat.13042

Li, G., Dong, H., Hou, W., Wang, S., Jiang, H., Yang, J., et al. (2016). Temporal succession of ancient phytoplankton Community in Qinghai Lake and Implication for paleo-environmental change. *Sci. Rep.* 6:19769. doi: 10.1038/srep19769

Li, Z., Gao, Y., Wang, S., Jia, J., Ha, X., and Lu, Y. (2023). Floodplain lake response to climate-nutrient-hydrological pressure revealed through phytoplankton community succession over the past century. *J. Hydrol.* 623:129838. doi: 10.1016/j.jhydrol.2023.129838

Li, X.-Y., Xu, H.-Y., Sun, Y.-L., Zhang, D. S., and Yang, Z. P. (2007). Lake-level change and water balance analysis at Lake Qinghai, West China during recent decades. *Water Resourc Manage* 21, 1505–1516. doi: 10.1007/s11269-006-9096-1

Liao, J., Shen, G., and Li, Y. (2013). Lake variations in response to climate change in the Tibetan plateau in the past 40 years. *Int J Digit Earth* 6, 534–549. doi: 10.1080/17538947.2012.656290

Lin, Q., Xu, L., Hou, J., Liu, Z., Jeppesen, E., and Han, B. P. (2017). Responses of trophic structure and zooplankton community to salinity and temperature in Tibetan lakes: implication for the effect of climate warming. *Water Res.* 124, 618–629. doi: 10.1016/j.watres.2017.07.078

Liu, X. C. (2013). Study of model of stable isotope fractionation in Lake-taking the Nam co Lake as an example. *Phys Numerical Simulat Geotech Engineer* 11:14.

Liu, X., Hou, W., and Dong, H. (2016). Distribution and diversity of cyanobacteria and eukaryotic algae in Qinghai–Tibetan Lakes. *Geomicrobiol. J.* 33, 860–869. doi: 10.1080/01490451.2015.1120368

Lu, S.-J., Si, J.-H., Hou, C.-Y., Li, Y. S., Wang, M. M., Yan, X. X., et al. (2017). Spatiotemporal distribution of nitrogen and phosphorus in alpine lakes in the Sanjiangyuan region of the Tibetan plateau. *Water Sci. Technol.* 76, 396–412. doi: 10.2166/wst.2017.091

Lv, J., Wu, H., and Chen, M. (2011). Effects of nitrogen and phosphorus on phytoplankton composition and biomass in 15 subtropical, urban shallow lakes in Wuhan, China. *Limnologica* 41, 48–56. doi: 10.1016/j.limno.2010.03.003

Nalley, J. O., O'Donnell, D. R., and Litchman, E. (2018). Temperature effects on growth rates and fatty acid content in freshwater algae and cyanobacteria. *Algal Res* 35, 500–507. doi: 10.1016/j.algal.2018.09.018

O'Connor Šraj, L., Almeida, M. I. G. S., Bassett, C., McKelvie, I. D., and Kolev, S. D. (2018). Gas-diffusion-based passive sampler for ammonia monitoring in marine waters. *Talanta* 181, 52–56. doi: 10.1016/j.talanta.2017.12.076

Paparazzo, F. E., Williams, G. N., Pisoni, J. P., Solís, M., Esteves, J. L., and Varela, D. E. (2017). Linking phytoplankton nitrogen uptake, macronutrients and chlorophyll-a in SW Atlantic waters: the case of the Gulf of san Jorge, Argentina. *J. Mar. Syst.* 172, 43–50. doi: 10.1016/j.jmarsys.2017.02.007

Preece, E. P., Hardy, F. J., Moore, B. C., and Bryan, M. (2017). A review of microcystin detections in estuarine and marine waters: environmental implications and human health risk. *Harmful Algae* 61, 31–45. doi: 10.1016/j.hal.2016.11.006

Ren, Z., Niu, D., Ma, P., Wang, Y., Fu, H., and Elser, J. J. (2019). Cascading influences of grassland degradation on nutrient limitation in a high mountain lake and its inflow streams. *Ecology* 100:e02755. doi: 10.1002/ecy.2755

Sheng, Z. (2022). Ecological stoichiometric characteristics of four halophytes in the Keluke Lake-Tuosu Lake nature reserve(in Chinese). doi: 10.27778/d.cnki.gqhzy.2022.000739,

Smith, V. H. (2003). Eutrophication of freshwater and coastal marine ecosystems a global problem. *Environ. Sci. Pollut. Res.* 10, 126–139. doi: 10.1065/espr2002.12.142

Song, C., Luo, S., Liu, K., Chen, T., Zhang, P., and Fan, C. (2022). Widespread declines in water salinity of the endorheic Tibetan plateau lakes. *Environ Res Commun* 4:091002. doi: 10.1088/2515-7620/ac9351

Song, W., and Sun, C. (2020). Diversity and distribution of bacteria and archaea in Tuosu Lake in Qaidam Basin. *Cell. Mol. Biol.* 66, 86–92. doi: 10.14715/cmb/2020.66.6.16

Sun, X. (2023). *Study on the spatial and temporal pattern and driving mechanism of phytoplankton communities in the Qinghai Lake basin(in Chinese)* Xi'an University of Technology.

Tadonléke, R. D. (2010). Evidence of warming effects on phytoplankton productivity rates and their dependence on eutrophication status. *Limnol. Oceanogr.* 55, 973–982. doi: 10.4319/lo.2010.55.3.0973

Tang, L., Duan, X., Kong, F., Zhang, F., Zheng, Y., Li, Z., et al. (2018). Influences of climate change on area variation of Qinghai Lake on Qinghai-Tibetan plateau since 1980s. *Sci. Rep.* 8:7331. doi: 10.1038/s41598-018-25683-3

Tang, H., and Ju, B. X. (2011). A preliminary study on the conservation of the wetlands of Keluke-Tuosu Lake(in Chinese). *Water Resources & Hydropower of Northeast China*, 29, 46–47. doi: 10.14124/j.cnki.dbslsd22-1097.2011.02.011

Trombetta, T., Vidussi, F., Mas, S., Parin, D., Simier, M., and Mostajir, B. (2019). Water temperature drives phytoplankton blooms in coastal waters. *PLoS One* 14:e0214933. doi: 10.1371/journal.pone.0214933

Wang, W. W., Jiang, X., Zheng, B. H., Chen, J. Y., Zhao, L., Zhang, B., et al. (2018). Composition, mineralization potential and release risk of nitrogen in the sediments of Keluke Lake, a Tibetan plateau freshwater lake in China. *R. Soc. Open Sci.* 5:180612. doi: 10.1098/rsos.180612

Wang, H., and Li, X. (2014). Survey and analysis of the Keluke Lake ecosystem in Qinghai-Tibet plain Lake district (in Chinese). *J Qinghai Normal Univ* 30, 62–66. doi: 10.16229/j.cnki.issn1001-7542.2014.02.023

Williams, W. D. (1998). Salinity as a determinant of the structure of biological communities in salt lakes. *Hydrobiol. J.* 381, 191–201. doi: 10.1023/A:1003287826503

Williams, W. D. (2002). Environmental threats to salt lakes and the likely status of inland saline ecosystems in 2025. *Environ. Conserv.* 29, 154–167. doi: 10.1017/S0376892902000103

Williams, W. D., Boulton, A. J., and Taaffe, R. G. (1990). Salinity as a determinant of salt lake fauna: a question of scale. *Hydrobiol. J.* 197, 257–266. doi: 10.1007/BF00026955

Winder, M., and Sommer, U. (2012). Phytoplankton response to a changing climate. *Hydrobiol. J.* 698, 5–16. doi: 10.1007/s10750-012-1149-2

Wu, L., Long, T.-y., Liu, X., and Guo, J. S. (2012). Impacts of climate and land-use changes on the migration of non-point source nitrogen and phosphorus during rainfall-runoff in the Jialing River watershed, China. *J. Hydrol.* 475, 26–41. doi: 10.1016/j.jhydrol.2012.08.022

Wu, Y., Wang, S., Ni, Z., Li, H., May, L., and Pu, J. (2021). Emerging water pollution in the world's least disturbed lakes on Qinghai-Tibetan plateau. *Environ. Pollut.* 272:116032. doi: 10.1016/j.envpol.2020.116032

Wu, S., Xie, P., Wang, S., and Zhou, Q. (2006). Changes in the patterns of inorganic nitrogen and TN/TP ratio and the associated mechanism of biological regulation in the shallow lakes of the middle and lower reaches of the Yangtze River. *Sci. China Ser. D Earth Sci.* 49, 126–134. doi: 10.1007/s11430-006-8112-x

Wu, Z., Yuan, X., Xiong, X., Ao, H., Wu, C., Liu, G., et al. (2023). Cladophora as ecological engineer: a new test from the largest lake of Qinghai-Tibet plateau with filamentous algal blooms. *Water Biol Secur* 3:100210. doi: 10.1016/j.watbs.2023.100210

Xu, H., Paerl, H. W., Qin, B., Zhu, G., and Gaoa, G. (2010). Nitrogen and phosphorus inputs control phytoplankton growth in eutrophic Lake Taihu, China. *Limnol. Oceanogr.* 55, 420–432. doi: 10.4319/lo.2010.55.1.0420

Yang, Y. (2016). *Response patterns of different phytoplankton to the interaction between temperature and phosphorus(in Chinese)* Nanjing Agricultural University.

Yao, T., Pu, J., Lu, A., Wang, Y., and Yu, W. (2007). Recent glacial retreat and its impact on hydrological processes on the Tibetan plateau, China, and surrounding regions. *Arct. Antarct. Alp. Res.* 39, 642–650. doi: 10.1657/1523-0430(07-510)[YAO]2.0.CO;2

Yao, W., Shi, J., Qi, H., Jianxin, Y., Li, J., and Tong, P. (2011). Study on the phytoplankton in Qinghai Lake during summer of 2006—2010(in Chinese). *Freshwater Fisher* 41, 22–28. doi: 10.3969/j.issn.1000-6907.2011.03.004

Zhang, X. (2019). SWOT analysis on the sustainable development prospect of tourism in Qinghai lake(in Chinese). *Territory Nat Resourc Study* 3, 72–74. doi: 10.16202/j.cnki.tnrs.2019.01.019

Zhang, Y., Gao, W., Li, Y., Jiang, Y., Chen, X., Yao, Y., et al. (2021). Characteristics of the phytoplankton community structure and water quality evaluation in autumn in the Huaihe River (China). *Int. J. Environ. Res. Public Health* 18:12092. doi: 10.3390/ijerph182212092

Zhang, M., Qin, B., Yu, Y., Yang, Z., Shi, X., and Kong, F. (2016). Effects of temperature fluctuation on the development of cyanobacterial dominance in spring: implication of future climate change. *Hydrobiol. J.* 763, 135–146. doi: 10.1007/s10750-015-2368-0

Zhang, Y., Zuo, J., Salimova, A., Li, A., Li, L., and Li, D. (2020). Phytoplankton distribution characteristics and its relationship with bacterioplankton in Dianchi Lake. *Environ. Sci. Pollut. Res.* 27, 40592–40603. doi: 10.1007/s11356-020-10033-6

Zhao, L., Wang, J., Zhang, Y., Chen, Y., Zheng, Y., and Wang, S. (1990). Enviroment of Keluke Lake and introduction of valuable fishes(in Chinese). *J Fisher China* 14, 286–296.

Zhao, M., Yao, D., Li, S., Zhang, Y., and Aweya, J. J. (2020). Effects of ammonia on shrimp physiology and immunity: a review. *Rev. Aquac.* 12, 2194–2211. doi: 10.1111/raq.12429

Zong-Xue, X. U., Tong-Liang, G., and Fang-Fang, Z. (2006). Analysis of climate change in Tibetan plateau over the past 40 years(in Chinese). *J Subtropic Resourc Environ* 1, 24–32. doi: 10.19687/j.cnki.1673-7105.2006.03.004

frontiers | Frontiers in Microbiology

TYPE Original Research
PUBLISHED 04 June 2024
DOI 10.3389/fmicb.2024.1396369

OPEN ACCESS

EDITED BY
Da Huo,
Chinese Academy of Sciences (CAS), China

REVIEWED BY
Meri J. Eichner,
Academy of Sciences of the Czech Republic (ASCR), Czechia
J. Michael Beman,
University of California, Merced, United States

*CORRESPONDENCE
Kunshan Gao
ksgao@xmu.edu.cn

RECEIVED 05 March 2024
ACCEPTED 20 May 2024
PUBLISHED 04 June 2024

CITATION
Zou C, Yi X, Li H, Bizic M, Berman-Frank I and Gao K (2024) Correlation of methane production with physiological traits in *Trichodesmium* IMS 101 grown with methylphosphonate at different temperatures.
Front. Microbiol. 15:1396369.
doi: 10.3389/fmicb.2024.1396369

Correlation of methane production with physiological traits in *Trichodesmium* IMS 101 grown with methylphosphonate at different temperatures

Chuze Zou[1], Xiangqi Yi[2], He Li[3], Mina Bizic[4,5], Ilana Berman-Frank[6] and Kunshan Gao[1,3]*

[1]State Key Laboratory of Marine Environmental Science, College of the Ocean and Earth Sciences, Xiamen University, Xiamen, China, [2]Polar and Marine Research Institute, College of Harbor and Coastal Engineering, Jimei University, Xiamen, China, [3]Co-Innovation Center of Jiangsu Marine Bio-industry Technology, Jiangsu Ocean University, Lianyungang, China, [4]Department of Environmental Microbiomics, Institute of Environmental Technology, Technical University of Berlin, Berlin, Germany, [5]Department of Plankton and Microbial Ecology, Leibniz Institute of Freshwater Ecology and Inland Fisheries (IGB), Stechlin, Germany, [6]Department of Marine Biology, Leon H. Charney School of Marine Sciences, University of Haifa, Haifa, Israel

The diazotrophic cyanobacterium *Trichodesmium* has been recognized as a potentially significant contributor to aerobic methane generation via several mechanisms including the utilization of methylphophonate (MPn) as a source of phosphorus. Currently, there is no information about how environmental factors regulate methane production by *Trichodesmium*. Here, we grew *Trichodesmium* IMS101 at five temperatures ranging from 16 to 31°C, and found that its methane production rates increased with rising temperatures to peak (1.028 ± 0.040 nmol CH_4 μmol POC^{-1} day^{-1}) at 27°C, and then declined. Its specific growth rate changed from 0.03 ± 0.01 d^{-1} to 0.34 ± 0.02 d^{-1}, with the optimal growth temperature identified between 27 and 31°C. Within the tested temperature range the Q_{10} for the methane production rate was 4.6 ± 0.7, indicating a high sensitivity to thermal changes. In parallel, the methane production rates showed robust positive correlations with the assimilation rates of carbon, nitrogen, and phosphorus, resulting in the methane production quotients (molar ratio of carbon, nitrogen, or phosphorus assimilated to methane produced) of 227–494 for carbon, 40–128 for nitrogen, and 1.8–3.4 for phosphorus within the tested temperature range. Based on the experimental data, we estimated that the methane released from *Trichodesmium* can offset about 1% of its CO_2 mitigation effects.

KEYWORDS

cyanobacteria, diazotroph, growth, methane, N_2-fixation, photosynthesis, phosphorus, *Trichodesmium*

1 Introduction

Methane (CH_4) is a crucial part of the carbon cycle and a potent greenhouse gas, with a global warming potential of more than 80 times that of CO_2 over a 20-year period (IPCC, 2013). Intriguingly, methane is typically supersaturated in the ocean's top mixed layer (Lamontagne et al., 1973; Scranton and Brewer, 1977; Weber et al., 2019), a phenomenon known as "the marine methane paradox." The paradoxical nature of this phenomenon stems

from the historically prevailing recognition that biogenic methane is produced exclusively by methanogenic archaea in a strictly anoxic environment, a condition incompatible with the oxic state of ocean top mixed layer (Karl and Tilbrook, 1994).

Recent studies show that phytoplankton, including cyanobacteria, can release methane in both oceanic and fresh surface waters (Karl et al., 2008; Bižić et al., 2020; Günthel et al., 2020; Klintzsch et al., 2020; Liu et al., 2022; Mao et al., 2022; Klintzsch et al., 2023). Precursors for aerobic CH_4 production include various methylated substances, such as C-P bond methylphosphonate (MPn) (Karl et al., 2008), C-N bond trimethylamine (Bižić et al., 2018), monomethylamine, and glycine betaine (Wang et al., 2021), as well as C-S bound methylsulfonyl propionate and methionine (Damm et al., 2010; Lenhart et al., 2016; Klintzsch et al., 2019). In addition, other phytoplankton groups, such as *Chrysochromulina* sp., *Emiliania huxleyi*, *Navicula* sp., and *Leptocylindrus danicus* (Günthel et al., 2020; Klintzsch et al., 2020, 2023), can also produce methane through photosynthesis-linked pathways that are yet to be explored. A notable source of CH_4 comes from the lysis of MPn C-P bond by specific microbes and cyanobacteria (Karl et al., 2008; Martinez et al., 2013; Repeta et al., 2016; Taenzer et al., 2020), making them primary contributors to methane production in the oceans.

The aerobic metabolism of MPn serves as a crucial source of phosphorus and subsequently a significant source of methane (Karl et al., 2008; Repeta et al., 2016; Von Arx et al., 2023). Despite dissolved inorganic phosphate (DIP) typically being the most bioavailable form of phosphorus, its availability is commonly limited in pelagic surface waters (Sañudo-Wilhelmy et al., 2001; Dyhrman et al., 2002). It has been documented that concentrations of dissolved organic phosphorus (DOP) in the open oceans are often much higher than those of DIP (Björkman and Karl, 2003; Karl and Björkman, 2015). The primary sources of DOP in the ocean originate from biological processes that include exudation, viral lysis, autolysis and cell death, and grazing (Karl and Björkman, 2015). C-P bond phosphonates are broadly distributed in the ocean, with the nuclear magnetic resonance (NMR) spectra of ultrafiltered dissolved organic matter (DOM) revealing that phosphonates (21%) are the second predominant components, after phosphate esters (73%), of high molecular weight dissolved organic phosphorus (HMWDOP) in the Pacific Ocean, the Atlantic Ocean, and the North Sea (Clark et al., 1998; Kolowith et al., 2001; Repeta et al., 2016). At station ALOHA, MPn and its precursor 2-hydroxyethylphosphonate (2-HEP) account for approximately 20% of the HMWDOP (Repeta et al., 2016). MPn can be synthesized by microbes, such as the archaeon *Nitrosopumilus maritimus* (Metcalf et al., 2012) and by other abundant marine bacteria, such as *Candidatus* Pelagibacter sp. (Born et al., 2017). The catabolism of MPn involves active transport into the cytoplasm through the phosphonate-specific ABC transporter system integrated by the phnCDE complex (Stasi et al., 2019) and subsequent degradation by the protein complex phnGHIJK (Kamat et al., 2011; Amstrup et al., 2023).

Trichodesmium, a prominent N_2-fixing organisms in the pelagic oceans, has long been recognized as a primary contributor to oceanic N_2 fixation (Capone et al., 1997; Bergman et al., 2013), supplying the "new" nitrogen within the euphotic zones of the tropical and subtropical regimes (Zehr and Capone, 2020). N_2 fixation and growth of *Trichodesmium* in the ocean is often constrained by the availability of inorganic phosphorus (Pi) (Sañudo-Wilhelmy et al., 2001; Frischkorn et al., 2018; Wang, 2022). Under Pi-limiting conditions, *Trichodesmium* exhibits weak competitiveness for Pi due to its lower specific affinities compared to other phytoplankton (Mccarthy and Carpenter, 1979; Sohm and Capone, 2006; Dyhrman, 2016). However, it can effectively utilize phosphate esters as a dependable source of phosphorus, supported by high levels of alkaline phosphatase (APase) activity (Mccarthy and Carpenter, 1979; Stihl et al., 2001; Sohm and Capone, 2006). Furthermore, *Trichodesmium* acquires phosphorus from phosphonate compounds, including MPn, through the C-P lyase pathway (Dyhrman et al., 2006), which leads to methane production as a byproduct (Karl et al., 2008). Hence, *Trichodesmium* is significant not only as a contributor to new nitrogen input for ocean but also as a potential source of ocean methane. However, little has been documented on the impacts of environmental drivers (e.g., temperature, P-availability) on methane production by *Trichodesmium*.

Trichodesmium's temperature tolerance ranges from18°C to 34°C when grown on the ingoranic phosphate, with optimal temperatures between 26–28°C (Breitbarth et al., 2007; Chappell and Webb, 2010; Fu et al., 2014). Rising temperatures impact diverse physiological and biochemical processes, including nitrogen fixation, respiration, carbon fixation, and growth (Breitbarth et al., 2007; Yvon-Durocher et al., 2012; Fu et al., 2014). As ocean warming intensifies, thermal stratification in the upper ocean stabilizes, reducing upward supply of dissolved inorganic phosphate (DIP) (Behrenfeld et al., 2006; Polovina et al., 2008; Somavilla et al., 2017; Ulloa et al., 2019). This may promote *Trichodesmium* to utilize more MPn, which may boost methane emission. Nevertheless, the thermal response of methane production by *Trichodesmium* has not been examined thus far. We hypothesize that changes in temperatures would alter levels of methane production by *Trichodesmium* grown on Mpn, since its utilization should correlate with the temperature-dependent assimilations of carbon, nitrogen, and phosphorus. To test this hypothesis, we employed MPn as the phosphorus source, grew *Trichodesmium* under various temperatures ranging from 16 to 31°C, and examined the correlations between methane production and several pivotal physiological processes, including assimilation of carbon, nitrogen, and phosphorus, as well as the specific growth rates. We found that changes in temperature affect the methane production of *Trichodesmium* grown on Mpn in parallel with the rates of C/N/P assimilations and growth.

2 Materials and methods

2.1 Culture conditions

Trichodesmium IMS101 stock culture was grown in nitrogen-free YBCII medium (Chen et al., 1996) containing 5 μM methylphosphonate (MPn, Aladdin, CAS 993-13-5, ≥98%). The stock culture was kept at 27°C, and the light intensity was set at 110 μmol photons m^{-2} s^{-1} with a light–dark cycle of 12:12 h (light source: white LED tubes; light period: 08:00 to 20:00 local time). The cultures were run at five different temperatures (16, 20, 23, 27, 31°C), with all other environmental conditions maintained identical to those of the stock cultures. No other P source or dissolved inorganic phosphorus (DIP) was intentionally added to the cultures. The experimental cultures were kept in the exponential growth phase through regular dilutions performed every 3–15 days depending on the temperatures and growth rates. The

semi-continuous cultures ensured that chlorophyll-*a* (Chl-*a*) concentrations consistently fell within the range of 0.005–0.05 μg mL^{-1}. The experimental cultures were acclimated to their respective temperatures for more than 6 months prior to measuring physiological and biochemical parameters.

2.2 Chl-*a* and specific growth rate

Chl-*a* concentration was determined using the spectrophotometric method. The cells were filtered onto GF/F filters and subsequently extracted in pure methanol overnight at 4°C in the dark. After extraction, the samples were centrifuged at 12,000 g for 4 min. The resulting supernatant was then scanned for absorbance across the wavelength range of 250–800 nm using a spectrophotometer (Cary 60, Agilent, CA, United States). Chl-*a* concentration was calculated using the following formula (Ritchie, 2006):

$$\text{Chl } a\left(\mu g \text{ mL}^{-1}\right) = 12.9447 \times \left(\text{OD}_{665} - \text{OD}_{750}\right),$$

where OD_{665} and OD_{750} were absorbance at wavelengths 665 nm and 750 nm, respectively. The following equation was used to calculate the specific growth rate (μ) based on the Chl-*a* concentration:

$$\mu\left(d^{-1}\right) = \frac{\ln m_2 - \ln m_1}{t_2 - t_1},$$

where m_2 and m_1 are the Chl-*a* values at time t_2 and t_1, respectively.

The following equation modified by Norberg (2004) was utilized to fit the thermal growth curve of *Trichodesmium*:

$$\mu(T) = \text{ae}^{\text{bT}}\left[1 - \left(\frac{T - z}{W}\right)^2\right],$$

where the specific growth rate (μ) is a function of temperature (T). In this equation, the coefficient w represents the thermal niche width, whereas the explicit biological significance of coefficients a, b, and z remain unspecific. Collectively, these four coefficients can be used to derive both the maximum growth rate and the optimum growth temperature (T_{opt}):

$$T_{\text{opt}} = \frac{\text{bz} - 1 + \sqrt{w^2 b^2 + 1}}{b},$$

2.3 Chl-*a* fluorescence

The effective photosynthetic quantum yield of photosystem II (Φ_{II}) and relative electron transport rate (rETR) were measured by Multi-color PAM (Multi-color PAM, Walz). Samples were acclimated to white actinic light with photon flux intensities similar to the growth conditions for 2 min to measure F_s, and then F_m' was measured using a saturating pulse (8,000 μmol photons m^{-2} s^{-1}, 0.8 s) to obtain the effective quantum yield (Φ_{II}) as follows (Genty et al., 1989):

$$\Phi_{\text{II}} = \left(F_m' - F_s\right) / F_m'.$$

Subsequently, rapid light curves (RLC) were measured at 11 actinic light levels [E], from 5 to 2,904 μmol photons m^{-2} s^{-1} with each light exposure lasting for 30 s. Relative electron transport rates (rETR) were calculated as follows (Ralph and Gademann, 2005):

$$\text{rETR} = E \times \Phi_{\text{II}}$$

The RLC was fitted by the following equation (Supplementary Figure S1) (Eilers and Peeters, 1988),

$$\text{rETR} = \frac{E}{a \times E^2 + b \times E + c},$$

where a, b, and c are the fitting coefficients. These three coefficients were used to derive the photosynthetic light-harvesting efficiency (α), maximum relative electron transport rate ($rETR_{max}$):

$$\alpha = 1 / \text{c},$$

$$\text{rETR}_{\max} = 1 / \left(b + 2 \times \sqrt{a \times c}\right).$$

2.4 Methane production

A Cavity Ring-Down Spectroscopy gas analyzer (Picarro Model G2308, CA, United States) was used to measure methane concentrations. A 350 mL sample (V_l) was placed within a polycarbonate (PC) bottle, leaving a 270 mL headspace (V_g). The PC bottle was sealed using a silicone stopper to ensure an airtight condition. The silicone stopper was equipped with two three-way valves for sampling. During the incubation of the samples at each of the temperatures (16, 20, 23, 27, 31°C) for methane measurement, 200 mL of gas in the bottle was replaced with sterile air every 12 h. The methane content in the headspace gas was shaken to equilibrate the dissolved gas with the headspace before subsequent measurement using the Picarro analyzer according to Lenhart et al. (2016). The total methane production rates (b_{CH_4}) were calculated based on the modified formula (Johnson et al., 1990):

$$C_g = \left(C_M \times 470 - C_{\text{air}} \times 200\right) / 270,$$

$$b_{\text{CH}_4}\left(\text{nmol day}^{-1}\right) = \left(C_{g2} - C_{g1}\right) \times \left(\beta / 22.356 \times \text{RT} + V_g / V_l\right) \times V_l / \Delta t,$$

where C_g indicates the methane concentration in the headspace (nmol L^{-1}), C_M represents the methane concentration in the headspace after replacing with the sterile air, C_{air} denotes the methane concentration of the sterile air, and C_{g1} and C_{g2} signify the methane concentrations at two time points, t_1 and t_2. Additionally, β is the Benson coefficient. V_g represents the headspace volume, while V_l corresponds to the volume of the culture medium. Methane production rates specific to *Trichodesmium* were determined based on the rates obtained from samples extracted from fractions containing heterotrophic bacteria. Several control experiments were

conducted to assess the potential influence of heterotrophic bacteria and to account for systematic errors. To test the bacterial contribution to methane production we filtered YBCII media through a 1.2 μm polycarbonate membrane, which lacked *Trichodesmium* but retained the heterotrophic bacteria in the cultures. It should be noted that the bacteria attached to the filaments of *Trichodesmium* might not be filtered off into the medium.

2.5 Carbon and nitrogen assimilation

In this study carbon and nitrogen assimilation rates were determined by assessing changes over time for particulate organic carbon (POC) and particulate organic nitrogen (PON) respectively. Briefly, samples for POC and PON measurements were taken at 0, 12, and 24 h after the start of the light period. The changes in particulate organic nitrogen (PON) and particulate organic carbon (POC) were then analyzed to determine the assimilation rate of carbon and nitrogen. Upon sampling, cells were filtered onto pre-combusted (450°C, 4 h) GF/F filters and rinsed with 100 mL fresh nitrogen-free YBCII. Subsequently, the filters were acidified for 24 h in HCl fumes and then dried for 24 h to remove unassimilated inorganic carbon. An elemental analyzer (Vario EL cube, Elementary, Germany) was used to quantify POC and PON. Changes in POC or PON between samples taken at 12 h and 0 h represented the assimilation during the light period, and changes between samples taken at 24 h and 0 h represented the daily assimilation. The results were comparable to the POC and PON production rates, which were calculated as POC or PON content (nmol Chl a^{-1}) × specific growth rate μ (d^{-1}, Supplementary Figure S2) (Tong et al., 2019).

We acknowledge that the POC changes effectively represent integrated assimilation of inorganic carbon and recycling of organic carbon leaked into the media by *Trichodesmium*. Similarly, the nitrogen assimilation rates, as determined in this study, are indicative of the sum of both N_2-fixation and the recycling of biogenic nitrogen leaked into the media by *Trichodesmium*.

2.6 Dissolved and particulate phosphorus measurement

To determine dissolved inorganic phosphorus (DIP), the samples were filtered through a 0.22 μm cellulose acetate membrane and were then analyzed using an auto-analyzer (AA3, Seal, Germany) at room temperature. For the measurement of particulate phosphorus (PP), we followed the Solórzano method (Solórzano and Sharp, 1980). In brief, the samples were filtered on pre-combusted (450°C, 4 h) GF/F filters (25 mm, Whatman, United States), and rinsed with 100 mL phosphorus-free YBCII artificial seawater. Subsequently, the filters were soaked with 0.017 M $MgSO_4$, dried at 95°C, and then baked for 2 h at 450°C. Before measurement, the samples were hydrolyzed with acid (0.2 M HCl) at 80°C for 30 min. These procedures convert PP to DIP, which was subsequently quantified with an auto-analyzer (see above). The assimilation rates of phosphorus during a daily cycle were calculated using the PP contents at 0 h, 12 h, and 24 h.

2.7 Thermal dependence of metabolic processes

The thermal dependence of methane production and the related assimilation of carbon, nitrogen and phosphorus was analyzed using the Boltzmann-Arrhenius equation (Padfield et al., 2016):

$$\ln\left(b\left(T\right)\right) = E_a\left(\frac{1}{k\,T_c} - \frac{1}{k\,T}\right) + \ln\left(b\left(T_c\right)\right),$$

where $b(T)$ represents the metabolic rate at temperature T (Kelvin, K), k Boltzmann's constant (8.62×10^{-5} eV K^{-1}), $b(T_c)$ the rate of metabolism normalized to an arbitrary reference temperature, $T_c = 25$°C, and E_a is the activation energy (in electron volts, eV) for the metabolic process. Supra-optimal temperatures could deviate the metabolic rate from the Boltzmann-Arrhenius equation. Therefore, corresponding values, usually those observed at 31°C, were excluded from this analysis.

The sensitivity of methane production and assimilation of carbon, nitrogen and phosphorus to temperature changes (Q_{10}) from 16°C to 27°C was assessed by the following model (Van't Hoff and Lehfeldt, 1899):

$$Q_{10} = \left(\frac{\mathrm{Rate}_2}{\mathrm{Rate}_1}\right)^{\frac{10}{T_2 - T_1}},$$

where $Rate_1$ and $Rate_2$ indicate metabolic rates at 16°C (T_1) and 27°C (T_2), respectively.

2.8 Statistical analysis

The data were provided as the means of three replicates (independent cultures) with standard deviation (SD) ($n = 3$). To examine the statistical differences between treatments, one-way ANOVA and Tukey's test were used. The Brown-Forsythe test and Shapiro–Wilk test were used to check data homoscedasticity and normality, respectively.

3 Results

3.1 Specific growth rates, ratio of Chl-*a* to POC, ratio of POC to PON and Chl-*a* fluorescence

The specific growth rate of *Trichodesmium* increased with temperature (Figure 1; one-way ANOVA, $p < 0.001$) and was sensitive to temperature changes, with a Q_{10} value (the rate increase fold for every 10-degree rise in the temperature) of growth rate for temperatures ranged from 16°C to 27°C reaching 8.6 ± 2.3. As the culture temperature increased from 16°C to 27°C, the specific growth rate exhibited a tenfold increase from 0.03 ± 0.01 d^{-1} to 0.34 ± 0.02 d^{-1} (Figure 1, Tukey's test, $p = 0.0001$). Increasing the growth temperature to 31°C did not significantly change the specific growth rate (0.32 ± 0.05 d^{-1}, Figure 1, Tukey's test, $p = 0.999$). According to the

Norberg equation, the optimal growth temperature (T_{opt}) was 29.2°C, corresponding to a maximum growth rate of 0.38 d^{-1}.

The ratio of Chl-*a* to POC increased with the rise in temperatures (one-way ANOVA, $p < 0.0001$). The Chl *a*: POC was 68 ± 1 ng Chl *a* µmol POC^{-1} at the lowest growth temperature of 16°C, and increased by 100% to 136 ± 3 ng Chl *a* µmol POC^{-1} at 31°C (Table 1; Tukey's test, $p < 0.0001$).

In contrast, the ratios of POC to PON were negatively correlated with temperatures (Table 1; one-way ANOVA, $p = 0.0004$). When the growth temperature increased from 16°C to 31°C, the ratios of POC to PON decreased by 15% from 6.60 ± 0.24 to 5.64 ± 0.26 (Table 1; Tukey's test, $p = 0.004$).

The effective quantum yield (Φ_{II}), a measure indicative of the photosynthetic efficiency of *Trichodesmium*, increased with rising temperature (one-way ANOVA, $p < 0.0001$). The value of Φ_{II} was 0.17 ± 0.02 at the lowest temperature of 16°C and increased by 188% to 0.49 ± 0.01 (Table 1; Tukey's test, $p < 0.0001$) at 31°C. The relative maximum electron transport rate ($rETR_{max}$) and photosynthetic light-use efficiency (α) showed a similar pattern to Φ_{II}. Specifically, $rETR_{max}$ increased by 207% from 73 ± 7 to 224 ± 4 µmol e $m^{-2} s^{-1}$ (Table 1, one-way ANOVA, $p < 0.0001$), while the value of α increased by 177% from 0.22 ± 0.02 to 0.61 ± 0.01 (Table 1, one-way ANOVA, $p < 0.0001$) with the temperature increasing from 16 to 31°C.

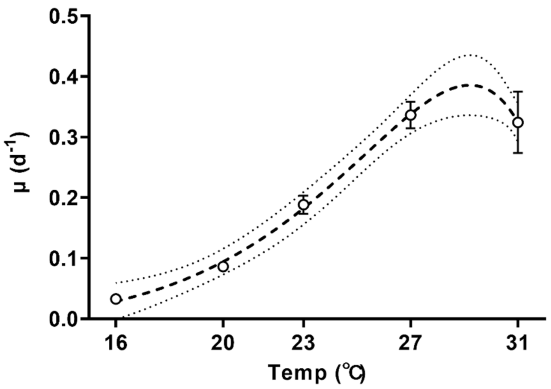

FIGURE 1
Specific growth rates of *Trichodesmium* IMS101 during the exponential stage after having acclimated at each of the specific temperatures [ranging from 16 to 31°C for 6 months]. The dotted line represents the 95% prediction bands of the best-fit line. Values represent the means ± SD of independent biological replicates ($n = 3$).

3.2 Methane production

Methane was produced during both the day and the night, exhibiting a typical temperature response curve (Figure 2, one-way ANOVA, $p < 0.0001$) and demonstrated sensitivity to temperature changes, with a Q_{10} value for temperature ranged from 16°C to 27°C, reaching 4.6 ± 0.7. At 16°C, the methane production rates during the light period and daily cycle were 0.120 ± 0.050 nmol CH_4 µm $POC^{-1} day^{-1}$ and 0.198 ± 0.042 nmol CH_4 µmol $POC^{-1} day^{-1}$, respectively (Figure 2). When the growth temperature increased to 27°C, the rate of methane production reached the maximum, with light-period and daily-cycle values increasing by 407% to 0.608 ± 0.018 nmol CH_4 µmol $POC^{-1} day^{-1}$ (Tukey's test, $p < 0.0001$) and by 419% to 1.028 ± 0.040 nmol CH_4 µmol $POC^{-1} day^{-1}$ (Tukey's test, $p < 0.0001$), respectively (Figure 2). The activation energy (E_a) for methane production was 1.09 ± 0.13 eV for light period and 1.08 ± 0.08 eV for daily-cycle. Notably, the amount of methane production in each treatment increased with incubation time (Supplementary Figure S3A) and showed a positive correlation with biomass (Supplementary Figure S4). Methane production was also observed in bacterial controls, and the production rate increased with rising temperature (Supplementary Figure S3B). *Trichodesmium* dominated the methane production, with heterotrophic bacterial contribution to the total production being 19.7% at 16°C, 1.5% at 20°C, 3.8% at 23°C, 1.9% at 27°C, and 11.4% at 31°C, respectively (Supplementary Figure S3A). Methane production by *Trichodesmium* was derived by subtracting the bacterial production from the total production, with the possible contribution of the attached heterotrophic bacteria to the filaments of *Trichodesmium* being ignored.

3.3 Carbon, nitrogen, and phosphorus assimilation

Carbon, nitrogen, and phosphorus assimilation rates increased with higher growth temperatures (Figure 3, one-way ANOVA, $p < 0.0001$, $p < 0.0001$, and $p < 0.0001$), demonstrating a high sensitivity to temperature changes. The Q_{10} values for temperature ranged from 16°C to 27°C for POC, PON and POP production were 4.9 ± 0.7, 2.6 ± 0.5, and 2.6 ± 0.3, respectively. When the temperature was raised from 16°C to 31°C, the light-period and daily rates of carbon assimilation increased by 577% from 81 ± 34 to 548 ± 128 nmol C nmol $POC^{-1} day^{-1}$ (Tukey's test, $p < 0.0001$) and

TABLE 1 Chlorophyll *a* content normalized to cellular particular organic carbon (Chl *a*: POC), ratio of POC to PON (POC: PON), effective quantum yield (Φ_{II}), photosynthetic light-gathering efficiency (α), maximum relative electron transport rate ($rETR_{max}$) of *Trichodesmium* IMS101 after having acclimated for 6 months to specific temperatures ranging from 16 to 31°C.

Growth Temp (°C)	Chl *a*: POC (ng: µmol)	POC: PON (mol: mol)	Φ_{II}	α	$rETR_{max}$ (µmol e $m^{-2} s^{-1}$)
16	68 ± 1^{a}	6.60 ± 0.24^{ab}	0.17 ± 0.02^{a}	0.22 ± 0.02^{a}	73 ± 7^{a}
20	101 ± 1^{b}	6.23 ± 0.04^{ac}	0.30 ± 0.02^{b}	0.46 ± 0.02^{b}	135 ± 10^{b}
23	78 ± 13^{ac}	7.00 ± 0.38^{b}	0.27 ± 0.02^{b}	0.35 ± 0.03^{b}	127 ± 9^{b}
27	120 ± 6^{d}	6.12 ± 0.14^{ac}	0.49 ± 0.01^{c}	0.63 ± 0.01^{c}	228 ± 4^{c}
31	136 ± 3^{d}	5.64 ± 0.26^{c}	0.49 ± 0.01^{c}	0.61 ± 0.01^{c}	224 ± 5^{c}

The $rETR_{max}$ and α were derived from the rapid light curves (Supplementary Figure S1). Values represent the means ± SD of independent biological replicates ($n = 3$).

10.3389/fmicb.2024.1396369

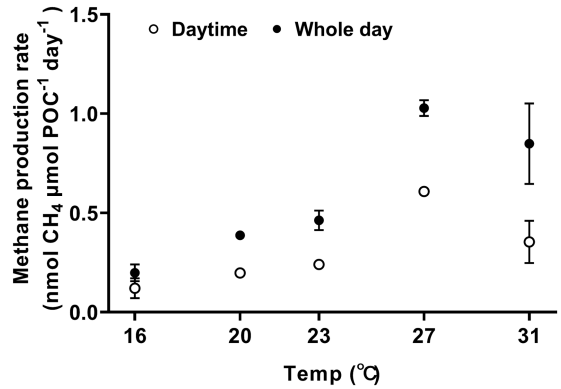

FIGURE 2
The effect of growth temperature on methane production by *Trichodesmium* IMS101. The cultures were acclimated to the temperatures for 6 months, and the methane production rates were normalized to particulate organic carbon (POC). The hollow circles represent methane production during the daytime (12 h), whereas the solid ones represent the diel production, summing that of light and dark periods. Values represent the means ± SD of independent biological replicates ($n = 3$).

by 650% from 56 ± 11 to 420 ± 103 nmol C µmol POC^{-1} day^{-1} (Tukey's test, $p = 0.0002$), respectively (Figure 3A). The activation energy (E_a) for carbon assimilation was 1.26 ± 0.15 eV for light period and 1.19 ± 0.19 eV for daily-cycle. As the growth temperature increased from 16°C to 31°C, the nitrogen assimilation rate increased by 475% from 16 ± 2 to 92 ± 12 nmol N µmol POC^{-1} day^{-1} (Tukey's test, $p < 0.0001$) during the light period, and increased by 250% from 26 ± 6 to 91 ± 14 nmol N µmol POC^{-1} day^{-1} (Tukey's test, $p < 0.0001$) (Figure 3B). The activation energy (Ea) for nitrogen assimilation was 1.19 ± 019 eV for light period and 0.78 ± 0.25 eV for daily-cycle. The phosphorous assimilation rate was 0.7 ± 0.2 nmol P µmol POC^{-1} day^{-1} for the light–dark period at 16°C, and increased by 228% from to 2.3 ± 0.5 nmol P µmol POC^{-1} day^{-1} at 31°C (Figure 3C; Tukey's test, $p < 0.0001$).

The methane production correlated positively with rates of C, N, and P assimilation, specific growth and relative electron transfer (Figures 4, 5). The daily methane production increased with higher carbon, nitrogen, and phosphorus assimilation (Figure 4). The correlation coefficients between the daily methane production and the assimilation of carbon, nitrogen and phosphorus were 0.83, 0.74, and 0.77, respectively (Figure 4, $p < 0.0001$, $p < 0.0001$, $p < 0.0001$). The methane production quotients (MPQ), ratio of the carbon, nitrogen or phosphorus assimilation rates to the methane production rates, were 253–494 for carbon, 40–128 for nitrogen, and 1.3–3.4 for phosphorus, respectively (Table 2).

The relationship between metabolic activity and growth rates to methane production rates, which was established based on the positive correlations of methane production with the specific growth rate (µ) and relative electron transport rate (rETR), provided the correlation coefficients (R-square) of 0.91 and 0.87, respectively (Figure 5, $p < 0.0001$, $p < 0.0001$). Under different growth temperatures, the ratio of specific growth rate to methane production rate ranged from 0.17 to 0.41 and that of rETR to methane production rate ranged from 118 to 215 (Table 2).

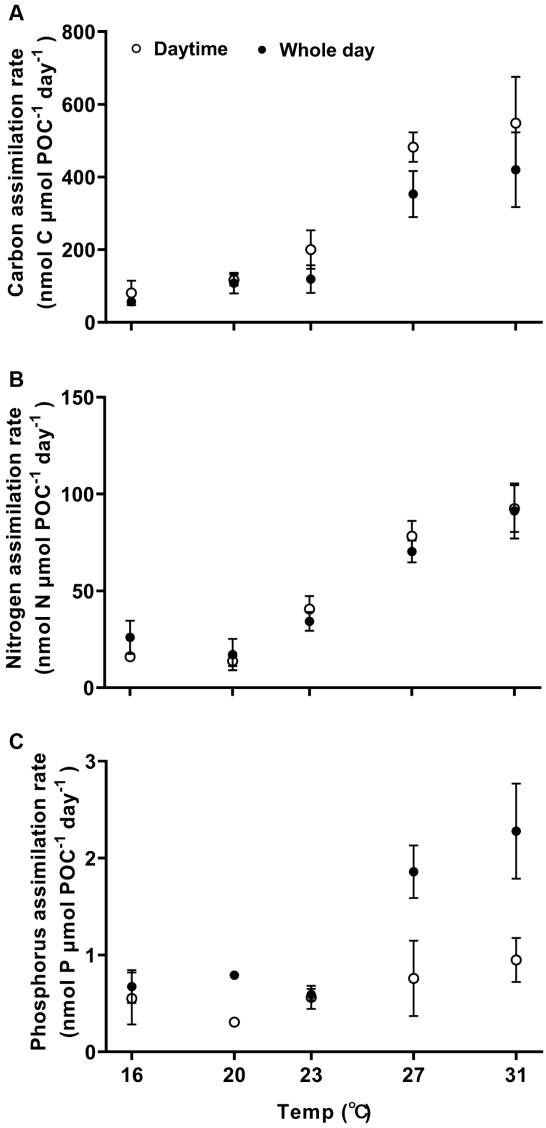

FIGURE 3
Carbon, nitrogen, and phosphorus assimilation rates **(A–C)** of *Trichodesmuim* IMS 101 normalized to particular organic carbon (POC) during the light period (hollow circle) or the diel cycle (solid circle) after being acclimated for 6 months to specific temperatures. Values represent the means ± SD of independent biological replicates ($n = 3$).

4 Discussion

The thermal dependence of key metabolic processes, including N_2 fixation, photosynthetic CO_2 fixation and specific growth rate, have been widely explored in *Trichodesmium* (Mulholland and Bernhardt, 2005; Breitbarth et al., 2007; Boatman et al., 2017). These studies have contributed to our understanding of its current distribution in natural environments and provided insights to predicting its future behavior under influence of climate change (Breitbarth et al., 2007; Fu et al., 2014; Jiang et al., 2018; Yi et al., 2020). This study presents the first report on how temperature impacts methane production in *Trichodesmium* and the relationship

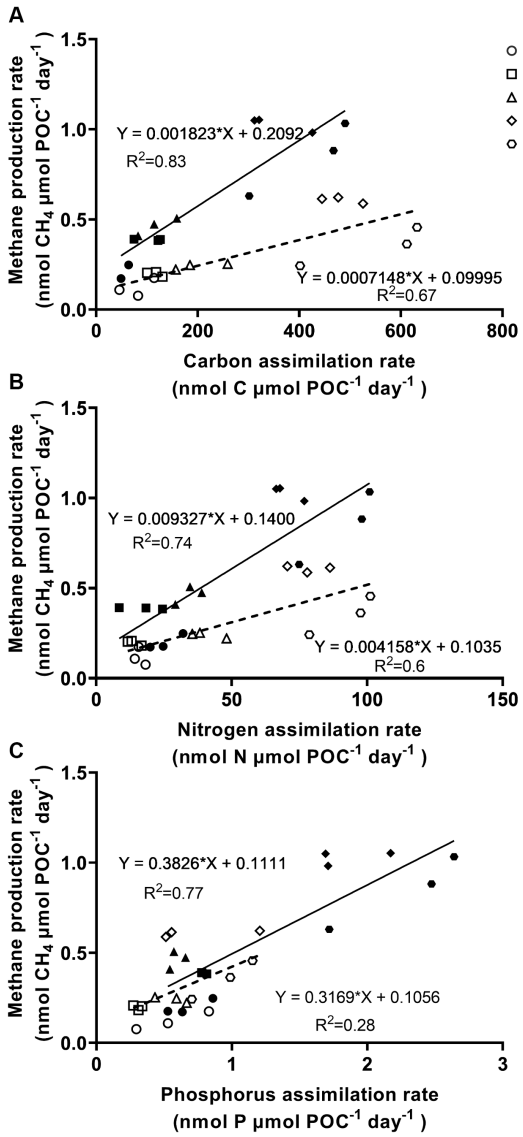

FIGURE 4
Methane production rates of *Trichodesmium* IMS101 correlated with assimilation rates of carbon **(A)**, nitrogen **(B)**, and phosphorus **(C)**, which were derived from Figures 2, 3. The hollow symbols and dotted line represent the correlations for the light period, while the solid symbols and lines represent the daily values. The numbers next to the different symbols indicate the growth temperatures (°C). Each data point represents an independent biological replicate, and different symbols represent different biological replicates.

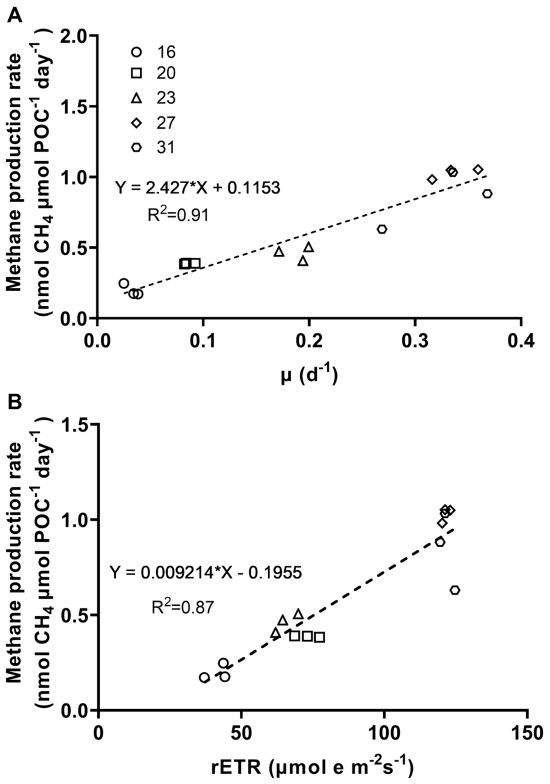

FIGURE 5
Methane production rates of *Trichodesmium* IMS101 as a function of specific growth rates **(A)** and relative electron transport rates (rETR) **(B)**. The rETR, were derived from the rapid light curves (Supplementary Figure S1), and represent rates measured at the acclimation light level. The correlation of methane production and the specific growth rates was based on Figures 1, 2. The numbers next to the symbols indicate the growth-acclimation temperatures (°C). Each data point represents an independent biological replicate, and different symbols represent different biological replicates.

of methane production to the assimilation of carbon, nitrogen and phosphorus, although it has been known to release methane for almost two decades (Karl et al., 2008; Beversdorf et al., 2010; Repeta et al., 2016). Within the experimental temperature range of 16 to 31°C, the daily methane production increased with growth temperature and saturated at 27°C, with a corresponding value of 1.028 ± 0.040 nmol CH_4 µmol POC^{-1} day^{-1} (Figure 2). Obvious linear positive correlations were detected between methane production and the assimilations of carbon, nitrogen and phosphorus (Figure 4).

Unlike the assimilation of carbon and nitrogen, which predominantly occurred during the light period (Figure 3), substantial methane production and phosphorus assimilation were observed during dark periods as well (Figure 2). In *Trichodesmium*, photosynthetic CO_2 fixation and biological N_2 fixation provide the substrates for other physiological and biochemical processes (Berman-Frank, 2001; Milligan, 2007). Moreover, the circadian clock of *Trichodesmium* confines the expression of genes related to CO_2 and N_2 fixation to light period (Ohki et al., 1992; Chen et al., 1996, 1998; Dodd et al., 2005; Masotti et al., 2007; Haydon et al., 2013). For MPn uptake and C-P cleavage, the required energy is directly provided by ATP (Kamat et al., 2011; Stasi et al., 2019). During the night, mitochondrial respiration likely served as the primary source of ATP, which consumes the organic carbon stored during the daytime period (Figure 3A). Within the temperature range of 16–31°C, the specific growth, the methane production rate and the assimilation rates of carbon, nitrogen and phosphorus exhibited high sensitivity to thermal changes with Q10 greater than 2 (Supplementary Table S1). The methane production of *Trichodesmium* saturated at 27°C and decreased when the temperature exceeded 31°C, indicating a threshold for warming to promote methane production. Methane production in the associated heterotrophic bacteria (control) also increased with rising temperatures

TABLE 2 The quotients of carbon (C_{as}: CH_{4pro}), nitrogen (N_{as}: CH_{4pro}) and phosphorus (P_{as}: CH_{4pro}) assimilations to methane production rate, and the ratio of specific growth rate (μ: CH_{4pro}) and relative electron transfer rate (rETR: CH_{4pro}) to methane production rate in *Trichodesmium* IMS101 after having acclimated for 6 months to specific temperatures ranging from 16 to 31°C.

Growth Temp (°C)	C_{as}: CH_{4pro}	N_{as}: CH_{4pro}	P_{as}: CH_{4pro}	μ: CH_{4pro}	rETR: CH_{4pro}
16	227 ± 18^{a}	128 ± 12^{a}	3.39 ± 0.35^{a}	0.17 ± 0.06^{a}	215 ± 37^{a}
20	278 ± 75^{a}	40 ± 21^{b}	2.04 ± 0.07^{b}	0.22 ± 0.01^{ac}	189 ± 13^{ab}
23	253 ± 57^{a}	74 ± 7.3^{b}	1.28 ± 0.14^{c}	0.41 ± 0.06^{b}	142 ± 8^{b}
27	345 ± 77^{ab}	69 ± 82^{b}	1.81 ± 0.23^{bc}	0.33 ± 0.01^{bc}	118 ± 4^{b}
31	494 ± 31 ^{b}	109 ± 11^{ac}	2.70 ± 0.13^{d}	0.39 ± 0.06^{b}	150 ± 42^{ab}

Values represent the means ± SD of independent biological replicates ($n = 3$).

and peaked at 31°C (Supplementary Figure S3), suggesting that future ocean warming may promote the growth of these bacteria and potentially stimulate degradation of organic matters with a possibility to indirectly affect MPn-based methane production by the diazotroph.

While the specific growth rates of *Trichodesmium* grown with the MPn as the main phosphorus source (Figure 1) were comparable to that of *Trichodesmium* grown on inorganic phosphate (Breitbarth et al., 2007; Jiang et al., 2018; Yi et al., 2020), *Trichodesmium* grown on MPn demonstrated resilience to temperature as low as 16°C, contrasting sharply with the constraints observed in *Trichodesmium* cultured with inorganic phosphate. Specifically, *Trichodesmium* IMS101 did not grow below 20°C when supplied with inorganic phosphate (Breitbarth et al., 2007). In studies involving three other strains of *Trichodesmium erythraeum* (KO4-20, RLI, 21–75), the minimum growth temperature was reported to be 18°C (Fu et al., 2014). In the oceans, *Trichodesmium* is predominately found in tropical and subtropical waters with temperatures exceeding 20°C (Laroche and Breitbarth, 2005; Luo et al., 2012). Although its presence in higher latitudes with colder waters is occasionally reported (Díez et al., 2012; Rees et al., 2016; Sabeur et al., 2016), it had been thought that these *Trichodesmium* cells were merely transported by ocean currents and were unable to establish a sustained presence (Laroche and Breitbarth, 2005). Our results provide an additional interpretation for *Trichodesmium*'s persistence in higher latitudes where temperatures drop below 20°C. When MPn was utilized as the primary phosphorus source, *Trichodesmium* demonstrated the capacity to acclimate and grow at temperatures as low as 16°C, possibly sustaining a seed community in colder regions (Shaika et al., 2023). However, the underlined mechanisms for the tolerance of the low temperature in *Trichodesmium* grown with Mpn need to be explored in future studies.

Based on the significant positive correlations between methane production and the assimilation of carbon, nitrogen, and phosphorus, as well as with the specific growth rate (μ) and relative electron transport rate (rETR) (Figures 4, 5), we established a series of methane production quotients (MPQ), representing the ratios between key metabolic rates and methane production rates (Table 2). Given that *Trichodesmium*'s capacity for carbon and nitrogen fixation has been extensively studied over the past few decades (Sañudo-Wilhelmy et al., 2001; Mulholland et al., 2006; Bergman et al., 2013), we applied the methane production quotients for carbon and nitrogen to estimate *Trichodesmium*'s counteractive roles in mitigating greenhouse effect. Based on the MPQ (Table 2), for every 227–494 nmol of CO_2 assimilated by *Trichodesmium*, 1 nmol of CH_4 is emitted. Given that the global warming potential of CH_4 is about 80 times that of CO_2 (Collins et al., 2013), and taking into account that the contribution of MPn accounts for 5–9.8% (Clark et al., 1998; Repeta et al., 2016; Sosa et al., 2020) of the other phosphorus sources in the oceanic areas where *Trichodesmium* thrives, the CH_4 emission via MPn demethylation from *Trichodesmium* can offset 0.25–1.12% of its CO_2 mitigation effects. This calculation does not take the oxidation of methane during diffusion processes into account (Hakemian and Rosenzweig, 2007). As *Trichodesmium* inhabit the upper 40 meters and form extensive sea surface blooms, it is plausible to assume that methane produced by *Trichodesmium* will be released to the atmosphere. Furthermore, methane production in *Trichodesmium* is mainly coupled with the utilization of MPn. Investigating the concentrations of MPn in different waters would promote more accurate estimates on a global scale.

Under the influence of global warming, concurrent ocean warming (Collins et al., 2013) is predicted to shoal thermal stratification within the upper layers of the oceans (Somavilla et al., 2017; Frischkorn et al., 2018; Ulloa et al., 2019) and reduce the upward transport of dissolved inorganic phosphate (DIP). Consequently, *Trichodesmium* may increasingly resort to utilizing MPn, potentially leading to enhanced methane production. Additional drivers may impact methane production. The optimal growth temperature changes in Fe-replete versus Fe-deplete cells (Jiang et al., 2018). The Fe and MPn availability may further affect methane production and requires future study.

Data availability statement

The raw data supporting the conclusions of this article will be made available by the authors, without undue reservation.

Author contributions

CZ: Writing – review & editing, Data curation, Formal analysis, Investigation, Methodology, Software, Validation, Visualization, Writing – original draft. XY: Visualization, Writing – review & editing. HL: Writing – review & editing, Investigation. MB: Writing – review & editing. IB-F: Writing – review & editing, Funding acquisition. KG: Writing – review & editing, Conceptualization, Funding acquisition, Project administration, Resources, Supervision.

Funding

The author(s) declare that financial support was received for the research, authorship, and/or publication of this article. This study was supported by National Natural Science Foundation of China (No. 42361144840) to KG and the joint NSFC-Israel Science Foundation (ISF) grant No. 3051/23 to IB-F.

Acknowledgments

The authors are grateful to Yuming Rao for methane measurements. We also thank the laboratory engineers Xianglan Zeng and Wenyan Zhao for their technical and logistical supports.

Conflict of interest

The authors declare that the research was conducted in the absence of any commercial or financial relationships that could be construed as a potential conflict of interest.

The author(s) declared that they were an editorial board member of Frontiers, at the time of submission. This had no impact on the peer review process and the final decision.

Publisher's note

All claims expressed in this article are solely those of the authors and do not necessarily represent those of their affiliated organizations, or those of the publisher, the editors and the reviewers. Any product that may be evaluated in this article, or claim that may be made by its manufacturer, is not guaranteed or endorsed by the publisher.

Supplementary material

The Supplementary material for this article can be found online at: https://www.frontiersin.org/articles/10.3389/fmicb.2024.1396369/full#supplementary-material

References

Amstrup, S. K., Ong, S. C., Sofos, N., Karlsen, J. L., Skjerning, R. B., Boesen, T., et al. (2023). Structural remodelling of the carbon–phosphorus lyase machinery by a dual ABC ATPase. *Nat. Commun.* 14:1001. doi: 10.1038/s41467-023-36604-y

Behrenfeld, M. J., O'Malley, R. T., Siegel, D. A., McClain, C. R., Sarmiento, J. L., Feldman, G. C., et al. (2006). Climate-driven trends in contemporary ocean productivity. *Nature* 444, 752–755. doi: 10.1038/nature05317

Bergman, B., Sandh, G., Lin, S., Larsson, J., and Carpenter, E. J. (2013). *Trichodesmium*-a widespread marine cyanobacterium with unusual nitrogen fixation properties. *FEMS Microbiol. Rev.* 37, 286–302. doi: 10.1111/j.1574-6976.2012.00352.x

Berman-Frank, I., Lundgren, P., Chen, Y. B., Kupper, H., Kolber, Z., Bergman, B., and Falkowski, P. (2001). Segregation of nitrogen fixation and oxygenic photosynthesis in the marine cyanobacterium Trichodesmium. *Sci.* 294, 1534–1537. doi: 10.1126/science.1064082

Beversdorf, L. J., White, A. E., Björkman, K. M., Letelier, R. M., and Karl, D. M. (2010). Phosphonate metabolism by *Trichodesmium* IMS101 and the production of greenhouse gases. *Limnol. Oceanogr.* 55, 1768–1778. doi: 10.4319/lo.2010.55.4.1768

Bižić, M., Ionescu, D., Günthel, M., Tang, K. W., and Grossart, H.-P. (2018). "Oxic methane cycling: new evidence for methane formation in oxic lake water" in *Biogenesis of hydrocarbons*, 1–22.

Bižić, M., Klintzsch, T., Ionescu, D., Hindiyeh, M., Günthel, M., Muro-Pastor, A. M., et al. (2020). Aquatic and terrestrial cyanobacteria produce methane. *Sci. Adv.* 6:eaax5343. doi: 10.1126/sciadv.aax5343

Björkman, K. M., and Karl, D. M. (2003). Bioavailability of dissolved organic phosphorus in the euphotic zone at station ALOHA, North Pacific subtropical gyre. *Limnol. Oceanogr.* 48, 1049–1057. doi: 10.4319/lo.2003.48.3.1049

Boatman, T. G., Lawson, T., and Geider, R. J. (2017). A key marine Diazotroph in a changing ocean: the interacting effects of temperature, CO_2 and light on the growth of *Trichodesmium erythraeum* IMS101. *PLoS One* 12:e0168796. doi: 10.1371/journal.pone.0168796

Born, D. A., Ulrich, E. C., Ju, K.-S., Peck, S. C., Van Der Donk, W. A., and Drennan, C. L. (2017). Structural basis for methylphosphonate biosynthesis. *Science* 358, 1336–1339. doi: 10.1126/science.aao3435

Breitbarth, E., Oschlies, A., and Laroche, J. (2007). Physiological constraints on the global distribution of *Trichodesmium*–effect of temperature on diazotrophy. *Biogeosciences* 4, 53–61. doi: 10.5194/bg-4-53-2007

Capone, D. G., Zehr, J. P., Paerl, H. W., Bergman, B., and Carpenter, E. J. (1997). Trichodesmium, a globally significant marine cyanobacterium. *Science* 276, 1221–1229. doi: 10.1126/science.276.5316.1221

Chappell, P. D., and Webb, E. A. (2010). A molecular assessment of the iron stress response in the two phylogenetic clades of *Trichodesmium*. *Environ. Microbiol.* 12, 13–27. doi: 10.1111/j.1462-2920.2009.02026.x

Chen, Y.-B., Dominic, B., Mellon, M. T., and Zehr, J. P. (1998). Circadian rhythm of nitrogenase gene expression in the diazotrophic filamentous nonheterocystous cyanobacterium Trichodesmium sp. strain IMS 101. *J. Bacteriol.* 180, 3598–3605. doi: 10.1128/jb.180.14.3598-3605.1998

Chen, Y. B., Zehr, J. P., and Mellon, M. (1996). Growth and nitrogen fixation of the diazotrophic filamentous nonheterocystous cyanobacterium Trichodesmium sp. Ims 101 in defined media: evidence for a circadian rhythm. *J. Phycol.* 32, 916–923. doi: 10.1111/j.0022-3646.1996.00916.x

Clark, L. L., Ingall, E. D., and Benner, R. (1998). Marine phosphorus is selectively remineralized. *Nature* 393:426. doi: 10.1038/30881

Collins, M., Knutti, R., Arblaster, J., Dufresne, J.-L., Fichefet, T., Friedlingstein, P., et al. (2013). "Chapter 12 - Long-term climate change: Projections, commitments and irreversibility," in *Climate Change 2013: The Physical Science Basis. IPCC Working Group I Contribution to AR5*. IPCC, Cambridge: Cambridge University Press.

Damm, E., Helmke, E., Thoms, S., Schauer, U., Nöthig, E., Bakker, K., et al. (2010). Methane production in aerobic oligotrophic surface water in the Central Arctic Ocean. *Biogeosciences* 7, 1099–1108. doi: 10.5194/bg-7-1099-2010

Díez, B., Bergman, B., Pedrós-Alió, C., Antó, M., and Snoeijs, P. (2012). High cyanobacterial nifH gene diversity in Arctic seawater and sea ice brine. *Environ. Microbiol. Rep.* 4, 360–366. doi: 10.1111/j.1758-2229.2012.00343.x

Dodd, A. N., Salathia, N., Hall, A., Kévei, E., Tóth, R., Nagy, F., et al. (2005). Plant circadian clocks increase photosynthesis, growth, survival, and competitive advantage. *Science* 309, 630–633. doi: 10.1126/science.1115581

Dyhrman, S. T. (2016). "Nutrients and their acquisition: phosphorus physiology in microalgae" in *The physiology of microalgae*, 155–183.

Dyhrman, S. T., Chappell, P. D., Haley, S. T., Moffett, J. W., Orchard, E. D., Waterbury, J. B., et al. (2006). Phosphonate utilization by the globally important marine diazotroph *Trichodesmium*. *Nature* 439, 68–71. doi: 10.1038/nature04203

Dyhrman, S. T., Webb, E. A., Anderson, D. M., Moffett, J. W., and Waterbury, J. B. (2002). Cell-specific detection of phosphorus stress in *Trichodesmium* from the Western North Atlantic. *Limnol. Oceanogr.* 47, 1832–1836. doi: 10.4319/lo.2002.47.6.1832

Eilers, P., and Peeters, J. (1988). A model for the relationship between light intensity and the rate of photosynthesis in phytoplankton. *Ecol. Model.* 42, 199–215. doi: 10.1016/0304-3800(88)90057-9

Frischkorn, K. R., Krupke, A., Guieu, C., Louis, J., Rouco, M., Salazar Estrada, A. E., et al. (2018). Trichodesmium physiological ecology and phosphate reduction in the western tropical South Pacific. *Biogeosciences* 15, 5761–5778. doi: 10.5194/bg-15-5761-2018

Fu, F.-X., Yu, E., Garcia, N. S., Gale, J., Luo, Y., Webb, E. A., et al. (2014). Differing responses of marine N_2 fixers to warming and consequences for future diazotroph community structure. *Aquat. Microb. Ecol.* 72, 33–46. doi: 10.3354/ame01683

Genty, B., Briantais, J.-M., and Baker, N. R. (1989). The relationship between the quantum yield of photosynthetic electron transport and quenching of chlorophyll fluorescence. *Biochim. Biophys. Acta* 990, 87–92. doi: 10.1016/S0304-4165(89)80016-9

Günthel, M., Klawonn, I., Woodhouse, J., Bižić, M., Ionescu, D., Ganzert, L., et al. (2020). Photosynthesis-driven methane production in oxic lake water as an important contributor to methane emission. *Limnol. Oceanogr.* 65, 2853–2865. doi: 10.1002/lno.11557

Hakemian, A. S., and Rosenzweig, A. C. (2007). The biochemistry of methane oxidation. *Annu. Rev. Biochem.* 76, 223–241. doi: 10.1146/annurev.biochem.76.061505.175355

Haydon, M. J., Mielczarek, O., Robertson, F. C., Hubbard, K. E., and Webb, A. A. (2013). Photosynthetic entrainment of the *Arabidopsis thaliana* circadian clock. *Nature* 502, 689–692. doi: 10.1038/nature12603

IPCC (2013). Climate Change 2013: The Physical Science Basis. Contribution of Working Group I to the Fifth Assessment Report of the Intergovernmental Panel on Climate Change eds. Stocker, T. F, D. Qin, G.-K. Plattner, M. Tignor, S.K. Allen, J. Boschung, et al. (Cambridge, United Kingdom and New York, NY, USA: Cambridge University Press), 1535.

Jiang, H.-B., Fu, F.-X., Rivero-Calle, S., Levine, N. M., Sañudo-Wilhelmy, S. A., Qu, P.-P., et al. (2018). Ocean warming alleviates iron limitation of marine nitrogen fixation. *Nat. Clim. Chang.* 8, 709–712. doi: 10.1038/s41558-018-0216-8

Johnson, K. M., Hughes, J. E., Donaghay, P. L., and Sieburth, J. M. (1990). Bottle-calibration static head space method for the determination of methane dissolved in seawater. *Anal. Chem.* 62, 2408–2412. doi: 10.1021/AC00220A030

Kamat, S. S., Williams, H. J., and Raushel, F. M. (2011). Intermediates in the transformation of phosphonates to phosphate by bacteria. *Nature* 480, 570–573. doi: 10.1038/nature10622

Karl, D. M., Beversdorf, L., Björkman, K. M., Church, M. J., Martinez, A., and Delong, E. F. (2008). Aerobic production of methane in the sea. *Nat. Geosci.* 1, 473–478. doi: 10.1038/ngeo234

Karl, D. M., and Björkman, K. M. (2015). Dynamics of dissolved organic phosphorus. in *Biogeochemistry of marine dissolved organic matter* eds. D. A. Hansell and C. A. Carlson (Elsevier), 233–334.

Karl, D. M., and Tilbrook, B. D. (1994). Production and transport of methane in oceanic particulate organic matter. *Nature* 368, 732–734. doi: 10.1038/368732a0

Klintzsch, T., Geisinger, H., Wieland, A., Langer, G., Nehrke, G., Bizic, M., et al. (2023). Stable carbon isotope signature of methane released from phytoplankton. *Geophys. Res. Lett.* 50:e2023GL103317. doi: 10.1029/2023GL103317

Klintzsch, T., Langer, G., Nehrke, G., Wieland, A., Lenhart, K., and Keppler, F. (2019). Methane production by three widespread marine phytoplankton species: release rates, precursor compounds, and potential relevance for the environment. *Biogeosciences* 16, 4129–4144. doi: 10.5194/bg-16-4129-2019

Klintzsch, T., Langer, G., Wieland, A., Geisinger, H., Lenhart, K., Nehrke, G., et al. (2020). Effects of temperature and light on methane production of widespread marine phytoplankton. *Journal of geophysical research. Biogeosciences* 125:e2020JG005793. doi: 10.1029/2020JG005793

Kolowith, L. C., Ingall, E. D., and Benner, R. (2001). Composition and cycling of marine organic phosphorus. *Limnol. Oceanogr.* 46, 309–320. doi: 10.4319/lo.2001.46.2.0309

Lamontagne, R., Swinnerton, J., Linnenbom, V., and Smith, W. (1973). Methane concentrations in various marine environments. *J. Geophys. Res.* 78, 5317–5324. doi: 10.1029/JC078i024p05317

Laroche, J., and Breitbarth, E. (2005). Importance of the diazotrophs as a source of new nitrogen in the ocean. *J. Sea Res.* 53, 67–91. doi: 10.1016/j.seares.2004.05.005

Lenhart, K., Klintzsch, T., Langer, G., Nehrke, G., Bunge, M., Schnell, S., et al. (2016). Evidence for methane production by the marine algae Emiliania huxleyi. *Biogeosciences* 13, 3163–3174. doi: 10.5194/bg-13-3163-2016

Liu, L. Y., Xie, G. J., Ding, J., Liu, B. F., Xing, D. F., Ren, N. Q., et al. (2022). Microbial methane emissions from the non-methanogenesis processes: a critical review. *Sci. Total Environ.* 806:151362. doi: 10.1016/j.scitotenv.2021.151362

Luo, Y.-W., Doney, S., Anderson, L., Benavides, M., Berman-Frank, I., Bode, A., et al. (2012). Database of diazotrophs in global ocean: abundance, biomass and nitrogen fixation rates. *Earth Syst. Sci. Data* 4, 47–73. doi: 10.5194/essd-4-47-2012

Mao, S.-H., Zhang, H.-H., Zhuang, G.-C., Li, X.-J., Liu, Q., Zhou, Z., et al. (2022). Aerobic oxidation of methane significantly reduces global diffusive methane emissions from shallow marine waters. *Nat. Commun.* 13:7309. doi: 10.1038/s41467-022-35082-y

Martinez, A., Ventouras, L. A., Wilson, S. T., Karl, D. M., and Delong, E. F. (2013). Metatranscriptomic and functional metagenomic analysis of methylphosphonate utilization by marine bacteria. *Front. Microbiol.* 4:340. doi: 10.3389/fmicb.2013.00340

Masotti, I., Ruiz-Pino, D., and Le Bouteiller, A. (2007). Photosynthetic characteristics of Trichodesmium in the Southwest Pacific Ocean: importance and significance. *Mar. Ecol. Prog. Ser.* 338, 47–59. doi: 10.3354/meps338047

Mccarthy, J. J., and Carpenter, E. J. (1979). Oscillatoria *Trichodesmium thiebautii* (cyanophyta) in the central North Atlantic Ocean. *J. Phycol.* 15, 75–82. doi: 10.1111/j.1529-8817.1979.tb02965.x

Metcalf, W. W., Griffin, B. M., Cicchillo, R. M., Gao, J., Janga, S. C., Cooke, H. A., et al. (2012). Synthesis of methylphosphonic acid by marine microbes: a source for methane in the aerobic ocean. *Science* 337, 1104–1107. doi: 10.1126/science.1219875

Milligan, A. J., Berman-Frank, I., Gerchman, Y., Dismukes, G. C., and Falkowski, P. G. (2007). Light-dependent oxygen consumption in nitrogen-fixing cyanobacteria plays a key role in nitrogenase protection. *J. Psychol.* 43, 845–852. doi: 10.1111/j.1529-8817.2007.00395.x

Mulholland, M. R., and Bernhardt, P. W. (2005). The effect of growth rate, phosphorus concentration, and temperature on N2 fixation, carbon fixation, and nitrogen release in continuous cultures of Trichodesmium IMS101. *Limnol. Oceanogr.* 50, 839–849. doi: 10.4319/lo.2005.50.3.0839

Mulholland, M. R., Bernhardt, P. W., Heil, C. A., Bronk, D. A., and O'Neil, J. M. (2006). Nitrogen fixation and release of fixed nitrogen by *Trichodesmium spp*. in the Gulf of Mexico. *Limnol. Oceanogr.* 51, 1762–1776. doi: 10.4319/lo.2006.51.4.1762

Norberg, J. (2004). Biodiversity and ecosystem functioning: a complex adaptive systems approach. *Limnol. Oceanogr.* 49, 1269–1277. doi: 10.4319/lo.2004.49.4_part_2.1269

Ohki, K., Zehr, J. P., and Fujita, Y. (1992). Regulation of nitrogenase activity in relation to the light-dark regime in the filamentous non-heterocystous cyanobacterium *Trichodesmium sp*. NIBB 1067. *Microbiology* 138, 2679–2685. doi: 10.1099/00221287-138-12-2679

Padfield, D., Yvon-Durocher, G., Buckling, A., Jennings, S., and Yvon-Durocher, G. (2016). Rapid evolution of metabolic traits explains thermal adaptation in phytoplankton. *Ecol. Lett.* 19, 133–142. doi: 10.1111/ele.12545

Polovina, J. J., Howell, E. A., and Abecassis, M. (2008). Ocean's least productive waters are expanding. *Geophys. Res. Lett.* 35:L03618. doi: 10.1029/2007GL031745

Ralph, P. J., and Gademann, R. (2005). Rapid light curves: a powerful tool to assess photosynthetic activity. *Aquat. Bot.* 82, 222–237. doi: 10.1016/j.aquabot.2005.02.006

Rees, A. P., Tait, K., Widdicombe, C. E., Quartly, G. D., Mcevoy, A. J., and Al-Moosawi, L. (2016). Metabolically active, non-nitrogen fixing, *Trichodesmium* in UK coastal waters during winter. *J. Plankton Res.* 38, 673–678. doi: 10.1093/plankt/fbv123

Repeta, D. J., Ferrón, S., Sosa, O. A., Johnson, C. G., Repeta, L. D., Acker, M., et al. (2016). Marine methane paradox explained by bacterial degradation of dissolved organic matter. *Nat. Geosci.* 9, 884–887. doi: 10.1038/ngeo2837

Ritchie, R. J. (2006). Consistent sets of spectrophotometric chlorophyll equations for acetone, methanol and ethanol solvents. *Photosynth. Res.* 89, 27–41. doi: 10.1007/s11120-006-9065-9

Sabeur, H. I., Wafa, F.-S., Asma, H., and Malika, B. H. (2016). Long term characterization of *Trichodesmium erythraeum* blooms in Gabès gulf (Tunisia). *Cont. Shelf Res.* 124, 95–103. doi: 10.1016/j.csr.2016.05.007

Sañudo-Wilhelmy, S. A., Kustka, A. B., Gobler, C. J., Hutchins, D. A., Yang, M., Lwiza, K., et al. (2001). Phosphorus limitation of nitrogen fixation by *Trichodesmium* in the Central Atlantic Ocean. *Nature* 411, 66–69. doi: 10.1038/35075041

Scranton, M. I., and Brewer, P. G. (1977). Occurrence of methane in the near-surface waters of the western subtropical North-Atlantic. *Deep-Sea Res.* 24, 127–138. doi: 10.1016/0146-6291(77)90548-3

Shaika, N. A., Alhomaidi, E., Sarker, M. M., An Nur, A., Sadat, M. A., Awal, S., et al. (2023). Winter bloom of marine cyanobacterium, Trichodesmium erythraeum and its relation to environmental factors. *Sustain. For.* 15:1311. doi: 10.3390/su15021311

Sohm, J. A., and Capone, D. G. (2006). Phosphorus dynamics of the tropical and subtropical North Atlantic: Trichodesmium spp. versus bulk plankton. *Mar. Ecol. Prog. Ser.* 317, 21–28. doi: 10.3354/meps317021

Solórzano, L., and Sharp, J. H. (1980). Determination of total dissolved phosphorus and particulate phosphorus in natural waters. *Limnol. Oceanogr.* 25, 754–758. doi: 10.4319/lo.1980.25.4.0754

Somavilla, R., González-Pola, C., and Fernández-Diaz, J. (2017). The warmer the ocean surface, the shallower the mixed layer. How much of this is true? *J. Geophys. Res. Oceans* 122, 7698–7716. doi: 10.1002/2017JC013125

Sosa, O. A., Burrell, T. J., Wilson, S. T., Foreman, R. K., Karl, D. M., and Repeta, D. J. (2020). Phosphonate cycling supports methane and ethylene supersaturation in the phosphate-depleted western North Atlantic Ocean. *Limnol. Oceanogr.* 65, 2443–2459. doi: 10.1002/lno.11463

Stasi, R., Neves, H. I., and Spira, B. (2019). Phosphate uptake by the phosphonate transport system PhnCDE. *BMC Microbiol.* 19:79. doi: 10.1186/s12866-019-1445-3

Stihl, A., Sommer, U., and Post, A. F. (2001). Alkaline phosphatase activities among populations of the colony-forming diazotrophic cyanobacterium Trichodesmium spp. (cyanobacteria) in the Red Sea. *J. Phycol.* 37, 310–317. doi: 10.1046/j.1529-8817.2001.037002310.x

Taenzer, L., Carini, P. C., Masterson, A. M., Bourque, B., Gaube, J. H., and Leavitt, W. D. (2020). Microbial methane from methylphosphonate isotopically records source. *Geophys. Res. Lett.* 47:e2019GL085872. doi: 10.1029/2019gl085872

Tong, S., Hutchins, D. A., and Gao, K. (2019). Physiological and biochemical responses of *Emiliania huxleyi* to ocean acidification and warming are modulated by UV radiation. *Biogeosciences* 16, 561–572. doi: 10.5194/bg-16-561-2019

Ulloa, H. N., Winters, K. B., Wüest, A., and Bouffard, D. (2019). Differential heating drives downslope flows that accelerate mixed-layer warming in ice-covered waters. *Geophys. Res. Lett.* 46, 13872–13882. doi: 10.1029/2019GL085258

Van't Hoff, J. H., and Lehfeldt, R. A. (1899). Lectures on Theoretical and Physical Chemistry. *Nature* 59:557. doi: 10.1038/059557b0

Von Arx, J. N., Kidane, A. T., Philippi, M., Mohr, W., Lavik, G., Schorn, S., et al. (2023). Methylphosphonate-driven methane formation and its link to primary production in the oligotrophic North Atlantic. *Nat. Commun.* 14:6529. doi: 10.1038/s41467-023-42304-4

Wang, X. (2022). Physiological and elemental changes of Trichodesmium in response to growth limitation by phosphorus, iron and zinc. PhD thesis, Christian-Albrechts-Universität.

Wang, Q., Alowaifeer, A., Kerner, P., Balasubramanian, N., Patterson, A., Christian, W., et al. (2021). Aerobic bacterial methane synthesis. *Proc. Natl. Acad. Sci. USA* 118:e2019229118. doi: 10.1073/pnas.2019229118

Weber, T., Wiseman, N. A., and Kock, A. (2019). Global Ocean methane emissions dominated by shallow coastal waters. *Nat. Commun.* 10:4584. doi: 10.1038/s41467-019-12541-7

Yi, X., Fu, F.-X., Hutchins, D. A., and Gao, K. (2020). Light availability modulates the effects of warming in a marine N_2 fixer. *Biogeosciences* 17, 1169–1180. doi: 10.5194/bg-17-1169-2020

Yvon-Durocher, G., Caffrey, J. M., Cescatti, A., Dossena, M., Giorgio, P. D., Gasol, J. M., et al. (2012). Reconciling the temperature dependence of respiration across timescales and ecosystem types. *Nature* 487, 472–476. doi: 10.1038/nature11205

Zehr, J. P., and Capone, D. G. (2020). Changing perspectives in marine nitrogen fixation. *Science* 368:eaay9514. doi: 10.1126/science.aay9514

frontiers | Frontiers in Microbiology

TYPE Original Research
PUBLISHED 26 June 2024
DOI 10.3389/fmicb.2024.1384435

OPEN ACCESS

EDITED BY
Man Xiao,
Chinese Academy of Sciences (CAS), China

REVIEWED BY
Anna Carratalà,
Swiss Federal Institute of Technology Lausanne, Switzerland
Martin T. Dokulil,
University of Innsbruck, Austria

*CORRESPONDENCE
Tomasz Lenard
✉ tomasz.lenard@kul.pl

RECEIVED 09 February 2024
ACCEPTED 17 June 2024
PUBLISHED 26 June 2024

CITATION
Lenard T and Ejankowski W (2024) The ice phenology as a predictor of *Planktothrix rubescens* bloom in vegetation season in temperate lakes.
Front. Microbiol. 15:1384435.
doi: 10.3389/fmicb.2024.1384435

The ice phenology as a predictor of *Planktothrix rubescens* bloom in vegetation season in temperate lakes

Tomasz Lenard[1]* and Wojciech Ejankowski[2]

[1]Department of Animal Physiology and Toxicology, Faculty of Medicine, The John Paul II Catholic University of Lublin, Lublin, Poland, [2]Laboratory of Research and Nature Protection, Krzczonów, Poland

Introduction: Global warming affects air and water temperatures, which impacts the phenology of lakes and aquatic ecosystems. These changes are most noticeable during winter, when the potentially toxic *Planktothrix rubescens* forms its inoculum for annual blooms. Mostly, research has been conducted on alpine lakes, where blooms have persisted for decades, while a few have focused on temperate lakes. Our study aimed to determine the factors influencing the dynamics of the development of *P. rubescens* in temperate lakes where blooms occasionally occur, with a particular emphasis on the role of ice phenology.

Methods: We investigated the vertical distribution of *P. rubescens* in an annual cycle in three temperate lakes. Samples were collected monthly in the winter and biweekly during the vegetative seasons. Overall, 434 samples were collected and analyzed according to biological and chemical parameters. Physical parameters were measured *in situ*.

Results: The vegetation seasons in temperate lakes showed a similar development pattern in the *P. rubescens* population as that in alpine lakes. Our results also show the influence of physical and chemical factors on the vertical distribution of this cyanobacterium. These results revealed the significant impact of *P. rubescens* filaments on phytoplankton biodiversity and biomass. Our data show the role of ice phenology in the establishment of the winter inoculum of *P. rubescens* and its further mass development until its disappearance in autumn.

Conclusion: A climate-zone-independent pattern of *P. rubescens* blooms was observed during the vegetation periods. The population of *P. rubescens* was more influenced by physical factors than by the availability of dissolved nutrients in the water. Despite the same etiology, global warming has been shown to cause different responses in aquatic ecosystems, which affect the different nature of *P. rubescens* appearances. We associated blooms in temperate lakes, in contrast to alpine lakes, mainly with the presence of ice cover during severe winters, when the species establishes its inoculum. Hence, blooms in temperate lakes occur at different time intervals. Therefore, the dynamics of periodic blooms of *P. rubescens* in temperate lakes provide novel knowledge to the case study and a counterpoint to permanent blooms found in deep alpine lakes.

KEYWORDS

***Planktothrix rubescens*, cyanobacterial blooms, vertical distribution, physical and chemical parameters of water, ice phenology, climatic conditions**

1 Introduction

Lakes are generally considered to be great sentinels for global change. Their relatively small scale enables observing rapid responses to environmental changes, which may translate to larger aquatic ecosystems (Hessen et al., 2009). A worldwide warming trend is reflected in increasing air and water temperatures, which directly affect seasonal anomalies, changes in the thermal regime of lakes, and, in turn, all biological processes in the aquatic environment (Dokulil, 2016; Lenssen et al., 2019; Kraemer et al., 2021; Woolway et al., 2020; Weiskopf et al., 2020; GISTEMP Team, 2024). This trend strongly supports the development of cyanobacteria in warm surface waters, where they often cause mass appearances called blooms (Paerl and Huismann, 2008; Ho et al., 2019). Most of these blooms occur because of the ability of cyanobacteria to grow under high light intensity and nutrient availability (Huisman et al., 2018). Therefore, phylogenetically old cyanobacteria have developed many environmental and physiological adaptations, such as the formation of filamentous or coccal colonies, heterocysts, production of mucilage and bioactive metabolites, which help them survive and outcompete other phytoplankton species in surface waters (Carey et al., 2012; Nandagopal et al., 2021).

Nevertheless, in this highly diverse phytoplankton group, species are also able to develop in lower, metalimnetic, or hypoloimnetic layers of water using other adaptations, such as the formation of gas vesicles (aerotopes), or using other pigments rather than green chlorophyll, to perform photosynthesis under low light intensities (Micheletti et al., 1998; Walsby and Schanz, 2002; Chorus and Welker, 2021). Hence, cyanobacteria can also survive in lower water columns or even cause blooms responsible for a deep chlorophyll maximum (DCM) phenomenon in deep lakes (Leach et al., 2018). From this perspective, the presence of cyanobacterial blooms in the metalimnion may sometimes be difficult to discover or even omitted, for example, in lake monitoring in some countries of the European Union, if the lower water column is not considered (Pasztaleniec, 2016; Lenard and Poniewozik, 2022).

Planktothrix rubescens (Gomont) Anagnostidis & Komárek is one of the most studied filamentous cyanobacteria that develop in deep-water layers, often causing DCM (Walsby and Schanz, 2002; Jacquet et al., 2005; Legnani et al., 2005; Yankova et al., 2016; Fernández Castro et al., 2021; Knapp et al., 2021). This species has a group of aerotopes that improve its buoyancy and support its vertical migration in lentic waters (Komárek and Anagnostidis, 2008; D'Alelio et al., 2011). This ability helps avoid high light intensity, light flashes, and vertical mixing of water, to which *P. rubescens* is vulnerable (Davis et al., 2003a; Oberhaus et al., 2007). As a consequence, it produces an additional photosynthetic pigment, phycoerythrin, which belongs to the phycobilins (Schanz, 1986; Davis et al., 2003b; Komárek and Komárková, 2004), which enables photosynthesis in dim light in the presence of blue or green light with high photosynthetic efficiency (Micheletti et al., 1998; Kromkamp et al., 2001; Walsby et al., 2001; Oberhaus et al., 2007). *P. rubescens* is a cyanobacterium devoid of heterocysts and must utilize biogenic compounds dissolved in water (Komárek and Komárková, 2004), which might limit its development. Nevertheless, its allelopathic capacity, manifested by its ability to produce toxins and other secondary metabolites, hampers the development of other primary producers, and it uses the entire pool of available nutrients in the water (Feuillade, 1994; Oberhaus et al., 2008; Salmaso et al., 2013; Kurmayer et al., 2016). Therefore, *P. rubescens* can develop well (Chorus et al., 2011) even with relatively low concentrations of dissolved nutrients in water, because of its ability to utilize organic forms of nitrogen and phosphorus or store nutrients in its cells (Feuillade et al., 1990; Reynolds, 2006; Kurmayer et al., 2016). Hence, its dense blooms in nutrient-poor metalimnion of deep and clear waters are mainly recorded in the mountain, alpine, and pre-alpine lakes (Micheletti et al., 1998; Walsby and Schanz, 2002; Jacquet et al., 2005; Legnani et al., 2005; Ernst et al., 2009; D'Alelio et al., 2011; Dokulil and Teubner, 2012; Hingsamer et al., 2014; Yankova et al., 2016; Copetti et al., 2017; Fernández Castro et al., 2021; Knapp et al., 2021; Carratalà et al., 2023), and less frequently in volcanic lakes (Messineo et al., 2006; Messyasz et al., 2012) and lowland temperate lakes (Wojciechowska and Krupa, 1992; Krupa and Czernaś, 2003; Padisák et al., 2003; Salmaso and Padisák, 2007; Lenard, 2009; Lenard, 2015; Lenard and Ejankowski, 2017; Lenard and Poniewozik, 2022; Kröger et al., 2023) or occasionally in lakes in semiarid Mediterranean climate (Naselli-Flores et al., 2007). Regardless of the location of the lakes, their common characteristics are great depth, the presence of stable stratification during summer providing an adequate light climate and a low-temperature gradient in the metalimnion, and the availability of nutrients. The recent studies from alpine lakes suggest also the positive effect of global warming on the existence and development of overwintering population of *P. rubescens* that constitute the first step for its annual development (Yankova et al., 2017; Knapp et al., 2021; Moiron et al., 2021; Carratalà et al., 2023). In contrast, some reports from temperate lakes suggest that *P. rubescens* blooms may have been influenced by "unusual" event of long lasting periods of ice in the year before the bloom occurred (Padisák et al., 2003).

Based on the permanent blooms of *P. rubescens* in alpine lakes, its mass development in temperate lakes is occasional and often restricted to short periods. Therefore, in this study, we aimed to (1) determine the dynamics of the annual bloom of *P. rubescens* that occurred in three lakes in the temperate zone of eastern Poland, and (2) determine the reason for the appearance of the bloom at different time intervals. We hypothesize that the ice phenology coupled with the presence of severe winter is the main reason for the establishment of the winter inoculum of *P. rubescens* in temperate lakes, which is crucial for its further mass development during the growing season.

2 Materials and methods

The study was carried out in three lakes, Rogóźno (51°22′ N 22°58′ E, 167.7 m a.s.l), Krasne (51°25′ N 22°57′ E, 164.0 m a.s.l), and Piaseczno (51°23′ N, 23°01′ E, 170.6 m a.s.l), located in the Łęczna-Włodawa Plain in eastern Poland, which is a part of the large cross-border Polesie region (Kondracki, 2002). All lakes were deep, dimictic, and mesotrophic. The maximum depth and lake area were 25.4 m and 57.1 ha in Lake Rogoźno, 33.0 m and 75.9 ha in Lake Krasne, and 38.8 m and 84.7 ha in Lake Piaseczno (Harasimiuk et al., 1998). The water level in Lake Piaseczno had highly fluctuated, at 1.68 m in the last 20 years. Moreover, it was estimated to decrease at a rate of *ca.* 1 cm per year, which is connected to a decrease in water resources in the chalk layer of the Lublin Upland and directions of underground outflow changes

from the catchment area of the upper Wieprz River (Michalczyk et al., 2017).

The phytoplankton biomass, chlorophyll-*a* concentration, as well as physical and chemical parameters of water, were studied during the annual appearance of *P. rubescens*, which lasted from January to September of 2006, 2010, and 2014 in lakes Rogóźno, Krasne and Piaseczno, respectively. Water samples for analyses were collected monthly in winter (January–March) and biweekly during the vegetation periods (April–September) from the deepest part of the lakes using a Ruttner-type water sampler (2.0 L capacity). A 3 liters samples of water were always taken from a depth of 0.5 m, from 1 m to 8 m in Lakes Rogóźno and Krasne, or from 1 m to 12 m in Lake Piaseczno, at one-meter intervals. Thereby, we always received nine (in lakes Rogóźno and Krasne) or 13 (in Lake Piaseczno) samples in every sampling date, giving a total of 126, 126, and 182 samples for lakes Rogóźno, Krasne, and Piaseczno, respectively.

In the laboratory, the water samples of 1 to 2 liters were filtered through Whatman GF/C microfiber filter with a particle retention of 1.2 µm. Next, the filters were frozen for further analyses of chlorophyll-*a*, and the filtered water was immediately used for analyses of dissolved nitrogen and phosphorus compounds. Unfiltered samples of water, after mineralization of organic matter, were used for determination of total nitrogen and phosphorus content. The samples were analyzed using spectrophotometric methods to determine the concentrations of chlorophyll-*a* with use of ethanol(Nusch, 1980), inorganic ($P–PO_4$) and total phosphorus (TP) with use of ammonium molybdate, and inorganic ($N–NO_3$ and $N–NH_4$) and total nitrogen (TN), with use of chromotropic acid or Nessler's reagent (Hermanowicz et al., 1999). A 100 mL samples of water for phytoplankton analyses were fixed with Lugol's iodine solution and a formalin–glycerin mixture. The abundance of phytoplankton was determined according to the standard Utermöhl method (Utermöhl, 1958), and the algal biovolume was calculated using the formula described by Hillebrand et al. (1999). The fixed water samples were transferred to a 5–50 mL settling chamber. After sedimentation, the algal abundance was evaluated using an inverted microscope (Zeiss Axiovert 135). Small phytoplankton species on the belts were counted in each chamber, whereas larger forms (filamentous or coccal colonies) were counted at the entire bottom of the chamber. The unit length of 100 µm and a surface of 300 μm^2 were one individual for filamentous and coccal colonies, respectively. Additionally, the samples for taxonomic analyses of phytoplankton were collected using a plankton net (20 µm mesh size) and were left without fixation to observe live specimens under a light microscope (Nikon Eclipse 80i). If possible, all phytoplankton organisms in the samples were identified to the species level. To determine the differences in phytoplankton species composition, the Shannon-Wiener diversity (Shannon and Wiener, 1963) and Pielou's evenness indices (Pielou, 1975) were calculated based on the abundance of the phytoplankton community.

Physical parameters such as water temperature (to calculate the range of the mixing zone, Z_{mix}), water transparency by Secchi disc visibility (SD), and photosynthetic active radiation (PAR), with the use of Li-Cor LI-250A light meter equipped with LI-192SA underwater quantum flat sensor were measured *in situ*. Additionally, the values of PAR were used to calculate the euphotic zone (Z_{eu}) range precisely. The mean air temperature in the study area was calculated using data from a meteorological station in Włodawa (Polesie region) obtained from an online service.[1]

Correlations between abiotic (physical and chemical) and biotic (phytoplankton biomass and chlorophyll-*a* concentration) parameters and *P. rubescens* biomass were evaluated using Spearman's rank correlation test (Sokal and Rohlf, 1995). The same test was used to analyze the relationship between the appearance of *P. rubescens* and air temperature in January–March. All calculations were performed using the PSPP (ver. 2.0.0) package.

3 Results

3.1 The effect of environmental conditions on *Planktothrix rubescens* development in winter

During the last 24 years (2000–2023), in which we monitored three deep lakes of Łęczna-Włodawa Plain, we noticed a certain increase in mean air temperature in winter (Figure 1A). During this time, *P. rubescens* found favorable conditions and started to develop only during the three winter periods of 2006, 2010, and 2014. The climatic conditions during winters with *P. rubescens* were generally similar. However, the bloom always appeared only in one lake each year, in Lake Rogóźno, Krasne or Piaseczno in 2006, 2010, and 2014, respectively. The minimum, maximum, and mean temperatures of air in January in these years were, on average, several degrees lower than those in the years without its appearance, for example, the mean air temperature in January was −7°C, while it was only −1.8°C in the periods without its development (Supplementary Figure S1). A high correlation indicated the strong link between air temperatures in January 2000–2023 and the occurrence of *P. rubescens* in the studied lakes (Spearman's test, $r_s = 0.5$, $p < 0.05$). In contrast, this effect was statistically insignificant, $r_s = -0.18$ and $r_s = 0.01$, $p < 0.05$ in February and March, respectively. Two of the studied winters (2006 and 2010) were extremely cold, with the mean air temperature for January close to −9°C (Figure 1B) and the lowest recorded temperature close to −30°C. Conversely, the mean air temperature in January in the last winter with *P. rubescens* appearance (2014) was *ca.* −4°C (Figure 1B), however, still with the lowest recorded temperature close to −21°C.

The climatic conditions recorded during these three winters affected lake functioning (Table 1). In severe winters (2006 and 2010), the duration of ice cover was almost 4 months, from mid-December to mid-April. The consequence of such long-lasting ice cover was great variability in snow thickness (0–0.18 m) and ice cover (0.11–0.45 m). These conditions caused water column stability and significantly reduced the amount of light (PAR) penetrating the water available to phytoplankton (Table 1). Hence, the snow/ice cover protected the water below from freezing and supported the existence of strong inverse thermal stratification, i.e., in January 2006, during sampling day in Lake Rogóźno with air temperature −22.1°C, the temperature of water below 0.25 m of ice layer was *ca.* 1.4°C and was similar to these noted in March 2010 in Lake Krasne under 0.1 m of snow and 0.35 m of ice (Table 1). The light passing through the thick snow and ice cover (thickness, *ca.*

1 www.tutiempo.net

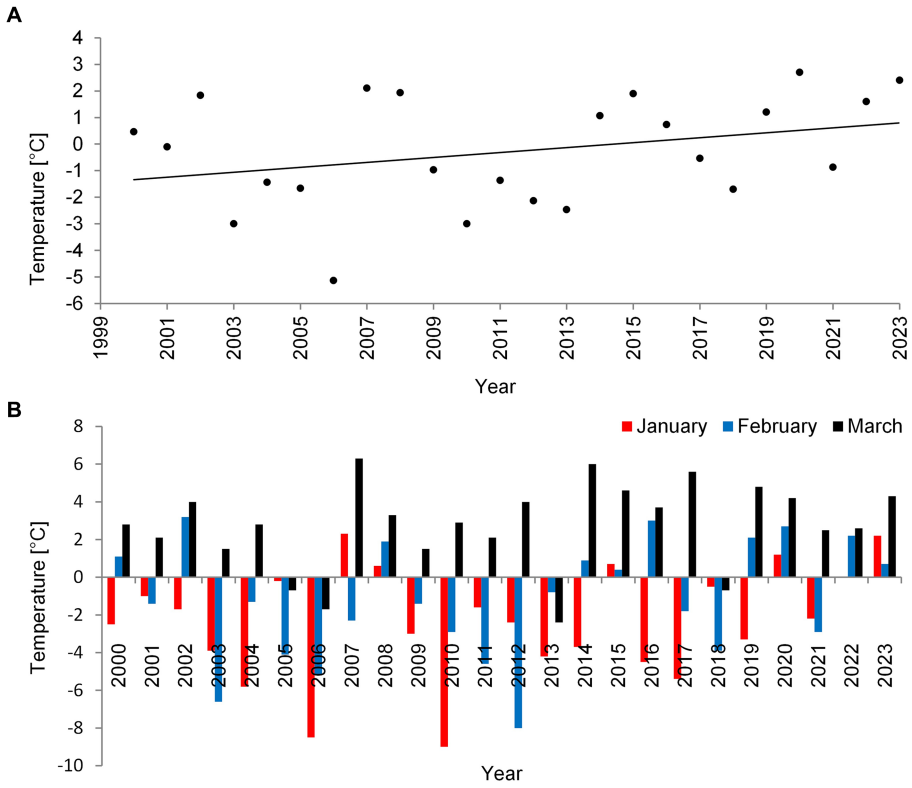

FIGURE 1
Mean air temperature values in °C for the winter (January–March) **(A)** and mean temperature values in °C in a particular month: January, February, and March **(B)** in the Łęczna-Włodawa Plain for 24 years.

TABLE 1 **Physical parameters measured in winter periods in Lake Rogóźno, Krasne, and Piaseczno in 2006, 2010, and 2014, respectively.**

Year	Month	Temperature [°C] in a sampling day		Thickness of		PAR [μmol m^{-2} s^{-1}]		Light absorption by the snow and ice [%]	Approximate duration of ice cover	
		of air	of water beneath the ice	snow[m]	ice [m]	above the ice	beneath the ice		beginning	breakup
2006	J	−22.1	1.4	0	0.25	204.29	43.51	78.7	23rd Dec. 2005	15th Apr. 2006
	F	−12.8	1.0	0.18	0.33	491.63	14.25	97.2		
	M	−16.2	0.9	0.05	0.45	386.21	8.95	97.7		
2010	J	−15.0	1.4	0.07	0.11	222.15	36.32	83.7	15th Dec. 2009	1st Apr. 2010
	F	−12.3	1.8	0.14	0.24	514.89	28.64	94.5		
	M	−6.0	1.6	0.10	0.35	841.14	75.55	91.1		
2014	J	1.8	3.3[a]	-	-	167.82	124.11[a]	26.0 [a]	19th Jan. 2014	14th Mar. 2014
	F	−10.6	1.3	0	0.21[b]	841.62	446.91	46.9		
	M	6.9	5.5[a]	-	-	170.81	108.71[a]	36.7 [a]		

PAR, photosynthetic active radiation; J, F, M, January, February, March. [a]The temperature or light just below the water surface; [b]The presence of "black ice."

0.5 m) often absorbed more than 90% of incoming light (February and March 2006 and 2010, Table 1). In these conditions, the highest mean values of the phytoplankton biomass (2.5–5.5 mg L^{-1}) and chlorophyll-*a* (14–22 μg L^{-1}) were noted mainly at a depth of 0.5 to 2–3 m (Figures 2A–D). In both lakes (Rogóźno and Krasne), high shares in the total phytoplankton biomass had mixotrophic species belonging to cryptomonads – *Cryptomonas marssonii* Skuja and *Cryptomonas curvata* Ehrenberg; however, the shares of *P. rubescens* in Lake Rogóźno in 2006 were low, while its shares in Lake Krasne in 2010 often exceeded 60% in the total phytoplankton biomass. Nevertheless, high light absorption fostered the development of *P. rubescens* under thick snow/ice cover by creating stable, dim light conditions in the water (Figures 2B,D). Simultanously, the vertical distribution of *P. rubescens* biomass was the highest in both lakes (Rogóźno and Krasne) at a depth

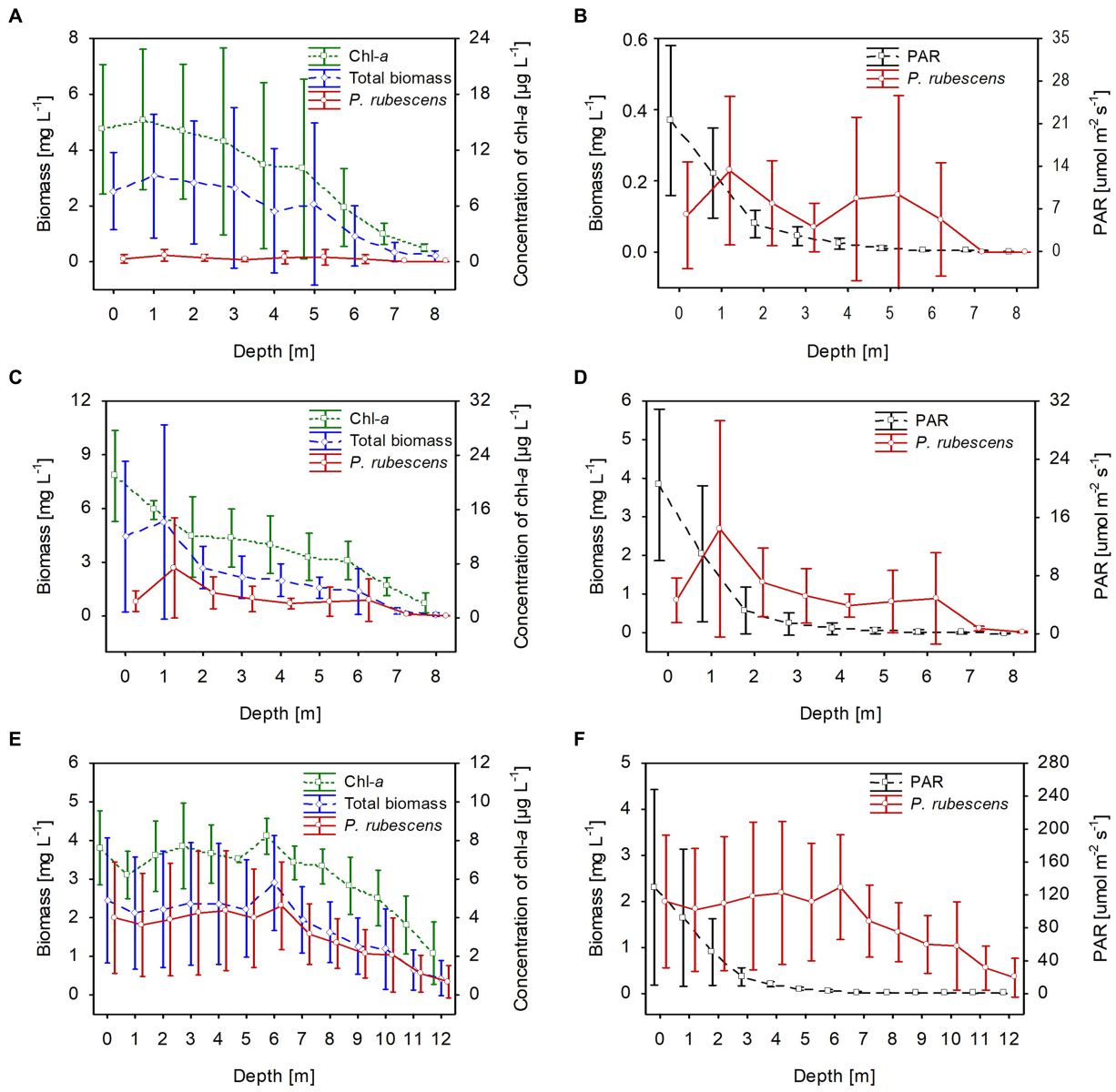

FIGURE 2
Vertical distribution of mean values (±standard deviations) of selected biological and physical parameters of water during winter in Lake Rogóźno in 2006 **(A,B)**; in Lake Krasne in 2010 **(C,D)**; in Lake Piaseczno in 2014 **(E,F)**. Chl-a, concentration of chlorophyll-a; PAR, photosynthetic active radiation; total biomass, the total phytoplankton biomass.

of 1 m, and decreased sharply with increasing depth (Figures 3A,B). However, in some cases, such as in February 2014 in Lake Piaseczno, the lack of snow cover and the presence of a thick layer (0.21 m) of so-called "black ice" devoid of air bubbles and almost perfectly transparent allowed more than 50% of the light reaching the surface to penetrate below the ice cover (Table 1). Under this highly transparent ice, the vertical distribution of *P. rubescens* biomass was almost homogenous at a depth of 0.5–6 m (*ca.* 3 mg L^{-1}, Figure 3C). This trend in its biomass distribution in the gradient of light was also maintained during mixing periods in winter (samples taken at 11th January and 24th March 2014), which resulted in higher mean values of chlorophyll-*a* (*ca.* 7 µg L^{-1}) and phytoplankton biomass (*ca.* 2.5 mg L^{-1}) at a depth of 0.5–6 m than in the deeper water column, 7–12 m (Figures 2E,F). Even if more than 60% of the light penetrated the water during mixing time, its amount just under the water surface was still minor (the values of PAR slightly above 100 µmol m^{-2} s^{-1}, Table 1) that still supported homogenous distribution of *P. rubescens* biomass to the depth of 6 m (Figure 3C).

The dissolved and total fractions of biogenic compounds (nitrogen and phosphorus) corresponded to the phytoplankton biomass distribution in all studied lakes. The mean values of dissolved nitrogen ($N\text{-}NH_4$ and $N\text{-}NO_3$) and phosphorus ($P\text{-}PO_4$) were generally homogeneously distributed in the water column; however, there was a slight increase at greater depths, at which the phytoplankton biomass was lower (Figure 4). The mean values of dissolved fractions varied from 0.05 to 0.3 mg L^{-1}, from 0.8 to 1.0 and from 0.008 to 0.017 for $N\text{-}NH_4$, $N\text{-}NO_3$ and $P\text{-}PO_4$, respectively. Contrarily, total nitrogen (TN) values were slightly higher in the upper water layers with high

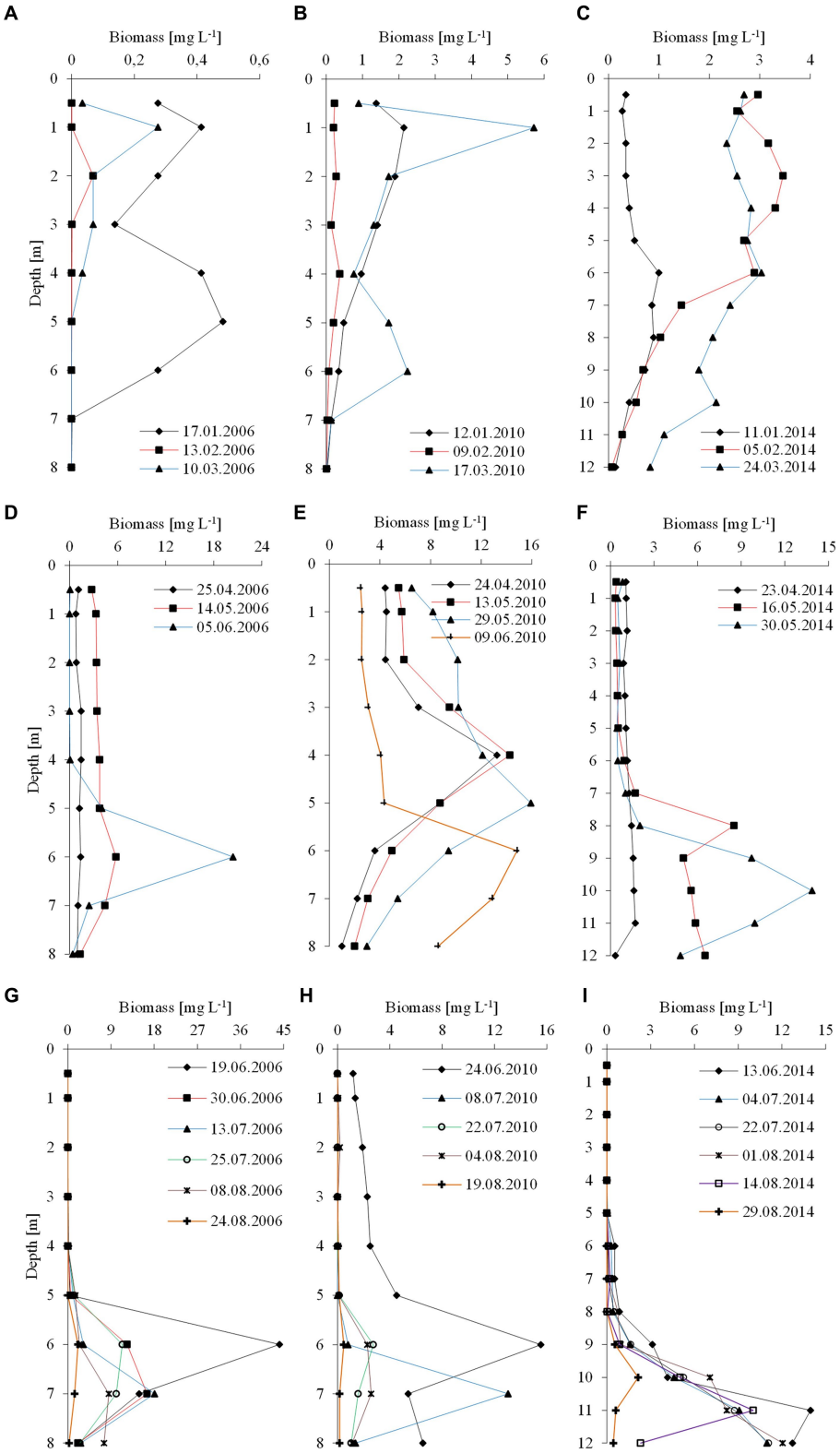

FIGURE 3
Vertical distribution of the biomass of *P. rubescens* during winter season (upper panel), spring season (middle panel) and summer season (lower panel) in the three studied lakes: **(A,D,G)** Rogóźno in 2006; **(B,E,H)** Krasne in 2010; and **(C,F,I)** Piaseczno in 2014.

phytoplankton biomass. They varied from 3.2 to 3.55 mg L^{-1}, from 2.0 to 2.6 mg L^{-1}, and from 2.0 to 2.4 mg L^{-1}, in lakes Rogóźno, Krasne, and Piaseczno, respectively (Figures 4A,C,E). A similar trend was noted with the values of total phosphorus (TP), with mean values in the range of 0.03–0.04 mg L^{-1} in lakes Rogóźno and Krasne and 0.04–0.06 mg L^{-1} in Lake Piaseczno (Figures 4B,D,F).

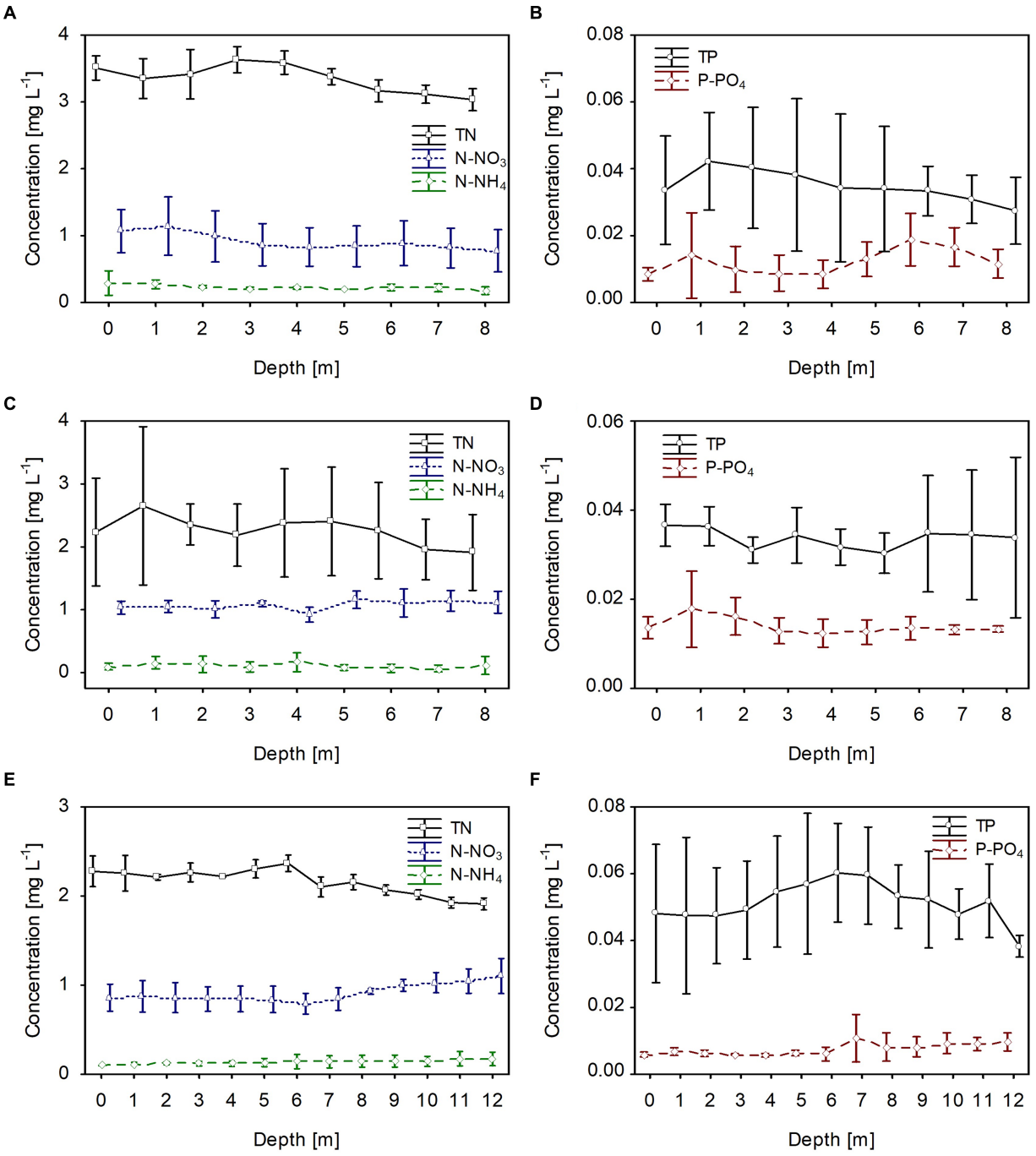

FIGURE 4
Vertical distribution of mean values (±standard deviations) of selected chemical parameters of water during winter in Lake Rogóźno in 2006 **(A,B)**; in Lake Krasne in 2010 **(C,D)**; in Lake Piaseczno in 2014 **(E,F)**. $N\text{-}NH_4$, concentration of ammonium nitrogen; $N\text{-}NO_3$, concentration of nitrate nitrogen; TN, concentration of total nitrogen; $P\text{-}PO_4$, concentration of phosphate phosphorus; TP, concentration of total phosphorus.

3.2 *Planktothrix rubescens* development in the vegetative season before the onset of thermal stratification

The appearance of *P. rubescens* in winter predicted its mass development in the months following a given year. The spring season, lasting from the end of March (30th March) to early June (9th June), was the time of permanent water mixing in the studied lakes and the first step in the onset of thermal stratification. During permanent water mixing (23rd–25th April of the individual years), the biomass of *P. rubescens* was generally evenly distributed throughout the water column in lakes Rogóźno and Piaseczno, except of Lake Krasne, in which the peak of biomass was stated on the depth of 4 m (Figures 3D–F). However, over time, the temperature of the upper water layers increased, leading to the slow establishment of thermal stratification, and its biomass increased significantly in the deeper

water layers of all lakes. These increases were particularly noticeable at the end of spring periods (29th May–9th June) when the highest values of *P. rubescens* biomass (often above 10 mg L^{-1}) were found at the depths of 6 m, 5–6 m, and 8–12 m in Lake Rogóźno in 2006, Lake Krasne in 2010 and Lake Piaseczno in 2014, respectively (Figures 3D–F).

3.3 *Planktothrix rubescens* development during summer stratification

Stable thermal stratification persisted in the studied lakes from 13th June to August. The metalimnion layer reached 4–8 m in lakes Rogóźno and Krasne and 7–12 m in Lake Piaseczno. The total biomass of phytoplankton in the metalimnion, in which the light intensities were extremely low (mean values of PAR mainly below 40 µmol m^{-2} s^{-1} that constituted less than 3% of surface light intensities), was almost completely dominated by *P. rubescens*. In contrast, its biomass in the epilimnion was negligible (Figure 5). The mean values of *P. rubescens* biomass and the concentration of chlorophyll-*a* were generally the highest in the middle of the metalimnion layer, giving deep chlorophyll maximum, i.e., in Lake Rogóźno at a depth of 6 m (13.8 mg L^{-1} and 44.8 µg L^{-1}), in Lake Krasne at a depth of 7 m (3.9 mg L^{-1} and 20.4 µg L^{-1}), and in Lake Piaseczno at a depth of 11 m (8.5 mg L^{-1} and 19.5 µg L^{-1}, Figures 5A,C,E). The share of *P. rubescens* often exceeded 80% in the total biomass of phytoplankton in lakes Rogóźno and Piaseczno, while in Lake Krasne, this species co-occurred with the biomass of other filamentous cyanobacteria, i.e., *Limnothrix planctonica* (Woloszynska) Meffert and *Planktolyngbya limnetica* (Lemmermann) Komarkova-Legnerova & Cronberg that explains its lower, still above 50% shares in the total biomass of phytoplankton in the metalimnion (Figure 5C). Additionally, Lake Krasne was the only lake in the epilimnion of which higher values of total phytoplankton biomass (mean values *ca.* 4 mg L^{-1}) were found. These water layers were dominated by the filamentous cyanobacteria *Aphanizomenon gracile* Lemmermann and the green alga *Closterium acutum* var. *variabile* (Lemmermann) W. Krieger.

In all lakes, changes in the biological parameters were reflected in the general trend of the mean values of the dissolved and total fractions of biogenic compounds. The mean concentrations of the dissolved fractions of nitrogen (N-NH_4 and N-NO_3) and phosphorus (P-PO_4) decreased, whereas the total fraction (TN and TP) increased with the growth of *P. rubescens* in the metalimnion of the studied lakes (Figures 5, 6). The mean concentration of N-NH_4 of *ca.* 0.25 mg L^{-1} was similar in all lakes. Conversely, the mean concentration of N-NO_3 varied between lakes and was about 0.6 mg L^{-1}, 0.8 mg L^{-1}, and 1.4 mg L^{-1} in lakes Rogóźno, Piaseczno and Krasne, respectively (Figures 6A,C,E). The mean values of P-PO_4 differed slightly between lakes and were approximately 0.007–0.012 mg L^{-1} (Figures 6B,D,F). The highest mean values of TN in the metalimnion were noted in lakes Rogóźno in 2006 and Piaseczno in 2014 (*ca.* 3.0 mg L^{-1}), whereas the lowest in Lake Krasne in 2010 (*ca.* 2.5 mg L^{-1}, Figures 6A,C,E). The mean values of TP sharply increased in the metalimnion and reached the values of *ca.* 0.08 mg L^{-1} in lakes Krasne and Piaseczno, while in Lake Rogóźno were almost two times higher and reached *ca.* 0.15 mg L^{-1} (Figures 6B,D,F).

A clear trend in the vertical distribution of *P. rubescens* biomass was observed in all lakes. In general, the upper water layers from 0 to 5 m in lakes Rogóźno and Krasne or from 0 to 8 m in Lake Piaseczno were almost devoid or only with a small share of the filaments of *P. rubescens*. Contrarily, the water layers in metalimnion were dominated by its biomass (Figures 3G–I). The highest values of biomass of *P. rubescens* were always recorded in mid-June (13th–24th June of the individual years) at the beginning of stable stratification periods, i.e., *ca.* 45 mg L^{-1} at a depth of 6 m in Lake Rogóźno (the highest value from all measurements that coupled with the highest values of chlorophyll-*a*, *ca.* 91 µg L^{-1}) or *ca.* 16 mg L^{-1} at a depth of 6 m in Lake Krasne and *ca.* 14 mg L^{-1} at a depth of 11 m in Lake Piaseczno (Figures 3G–I). In light overexposure, the population of *P. rubescens* in all the studied lakes changed its position to actively migrate down or up the metalimnion layer. Hence, the highest biomass values were often found at different depths, even at biweekly intervals (Figures 3G–I).

3.4 The end of *Planktothrix rubescens* bloom

The development of *P. rubescens* in all studied lakes just suddenly ended in September when the thermal stratification started to be weaker and the mixing conditions reached the bottom of metalimnion – 8 m in lakes Rogóźno and Krasne and 12 m in Lake Piaseczno. The total biomass of phytoplankton significantly decreased and varied from 1.2 to 6.1 mg L^{-1}, whereas the niche previously occupied by *P. rubescens* was dominated by the new species. In Lake Rogóźno, as in the winter season, by the cryptomonads *C. marssonii* and *C. curvata,* and in the other two lakes by filamentous cyanobacteria – in Lake Krasne by *Planktolyngbya limnetica*, which was already present in the metalimnion of this lake in August, and in Lake Piaseczno by *Limnothrix planctonica* (Woloszynska) Meffert and *Aphanizomenon gracile* Lemmermann.

3.5 *Planktothrix rubescens* biomass concerning biological and physicochemical parameters during its annual occurrences

The annual appearance of *P. rubescens* in the studied lakes was directly related to thermal and light conditions changes. In general, the first appearance of *P. rubescens* with different values of biomass were recorded in winter (January–March) just below the ice cover and the highest values of its biomass were noted in summer (June–August) in the metalimnion layer (Figure 7). During spring periods (23rd April–9th June), water transparency measured with Secchi Disk (SD) in lakes Rogóźno and Krasne was only 1–2 m, which corresponded to the smaller range of the euphotic zone (4–5.5 m). Such conditions affected the migration of *P. rubescens* into the upper 4–5 m water layers, which were susceptible to mixing (Figures 7A,B). In Lake Piaseczno, the SD values in spring were much higher (4–5.5 m), which influenced the greater range of the euphotic zone (8–11 m) and thus the presence of *P. rubescens* in deeper water layers outside the mixing zone (Figure 7C). The ecological niche in the metalimnion, once occupied in spring, remained a habitat for the development of *P. rubescens* throughout the summer stratification period, in which the highest values of biomass of this cyanobacterium were found at or below the euphotic zone at very low light intensities,

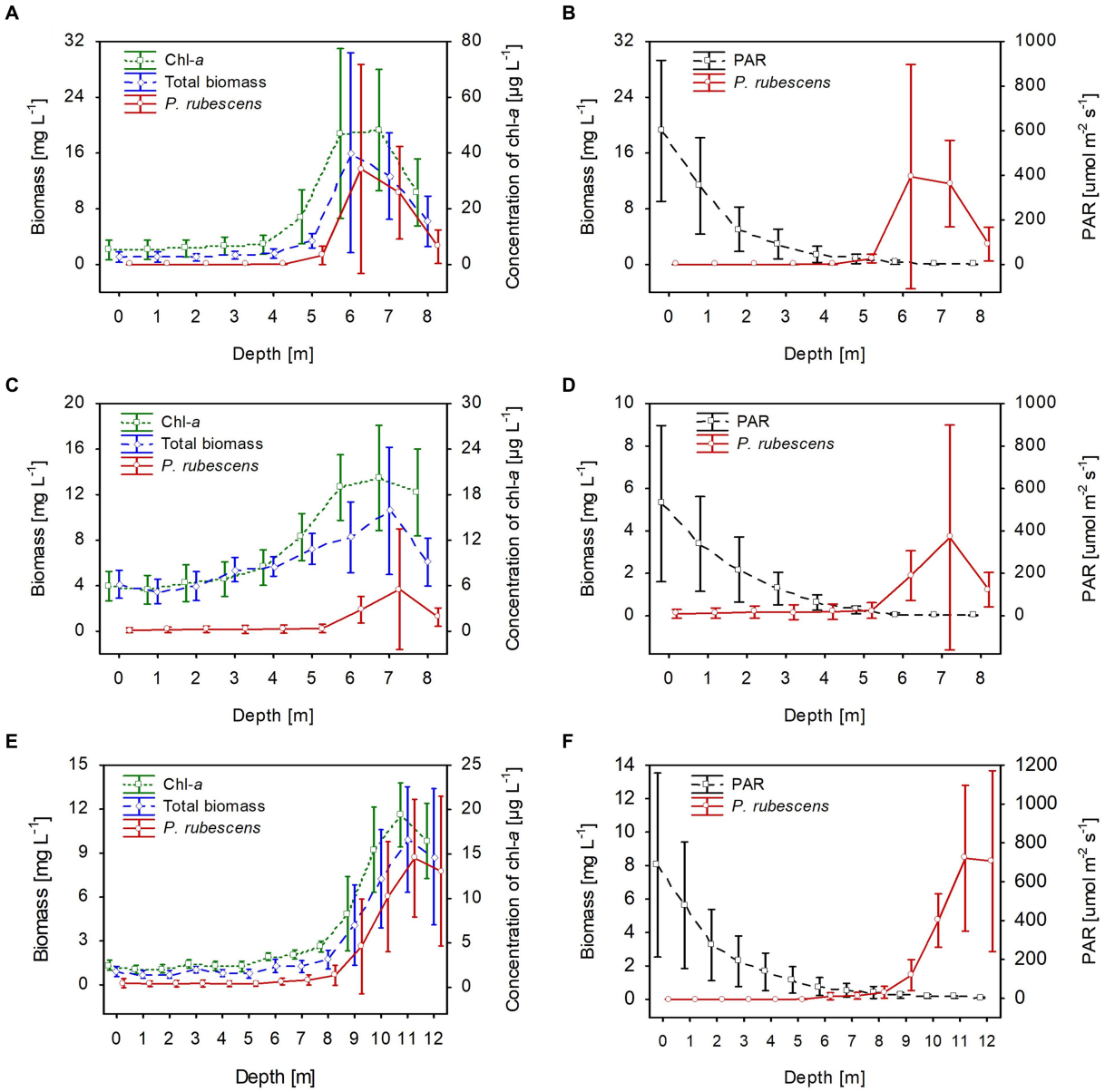

FIGURE 5
Vertical distribution of mean values (±standard deviations) of selected biological and physical parameters of water during summer thermal stratification in Lake Rogóźno in 2006 **(A,B)**; in Lake Krasne in 2010 **(C,D)**; in Lake Piaseczno in 2014 **(E,F)**. Chl-a, concentration of chlorophyll-a; PAR, photosynthetic active radiation; total biomass, the total phytoplankton biomass.

PAR 0.6–27 µmol m^{-2} s^{-1} that constituted 0.05–1% of surface light intensities. This situation persisted until the end of August (Figures 3G–I). During the beginning of September, the metalimnetic bloom of *P. rubescens* underwent a complete breakdown, which corresponded to a disruption in the stability of thermal stratification caused by an increase in the range of the mixing zone in all lakes (Figure 7). Nevertheless, its annual development, lasting 8 months, had a significant impact on phytoplankton composition; when the biomass of *P. rubescens* reached *ca.* 2.5, 3.0, and 1.0 mg L^{-1} in Lakes Rogóźno, Krasne, and Piaseczno, respectively, its dominance in the total biomass of phytoplankton was at a level higher than 60% (Supplementary Figure S2). The high proportion of *P. rubescens* in the total biomass of phytoplankton affected the decrease in species richness and biodiversity (Shannon-Wiener index, H′), as well as evenness (Pielou's index), which were within a similar range in all lakes. The values of H′ were higher in the epilimnion (1.5–2.7) than those in the metalimnion (0.7–1.5). Similarly, the evenness index and species richness ranged from 0.5–0.7 and 19–40 and 0.2–0.6 and 8–30 in the epilimnion and metalimnion, respectively. Hence, in all the studied lakes, negative Spearman correlations at a high level of significance ($p < 0.001$) were observed between *P. rubescens* biomass and these parameters (Table 2). Therefore, the biomass of *P. rubescens* was strongly positively correlated with biological factors (total biomass of phytoplankton and concentration of chlorophyll-*a*) and negatively correlated ($p < 0.001$) with the measured values of physical

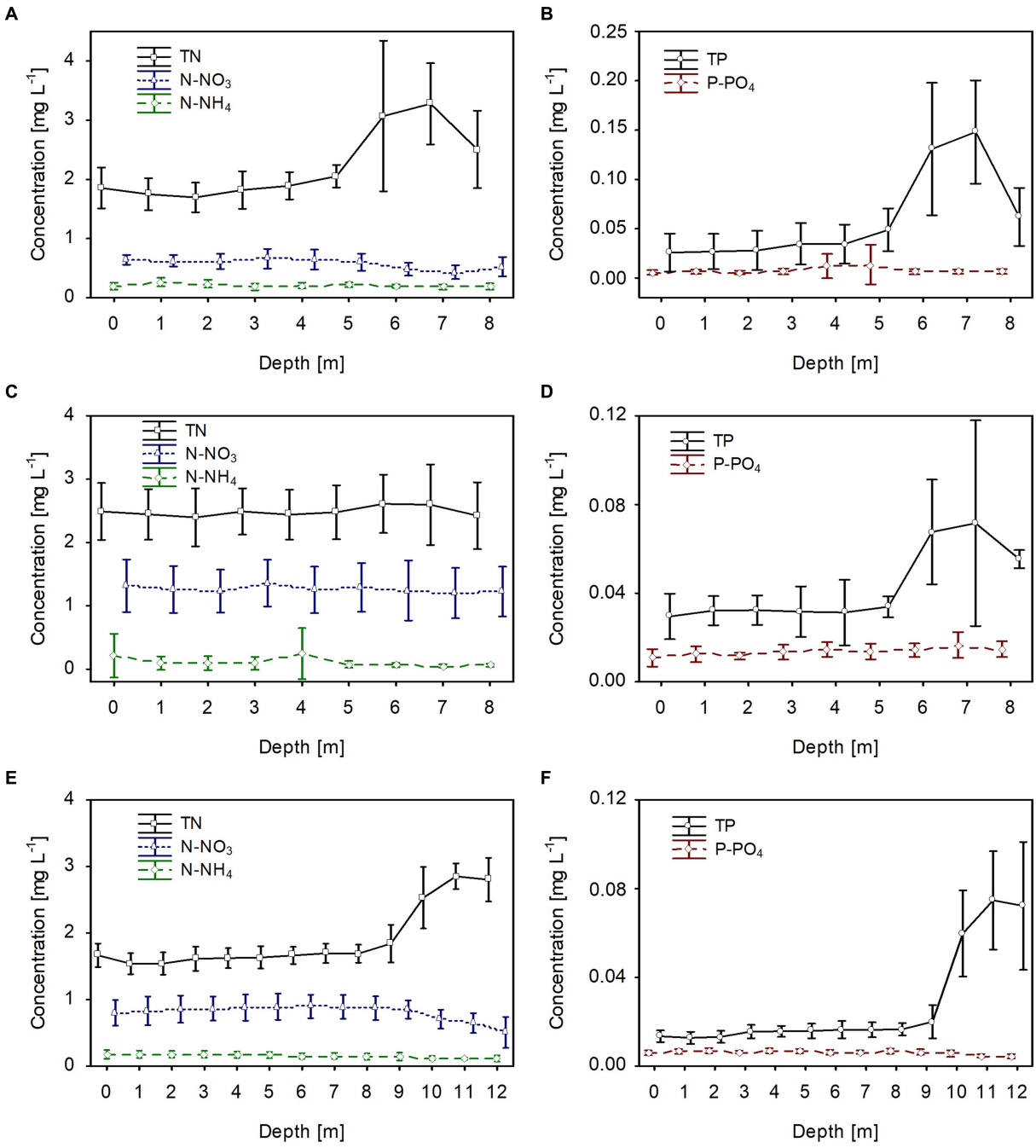

FIGURE 6
Vertical distribution of mean values (±standard deviations) of selected chemical parameters of water during summer thermal stratification in Lake Rogóźno in 2006 **(A,B)**; in Lake Krasne in 2010 **(C,D)** in Lake Piaseczno in 2014 **(E,F)**. $N\text{-}NH_4$, concentration of ammonium nitrogen; $N\text{-}NO_3$, concentration of nitrate nitrogen; TN, concentration of total nitrogen; $P\text{-}PO_4$, concentration of phosphate phosphorus; TP, concentration of total phosphorus.

factors, such as light intensity (PAR) and water temperature (Table 2). The biomass of *P. rubescens* was also correlated with the chemical parameters. In general, low negative correlations, at a significance level of $p < 0.05$, were found with the dissolved fractions of nitrogen ($N\text{-}NH_4$ and $N\text{-}NO_3$) and phosphorus ($P\text{-}PO_4$), whereas the values of the total fractions (TN and TP) correlated positively ($p < 0.001$) with biomass. Only in Lake Krasne was the lack of correlation with TN and $P\text{-}PO_4$ noted (Table 2).

4 Discussion

Most climate warming scenarios indicate an increasing temperature trend, which is particularly significant during winter; this is directly related to the presence or absence of snow/ice cover and the consequent disruption of thermal water conditions during winter periods (Samuelsson, 2010; Dokulil, 2016; Woolway et al., 2020). The deep lakes of temperate zones, where the increase in surface water

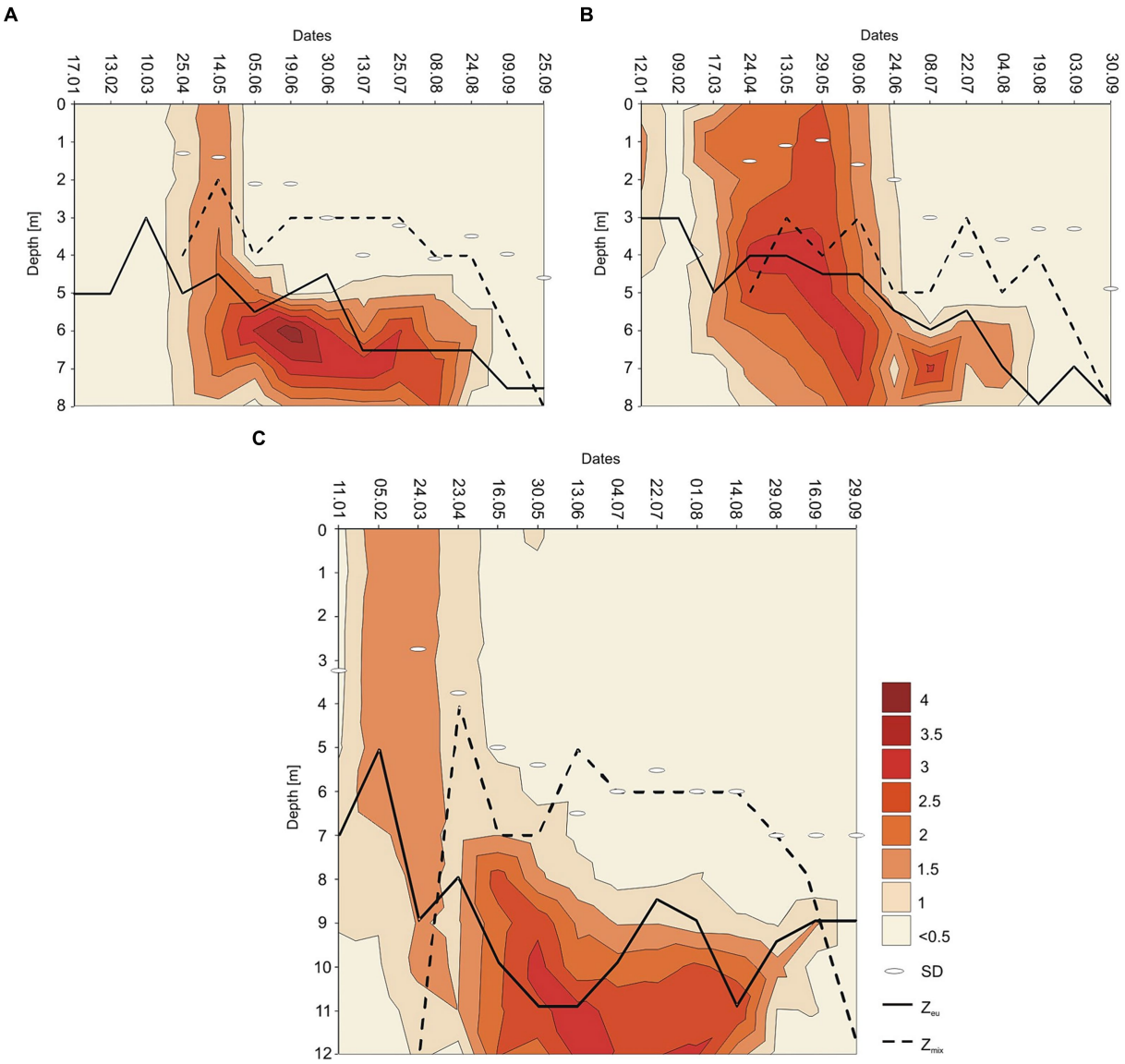

FIGURE 7
Contour plot of the annual distribution of the *Planktothrix rubescens* biomass as ln (x + 1) with euphotic depth (Z_{eu} in m, continuous line), mixing depth (Z_{mix} in m, dashed line), and Sechi Disk visibility (SD) in Lake Rogóźno in 2006 **(A)**; in Lake Krasne in 2010 **(B)**; in Lake Piaseczno in 2014 **(C)**.

temperature during winter is the highest, are particularly susceptible (Dokulil et al., 2010). This trend was also observed in the lakes studied in eastern Poland under the influence of a temperate climate (Figure 1). Water warming directly impacts the functioning of aquatic organisms, especially small primary producers. One such species is *P. rubescens*, whose blooms are frequently recorded in various European lakes (Jacquet et al., 2005; Ernst et al., 2009; Dokulil and Teubner, 2012; Posch et al., 2012; Copetti et al., 2017). However, its response to changes and development during winter can vary depending on the location and characteristics of the lake. Thus, the same trend in climate change can generate differences in the appearance and pattern of *P. rubescens* development, especially during winter, which are important for establishing a novel population; this is particularly evident in alpine lakes where blooms of this cyanobacterium have been recorded permanently for many decades, with some data dating back to the 19th century (Walsby and Schanz, 2002; Jacquet et al., 2005; Legnani et al., 2005; Ernst et al., 2009; D'Alelio et al., 2011; Dokulil and Teubner, 2012; Hingsamer et al., 2014; Yankova et al., 2016; Copetti et al., 2017; Fernández Castro et al., 2021; Knapp et al., 2021; Carratalà et al., 2023). Recent studies of alpine lakes have indicated that warming water masses have multidirectional effects on *P. rubescens* bloom dynamics.

Moreover, a paradox related to the positive impact of climate warming has been found: a small population of *P. rubescens* after periods of warmer winters produces a more intense bloom during periods of thermal stratification than a large population after periods of cold winters (Knapp et al., 2021). Temperate lakes in the lowlands appear to respond differently to such changes, as evidenced by reports of occasional blooms of *P. rubescens*, often recorded at different time intervals (Krupa and Czernaś, 2003; Padisák et al., 2003; Salmaso and Padisák, 2007; Kröger et al., 2023). Some reports suggest that *P. rubescens* blooms in winter may have been influenced by prolonged periods of ice

TABLE 2 Spearman rank correlation matrix (r_s) of the biomass of *Planktothrix rubescens* and selected environmental parameters (bold numerals for $p < 0.001$; bold italic numerals for $p < 0.05$).

Parameters	Lake Rogóźno ($n = 126$)	Lake Krasne ($n = 126$)	Lake Piaseczno ($n = 182$)
Depth	**0.36**	0.10	**0.47**
Total nitrogen (TN)	**0.57**	−0.07	**0.29**
Ammonium nitrogen (N-NH_4)	***−0.28***	***−0.25***	**−0.31**
Nitrate nitrogen (N-NO_3)	***−0.26***	***−0.21***	**−0.43**
Phosphate phosphorus (P-PO_4)	**−0.34**	0.08	**−0.32**
Total phosphorus (TP)	**0.36**	**0.71**	**0.72**
Photosynthetic Active Radiation (PAR)	**−0.31**	**−0.28**	**−0.54**
Temperature of water	**−0.36**	**−0.27**	**−0.70**
Concentration of chlorophyll-*a*	**0.86**	**0.70**	**0.76**
Total biomass of phytoplankton	**0.87**	**0.62**	**0.72**
Shannon-Wiener diverity index	**−0.58**	**−0.36**	**−0.72**
Pielou evenness index	**−0.56**	**−0.42**	**−0.64**
Number of species	**−0.37**	***−0.21***	**−0.62**

in the year before the bloom occurred (Padisák et al., 2003). Our study extends this conjecture to a certain extent. During the 24 years considered (2000–2023), *P. rubescens* was found only three times, and its appearance was associated with extremely low temperatures in January. In eastern Poland, such conditions are associated with Arctic or polar continental air masses heralding prolonged periods of ice cover, ensuring the thermal stability of lake waters during winter. The blooms discussed in this study, separated by 4-year intervals, occurred under such conditions and began with low intensity during winter periods; the lowest values of *P. rubescens* biomass (below 0.6 mg L^{-1}) were found in Lake Rogóźno in 2006, while much higher values (often above 2 mg L^{-1}, Figures 3A–C) were found in Lakes Krasne and Piaseczno. In deep alpine lakes, climate warming has a limiting effect on the mixing depth, significantly reducing the internal release of biogenic compounds from the hypolimnetic layers and decreasing their availability in the upper water layers. This process limits the development of eukaryotic phytoplankton, such as diatoms and cryptomonads, and increases the development of prokaryotic species, such as *P. rubescens* (Yankova et al., 2017; Knapp et al., 2021). This effect was not observed in the temperate lakes studied, in which an even distribution of nutrients was observed throughout the water column in winter. This is probably influenced by the almost 10-fold lower maximum depth of the studied lakes (25–39 m) compared to that of the Alps, which allows the release of internal nutrients deposited in the bottom sediments during the autumn mixing of waters preceding the occurrence of ice periods. Thus, our observations suggest that winter appearances of this cyanobacterium in temperate lakes, unlike those in alpine lakes, are related to extremely cold winter coupled with long-lasting periods of ice cover. Owing to their occasional character and relatively shallow depth, blooms are not limited by the availability of nutrients.

This study also showed that physical factors affected by ice phenology, such as thermal and light conditions, are important for the development of the winter population of *P. rubescens*. Under the thick snow/ice cover, specific, albeit stable conditions of dim light climate occurred, which combined with reverse thermal stratification to support the vertical migration of *P. rubescens*, with highest values of biomass were often found just under the ice cover in lakes Rogóźno and Krasne in 2006 and 2010, respectively. The bloom recorded in Lake Piaseczno in the winter of 2014 occurred during a warmer period, and the biomass of *P. rubescens* was often evenly distributed in the 0–6 m water layer. Nevertheless, polar continental air masses were also recorded during this winter, resulting in an ice cover that lasted almost 2 months. In addition, even if no ice cover was present in winter, the light conditions were moderate because of the long-lasting cloudy and rainy weather, which effectively hindered solar radiation and indirectly protected the biomass of *P. rubescens* against photoinhibition. Since 2014, all three lakes have been monitored yearly during winter and summer. Still, the presence of *P. rubescens*, which we associate with unusually warm winters, has not been recorded once. The paradox presented in alpine lakes by Knapp et al. (2021) related to the more intensive development of *P. rubescens* in the metalimnion in summer after a period of weaker development of its population during warmer winters in a sense also occurred in the studied temperate lakes. However, this is not regarding the type of winter (warm or cold) but of the appearance of a much more intense bloom of *P. rubescens* during summer stratification after a winter inoculum with very low biomass, which occurred in Lake Rogóźno in 2006 and did not occur in the other lakes (Figures 3A–C,G). Low biomass persisted in this lake during the spring mixing period (Figure 3D); however, in late spring (9th June), its population visibly increased in the metalimnion after the establishment of thermal stratification of the waters. The highest value of *P. rubescens* biomass (44.8 mg L^{-1}) was recorded 2 weeks later at a depth of 6 m. Similar dynamics in population development, although with lower biomass values, have also been observed in other temperate lakes (Krasne and Piaseczno). This bloom scheme reflects the three phases of the annual development of *P. rubescens* in the alpine Lake Mondesee (Dokulil and Teubner, 2012). From vertical migration to the metalimnion, *P. rubescens* remained until the end of the thermal stratification period (end of August), maintaining its biomass at approximately 15 mg L^{-1}. Thus, we conclude that the presence of *P. rubescens* in temperate lakes during the winter period, regardless of its biomass, is a guarantee of its bloom during the summer period, often with high intensity.

Therefore, monitoring of deep temperate lakes where *P. rubescens* has previously appeared should take place during winter periods, as

this provides an opportunity to plan future research during the summer stratification period. Based on the available literature, only one lake, Piaseczno, had a previous occurrence of *P. rubescens*, which was more than 20 years earlier (1986–1996); its appearance was of low intensity and it was occasionally found (every few years). In addition, the studies were carried out only during the growing season (spring-autumn) and at large time intervals (one sample representative of the season), thus unintentionally ignoring the important role of ice phenology in creating the inoculum for further annual development of *P. rubescens* populations (Krupa and Czernaś, 2003). Only once, in 1989, a bloom of this cyanobacterium was reported in Lake Piaseczno and was linked with the increase in nutrients level; however, the study focused mostly on its effect on the qualitative and quantitative structure of phytoplankton. Therefore, it was concluded that the presence of this species was a symptom of the eutrophication of Lake Piaseczno (Wojciechowska and Krupa, 1992; Krupa and Czernaś, 2003). However, after the blooms disappeared, the lake returned to a mesotrophic state.

The summer period in the studied lakes, along with stable thermal stratification, presented a typical course of *P. rubescens* bloom dynamics in various European lakes (Micheletti et al., 1998; Walsby and Schanz, 2002; Jacquet et al., 2005; Legnani et al., 2005; Dokulil and Teubner, 2012; Posch et al., 2012; Yankova et al., 2016; Fernández Castro et al., 2021; Knapp et al., 2021; Moiron et al., 2021; Carratalà et al., 2023). Notably, different depths at which this species developed were recorded in the studied lakes during summer. The major reason was the location and thickness of the metalimnion layer, which was 4–8 m in lakes Rogóźno and Krasne and 7–12 m in Lake Piaseczno. The occurrence of the bloom of *P. rubescens* on higher depths in Lake Piaseczno was also influenced by the high transparency of the waters (5.5–6.5 m) and the large range of the euphotic zone (8.5–11 m), which were much deeper compared to the other lakes. Nevertheless, a similar pattern of vertical migration of this species into the metalimnion layer and the movement of its populations within this layer in response to changing light conditions has been recorded in all lakes during summer, which is called light-driven buoyancy regulation (Micheletti et al., 1998; Dokulil and Teubner, 2012; Knapp et al., 2021). This is mainly due to the need to avoid mixing of the water and too high light intensity, which was particularly noticeable at the point of maximum bloom recorded in lakes Rogóźno and Krasne at depths of 6–7 m and in the much more transparent Lake Piaseczno almost twice as deep at a depth of 11 m (Figures 3G–I, 7). The highest biomass of *P. rubescens* in the metalimnion of studied lakes occurred at very low values of photosynthetically active radiation (PAR, 0.6–27.1 $\mu mol\, m^{-2}\, s^{-1}$) and in low values of water temperature (8–12°C), which was confirmed by strong negative correlation with these parameters (Table 2). Such conditions were often measured below the euphotic zone in the dim light layer, close to 0.1% of light intensity, and are similar to the values noted during summer periods in alpine lakes by other authors (Micheletti et al., 1998; Walsby and Schanz, 2002; Jacquet et al., 2005; Dokulil and Teubner, 2012; Fernández Castro et al., 2021; Knapp et al., 2021; Carratalà et al., 2023); this suggests the existence of a certain summer bloom pattern independent of the type of lake and climatic zone in which it is located.

The values of dim light climate in the studied lakes, in which *P. rubescens* developed well in the summer periods, were comparable to those noted under thick snow/ice cover during severe winters. The role of dim light was also confirmed in a laboratory experiment that demonstrated the positive effect of low quantities of green light and the strong negative effects of high intensities of white light on the development of *P. rubescens* (Oberhaus et al., 2007). However, the dim light climate in winter is used to establish an inoculum for the population so that later in summer, similar light conditions represent the optimum conditions for an intensive metalimnetic bloom. In addition the bloom of *P. rubescens* was associated with almost complete dominance in the phytoplankton, often reaching 60–90%. Similar dominance values were also found in Alpine Lake Pusiano (Legnani et al., 2005). The high proportion of *P. rubescens* in the phytoplankton of the studied lakes was most likely due to the allelopathic effect of this species, which had a limiting effect on the total biomass of phytoplankton, not only in the metalimnion but also in the upper water layers (Kurmayer et al., 2016). This activity ensured an optimal light climate for blooms in the metalimnion. The allelopathic interactions of this cyanobacterium are related to the secretion of toxins (microcystins) and secondary metabolites, described previously in mixed culture experiments (Oberhaus et al., 2008). In this study, the allelopathic effect of *P. rubescens* populations was also associated with a significant decrease in the biodiversity and species richness of the phytoplankton community, as confirmed by Spearman correlations (Table 2). Similar decreases in phytoplankton biodiversity indices were found earlier in the bloom layer of Lake Pusiano (Legnani et al., 2005). Recent reports from Alpine Lake Geneva also suggest a limiting effect of the biomass of *P. rubescens* on the taxonomic and functional diversity of bacterioplankton (Carratalà et al., 2023).

Chemical factors, especially the dissolved nitrogen and phosphorus fractions, influenced the development of *P. rubescens* in the temperate lakes studied, as confirmed by Spearman's correlations (Table 2). Particularly in summer, decreases in dissolved nutrients ($N\text{-}NO_3$, $N\text{-}NH_4$ and $P\text{-}PO_4$) were found in the bloom layer in lakes Rogóźno and Piaseczno, which was not so evident in lake Krasne (Figure 6). This may be due to the higher proportion of other cyanobacterial species, *Limnothrix planctonica* and *Planktolyngbya limnetica* in the metalimnion layer of this lake. However, during annual blooms, the pool of available nutrients did not limit the development of the *P. rubescens* population. We attribute this to the high concentrations of dissolved nutrients recorded in winter and in the upper water layers of the studied lakes during summer. Similarly, high concentrations of $P\text{-}PO_4$ have been recorded in alpine lakes during the winter (Legnani et al., 2005). There are also mechanisms by which *P. rubescens* can utilize, in addition to the nitrate fraction, the ammonium fraction of nitrogen, which increases the pool of available nitrogen compounds and gives it a competitive advantage over other algae (Köster and Jüttner, 1999). Furthermore, the low concentrations of phosphate ($P\text{-}PO_4$) available in the water of the studied lakes (4–18 ug L^{-1}) probably did not limit the development of *P. rubescens*. Similar values of $P\text{-}PO_4$ (0–10 ug L^{-1}) were often found during its blooms in Dutch lakes, as well as in alpine and temperate lakes (Schreurs, 1992; Chorus et al., 2011; Moiron et al., 2021). Even in the limitation of $P\text{-}PO_4$, *P. rubescens* can utilize organic forms of phosphorus due to the presence of alkaline phosphatase or other sources of phosphorus decomposed from organic matter by heterotrophic bacteria (Feuillade et al., 1990; Jacquet et al., 2005).

The development of *P. rubescens* promptly ended in early September, when the extent of the mixing zone increased rapidly, reaching the lower layer of metalimnion (8 m in lakes Rogóźno and Krasne, 12 m in Lake Piaseczno); this led to a breakdown of the population and the complete disappearance of this species from the studied water layers. The ecological niche left by *P. rubescens* was filled by species belonging to

cryptomonads in Lake Rogóźno or other filamentous cyanobacteria in Lakes Krasne and Piaseczno. A similar scheme of complete breakdown of the population of *P. rubescens* and the development of other phytoplankton groups, diatoms, and chlorophytes in autumn has been found in temperate Lake Stechlin (Padisák et al., 2003; Salmaso and Padisák, 2007); this confirms the different dynamics of *P. rubescens* bloom in temperate lakes, which ends with the complete disappearance of its population with an undetermined moment of the next appearance. In alpine lakes, there are temporary decreases in the biomass of this species in autumn and the initiation of a new population in the following winter. Global warming has a positive influence on the development of blooms in alpine lakes, increasing water temperature, which reduces the range of the mixing zone and protects the gas vesicles in the filaments of *P. rubescens* from damage caused by high hydrostatic pressure during convective mixing, which in turn has a positive influence on the dispersion and buoyancy of this species and the initiation of a new population during the forthcoming winter (D'Alelio et al., 2011; Carey et al., 2012; Posch et al., 2012; Yankova et al., 2016, 2017; Fernández Castro et al., 2021; Knapp et al., 2021). Our research shows that such a phenomenon does not occur in temperate lakes in the lowlands. In contrast, although global warming causes similar increases in water temperatures in winter, it simultaneously reduces the occurrence of severe winters and the duration of ice cover, the presence of which is extremely important because of the establishment and persistence of *P. rubescens* populations during winter periods under stable ice cover. The lack of ice periods in winter often results in the mixing of water masses, which can persist continuously from autumn to spring, as it was at the turn of 2006 and 2007 in Lake Rogóźno when the mixing period lasted for 7 months. Such conditions negatively affect the possibility of initiating a new bloom of this cyanobacterium; however, they also support the development of other phytoplankton groups, such as diatoms (Lenard and Ejankowski, 2017).

Our study showed that the development of *P. rubescens* populations during the annual cycle in the temperate lakes studied was more influenced by physical conditions (ice phenology, low light intensity, and water temperature) than by chemical parameters (dissolved and total fractions of nitrogen and phosphorus). However, the following question arises: why did blooms not appear simultaneously in the studied lakes? We can only partially answer this question. One of the reasons for the absence of *P. rubescens* blooms in Rogóźno Lake in 2010 and 2014, when the blooms were found in the other lakes, was a significant change in the water color of this reservoir caused by a rapid rise in the water level (by more than 0.5 m), which took place in 2007; this led to the flooding of the peatlands adjacent to the lake and the release of deposited humic compounds, resulting in intense brownification of lake water. The effect of the color change was a drastic decrease in water transparency, a significant deterioration in light conditions, and consequently, a complete qualitative and quantitative remodeling of the phytoplankton community combined with the dominance of flagellate species (Lenard and Ejankowski, 2017). High watercolor is maintained in Lake Rogóźno to the present (almost 20 years), affecting the small range of the euphotic zone, which is even shallower than the mixing zone. Such conditions negatively affected the possibility of *P. rubescens* blooms in this lake, even during severe winter in 2010 and 2014, when blooms were noted in lakes Krasne and Piaseczno, respectively. The absence of this cyanobacterium in Lake Krasne in 2006 and 2014 was likely due to the occurrence of high biomass of diatoms, e.g., *Stephanodiscus medius*, and cryptomonads, e.g., *Cryptomonas curvata* and *Plagioselmis nannoplanctica* in winter periods (Lenard and Wojciechowska, 2013) and the frequent blooms of other filamentous cyanobacteria, e.g., *Limnothrix planctonica*, *Limnothrix redekei* and *Planktolyngbya limnetica*, in the upper water layers (0–4 m) during summer periods, which significantly reduced the light climate in the lake and the possibility of the development of *P. rubescens*. However, blooms did not occur in Lake Piaseczno in 2006 and 2010, when the phytoplankton biomass in winter was dominated by green algae such as *Botryococcus braunii*, *Closterium acutum* var. *variabile,* and cryptomonads, for example, *Cryptomonas* sp. (Wojciechowska and Lenard, 2014), whereas coccal cyanobacteria, such as *Aphanothece clatrata* and *Radiocystis geminata*, dominated the phytoplankton biomass in the upper water layers (0–8 m) during summer. Another question remains: What happens to *P. rubescens* filaments in temperate lakes during periods of prolonged absence of blooms? A similar dilemma regarding the return of the bloom after an absence of several years has appeared in Alpine Lake Bourget, but it has still not been clarified (Moiron et al., 2021). In our opinion, presumably during the autumn period, filaments are shortened, they lose the aerotopes, form hormogonia, and then relocate to the bottom sediments, which is characteristic of the population of *Planktothrix agardhii* (Poulíčková et al., 2004). It is likely that, in this form, the population waits until the establishment of a new winter inoculum only if favorable conditions occur in the lake from a certain climatic zone.

In conclusion, the blooms in temperate lakes in the lowlands present similar patterns of *P. rubescens* population development during the growing season (spring–summer) as in alpine lakes. However, these species differ significantly in the formation of winter inocula during annual blooms (Walsby et al., 1998; Salmaso, 2000; Moiron et al., 2021). An important role in this process is provided by the specific conditions of severe winters affecting lake ice phenology, which allow the initiation of the appearance of *P. rubesens* under ice cover. Our studies show that Global warming, manifested by the occurrence of increasingly warmer winters devoid of ice cover, has a negative impact on the possibility of establishing a new population of *P. rubescens* in temperate lakes during winter, which is not the case for alpine lakes (Yankova et al., 2017; Knapp et al., 2021; Moiron et al., 2021; Carratalà et al., 2023). The consequence of the lack of winter inoculum was the absence of *P. rubescens* throughout the year. In the lakes studied, blooms were found in 4 years intervals (2006, 2010, and 2014) that occurred over approximately 10 years, when severe winters with ice cover were noted as many as three times. Since the last bloom in Lake Piaseczno in 2014, another *ca.* 10 years have passed, during which no single occurrence of severe winters has been recorded, resulting in the absence of *P. rubescens*. Therefore, the occasional presence of this species in shallower temperate lakes seems particularly interesting, as it constitutes a counterpoint to the permanent blooms of this cyanobacterium found in very deep alpine lakes.

Data availability statement

The raw data supporting the conclusions of this article will be made available by the authors, without undue reservation.

Author contributions

TL: Conceptualization, Data curation, Formal analysis, Investigation, Methodology, Resources, Supervision, Validation, Visualization, Writing – original draft, Writing – review & editing. WE: Data curation, Investigation, Methodology, Writing – review & editing.

Funding

The author(s) declare that no financial support was received for the research, authorship, and/or publication of this article.

Conflict of interest

The authors declare that the research was conducted in the absence of any commercial or financial relationships that could be construed as a potential conflict of interest.

Publisher's note

All claims expressed in this article are solely those of the authors and do not necessarily represent those of their affiliated organizations, or those of the publisher, the editors and the reviewers. Any product that may be evaluated in this article, or claim that may be made by its manufacturer, is not guaranteed or endorsed by the publisher.

Supplementary material

The Supplementary material for this article can be found online at: https://www.frontiersin.org/articles/10.3389/fmicb.2024.1384435/full#supplementary-material

SUPPLEMENTARY FIGURE S1
Relation, in the average values of minimum **(A)**, maximum **(B)**, and mean **(C)** temperatures of air in January 2000–2023, between the years with or without the presence of *Planktothrix rubescens*. 0, periods without *P. rubescens*; 1, periods with *P. rubescens*.

SUPPLEMENTARY FIGURE S2
The relative contribution of the biomass of *Planktothrix rubescens* to the biomass of total phytoplankton in Lake Rogóźno in 2006 **(A)**; in Lake Krasne in 2010 **(B)**; in Lake Piaseczno in 2014 **(C)**.

References

Carey, C. C., Ibelings, B. W., Hoffmann, E. P., Hamilton, D. P., and Brookes, J. D. (2012). Eco-physiological adaptations that favour freshwater cyanobacteria in a changing climate. *Water Res.* 46, 1394–1407. doi: 10.1016/j.watres.2011.12.016

Carratalà, A., Chappelier, C., Selmoni, O., Guillaume, A. S., Chmiel, H. E., Pasche, N., et al. (2023). Vertical distribution and seasonal dynamics of planktonic cyanobacteria communities in a water column of deep mesotrophic Lake Geneva. *Front. Microbiol.* 14:1295193. doi: 10.3389/fmicb.2023.1295193

Chorus, I., Dokulil, M., Lammens, E., Manca, M., Naselli-Flores, L., Nixdorf, B., et al. (2011). "Restoration responses of 19 lakes: are TP thresholds common?" in Oligotrophication of Lake Tegel and Schlachtensee, Berlin analysis of system components, causalities and response thresholds compared to responses of other waterbodies, Federal Environment Agency (Umweltbundesamt), Dessau-Roßlau. eds. I. Chorus and I. Schauser (Germany), 84–102.

Chorus, I., and Welker, M. (2021). Toxic cyanobacteria in water: a guide to their public health consequences, monitoring and management. London: CRC Press, Taylor & Francis, 858.

Copetti, D., Salerno, F., Valsecchi, L., Viviano, G., Buzzi, F., Agostinelli, C., et al. (2017). Restoring lakes through external phosphorus load reduction: the case of Lake Pusiano (southern Alps). *Inland Waters* 7, 100–108. doi: 10.1080/20442041.2017.1294354

D'Alelio, D., Gandolfi, A., Boscaini, A., Flaim, G., Tolotti, M., and Salmaso, N. (2011). Planktothrix populations in subalpine lakes: selection for strains with strong gas vesicles as a function of lake depth, morphometry and circulation. *Freshw. Biol.* 56, 1481–1493. doi: 10.1111/j.1365-2427.2011.02584.x

Davis, P. A., Beard, S. J., and Walsby, A. E. (2003b). Variation in filament width and gas vesicles of red and green isolates of *Planktothrix* spp. *Algol. Stud.* 108, 15–29. doi: 10.1127/algol_stud/108/2003/15

Davis, P. A., Dent, M., Parker, J., Reynolds, C. S., and Walsby, A. E. (2003a). The annual cycle of growth rate and biomass change in *Planktothrix* spp. in Blelham Tarn, English Lake District. *Freshwat. Biol.* 48, 852–867. doi: 10.1046/j.1365-2427.2003.01055.x

Dokulil, M. T. (2016). Climate impacts on ecohydrological processes in aquatic systems. *Ecohydrol. Hydrobiol.* 16, 66–70. doi: 10.1016/j.ecohyd.2015.08.001

Dokulil, M. T., and Teubner, K. (2012). "Deep living *Planktothrix rubescens* modulated by environmental constraints and climate forcing" in Phytoplankton responses to human impacts at different scales. eds. N. Salmaso, L. Naselli-Flores, L. Cerasino, G. Flaim, M. Tolotti and J. Padisák, *Developments in Hydrobiology*, vol. *221* (Dordrecht: Springer), 29–46.

Dokulil, M. T., Teubner, K., Jagsch, A., Nickus, U., Adrian, R., Straile, D., et al. (2010). "The impact of climate change on lakes in Central Europe" in The impact of climate change on European Lakes. ed. D. G. George. Dordrecht: Springer, vol. 4, 387–410.

Ernst, B., Hoeger, S. J., O'Brien, E., and Dietrich, D. R. (2009). Abundance and toxicity of *Planktothrix rubescens* in the pre-alpine Lake Ammersee, Germany. *Harmful Algae* 8, 329–342. doi: 10.1016/J.HAL.2008.07.006

Fernández Castro, B., Sepúlveda Steiner, O., Knapp, D., Posch, T., Bouffard, D., and Wüest, A. (2021). Inhibited vertical mixing and seasonal persistence of a thin cyanobacterial layer in a stratified lake. *Aquat. Sci.* 83:38. doi: 10.1007/s00027-021-00785-9

Feuillade, J. (1994). The cyanobacterium (blue-green alga) *Oscillatoria rubescens* D. C. *Archiv für Hydrobiologie – Ergebnisse der Limnologie Beiheft. Adv. Limnol.* 41, 77–93.

Feuillade, M., Feuillade, J., and Blanc, P. (1990). Alkaline phosphatase activity fluctuations and associated factors in a eutrophic lake dominated by *Oscillatoria rubescens*. *Hydrobiologia* 207, 233–240. doi: 10.1007/BF00041461

GISTEMP Team. (2024). GISS surface temperature analysis (GISTEMP), version 4. NASA Goddard Institute for Space Studies. Available at: https://data.giss.nasa.gov/gistemp/

Harasimiuk, M., Michalczyk, Z., and Turczyński, M. (1998). "Jeziora łęczyńsko-włodawskie. Monografia przyrodnicza" in Biblioteka Monitoringu Środowiska; Studia Ośrodka Dokumentacji Fizjograficznej (Lublin, Poland).

Hermanowicz, W., Dojlido, J., Dożańska, W., Koziorowski, B., and Zerbe, J. (1999). Fizyczno-chemiczne badanie wody i ścieków. Warszawa, Poland: Arkady.

Hessen, D. O., Andersen, T., Larsen, S., Skjelkvåle, B. L., and De Wit, H. A. (2009). Nitrogen deposition, catchment productivity, and climate as determinants of lake stoichiometry. *Limnol. Oceanogr.* 54, 2520–2528. doi: 10.4319/lo.2009.54.6_part_2.2520

Hillebrand, H., Dürselen, C. D., Kirschtel, D., Pollingher, U., and Zohary, T. (1999). Biovolume calculation for pelagic and benthic microalgae. *J. Phycol.* 35, 403–424. doi: 10.1046/j.1529-8817.1999.3520403.x

Hingsamer, P., Peeters, F., and Hofmann, H. (2014). The consequences of internal waves for phytoplankton focusing on the distribution and production of *Planktothrix rubescens*. *PLoS One* 9:e104359. doi: 10.1371/journal.pone.0104359

Ho, J. C., Michalak, A. M., and Pahlevan, N. (2019). Widespread global increase in intense lake phytoplankton blooms since the 1980s. *Nature* 574, 667–670. doi: 10.1038/s41586-019-1648-7

Huisman, J., Codd, G. A., Paerl, H. W., Ibelings, G. W., Verspagen, J. M. H., and Visser, P. M. (2018). Cyanobacterial blooms. *Nat. Rev. Microbiol.* 16, 471–483. doi: 10.1038/s41579-018-0040-1

Jacquet, S., Briand, J. F., Leboulanger, C., Avois-Jacquet, C., Oberhaus, L., Tassin, B., et al. (2005). The proliferation of the toxic cyanobacterium *Planktothrix rubescens* following restoration of the largest natural French lake (lac du Bourget). *Harmful Algae* 4, 651–672. doi: 10.1016/j.hal.2003.12.006

Knapp, D., Fernández Castro, B., Marty, D., Loher, E., Köster, O., Wüest, A., et al. (2021). The red harmful plague in times of climate change: blooms of the cyanobacterium *Planktothrix rubescens* triggered by stratification dynamics and irradiance. *Front. Microbiol.* 12:705914. doi: 10.3389/fmicb.2021.705914

Komárek, J., and Anagnostidis, K. (2008). Cyanoprokaryota, 2. Teil/part 2: Oscillatoriales, Süswasser Flora von Mitteleuropa. Heidelberg: Elsevier, Freshwater Flora of Central Europe.

Komárek, J., and Komárková, J. (2004). Taxonomic review of the cyanoprokaryotic genera Planktothrix and Planktothricoides. *Czech Phycol.* 4, 1–18.

Kondracki, J. (2002). Geografia regionalna Polski. Warszawa, Poland: PWN.

Köster, O., and Jüttner, F. (1999). NH4+ utilization and regeneration rates in freshwater lakes determined by GC–MS of derivatised dihydroindophenol. *J. Microbiol. Methods* 37, 65–76. doi: 10.1016/S0167-7012(99)00042-1

Kraemer, B. M., Pilla, R. M., Woolway, R. I., Anneville, O., Ban, S., Colom-Montero, W., et al. (2021). Climate change drives widespread shifts in lake thermal habitat. *Nat. Clim. Chang.* 11, 521–529. doi: 10.1038/s41558-021-01060-3

Kröger, B., Selmeczy, G. B., Casper, P., Soininen, J., and Padisák, J. (2023). Long-term phytoplankton community dynamics in Lake Stechlin (north-East Germany) under sudden and heavily accelerating eutrophication. *Freshw. Biol.* 68, 737–751. doi: 10.1111/fwb.14060

Kromkamp, J. C., Domin, A., Dubinsky, Z., Lehmann, C., and Schanz, F. (2001). Changes in photosynthetic properties measured by oxygen evolution and variable chlorophyll fluorescence in a simulated entrainment experiment with the cyanobacterium *Planktothrix rubescens*. *Aquat. Sci.* 63, 363–382. doi: 10.1007/PL00001360

Krupa, D., and Czernaś, K. (2003). Mass appearance of cyanobacterium *Planktothrix rubescens* in Lake Piaseczno, Poland. *Water Qual. Res. J.* 38, 141–152. doi: 10.2166/wqrj.2003.009

Kurmayer, R., Deng, L., and Entfellner, E. (2016). Role of toxic and bioactive secondary metabolites in colonization and bloom formation by filamentous cyanobacteria *Planktothrix*. *Harmful Algae* 54, 69–86. doi: 10.1016/j.hal.2016.01.004

Leach, T. H., Beisner, B. E., Carey, C. C., Pernica, P., Rose, K. C., Huot, Y., et al. (2018). Patterns and drivers of deep chlorophyll maxima structure in 100 lakes: the relative importance of light and thermal stratification. *Limnol. Oceanogr.* 63, 628–646. doi: 10.1002/lno.10656

Legnani, E., Copetti, D., Oggioni, A., Tartari, G., Palumbo, M. T., and Morabito, G. (2005). Planktothrix rubescens' seasonal dynamics and vertical distribution in Lake Pusiano (North Italy). *J. Limnol.* 64, 61–73. doi: 10.4081/jlimnol.2005.61

Lenard, T. (2009). Metalimnetic bloom of *Planktothrix rubescens* in relation to environmental conditions. *Oceanol. Hydrobiol. Stud.* 38, 45–53.

Lenard, T. (2015). Winter bloom of some motile phytoplankton under ice cover in a mesotrophic lake: vertical distribution and environmental factors. *Oceanol. Hydrobiol. Stud.* 44, 164–171. doi: 10.1515/ohs-2015-0016

Lenard, T., and Ejankowski, W. (2017). Natural water brownification as a shift in the phytoplankton community in a deep hard water lake. *Hydrobiologia* 787, 153–166. doi: 10.1007/s10750-016-2954-9

Lenard, T., and Poniewozik, M. (2022). *Planktothrix agardhii* versus Planktothrix rubescens: separation of ecological niches and consequences of cyanobacterial dominance in freshwater. *Int. J. Environ. Res. Public Health* 19:14897. doi: 10.3390/ijerph192214897

Lenard, T., and Wojciechowska, W. (2013). Phytoplankton diversity and biomass during winter with and without ice cover in the context of climate change. *Pol. J. Ecol.* 61:739–748.

Lenssen, N., Schmidt, G., Hansen, J., Menne, M., Persin, A., Ruedy, R., et al. (2019). Improvements in the GISTEMP uncertainty model. *J. Geophys. Res. Atmos.* 124, 6307–6326. doi: 10.1029/2018JD029522

Messineo, V., Mattei, D., Melchiorre, S., Salvatore, G., Bogialli, S., Salzano, R., et al. (2006). Microcystin diversity in a *Planktothrix rubescens* population from Lake Albano (Central Italy). *Toxicon* 48, 160–174. doi: 10.1016/j.toxicon.2006.04.006

Messyasz, B., Czerwik-Marcinkowska, J., Lücke, A., and Uher, B. (2012). Differences in the ultrastructure of two selected taxa of phytoplankton in a thermally stratified Lake Holzmaar (Germany). *Biodiv. Res. Conserv.* 28, 55–62. doi: 10.2478/v10119-012-0029-y

Michalczyk, Z., Mięsiak-Wójcik, K., Sposób, J., and Turczyński, M. (2017). The state of and changes in water conditions in the Łęczna-Włodawa Lake District. *Przegląd Geograficzny* 89, 9–28. doi: 10.7163/PrzG.2017.1.1

Micheletti, S., Schanz, F., and Walsby, A. E. (1998). The daily integral of photosynthesis by *Planktothrix rubescens* during summer stratification and autumnal mixing in Lake Zurich. *New Phytol.* 139, 233–246. doi: 10.1046/j.1469-8137.1998.00196.x

Moiron, M., Rimet, F., Girel, C., and Jacquet, S. (2021). Die hard in Lake Bourget! The case of *Planktothrix rubescens* reborn. *Ann. Limnol. Int. J. Lim* 57:19. doi: 10.1051/limn/2021014

Nandagopal, P., Steven, A. N., Chan, L. W., Rahmat, Z., Jamaluddin, H., and Mohd Noh, N. I. (2021). Bioactive metabolites produced by cyanobacteria for growth adaptation and their pharmacological properties. *Biology* 10:1061. doi: 10.3390/biology10101061

Naselli-Flores, L., Barone, R., Chorus, I., and Kurmayer, R. (2007). Toxic cyanobacterial blooms in reservoirs under a semiarid Mediterranean climate: the magnification of a problem. *Environ. Toxicol.* 22, 399–404. doi: 10.1002/tox.20268

Nusch, E. A. (1980). Comparison of different methods for chlorophyll and phaeopigment determination. *Arch. Hydrobiol Beih. Ergebn. Limnol.* 14, 14–36.

Oberhaus, L., Briand, J. F., and Humbert, J. F. (2008). Allelopathic growth inhibition by the toxic bloom-forming cyanobacterium *Planktothrix rubescens*. *FEMS Microbiol. Ecol.* 66, 243–249. doi: 10.1111/j.1574-6941.2008.00567.x

Oberhaus, L., Briand, J. F., Leboulanger, C., Jacquet, S., and Humbert, J. F. (2007). Comparative effect of the quality of light and temperature on the growth of *Planktothrix agardhii* and *Plankttthrix rubescens*. *J. Phycol.* 43, 1191–1199. doi: 10.1111/j.1529-8817.2007.00414.x

Padisák, J., Scheffler, W., Kasprzak, P., Koschel, R., and Krienitz, L. (2003). Interannual variability in the phytoplankton composition of Lake Stechlin (1994–2000). *Arch. Hydrobiol. Spec. Issues Advanc. Limnol.* 58, 135–155.

Paerl, H. W., and Huismann, J. (2008). Blooms like it hot. *Science* 320, 57–58. doi: 10.1126/science.1155398

Pasztaleniec, A. (2016). Phytoplankton in the ecological status assessment of European lakes – advantages and constraints. *Environ. Protect. Nat. Resour.* 27, 26–36. doi: 10.1515/oszn-2016-0004

Pielou, E. C. (1975). Ecological diversity. John Wiley & Sons: New York.

Posch, T., Köster, O., Salcher, M. M., and Pernthalen, J. (2012). Harmful filamentous cyanobacteria favoured by reduced water turnover with lake warming. *Nat. Clim. Chang.* 2, 809–813. doi: 10.1038/nclimate1581

Poulíčková, A., Hašler, P., and Kitner, M. (2004). Annual cycle of *Planktothrix agardhii* (Gom.) Anagn. & Kom. Nature population. *Int. Rev. Hydrobiol.* 89, 278–288. doi: 10.1002/iroh.200310716

Reynolds, C. S. (2006). Ecology of phytoplankton. United Kingdom, New York: Cambridge University Press.

Salmaso, N. (2000). Factors affecting the seasonality and distribution of cyanobacteria and chlorophytes: a case study from the large lakes south of the Alps, with special reference to Lake Garda. *Hydrobiologia* 438, 43–63. doi: 10.1023/A:1004157828049

Salmaso, N., Boscaini, A., Shams, S., and Cerasino, L. (2013). Strict coupling between the development of *Planktothrix rubescens* and microcystin content in two nearby lakes south of the Alps (lakes Garda and Ledro). *Ann. Limnol.* 49, 309–318. doi: 10.1051/limn/2013064

Salmaso, N., and Padisák, J. (2007). Morpho-functional groups and phytoplankton development in two deep lakes (Lake Garda, Italy and Lake Stechlin, Germany). *Hydrobiologia* 578, 97–112. doi: 10.1007/s10750-006-0437-0

Samuelsson, P. (2010). "Using regional climate models to quantify the impact of climate change on lakes" in The impact of climate change on European Lakes. ed. D. G. George, Dordrecht: Springer 4, 15–32.

Schanz, F. (1986). Depth distribution of phytoplankton and associated spectral changes in downward irradiance in Lake Zürich (1980/81). *Hydrobiologia* 134, 183–192. doi: 10.1007/BF00006740

Schreurs, H. (1992). Cyanobacterial dominance. Relations to eutrophication and lake morphology. Doctoral thesis, University of Amsterdam.

Shannon, C. E., and Wiener, W. (1963). The mathematical theory of communication. Urbana, Illinois: University of Illinois Press.

Sokal, R. R., and Rohlf, F. J. (1995). Biometry: The principles and practice of statistics in biological research. *3rd* Edn. New York: W. H. Freeman and Co.

Utermöhl, H. (1958). Zur Vervollkommung der quantitative Phytoplankton-Methodik. *Mitt. Int. Verein. Theor. Angew. Limnol.* 9, 1–38.

Walsby, A. E., Avery, A., and Schanz, F. (1998). The critical pressures of gas vesicles in *Planktothrix rubescens* in relation to the depth of winter mixing in Lake Zurich (Switzerlaand). *J. Plankton Res.* 20, 1357–1375. doi: 10.1093/plankt/20.7.1357

Walsby, A. E., Dubinsky, Z., Kromkamp, J. C., Lehmann, C., and Schanz, F. (2001). The effects of diel changes in photosynthetic coefficients and depth of *Planktothrix rubescens* on the daily integral of photosynthesis in Lake Zürich. *Aquat. Sci.* 63, 326–349. doi: 10.1007/PL00001358

Walsby, A. E., and Schanz, F. (2002). Light-dependent growth rate determines changes in the population of Planktothrix rubescens over the annual cycle in Lake Zürich, Switzerland. *New Phytol.* 154, 671–687. doi: 10.1046/j.1469-8137.2002.00401.x

Weiskopf, S. R., Rubenstein, M. A., Crozier, L. G., Gaichas, S., Griffis, R., Halofsky, J. E., et al. (2020). Climate change effects on biodiversity, ecosystems, ecosystem services, and natural resource management in the United States. *Sci. Total Environ.* 733:137782. doi: 10.1016/j.scitotenv.2020.137782

Wojciechowska, W., and Krupa, D. (1992). Many years and seasonal changes in phytoplankton of lakes of Polesie National Park and its protection zone. *Ekol. Polska* 40, 317–332.

Wojciechowska, W., and Lenard, T. (2014). Effect of extremely severe winters on under-ice phytoplankton development in a mesotrophic lake (Eastern Poland). *NOceanol. Hydrobiol. Stud.* 43, 147–153. doi: 10.2478/s13545-014-0127-X

Woolway, R. I., Kraemer, B. M., Lenters, J. D., Merchant, C. J., O'Reilly, C. M., and Sharma, S. (2020). Global lake responses to climate change. *Nat. Rev. Earth Environ.* 1, 388–403. doi: 10.1038/s43017-020-0067-5

Yankova, Y., Neuenschwander, S., Köster, O., and Posch, T. (2017). Abrupt stop of deep water turnover with lake warming: drastic consequences for algal primary producers. *Sci. Rep.* 7:13770. doi: 10.1038/s41598-017-13159-9

Yankova, Y., Villiger, J., Pernthaler, J., Schanz, F., and Posch, T. (2016). Prolongation, deepening and warming of the metalimnion change habitat conditions of the harmful filamentous cyanobacterium *Planktothrix rubescens* in a prealpine lake. *Hydrobiologia* 776, 125–138. doi: 10.1007/s10750-016-2745-3

Frontiers in Microbiology

Explores the habitable world and the potential of microbial life

The largest and most cited microbiology journal which advances our understanding of the role microbes play in addressing global challenges such as healthcare, food security, and climate change.

Discover the latest Research Topics

See more →

Frontiers

Avenue du Tribunal-Fédéral 34
1005 Lausanne, Switzerland
frontiersin.org

Contact us

+41 (0)21 510 17 00
frontiersin.org/about/contact